A taphonomic and palaeoecological approach to the study of palaeocolour

Fiann Michael Smithwick

A dissertation submitted to the University of Bristol in accordance with the requirements for award of the degree of Doctor of Philosophy in the Faculty of Science, School of Earth Sciences. **March 2019.**

Word count: 71,600

Artwork: Lisa Sanchez

Abstract

The field of palaeocolour has greatly improved our understanding of how many extinct animals looked and behaved. Preservation of the pigment melanin allows for several aspects of colour patterns to be revealed and inferences of likely ecologies and behaviours made based on comparisons to living taxa. Additionally, important aspects of soft tissue taphonomy in fossils have been ascertained through the study of fossil melanin. The field is still in its infancy however, leaving much to be understood in terms of what is preserved, how and what biases may exist. There is also debate as to the nature and preservation of soft tissue features important to palaeocolour, such as feathers and skin. In this thesis, I explore the nature of soft tissue preservation in the integument of several non-avian dinosaurs, crown group avians and Jurassic ichthyosaurs, revealing their melanin-based colouration using chemical and microscopy approaches. Issues surrounding previous interpretations of soft tissue anatomy in ichthyosaurs and the Early Cretaceous theropod *Sinosauropteryx* are addressed and comprehensive re-descriptions carried out allowing palaeocolours to be reconstructed and ecological implications explored. The palaeocolour of the non-avian theropod, *Caudipteryx* is also investigated in the same manner. Methods for revealing melanosomes (organelles containing melanin) from modern feathers are investigated and revised, allowing comparisons to fossil examples. Using these revised methods, the palaeocolours of several extinct Eocene birds are reconstructed and their likely habitats and ecologies investigated in a phylogenetic framework using melanosome data from their closest living relatives. Novel data on modern melanosomes and the evolution of iridescent colouration in several crown group bird clades are also revealed. My work advances the field of palaeocolour in terms of taphonomic biases involved, how to sample and infer colour patterning with these in mind and finally how to integrate extant and fossil colour data in a phylogenetic comparative framework.

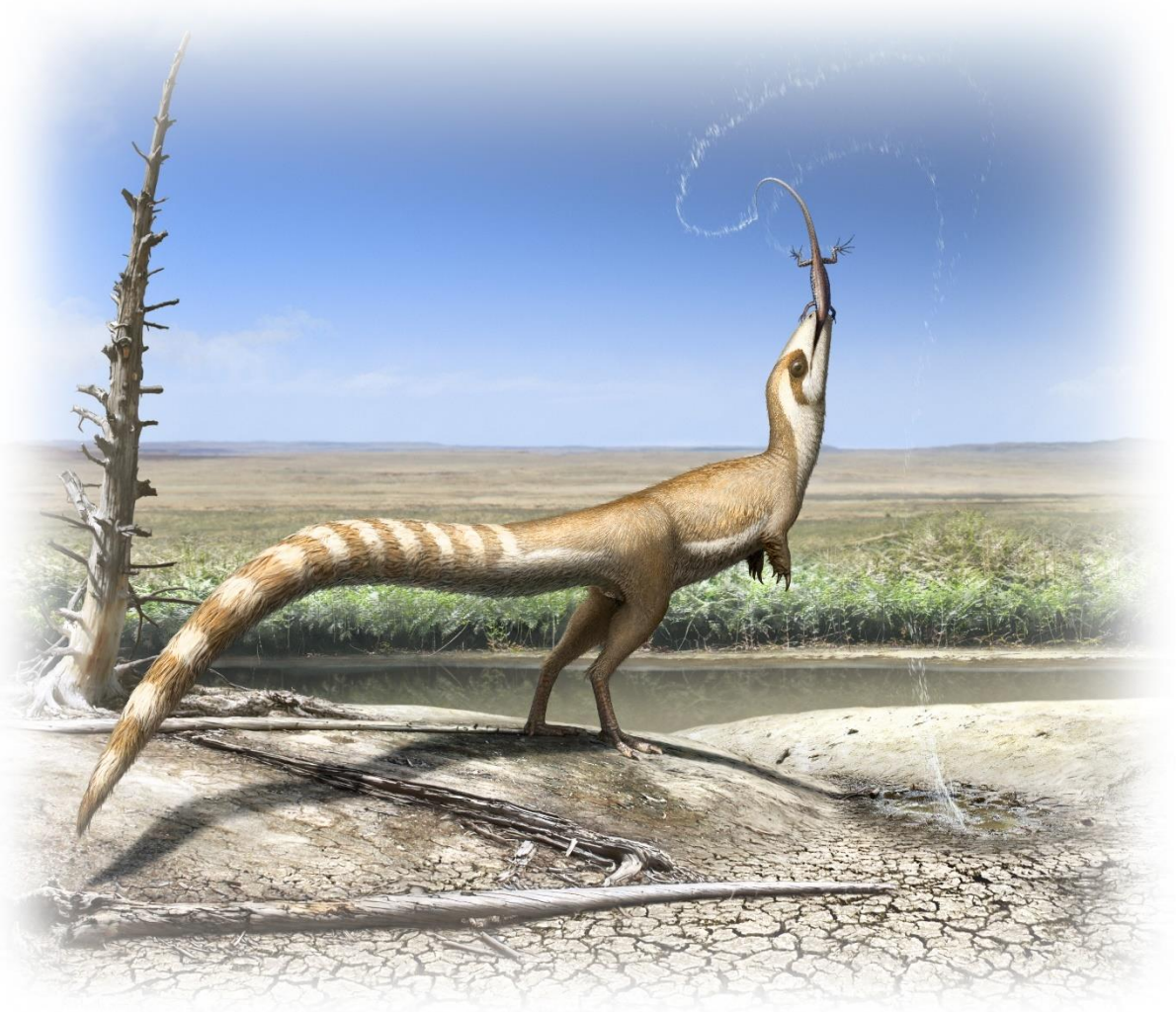

Artwork: Bob Nicholls

Dedication and acknowledgements

This thesis is dedicated to my parents for encouraging and supporting me in all of my endeavours and giving me the space and encouragement to do what I am most passionate about in life, my brother and sister for being supportive friends as well as siblings and Flora Beverley for being my (non-geological) rock and saviour.

I would like to thank Mike Benton for guiding me along my academic path and Mary Benton for letting me get started on it in the first place. I would also like to thank Gerald Mayr for his help and support with museum collections of the Messel material and advice on avian evolution, Daniel Field for guiding my writing and ideas and inspiring the bird nerd in me, Innes Cuthill for making me think like an ecologist as well as a palaeontologist and Sally Hobson for helping me hone my technical skills. Frane Babarović, Klara Nordén and Jaeike Faber provided invaluable help with my investigations into modern melanosomes and techniques for their extraction from feathers. Robert Nicholls and Lisa Sanchez provided the beautiful artwork that brings the extinct animals in this thesis back to life. Finally, I would like to thank Jakob Vinther for getting me into this whole subject area and making me think like a scientist.

I would also like to thank my funding body, the Natural Environment Research Council (NERC) for making all of this possible and for providing the generous financial and training support of the GW4+ Doctoral Training Partnership (DTP).

Artwork: Fiann Smithwick

Artwork: Bob Nicholls

Author’s declaration

I declare that the work in this dissertation was carried out in accordance with the requirements of the University's *Regulations and Code of Practice for Research Degree Programmes* and that it has not been submitted for any other academic award. Except where indicated by specific reference in the text, the work is the candidate's own work. Work done in collaboration with, or with the assistance of, others, is indicated as such. Any views expressed in the dissertation are those of the author.

SIGNED: ..... DATE: .....

Artwork: Lisa Sanchez

Table of Contents

List of figures

Introduction

Chapter 1

Chapter 2

Chapter 5

Chapter 6

Chapter 7

Chapter 8

General discussion and conclusions

List of tables

Chapter 3

Chapter 5

Chapter 6

Chapter 7

Chapter 8

General introduction

Until about a decade ago it was thought that certain aspects of extinct organisms and their appearance were impossible to determine. One of these aspects was original colouration (Turner 2007). With the discovery that the pigment melanin can preserve in fossils (Vinther et al. 2008), and the subsequent advent of the field of "palaeocolour", this has been turned on its head (Cleland 2011). Since 2008, the likely colour patterns of several extinct avian and non-avian dinosaurs have been revealed (Vinther et al. 2008; Li et al. 2010, 2012; Zhang et al. 2010; Vinther et al. 2016; Brown et al. 2017; Hu et al. 2018). This in turn has permitted more detailed inferences to be made about the ecologies and behaviours of these animals as well as the nature of ecological interactions, such as predator-prey dynamics in deep time (Vinther 2015*a*; Vinther et al. 2016; Brown et al. 2017). This field is still in its infancy however - novel methods are being developed and new data revealed that are changing how we look at extinct animals. The field is also helping to advance our understanding of taphonomy more generally through investigations into the nature of soft tissue preservation as we try to better understand how and why melanin preserves when so many other soft tissues are lost during decay and/or diagenesis (Glass et al. 2010, 2012; Colleary et al. 2015; Vinther 2015*a*; Saitta et al. 2017; Parry et al. 2018).

Colour in modern animals

In order to understand colour and its likely function and evolution in extinct animals, we first need to appreciate the types of colour pattern present in extant animals and potential related functions. Colour plays a pivotal role in the ecology of most animal clades (Thayer 1896; Cott 1940; Endler 1990; Hill and McGraw 2006*a*; Stevens and Merilaita 2008; Ruxton et al. 2018). Colour patterns can evolve in response to the visual perception of a receiver due to optical properties, nonoptical functions or a mixture of the two (Endler et al. 2005; Bortolotti 2006; Stoddard and Prum 2011). Colour patterns that have evolved due to their optical properties have likely been important since the evolution of the eye at least as far back as the early

Cambrian (Goldsmith 1990; Land and Fernald 1992; Fernald 2000; Collin et al. 2003; Nilsson 2009; Strausfeld et al. 2016) and can impact all aspects of animal ecology (Hill and McGraw 2006*a*). Nonoptical functions of colour still usually have an optical element, as trade-offs are needed between non-visual functions and the need to either be seen by others (conspicuousness) or to remain hidden from predators (crypsis) (Osorio and Srinivasan 1991; Bortolotti 2006; Stevens 2007; Rowland 2009; Caro 2011; Ruxton et al. 2018). Few animals live in an environment completely devoid of light, and so colour patterns will almost always be seen by other animals. Because colour patterns that have evolved for their optical properties are dependent on the intended receiver, they can inform about more than just an individual animal (Osorio and Srinivasan 1991; Guilford and Dawkins 1991; Bortolotti 2006; Stevens 2007). Dynamic animal interactions, such as predator-prey landscapes, can be informed by the colouration of different taxa (Thayer 1896, Cott 1940; Osorio and Srinivasan 1991; Brown et al. 2017), for example by providing a better understanding of the visual capabilities of both predators and prey (Osorio and Srinivasan 1991; Stevens 2007; Stuart-Fox et al. 2008). Conversely, understanding the vision of one animal can inform the potential function of colour patterns in another (Osorio and Srinivasan 1991; Stevens 2007; Stuart-Fox et al. 2008).

Colour can be a highly labile trait resulting in rapid phenotypic evolution (Endler et al. 2005; Hill and McGraw 2006*a*), helping to explain the vast and dazzling array of colours present in living animals that include hues far beyond the visual range of humans (Stoddard and Prum 2011). Despite centuries of study, the function and evolution of colour in animals is still incompletely understood (Bortolotti 2006). We do know that vision-driven colour patterns can serve to increase or decrease conspicuousness for a multitude of functions (Hill and McGraw 2006*a*; Stevens and Merilaita 2008).

Decreasing conspicuousness through colour patterning is key to camouflage in many animals (Thayer 1909; Ruxton et al. 2018). Colouration that helps to mask the presence of an animal, helping it avoid predation is common in all animal groups (Stevens and Merilaita 2008, 2011; Ruxton et al. 2018). These cryptic colour patterns often relate to background matching, having colours that help an animal blend into its surroundings making it harder to detect (Fig. I1a-c; Merilaita and Lind 2005; Stevens and Merilaita 2008, 2011). Background matching can be

achieved through either static colouration (most cases; Fig. I1a) or dynamic colour change (e.g., some cephalopods (Fig. I1b) and chameleons (Fig. I1c)) and will depend on the environment in which an animal lives and is attempting to blend into (Bortolotti 2006; Hanlon et al. 2008; Stevens and Merilaita 2008, 2011; Ruxton et al. 2018).

Figure I1. Examples of common camouflage patterns seen in extant animals. **a**. The Egyptian Nightjar (*Caprimulgus aegyptius*) showing background matching camouflage. **b**. A juvenile cuttlefish showing dynamic background matching. **c**. Jackson's Chamaeleon (*Trioceros jacksonii*) showing dynamic background matching. **d**. The Shortfin Mako shark (*Isurus oxyrinchus*) exhibiting typical countershading (a dark dorsum and light ventrum). **e**. The Pronghorn (*Antilocapra Americana*) showing countershading that can inform as to its likely habitat. **f-g**. The Tau Emperor (*Aglia tau*) caterpillar showing reverse countershading with a light dorsum and dark ventrum which is

conspicuous when on top of a branch (f) but counterbalances the illumination gradient when under a branch (g). **h**. The American Bittern (*Botaurus lentiginosus*) in an erect posture mimicking the reeds it inhabits. **i**. The Common Potoo (*Nyctibius griseus*) mimicking a dead branch by holding itself erect. **j**. The Great Oak Beauty caterpillar (*Hypomecis roboraria*) showing masquerade camouflage by imitating a twig. **k**. The Giant Leaf Insect (*Phyllium giganteum*) masquerading as a leaf. **l**. The Edible Frog (*Rana esculenta*) showing coincident disruptive colouration across the legs. **m**. The Southern Leopard Frog (*Rana sphenocephala*) with disruptive colouration running through the eye. **n**. A moth displaying both contrasting colour patterns that break up the body outline and blend into the mottled background. Image credits: (a) Wikipedia user "K", (b) Wikipedia user "Raul645", (f-g) Wikipedia user "Gopp pi", (h) Flickr user "seabamirum", (i) Julian Londono Jaramillo, (j) Gyorgy Csoka, (k) Bernard Dupont and (m) Trish Hartmann. All other images marked as public domain.

Another common form of camouflage in extant animals is countershading – typically having a darker dorsum than ventrum (Fig. I1d-e; Thayer 1896; Rowland 2009, 2011; Allen et al. 2012; Ruxton et al. 2018). Countershading acts to reduce the three-dimensionality of an object by optically flattening the appearance of the body by reducing self-shadowing (Thayer 1896; Rowland 2009, 2011; Allen et al. 2012; Vinther et al. 2016). Self-shadowing is an important visual cue (shape from shading) in practically all animal visual systems (Allen et al. 2012). This may help to explain why countershading has evolved in animal groups as disparate as sharks, mammals, reptiles, insects and cephalopods (Fig. I1d-g; Ferguson and Messenger 1991; Edmunds and Dewhirst 1994; Rowland et al. 2008; Rowland 2009, 2011; Allen et al. 2012; Ruxton et al. 2018). The precise pattern of countershading can inform as to the habitat certain animals are best adapted to, based on the ambient lighting conditions (Allen et al. 2012). Reverse-countershading, having a darker ventrum than dorsum also exists in some animals, and is particularly prevalent in insects that hide underneath branches (Fig. I1f-g), reversing the part of the body illuminated by the environmental lighting conditions (Rowland 2011). Alternative (but not necessarily contradicting) functions of countershading have also been proposed, including background matching, UV protection and thermoregulation (Stevens and Merilaita 2008; Rowland 2009, 2011).

Behaviour and posture are also clearly important in camouflage (Bortolotti 2006; Kamilar and Bradley 2011; Merilaita and Stevens 2011; Webster et al. 2011). Some

countershaded animals have been shown to orientate themselves so that their darker surface always faces the direction of illumination, even when that direction is artificially changed (Rowland et al. 2008; Rowland 2011). Background matching may only work if an animal remains motionless when predators are nearby (Ioannou and Krause 2009; Hultgren and Stachowicz 2011; Merilaita and Stevens 2011). Behaviours have evolved to facilitate this. For example, the American Bittern, a reed-inhabiting bird, erects its neck and head so that its stripes blend in with the reeds and even sways back and forth to imitate reeds blowing in the wind (Fig. I1h; Bortolotti 2006). Potoos will mimic broken tree branches by displaying erect postures which, combined with their highly cryptic plumage, allows them to blend seamlessly into the trees in which they perch (Fig. I1i). Some animals have taken this a step further and have evolved to look like inanimate objects in their environment (a strategy called masquerade) and often must pose in a way that aids the deception to avoid predation (Fig. I1j-k).

Colouration that increases conspicuousness is common throughout all animal clades and usually serves as either intraspecific or interspecific communication (Hill and McGraw 2006*a*). The function of these colour patterns therefore depends on the intended receiver (Guilford and Dawkins 1991; Stevens 2007). Camouflage through conspicuous patterning is also common. "Coincident disruptive colouration", having colour patterns that break up the outline of a body or body part in an attempt to mask its identity, can serve as camouflage (Fig. I1l-n; Cott 1940; Schaefer and Stobbe 2006; Stevens and Merilaita 2008; Cuthill and Székely 2011; Ruxton et al. 2018). Highly contrasting colour patterns that disrupt anatomical boundaries can reduce object recognition, particularly when they occur at the body's edge (Cott 1940; Cuthill and Székely 2009). These colour patterns can occur over the whole body or in restricted regions such as the limbs (Fig. I1l), head or across the eyes (Fig. I1m) (Cott 1940; Cuthill and Székely 2009). Disruptive camouflage and background matching may also work in tandem, for example breaking the outline of the body while also showing a pattern that blends into a specific background (Fig. I1n; Schaeffer and Stobbe 2006). A further possible camouflage function of conspicuous patterns is "dazzle camouflage", whereby the presence of bold contrasting colours may serve to confuse predators by making motion hard to predict in a prey animal (Stevens et al. 2011). Distractive markings can serve to confuse predators or draw the attention of a

predator away from the body outline (Stevens et al. 2012; Caro and Allen 2017). However, both dazzle camouflage and distraction markings have limited empirical support and have long been a source of debate (Stevens et al. 2012; Hughes et al. 2014). Non-camouflage interspecific conspicuous colour patterns can also serve multiple functions, including deimatism (startling a predator to deter attack), flushing (startling a prey animal to make it easier to catch), luring prey and mimicking of innocuous prey (all reviewed in Caro and Allen 2017).

Conspicuous colour patterns may serve a multitude of functions along with camouflage, including intraspecific communication and aposematism (warning colouration) (Cott 1940; Bortolotti 2006; Stevens and Merilaita 2011). Aposematic warning colouration (Fig. I2a) can indicate to a potential predator that an animal is toxic, unpalatable or highly aggressive (Mappes et al. 2005; Caro 2011). Conspicuous colour patterns used in intraspecific communication can be intended for members of the same sex, such as rival males in territorial or highly competitive species (Fig. I2b; Seehausen and Schluter 2004; Dijkstra et al. 2005; Senar 2006), potential mates (Fig. I2c; Hill 1990, 2006) or both sexes in species or kin recognition (Dale 2006). Intraspecific colour signalling is a key driver in sexual selection, particularly in highly colourful clades such as birds (Hill and McGraw 2006*a*).

While broad relationships between colour patterning and functions can often be determined, it is likely that in most cases there is an interplay between multiple functions (Bortolotti 2006). Dark stripes or patches around the eyes are common in multiple animal clades (Fig. I2d-e) and have had several possible functions hypothesised, which are not necessarily mutually exclusive. These include reducing glare from surrounding fur or feathers, targeting lines for binocular predators, sexual ornaments or aposematic warnings of aggressive behaviour (Ficken and Wilmot 1968; Ortolani 1998; Caro 2005, 2013; Bortolotti 2006). Spots and bands/stripes are common in many clades and can have mixed functions. Banded feathers in birds and stripes in fishes are examples of this - empirical data have shown that in some cases they can serve the dual purpose of sexual signalling and camouflage depending on the distance at which they are viewed (Fig. I2e-f; Marshall 2000; Gluckman and Cardoso 2010; Marques et al. 2016).

Non-visual functions of colour patterns have also been proposed but have received far less attention than those inferring optical properties (Bortolotti 2006). Functions including thermoregulation, UV protection, abrasion resistance, integumentary hardening and bacterial protection have been proposed (Bortolotti 2006). Further novel functions are still been described; for example, dark dorsal wing surfaces in seabirds providing extra lift through thermal reduction of skin drag forces (Hassanalian et al. 2017).

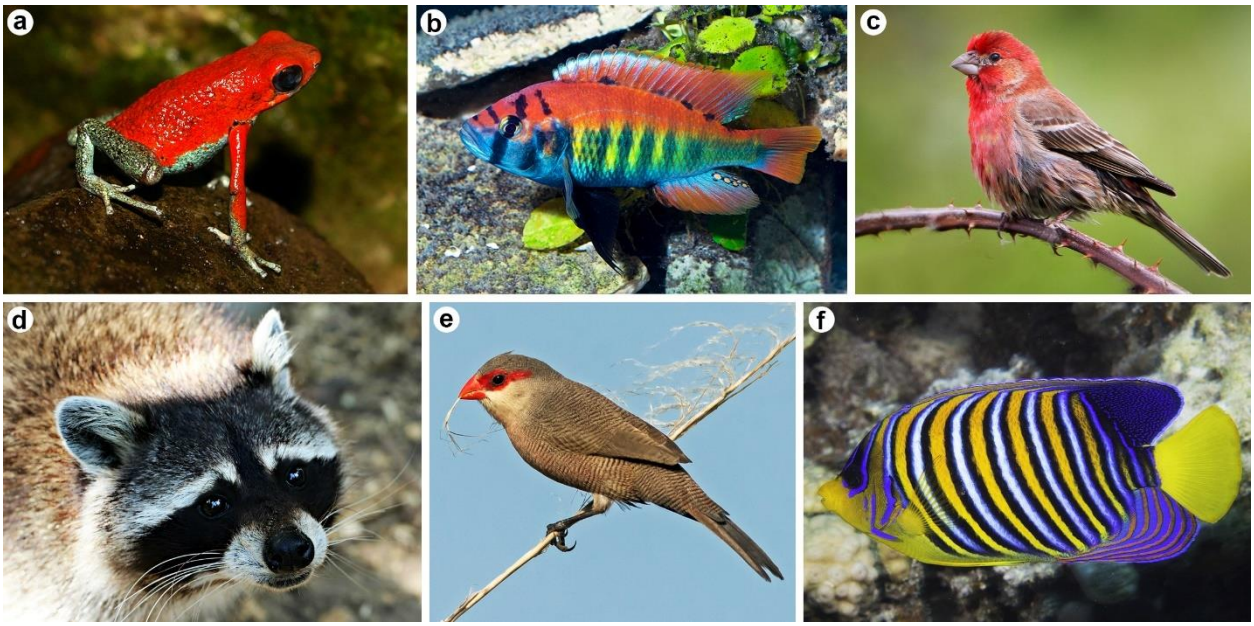

Figure I2. Conspicuous colour patterns in modern animals. **a**. The Granular Poison Frog (*Oophaga granulifera*) showing conspicuous aposematic warning colours to advertise its toxicity to potential predators. **b**. The Lake Victorian cichlid *Pundamilia nyererei* whose bright conspicuous colours are driven at least in part by male-male competition **c**. The male House Finch (*Haemorhous mexicanus*), a bird whose conspicuous colours are driven by female preference. **d**. The raccoon (*Procyon lotor*) with a "bandit mask" dark colour around the eyes which has had multiple functions hypothesised. **e**. The Common Waxbill (*Estrilda astrild*) with a coloured eye stripe and fine banding across the body that confers both camouflage at distance and acts as a sexual ornament at close range. **f**. The Regal Angelfish (*Pygoplites diacanthus*) showing strong banding that acts as an intraspecific signal at close range and blurs at greater distances providing camouflage against predators. Image credits: (a) Patrick Gijsbers, (b) Kevin Bauman, (c) Flickr user "Nigel", (d) public domain image, (e) Juan Emilio, (f) Flickr user "zsispeo".

Investigating colour in extinct animals

Extending our understanding of colour patterns into deep (geological) time can allow us to explore the evolution of colour patterns as well as possible functions and behaviours in the past based on knowledge of extant animals. As colour patterning often depends on the environment in which an animal lives (Marchetti 1993; Fuller 2002; McNaught and Owens 2002; Merilaita and Stevens 2011) and the visual capabilities of other animals in the same environment (Guilford and Dawkins 1991; Cuthill 2006; Stevens et al. 2009; Zylinski and Osorio 2011), reconstructing colour in extinct taxa can inform both of these. However, certain factors must be taken into account when transferring inferences of colour from living animals to extinct.

One key assumption when looking at colour in extinct taxa is that the principals governing colouration in living animals hold true in the past. As certain colour features, such as countershading, background matching and disruptive colouration are present across disparate clades and visual systems (Stevens and Merilaita 2008; Rowland 2009, 2011) and have been detected in fossil taxa (Vinther et al. 2016; Brown et al. 2017), it is likely that they served similar functions in the past. Confidence can be increased further when we know about the visual systems of animals around at any given point in time (Guilford and Dawkins 1991). This is achievable when the phylogenetic placement of the animals in question is taken into account. When investigating colour in an extinct avian dinosaur for example, we can look at the visual system of modern birds and their closest relatives, crocodilians, to get an idea of its likely visual capabilities (Stevens 2006; Li et al. 2010, 2012). Most birds today are tetrachromatic (Bowmaker 1980; Vorobyev et al. 1998) and crocodilians are trichromatic (Nagloo et al. 2016), making it likely that dinosaurs had good colour discrimination capabilities (Stevens 2006). As dinosaurs constituted both predators and prey in the Mesozoic (Farlow and Holtz 2002; Stevens 2006), this can inform a range of potential colour pattern adaptations.

However, we also need to understand potential differences between the environment and predator-prey landscape today and in the past. It is not just the visual capabilities of animals that must be considered, but also likely behaviours and associated ecologies. Although many dinosaurs may have had visual capabilities similar to modern birds (Stevens 2006), their

ecologies may have been more analogous to extant mammals which fill similar niches today (Vinther et al. 2016; Brown et al. 2017). While birds are dinosaurs (Ostrom 1976), most extinct dinosaurs could not fly and so likely had behaviours and ecologies more analogous to today's mammals or the flightless palaeognath birds (Brown et al. 2017). Small ground-dwelling dinosaurs would have been prey to larger theropods with likely better visual capabilities than today's large mammals (that are mostly dichromatic; Li and DeVries 2006), however. Camouflage may therefore have been even more important in the Mesozoic than today, and this is something that can be investigated through palaeocolour. Looking at both bird and mammal colouration and considering the likely predator-prey landscape in the past can give a more informed insight into potential functions of colour in dinosaurs. The same can be said for taxa such as extinct Mesozoic marine reptiles. While ichthyosaurs are reptiles, their ecology was more analogous to living sharks and cetaceans (Motani 2002; Lingham-Soliar and Plodowski 2007), so it is to these taxa we must turn to fully understand potential colour patterning and associated behaviours and ecologies.

Soft tissue taphonomy

In order to comprehensively study colour patterns in extinct taxa, an appreciation of the taphonomy of the fossils is also necessary. Taphonomy refers to all of the processes that are involved in the fossilisation of an organism, from death and transportation, through burial, compaction and the chemical processes of mineralisation and tissue stabilisation to eventual exhumation, exposure and weathering (Fig. I3; Parry et al. 2018). Understanding taphonomy is especially important in palaeocolour, because it is soft tissues that hold the key to revealing likely original colour patterns (Vinther et al. 2008; Vinther 2015*a*). Colour producing features, including pigments and structural colours, are generally found in soft tissues in living animals (reviewed in Chapter 1; Hill and McGraw 2006*b*). Soft tissues are however much rarer in the fossil record than hard mineralised tissues and can be lost and/or modified at every stage of taphonomy of an animal (Parry et al. 2018). A thorough understanding of how taphonomy has affected these tissues is therefore essential if palaeocolours are to be investigated. Only in

exceptional circumstances will features that inform of original colours be present in fossils, making samples sizes generally low.

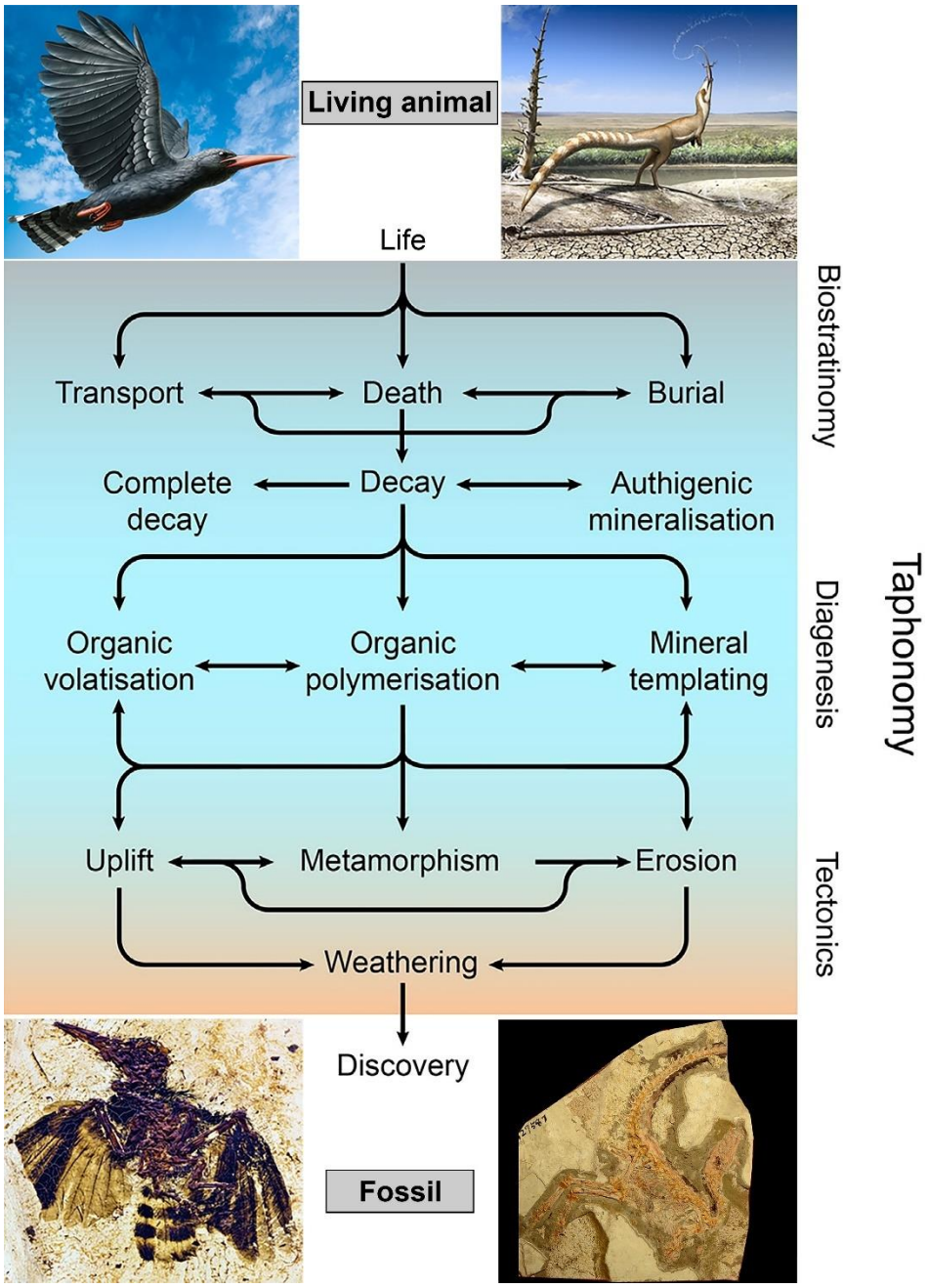

Figure I3. The taphonomic processes involved in the fossilisation of an organism. Modified from Parry et al. (2018).

It is also important to understand the chemical nature of fossil soft tissue preservation as well as the physical (Colleary et al. 2015; Parry et al. 2018). Understanding the chemical nature of certain soft tissues helps to determine how they have been preserved. This in turn can provide key information about the origins of the tissues, which is not always obvious from their physical appearance in fossils (Parry et al. 2018). While most fossil tissues are replaced by minerals (e.g., authigenic mineralisation; Allison and Briggs 1993; Briggs et al. 1993), specific features can retain original organics (or products derived from the original organics) under certain circumstances (Parry et al. 2018). As I will explore in Chapter 1, this is of key importance in palaeocolour studies, as melanin is often preserved organically, which opens a window to understating the original chemistry of the pigment in deep time.

To fully appreciate and understand the colour of extinct animals therefore, a combined approach of palaeontology (including taphonomy, phylogenetics and palaeoecology) and neontology (including visual and behavioural ecology, colour production mechanics and the study of colour pattern function) is needed. In this thesis, I deploy these approaches to explore the colour patterns and their likely behavioural, ecological and evolutionary implications in a range of diapsid taxa spanning multiple time periods and environments. These taxa include Jurassic ichthyosaurs and several extinct Cretaceous non-avian dinosaurs and Eocene crown group neognath birds. I also advance the methodology used to investigate colour in extinct vertebrates by revising the most commonly used protocol to extract melanosomes from extant feathers to aid future palaeocolour studies.

In my first chapter, I provide background about the production of colour in the most important clade in terms of palaeocolour – the birds, as well as the most up-to-date and thorough review of the state of the art of palaeocolour. This includes a review of how the field came about, the key studies that helped to advance the field from its origins to the present day and the methodology that has been used to probe the nature of colour preservation. I provide new taphonomic data using exceptionally preserved fossil feathers from the Eocene age Messel Formation to show how melanosomes (the organelles in which melanin is stored in vertebrates) account for the preservation of the feather structure when no traces of keratin remain. I use these feathers to demonstrate how the most commonly used palaeocolour techniques can

reveal their likely original colour and how the chemical makeup of the constituent melanin compares to modern and other fossil melanin samples. This provides all the background for the following chapters.

Chapter two investigates the nature of soft tissue preservation in a Jurassic ichthyosaur (*Stenopterygius quadriscissus*) from the Posidonia Shale Formation of Germany and the Early Cretaceous non-avian theropod dinosaur *Sinosauropteryx* from the Jehol Biota of China. These taxa are of particular importance to palaeocolour work, vertebrate soft tissue taphonomy and the early evolution of feathers. Several studies have claimed that purported feathers or feather homologues in *Sinosauropteryx* are more likely remnants of degraded dermal collagen, similar to structures identified in the Jurassic ichthyosaurs (Lingham-Soliar et al. 2007; Lingham-Soliar 2012). Previous work identifying the colour of *Sinosauropteryx* based on melanosomes in the feathers (Zhang et al. 2010) has been questioned based upon these reports. These issues are addressed in Chapter 2 and new evidence provided confirming the structures seen on *Sinosauropteryx* as feather or feather homologues. This is key to the following work on the colour of this theropod.

In the third chapter, a comprehensive account of the nature and preservation of soft tissues of Jurassic ichthyosaurs is provided, including several specimens from the UK and Germany in order to clarify the discrepancies identified in Chapter 2 and to investigate their palaeocolour. The presence of phosphatised impressions of dermal fibres are presented, but with a very different morphology and preservation to the structures in *Sinosauropteryx*. Melanosomes are also identified from multiple tissue types in the ichthyosaurs that inform as to the original colour of the animals and helps to unravel the taphonomic pathways and processes that led to the exceptional preservation of the integument in these fossils. Additionally, multiple tissues from the eye are identified based on differences in preserved melanosome morphologies.

The fourth chapter investigates the colour patterns of *Sinosauropteryx* in detail. Through detailed mapping of the distribution of pigmented plumage and 3D modelling of how shadows would have been cast across the body based on methods developed for modern animals (Allen

et al. 2012; Vinther et al. 2016), the complete plumage patterns of *Sinosauropteryx* are reconstructed. Along with the previously noted banded tail, these reconstructions reveal a dark stripe across the eyes (a "bandit mask") and a countershaded body, all of which are patterns seen in living animals (Fig. I1d-e and I2d). Comparisons to modern avian and mammalian analogues are used to suggest potential behaviours and ecologies exhibited by *Sinosauropteryx* based on these colour patterns. By investigating the nature of the countershaded pattern quantitatively, the likely habitat preference of *Sinosauropteryx* is also explored (Allen et al. 2012). This chapter highlights how an understanding of the link between colour patterning and ecology in extant taxa can inform as to the ecology and behaviour of extinct taxa with no direct living relatives.

Chapter five focuses on reconstructing the colour of another theropod dinosaur from the Jehol Biota; *Caudipteryx*. Colour patterns are revealed through comparison of preserved melanosomes from across the body with a dataset of extant melanosome morphologies (Li et al. 2012). Again, modern animals are used as potential analogues for the observed colour patterns and potential functions and behaviours explored. Both *Sinosauropteryx* and *Caudipteryx* are contemporaneous small cursorial flightless theropods - revealing their colour patterns and potential divergences in behaviours helps to create a clearer picture of the dynamics of the Jehol ecosystem.

In chapter six methodologies for revealing melanosomes from inside modern bird feathers are investigated and revised specifically for palaeocolour investigations. This is of key importance because studies of colour in extinct taxa rely heavily on the morphology and chemical makeup of extant melanosomes which must be exposed from the feather keratin first. Current techniques have limitations including degradation of some melanosome types (Liu et al. 2005*a*). The effectiveness of a number of techniques, both mechanical and chemical, are assessed to determine which is the most appropriate for revealing melanosomes for SEM imaging (the most common way to investigate fossil melanosomes). A substantially revised version of the most commonly used enzyme extraction protocol (Liu et al. 2003; Colleary et al. 2015) is presented. This technique allows for significantly more samples to be processed in a

shorter timeframe and was used in the final two chapters to compile new datasets of modern melanosome morphologies.

Chapter seven investigates the palaeocolour of the stem upupiform bird *Messelirrisor* from the Messel Formation (Germany), which is sister to living hoopoes and wood hoopoes. The revised enzymatic extraction protocol (Chapter 6) was used to create a large new dataset of melanosome morphologies from extant taxa with known colours. Importantly, this dataset focuses on Upupiformes and their nearest relatives, making this the first study to perform a palaeocolour reconstruction in a specifically phylogenetic framework (all have previously used a wide phylogenetic sample). Colour patterns are explored in terms of both their ecological context and the ancestral condition of Upupiformes and their closest relatives. Additionally, the modern melanosome data are used to test whether melanosome morphology correlates strongly to colour when a restricted phylogeny vs a wide phylogenetic sample is used (see Chapter 1.1).

Chapter eight investigates the palaeocolour of the neognath bird clade Strisores. Six extinct Eocene taxa from this group from Messel, and the Fur Formation in Denmark are reconstructed based on a comprehensive new dataset of extant Strisores melanosomes extracted under the revised protocol from Chapter 6. Modern Strisores show dichotomous colouration patterns related to their divergent activity patterns and ecologies – the nocturnal (and paraphyletic) caprimulgiform birds are all cryptically coloured with earthy tones while the diurnal Apodiformes (including hummingbirds) show conspicuous colouration including bright iridescence related to signalling. I use the extant melanosome database and reconstructed colour patterns in the fossils to investigate the ancestral activity patterns of the clade. Additionally, novel observations about iridescent melanosome morphologies in extant Apodiformes allow hypotheses to be put forward about the evolution of this trait and the general evolution of the clade post-Eocene.

In my concluding statements I reflect on how my thesis has advanced the field of palaeocolour and provide some perspectives on the direction of future research in the field. Supplementary data from the main chapters are included as an appendix along with a list of

publications I have been involved with during my PhD, both directly resulting from this thesis and other collaborations. All other data from each chapter are included in the text, figures and tables.

Chapter 1 – Palaeocolour: a history and state of the art

Abstract: The past decade has seen a revolution in our understanding of how colour influenced vertebrate evolution in deep time. Once thought impossible, we can now investigate likely colour patterns displayed by extinct animals with a high degree of confidence. In turn, this allows exploration of possible functions and the wider evolution of colour patterns through time. In this chapter, I provide an overview of colour production in living animals and a review of the development of the field of palaeocolour; from the overturning of the paradigm that lithified bacteria were responsible for vertebrate integumentary preservation to the development of analytical techniques used to probe pigment preservation. As birds have received the most attention in both palaeocolour and extant animal colouration studies and are the most relevant taxa for the bulk of the research presented in this thesis, they will be the focus of this chapter. I also explore how palaeocolour reconstructions in extinct dinosaurs have informed us about the ecologies and behaviours of long extinct taxa that would otherwise be difficult to determine. This exemplifies the utility of palaeocolour in deepening our understanding of past life, particularly early avian evolution. Palaeocolour work is also helping unravel the intricacies of feather preservation and in turn has furthered our understanding of soft tissue taphonomy more generally.

A version of this chapter has been **accepted for publication** in an upcoming book entitled "*The evolution of feathers: a palaeontological perspective*" to be published in the second half of 2019 by Springer (Editors Christian Foth and Oliver Rauhut).

Author contributions – The concept for this chapter was devised by the author along with Jakob Vinther. The author wrote the chapter and produced the figures with feedback from Jakob Vinther.

1.1. Introduction

A plethora of described colouration strategies are found in most living groups of animals (see general introduction), but two clades show some of the most remarkable ranges of colours today; teleost fishes in the water (Cuthill 2006; Nelson et al. 2016) and the birds on land (Baker and Parker 1979; Hill and McGraw 2006*a*; Stoddard and Prum 2011). Thanks to features such as tetrachromacy and ultraviolet (UV) vision, many birds can see colours invisible to di- or trichromatic mammals (Vorobyev et al. 1998). The range of colours exhibited by birds can likely be explained, at least in part, by the importance of visual cues in avian signalling due to their excellent tetra-chromatic visual capabilities (Vorobyev et al. 1998; Koschowitz et al. 2014) along with the visual requirements of flight. Bird colouration has fascinated naturalists and scientists for centuries and helped to galvanise the theories of evolution by both natural and sexual selection (Baker and Parker 1979; Darwin 1859, 1871).

The dazzling array of colours seen in birds has traditionally been attributed to two mechanisms of colour production; the utilisation of pigments, biopolymers that differentially absorb and reflect specific wavelengths of light, and nanostructural arrays within feathers (McGraw et al. 2005; McGraw 2006*a*; 2006*b*; 2006*c*; Prum 2006). Structural colours are produced in two primary ways in bird plumage. Iridescence is angle dependent refraction, most often associated with pigment layers and keratin interacting with incident light to modulate it resulting in the reflection of specific wave lengths of light (McGraw 2006*b*; Prum 2006; Igic et al. 2016). Non-iridescent structural colour is produced by a complex network of quasi-ordered air bubbles inside the keratin matrix. This serves to scatter certain light waves, while an underlying melanin layer usually serves to absorb the remaining un-scattered light (Prum 2006).

The hues, saturation and brightness of pigmentary colours are also controlled in part by their arrangement within the keratin matrix. Thus, a likely continuum in colour production involving both structural and pigmentary mechanisms, rather than a strictly dichotomous division of pigmentary and structural production exists (McGraw et al. 2005; McGraw 2006*b*; Prum 2006; Galván and Solano 2016). Novel nuances of bird colour production are still being

recognised, and it is likely that we are far from fully appreciating the variations that exist in how certain hues are produced in extant bird plumages (Igic et al. 2016).

Pigmentary colour production involves the use of multiple different pigment types in birds. These include melanins, carotenoids, porphyrins, flavins, psittacofulvins, pterins and purines among others (McGraw 2006*a*; 2006*b*; 2006*c*; Galván and Solano 2016). The most ubiquitous and likely ancient of these are the melanins (McGraw 2006*b*; Galván and Solano 2016; D'Alba and Shawkey 2018). Melanins are synthesised within the animal, whereas numerous other pigment classes including carotenoids, porphyrins and pterins are obtained directly from the diet. These diet-derived pigments may however be altered in their molecular structure after ingestion (McGraw 2006*a*; 2006*c*). These less common pigment classes usually confer different hues to melanins, such as the reds, oranges and yellows of carotenoids and psittacofulvins. They are presumed to often be honest indicators of quality due to the need to obtain them through the diet (Olson and Owens 1998; McGraw 2006*a*; LaFountain et al. 2015).

Two distinct types of melanin are known in vertebrates (McGraw 2006*b*; Galván and Solano 2016). Eumelanin, which is the most common of the two, imparts black, dark grey and dark brown hues (Fig. 1.1a-d) (McGraw 2006*b*; Vinther 2015*a*). Phaeomelanin produces lighter brown, yellow and reddish hues (Fig. 1.1e-f) (McGraw 2006*b*; Vinther 2015*a*). The two melanin types have distinct chemistries and are synthesised through different pathways (McGraw 2006*b*; Galván and Solano 2016).

The evolutionary origins of melanin are currently unclear. Due to its ubiquity throughout vertebrates, the occurrence in fossils as far back as at least the Carboniferous and the presence of eumelanin in invertebrate clades as well as fungi, the pigment and its synthesis pathway likely has ancient origins (Glass et al. 2012; Clements et al. 2016; Galván and Solano 2016; D'Alba and Shawkey 2018). Cambrian vertebrate fossils, like *Haikouichthys* and *Metaspriggina* (Shu et al. 2003, Morris and Caron 2014), for example preserve their eyes and liver as an organic stain, which has been shown to be due to preserved melanin in younger occurrences. It has been suggested that due to melanin's ability to protect cells from UV radiation, owing to its broadband absorbance spectrum, it may have been essential for the evolution of life on Earth

(Galván and Solano 2016). This may have been particularly the case when microorganisms began to inhabit environments exposed to the harmful effects of the sun. While these concepts relate to the darker melanin form, eumelanin, the origin and original functional role of phaeomelanin is much less clear (Galván and Solano 2016). Although the origins of phaeomelanin are uncertain, its importance in colouring the vertebrate integument, and in particular that of birds and mammals is undoubted.

Vertebrates synthesise melanin within organelles called melanosomes (McGraw 2006*b*; Vinther 2015*a*; Clements et al. 2016). Melanosomes are found in multiple tissue types, including the eyes, internal organs and integument (Vinther 2015*a*; Clements et al. 2016; McNamara et al. 2018). It is those of the integument that are involved in the key role of colour production, although they serve multiple other functions alongside this including thermoregulation, as antimicrobial barriers and protection against UV radiation (McGraw 2006*b*; Margalida et al. 2008; Vinther 2015*a*; Galván and Solano 2016). In birds, most melanin involved in colour production is found in the feathers, where it is deposited as melanin granules by keratinocytes after being synthesised in melanocytes (McGraw 2006*b*; Galván and Solano 2016).

Much work has been performed in recent decades to better characterise the way in which melanosomes contribute to colour production in bird feathers (McGraw et al. 2005; McGraw 2006*b*; McGraw 2008; Galván and Solano 2016; Igic et al. 2016). The physical structures of bird melanosomes vary depending on the colours they produce (Vinther 2015*a*; Fig. 1.1). Eumelanin-rich melanosomes (commonly referred to as “eumelanosomes”) generally exhibit an oblong morphology (Fi. 1.1a-d). Phaeomelanin-rich melanosomes (referred to as “phaeomelanosomes”) show a spherical to ovoid morphology (Fig. 1.1f; Vinther 2015*a*). However, this is likely an over-simplification because a wide range of morphologies exist with potentially varied eumelanin-phaeomelanin compositions (McGraw et al. 2005; McGraw 2006*b*; Galván and Solano 2016; Galván and Wakamatsu 2016). To date, most studies that have looked in detail at the melanin composition of extant bird feathers has concluded that both melanin types are present in almost every instance of melanised colouration. Until better chemical characterisation of each of the observed types is available, I will refer to melanosomes that

typically impart black and grey colours and have oblong morphologies as “eumelanin-rich”, and those imparting brown and rufous tones with spherical-ovoid shapes as “phaeomelanin-rich” rather than using the potentially controversial terms “eumelanosome” and “phaeomelanosome”. While the relative ratios of eumelanin-phaeomelanin are unclear, a correlation with melanosome morphology to colours (in birds and mammals – see below) produced does appear to exist (Li et al. 2010, 2012) and this is something I will explore further in later chapters.

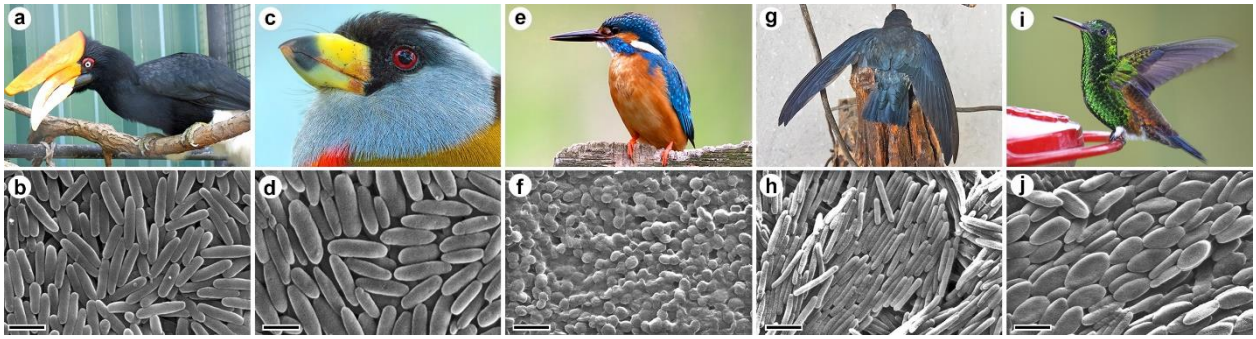

Figure 1.1. Example of melanised colours in birds and the associated melanosome morphologies. **a**. Black - *Buceros rhinoceros*. **b**. Ellipsoidal (likely eumelanin-rich) melanosomes commonly referred to as eumelanosomes extracted from a black feather of *B. rhinoceros*. **c**. Grey – *Semnornis ramphastinus.* **d**. Large ellipsoidal eumelanin-rich melanosomes extracted from a grey feather of *S. ramphastinus.* **e**. Rufous – *Alcedo atthis.* **f**. Spherical phaeomelanin-rich melanosomes commonly referred to as phaeomelanosomes extracted from a rufous feather of *A. atthis.* **g**. Glossy iridescence - *Collocalia isonata.* **h**. Long, thin melanosomes extracted from *C. isonata.* **i**. Bright iridescence – *Amazilia tobaci.* **j**. Flattened hollow plate-like melanosomes extracted from a green feather of *A. tobaci.* Scale bars represent 1 µm. Modern bird images from Pixabay, Flickr and Wikipedia: Perry Quan (a), Luis Fernando Serna Agudelo (c), Obsidian Soul (g) and Dominic Sherony (i).

Outside of birds, melanosomes are also the key colour component of all other vertebrate clades (Bagnara et al. 1968; Jimbow et al. 1986; Landmann 1986; Wasmeier et al. 2008; Li et al. 2014). Mammals impart colour in their skin and hair through melanosomes synthesised in melanocytes in a similar fashion to birds and only rarely use any other pigments

for colour which are restricted to the skin (Jimbow et al. 1986; Wasmeier et al. 2008). Without hair or feathers, reptiles and amphibians impart colour directly into their skin, mainly through a class of pigment cells called chromatophores found in the dermis, along with melanocytes in the epidermis (Bagnara et al. 1968; Landmann 1986). These chromatophores are divided into different classes based on their composition and the resulting colours they produce (Landmann 1986). Several classes exist, but the most relevant to palaeocolour are the xanthophores (containing carotenoids and/or pteridines and generally imparting yellow colours), iridophores (that contain platelets of guanine, hypoxanthine and/or adenine and produce reflective/iridescent colours) and melanophores that contain melanosomes and impart black/dark brown colours (McNamara et al. 2016*a*). Unlike birds and mammals, some reptiles and amphibians can dynamically change their skin colouration rapidly by migrating specific chromatophores up and down in the dermis (Fig. I1c; Landmann 1986). Melanosome morphology has been shown to only correlate to colour in birds and mammals, with those of amphibians and reptiles showing homogenous shapes irrespective of colour (Li et al. 2014).

1.2. Overturning the paradigm: from bacteria to coloured dinosaurs

Soft tissues, that is those that are not mineralised in life, are generally rare in the fossil record (Allison and Briggs 1993; Parry et al. 2018). When found however, they can offer unique additional insights (Allison and Briggs 1993; Briggs and Kear 1993; Wilby and Briggs 1997; Parry et al. 2018). Integumentary preservation in vertebrates is known from several exceptional fossil localities, and includes scales, skin, hair and importantly for the understanding of avian evolution, feathers (Davis and Briggs 1995; Vinther 2015*a*). The first fossil feather was found in the lithographic limestone of Solnhofen, in around 1860 (von Meyer 1861*a*, 1861*b*, 1862; Griffiths 1996; Carney et al. 2012). This well preserved and very detailed feather is preserved as a dark organic film in a buff coloured limestone and was used to erect a new taxon: *Archaeopteryx lithographica* (Carney et al. 2012; Fig. 1.2a). The discovery of this single isolated feather was followed just a year later by that of a remarkably complete animal from which it was assumed the isolated feather came (Fig. 1.2b) (von Meyer 1861*a*, 1861*b*, 1862; Griffiths

1996). *Archaeopteryx* displayed a mixture of bird-like and reptile-like features. Importantly, this included a full covering of pennaceous feathers that helped to spark the now near-universally accepted idea that birds are directly descended from, and for all intents and purposes are living representatives of, dinosaurs (Ostrom 1974; Carney et al. 2012; Foth et al. 2014; Brusatte et al. 2015). The feathers of the first complete *Archaeopteryx* specimen, the London specimen, as well as the later Berlin specimen (Fig 1.2b) were preserved as inorganic impressions just like all subsequent finds. It should be noted that a recent study has called into question the identity of the original isolated feather as coming from *Archaeopteryx*, due to its organic preservation and gross morphology (Kaye et al. 2019).

Figure 1.2. The iconic Late Jurassic paravian theropod *Archaeopteryx* from Solnhofen, Germany. **a**. The first fossil feather to be discovered in 1860 - an organically preserved isolated wing feather assigned to *Archaeopteryx* and recently shown to contain abundant melanosomes (Carney et al. 2012). **b**. The "Berlin Specimen" (HMN 1880) showing the complete animal with feathered wings and tail displayed. Scale bars represent 5 mm in (a) and 50 mm in (b). Reproduced and modified with permission from Nature Publishing.

In the 160 years since the initial iconic discovery of *Archaeopteryx*, numerous fossil localities have been uncovered globally where feathers have been found to preserve (Vinther 2015*a*). Among the most important of these include the Early Eocene formations of Messel (near Darmstadt, Germany), Fur (Denmark) and Green River (Wyoming, USA), exceptional Early Cretaceous deposits such as the Jehol Biota of Liaoning Province (China) and the Santana Formation (Brazil) and the Mid-Cretaceous Burmese amber deposits of Myanmar (Davis and Briggs 1995; Kellner 2002; Chang 2003; Vinther et al. 2008; Prado et al. 2016; Xing et al. 2016).

Despite fossil feathers being well known for over 150 years, in depth questioning of the nature of their preservation did not start until electron microscopic investigations became commonplace in geology and palaeontology in the late 20th century (Wuttke 1983; Davis and Briggs 1995; Vinther 2015*a*). The ultrastructure of fossil feathers was first examined alongside fossil hair and frog integument from the extraordinary Messel Formation using electron microscopy in the early 1980s (Wuttke 1983; Vinther 2015*a*). All integumentary structures were shown to be preserved due to the presence of abundant tiny sausage-shaped microbodies, around a micron each in length that were only found within the dark patches of the integumentary structures. In feathers, they were aligned together along the axis of the barbs and barbules (shown in Fig. 1.3 of an undescribed isolated Messel feather). It was argued that these microbodies represented bacterial colonies and bacterial glycocalyx, which was preserving an outline of the features on which they grew (Wuttke 1983). Several mechanisms through which feathers could become preserved were subsequently postulated by Davis and Briggs (1995). These included preservation as carbonised mats, bacterial autolithification and imprintation, all of which showed similar microstructures attributed to preserved bacteria. This paradigm, that feathers (and other integumentary structures) were preserved due to the presence of the bacteria that were involved in their decay pervaded for another decade. That is, until a novel realisation came about through an investigation of exceptional preservation in an invertebrate.

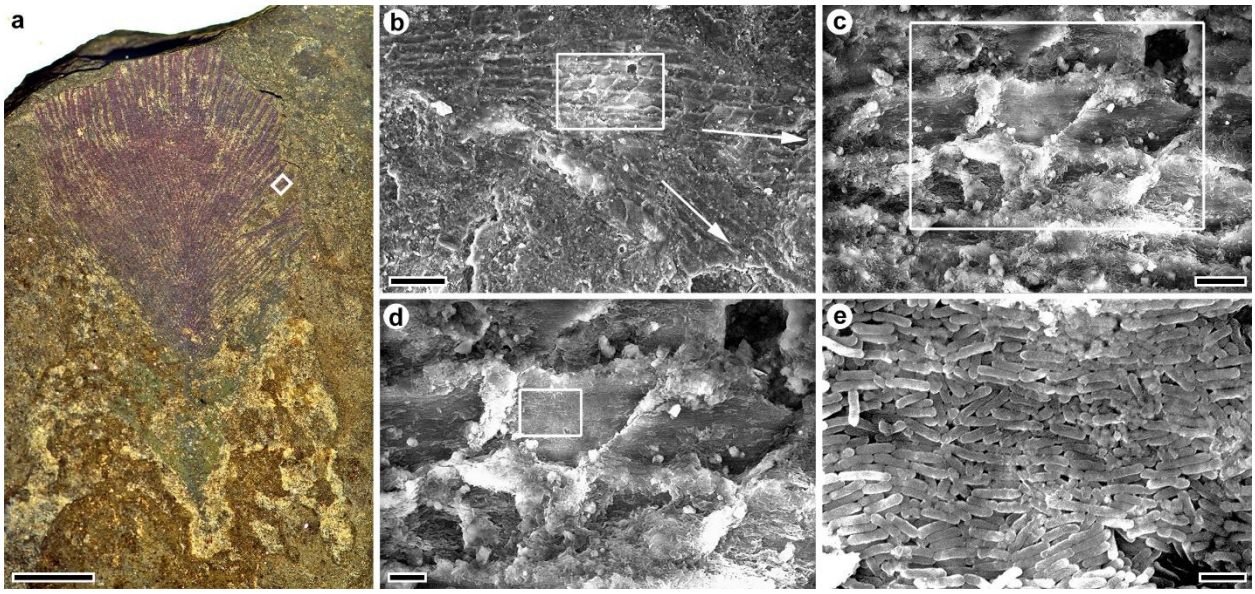

Figure 1.3. The preservation and arrangement of melanosomes (previously identified as lithified bacteria) in an exceptional fossil feather from the Eocene Messel Formation, Germany. White boxes indicate the next SEM image in the series. **a**. An isolated feather from an unknown bird (SMF-ME 3937) showing exceptional preservation of barbs and barbules. **b**. SEM image of a barb showing preservation of individual barbules arranged as in a modern pennaceous feather. White arrows show the orientation of the barbules. **c**. SEM image of the barbules showing apparent cell-like structure with each cell measuring around 10 µm in length. **d**. Close up SEM image of four individual cell-like structures. **e**. SEM image of the melanosomes that explain the preservation of the barb and barbule structures, with no other original feather features (including keratin) present. The melanosomes are in their original arrangement sitting on the matrix and it is clear that all keratin has degraded away. Scale bars represent 5 mm in (a), 50 µm in (b), 10 µm in (c), 5 µm in (d) and 1 µm in (e).

Coleoid cephalopods have been known to preserve soft tissue for around 170 years (Owen 1863). An unusual feature of their preservation often observed is that the ink sacs are usually three-dimensionally preserved due to preservation of the melanin pigment that constitutes the ink inside the organ. The rest of the soft tissues (including the muscular mantle) are most often preserved two-dimensionally compressed (Fig. 1.4a) (Vinther 2015*a*). It has long been recognised that fossil coleoid ink reveals an infrared spectroscopy chemical signature consistent with melanin (Beyerman and Hasenmaier 1973). In the late 2000s researchers examined the microstructure of Jurassic coleoid ink under an electron microscope. The

preserved ink was composed of tightly packed spherical granules (Fig. 1.4c) (Vinther 2015*a*) identical in size and shape to modern cephalopod ink granules, which are composed of pure eumelanin (Doguzhaeva et al. 2004). The fossil ink therefore appears to be little-changed over 196 million years (Fig. 1.4b) (Vinther 2015*a*). That the fossilised cephalopod ink sacs often showed three-dimensional preservation, despite compression of the rest of the animal, highlighted a key feature of melanin, its high recalcitrancy and resistance to degradation (Vinther 2015*a*, 2015*b*). Subsequent work found that the precise chemical nature of the fossil ink was similar to that of modern melanin from the cuttlefish *Sepia officinalis* (Glass et al. 2012, 2013).

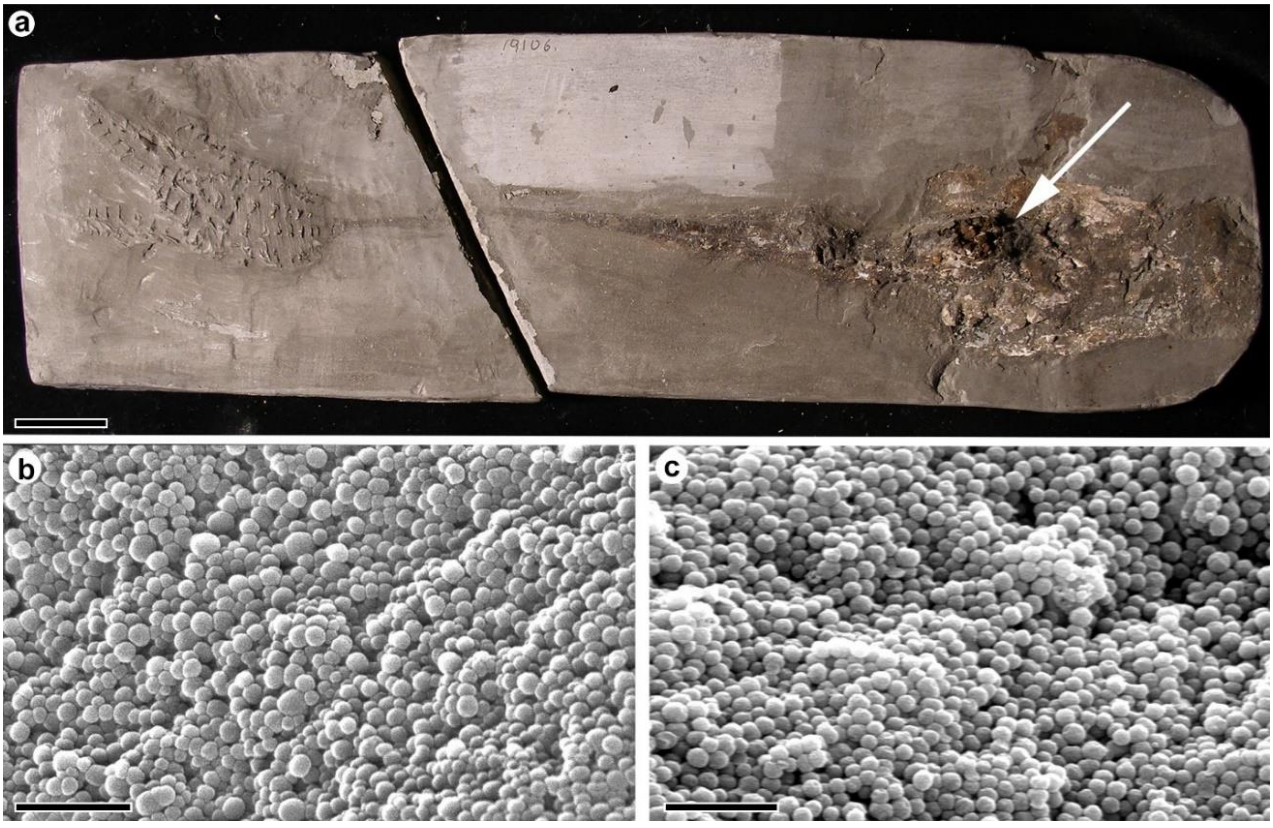

Figure 1.4. Preserved melanin granules in fossil coleoid cephalopod ink demonstrating the remarkable recalcitrancy of the pigment. **a**. A complete coleoid fossil of the genus *Geoteuthis* from the Early Jurassic of Lyme Regis, UK (YPM 19106) showing compressed soft tissue preservation apart from the 3D black ink sac (white arrow), uncompressed due to its constituent melanin. **b**. SEM image of modern coleoid cephalopod (*Sepia*) ink showing the morphology of the melanin granules. **c**. SEM image of the preserved ink from YPM 19106 showing identical melanin granule morphology to the extant *Sepia* ink. Scale bars represent 2 cm in (a) and 1 µm in (b-c).

As modern bird feathers have been long known to be predominantly coloured by melanin, fossil feathers were an obvious next step in looking for melanin in the geological record. In 2008, Vinther et al. analysed a fossil feather from the Early Cretaceous Crato Formation of Brazil which showed distinct dark and light transverse bands (Fig. 1.5a). Within the dark bands of the feather they found abundant oblong structures around 1-2 µm in length aligned along the barbs and barbules, identical to those previously identified as lithified bacteria in feathers from Messel (Fig. 1.5b; Vinther et al. 2008). In contrast, the light bands showed no microstructures other than the matrix itself (Fig. 1.5c). Vinther et al. (2008) noted that the oblong structures were identical to eumelanin-rich melanosomes found in modern bird feathers (Fig. 1.1).

Due to the newly appreciated preservation potential of melanin together with their unique arrangement and dimensions, it was considered more parsimonious that these micrometre-sized structures were in fact exceptionally preserved melanosomes rather than lithified bacteria. Furthermore, they were still arranged roughly as they would have been in the feather in life, although all remnants of the keratin matrix in which they sat had been lost. They suggested therefore that the feather was showing its original colour pattern of pigmented and unpigmented banding, i.e., the presence and absence of melanin. Based on their shape, it was surmised that the feather would have been striped black and white since it was known that reddish brown phaeomelanin is contained in spherical/oblate melanosomes (Vinther et al. 2008). The bacterial explanation for this preservation was harder to justify, given that bacteria are associated with all parts of an animal during decay, and thus would be highly unlikely to form distinct bands within individual structures or precisely mirror the morphology and arrangement of feather melanosomes (Vinther 2015*a*). Energy-dispersive X-ray spectroscopy (EDX) of the dark bands backed this up, showing high concentrations of carbon whereas no carbon was present in the light bands. Alongside this isolated feather, a complete bird skull from the Fur Formation was also analysed in the study, which showed the same oblong-shaped structures that were aligned along the barbs and barbules in the preserved plumage forming a halo around the skull (Vinther et al. 2008). Furthermore, a dark patch within the eye orbit of the

bird showed both oblong and sub-spherical microstructures which resembled melanosomes found within the retinas of modern birds (Hu et al. 2008; Vinther et al. 2008; Vinther 2015*b*).

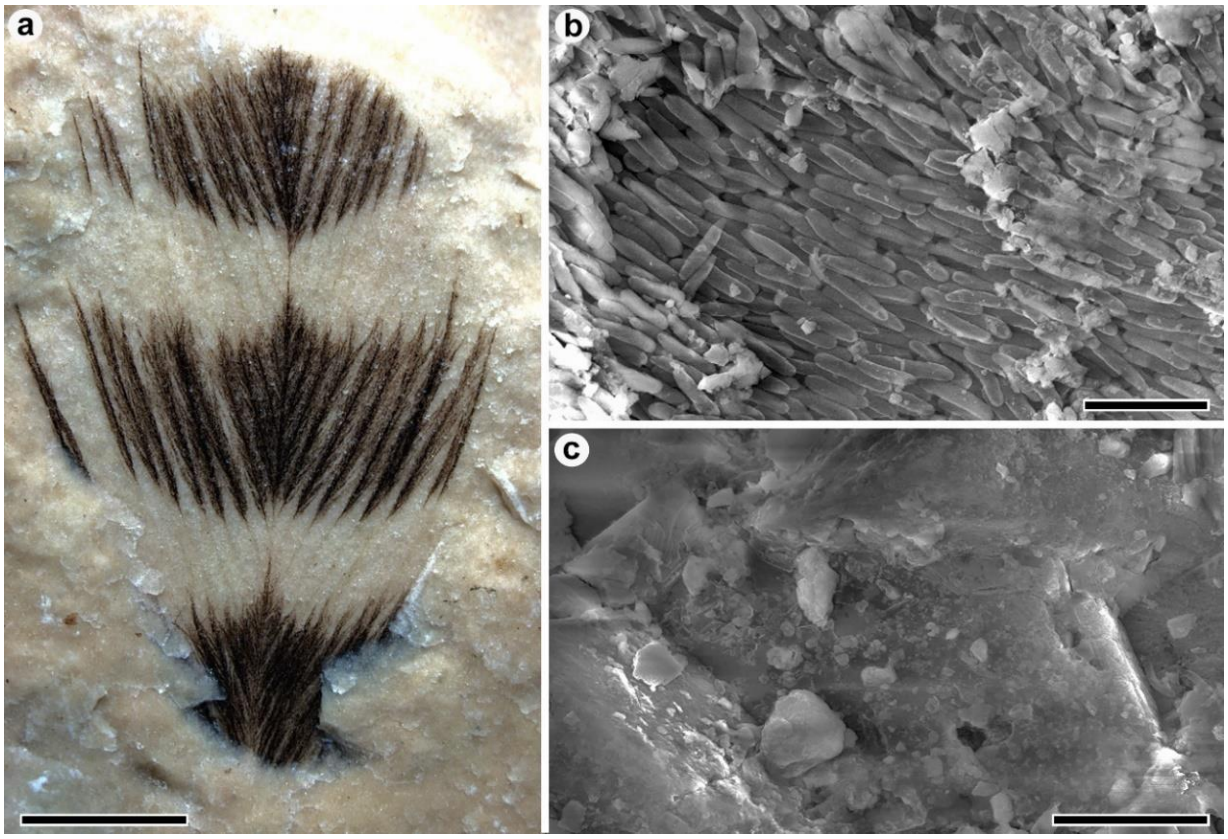

Figure 1.5. A fossil feather from the Early Cretaceous Crato Formation, Brazil, the first to be unequivocally shown to preserve due to the presence of melanin (Vinther et al. 2008). **a**. The isolated feather (LEIUG 115562) showing distinct dark and light banding. **b**. SEM image of a sample taken from a dark band showing abundant aligned melanosomes. **c**. SEM image of a sample taken from a light band showing no melanosomes, only the rock matrix. This shows that the striping is due to preservation of original colour patterning and the presence and absence of melanin in the dark and light bands respectively. Scale bar represent 3 mm in (a), 2 μm in (b) and 5 μm in (c).

This study overturned the orthodoxy that lithified bacteria were the chief explanation for integumentary preservation in vertebrate fossils and proposed that instead, exceptionally preserved melanosomes were a more likely scenario (Vinther 2015*a*, 2015*b*). The palaeocolour literature has subsequently adopted the term melanosome for their occurrence in fossils,

however some have advocated use of the term melanin granules instead (Galván and Solano 2016). The term melanosome refers to the living organelle within a cell while palaeocolour most often deals with melanin deposited into inert keratin. However, the morphology of the two is identical as the melanin granules are formed through dense packing of melanin inside the organelle's membrane, which is then lost as they are transported to the keratin. For consistency with the literature, both the living organelle and the fossil occurrences are referred to as melanosomes throughout this thesis.

More recently, the bacterial hypothesis has been revisited, with suggestions that bacteria fossilise easily and are indistinguishable from melanosomes (Moyer et al. 2014; Lindgren et al. 2015; Schweitzer et al. 2015). However, these criticisms fall short in their consideration of their relative preservation potential, the actual dimensions that bacteria exhibit and the unique fashion in which melanosomes localise themselves in fossil tissues (Vinther 2015*a*, 2015*b*). Bacteria are certainly key to inducing conditions that make soft-tissue fossilisation possible and promoting many of the processes that lead to exceptional preservation (Briggs and Kear 1993; Parry et al. 2018 and references therein). As yet however, they have not been conclusively demonstrated to be organically preserved themselves in any fossil vertebrate. Furthermore, the bacterial model does not explain why only tissues that are known to contain melanin preserve as organic stains and not other tissues that would be likely to host thriving microbiomes, such as muscles and the intestinal tract.

1.3. Mechanism of melanin preservation

The ubiquity and varied functions of modern melanins have made them a focus of scientific study since the 19th Century (Wolfenden 1884; Chittenden and Albro 1899; Galván and Solano 2016). Despite such a long history of research, certain aspects of the structure and synthesis of melanin are still incompletely understood in living animals (Galván and Solano 2016). Melanins are complex biopolymers thought to be formed through subtly different pathways depending on the exact melanin type. In modern vertebrates, melanins are synthesised in melanocytes through a process known as melanogenesis (Galván and Solano 2016). The current state of

knowledge of the full process is described in detail elsewhere (Galván and Solano 2016), but in brief melanogenesis involves a number of steps which differ between eumelanin and phaeomelanin. The initial step common to both melanin types is the oxidation of L-tyrosine to L-dopaquinone by oxygen, catalyzed by the enzyme tyrosinase (Galván and Solano 2016). After this step, the chemical composition of the solution appears to determine whether eumelanogensis or phaeomelanogenesis follows through different polymerisation reactions resulting in the final large and complexely cross-linked pigment molecules (Galván and Solano 2016). The chemical structures of eumelanin and phaeomelanin differ in key aspects that have significant implication for fossil melanin. Eumelanin comprises cross-linked 5,6 dihydroxyindole (DHI) and 5,6 dihydroxiindole-2-carboxylic acid (DHICA) polymers. Phaeomelanin incorporates monomers of benzothiazines and benzothiazoles rather than DHI and DHICA. This presence of these distinctive sulphur compounds distinguishes phaeomelanin and also provides key signatures that can be looked for in the fossil record (Glass et al. 2012; Brown et al. 2017). The complex cross-linking of melanin may help to explain its remarkable recalcitrance and ability to survive diagenetic processes.

Despite numerous studies into the preservation of melanin in fossils, its precise taphonomy and preservation is at present still to be fully understood. This is in part due to the lack of complete clarity on the molecular structure of modern melanin, but also due to the relative novelty of the field. Although a small number of references to melanin being inferred to be present in fossils were made throughout the 20th century (e.g., Voigt 1936, 1988; Whitear 1956; Beyerman and Hasenmaier 1973; Gottfried 1989; Mapes and Davis 1996), it has only been the past decade that has seen any serious advances made in unravelling the intricacies of the pigment's preservation in deep time (Vinther 2015*a*). Since the initial confirmation that melanin survives in fossils, it has become apparent that the pigment may be relatively common in the fossil record where soft tissues are present (Glass et al. 2012; Vinther 2015*a*, 2015*b*; Clements et al. 2016). Why the pigment is so recalcitrant is still an open question. It may be that the complexity of the cross-linked structure confers its long-term stability or alternatively it could be due to how it is diagenetically altered (for example through vulcanisation – see below). While it is generally accepted that melanin can survive taphonomic and diagenetic

processes, work to better elucidate the mechanisms by which the pigment can become preserved has thus far been comparatively limited and the subject is still in its infancy. A small number of important studies over the past decade have however attempted to further our understanding of the nature of melanin preservation and have provided key information.

Identifying chemical signatures for melanin and its diagenetic products has been attempted using a number of different techniques (e.g., Vinther et al. 2009; Barden et al. 2011; Wogelius et al. 2011; Glass et al. 2012; Lindgren et al. 2012; Glass et al. 2013; Colleary et al. 2015; Pan et al. 2016; Gren et al. 2016). Maturation experiments have also been performed to investigate how the effects of heat and pressure (both key factors in diagenesis) affect the morphology and chemical structure of melanin and melanosomes (McNamara et al. 2013; Colleary et al. 2015; Saitta et al. 2017).

While preliminary work in the 1970s studied fossil melanin using infrared spectrometry in order to understand melanin preservation (Beyerman and Hasenmaier 1973), only more recently after the discovery of widespread melanin preservation have scientists attempted to understand the chemical make-up of fossil melanins. Some studies were able to identify chelating metals associated with melanin using synchrotron X-ray fluorescence (XRF) (Wogelius et al. 2011). These could be mapped across a whole specimen. Similar elemental mapping confirmed the carbonaceous nature of melanosomes, using scanning electron microscopy (SEM) and EDX (Vinther et al. 2008). While melanin is unique for its ability to chelate an assortment of metals (Liu and Simon 2005), the use of these techniques in identifying fossil melanins is limited because other organic fossils will bind metals in life and after death (Vinther 2015*a*). Furthermore, the elemental mapping does not identify areas in which melanosomes have dissolved due to oxidation, but can be identified as impressions, giving a false appearance of colour pattern (Vinther 2015*a*).

Studies into the chemical nature of melanin in fossils using techniques other than whole-specimen elemental surface mapping have provided more insight into the nature of its preservation. Barden et al. (2011) performed Fourier transform infrared spectroscopy (FTIR), electron paramagnetic resonance (EPR) and pyrolysis gas chromatography mass spectrometry

(py-GCMS) alongside SEM and EDS on isolated fossil feathers from the Early Cretaceous Xiagou Formation of China attributed to the amphibious bird *Gansus yumenensis*. Imaging demonstrated the presence of melanosomes and the infrared spectra and chromatograms of the organics were very similar to a modern eumelanin standard. FTIR allow for the identification and quantification of functional groups, such as hydroxyl, ketone and carboxyls. Hydroxyl and carboxyl groups tend to be lost during maturation and hence allow for understanding the alterations of melanins. While the py-GCMS did not serve to identify melanin markers in this study, it importantly showed no significant contribution of bacterial hopanoid biomarkers, which helped to rule out the possibility of a bacterial origin of the microbodies.

In 2012, Glass et al. performed what is still one of the most comprehensive chemical studies into fossil melanin preservation to date. The study focussed on one of the least controversial and likely purest sources of eumelanin in the fossil record, that of coleoid cephalopod ink sacs. Using a suite of analytical techniques, including py-GCMS, Alkaline Hydrogen Peroxide Oxidation, FTIR and X-ray Photoelectron Spectroscopy (XPS), Glass et al. determined that the fossil ink of coleoids from the Middle Jurassic of Christian Malford (Wiltshire, UK) and Early Jurassic of Lyme Regis (Dorset, UK) was unequivocally preserved as eumelanin and its breakdown products. In fact, around 10-15% of the preserved ink was still composed of intact eumelanin with carboxyl and hydroxyl groups intact. This further demonstrated the incredible recalcitrance of the pigment and its ability to survive relatively unchanged for over 190 million years. Numerous melanin-derived products were found in the Jurassic ink as well as multiple diagenetic components using py-GCMS. Some had been secondarily sulphurised, that is they had reacted with sulphur to form various thiophenes (Glass et al. 2012; Vinther 2015*a*).

A follow-up study by Glass et al. (2013) examined ink from coleoids found at the late Early Jurassic locality of Holzmaden (Germany). Although these were of an age intermediate to the two English coleoids studied previously, the melanin content was found to be just 1% that of those specimens and just 0.1% that of a modern eumelanin extract. The only major difference between the fossils was the burial, and thus diagenetic history of the formations. The Posidonia Shale of Holzmaden was buried deeper than the other two Jurassic localities. This

meant it had entered the oil window (the point at which insoluble organic matter, kerogen, thermally matures into oil, which is dependent on burial depth-controlled temperature; Vandenbroucke and Largeau 2007). The level of organic maturation was therefore significantly higher, resulting in the alteration and enhanced breakdown of the original melanin. Despite this, numerous pyrolysate compounds were found in the Holzmaden specimens that were similar to the other, less matured fossils. This showed that py-GCMS is capable of detecting melanin-derived breakdown products even in heavily matured specimens (Glass et al. 2013; Vinther 2015*a*). Py-GCMS is a destructive technique however (although modern GCMS machines can analyse down to 50 µg), meaning that samples are destroyed in the analysis. This destructive technique may therefore prove unsuitable for particularly rare specimens, as is often the case with exceptionally preserved fossils.

A recent development for exploring fossil melanins is the relatively non-destructive Time-of-Flight Secondary Ion Mass Spectrometry (ToF-SIMS). This sensitive technique involves firing a pulsed ion beam at small areas of the surface of samples and determining the mass of secondary ions removed from the outermost surface (Vickerman and Briggs 2001). Both positively and negatively charged ions can be detected but have to be collected separately in successive runs. These secondary ions can give information about the elemental and molecular makeup of the sample surfaces (Vickerman and Briggs 2001; Lindgren et al. 2012; Colleary et al. 2015). For melanins the technique is best suited to characterise low molecular weight secondary ions - fragments of the larger and poorly understood molecule. Spectra can be generated and compared to those of other samples with known compositions (Colleary et al. 2015). Importantly, each individual peak, composed of a single or a couple of secondary ions, is not diagnostic of melanin, but the relative intensity creates a spectral fingerprint that can be compared between samples.

Lindgren et al. (2012) used ToF-SIMS to probe the preserved eye of a fish from the early Eocene Fur Formation, and compared the resulting spectra to the surrounding sediment, other body regions, and importantly a modern melanin standard. The results from this showed that the mass spectra derived from the eye was very similar to that of the modern melanin standard, and dissimilar to that of the surrounding sediment (Lindgren et al. 2012). ToF-SIMS

has its limitations however, as it only provides fragments of the molecular make up from a sample surface. The fragmentation of the molecules in-situ lead to complex arrays of secondary ion fragments that could be derived from several sources in a heterogenous sample. Furthermore, the mass of the secondary ions is obtained from the time-of-flight from the sample to the detector, which gives poor mass resolution, further conflating the ability to characterise distinct ions of similar relative mass.

In spite of its limitations, ToF-SIMS has now become something of a standard in analysing melanin in the fossil record. It is currently considered to be one of the most suitable and easily applicable techniques to probe the molecular makeup of fossil samples without excessive damage to the specimen (Colleary et al. 2015; Clements et al. 2016; Gabbott et al. 2016; Gren et al. 2017). The use of multivariate statistics, such as principal component analysis (PCA) also allows more objective comparison of the appearance of the ToF-SIMS spectra. Incorporating PCA provides both the ability to distinguish melanin from negative non-melanin samples in an objective fashion (Fig. 1.6c), and the possibility of identifying alterations to melanin that occurred during maturation (Colleary et al. 2015).

1.3.1. Maturation experiments

It has become apparent that melanin, while recalcitrant, does not survive molecularly intact. Instead, it must undergo alterations similar to other fossil organic materials (Eglinton and Logan 1991). Hence researchers have begun to experimentally understand the nature of alterations to melanins during fossilisation, driven by maturation under elevated heat and pressure (McNamara et al. 2013; Colleary et al. 2015). Artificial maturation experiments have been carried out on both feathers and pure melanin samples under experimental conditions to elucidate how the pigment may alter during diagenesis (McNamara et al. 2013; Colleary et al. 2015; Saitta et al. 2017). As the geologic processes of organic alteration are contingent on time and the levels of temperature and pressure they have experienced, experimentalists resort to using more elevated P/T conditions in a shorter time window to speed the process up.

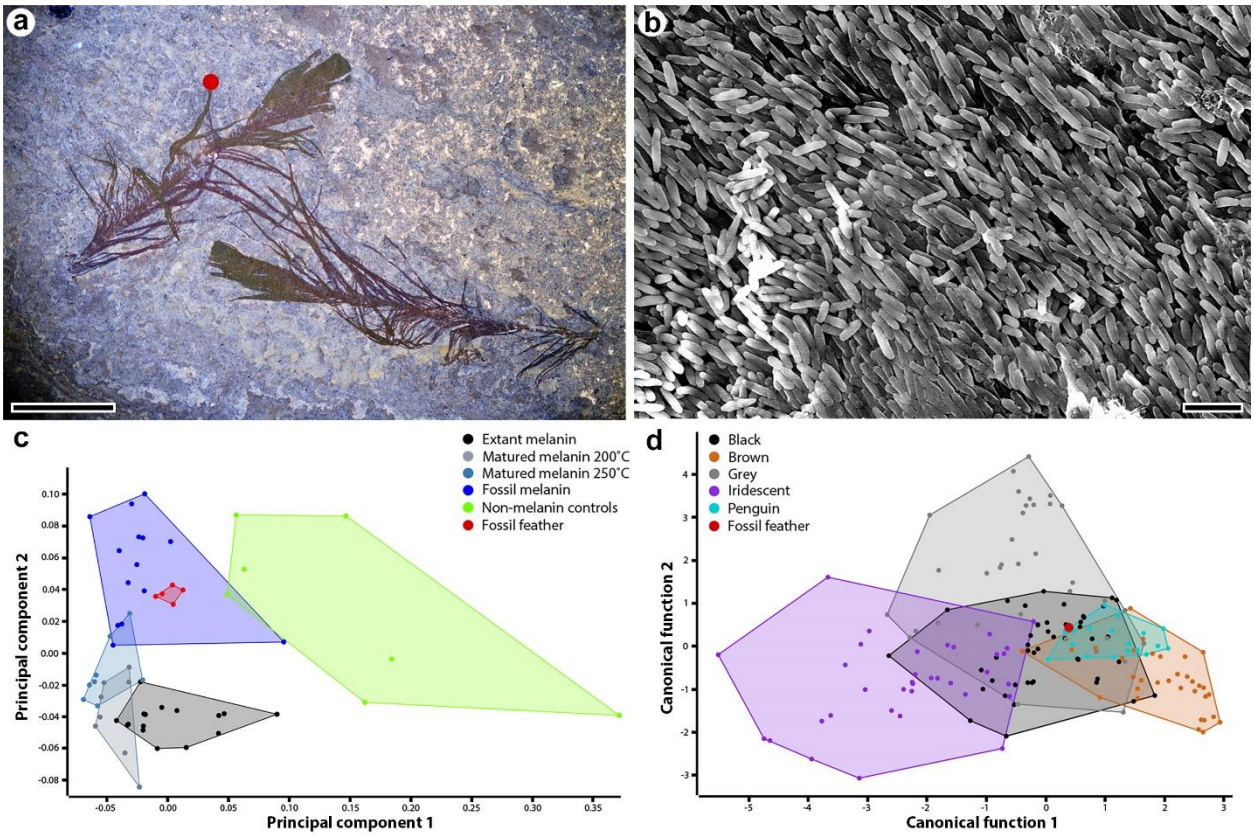

Figure 1.6. Melanin preservation in Eocene feathers and palaeocolour inferences possible from minimal sampling. **a**. A pair of feathers (SMF-ME 3855) from an unknown bird from the Eocene Messel Formation, Germany. The red dot indicates the point at which a sample was removed for analysis. **b**. SEM image of melanosomes that mark out the barbules of the fossil feather. **c**. Time of Flight Secondary Ion Mass Spectrometry (ToF-SIMS) principal component analysis (PCA) plot showing the distribution of extant, matured and fossil melanin samples based on the first two PC axes derived from 54 mass peaks known to be associated with melanin (adapted using data from Colleary et al. 2015). The isolated fossil feather plots in the centre of the range of other fossil melanin samples, separate from the non-melanin controls, confirming a likely melanin affinity. **d**. Canonical discriminant analysis (CDA) results showing the relationship between melanosome morphology and colours produced. Modern feather melanosomes with known associated colours were categorised by colour and used to predict the likely colour of the fossil feather, shown here to fall within the range of black and "penguin" feather melanosomes. Data adapted from Li et al. (2012). Scale bars represent 1 cm in (a) and 2 µm in (b).

It has been observed that impressions of fossil melanosomes are often larger than the actual preserved ones (Clarke et al. 2010, Carney et al. 2012). Maturation experiments have demonstrated that this difference can be explained by dehydrating alterations taking place during maturation causing condensation reactions (Eglinton and Logan 1991) and hence shrinkage without affecting the preservation and overall morphology of the melanosome (McNamara et al 2013). Melanosome geometry has been shown to change by between 7.6 and 20% depending on the conditions to which they were exposed (lower temperature regimes result in less shrinkage). Although the potential shrinkage of melanosomes had been highlighted previously (Clarke et al. 2010; Carney et al. 2012), this study (McNamara et al. 2013) highlighted how the effect of thermal maturation can induce the phenomenon. As the temperature controlled the degree of shrinkage, burial history, and in particular the level of thermal maturation should therefore ideally be taken into account when melanosomes are analysed for palaeocolour reconstructions by their morphology. However, as the shrinkage appears to be isometric (i.e., the aspect ratio of melanosomes remains the same) it is observed to have a negligible effect. This is because it has been shown that aspect ratio is one of the most important variables in statistical comparisons for colour prediction by melanosome morphology (see below). Shrinkage can in theory be mitigated by scaling up fossil melanosome measurements in statistical analyses. Additionally, measuring both mouldic impressions and actual 3D preserved melanosomes (if present within a single sample) could allow the potential degree of shrinkage to be examined.

While melanosomes may shrink during diagenesis, the presence and absence of the pigment should not change, therefore original colour patterns are likely to be visible even in highly matured deposits provided that soft tissue preservation occurs (Vinther et al. 2008; Vitek et al. 2013; Colleary et al. 2015; Vinther 2015*a*). This is highlighted by deposits such as those of the Jehol Biota, which are thought to have undergone a deeper burial history than many other feather-bearing sites, yet still show remarkable integumentary structure preservation including original colour patterning (McNamara et al. 2013; Vinther 2015*a*, Vinther et al. 2016, Smithwick et al. 2017*a*, 2017*b*). Younger deposits that have undergone less harsh burial conditions, such

as Messel, can also preserve colour patterns in exquisite detail, suggesting minimal alteration (Fig. 1.7).

The most recent and comprehensive maturation study looked at the effects of elevated temperatures and pressures on melanins in conjunction with ToF-SIMS (Colleary et al. 2015). In addition to effects on the morphology of melanosomes, Colleary et al. (2015) also investigated how the chemical structure of melanin was altered. They analysed a range of fossil taxa, including bird feathers, mammal hair, fish eyes, amphibian skin and coleoid cephalopod ink. This provided for a broad sample straddling almost 300 million years of the fossil record, bracketing bilaterian metazoans and included melanosomes of varying morphology and hence likely different eu- and phaeomelanin composition.

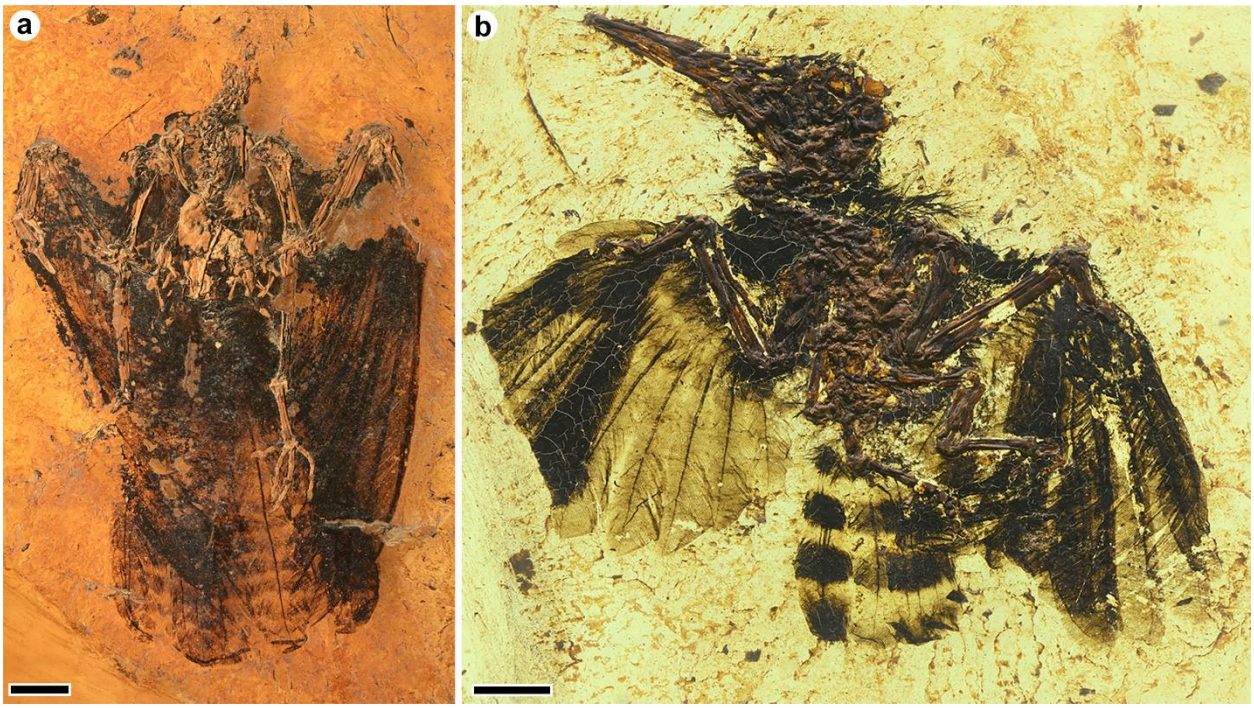

Figure 1.7. Examples of preserved original colour patterns in fossil birds from the Eocene Messel Formation, Germany. **a**. A near-complete specimen of the species *Hassiavis laticauda* (SMF-ME 9047a) missing the head but showing exceptional feather preservation including dark pigmented wings and a finely banded tail. **b**. A complete specimen of the species *Messelirrisor grandis* (HLMD-Be 178) showing a striking thickly banded tail. These colour patterns are retained due to the presence of melanosomes. Scale bars represent 10 mm.

Maturation experiments were also run on extracts of pure melanin from modern bird feathers. As with previous experiments, samples were subjected to elevated temperatures and pressures (200 and 250 °C and 250 bar) for 24 hours sealed in gold tubes. To compare the more than 55 ToF-SIMS spectra, PCA was used. Most significantly, the ToF-SIMS spectra could show that fresh and fossil melanin are distinct from negative samples, but that they in turn have subtle differences with matured melanins being intermediate in spectral composition (reproduced in Fig. 1.6c). Furthermore, the spectra showed differences correlating the morphology of fossil melanosomes, suggesting that ToF-SIMS is also able to characterise different compositions of eu- and phaeomelanin. These results also show that the fossil samples did not cluster according to lithology, age or locality, showing that the framework mainly allows for characterising differences in original melanin chemistry. Some differences in how melanin chemistry spread in extant and fossil samples in PCA needs further scrutiny and is the focus of current research (Colleary et al. 2015).

1.3.2. Melanin and sulphurisation

In the comprehensive chemical characterisation of cephalopod ink by Glass et al. (2012) it was shown that the eumelanin had reacted with sulphur to form a host of thiophenes among the pyrolysates in the py-GCMS spectrum. Sulphurisation is a well-known phenomenon in organic geochemistry (Sinninghe Damste et al. 1989) and is noted to likely be an important pathway for preserving both bone marrow and muscle tissue in a particularly sulphuric Miocene fossil deposit (McNamara et al. 2006, 2010). Since phaeomelanin is composed of monomers of benzothiazines and benzothiazoles, which contain sulphur, concerns had been raised about whether secondary sulphurisation could lead to unwanted conflation between original pheomelanin and secondarily sulphurised eumelanin (McNamara et al. 2016*b*). However, thiophenes and thiazines/thiazoles are molecularly distinct by the presence of nitrogen in the latter. Hence, the secondary ions chosen by Lindgren et al. (2014) to characterise pheomelanin in ToF-SIMS analyses (of which many combine C, N and S) would be distinct from the

thiophenes (which would not contain N). It is therefore observed that the sulphurised fossil coleoid ink analysed by Colleary et al. (2015) is not conflated with both modern and fossil melanins that contain benzothiazoles (Brown et al. 2017) or modern and fossil melanosomes that possess the distinct small and ovoid morphology characteristic of phaeomelanin-rich compositions (Colleary et al. 2015).

1.4. Non-pigmentary feather preservation

A feature that has been frequently noted in studies on fossil feathers is the absence of any feather ultrastructure apart from the preserved melanosomes (Vinther et al. 2008, 2009; Carney et al. 2012; Li et al. 2012; Field et al. 2013; Vitek et al. 2013; Vinther 2015*a*). Most SEM analyses of fossil feathers to date have shown that when feathers are preserved, melanosomes mark out the structure of the barbs and barbules, but lie freely in the matrix with little morphological evidence of the other key component of feathers, keratin, present (highlighted in Fig. 1.3, also clear in Figs. 1.5, 1.6 and 1.8; Vinther et al. 2008, 2009; Carney et al. 2012; Li et al. 2012; Field et al. 2013; Vitek et al. 2013; Vinther 2015*a*, 2015*b*). As keratin is the key component in structural colours (Prum 2006), it is important to consider in palaeocolour work. Maturation experiments have shown that keratin, like other proteins, does not survive in diagenetic environments and becomes fluid and water soluble readily when temperatures and pressures are elevated (Saitta et al. 2017), leaving only melanosomes (Colleary et al. 2015). McNamara et al. (2013) reported on experiments in which feather keratin appeared to survive, but it turned out that there was a mix up in the presentation of their experimental protocol and only experiments that had been performed under brief intervals (1 hour vs. 24 hours) were reported (McNamara et al. 2017, recent correction), which is not standard protocol.

Some have however claimed that keratin preserves organically in fossil feathers, and that molecular signatures remain (Schweitzer et al. 1999; Moyer et al. 2016; Pan et al. 2016, 2019). Recent studies of theropods from the Early Cretaceous Jehol Biota of China have investigated the possibility of keratin being preserved using immunohistochemistry techniques alongside SEM imaging, transition electron microscopy (TEM) and ChemiSTEM techniques (Pan

et al. 2016, 2019). Antibody antigen binding suggested that original components of the feather beta keratin are preserved, and melanosomes are present within a presumed filamentous keratin matrix. Issues surrounding the immunohistochemistry techniques have however been raised, including their propensity to provide false positives (e.g., from consolidants used to conserve fossils) and statistical artefacts (Saitta et al. 2017, 2018).

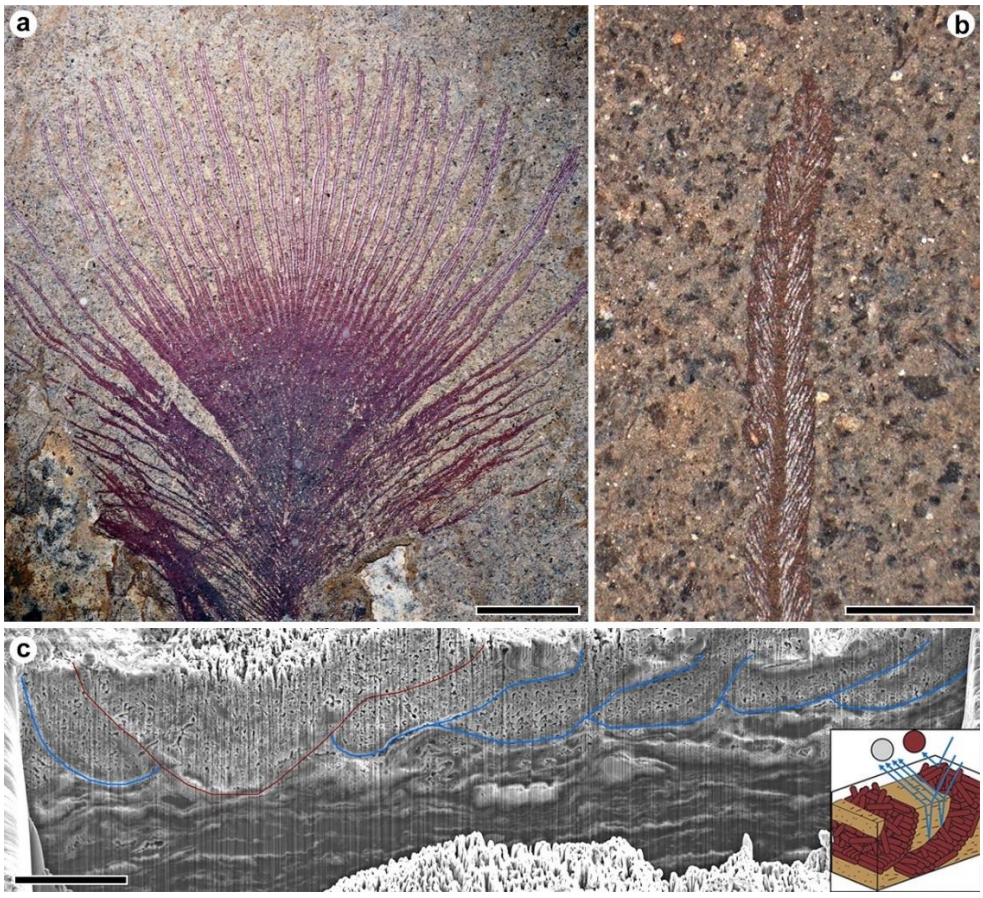

Figure 1.8. Three-dimensional preservation in a fossil feather from the Eocene Messel Formation, Germany shown to be originally iridescent (from Vitek et al. 2013). **a**. Overview of the pennaceous portion of an isolated feather (SMF ME 3850) from an unknown bird. **b**. Close up of an individual barb showing preserved barbules and a silver-sheen. **c**. SEM image of a cross section of a barb and associated barbules cut using a focused ion beam (FIB). The barb is outlined in red and the individual barbules are marked in blue. The structures can be seen to be three-dimensionally preserved thanks to the presence of melanosomes. All keratin has degraded away but the melanosomes sit in their original arrangement on the rock matrix and show distinct similarity in their arrangement to modern iridescent feathers. The silver sheen visible to the naked eye is caused by the three-dimensional arrangement of melanosomes layers and a thin layer of sediment (inset diagram). Scale bars represent 5 mm in (a), 1 mm in (b) and 10 µm in (c).

Other studies have maintained the possibility of keratin protein preservation using antibody experiments (Lindgren et al. 2017). However, the observation that these fossils preserve melanosomes liberated from their keratin matrix and that un-melanised keratinous tissues preserve no organic residues (Vinther et al. 2008) in addition to previous knowledge on protein stability (Logan and Eglinton 1991, Demarchi et al. 2016; Saitta et al. 2017) goes against the claimed presence of these highly unstable molecules in such ancient samples. Additionally, the mass spectroscopic methods employed fail to recover a protein signal. Antibody experiments are therefore demonstrably unsuitable for analysing fossil samples due to the well-known problems with frequent unspecific binding of antibodies (Saitta et al. 2017, 2018).

While organically preserved keratin is controversial, some originally keratinous structures can survive in the fossil record under certain circumstances through authigenic mineralisation. Claw sheaths for example are relatively common in deposits such as Jehol (e.g., Gong et al. 2012; Smithwick et al. 2017*a*, 2017*b*) and Solnhofen (e.g., Frey et al. 2003 and Fig. 1.2b) and fossil baleen has been shown to be prevalent in whales from the Neogene Pisco Formation of Peru (Esperante et al. 2008; Gioncada et al. 2016). The preservation of these features is likely due to the presence of hardening calcium phosphate salts (apatite) (Saitta et al. 2017). Hard keratinous tissues in living animals can contain up to 15% calcium phosphate by dry weight (O'Connor et al. 2015; Gioncada et al. 2016). Apatite is one of the most important minerals in both hard and soft part preservation in vertebrate fossils (Briggs and Kear 1993; Briggs et al. 1993; Briggs and Wilby 1996; Parry et al. 2018 and references therein), and its presence in keratinous tissues likely aids its mineralisation and preservation in fossils. These mineralised keratinous tissues can retain the structure's original morphology but are highly unlikely to preserve any organic traces of the original decay-prone and labile proteins (Saitta et al. 2017). The only part of feathers that has been shown to be hardened in this manner is the rachis (Blakey et al. 1963; Saitta et al. 2017) but none have been found preserved in fossils with intact ultrastructure. While it is plausible that apatite is present in other parts of feathers (Blakey et al. 1963), it seems that levels are not sufficient to allow for authigenic mineralisation of feather keratin in most circumstances. An alternative proposed pathway for mineralisation of organic features (mineral preserved organics - MPO) such as keratin has been proposed based

on close association with metal that could coat and/or invade the tissues, promoting preservation (O'Connor et al. 2015). As yet however, this has not been identified in fossil feathers and is more relevant to much younger archaeological remains.

1.5. Bringing the past to life: palaeocolour reconstructions of extinct dinosaurs

Alongside research into how and why melanin may preserve, much work has been carried out since the initial studies of fossil melanosomes (Vinther et al. 2008, 2009, Vinther 2015a) to better understand what the preservation of melanin and other pigments can tell us about the colouration of extinct animals, particularly birds and other dinosaurs, and how we can use that information to better inform understanding of past ecologies.

Once it had been established that melanosomes could be found preserved with high fidelity in fossil feathers, attention turned to whether the original arrangement of the melanosomes within a fossil feather could be found and thus provide information about potential structural colouration in extinct taxa. In 2009, Vinther et al. looked at isolated fossil feathers from Messel, some of which showed a silvery sheen in the barbules visible to the naked eye (Fig. 1.8a-b). The aim was to determine whether this was a preservational artefact or remnants of original structural arrangements of melanosomes. In one particular contour feather, which became the focus of the study, the arrangement of the melanosomes distinctly varied with a contrast being apparent between the proximal and distal portions. This variation matched the visible differences in the feather. Proximally, melanosomes were arranged in an aligned but loosely packed configuration in the barbs and barbules as well as the rachis. In the distal portion however, the barbs formed an open and pennaceous arrangement with the barbule melanosomes forming solid, smooth and continuous dense external layers. Underlying these layers, further melanosomes were more loosely packed and less densely arranged. This arrangement is similar to the single thin-film nanostructural array seen in many modern bird feathers exhibiting iridescence (Prum 2006; Vinther et al. 2009; Vitek et al. 2013).

Subsequent work on the same originally iridescent feathers from Messel revealed that the silvery sheen was related to the original structural arrangement of melanosomes in the

feather (Fig. 1.8c). Focussed ion beam scanning electron microscopy (FIB-SEM), a technique that cuts a micrometre-scale trench in a sample allowing three dimensional structures to be observed was used to examine this. Thin wedges of sediment were found to be acting in place of the original keratin as a material with a different refractive index than the underlying melanosomes (Vitek et al. 2013). Due to the variable thickness of the wedge of sediment, all light waves were scattered, like in a chirped mirror, hence creating the observed silvery sheen. This showed that the feather was most likely strongly iridescent in life.

Most fossil feathers do not show evidence of original structural colours. Instead, we must rely on the morphology, density and chemistry of the melanosomes to infer original colouration. Since melanosome morphology provides the ability to distinguish pigmentary colours in extant taxa (Fig. 1.1), methods for predicting colour from melanosome shape in fossils have been investigated. In 2010, two research groups independently analysed the integument of Mesozoic feathered dinosaurs. Zhang et al. (2010) were able to demonstrate the preservation of both elongate and smaller ovoid melanosomes in theropods and pygostylians from the Jehol Biota. Li et al. (2010) described melanosomes from the late Jurassic paravian *Anchiornis huxleyi* from the Tiaojishan Formation of China. SEM imaging of 29 samples from feathers across the body of *Anchiornis* revealed abundant impressions of oblong structures again identical to modern melanosomes. These melanosomes preserved the original alignment along feather structures in most places. Some light-coloured feather impression samples were barren of melanosomes and organic remains and hence were considered unpigmented. From the preserved melanosomes and impressions in the rock matrix, measurements were taken of the long and short axis of each structure and added to a database of measurements from modern bird feathers with known associated colours (10 black, 10 brown and 10 grey samples). A canonical discriminant analysis (CDA) was performed on this database which predicted the likely colour of *Anchiornis*. An example of how this method can be done is presented for a Messel feather in Fig. 1.6. Samples from different areas of *Anchiornis* were predicted as black, brown and grey with different, but generally high P-values. This was used to create a complete reconstruction of the plumage of this dinosaur (Fig. 1.9a-b). The body of the animal was predicted as a mixture of grey and black with unpigmented white bands on the fore and hind

wings with spangled, black tips. Melanosomes taken from the feathers on the distal crown feathers were particularly small, clustering with rufous red feathers in the brown category in the CDA. This contrast to the body melanosomes suggests a display function. This method of statistically comparing fossil melanosome morphologies to extant feather melanosomes with known colours has become the standard for many palaeocolour predictions (Fig. 1.6).

Further studies of dinosaur integumentary structures expanded the extant colour database to include iridescence as a category (Li et al. 2012; Hu et al. 2018). Generally, iridescent melanosomes are consistently longer and thinner than black melanosomes apart from certain clades such as hummingbirds (Fig. 1.1h and j). These works have shown that some dinosaurs likely exhibited iridescence in a similar fashion to modern birds. In 2012, Li et al. looked at the paravian *Microraptor gui*, an unusual 'four-winged' dinosaur from the Jehol Biota. The morphology of the melanosomes in *Microraptor*, being relatively longer and thinner and preserved as aligned impressions, predicted them as iridescent. The limited evidence of the original keratin nanostructure, and thus structural colouration, but with the dense end to end arrangement of the melanosomes in *Microraptor* allowed for a conservative interpretation that it would have most likely exhibited thin film iridescence. This type of iridescence is common to some extant birds such as members of the family Corvidae (Li et al. 2012; Lee et al. 2016), which only show weak iridescence (Fig. 1.9c-d). As aforementioned, since the overlying keratin layer which is integral in determining exact iridescent hues doesn't fossilise, this cannot be inferred from the fossils. From this reconstruction, inferences were also made about the potential ecology of *Microraptor*. Previous analysis of the scleral ring morphology of the dinosaur indicated a nocturnal lifestyle, however dark glossy plumage is more common in diurnal modern birds (Li et al. 2012). More recently another paravian, *Caihong juji* (Hu et al. 2018), was described with solid platelet-shaped melanosomes, which is a feature only known from brightly iridescent extant birds such as hummingbirds and tree swifts (Fig. 1.1j), thus extending this colour-producing feature back into the Jurassic.

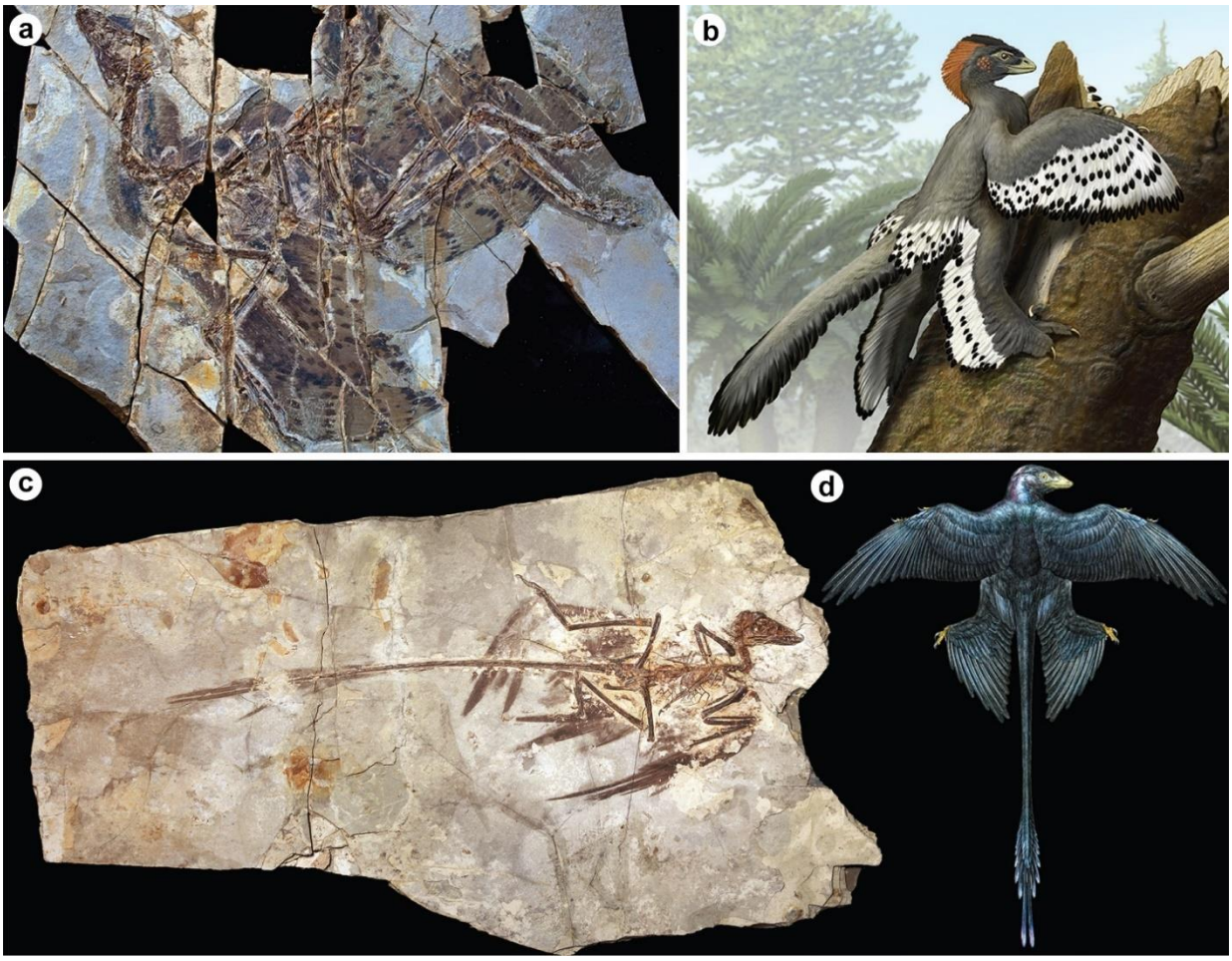

Figure 1.9. Palaeocolour reconstructions of paravian dinosaurs. **a**. *Anchiornis* from the Middle Jurassic of Liaoning, China. **b**. Palaeocolour reconstruction of *Anchiornis* based on melanosome sampling showing a black and grey body with mottled wings and a rufous head crest. **c**. *Microraptor*, a four-winged dinosaur from the Early Cretaceous of Liaoning, China. **d**. Palaeocolour reconstruction of *Microraptor* showing subtle corvid-like iridescence based on melanosome sampling. Reconstructions courtesy of Robert Clark (a), Carl Zimmer (Commissioner) and Carl Buell (Illustrator), from 'Evolution – making sense of life' (Zimmer and Emlen, Roberts and Co. Publishers) (b) and Mick Ellison (c-d).

More recent studies utilising palaeocolour have started to further explore the intricacies of behaviour and ecology in dinosaurs outside of Maniraptora. Integumentary structures suggested as potentially homologous to feathers are present in certain ornithischian taxa

(Zheng et al. 2009; Godefroit et al. 2014*a*) as well as the so-called protofeathers present in basal theropods (Chen et al. 1998; Rauhut et al. 2012). These structures have also been contended as possible decayed scales or collagen fibres rather than feathers of feather antecedents (Lingham-Soliar et al. 2007). The presence of melanosomes preserved in these features (Zhang et al. 2010; Godefroit et al. 2014*a*) however makes it possible to characterise them as genuine integumentary appendages rather than dermal collagen (which does not contain melanosomes). Further, significant issues surrounding the identification of the structures as dermal in origin have been highlighted (Chapter 2; Smithwick et al. 2017*b*). Along with likely feathers (or at least feather homologues) in some early theropod dinosaurs, certain cases of exceptional preservation of genuine scales with original melanised colour patterns have been described.

Fossil colour patterns in these ancient and ground dwelling dinosaurs are able to provide important clues to the nature of the terrestrial predator-prey landscape and how these adapted to it. A well-preserved specimen of the small ceratopsian, *Psittacosaurus* sp. from the Jehol Biota preserves visible colour patterns (Lingham-Soliar and Plodowski 2010; Vinther et al. 2016). SEM imaging of samples of dark patches on the externally scaled integument of *Psittacosaurus* revealed abundant melanosome impressions which resembled "phaeomelanosomes" and were predicted as being brown in quadratic discriminant analysis (Vinther et al. 2016). The distribution of the melanosome-containing organic material exhibits distinct patterns that resemble those seen in extant animals, such as stripes, spots and countershading (Fig. 1.10a). Unpigmented scales are also discernible across the whole body of *Psittacosaurus* by their modest relief, but they preserve as films of calcium phosphate (see above) that fluoresce in UV and laser stimulated fluorescence (LSF) imaging (Vinther et al. 2016). To understand the distribution of the observed colour patterns, an anatomically accurate 3D model was made of the dinosaur which had the pigment distribution carefully projected onto it (Fig. 1.10b). This allowed further investigation of the countershading pattern, and in turn the likely habitat that the animal live in.

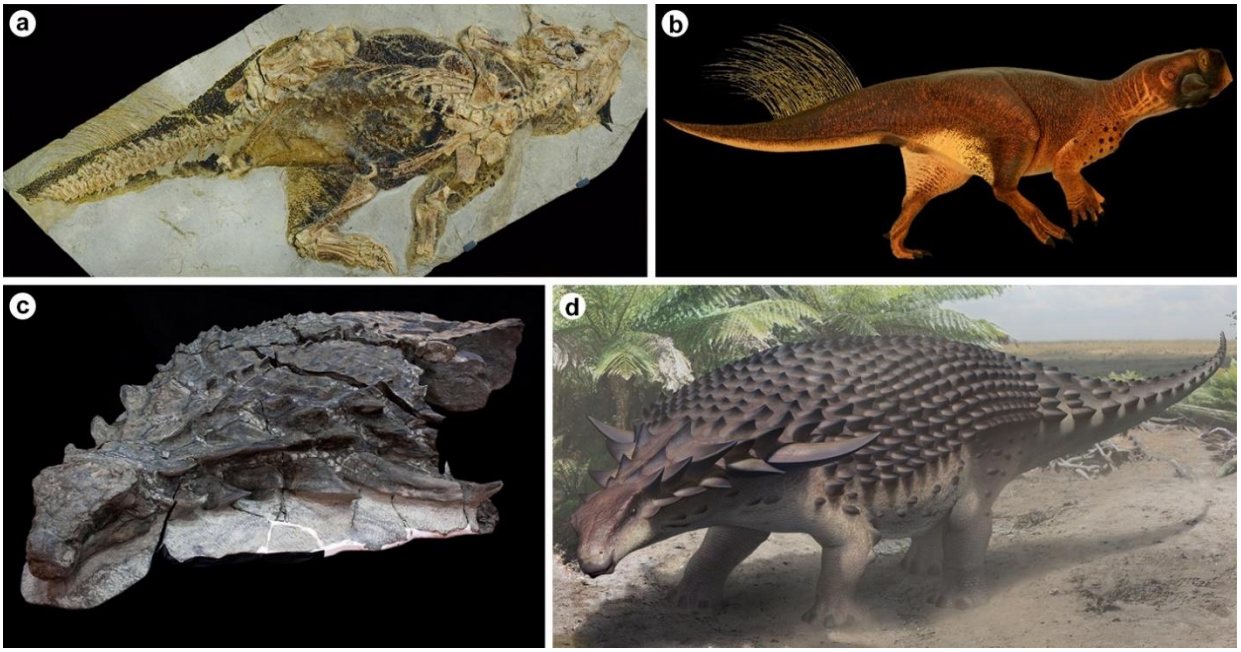

Figure 1.10. Palaeocolour reconstructions of non-maniraptoran dinosaurs. **a**. *Psittacosaurus*, a ceratopsian from the Early Cretaceous of Liaoning, China. **b**. 3D palaeocolour model of *Psittacosaurus* based on melanosome sampling and pigment distributions showing a low countershaded pattern and dark brown hue. **c**. *Borealopelta*, a large armoured ankylosaur from the Early Cretaceous of Alberta, Canada. **d**. Palaeocolour reconstruction of *Borealopelta* showing a phaeomelanised countershaded pattern, based on the distribution of pigment across the body and the chemistry of the preserved melanin. Reconstructions courtesy of Robert Nicholls.

Studies have shown that there is distinct relationship between extant animals living in closed versus open habitats and the transition in countershading, being sharper and higher on the body when directly illuminated versus more gradual and further down the body in closed habitats (Allen et al. 2012). To understand the light environment that the countershading gradient of *Psittacosaurus* would have been best adapted for, a further 3D model (painted grey) was imaged under different lighting conditions found in open and closed habitats. By comparing the shadows produced under each lighting condition with the actual preserved colour patterns it was shown that *Psittacosaurus* would have been best adapted to living in a closed forested habitat.

Countershading has also recently been observed in a large Cretaceous nodosaurid ankylosaur, *Borealopelta markmitchelli* (Brown et al. 2017). This provided an opportunity for

understanding the non-actualistic nature of Mesozoic predator-prey landscapes. The frequency of countershading occurring in living terrestrial mammals drops with increasing body size and is lost above 1000 kg (Brown et al. 2017). This is due to the safe haven provided by gigantism at this threshold and the fact that larger objects are likely harder to camouflage. Showing that a heavily armoured ornithischian dinosaur, estimated to have weighed more than 1300 kg, was countershaded (Fig. 1.10c-d) demonstrates the difference in the nature of the predator-prey balance in the Mesozoic to today. This was likely due to the presence of large theropodan predators that meant the safety of large body sizes was only effective at even greater magnitudes than would be necessary today, as exemplified by the giant sauropods (Brown et al. 2017).

Fossil colour patterns therefore provide important insights to extinct ecologies, which would be limited from conventional lines of evidence, such as osteology, trace fossils and stable isotopes. As our ability to reconstruct colour in extinct taxa improves, a more comprehensive picture of the past landscape is becoming clearer.

1.6. Limitations

While a wealth of information on past animal colour has been revealed since the discovery of melanin preservation in birds and extinct dinosaurs, there are currently limitations. These include inferences of specific hues, detection of other pigments and some taphonomic considerations.

Although melanin is the most common pigment utilised by vertebrates for colouration, the myriad of less common pigments contributes a significant extra gamut of possible colours (McGraw 2006*a*, 2006*c*). By contrast, melanised colours are limited to black, browns, rufous red and greys (McGraw 2006*b*).

Carotenoids are the most widespread pigment in extant avian clades after melanin. This pigment is taken up through diet and appear with little phylogenetic constraint in different groups. Passerines most commonly exhibit carotenoid-based patches of plumage in about 40%

of taxa (Thomas et al. 2014*a*), while in non-passerines it is much more restricted to only 13% (Thomas et al. 2014*a*). It is likely that dinosaurs could have exhibited carotenoid-based plumage and integument. It is a common feature in other diapsids. The pigment *does* have a preservation potential (Damsté and Koopmans 1997; Summons 2014) but is not hosted inside organelles with a preservation potential as the pigment does not form polymerised macromolecules like melanin does. Carotenoid preservation, or the vesicles containing them, has been proposed in a Late Miocene snake (as xanthophores along with iridophores; McNamara et al. 2016*a*), but no evidence of the pigment has been found in any fossil feather (Thomas et al. 2014*b*; Vinther 2015*a*), which may be due to preservation and its utmost rarity. A number of other non-melanin pigments found in modern birds are clade-specific (e.g., psittacofulvins in the Psittaciformes and green turacoverdin in turacos; McGraw 2006*c*) and are therefore unlikely to have been present in any birds outside of these groups. Whether any extinct birds or other dinosaurs had their own unique class of pigments is an open question but given the rarity in modern birds it is unlikely.

In order to detect non-melanin pigments, mass spectroscopic or other chemical methods would have to be employed and most of these are highly destructive. Porphyrins have been characterised compellingly with the otherwise less diagnostic ToF-SIMS (Greenwalt et al. 2014). How much of a concern is this when proposing broad colour patterns from a non-avian dinosaur?

First, these pigments are generally uncommon as previously mentioned. Hence, the likelihood of having to entertain non-melanin pigments outside of passerines, turacos, owls and parrots is small. Second, co-occurring melanin pigments mask the colour of these pigments (McGraw 2006*a*, 2006*b*, 2006*c*; Vinther 2015*a*). Hence, only feathers lacking melanosomes are likely to have been either white or patterned with alternative pigments. It is possible that labile non-melanin pigments could have been present in these presumed unpigmented areas and have since been lost through diagenesis. However, the most parsimonious interpretation would be that these regions could have been white, given its higher abundance than these pigments. Alternatively, one can entertain exploring for these pigments in these particular regions of the body. However, if the white region forms a dorsoventral gradient, it is most likely that it

represents countershading transition as this is one of the commonest colour patterns in modern animals (Rowland 2009).

While pigments other than melanin have been found in certain fossils and sediments (e.g., flavonoids in leaves (Rieseberg et al. 1987) and geoporphyrins, derived from haem, in a mosquito (Greenwalt et al. 2014)), assigning them as endogenous to a specific fossil is often problematic due to the propensity of the pigments to remobilise during decay and diagenesis (Vinther 2015*a*). While it may be possible to find other pigments in fossil birds and dinosaurs, ruling out contamination from remobilisation (e.g., from decaying algae) would require careful comparison of integumentary features to surrounding sediments (Vinther 2015*a*).

Another limitation of palaeocolour reconstructions is the preservation potential of keratin. As keratin is lost early on in diagenesis (e.g., within decades to millennia in archaeological sites of otherwise promising preservation potential; O'Connor et al. 2015), original non-iridescent structural colouration, that is formed via light scattering air bubbles inside the keratin is also lost (Saitta et al. 2017). As outlined previously, iridescence, which is generated by organised melanosomes can be identified however, through either the preserved arrangement of the melanosomes (Vitek et al. 2013) or through their characteristic shape (Li et al. 2012; Hu et al. 2018).

As it stands, palaeocolour can only provide information on broad melanic hues and iridescence. Non-iridescent structural colour cannot be identified and detecting albeit rare non-melanin pigments is complicated. However, inferences about distinct colouration strategies have been performed from fossils such as display (Li et al. 2010, 2012) and camouflage (Vinther et al. 2016, Brown et al. 2017). In addition, broad-scale colour patterns such as countershading, stripes and spots can be highly informative as to an animal's ecology and behaviour irrespective of the precise hues.

1.7. Conclusions

Over the last decade palaeocolour has evolved significantly as a discipline. The preservation potential of melanin and other pigments under exceptional circumstances has allowed for

inferring aspects of dinosaurian appearance and ecology that was thought to be impossible. While palaeocolour is limited to a few fossils from few localities, it has shown its potency for contributing crucial input to evolutionary and ecological studies of extinct ecosystems.

Palaeocolour has contributed significantly to our understanding of the evolution and origin of avian plumage and its colour gamut and many discoveries are still to be made. Colour reconstructions have helped to advance our knowledge of the predator-prey landscape in the Mesozoic, further highlighting major differences to today, but also some important similarities. Understanding which types of camouflage were present and in which groups helps to elucidate how Jurassic Park would have played out, if the book were written today.

Chapter 2 - On the purported presence of fossilised collagen fibres in an ichthyosaur and a theropod dinosaur

Abstract: Since the discovery of exceptionally preserved theropod dinosaurs with soft tissues in China in the 1990s, there has been much debate about the nature of filamentous structures observed in some specimens. *Sinosauropteryx* was the first non-avian theropod to be described with these structures and remains one of the most studied examples. Despite a general consensus that the structures represent feathers or feather homologues, a few identify them as degraded collagen fibres derived from the skin. This latter view has been based on observations of low-quality images of *Sinosauropteryx*, as well as the suggestion that because superficially similar structures are seen in Jurassic ichthyosaurs, they cannot represent feathers. Here, issues with the evidence put forward in support of this view are highlighted, showing that integumentary structures have been misinterpreted based on sedimentary features and preparation marks, and that these errors have led to incorrect conclusions being drawn about the nature of soft tissue features of *Sinosauropteryx* based on comparative data to the ichthyosaur *Stenopterygius*. No evidence is found to support the idea that the integumentary structures seen in *Sinosauropteryx* are degraded collagen fibres and I confirm that the most parsimonious interpretation of fossilised structures that look like feather homologues is that they are indeed the remains of feather homologues.

This chapter was **published in the journal *Palaeontology*** in July 2017 (https://doi.org/10.1111/pala.12292). See Appendix 2 for full details of publication.

Author contributions – The author devised this chapter, analysed all data, wrote the chapter and produced all figures. Contributions to the writing of the original manuscript were provided from Gerald Mayr, Evan T. Saitta, Michael J. Benton, Jakob Vinther. Jakob Vinther took the photographs of *Sinosauropteryx.*

2.1. Introduction

The debate on the origins of birds is one of the oldest in palaeontology (Huxley 1870; Heilmann 1926), and there has been a substantial increase in research on this question in the past two decades thanks to the discovery of numerous exceptionally preserved fossils in China (reviewed, Zhou et al. 2003; Xu 2006). These discoveries included extraordinarily well-preserved stem birds and theropod dinosaurs complete with integumentary preservation (Ji and Ji 1996; Zhou et al. 2003; Xu 2006; Zhang et al. 2006). The first of these theropods to be described with features attributed to filamentous integumentary structures was the compsognathid *Sinosauropteryx* (Ji and Ji 1996; Fig. 2.1). These authors noted the unique integumentary structures found mostly across the dorsum and tail of the animal, which have subsequently been observed in all known specimens (Ji and Ji 1996; Currie and Chen 2001; Ji et al. 2007). Through the original descriptions and a series of subsequent studies, a general consensus has arisen that the structures represent feather homologues or 'protofeathers' (see Prum (1999) and Xu (2006) for discussions on feather evolution and nomenclature). This consensus conforms to previous phylogenetic hypotheses about the origins of birds and their nesting within Theropoda, established before any theropod with proposed feathers had been discovered (Ostrom 1976; Prum 2002; Prum 2003; Norell and Xu 2005; Smith et al. 2015).

Evidence supporting a feather affinity of integumentary structures in *Sinosauropteryx* includes morphological analysis of the structures, their distribution across the body which is conserved in multiple specimens (Fig. 2.1), SEM data showing the presence of melanosomes within the structures, and both morphological and molecular phylogenetics (Currie and Chen 2001; Prum 2002; Prum 2003; Norell and Xu 2005; Li et al. 2010, 2012; Zhang et al. 2010; Smith et al. 2015). Alternative explanations have however been put forward for the structures, with suggestions that they represent partially degraded collagen fibres from the skin rather than feathers (Ruben and Jones 2000; Lingham-Soliar 2003*a*; Feduccia et al. 2005; Lingham-Soliar et al. 2007).

Figure 2.1. The three best preserved described specimens of *Sinosauropteryx* from the Early Cretaceous Jehol Biota of Liaoning Province, China. All three specimens show the preservation of integumentary structures identified by some as feathers, and others as degraded collagen fibres. The integument can be seen as the dark brown patches across the dorsum and tail. **a**. NIGP 127586. Counterpart of the holotype. **b**. NIGP 127587. **c**. IVPP V12415. Orange staining is present across the matrix likely due to oxides which is different from the clearly darker colour of the integument. Scale bars represent 50 mm in (a), and 100 mm in (b-c).

The idea that the integumentary structures first identified as feathers in *Sinosauropteryx* could actually represent degraded collagen fibres originated soon after the original description of the theropod, based on similarities to modern snake and lizard collagen (Gibbons 1997; Ruben and Jones 2000). The claim was then further fuelled by the observations of similar structures in ichthyosaur fossils (Feduccia 1999; Lingham-Soliar 2003*a*). A description of the integumentary structures on a *Sinosauropteryx* specimen (IVPP V12415: Fig. 2.1c) using light microscopy was used to suggest that they were collagen fibres (Lingham-Soliar et al. 2007). This work has formed the basis of most criticisms and rebuttals of the feathered theropod hypothesis (Lingham-Soliar et al. 2007; Lingham-Soliar 2010*a*, 2012; Feduccia 2013). One of the key observations made about the structures of IVPP V12415 as evidence of a collagen affinity is the beaded appearance of the fibres (Fig. 2.2; Lingham-Soliar et al. 2007, fig. 2). Beading is said to occur in modern collagen due to contraction caused by dehydration (Lingham-Soliar et al.

2007; Lingham-Soliar and Wesley-Smith 2008). Further evidence for a collagen affinity came from the pattern and orientation of their arrangement. In certain regions, an overlap of "geometrically precise bands of parallel fibres" is said to be consistent with structural reinforcement of the skin when compared to modern animals (Lingham-Soliar et al. 2007). Observations of decaying dolphin tissues were also used to demonstrate how collagen can show a similar morphological appearance to feathers (Lingham-Soliar 2003*b*).

The integumentary structures in *Sinosauropteryx* were interpreted by Lingham-Soliar et al. (2007) as remnants of a frill along the dorsum, reinforced with structural collagen fibres, thus accounting for the way in which the integument extends dorsally from the vertebrae. This was suggested to add stiffening support to the long tail, to protect against injury, as well as to provide a decorative display organ (Lingham-Soliar et al. 2007). The banded pattern of the integument was interpreted as "scalloping", analogous to features in modern basilisk lizards such as *Basiliscus basiliscus* and *B. plumifrons* (Lingham-Soliar et al. 2007; Lingham-Soliar 2012, 2013). It has been further suggested that the purported frill could be used to aid swimming in *Sinosauropteryx* as the dinosaur was found in a lacustrine environment (Lingham-Soliar 2012, 2013).

In addition to the hypothesis that the structures on *Sinosauropteryx* are collagen fibres rather than feathers, it has been claimed that scales are present overlying the fibres making them unlikely to represent feathers. Martin and Czerkas (2000) were the first to suggest that scales were present in *Sinosauropteryx* four years after its original description, when it was stated that a slab with scale impressions was originally removed from a specimen. No evidence to support this claim was ever provided, however, nor any images (Martin and Czerkas 2000 p 688; Lingham-Soliar 2013 p. 460). More recently, scales have been purportedly identified on another specimen and used as evidence of a frill as well as to refute the presence of feathers (Lingham-Soliar 2013).

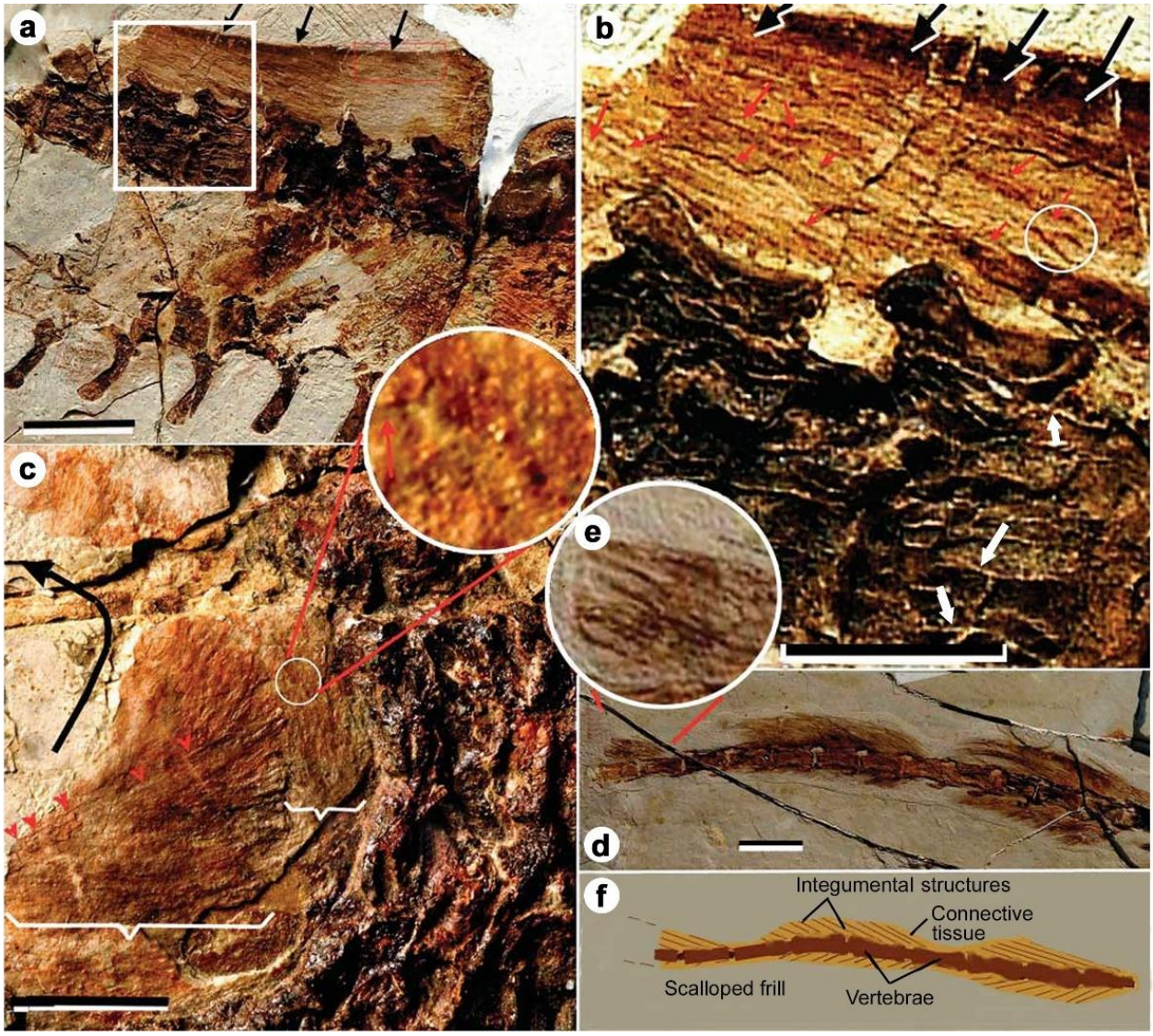

Figure. 2.2. Original figure published in Lingham-Soliar et al. (2007, fig. 2) of the integument of *Sinosauropteryx* specimen IVPP V12415. **a**. The integument preserved next to the skeleton in the proximal tail region. **b**. A close up of the area denoted by a rectangle in (a) purportedly showing an aberrant association of fibres (highlighted by the white circle). White arrows indicate areas of the internal structure of the vertebrae misidentified as collagen fibres (Fig. 2.5e). **c**. Purported collagen fibres of the dorsal cervical region, apparently showing beading indicative of degraded collagen (highlighted in the expanded circle). **d**. The mid-tail region showing the integument with an expanded area (inset circle; **e**) purporting more beading of individual fibres. **f**. A schematic illustration of the mid tail region depicting the fibres as running straight and parallel posteriorly outwards from the vertebrae from the axial skeleton, contrary to the genuine pattern of orientation of the integumentary structures seen in the specimen where they recurve back towards the vertebrae (d) (Fig. 2.4a). Scale bars represent 20 mm in (a) and (d) and 10 mm in (b-c). Reproduced with original labelling from Lingham-Soliar et al. (2007) with permission from Springer.

Many of the flaws in arguments given by proponents of the collagen hypothesis have been noted (e.g. Mayr 2010*a*; Smith *et al.* 2015; van der Reest et al. 2016) but claims of a likely collagen affinity have propagated through the literature. Often, when avian origins and theropod integuments are discussed, both feather and collagen hypotheses are treated as equally parsimonious and credible (Perrichot et al. 2008; Dhouailly 2009; Geist 2009; Ruben 2010; Dove and Straker 2012). The debate is clearly an important one, with major implications for our understanding of the early evolution of birds, feathers and flight, and thus scrutiny over proposed evidence is essential. As *Sinosauropteryx* has been the focus of the majority of the debate on theropod integumentary structures, a clearer understanding of the known specimens is essential.

Here, the evidence given for the collagen model of theropod integumentary structures in *Sinosauropteryx* as well as similar structures observed in ichthyosaurs is reviewed. A shortcoming in this model is highlighted, in that nearly all the evidence comes from low-resolution photographic images. New results based on close study of the three best-preserved *Sinosauropteryx* specimens are presented (Fig. 2.1). From new observations and photographs, previous work using lower resolution images is reconsidered, and errors arising in earlier interpretations discussed. The aim of this paper is to clarify a number of misconceptions surrounding soft tissue preservation in ichthyosaurs and the theropod *Sinosauropteryx* as well as to highlight errors used in many of the arguments surrounding theropod integumentary structures.

Institutional abbreviations: GMV – Vertebrate Collections of the Geological Museum of China, Beijing; NIGP – Nanjing Institute of Geology and Palaeontology, Chinese Academy of Sciences, Nanjing, Jiangsu Province; IVPP – Institute of Vertebrate Palaeontology and Palaeoanthropology, Chinese Academy of Sciences, Beijing; SMF – Senckenberg Research Institute, Frankfurt am Main, Germany.

2.2. Evidence for collagen fibres in ichthyosaurs and *Sinosauropteryx* reappraised

While the evidence for a feather affinity of the integumentary structures in *Sinosauropteryx* has been criticised heavily since the hypothesis was first put forward (Gibbons 1997; Feduccia 1999; Lingham-Soliar et al. 2007; Feduccia 2013), the evidence for the collagen model has never been rigorously tested. The statements provided by proponents of the collagen hypothesis will be evaluated in turn, highlighting errors that include misidentification of sedimentary structures, surface topography and marks made during the fossil preparation process. New, high resolution images (saved in TIFF format at 60-160mb) of three *Sinosauropteryx* specimens (IVPP V12415, NIGP 127586 and NIGP 127587; Fig. 2.1) were taken using a Nikon D800 camera with a Micro Nikkor 60 mm lens mounted on a tripod with a ten second delayed timer to maximise image sharpness. Specimens were illuminated from overhead with a tripod-mounted tungsten light source with a polarising filter attached. Images were taken under these lighting conditions and using a Tiffen Warm Polariser lens filter on the camera to allow cross-polarisation to reduce glare (Bengtson 2000). These methods provided very accurate and detailed images with two lighting conditions per image – normal and cross-polarised. Images of the ichthyosaur *Stenopterygius quadriscissus* (SMF R 457) were taken by Sven Tränkner (SMF) under artificial lighting without cross-polarisation.

2.2.1 Fibres in ichthyosaurs

Further study of purported ichthyosaur collagen fibres used in comparisons to the integumentary structures of *Sinosauropteryx* has revealed a number of misinterpretations in the original descriptions. Identified fibres on *Stenopterygius quadriscissus* (SMF R 457) said to show three-dimensional preservation and resemblances to theropod fossil fibres are, in many cases, actually preparation marks made when the matrix of the ichthyosaur was being smoothed around the genuine preserved soft tissue (Fig. 2.3). The new images of the same specimen clearly show that these marks are deep scratches within the matrix, which is not so obvious from the original black and white images (Fig. 2.3a). These scratch marks, frequently described as “class 2” or “radial” fibres were said to show superficial resemblance to a feather

rachis (referred to as pseudo-rachis), an argument against genuine feather preservation in theropods (Lingham-Soliar 2001, 2003*a*; figure 1d). These fibres are noted as only being present on SMF R 457, which is presumably because the other fossils studied do not have these preparation marks still on the matrix or fossil. Further purported "radial" fibres can now also be shown to be misidentified cracks running through the matrix which had been repaired when the multiple blocks of the fossil were put back together (Figs. 2.3a and b).

It was claimed that mineralisation patterns of a "dorsal longitudinal fibre" (DLF) in SMF R 457 also resembled that of filaments in *Sinosauropteryx* (Fig. 2.3a and c; Lingham-Soliar 2001, 2003*a*). This feature can be seen to run parallel to the body, separating the soft tissue from the preparation marks misidentified as "radial fibres" in the ichthyosaur (Fig. 2.3a; Lingham-Soliar 2001, figs. 5 and 9). The "DLF" runs continually, marking the boundary between soft tissue and matrix (Lingham-Soliar 2001). Re-examination of the specimen indicates that rather than a single primary feature, this is in fact a deep trench within the matrix, with the three-dimensional structure creating a light centre with darker ridges due to shadowing (Fig. 2.3b and d). This is therefore not a pattern created by mineralisation, but is likely also a preparation mark, and is therefore not an appropriate analogue for any structure seen on *Sinosauropteryx.*

While many of the soft tissue features preserved within the halo of the body of SMF R 457 do appear to be remnants of organic structures, none that resemble the filaments found on *Sinosauropteryx* stands up to scrutiny. Therefore, references to the similarities of ichthyosaur fibres and theropod integumentary structures can be shown to be baseless. Published SEM images of purported ichthyosaur soft tissue (Lingham-Soliar and Wesley-Smith 2008; Zhang et al. 2010; Lingham-Soliar 2011) and that of *Sinosauropteryx* show no microstructural resemblance, with ichthyosaur tissue forming a rope-like structure of fine filaments and the integumentary structures of *Sinosauropteryx* showing preserved melanosomes with no fibre-like features.

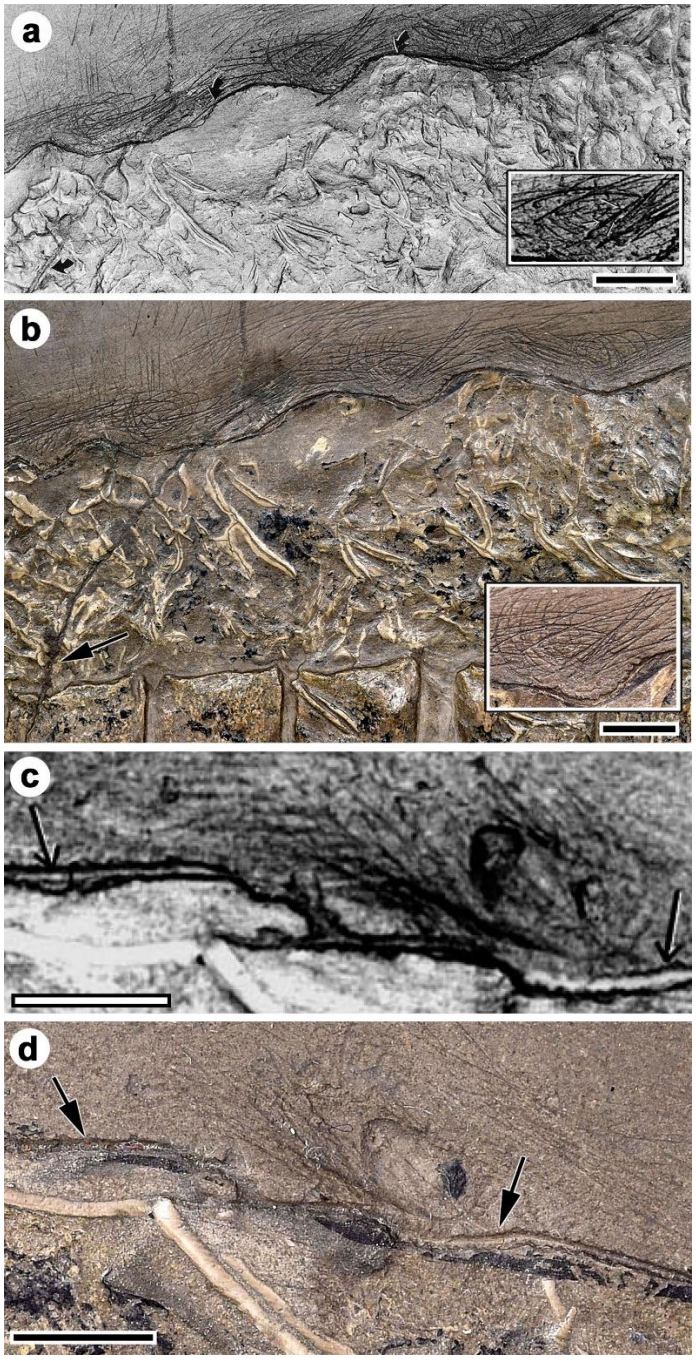

Figure 2.3. Soft tissue preservation in the ichthyosaur S*tenopterygius quadriscissus* (SMF R 457). **a**. The original image provided by Lingham-Soliar (2001, fig. 5a) showing purported preserved collagen fibres. Black arrows mark suggested fibre types including a dorsal longitudinal fibre (DLF). Inset shows an area above the DLF of purported fibres resembling feather rachis and barbs (from Lingham-Soliar 2003*a*, fig. 1d). **b**. A new colour image of the same area depicted in A showing that a previously identified fibre can be seen to be a crack in the matrix (black arrow) and the purported collagen fibres said to resemble feathers in *Sinosauropteryx* appear to be deep scratches in the matrix made during preparation of the fossil (inset). **c**. A close up of the DLF (indicated by arrows) allegedly

indicating mineralisation patterns similar to those seen in *Sinosauropteryx* (from Lingham-Soliar 2003*a*, fig. 1f). **d**. A new image showing the DLF to actually be a deep trench in the matrix (indicated by arrows) which casts a strong shadow, thus creating an illusion of differential mineralisation. Scale bars represent 10 mm in (a-b) and 5 mm in (c-d). (a) reproduced with original labelling from Lingham-Soliar (2001) with permission from the Wiley and (c) reproduced with original labelling from Lingham-Soliar (2003*a*) with permission from Springer.

2.2.2. Evidence of beading in Sinosauropteryx

The purported evidence that the structures found on *Sinosauropteryx* are beaded, conforming to collagen, falls short for a number of reasons. Beading in collagen is not a commonly observed phenomenon in modern vertebrate tissue. It has only been reported in decaying collagen from marine vertebrates (Lingham-Soliar 2003*b*; Lingham-Soliar and Wesley-Smith 2008). The images of beading in this modern collagen (Lingham-Soliar 2003*b*; Lingham-Soliar et al. 2007) are of insufficient quality to determine any genuine resemblance to structures seen in the fossils. References to observations of beading in modern mammal collagen are scant, and in the cited publications the authors note only sub-micrometre scale granular textures sometimes induced by experimental procedures, and these would not be visible without high magnification, and this was not used in the description of the *Sinosauropteryx* integument (Lewis and Johnson 2001; Young 2003; Reichlin et al. 2005; Lingham-Soliar et al. 2007). In other words, beading in collagen is not ubiquitous, and in any case the scale differs from that supposedly seen in *Sinosauropteryx*.

There are also issues in the identification of a purported beaded structure in the *Sinosauropteryx* integument. The high-resolution images in the same areas as those depicted in Lingham-Soliar et al. (2007) show that the structures present no evidence of beading (Figs. 2.4 and 2.5). When well preserved, the structures instead appear as long, smooth filaments tapering distally (Fig. 2.4). In figure 3b in Lingham-Soliar et al. (2007) isolated fibre structures are shown suggesting beading, which have been digitally cut and reorientated to one another with a background mimicking matrix (Fig. 2.5c). For most of these structures it is not clear from where they have been cut, and so comparison to the original cannot be made. One of the structures however is noted in a larger figure (Fig. 2.2b) and is said to show aberrant

associations between multiple beaded fibres, forming a 'Y' shape (Lingham-Soliar et al. 2007, fig. 2b). The new specimen photograph, however, shows no such structure other than a slight undulation in the sediment of the matrix, with no clear association between the integumentary structures (Fig. 2.5b and d). The digitally cut and reproduced fibres also show large discrepancies in scale, with the Y-shaped fibre depicted as around 633 µm (Fig. 2.5c) while in larger figures it can be seen to measure around 3000 µm (Figs. 2.2b and 2.5d; measured using ImageJ).

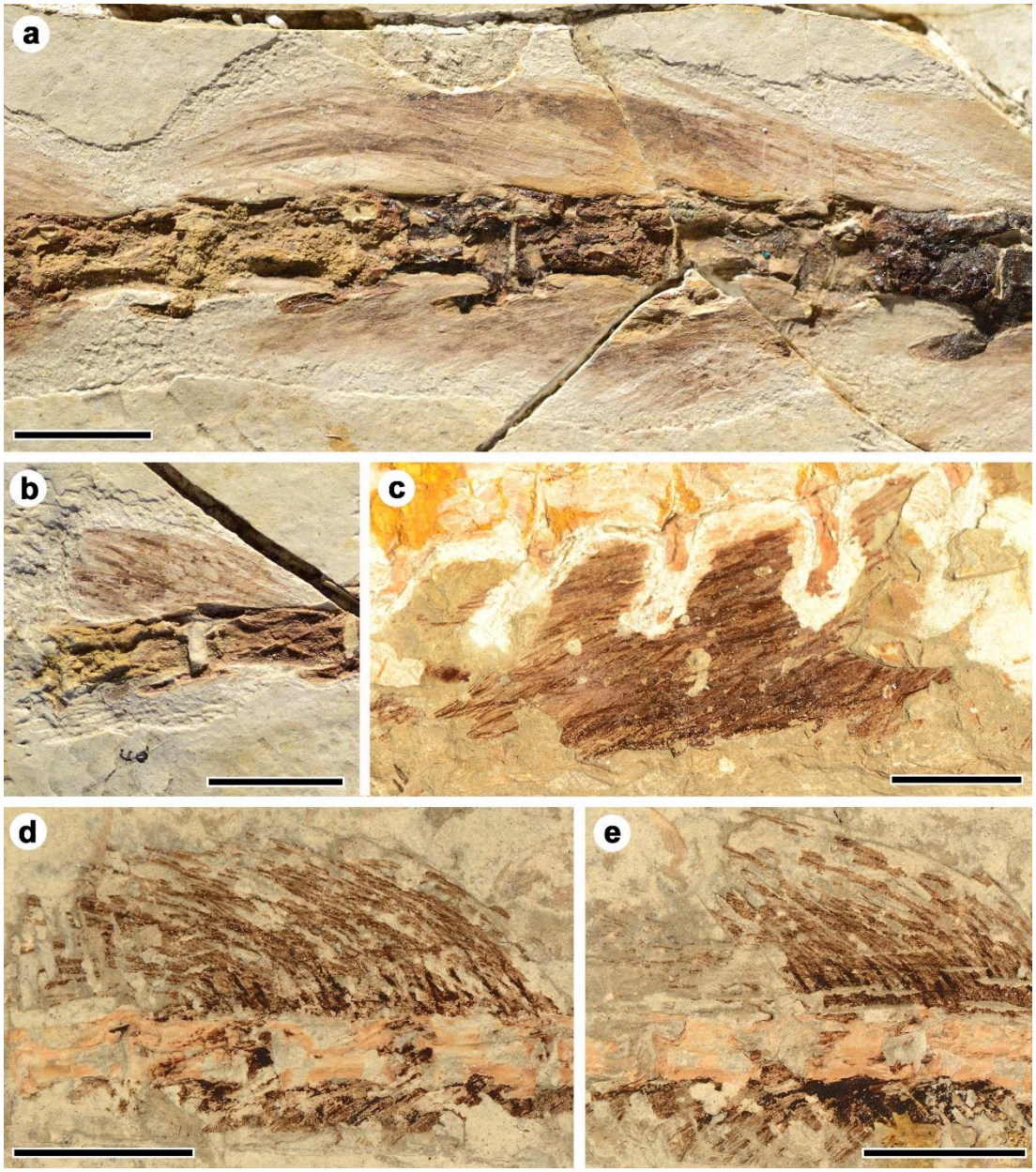

Figure 2.4. Areas of well-preserved integumentary structures on the tail of *Sinosauropteryx*. All regions show smooth filament-like structures which taper towards their tips, with no evidence of beading, as is suggested for degraded collagen. **a**. The mid-tail region of IVPP V12415, showing long smooth filaments protruding from the tail axis before recurving back in towards it. **b**. A region of integument at the break of the tail in IVPP V12415. **c**. Ventral integumentary structures in the mid-tail region of NIGP 127587, again showing long smooth filaments with a clearly flexible structure allowing curvature and overlap. (**d-e**). Posterior regions of the tail in NIGP 127586 showing further flexible filaments recurving posteriorly after protruding from the tail. Scale bars represent 10 mm

Beaded integumentary structures are also identified as overlying the vertebrae, showing apparent branching (Fig. 2.2b; Lingham-Soliar et al*.* 2007, fig. 2b). Close inspection of the new images however shows that these are three dimensionally preserved parts of the bones themselves, likely part of the internal structure as they appear broken when compared to a number of complete bones adjacent to them, which readily cast shadows that appear to have been misidentified as integument (Fig. 2.5b and d). One of these skeletal structures was digitally cut from the bone and again presented as an isolated collagen fibre (Fig. 2.5c; Lingham-Soliar et al. 2007, fig. 3b). It cannot be assumed that any of these cut fibres are integumentary features showing beading, as the only two that have their original location shown are not fibres, as noted. In conclusion, it seems that the illustrations of supposedly beaded collagen fibres from the *Sinosauropteryx* specimens are based on undulations of the matrix which create differential lighting and shadowing. Furthermore, no examples of these beaded structures were observed on close inspection of the actual specimens.

2.2.3. Orientation of the filaments in Sinosauropteryx*: parallel and cross-fibre patterning*

Cross-fibre patterning of the dermis reported from NIGP 127587 and IVPP V12415, used to support the collagen hypothesis, also fails to stand up to scrutiny (Lingham-Soliar et al. 2007; Lingham-Soliar 2012, 2013). In Lingham-Soliar (2013), figure 4 shows a section of the tail of IVPP V12415 which has broken and separated, with arrows indicating the proposed opposing direction of fibre orientation suggested to represent the original collagen structural arrangement (Fig. 2.6a; Lingham-Soliar 2013 p. 457). The new photographs, however, show that

the so-called 'fibres' are in fact deep scratches made during preparation of the specimen, likely from a pneumatic air scribe, and so with no biological significance (Fig. 2.6c). Similar preparatory scratch marks can be seen across the matrix around the entire animal (Fig. 2.7). The same marks are found in NIGP 12586, with some even cutting through the genuine integumentary structures (Fig. 2.7c). These marks cast shadows, which appears to have led to their misidentification. Interestingly, these preparation marks are clear and obvious in the region where the tail has been displaced, in IVPP V12415 (Fig. 2.6d), a feature blocked out on the original image by a black square with no explanation in Lingham-Soliar (2013, fig. 1).

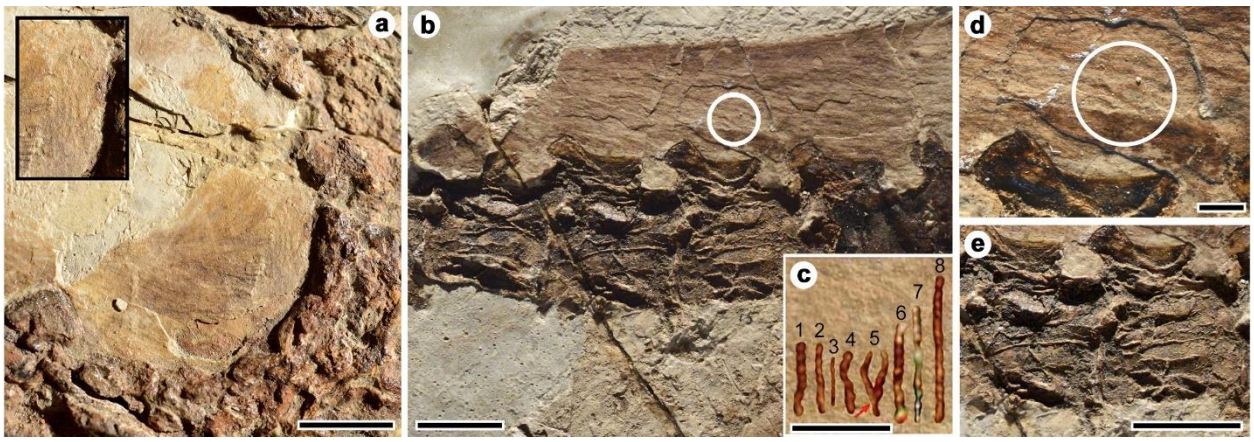

Figure 2.5. Areas of well-preserved integument in *Sinosauropteryx* specimen IVPP V12415A. **a**. The integument dorsal to the cervical vertebrae previously depicted in Lingham-Soliar et al. (2007; Fig. 2.2c). The structures appear as long, smooth filaments, with no evidence of beading even when viewed close up (inset). Despite the extreme arching of the neck, the filaments remain straight and parallel. **b**. Dorsal integumentary structures of the anterior tail region with purported associated collagen fibres (white circle). **c**. The original figure from Lingham-Soliar *et al.* (2007, fig. 3b) showing digitally cut, and reorientated fibres including an aberrant association forming a 'Y' shape (fibre 5) cut from the integument shown in (b). **d**. A close up (circled) of the purported aberrant association of fibres in (c). From this image it is unclear whether the structures preserved are associated, or if undulations in the matrix have caused the apparent shape of the structures. A large discrepancy in size can be seen between the cut fibre (633 µm) and the original area of interest (3000 µm). **e**. The vertebrae of the same region imaged under bright conditions to highlight the shadows cast by the three-dimensional structure of the bones, which have previously been misidentified as part of the integument (Fig. 2.2d; Lingham-Soliar et al. 2007). One of these ridges running across the bone was digitally cut and presented as collagen fibre 7 in Lingham-Soliar et al. (2007; c). Scale bars represent 10 mm in (a-b) and (e), 1 mm in (c) and 2 mm in (d). (c) reproduced with original labelling from Lingham-Soliar et al. (2007) with permission from Springer.

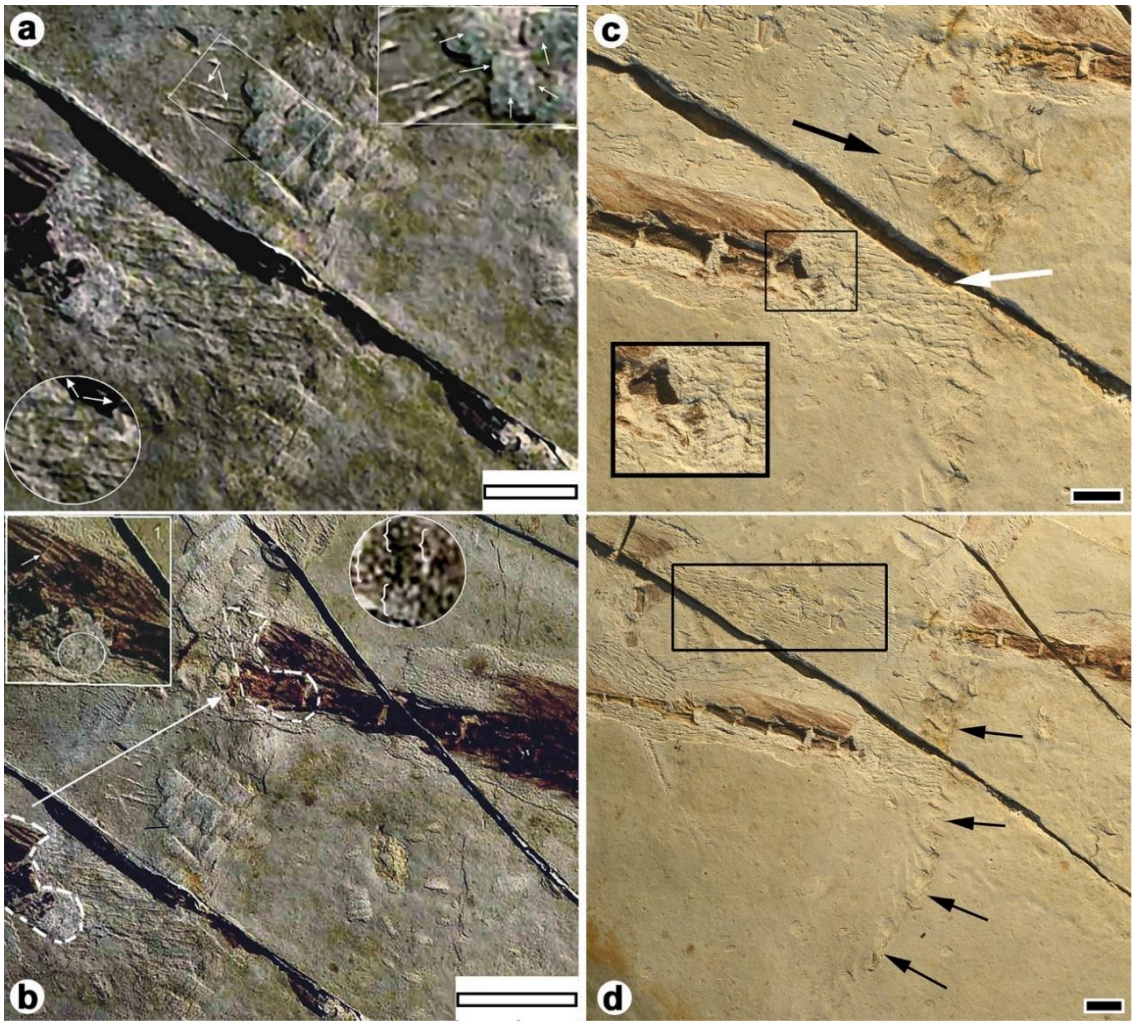

Figure 2.6. Images of a break in the mid-tail of *Sinosauropteryx* specimen IVPP V12415 reported in Lingham-Soliar (2012, figs. 3 and 4) alongside new high-resolution images of the same area. **a**. A region between the broken tail sections purportedly showing cross orientated collagen fibres (inset circle) and scales with attachment fibres (inset rectangle). **b**. The same region showing purported organic scale preservation shown in the inset circle. Despite attempts to highlight the scales and a papulose pattern by brackets, no clear structures can be made out due to the low resolution of the image. **c**. A new high-resolution image of the same region, showing that the structures identified as cross fibres (white arrow) and scale attachment fibres (black arrow) in (a) are in fact preparation marks which appear throughout the matrix, likely made by a pneumatic air scribe. Inset shows the area of purported scales in (b) with no clear structure being present. **d**. An expanded view of the same area, showing potential sedimentary structures and undulations in the matrix misidentified as scales in (a), which run across the matrix far from the animal itself (black arrows). The highlighted rectangle shows extensive preparation scratches resembling identified fibres in (a), which were blocked out of an original image in Lingham-Soliar (2013). Scale bars represent 10 mm. (a-b) reproduced with original labelling from Lingham-Soliar (2013) with permission from Springer.

Figure 2.7. Evidence of preparations scratches likely made by pneumatic air scribes in multiple specimens of *Sinosauropteryx* which conform to structures previously identified as primary collagen fibres (Fig. 2.6). Black arrows show the orientation of the preparation scratches. **a**. The anterior tail region of IVPP V12415 with long preparation marks running at the same angle as the integumentary structures. **b**. The mid-tail region of IVPP V12415 showing further preparation scratches running parallel to the genuine integument. **c**. NIGP 127586 mid-tail region showing preparation scratches cross-cutting the genuine integumentary structures. Scale bars represent 10 mm.

The layer containing the purported fibres clearly sits underneath the main integumentary layer, as can be seen from the shadow cast by the overlying layer. New specimen photographs show that subsequent preparation of the specimen has removed most of the overlying layer of integumentary structures, and the matrix now sits entirely at the level of the aforementioned purported parallel fibres (Fig. 2.8). This new preparation work was presumably done in order to reveal more depth around the bones themselves, as can be seen in the more exposed ventral side of the vertebrae in the new image (Fig. 2.8) in comparison to the pre-preparation image. Due to this preparation, information from the integument in the region has been lost. However, it reveals that the identified purported fibres are actually sedimentary layers of the matrix (Fig. 2.8). The area where the suggested fibres were in the original figure is still present after the preparation, but all that can be seen are contrasting coloured sediment layers exactly conforming to the outer margin of the 'fibres' described in the original image. The same appearance can be seen on the dorsal side of the same area, with another clear boundary created by sedimentary changes (Figs. 2.8b and 2.9). From close observation of these and other areas of the specimen, it is clear that a superficial halo is

present where the sedimentary layers are visible around the animal's body, creating a transition from dark to light matrix (Figs. 2.8b and 2.9). The preserved integument is markedly different in colour, being a deep brown in contrast to the lighter grey and buff sediment, a feature that is highlighted when the whole specimen is observed under strong light (Fig. 2.10a). In conclusion, the purported 'fibres' are in fact shadow effects caused by surface undulations in the rock and overlying layers prior to preparation (compare the shadows in Fig. 2.8a compared to Fig. 2.8b). The same error occurs in a more recent paper (Lingham-Soliar 2012, fig. 3), where even lower-quality images of the same area are used to identify "dermal tissues" showing "fine horizontal geometric fibres" "unique to dermal tissue" which are the sedimentary layering features already noted. In this paper, images of the whole specimen prior to the recent preparation are presented where the region of interest can clearly be seen to form part of the sedimentary halo shown here (Lingham-Soliar 2012, fig. 1). From a reconstruction in the same paper (Lingham-Soliar 2012, fig. 6) it appears that this halo has been misinterpreted as the remnants of the outline of the skin of the animal in the form of a frill. This has been used as evidence in support of a collagen affinity (Lingham-Soliar et al*.* 2007; Feduccia 2013). The halo present on NIGP 127587 is not seen in the other two fossils (Fig. 2.1), which both sit on a more uniform flat surface layer, highlighting the fact that only where the sediment layers are cut through in NIGP 127587 can the lines suggested as 'fibres' be seen. Shadowing effects on fossil specimens from images in previous work have also been misinterpreted as genuine biological structures in a similar fashion, as noted by Mayr (2010*a*).

The orientation of the genuine integumentary filaments (outwards and posteriorly along the body axis), conforms to pliable integumentary appendages such as feather homologues rather than collagen fibres, especially as they often curve back in towards the body distally, showing apparent flexibility (Currie and Chen 2001). This is most obvious in the tail region in IVPP V12415 (Fig. 2.4a-b) and is also clear in the tails of NIGP 127586 (Fig. 2.4d-e) and NIGP 127587 (Fig. 2.4c). A schematic figure in Lingham-Soliar et al. (2007, fig. 2f) ignores the actual pattern of orientation of the filaments and depicts them as being aligned straight and parallel, running posteriorly and outwards from the skeletal axis, in support of a structural collagen fibre affinity. This is in spite of the fact that the genuine orientation of the fibres is presented in a

panel in the same figure (Fig. 2.2e). The new high-quality images of the filaments (Fig. 2.4) also clearly refute the suggestion that they become progressively more degraded towards their tips, a feature suggested to support identification as collagen (Lingham-Soliar et al. 2007).

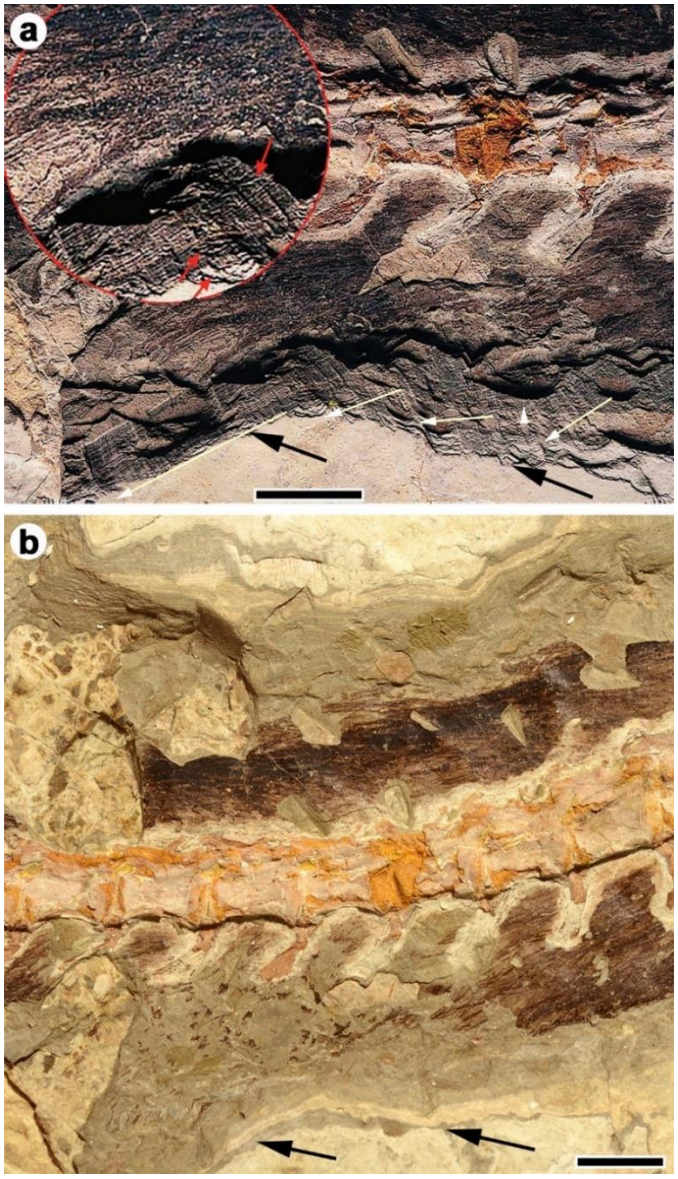

Figure 2.8. The mid-tail region of NIGP 127587 before (**a**) and after (**b**) preparation. In the description of the integument in this region by Lingham-Soliar et al*.* (2007, fig. 4), large areas of sediment underlying the integumentary layer were misidentified as primary structures. Small arrows (a) were placed by Lingham-Soliar *et al.* (2007) to show apparent orientations and positions of fibres. From the new image (b) it can be seen that these are most likely shadow effects of the change in sediment layer height, the outline of which exactly conforms to the original image prior to preparation (large black arrows indicate the same area in both images). The transition from

dark to light matrix is clear, and also present on the dorsal side of the tail, forming a superficial halo around the animal. The genuine integument is markedly different, with a dark brown preservation contrasting the lighter matrix. Scale bars represent 10 mm. (a) originally published in Currie and Chen (2001) and reproduced with original labelling from Lingham-Soliar et al. (2007) with permission from Springer.

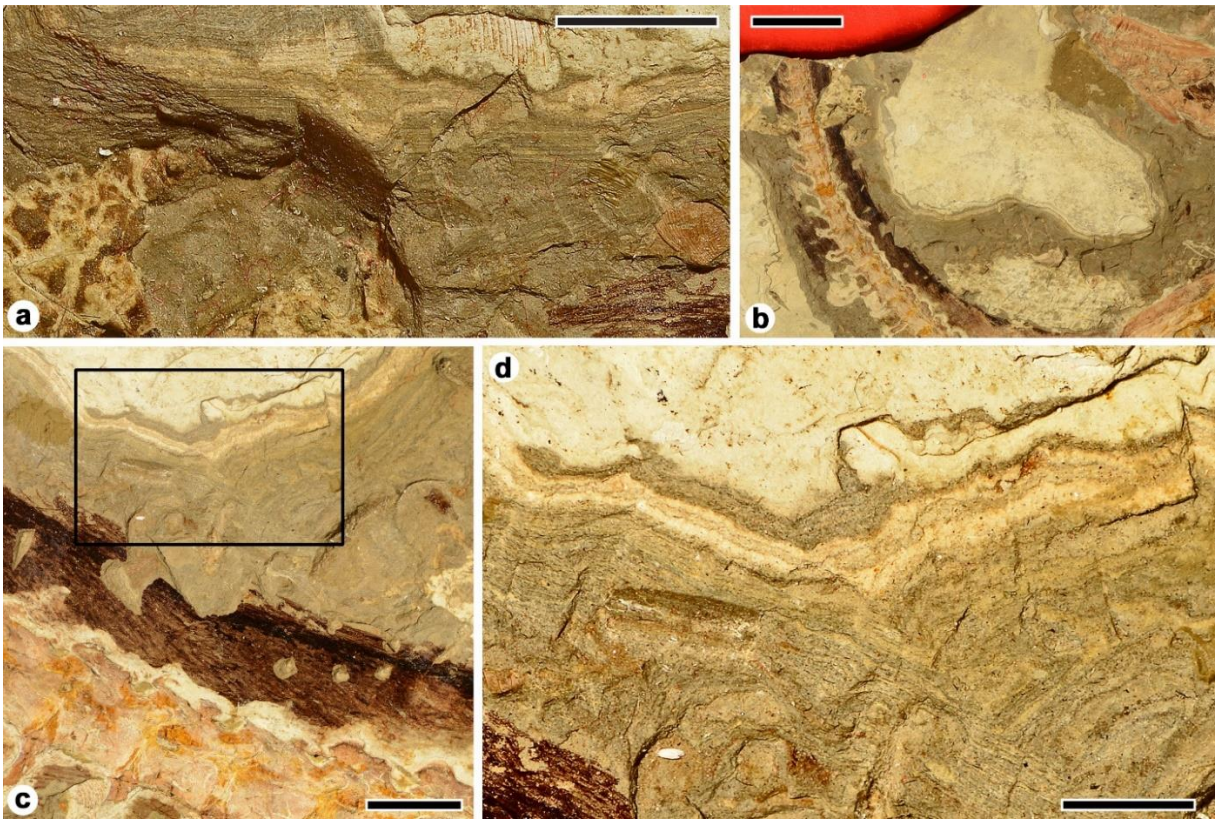

Figure 2.9. The sedimentary halo surrounding NIGP 127587 which has previously been misinterpreted as a corona of skin around the animal. **a**. A close up of the area dorsal to the tail shown in Fig. 2.8. The distinct layers of matrix can be seen to form parallel rows, previously identified as collagen fibres from low-resolution images. **b**. The change in sediment colour from dark to light forming a halo around the entire animal previously misidentified as skin in Lingham-Soliar *et al.* (2007) and Lingham-Soliar (2012). The areas of genuine integumentary preservation are clear from the dark brown patches close to the skeleton, the colour of which is most likely due to the presence of preserved melanosomes. **c**. A region dorsal to the anterior tail, showing clear dark integumentary structures above the vertebrae, followed by the dark grey matrix which transitions to light grey creating a series of parallel lines. **d**. Close up of the area highlighted in (c), showing the parallel lines of sediment layers in detail, which conform to previous images in Lingham-Soliar *et al.* (2007) where they were identified as collagen fibres (Fig. 2.8). The clear dark integument can be seen in the bottom left-hand corner. Scale bars represent 10 mm in (a) and (c), 50 mm in (b) and 5 mm in (d).

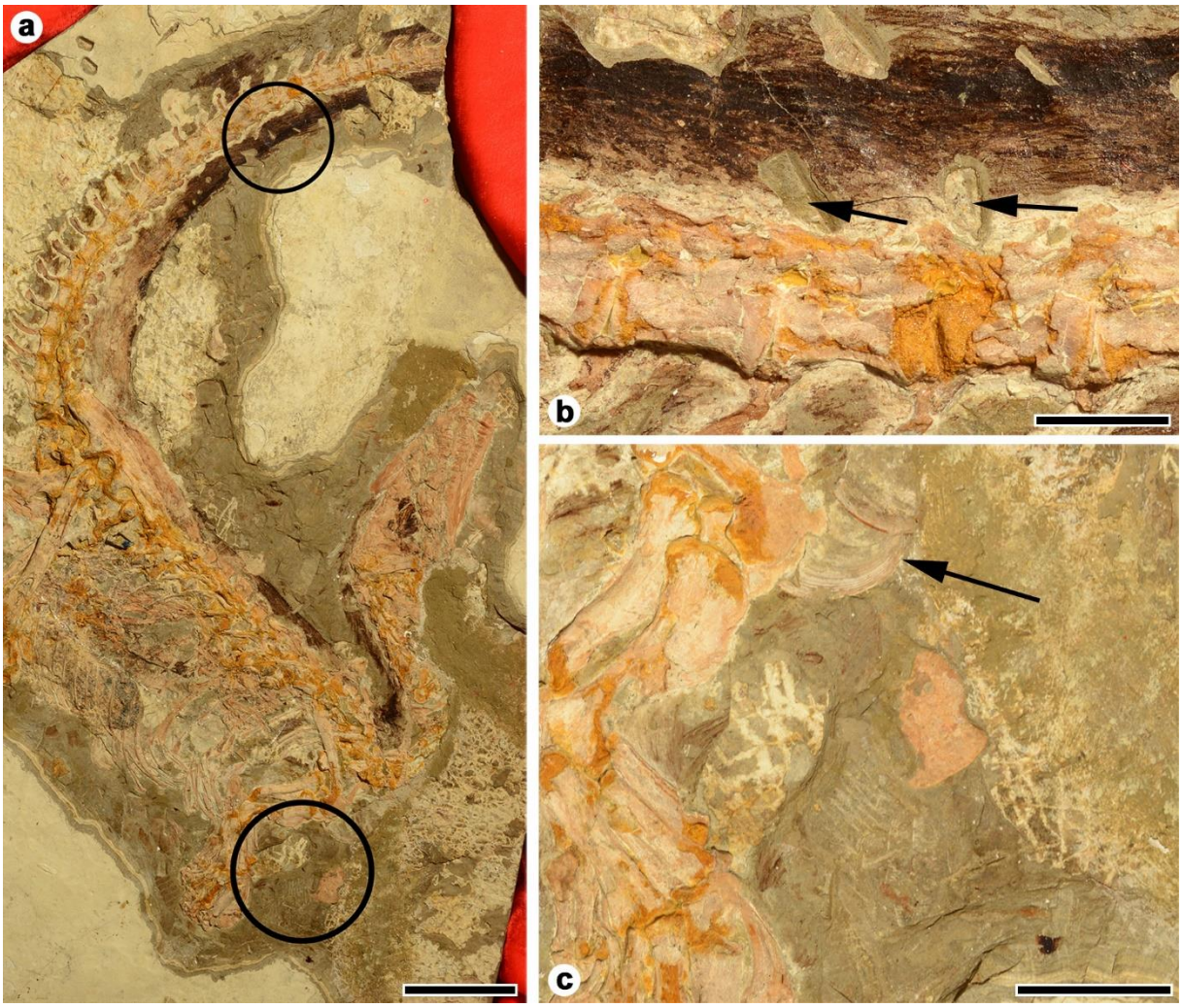

Figure 2.10. Examples of misidentifications of non-biological structures in previous work using low-resolution images. **a**. NIGP 127587 showing the two areas where the erroneous identifications have been made. Note the sedimentary halo previously identified as the outline of the animal's integument and the starkly darker genuine integument. **b**. Clear holes in the matrix, devoid of any primary structures (highlighted by black arrows) which have been previously identified as neural spines in Lingham-Soliar (2012; fig. 3). **c**. An area ventral to the cervical region of the animal, which has been previously identified as a preserved trachea in Lingham-Soliar (2012; fig. 1) with only conchostracans potentially resembling tracheal rings at the centre top of the image (black arrows). Scale bars represent 100 mm in (a) and 10 mm in (b-c).

Further misidentification of non-organic structures occurs through the use of low-resolution images of NIGP 127587. Holes in the matrix which cut through the genuine integumentary structures were identified as neural spines with geometrically parallel fibres

impressed into them (Lingham-Soliar 2012, fig. 3a). The new images show that these holes are not part of the theropod fossil, nor do they show any evidence of fibre association (Fig. 2.10b). It is also claimed that a cartilaginous trachea is preserved in NIGP 127587 (Lingham-Soliar 2012, fig. 1). In fact, the high-resolution images show that no tracheal structure is present (Fig. 2.10c). In the original figure, a vague bend has been highlighted to create the impression of a structure, which the new images reveal as a joining of unrelated features of the matrix. It is also possible that the conchostracans that appear throughout the matrix were interpreted as tracheal rings (Li et al. 2007). Genuine tracheal preservation is rare but has been found in some exceptional fossils including a mosasaur where tracheal rings were present in the throat region of the animal (Lindgren et al. 2010, fig. 3) and the theropod *Scipionyx samniticus* (Dal Sasso and Signore 1998). When present in fossils however, these tracheal features bear no resemblance to any structure seen in *Sinosauropteryx* (Dal Sasso and Signore 1998; Lindgren et al. 2010).

2.2.4. Evidence of scales in Sinosauropteryx

In IVPP V12415, a dark patch found at a break in the tail was identified as comprising four distinct scales with papulose surface patterns (Fig. 2.6b; Lingham-Soliar 2013, fig. 3). The original figure is of such low resolution however, that no features can be seen. Even using the highest resolution of the new images obtained, identifiable structures cannot be made out within the organic patch (Fig. 2.6c).

A further area is also claimed to represent scales, this time with ‘attachment fibres’ as further evidence of their affinity (Fig. 2.6a; Lingham-Soliar 2013, fig. 4). Superficially these appear more convincing, and scale-like shapes can be made out along with apparent fibres protruding from them (Fig. 2.6a). Examination of the high-resolution images however reveals that these scales are sedimentary features of the matrix, which continue not only between the tail break, as in the original figure, but right across the matrix far from the animal in a distinct linear arrangement, with those furthest from the fossil showing no scale-like structures (Fig. 2.6d). The claim that these structures also show a papulose pattern is incorrect, and no evidence of this is seen in the specimen or the new images (Fig. 2.6). The proposed ‘attachment

fibres' are also misidentified on closer inspection of the high-quality images, which clearly show these to be scratch marks likely made by an air scribe during the preparation of the fossil, further matching those made throughout the matrix of the specimen (Figs. 2.6 and 2.7).

Along with the misidentification of preparation marks as collagen fibres in both *Sinosauropteryx* and *Stenopterygius*, similar features were misinterpreted as biological structures in other important fossils, as in the critique of work showing feathers in an ornithomimid dinosaur from Canada (Van der Reest et al*.* 2016). Similarly, preparation marks were misinterpreted in support of the view that integumentary structures on the ornithischian *Psittacosaurus* (Mayr et al. 2002) were collagen, in a critique by Lingham-Soliar (2010*a,* 2010*b*) who misidentified a sand-blasted bristle as primarily "degraded" (Mayr 2010*a*).

2.3. Contemporaneous Jehol fossils refute collagen interpretation

Following these discussions, there is no evidence of scales on the known specimens of *Sinosauropteryx*. On the other hand, scaled dinosaurs have been found in the Jehol Biota, and so there is evidence available of what preserved scales look like in these lithologies. The ornithischian dinosaur *Psittacosaurus* shows a covering of well-preserved scales complete with pigment preservation (Mayr et al*.* 2002, 2016; Lingham-Soliar and Plodowski 2010, Smith et al. 2015; Vinther et al. 2016). Despite this, no evidence of any structures similar in appearance to the integumentary structures of *Sinosauropteryx* are present, other than long bristles on the dorsal side of the tail of *Psittacosaurus* (Mayr et al*.* 2016). It seems implausible that one scaled dinosaur would be preserved with no scales but with the underlying collagen fibre structure in situ, when another in the same deposit would have a covering of scales but no evidence of collagen preservation. Furthermore, the scales of *Psittacosaurus* are likely preserved because of the refractory properties of melanin (in melanosomes) and calcium phosphate, residues of which are embedded in mineral salts commonly found in the vertebrate epidermis, rather than through mineralisation or organic preservation of collagen or keratin (Pautard 1964; Mayr et al. 2016; Vinther et al. 2016).

The exceptionally preserved feathers in stem birds in the same deposits show similarities to the integument of *Sinosauropteryx*, including pigment preservation, but no evidence of preserved collagen fibres (Clarke et al. 2006; Zhang et al. 2006, 2010; Wogelius et al. 2011). Furthermore, pterosaurs from the Jehol Biota show both dermal soft tissue preservation (actinofibrils) and integumentary appendages (pycnofibres) which are preserved in different manners within individual specimens (Kellner et al. 2010). The actinofibrils are lightly coloured, geometrically arranged structures (herein shown not to exist in *Sinosauropteryx*) while the pycnofibres are darkly coloured filaments similar to those of *Sinosauropteryx*, which are most likely preserved by their pigment content (Kellner 2010). Original colour patterns have been found in pterosaur integuments indicating the high likelihood of pigment preservation (Vinther 2015*a*). The presence of dark organic preservation of the integumentary appendages of vertebrates including theropods, ornithischians, pterosaurs and early representatives of Aves in the Jehol Biota, which is due to the retention of melanin is a key piece of evidence uniting these with those of *Sinosauropteryx*. Thus far no satisfactory alternative explanation for the dark colour of these structures has been provided (Vinther 2015*a*, 2015*b*), although it has been suggested by some using antibody immunisation experiments that keratin should also preserve (Pan et al. 2016), which would need direct chemical confirmation (see Chapter 1.4).

The melanosomes found in *Sinosauropteryx* conform to the morphology of modern phaeomelanin-rich melanosomes, which are known to impart rufous or chestnut hues to feathers (Chapter 1; Zhang et al. 2010; Vinther 2015*a*). Criticisms of the presence of melanosomes in the integument of *Sinosauropteryx* (Lingham-Soliar 2011) are poorly supported and include observations that a chestnut colour appears throughout the matrix, which does not conform to our understanding of the nature of pigment preservation and the taphonomy of melanin (Colleary et al. 2015; Vinther 2015*a*). Preserved pigments rarely retain their original colour through diagenesis, and no case is known where phaeomelanin-rich melanosomes provide rufous or chestnut colours in a fossil (Li et al. 2010; Colleary et al. 2015; Vinther 2015*a*). This can be seen in the integument of all specimens of *Sinosauropteryx,* which is preserved as dark brown-black pigment, differing markedly from any other features of the matrix except for the eyes and abdominal soft tissues (Fig. 2.1), which also contain abundant melanin in modern

animals (Lindgren et al. 2012; Vinther 2015*a*; McNamara et al. 2018). In *Sinosauropteryx*, the preserved dark integumentary pigment is confined to the filaments themselves, marking out their structure, and is not found outside the filaments as would likely be the case if claims that leaching from overlying skin were true (Lingham-Soliar and Plodowski 2010). Orange colours in the matrix are likely produced by iron oxides and are not related to biological pigments. Claims that SEM images of melanosomes in *Sinosauropteryx* resemble collagen 67 nm *D*-banding are based on low resolution expanded images of the originals, which show little more than groups of pixels highlighted to infer a desired pattern (Zhang et al. 2010; Lingham-Soliar 2011, fig. 2).

An ornithischian dinosaur (*Kulindadromeus*) from Siberia has been described with both scales and feather-like structures preserved together, with extensive comparison made between the preservation and morphology of each structure type (Godefroit et al. 2014*a*). This is further evidence that scales and feathers have a similar propensity for preservation within specific deposits, and the specimens show that when scales and feathers are preserved in the same specimen they can readily be distinguished. Reinterpretations of the feathers in *Kulindadromeus* as collagen fibres by Lingham-Soliar (2014) have been rebutted and cannot be considered likely in the absence of evidence (Godefroit et al. 2014*b*).

2.4. Conclusions

The debate about avian origins has generated a great deal of controversy in the past few decades. Despite an accumulation of substantial evidence that birds are dinosaurs, some voices continue to challenge this evidence. The focus here has been on the papers that criticise the evidence for feathers in *Sinosauropteryx*, and it is shown that these studies have largely misinterpreted sedimentary and preparation structures as primary anatomical features. The use of low-quality images instead of first-hand study of the specimens has made it difficult to determine which traces in the fossils might be bone, feathers, sedimentary features or preparation marks. Re-examination of the specimens and use of high-quality images has shown how these features have been misidentified. Reanalysis of the specimens shows that the studies arguing that feathers are in fact degraded collagen in *Sinosauropteryx* based on the soft tissue anatomy of *Stenopterygius* are thus refuted.

Chapter 3 – Exceptional soft tissue preservation in Jurassic ichthyosaurs reveals countershading, skin architecture and ocular tissues

Abstract: Soft tissues are less likely to preserve in fossils than hard mineralised tissues due to their inherent instability during decay but can provide a wealth of information when present. Understanding the taphonomic pathways that lead to loss and preservation of different soft tissues is inherent in understanding fossils as once living animals. Ichthyosaur fossils occasionally preserve soft tissues such as components of the integument, revealing important aspects of their anatomy, however these have proven contentious. Here the soft tissues of three different genera of ichthyosaurs from three different Lagerstätten in the UK and one from Germany are examined in detail. Remains of the epidermis, including in-situ melanocytes, dermis with a dispersed layer of melanophore-derived melanosomes and hypodermis as well as some organic internal tissues and melanosomes preserving the eye are all observed. A phosphatised dermal fibrous network preserved as impressions in the mineralised matrix is also described. Fibrous features have been described previously, but were partially conflated with artefacts, such as cracks and preparation marks (chapter 2), complicating the full understanding of their nature, which is resolved here. Distribution of melanocytes and dermal melanosomes reveal a countershaded pattern in at least three specimens suggesting this was a common colour pattern in Jurassic ichthyosaurs.

This chapter is currently **unpublished** but will soon be submitted to a general science journal.

Author contributions – The author devised the project along with Jakob Vinther and gathered and analysed all data with the assistance of Kieran Goss, apart from the ToF-SIMS analysis which was performed by Ian Fletcher. Kieran Goss gathered the CT data. The author wrote the chapter and constructed all figures with contributions from Kieran Goss and Jakob Vinther.

3.1. Introduction

The majority of the vertebrate fossil record consists only of hard-part preservation, which can limit our understanding of the appearance, behaviour and physiology of many extinct taxa (Parry et al. 2018). Greater insights can be gained when soft tissues are preserved as well. Most soft tissue preservation occurs in deposits known as Konservat-Lagerstätten (Parry et al. 2018) which provide unique windows into the nature of extinct animals and allow for investigation of the taphonomic processes leading to their preservation.

Extensive recovery of ichthyosaur material from the UK and Germany over the past two centuries has provided many specimens with preserved soft tissue, including several that show full or partial body outlines (de la Beche and Conybeare 1821; Owen 1841; Broili 1942; Wiman 1946; Whitear 1956; Delair 1966; Howe et al. 1981; McGowan 1992; Lingham-Soliar 1999; 2001; Martill 1995; Lindgren et al. 2014; Lindgren et al. 2018). These have revealed the body shape of ichthyosaurs including dorsal fins and tail flukes in derived 'thunniform' taxa (Howe et al. 1981); features that would not have been known if only the bones were preserved. Soft tissue features have also been used to infer likely behaviours such as modes of locomotion (Massare 1988; Buchholtz 2001; Motani 2002) and organically preserved pigmentary colours have been proposed (Lindgren et al. 2014, 2018).

Melanosomes, the organelle containing the pigment melanin in vertebrates (Chapter 1), and even melanocytes have been observed in ichthyosaurs from the Early Jurassic of the UK (Whitear 1956; Lindgren et al. 2014) and Germany (Lindgren et al. 2018). Countershading and uniformly dark body colours have been proposed for Jurassic ichthyosaurs (Lindgren et al. 2014, 2018), however the latter was based on a single spot sample showing melanosomes from the tail of one individual, making it difficult to confirm the interpretations of a dark colour all over (Lindgren et al. 2014).

Fibrous structures have also been identified in a number of ichthyosaur fossils and were noted in several studies throughout the 20th Century (e.g., Broili 1942; Wiman 1946; Delair 1966; Lingham-Soliar 1999). The morphology and arrangement of these fibres were described in specimens from both Germany and the UK. Delair (1966) described a single layer of parallel

fibres preserved on the surangular of an ichthyosaur skull from the UK. In a more recent study of the same specimen, Lingham-Soliar (1999) described two layers of fibres overlying one another. Subsequent work on exceptionally preserved ichthyosaurs from the Posidonia Shale Formation of Holzmaden, Germany, suggested the presence of three distinct classes of fibres sometimes superimposed on top of one another in an apparent meshwork on the body and fins (Lingham-Soliar 2001; Lingham-Soliar and Plodowski 2007). However, many of the purported layers were in fact misidentifications of other structures including folds in preserved skin, cracks in the rock matrix or preparation marks (Chapter 2.2.1; Smithwick et al. 2017*b*), calling into question the identification of the proposed fibre classes. Furthermore, specimens from Holzmaden are well known to have been enhanced or embellished by preparators including recreation of lost or damaged features and adding or enhancing soft tissue structures (Martill 1987; McGowan 1992).

Accounts of the nature, arrangement and preservation of fibrous structures in ichthyosaurs are inconsistent between deposits and taxa, and further investigations into their likely colouration may identify common patterns and allow comparison to living analogues. To investigate this further, here soft tissue features including fibrous structures and organics in multiple exceptionally preserved ichthyosaur specimens representing four different taxa from three separate Lagerstätten in the UK as well as one of the Holzmaden fossils described previously (Lingham-Soliar 2001) are examined in detail. Importantly, many of the specimens from the UK have only been half-prepared out of the rock, and one is a recent discovery, and so do not have any of the potential issues with alteration or enhancement seen in other historical specimens. Light microscopy, SEM imaging and ToF-SIMS are used to investigate the nature of the soft tissues with particular attention paid to the morphology and arrangement of the fibrous features, the nature and likely origin of organics and the layering of different soft tissues. In addition, soft tissues found within the eye orbits of two specimens is investigated to determine whether melanosomes from different ocular layers are present, as has been proposed for other vertebrate fossils (e.g., Vinther et al. 2008; Clements et al. 2016).

3.2. Materials and methods

3.2.1. Specimens

Specimens from three UK Lagerstätten were investigated (Fig. 3.1): four individuals representing two taxa from the Early Jurassic (Toarcian) Strawberry Bank Formation, Ilminster, Somerset (M1401, M1405, M1408 and M1409, Fig. 3.1a-e), one specimen from the Late Jurassic (Kimmeridgian) Kimmeridge Clay Formation of Kimmeridge, Dorset (K1747, Fig. 3.1f) and one specimen from the Early Jurassic (Sinemurian) Gumption Shales member of the Blue Lias Formation, Lyme Regis, Dorset (Fig. 3.1g). A further specimen from the Holzmaden Posidonia Shale Lagerstätten (SMF R 457, Fig. 3.1h) was also investigated to allow comparison with the UK material and to reassess previous characterisation of the soft tissues shown to contain misidentifications (Lingham-Soliar 2001; Smithwick et al. 2017*b*). Six of the seven specimens examined in this study are small in overall body size for their species with large heads relative to body length, suggesting that they represent juveniles. High resolution photographs were taken of all specimens.

3.2.2. Specimen imaging

The Strawberry Bank and Lyme Regis ichthyosaurs were photographed using a Nikkon D5300 DLSR with an 18-300 mm VR lens under artificial lighting using a 3200K halogen light source (Lowell Tota-light, 400W). Photographs were taken with angles of illumination at both North-West to North-East to highlight three-dimensional features better that may not be visible under a single condition. Images of K1747 were provided by the Etches Collection and SMF R 457 was imaged by Sven Tränkner (SMF).

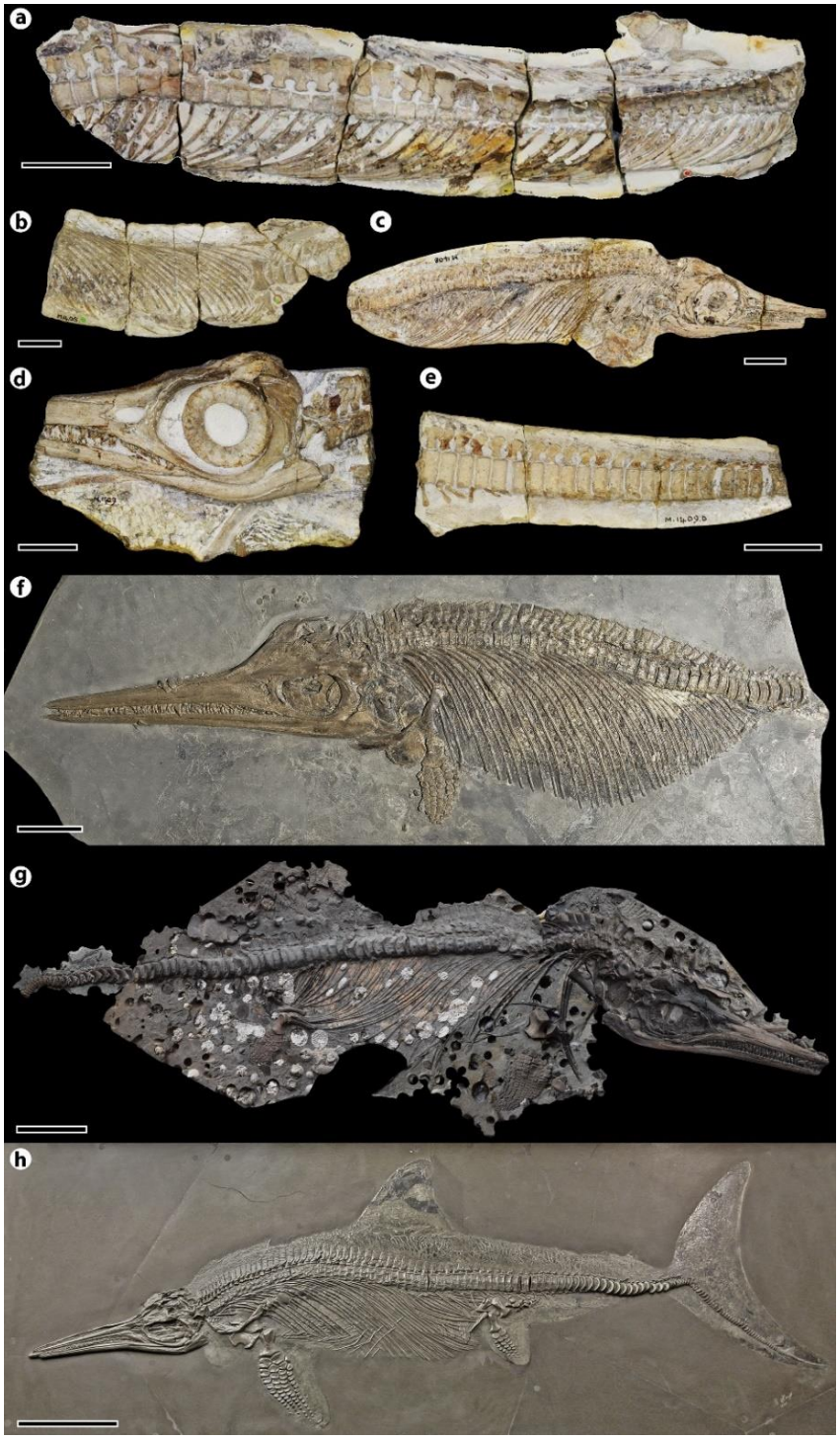

Figure 3.1. Exceptionally preserved ichthyosaur fossils showing extensive soft tissue preservation. **a**. *Hauffiopteryx typicus* (M1401) from the Strawberry Bank Formation, Ilminster, Somerset UK. **b**. *Stenopterygius triscissus* (M1405) from Strawberry Bank. **c**. *S. triscissus* (M1408) from Strawberry Bank. **d-e**. *S. triscissus* (M1409 and M1409D) from Strawberry Bank. **f**. An undescribed specimen (K1747) from the Kimmeridge Clay Formation, Kimmeridge, UK. **g**. An

undescribed specimen from the Blue Lias Formation of Lyme Regis, Dorset UK likely of the species *Ichthyosaurus communis*. White circles are where holes in the matrix created by the Common Piddock (*Pholas dactylus*; as the fossil was exposed on the foreshore) have been filled with plaster. **h**. *Stenopterygius quadriscissus* (SMF R 457) from the Posidonia Shale Formation of Holzmaden, Germany. Scale bars represent 10 cm in (a, f-g), 5 cm in (b-e) and 30 cm in (h).

3.2.3. Specimen sampling

The Strawberry Bank and Lyme Regis ichthyosaurs were sampled to allow further morphological and chemical investigation of the soft tissues. Small chips of material were removed from the fossils using a sterile scalpel and stored in aluminium foil to avoid contamination. Both pale phosphatised material (including fibrous features) and dark organics were sampled. Because dark organic material in vertebrate soft tissues is often the remains of the original melanin pigment (Vinther 2015*a*), organics from multiple regions of the body were sampled to first determine whether they derived from different original tissues and then to identify possible colour patterns. Organic samples from within the eye orbits of the Lyme Regis fossil and M1408 were also taken to determine whether they represent ocular melanin. Locations of the samples are shown in Figure S3.1. The samples were mounted onto SEM stubs using double sided copper tape to allow for light microscopy, SEM and ToF-SIMS investigation. Samples of integumentary soft tissue from the Lyme Regis specimen were also set into Epofix epoxy resin (Agar Scientific) and cut and polished to create clean cross sections using a Buehler Isomet 1000 diamond saw and Buehler Ecomet 250 Grinder-Polisher using MetaDi Supreme Polycrystalline diamond suspensions down to 1 micron. Samples were set on edge in the resin to ensure the cut went laterally through the soft tissue layers.

3.2.4. Light and SEM microscopy

Light microscopy and imaging were conducted using a LEICA MZ 125 microscope, with an attached QImaging MicroPublisher 5.0 RTV camera. Removed samples and cut cross sections as well as smaller areas of the fossils showing high levels of soft tissue preservation were

investigated. Both overhead and angled light sources were used to highlight three-dimensional features of the soft tissues. To prepare the samples for SEM imaging, they were sputter coated with 10 nm of gold using a Quorum Q150R ES sputter coater. Imaging was then conducted using a Zeiss EVO15 ESEM at the University of Bristol Life Sciences Building. Samples were imaged at a working distance of 10 mm using an accelerating voltage of 5-30 KeV (this depended on the amount of charging in the samples, which varied).

3.2.5. ToF-SIMS analysis

Four samples from the Lyme Regis specimen were chemically analysed using ToF-SIMS. This was carried out to determine whether the dark apparently organically preserved soft tissue features in the fossil were indeed organics and to ascertain whether they represent melanin (Vinther 2015). The samples were first washed in acetone and Purite water (Purite Ltd) to remove possible modern contamination and were not gold coated.

Static SIMS analyses were performed using an ION-TOF 'TOF-SIMS IV – 200' Time of Flight Secondary Ion Mass Spectrometer (ION-TOF GmbH, Münster, Germany; single-stage reflectron design; Schwieters et al. 1991). This was carried out at the NEXUS facility, Newcastle University. Positive and negative ion spectra were obtained using a Bi_3^+ focused liquid metal ion gun at an energy of 25 keV. It was fired at 45° to the sample surfaces and operated in 'bunched' mode for high mass resolution (using 20 ns wide ion pulses at 10 kHz repetition rate). The sample surface topography and the ion gun mode of operation limited the mass resolution resolvable to around m/Dm = 2000. The spatial resolution was around 4 µm (limited by the primary ion beam diameter).

Positive and negative ion static SIMS spectra were obtained from the outermost sample surfaces (around 1 nm in depth) for each fossil sample at room temperature. Raw data containing the secondary ions recorded at each pixel were acquired with a 128 × 128-pixel raster and a field of view of 50 µm × 50 µm.

While ToF-SIMS provides useful information on the molecular makeup of a sample surface in the form of a spectrum of mass peaks that can be qualitatively compared to samples with known spectra (Colleary et al. 2015), it is most informative when results are quantitatively compared to samples with known molecular makeup (see Chapter 1.5). The results were therefore added to a database of modern and fossil melanin samples and non-melanin controls (from Colleary et al. 2015) and a principal component analysis (PCA) produced. Fifty-six mass peaks were selected as the variables in the PCA based on those selected as representative of modern melanin in previous works (Lindgren et al. 2014; Colleary et al. 2015). To ensure that each peak was given the same weight in the PCA, the peak signal intensities of each mass were normalised to the standard deviation of all peak intensities of the same mass from all samples in the analysis, as per previous ToF-SIMS work on fossil melanin (Colleary et al. 2015).

3.2.6. Modern tissue CT scanning

In order to analyse soft tissue features in modern animals that could function as analogues for the ichthyosaur tissues, a 5 cm^3 piece of ethanol-preserved porpoise epidermis was imaged using a Nikon XT H 225 ST CT scanner at the University of Bristol. The scan was conducted with X-ray energies of 150 keV and a current of 87 uA.

3.2.7. Measurement of fibres and melanosomes

The widths of fibrous features were measured in ImageJ (Abràmoff et al. 2004). The number of fibres per centimetre was calculated and from this the average fibre diameter taken. For each specimen, multiple measurements were taken and averaged for the final result. The features were shown to be preserved as impressions rather than three dimensionally (see Results), and so measurements of individual impressions (from SEM images) were taken for the Lyme Regis and Strawberry Bank fossils (again averaged from multiple measurements). Measuring the troughs from light images was more difficult and considered too inaccurate to be representative. Similar structures observed in the CT scans of the porpoise epidermis were measured in the same way as the fossils in ImageJ.

Microbodies found in the organics (identified as melanosomes – see results) had their long and short axis measured and from these the aspect ratio was calculated. These data were compiled for melanosomes from several different locations, each likely representing different original tissues. These comprised dark spots within the upper-most phosphatised integumentary layer (putative melanocytes), internal organics underlying the fibrous layers (putative internal organ remains), dark organics on the matrix forming a halo dorsal to the neural spines and around the pelvic girdle (presumably from the skin) and from within the eye (known to contain abundant melanosomes in extant vertebrates; Liu et al. 2005*b*; Hu et al. 2008).

3.2.8. Statistical analyses

T-tests were performed on the measurement data of melanosomes from each different location to determine whether they represent distinct morphologies. In extant reptiles, melanosome shape and size differ between different locations within the integument. Those of the epidermal melanocytes are smaller than those of underlying dermal melanophores (Landmann 1986). It has also been shown that melanosomes deriving from the internal organics can differ in morphology to those of the integument (McNamara et al. 2018). Melanosomes from within the eye differ in morphology in relation to the exact tissue layer from which they derive (Liu et al. 2005*b*; Hu et al. 2008, Clements et al. 2016). Each melanosome population from the different locations on the body of the Lyme Regis specimen (which showed the best preservation of melanosomes) was tested against each other for length, width and aspect ratio to identify any significant differences. All tests were carried out in SPSS 25 (IBM Corp).

3.3. Results

3.3.1. Specimen descriptions.

Soft tissues are extensive throughout all of the studied specimens (Figs. 3.2-3.6) and fall into two broad categories; white to buff phosphatised material (Figs. 3.2-3.3) and dark organics

(Figs. 3.5, 3.6 and S3.2). Much of the phosphatic material shows a distinct fibrous structure with a consistent morphology in all specimens of fibres arranged in parallel rows (Figs. 3.2-3.3).

Strawberry Bank

The Strawberry Bank specimens (M1401, M1405, M1408 and M1409, Fig. 3.1a-e) were excavated in the mid-1800s by Charles Moore (Williams et al. 2015) and reside in the collections of the Bath Royal Literary and Scientific Institution (BRLSI) collections. All of the Strawberry Bank ichthyosaur material appears to preserve abundant soft tissues features, mostly in the form of white, apparently phosphatised remains (including fibrous material) as well as some darker organics. Organics were occasionally associated with the fibrous layers, but for the most part the phosphatised soft tissues and organically preserved tissues were separate. While much is visible in the specimens, it is likely that most has been prepared away on the exposed areas of the fossils, particularly from above the bones. It is also likely that more soft tissues are still present in the un-prepared regions of the fossils, as evidenced by thin dark halos surrounding the unexposed bones. Unlike all the other specimens, which are compressed laterally with soft tissues compacted onto and surrounding the bones, the Strawberry Bank fossils are generally three-dimensionally preserved. Rather than being compressed onto the bones, much of the integumentary soft tissues appear to have been close to their original positions above the bones and were thus likely removed during preparation. It was noted that soft tissue material readily came away from the bones in the few areas it was present, suggesting it may have been hard to not remove during the preparation process which was likely aimed at revealing the bones. Therefore, it is likely that the fibrous material was present across the whole body of each specimen originally. When samples of fibrous layers were removed, no other layers were found underneath.

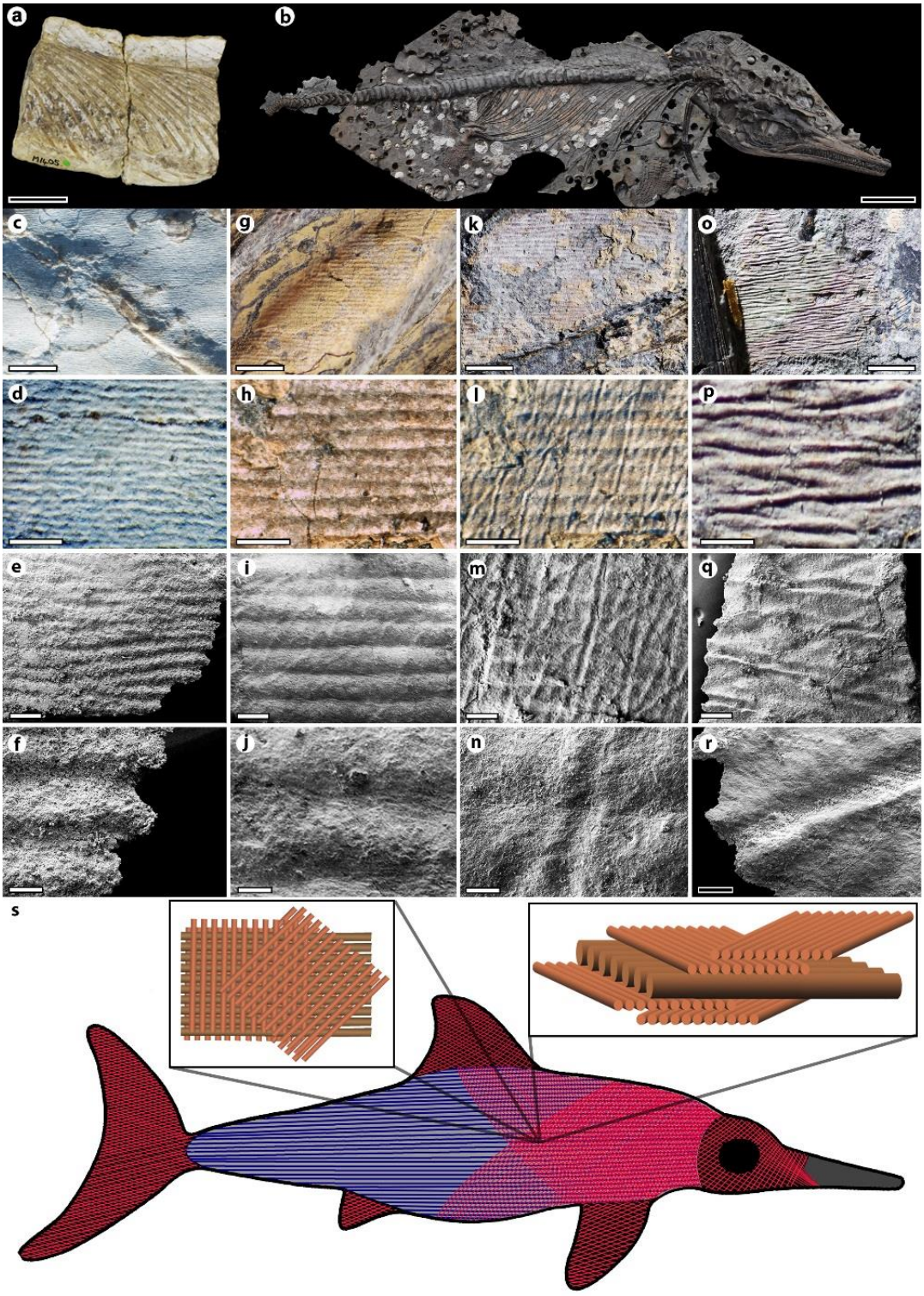

Figure 3.2. Dermal fibre preservation in Jurassic ichthyosaurs from the Blue Lias Formation of Lyme Regis, Dorset UK and the Strawberry Bank Formation of Ilminster, Somerset UK. Phosphatised soft tissue layers show impressions of dermal fibres with no evidence of 3D fibre preservation. Each column shows two light microscopy

images and two SEM images of each sample. **a**. *Stenopterygius triscissus* (M1405) from the Strawberry Bank Formation. **b**. An undescribed specimen from the Blue Lias of Lyme Regis. **c-f**. A single layer of parallel fibres running at the same orientation to the body axis in the Strawberry Bank specimen M1405. **g-j**. Parallel fibres running at the same orientation to the body axis in the Lyme Regis specimen. **k-n**. A layer of finer fibres running orthogonally to the main parallel fibres in the Lyme Regis specimen. **o-r**. A fabric of obliquely orientated interweaving fibres from the Lyme Regis specimen. **s**. Reconstruction of the likely fibre architecture in the dermis of Jurassic ichthyosaurs based on all available data. A layer of larger fibres runs parallel to the body axis (blue in the main image) with smaller fibres cross orientating with it (red fibres). Scale bars represent 5 cm in (a), 10 cm, (b), 2 mm in (c), (g), (k) and (o), 500 µm in (d), (h), (l) and (p), 200 µm in (e), (i), (m) and (q) and 50 µm in (f), (j), (n) and (r). Reconstruction (s) not drawn to scale.

M1401

Specimen M1401 (Fig. 3.1a) is described as *Hauffiopteryx typicus* (von Huene, 1931) and consists of a near-complete individual preserved in multiple sections (Caine and Benton 2011). Five sections of vertebral column and ribcage in joining pieces of concretion were examined, labelled M1401C-G (Caine and Benton 2011). M1401A-B consists of the skull and anterior-most postcrania with limited soft tissues preserved. The animal is preserved three-dimensionally with the dorsal side exposed. Extensive organics are present on many bones and on the matrix dorsal to the neural spines as well is internal to the ribcage.

M1405

Specimen M1405 (Fig. 3.1b) was described as belonging to *Stenopterygius triscissus* (Caine and Benton 2011) and consists primarily of postcranial material. Extensive soft tissues are present both inside the ribcage and on the matrix surrounding the bones. A white presumably phosphatised layer runs dorsal to the vertebrae and contains abundant fibrous features running parallel to the body axis. The specimen is preserved partially dorsoventrally and laterally compressed, meaning that there is no obvious dorsal or ventral exposure. A small block with abundant soft tissues on (sample 39-20110353; Fig. S3.1c) came from the dorsal region of M1405. This piece also shows extensive white/buff-coloured soft tissue corresponding to the same material in the larger block from which this piece derives.

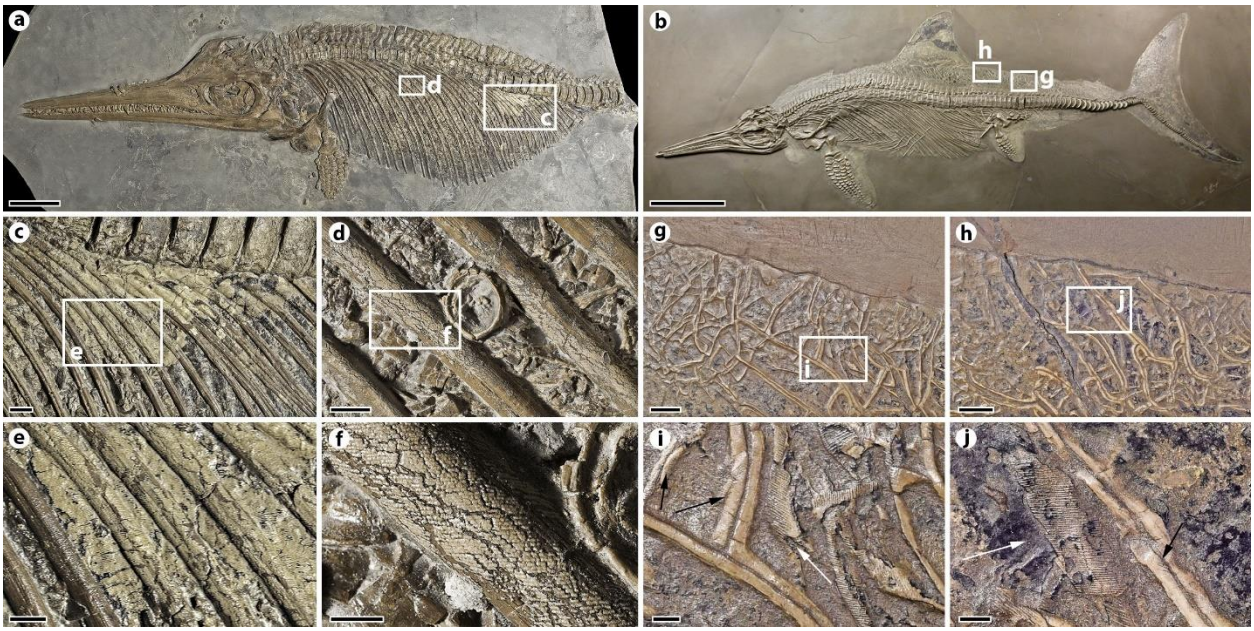

Figure 3.3. Dermal fibres preserved in ichthyosaurs from the Kimmeridge Clay Formation of Kimmeridge Bay, Dorset, UK and the Posidonia Shale Formation, Holzmaden, Germany. White rectangles mark the location of the next respective panels. **a**. An undescribed ichthyosaur from Kimmeridge (K1747) with fibres across parts of the abdomen. **b**. *Stenopterygius quadriscissus* from Holzmaden with fibres across most of the animal including a halo of soft tissue demarking the body outline (SMF R 457). **c**. A patch of phosphatic fibres overlying the ribs and vertebrae with organics underneath. **d**. Further fibres on top of the ribs that had pulled apart prior to fossilisation. **e**. Detail of the sheet of parallel fibres. **f**. Detail of the pulled-apart fibres. **g-h**. Overview of the soft tissues on the dorsum of SMF R 457 showing mixed phosphatic and organic remains. **i-j**. Fibrous tissue layers running at different angles to one another. Larger features previously identified as "class 1" collagen fibres (black arrows) have the smaller fibrous texture on their lower margins, while the tops have been artificially flattened. These therefore appear to be wrinkles in the integument that have been ground down, revealing sediment in the gap underneath. Organics are present underneath and overlying the fibrous layers (white arrows). Scale bars represent 10 cm in (a), 30 cm in (b), 1 cm in (c) and (g-h), 5 mm in (d-e) and 2 mm in (f) and (i-j).

M1408

This specimen represents the smallest individual studied and is of the species *S. triscissus* (Caine and Benton 2011). The individual is complete apart from the tail and limbs, is preserved laterally with the right flank exposed and measures 52 cm (Fig. 3.1c). It has extensive soft tissues covering the rib cage, inside the abdomen and surrounding the bones on the matrix. Organics are only present on the dorsal side with soft tissue on the ventrum consisting of white

phosphatised material. More soft tissues were likely present but were lost during preparation. Dark organics are also present within the sclerotic ring of the eye.

M1409

Specimen M1409 (Fig. 3.1d-e) is also identified as *S. triscissus*. The specimen consists of multiple blocks representing a near-complete individual. Soft tissues are most pronounced in the skull and tail blocks (Fig. 3.1d-e), so these were the only ones studied in detail. The skull shows good preservation and has abundant fibrous soft tissue underlying the mandible. The caudal section lacks the distal-most region and shows pale-coloured soft tissues around the vertebral column as well as some organics dorsally. A fibrous layer is present ventral to the mandible which undulates in a way that suggests that the entire soft tissue layer became folded during decay of the animal.

Kimmeridge

The Kimmeridge specimen was found by Steve Etches at Kimmeridge Bay and resides in the Etches Collection at Kimmeridge Bay, Dorset. Specimen K1747 (Fig. 3.1f) is an undescribed near-complete specimen. It is preserved laterally compressed with the left flank exposed and measures around 120 cm in length (though it is missing the tail). Soft tissues are present throughout the specimen including dark organics and fibrous buff coloured material. Dark organic material is present across the specimen but mostly not associated with the buff fibrous material except in one region where organics appear to underlie the fibrous layer (Fig. 3.3c-d). The organics lie over some bones (such as the anterior neural spines) as well as internal to the ribcage). Samples could not be obtained but high-resolution photographs were used to assess soft tissue features.

Lyme Regis

The Lyme Regis specimen (Fig. 3.1g) was discovered by Chris Moore who kindly donated samples of soft tissue which are now housed in the University of Bristol Collections. The ichthyosaur was collected from the *Arietites bucklandi* (Sowerby 1816) Zone (Blue Lias Formation) in 2016 and is therefore early Sinemurian in age. It is a near-complete individual

most likely of the species *Ichthyosaurus communis* (Conybeare 1822) preserved laterally compressed with the right-hand side exposed. The postcranial material has only been partly prepared as to not disturb the soft tissues, which are easily destroyed using traditional preparation methods such as air abrasive (Chris Moore 2018, pers. comm.). The body extends from the skull to just beyond the tail deflection, and the front and rear limbs are present roughly in life position, though the front limb shows minor detachment from the pectoral girdle. The fossil is 114 cm in length but is missing the distal-most part of the tail.

Soft tissues are preserved throughout the specimen, including overlying many of the bones and on the matrix between bones and surrounding the animal. The soft tissues consist of layers of dark organic material as well as buff-coloured layers often showing the distinctive fibrous features. Multiple layers of different fibre orientations are present. Dark organics are abundant throughout the Lyme Regis specimen, both separate from and apparently associated with the buff fibrous layers (Figs. 3.5 and S3.2). In some areas a black organic layer overlies the fibrous layer and in others it appears to lie underneath the fibres (e.g., Fig S3.2b). Occasionally, fibre impressions can be seen in the organics themselves (Fig. 3.5d). Dark patches of organics also occur directly on the matrix dorsal to the neural spines in multiple locations (e.g., Fig. 3.5c) as well as ventral to the tail bend (Fig. S3.4b). Further dark organics are present within the sclerotic ring of the eye. Much soft tissue remains underneath the matrix in certain areas and so could be freshly sampled knowing overlying layer had not been lost during preparation

Holzmaden

A specimen was examined from the Posidonia Shale of Holzmaden, Germany housed in the collections of the Senckenberg Research Institute, Frankfurt (SMF R 457) for comparison with the British material. This specimen has been previously described in terms of its soft tissue anatomy (Lingham-Soliar 2001), however owing to the issues surrounding this (Chapter 2) I re-describe it here for clarity. The specimen is of the species *S. quadriscissus*, measures around 2.3 metres in length and shows a complete body outline of soft tissue including caudal and dorsal fins (Lingham-Soliar 2001), although the apparently perfect body outline was most likely enhanced during preparation (Smithwick et al. 2017*b*). Fibrous material and dark organics are

present throughout the specimen. The genuine fibrous layers (see Chapter 2 and Results for discussion on previous misidentifications of other features) on the Holzmaden specimen appear to run in multiple directions relative to the body, with some parallel to the body's long axis and some running obliquely and obtusely to this. The significant distortion and folding in the integument makes it difficult to determine precise orientations however, or to say for certain whether a single or multiple fibrous layers are present (Fig. 3.3i-j).

3.3.2. Fibre morphology and layering

SEM images reveal that the fibrous layers consist of a series of parallel peaks and troughs rather than being composed of three-dimensionally preserved fibres (Fig. 3.2 and S3.6). Cut and polished cross sections also reveal that no 3D fibre morphology is present (Fig. 3.4). Close-up inspection of this material confirmed that it was phosphatically preserved as evidenced by the microstructure of phosphate mineral grains (Fig. S3.6) being similar to those observed in other phosphatised fossil tissues and artificially phosphatised material (Martill 1990; Briggs et al. 1993). The "fibres" are therefore preserved as moulds/impressions in an amorphous phosphatised surface rather than as authigenically mineralised or organically preserved elements. For clarity, the term "fibres" is hereafter used to refer to these fibre impressions.

All the UK specimens show expansive sheet-like layers of fibres that run parallel or near-parallel to the body's long axis (Fig. S3.3). In the Kimmeridge and most Strawberry Bank specimens, these sheet-like layers are generally not accompanied by any other fibrous layers. The only exception to this is M1409, where a second layer of fibres appears to sit under the main layer but is rarely exposed. In the Lyme Regis specimen, multiple clearly defined fibrous layers are present throughout with different sizes (Fig. S3.6). The layers easily came away from one another during sampling indicating that they were not cemented together during diagenesis. The widest of these phosphatised layers shows the same sheet-like fabric running in a single orientation parallel to the body long axis like the other UK specimens (Fig. 3.2d and h and S3.3). There are also multiple further layers of parallel fibres sitting on top of one another running at different angles to this main layer. In places, this creates an orthogonally-orientated

meshwork of fibres (Fig. 3.2f, j and n) while in others the orientation is more oblique (Fig. 3.2e, I and m). When illuminated from different angles, the same patches can show multiple layers of fibre orientations not obvious when only one angle of illumination is used (Fig. S3.7). The same phenomenon is apparent under SEM imaging, depending on the angle at which the electron beam hits the samples (Fig. 3.2l and m). Much of the fibrous soft tissue material is preserved in patches seemingly disconnected to one another (Fig. S3.6). Whether the fibre layers were once all connected as a single sheet as in the other specimens is unclear, but I consider it likely that the apparent disconnect between the layers is a taphonomic artefact or due to uneven splitting upon removal of the matrix during preparation of the fossil (due to the ease with which separate layers spall apart). It is likely therefore that originally a layered meshwork of fibres was present throughout the animal. As well as the fibrous layers, some patches of a paler phosphatised tissue with an amorphous surface texture are present in the Lyme Regis specimen, underneath the fibrous layers forming a basal layer (Fig. S3.2c).

There are two distinct size classes of fibre in the Lyme Regis specimen; one larger fabric (parallel to the body long axis; Fig. S3.3), and another class of much smaller fibres that always seem to cross-orientate with the larger fibres and occasionally with each other (e.g., Figs. 3.2, and S3.5-S3.7). The number of layers appears to vary from region to region. It is difficult to ascertain the exact number present, but there are multiple examples of at least three distinct layers overlying one another based on the orientation of the fibres (Fig. S3.6-3.7). It is likely that more than three layers in total were originally present. Another feature not seen in any other specimen is the presence of a layer of apparently interweaving fibres (Fig. 3.2f, j and n, S3.2c and S3.5). This distinct layer has two separate fibre orientations in a single layer that overlap one another creating a rhomboidal fabric (Fig. S3.5 and S3.6a-b). This layer always overlies any other fibres when it is present and has a lighter colour to the deeper fibrous layers.

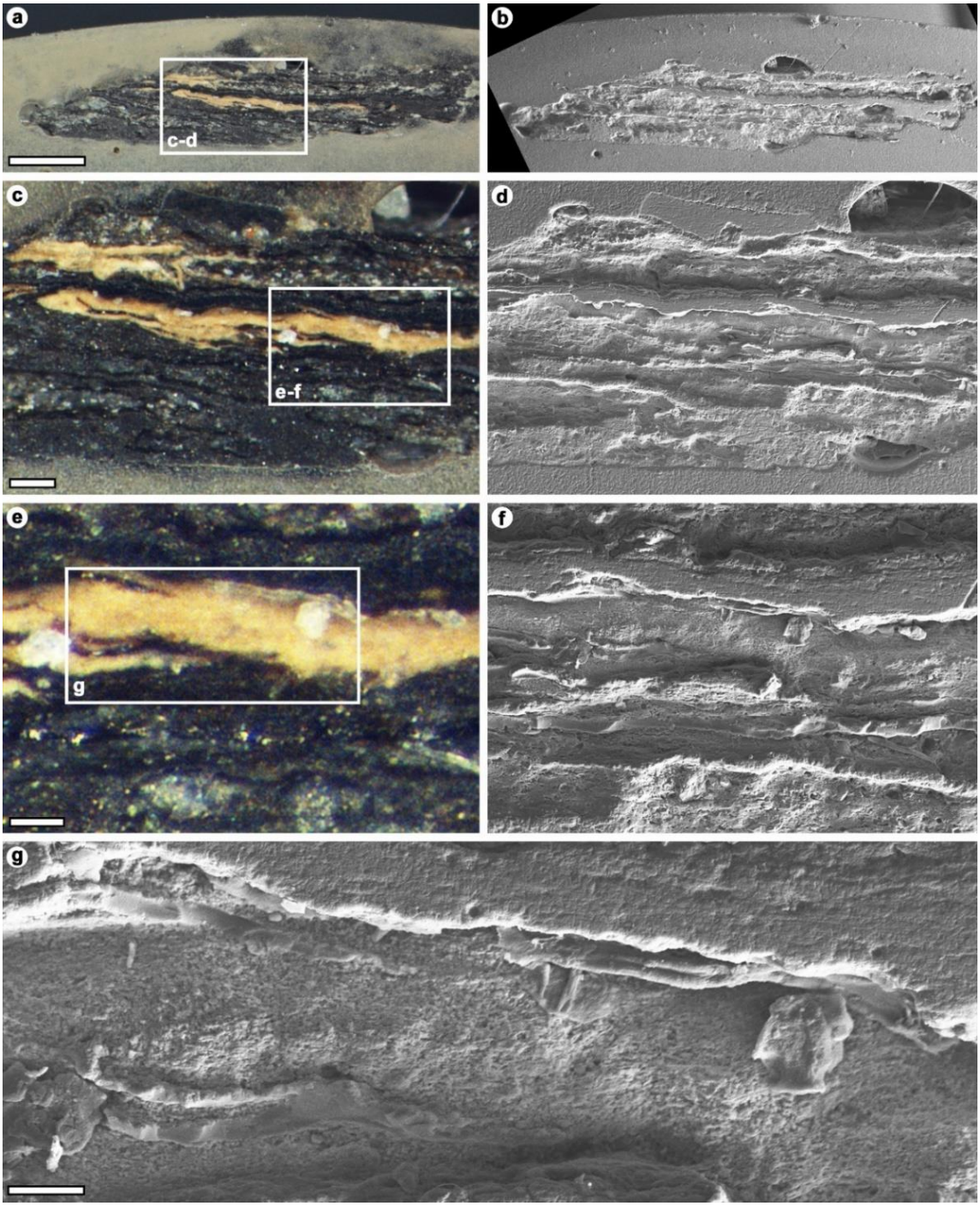

Figure 3.4. Polished cross sections of ichthyosaur integumentary soft tissue from the Lyme Regis specimen imaged using both light microscopy (**a**) (**c**), and (**e**) and SEM (**b**), (**d**) and (**f-g**). White rectangles represent the next images in the series. The section contains buff-coloured phosphatised layers that have the fibre impressions on their surface, black organics and dark grey mineralised matrix. No evidence exists of three-dimensional fibres at any level of magnification (**a-g**). Scale bars represent 500 µm in (a-b), 100 µm in (c-d), 50 µm in (e-f) and 20 µm in (g).

In the Holzmaden specimen (Fig. 3.3b) fibres are present throughout, but rather than being exposed in expansive sheets, appear in patches with apparently random orientation to one another (Fig. 3.3g-j). Due to extensive distortion of the integument it is difficult to determine if these layers overlap one another in the same fashion as the Lyme Regis specimen, but multiple fibrous layers appear present in a single size class.

Much larger structures are also present in SMF R 457 (Fig. 3.3g-j), previously identified as "class 1" and "class 2" collagen fibres (Chapter 2.2.1; Lingham-Soliar 2001). Many of these structures however have the smaller fibrous fabric seen throughout the specimens impressed into them, which fades towards the most exposed portions of these larger structures (Fig. 3.3i-j). The small fibres disappear from these larger features in a way that suggests that they have been worn away and the tops of the large structures have clearly been artificially flattened. This is most pronounced on the features with the greatest relief, while those closer to the matrix, and therefore relatively shallower in relation to the others, have more pronounced fibrous texture. The matrix of this specimen appears to have been ground down during preparation (Chapter 2.2.1; Smithwick et al. 2017*b*), which may explain why many of the soft tissue features with the greatest relief have had their surfaces worn away. It seems likely that when the matrix around the bones was ground down, some of the top layers of the integumentary soft tissues were worn away as well. Wrinkles in the overall preserved skin layer appear to have had their peaks ground away during preparation revealing a gap of sediment creating the appearance of fibre-like features. Skin wrinkles are also present in some of the Strawberry Bank specimens and therefore seem common (see section 3.3.7). It therefore seems that there is only a single morphology of fibre in this specimen, which resembles the UK material.

3.3.3. Fibre size

The Strawberry Banks fossils show the smallest average fibre impression diameter of the parallel-to-body-long-axis fibre layers (Table 3.1). The largest fibre impressions were seen in the Kimmeridge fossil (Table 3.1). Two distinct fibre size classes are present in the Lyme Regis fossil, with the layers running parallel to the body long axis being of similar diameter to the other

fossils, but the cross-orientating fibre impressions being much smaller (by almost three times; table 3.1). The diameter of the Holzmaden fibres, averaging 130 µm matches well with the fibres in the Kimmeridge fossil as well as the largest size class in the Lyme Regis fossil (Table 3.1).

3.3.4. Modern Porpoise tissue

The CT scan of the piece of porpoise epidermis shows structures that resemble the fibrous features in the ichthyosaurs. Fibrous structures that derive from the dermis are arranged to create a parallel fabric similar to the large sheets of fibre impressions in the ichthyosaurs (Fig. S3.8). The orientation of the fibres relative to the body could not be deduced because the original position on the body was unknown. The diameter of the fibres match well with the diameters of the larger fibre impressions in the ichthyosaur fossils (Table 3.1).

Table 3.1. Measurements of the dermal fibres from each fossil specimen and modern porpoise dermis. The average number of fibres per cm was calculated from multiple measured regions and averaged for each specimen. From this the average fibre diameter was calculated. Samples for which SEM images were available had individual fibre impressions measured.

Specimen	Fibres per cm	Avg. fibre impression per cm	Individual fibre impressions
Lyme Regis (large fibres)	6.706	150.259 µm	134.160 µm
Lyme Regis (small fibres)	17.366	57.583 µm	59.960 µm
Strawberry Bank	11.057	90.444 µm	66.956 µm
Kimmeridge	5.819	171.857 µm	N/A
Holzmaden	7.714	129.636 µm	N/A
Modern porpoise	6.730	148.961 µm	N/A

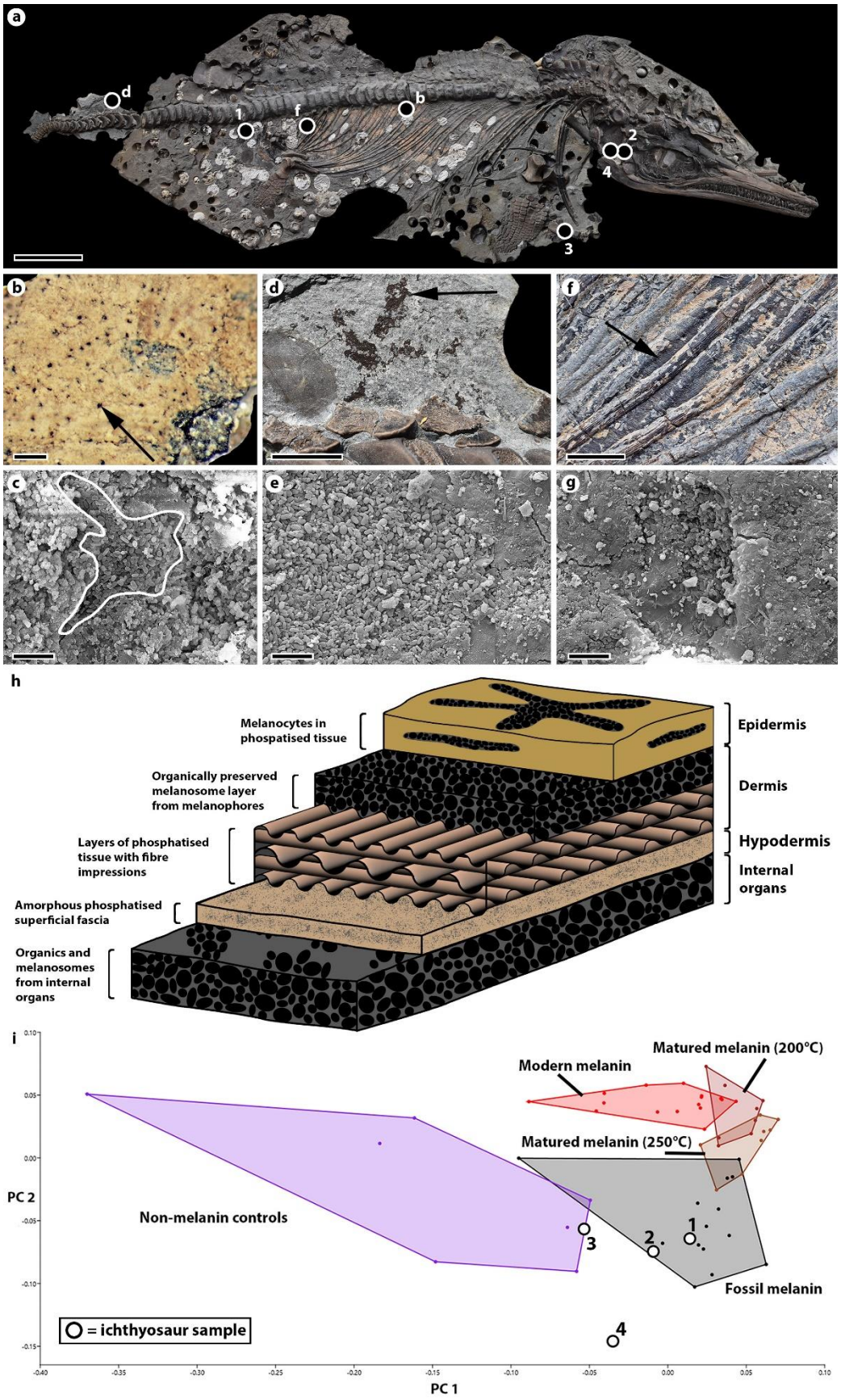
a
d
1
f
b
2
4
3
b
d
f
c
e
g
h
Melanocytes in phospatised tissue
Epidermis
Organically preserved melanosome layer from melanophores
Dermis
Layers of phosphatised tissue with fibre impressions
Hypodermis
Internal organs
Amorphous phosphatised superficial fascia
Organics and melanosomes from internal organs
i
Matured melanin (200°C)
Modern melanin
Matured melanin (250°C)
Non-melanin controls
Fossil melanin
= ichthyosaur sample
PC 2
PC 1

Figure 3.5. Organic soft tissues including melanin in the form of melanosomes from different tissues in the Lyme Regis ichthyosaur. **a**. Overview image of the specimen showing location of the following panels (lettered) and samples taken for ToF-SIMS analysis. **b**. Light microscope image of a layer of soft tissue likely representing a phosphatised epidermis with in-situ melanocytes as black dots (black arrow). **c**. SEM image of a single black dot showing melanosomes in a cluster (outlined in white) resembling a modern reptile melanocyte. **d**. A patch of dark organics sitting directly on the matrix above the caudal vertebrae. **e**. SEM image of the same patch of organics showing abundant melanosomes in a thick layer. These melanosomes are significantly larger than those found in the melanocytes. **f**. A patch of soft tissue overlying the ribcage showing extensive phosphatised material and underlying dark organics. **g**. SEM image of the same internal organics showing patches of melanosomes in a more amorphous organic matrix. **h**. A schematic showing the hypothesised tissue layers preserved in the Lyme Regis ichthyosaur. **i**. PCA based on the first two principal component (PC) axes of the ToF-SIMS analysis of previous data on modern, matured and fossil melanin plus controls (from Colleary et al. 2015) with the four numbered ichthyosaur samples. These two axes account for 47% and 23% of the observed variance respectively. Scale bars represent 10 cm in (a), 100 µm in (b), 5 µm in (c), (e) and (g) and 1 cm in (d) and (f).

3.3.5. Preservation and distribution of pigment

Patches of dark organic material are present throughout all of the specimens but likely derive from different sources due to their location relative to other soft tissues. SEM images show that most of the dark organic samples in the Lyme Regis specimen comprise abundant three-dimensional ellipsoids identical in size and morphology to extant reptile melanosomes (Figs. 3.5, 3.6 and S3.9). The ToF-SIMS analysis highlighted the preservation of key organics known to be associated with both modern and fossil melanin (Fig. 3.5). The first two principal components (PCs) in the PCA accounted for around 70% of the total observed variance (47% and 23% respectively) with further PCs accounting for rapidly decreasing percentages of the variance which never explained more than 10% (Table S3.1). This is why only the first two PCs were used to plot the data (Fig. 3.5). The relative loadings of each variable (mass peak) for the first two PCs are shown in Figure S3.10. Two dark organic samples with melanosome-like bodies present clustered with other fossil melanin samples in the PCA (Fig. 3.5i). One organic sample with no melanosomes present and a single sample with only phosphatic fibres clustered with non-melanin controls and outside of any other group respectively. These results confirm that melanin in melanosomes is organically preserved and accounts for most of the dark organics in

the Lyme Regis specimen. While the specimens from other UK locations and Holzmaden were not chemically analysed, the similarity of the dark organics, presence of melanosomes in the Strawberry Bank fossils (Fig. 3.6), as well as their prevalence in other fossil vertebrate integumentary organics (Chapter 1; Vinther 2015*a*) suggests that melanin is also responsible for the organics in these fossils.

The Lyme Regis specimen has the greatest number of potential different organic tissue remains present. In the upper-most phosphatised integumentary layer, black spots are present (Fig. 3.5 and S3.11). When imaged under the SEM, these spots comprised abundant melanosomes (Fig. 3.5e and S3.9) in an otherwise phosphatised matrix. The clusters of melanosomes resemble the dendritic shape of extant reptile melanocytes (Landmann 1986). In some cases, the clusters were sandwiched between phosphate layers apparently in their original arrangement in what would have presumably been the epidermis (Fig. S3.9). In other areas of the Lyme Regis specimen where organics were present (and unlikely to represent internal organs; e.g., on the matrix dorsal to the neural spines and above some phosphatic layers), higher abundances of melanosomes were observed within a phosphatic matrix (Fig. 3.5f). In some cases, the samples consisted almost entirely of melanosomes without phosphate (Fig. S3.4). These melanosomes differed significantly in length, width and aspect ratio from those of the melanocytes (Tables 3.2-3.3) suggesting that they derive from different tissues (Landmann 1986). Melanosomes were also found in the black layer underlying the fibres in the ribcage of the Lyme Regis specimen (Fig. 3.5g). These also differed significantly from all other sampled melanosomes (Tables 3.2-3.3) and were preserved in a more amorphous, apparently organic matrix, suggesting that they also derive from a different tissue. Due to their location underneath the fibres and in the ribcage (Fig. 3.5d), I propose that they derive from the internal organs (McNamara et al. 2018).

Table 3.2. Results from the t-tests to determine any difference in the mean length, width and aspect ratios of the melanosomes from presumed different tissues from the Lyme Regis ichthyosaur. P-values are considered significant if they are below 0.05. All tests between the putative melanocytes, the free organic layer presumed to be derived from dermal melanophores and the internal melanin layer returned significant results, as did the separate layers of the eye.

Melanocytes length	**p-value**	**t stat**	**Eye top layer length**	**p-value**	**t stat**
Free melanosome layer	4.13E-34	10.244	Eye middle layer	2.42E-31	-10.66
Internal organics	0.0187	2.0943	Eye bottom layer	4.52E-22	6.756
Melanocytes width	**p-value**	**t stat**	**Eye top layer width**	**p-value**	**t stat**
Free melanosome layer	3.75E-67	17.719	Eye middle layer	2.75E-44	15.571
Internal organics	7.05E-17	-4.955	Eye bottom layer	1.76E-32	10.315
Melanocytes aspect ratio	**p-value**	**t stat**	**Eye top layer aspect ratio**	**p-value**	**t stat**
Free melanosome layer	7.25E-18	-4.867	Eye middle layer	9.45E-61	-22.423
Internal organics	1.35E-22	7.009	Eye bottom layer	4.52E-04	-3.357

Melanosomes in the Strawberry Bank fossils are preserved in a different manner to those of the Lyme Regis fossil. In most cases, melanosomes were preserved as moulds in an amorphous organic matrix (Fig. 3.6g-h). 3D melanosomes that were present appear to have shrunk markedly in specimens M1405 and M1409, often still remaining inside the much larger moulds (Fig. 3.6h). A contrast to this was seen in M1408, which had both moulds and 3D melanosomes of similar size present (Fig. 3.6i). No melanosomes were observed in samples taken from the abdomen underneath the ribs or in any sample of soft tissue from the ventrum.

In the Holzmaden specimen a dark organic layer sits on top of the fibres (Fig. 3.3j) and is therefore likely derived from the integument rather than internal organs. The organics in the Kimmeridge specimen appear both on top of the bones and inside the ribcage, suggesting that both integumentary and internal organ melanins are present (Fig. 3.3a-f).

Table 3.3. Mean length, width and aspect ratios for all measured melanosomes from presumed different tissue layers.

Melanosome location	Length (nm)	Width (nm)	Aspect ratio	n melanosomes
Melanocytes	822.279	434.636	1.925	302
Free melanosome layer	944.616	543.876	1.769	431
Internal organics	871.075	391.760	2.292	115
Eye top layer	882.599	684.230	1.313	133
Eye middle layer	1312.257	368.421	3.625	75
Eye bottom layer	742.731	526.854	1.422	135

The abundance and distribution of dermal organics (including melanosomes) and epidermal melanocytes in different areas of the fossils were analysed to predict likely palaeocolours. The Strawberry Bank fossils all have organics (and associated melanosomes) only on the dorsal side where both dorsum and ventrum are exposed, with any ventral soft tissue comprising only phosphatic material (Fig. 3.6). In the specimen with the best exposure of both the dorsal and ventral side, M1409D, darker organics are clearly present dorsally but absent ventrally (Fig. 3.6j). In the Lyme Regis fossil, the large expanses of melanosomes were only present in samples removed from the dorsal regions of the specimens with none being found in the ventral areas (Fig. S3.4). Melanocytes were also only found on the dorsal side and on the flank, but not on the ventrum (Fig. S3.11).

3.3.6. Ocular melanosomes

Melanosomes were found in organic samples taken from within the eye orbits of the Lyme Regis specimen (Fig. 3.7) and one Strawberry Bank specimen (M1408, Fig. S3.12). In the Lyme Regis specimen different layers of melanosomes were present with significantly different melanosome morphologies in each (Tables 3.2-3.3). A layer of spherical melanosomes overlay of a layer of rod-shaped melanosomes which was itself underlain by another, thicker layer of spherical melanosomes (Fig. 3.7). Only one melanosome type was observed in M1408 in a thick amorphous organic layer (Fig. S3.12).

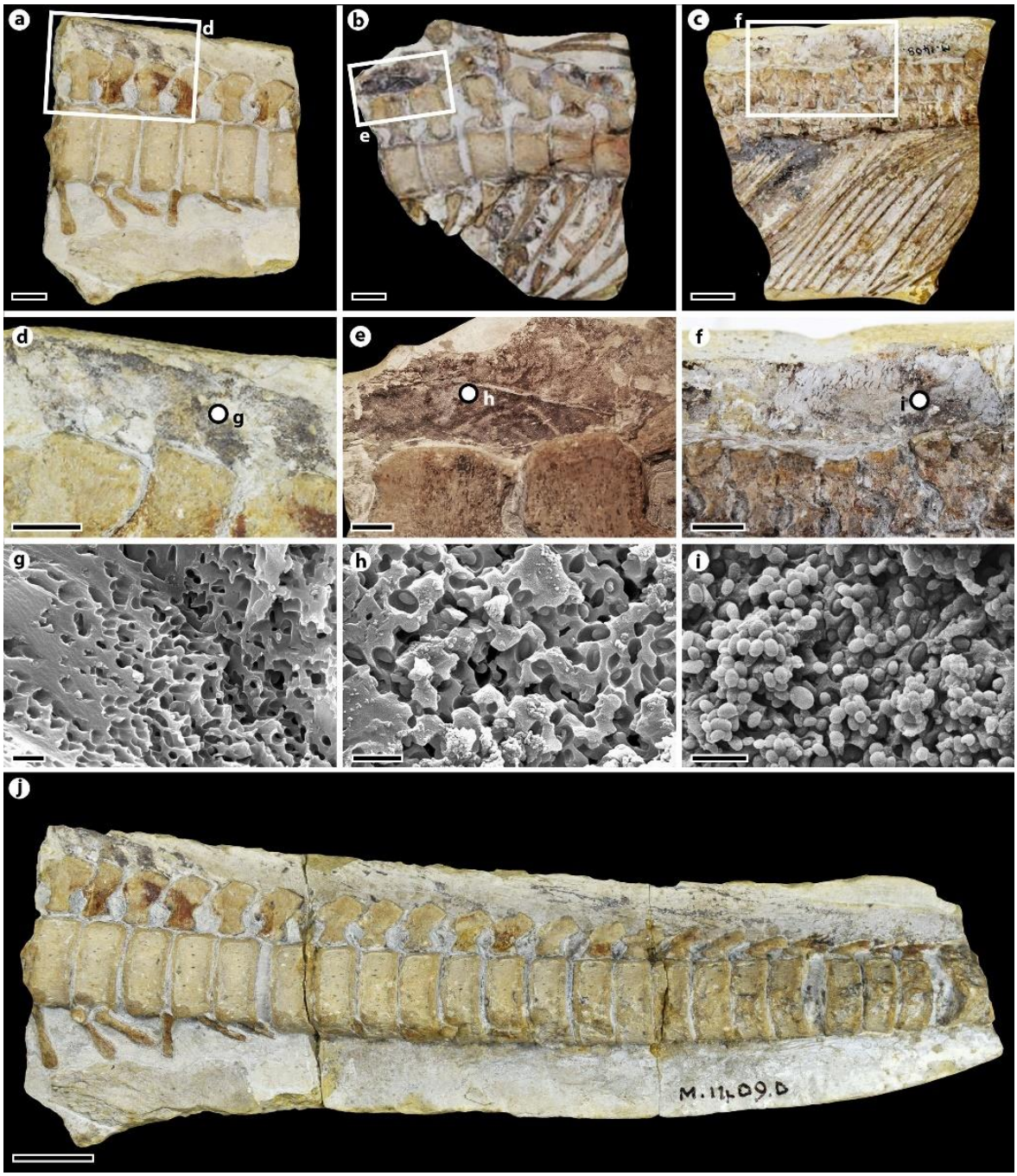

Figure 3.6. Organic soft tissue preservation in the Strawberry Bank ichthyosaurs. **a-c**. Three specimens (M1409; M1401; M408) showing dark organics predominantly on the matrix around the bones. White rectangles indicate the following panels. **d-f**. Detail of the dark organics dorsal to the neural spines in M1409, M1401 and M1408. White dots indicate the locations of samples taken for SEM imaging. **g-i**. SEM images of melanosomes from the three samples. Melanosomes are predominantly preserved as moulds in amorphous organics in the sample from

M1409, as shrunken melanosomes inside moulds in M1401 and as apparently un-altered 3D melanosomes in M1409. Scale bars represent 1 cm in (a) and (d-f), 2 cm in (b), (c) and (j) and 2 µm in (g-i).

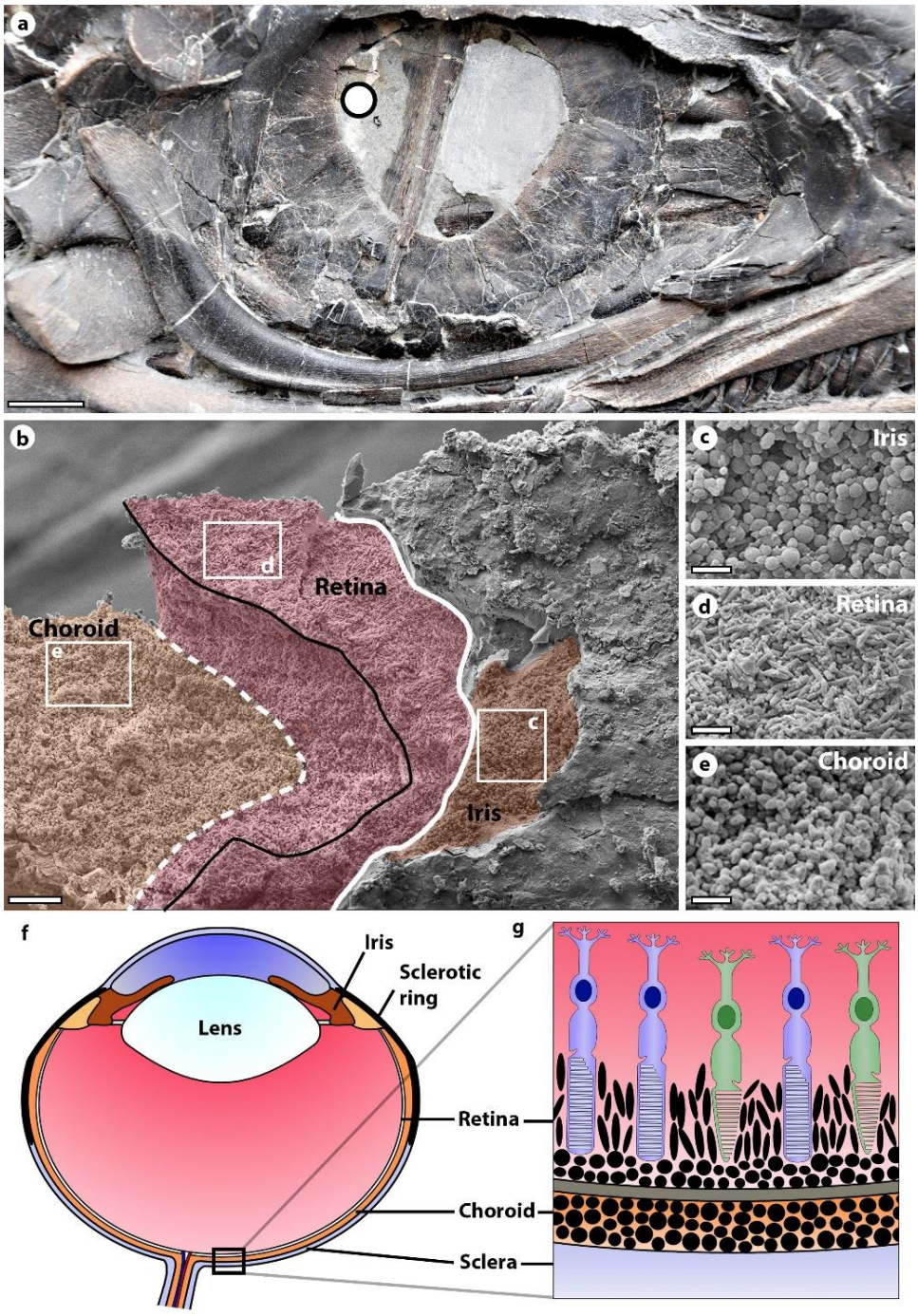

Figure 3.7. Organic preservation of melanosomes from different tissues within the eye of the Lyme Regis specimen. **a**. The eye orbit of the ichthyosaur with the sample location (white dot). **b**. SEM image of the layers of

melanosomes, colour coded to show the different layers. The solid black and white lines mark the definite boundary between layers. The white dotted line represents a hypothesised boundary between the spherical melanosome layer of the choroid and retinal pigment epithelium (RPE). As these two layers are adjacent in extant taxa and no soft tissues other than the melanosomes (known to be spherical in both layers) are preserved, they likely merged during decay. White rectangles mark the following panels. **c**. Spherical melanosomes from the iris. **d**. Rod-shaped melanosomes from the upper-RPE. **e**. Spherical melanosomes from the choroid. **f**. A hypothesised schematic of an ichthyosaur eye showing the position of the iris, retina and choroid. Only melanised and mineralised tissues remain in the fossil. **g**. The arrangement of melanosomes from the choroid and RPE based on comparison to living taxa (Clements et al. 2016). Spherical melanosomes of the RPE lie at the base of the photoreceptors (rods – blue, cones – green) while rod-shaped melanosomes extend up between the photoreceptors. Scale bars represent 1 cm in (a), 10 µm in (b) and 2 µm in (c-e).

3.3.7. Soft tissue deformation/wrinkling

A feature noted in multiple specimens is the apparent flexibility/pliability of the original soft tissues prior to their fossilisation. This has been noted before and therefore appears common in ichthyosaur fossils with soft tissues preserved (Lingham-Soliar 1999; Lingham-Soliar 2001; Lindgren et al. 2018). Multiple regions where the soft tissue layers undulate in a way that suggests distortion post-mortem were identified, mostly on the Strawberry Bank and Holzmaden specimens (Figs. 3.3 and S3.13). This includes both the fibrous layers and in soft tissues without obvious fibres (Fig. S3.13). The specimen with the most pronounced structural deformation reminiscent of tissue flexibility is SMF R 457 (Fig. 3.3b). In this fossil, wrinkling of the tissue layers appears to have been extensive throughout, making identification of individual tissue layers difficult. The Lyme Regis specimen has no discernible wrinkling of the tissues (Figs. 3.1 and S3.1), which aids in the identification of different tissue layers.

3.4. Discussion

3.4.1. Fibre preservation

The new observations presented here combined with previous studies into ichthyosaur soft tissue preservation suggest that phosphatised fibrous material is common where exceptional

preservation occurs (Delair 1966; Lingham-Soliar 1999, 2001, Lingham-Soliar and Plodowski 2007). Contrary to previous reports that the fibres are themselves mineralised (Lingham-Soliar and Wesley-Smith 2008), or organically preserved (Delair 1966), the fibrous layers studied here consist of impressions in a phosphatic matrix (Figs. 3.2 and S3.5). Phosphatisation appears to have occurred around the fibres which were subsequently lost (presumably during the decay process), leaving "ghost fibres". A similar mechanism has been proposed for "scale ghosts" preserved in a marine lizard from the Late Cretaceous of Italy (Paparella et al. 2018). Where multiple fibrous layers are present in the ichthyosaurs, each layer appears to have become mineralised separately (evidenced by their propensity to spall away from one another with ease, F.S. pers. obs.), ruling out the possibility that an underlying tissue (such as the superficial fascia) was responsible for retaining the impressions as suggested in other similar cases (Paparella et al. 2018).

Phosphatisation of soft tissues has been shown to be possible over short timescales during decay under the right conditions (Briggs et al. 1993; Parry et al. 2018 and reviews therein). This bacterially mediated process requires a source of phosphate which can come from surrounding sediment or from the decaying carcass itself (Briggs et al. 1993; Wilby and Briggs 1997). It has been suggested that when vertebrate material shows extensive soft tissue phosphatisation, the phosphate source is likely external due to a limited pool of phosphate in the animal itself (Wilby and Briggs 1997). A combination of phosphate derived externally from surrounding sediment and from microbially released phosphate ions during decay is also possible (Wilby and Briggs 1997).

That the different fibre layers in the Lyme Regis specimen show subtly different colours and were phosphatised individually may indicate different sources of phosphate were involved. The outer-most layers may have been more influenced by phosphate from an external sedimentary source while underlying layers had a stronger influence from internal phosphate sources. Without precise chemical characterisation of each individual layer and the surrounding sediment however, this is speculative at this stage but would be an interesting area for future work and could yield insights into phosphatisation in vertebrate soft tissues.

3.4.2. Tissue origin of the fibrous layers

Fibres are present in multiple tissues in extant animals. The most likely of these tissues represented by the ichthyosaur fibres are considered.

One possibility is that the fibres could represent muscle tissue, as seen in other exceptional vertebrate fossils such as the fishes from the Santana Formation (Early Cretaceous, Brazil; Martill 1990). This is considered unlikely due to the position on the fossils (including as a halo around SMF R 457 and M1405 and underneath the mandible of M1409) and the difference in ultrastructure between the ichthyosaur samples and those of undisputed fossil muscle tissues (which often retain their three-dimensional structure – see Martill 1990 and Long et al. 2010) or experimentally phosphatised modern muscle tissues (e.g., Briggs et al. 1993).

A cross-orientated fibrous meshwork is found in the collagen fibres of the subdermal connective tissue sheath (SDS) of at least some extant cetaceans (Pabst 1996). This feature surrounds and connects to the axial musculature, acting as a peripheral skeletal element (Pabst 1996). It is possible the ichthyosaurs could have convergently evolved an SDS-like structure. However, the SDS is orientated at oblique angles to the body in cetaceans and is restricted to the trunk (Pabst 1996). The main fibres of the ichthyosaurs run parallel to the body and extend to at least the lower jaws (Delair 1966).

The most plausible origin of the fibrous material is the integument, in particular the dermis, which contains abundant layers of collagen and elastin fibres (or fibre bundles) in extant taxa (Landmann 1986). This is indicated in the porpoise CT scan (Fig. S3.8). Previous work also identified fibrous material in ichthyosaurs as being dermal in origin (Lingham-Soliar 1999, 2001; Lingham-Soliar and Wesley-Smith 2008). While some discrepancies occur between the material previously identified and that which is described here (Smithwick et al. 2017*b*), I concur that this is the most likely origin of the preserved fibres.

Reptile dermis (in particular the ‘deep dermis’) is comprised of densely packed cross-orientated layers of collagen and elastin fibres creating a meshwork similar to the ichthyosaur material (Figure 17 in Landmann 1986). Underlying the dermis in modern reptiles is the

superficial fascia (hypodermis), a layer of loose connective tissue and fat cells between the integument and underlying muscles (Landmann 1986). This is considered an unlikely origin of the fibres, however the amorphous phosphatised basal layer in the Lyme Regis specimen (Fig. S3.2c) may represent remains of this tissue (Fig. 3.5h).

3.4.3. Fibre morphology and architecture

Previously, three classes of fibres ranging in diameter from 100-500 µm (averaging 100, 250 and 450 µm respectively) have been suggested (Lingham-Soliar 2001), mainly from Holzmaden specimens including SMF R 457. These three classes were all said to show different morphologies and preservation. Evidence of fibres with diameters ranging from ~ 50-200 µm showing a remarkably consistent morphology is only found in the current study.

I propose that a class of fibre exists in Jurassic ichthyosaurs that runs parallel to the body long axis with each fibre averaging 136 µm in diameter. A size discrepancy exists in this class between the smaller fibre impressions found in the Strawberry Bank fossils and all others (Table 3.1), but as the fabric runs parallel to the body long axis and the morphology is so similar to other specimens, I still consider this to be the same class of fibre. The difference in size may be due to taphonomic, taxonomic or biological factors. For example, muscle fibres of Northern elephant seals, animals with similar deep diving habits to ichthyosaurs, increase significantly in diameter with age (Moore et al. 2014). The only specimen that does not show the fibre fabric running parallel to the body long axis is SMF R 457, however due to the extensive deformation of the soft tissue layers, precise orientations and layering are hard to identify.

A further distinct fibre class appears to exist but is only unequivocally present in the Lyme Regis specimen. Fibres in this class are significantly narrower than those of the first class and cross-orientate with the layer that runs parallel to the body long axis creating a meshwork (Figs. 3.2 and 3.5). The total number of layers in this meshwork is unclear from the present data.

The fibres observed in the specimens likely correspond to those previously described as "class 3 fibres" by Lingham-Soliar (2001, 2016) and those described by Delair (1966). This includes specimen SMF R 457, where I consider only the "class 3 fibres" on the trunk of the animal to be genuine integumentary fibres. Issues surrounding several of the other previously described fibre types, including the purported "dorsal longitudinal fibres" have already been highlighted (Chapter 2.2.1; Smithwick et al. 2017*b*). Further to this, here it is proposed that the largest fibres described previously (Lingham-Soliar 2001, 2016) are more likely to be wrinkles in the finer fibrous layer that have been worn down through preparation to give the appearance of a large class of fibre (Fig. 3.3bg-j). Further fibres showing cross-orientations similar to the Lyme Regis specimen have been noted previously in SMF R 457, however these were found on the dorsal and caudal fins and show similar morphology to fibre observations in the UK material suggesting this feature extended across the whole integument (Lingham-Soliar and Plodowski 2007).

Rather than having a range of fibre morphologies of highly varied sizes and three separate classes, I instead propose that in Jurassic ichthyosaurs a layer of fibres ran parallel to the body axis along the trunk with an unknown number of additional finer fibrous layers creating a meshwork that extended to the fins (Lingham-Soliar and Plodowski 2007) and at least part of the head (Delair 1966). A schematic based on our current knowledge of the fibre network (from this study and previous work) is presented in Figure 3.1s. This meshwork is similar to that proposed previously (Lingham-Soliar 2001, 2016), but excludes the fibres whose identity is questionable (Chapter 2.2.1; Smithwick et al. 2017*b*).

The supporting meshwork of fibres proposed here likely strengthened the skin while still allowing flexibility, as seen in many modern marine taxa with similar modes of locomotion (Motta 1977; Pabst 2000; Meyer and Seegers 2012). Dermal fibre networks like the one seen in ichthyosaurs act in an exoskeleton-like fashion in tandem with the musculature in extant sharks and teleosts, allowing the body to remain stiff and store energy during fast swimming (Meyer and Seegers 2012). As the Jurassic "thunniform" ichthyosaurs would have swum in a similar fashion to these extant taxa (Buchholtz 2001; Motani 2002), they are the best living analogues

available. A unique feature identified here in ichthyosaurs and not observed before is the extensive layer of large fibres running parallel to the body long axis. I suggest that these likely contributed significantly to the stiffening of the body during swimming (Lindgren et al. 2011) and could have provided further elastic tension to aid in axial undulation. Similar longitudinal fibres have been identified in an Upper Cretaceous Mosasaur but associated with overlying scales (Lindgren et al. 2011). Whether the ichthyosaur fibres represent remnant impressions of collagen or elastin remains an open question, but extant dolphins show high levels of elastin in their dermis making it more unusually elastic (Palmer and Weddell 1964). I consider it plausible that ichthyosaurs too had high levels of elastin in their dermis, allowing for the flexibility plus rigidity required for fast swimming.

3.4.4. Organically preserved melanin and palaeocolour implications

ToF-SIMS and SEM imaging confirm preserved organics to be melanin (Fig. 3.5). Melanosomes from multiple different tissues are preserved in at least the Lyme Regis and Strawberry Banks specimens (Tables 3.2 and 3.3). Melanocytes are present apparently in-situ in a phosphatised epidermis overlying the dermal fibres in the Lyme Regis ichthyosaur (Figs. S3.9 and S3.11). Associated with the dermal fibres in places, and in patches dorsal to the neural spines, are more continuous layers of melanosomes (Fig. 3.5f and S3.4). Due to their location, it is likely that these represent dispersed melanosomes from the basal pigment layer of melanophores found underlying other chromatophores in the upper-dermis of extant reptiles (Landmann 1986). The melanosomes in dermal chromatophores are significantly larger than those from the epidermal melanocytes in both extant reptiles (Landmann 1986) and the ichthyosaur samples (Table 3.2). Chromatophores contribute the majority of the dark colour in reptiles (Landmann 1986). The high abundance of chromatophore-derived melanosomes on the dorsum and lack of melanosomes or melanocytes on the ventrum suggests that the Lyme Regis and at least two of the Strawberry Bank specimens exhibited countershading (Palmer and Weddell 1964; Rowland 2009; Caro et al. 2011). Although melanin from the integument is likely present on the

Kimmeridge and Holzmaden fossils, without being able to sample them it cannot be determine whether it derives from the melanocytes or melanophores.

Previous work on ichthyosaurs has suggested that at least some may have shown a uniformly dark colouration which would have been beneficial as camouflage when diving deep to find food (Lindgren et al. 2014). This was however extrapolated from a single spot sample containing melanosomes in one specimen from Lyme Regis and observations of dark colour being present on both the dorsum and ventrum of some Holzmaden specimens. Owing to the previously described issues of preparators colouring and adding false soft tissue outlines in these specimens however (Martill 1987; McGowan 1992; Smithwick et al. 2017*b*) this conclusion is questionable. It is shown here that all of the ichthyosaurs that could be sampled sufficiently for palaeocolour reconstructions show countershading in agreement with a more recent interpretation of another Holzmaden specimen (Lindgren et al. 2018), indicating that this was the most common colour pattern in Jurassic ichthyosaurs. As the specimens studied here are mostly juveniles, the suggestion that ontogenetic changes in colour from monotonal to countershading are unlikely (Lindgren et al. 2018).

Countershading is one of the most common colour patterns seen in large marine vertebrates today and likely serves similar functions to better-studied terrestrial vertebrates (Rowland 2009; Caro et al. 2011). Countershading is particularly prevalent in marine animals that spend much time in clear waters near the surface, as ichthyosaurs would have done as air breathers. This is seen in similar sized cetaceans today (Caro et al. 2011). It has also been shown that cetaceans that hunt fast-moving prey like fishes and squid are more likely to show countershading (Caro et al. 2011). Small to medium sized ichthyosaurs also ate fast swimming fishes and squid-like coleoid cephalopods (Massare and Young 2005; Lomax 2010), thus conforming to this interpretation. There is debate as to whether countershading in aquatic taxa provides camouflage through self-shadow concealment or through background matching (Kelley and Merilaita 2015; Kelley et al. 2017) along with hypotheses of non-visual functions such as UV protection and thermoregulation (Rowland 2009). Due to the optical characteristics of water (being less directional and more diffuse than in terrestrial systems; Ruxton et al. 2004),

background matching has been suggested as a more likely camouflage function (Kelley and Merilaita 2015; Kelley et al. 2017). While evidence exists for background matching adaptations in shallow-water inhabiting fish (Kelley et al. 2017), I consider this unlikely in Jurassic ichthyosaurs due to the water depths at which they presumably lived. A dark dorsum would likely provide good background matching camouflage when viewed from above due to a lack of backscattered light from the seafloor in the open ocean. For a light ventrum to confer background matching camouflage however, backscattered light would be necessary to illuminate the body to some extent (in the absence of light, a white object will still appear as a black silhouette against the light coming from above unless it produces its own illumination; Young and Roper 1976; Kelley et al. 2017). Further work on aquatic animals that live in the open ocean where light does not come from below is needed to better understand the functions of countershading in these cases.

The difference in preservation of melanosomes between specimens and locations is informative to melanosome taphonomy. All melanosomes in the Lyme Regis specimen are preserved three-dimensionally with a high fidelity of their original arrangement in the tissues (Figs. 3.5, S3.4, S3.9 and S3.11). Those of the Strawberry Bank however varied between specimens with most showing just mouldic impressions (Fig. 3.6) similar to those seen in other deposits such as the Jehol Biota of China (Zhang et al. 2010) and only M1408 showing 3D melanosomes in large numbers. Burial conditions are thought to control melanosome shrinkage during diagenesis, with deeper burial and associated elevated temperatures causing more shrinkage (McNamara et al 2013; Vinther 2015*a*). As all of the Strawberry Bank fossils have undergone the same burial conditions, this cannot explain why some show total loss of melanosomes leaving only moulds, while some show extensive preservation of 3D melanosomes. Instead, oxidation of melanosomes may account for the observed differences. The Strawberry Bank material is highly weathered, suggesting extensive exposure to oxygen. Differences in the level of exposure between specimens may account for different degrees of melanosome shrinkage and loss.

3.4.5. Ocular tissue preservation

Melanosomes are present in various ocular tissues in modern vertebrates including the retina (specifically the retinal pigment epithelium – RPE), the choroid and the iris. The RPE of extant animals contains both spherical and rod-shaped melanosomes, while the iris and choroid generally only have spherical morphologies (Liu et al. 2005*b*; Clements et al. 2016). The RPE has a base layer of spherical melanosomes with rod-shaped melanosomes protruding outwards between the rods and cones (Fig. 3.7f-g; Clements et al. 2016). The whole RPE complex overlies the choroid with the iris at the front (Fig. 3.7f; Hu et al. 2008). The spherical-rod-spherical melanosome layering in the Lyme Regis ichthyosaur eye suggests that all three layers may be present with the spherical choroid and RPE melanosomes together forming the thick layer at the base below the RPE rod melanosomes with the thin top layer of spherical iris melanosomes (Fig. 3.7f-g). Significant differences in melanosome morphology between each layer backs this assumption up (Table 3.2). This is the first time all three tissue layers have been identified in any fossil and is a significant discovery in ichthyosaurs.

Retinal melanin helps to screen stray light, preventing it reaching photoreceptive cells, and ocular pigments generally likely have UV protection functions (Fein and Szuts 1982; Hu et al. 2008; Clements 2016). Ichthyosaur eyes would have to have been adapted for very different lighting environments to extant terrestrial vertebrates, the only animals from which comparative data can be currently derived (Liu et al. 2005*b*), making comparisons with living analogues difficult. Data on the tissue layering of an extinct animal for which vision was of key importance is however significant and warrants further study when better extant data become available.

3.5. Conclusions

Soft tissue features preserved in several British and German ichthyosaur specimens help to clarify multiple features of the ichthyosaur integument. Layers of fibre impressions in phosphatic matrices are common to all studied specimens and most likely represent dermal

collagen or elastin fibres arranged in a meshwork with the largest fibres orientated parallel to the body long axis. Contrary to previous reports, these fibres are restricted in size and morphology. Melanosomes account for much of the preserved organic material and derive from multiple tissue types including melanocytes within a phosphatised epidermis, dispersed dermal melanophores and internal organ melanin. The distribution and relative abundance of integumentary melanosomes suggests that countershading was a common colour pattern in Jurassic ichthyosaurs, as is the case for similarly sized marine vertebrates today. Additionally, the three pigmented layers of the eye, likely representing the choroid, retina and iris, are preserved in at least one specimen showing a remarkable similarity to extant vertebrates.

Chapter 4 – Countershading and stripes in the theropod dinosaur *Sinosauropteryx* reveal heterogeneous habitats in the Early Cretaceous Jehol Biota

Abstract: The preservation of pigmentary colour patterns has revealed camouflage patterns including countershading in deep time. As yet, countershading has not been identified in any extinct feathered dinosaur however. Applying the principles of modern colour patterning, the pattern of countershading in the theropod dinosaur *Sinosauropteryx* from the Jehol Biota of Liaoning, China is described in detail. From reconstructions based on exceptional fossils, the colour pattern is compared to predicted optimal countershading transitions based on 3D reconstructions of the animal's abdomen imaged in different lighting environments. Reconstructed patterns match well with those predicted for animals living in open habitats. Jehol is presumed to have been a predominantly closed forested environment which is also evident from countershading gradients in the ornithischian, *Psittacosaurus*. The colouration of *Sinosauropteryx* indicates a heterogeneous range of habitats explored by dinosaurs in the vicinity of the Jehol lakes. In addition to a striped tail *Sinosauropteryx* also exhibits a 'bandit mask', which is a common pattern in many living vertebrates and serves multiple functions.

A version of this chapter was **published in the journal *Current Biology*** in November 2017 (https://doi.org/10.1016/j.cub.2017.09.032). See Appendix 2 for full details of publication.

Author contributions – The author and Jakob Vinther devised the concepts of this chapter. The author created and imaged the 3D models, produced all figures (apart from the reconstruction in Figure 4.2b which was illustrated by Robert Nicholls) and wrote the chapter. Jakob Vinther photographed the fossils. Innes Cuthill produced the Matlab models and performed the statistical analyses of countershading predictions.

4.1. Introduction

Countershading is common across a variety of lineages and ecological time (see General Introduction; Fig. I1d-g; Thayer 1896; Rowland 2009; Allen et al. 2012; Vinther et al. 2016). One of the most important visual cues used by animals with complex visual systems, including vertebrates and coleoid cephalopods, is the detection of a three-dimensional shape created by gradients in shadowing caused by the body depth of an animal (Horn 1975; Harris 2004). Countershading reduces the degree to which an animal stands out as a three-dimensional object by reducing self-shadow contrast, thus making the animal appear more optically flat (Rowland 2009; Allen et al. 2012; Penacchio et al. 2013). For countershading to be effective in obliterating 3D cues of an animal's presence, the pattern of pigmentation from the dorsal to ventral body regions should match the illumination gradient created by the lighting environment in which it lives (Allen et al. 2012; Penacchio et al. 2015; Cuthill et al. 2016; Vinther et al. 2016). This allows the determination of likely habitats of animals based on quantification of colour patterns (Allen et al. 2012; Vinther et al. 2016). Those that inhabit open environments with direct lighting conditions generally exhibit a sharp transition from dark to light colour high up on the flanks of the body (Allen et al. 2012; Vinther et al. 2016). Conversely, animals inhabiting a more closed habitat with diffuse lighting coming in at many angles often show a smoother gradation from dark to light lower down on the body (Allen et al. 2012; Vinther et al. 2016).

With the discovery of fossil melanin (Chapter 1; Vinther et al. 2008; Vinther 2015*a*) it is possible to infer original colour patterns from fossils, including countershading (Li et al. 2010, 2012; Vinther et al. 2016). Fossil feathered dinosaurs provide a unique opportunity to investigate colour patterns in long-extinct taxa (Chapter 1.5). One such feathered dinosaur is *Sinosauropteryx prima* from the Jehol Biota (Chapter 2; Currie and Chen 2001). A number of specimens of this theropod show exceptional preservation of integumentary structures identified as feathers which can be found across distinct regions of the body (Chapter 1; Figs. 2.1 and 4.1). The exquisite preservation of these feathers allows the colour patterns of *Sinosauropteryx* to be evaluated in depth. The presence of pigmented plumage on the dorsum

but absence on the ventrum indicates a countershaded colour pattern, allowing potential habitat preference to be investigated.

Here, the relationship between countershading and habitat is explored in a theropod dinosaur for the first time. The three best-preserved *Sinosauropteryx* specimens are used to map out the distribution of plumage through the presence and absence of pigmented feathers across the body. A detailed reconstruction of the colour patterns of the dinosaur is then tested against predicted countershading configurations which are dependent upon illumination gradients induced across the body by different lighting environments. 3D reconstructions of the theropod's abdomen are used to test expected illumination gradients against the genuine colour pattern of the animal to determine the likely habitat in which it lived, thus adding to our knowledge of camouflage strategies in deep time and helping to build a clearer picture of the Jehol Biota.

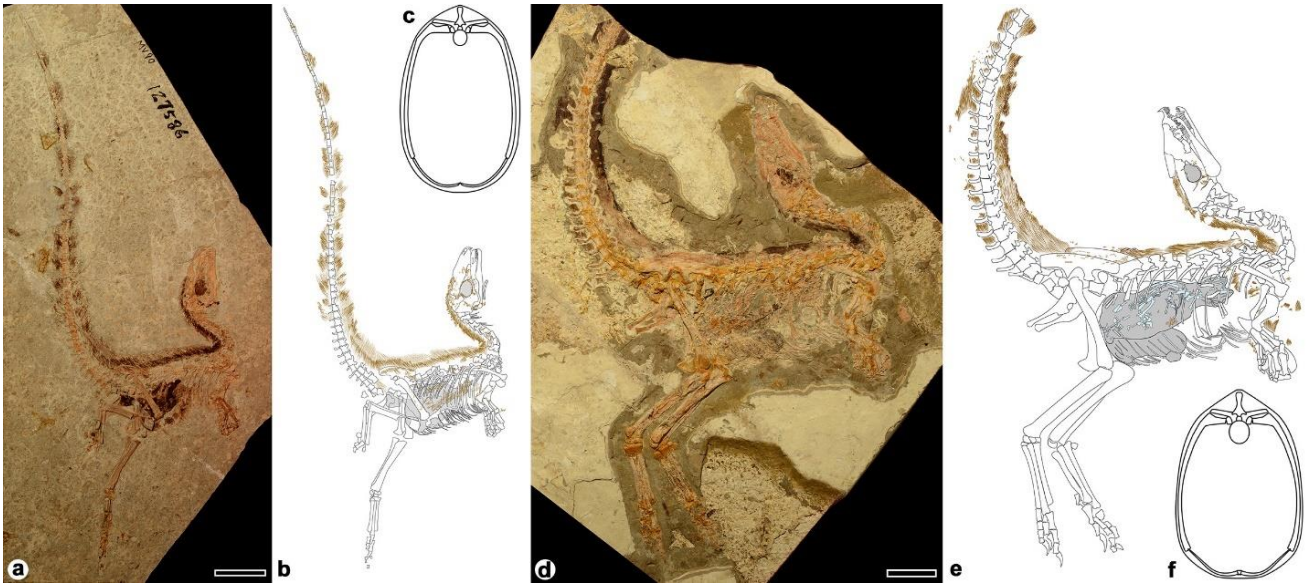

Fig. 4.1. *Sinosauropteryx prima* fossils and interpretive drawings. The plumage distribution is mapped out across each specimen with feathers shown in brown, internal soft tissues and pigment from the eyes shaded grey and vertebrate stomach contents in light blue. **a.** NIGP 127586 counterpart to the holotype. **b.** Interpretive drawing of NIGP 127586. **c.** Reconstructed transverse section through the abdomen of NIGP 127586. **d.** NIGP 127587. **e.** Interpretive drawing of NIGP 127587. **f.** Reconstructed cross-section through the abdomen of NIGP 127587. Scale bars represent 50 mm. Abdominal transverse sections not to scale.

4.2. Materials and Methods

4.2.1. Institutional abbreviations

GMV – Vertebrate Collections of the Geological Museum of China, Beijing; NIGP – Nanjing Institute of Geology and Palaeontology, Chinese Academy of Sciences, Nanjing, Jiangsu Province; IVPP – Institute of Vertebrate Palaeontology and Palaeoanthropology, Chinese Academy of Sciences, Beijing.

4.2.2. Specimen imaging

Three of the best-preserved specimens of *Sinosauropteryx* (IVPP V12415, NIGP 127586 and NIGP 127587; Figs. 2.1c and 4.1a and d) were imaged using a Nikon D800 camera with a Micro Nikkor 60 mm macro lens and polarising filter attached. The camera was mounted on a tripod and a ten second delayed timer used to maximise image sharpness. TIFF format (5520 x 3680 pixels) was used to capture the images in high resolution. Specimens were illuminated with a mounted tungsten light source (Lowell Tota-light, Tiffen, Hauppauge, NY, USA) with a linear polarising gel attached. Images were taken under both normal lighting conditions and using the polarised filter on the camera adjusted to allow cross-polarisation to reduce glare from the specimen (Boyle 1992; Rayner 1992; Bengtson 2000).

4.2.3. 2D illustrations and plumage distribution

Illustrations of specimens IVPP V12415 and NIGP 127586 were created using Adobe Illustrator (Adobe, San Jose, CA, USA), as these specimens show the best preservation of the integument and are the most articulated. Feathers were mapped across each specimen, with particular attention paid around the abdomen to ensure that the ventral extent of the preserved plumage was accurately depicted. Across the stomach region, other soft tissues are preserved which likely represent remains of internal organs, which are known to contain the pigment melanin (Vinther 2015*a*; McNamara et al. 2018). Differentiating between organ melanin and feather melanin is possible as the feathers can be seen preserved on top of the internal soft tissues as clear linear features representing filaments (Fig. 4.2f-g).

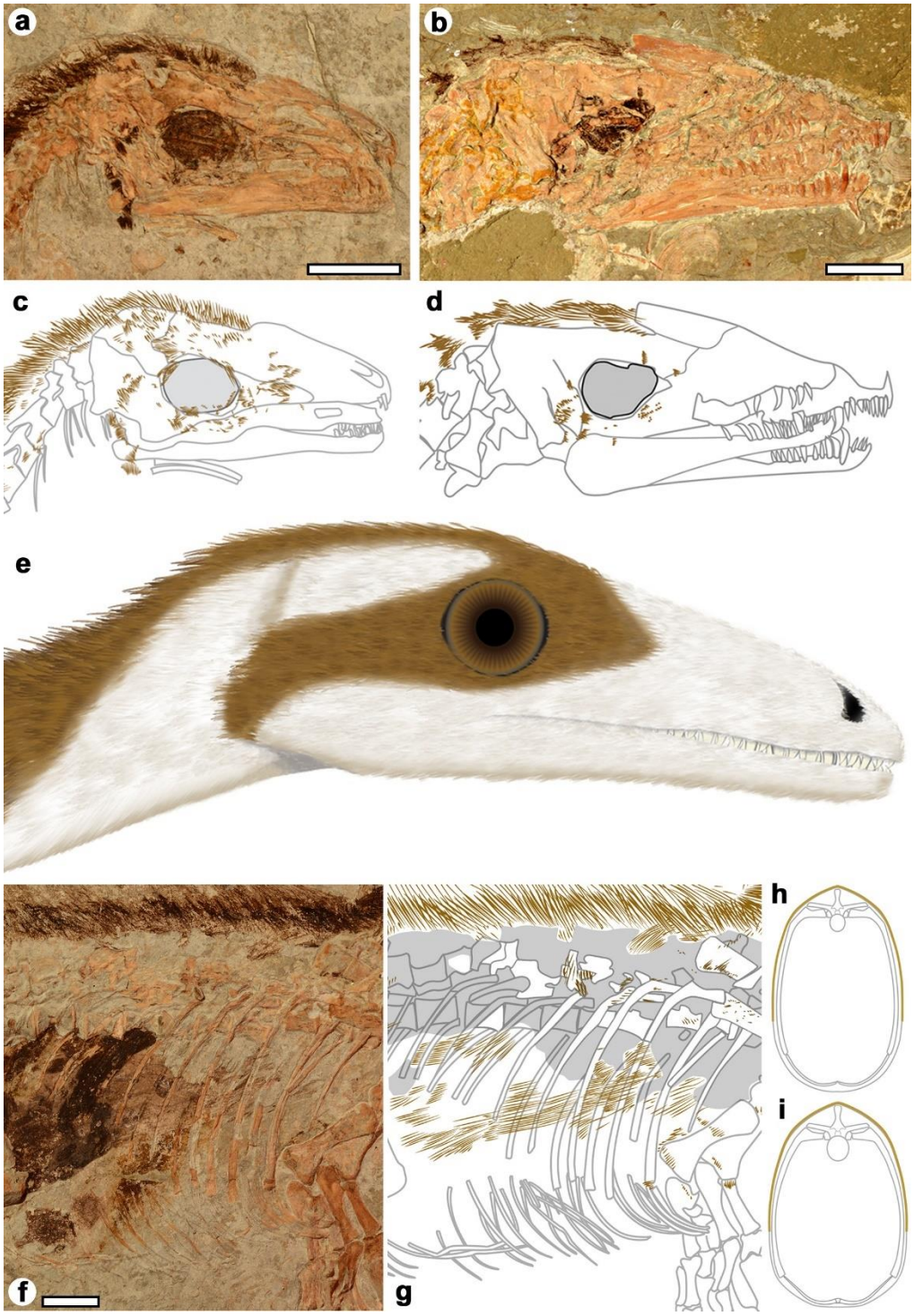

Figure 4.2. Detail of the pigmented plumage distribution across the face and abdomen of *Sinosauropteryx.* **a.** The skull of NIGP 127586 showing pigmented feathers forming a crest on the top of the head running along the dorsal side of the neck and patches of plumage on the posterioventral margin of the lower jaw and around the eye orbit. The orbit shows abundant pigment likely from retinal melanin. Pigmented feathers can also be seen anterior to the orbit and in patches joining those around the orbit to the dorsal crest, indicating a stripe of pigment running across

the eye. **b.** The skull of NIGP 127587 showing a similar pigmented plumage distribution to NIGP127586 but with poorer preservation. **c.** Interpretive drawing of the skull of (a) showing the distribution of pigmented feathers. **d.** Interpretive drawing of (b). **e.** Full reconstruction of the head of *Sinosauropteryx* based on the distribution of the plumage in the two specimens. This pattern conforms to a 'bandit mask' seen in many modern taxa. **f.** The abdomen of NIGP 127586, showing feather filaments running across internal melanised soft-tissues. **g.** Interpretive drawing of the abdomen of NIGP 127586 showing the ventral extent of feathers (brown) and overlying sediment covering feathers dorsally (grey area). **h.** Transverse section of NIGP 127586 showing the proposed ventral extent of pigmented plumage (brown). **i.** Transverse section of NIGP 127587 showing the proposed ventral pigmented plumage extent. Scale bars represent 20 mm in (a-d) and 10 mm in (f-g). Reconstruction and transverse sections not to scale.

Previous work identified preserved pigment remains in the feathers of another reported *Sinosauropteryx* specimen IVPP 14202 in the form of "phaeomelanosome"-like spherical granules, indicating that the pigmented plumage was likely a rufous or light brown tone (Zhang et al. 2010). Caution must be taken, however, in reconstructing colour patterns across an animal from single, small spot samples between individual fossil specimens. Unfortunately, IVPP 14202 was not available for this study. Here, the distribution of pigmentation in the plumage and its overall pattern across the body is focussed on rather than further attempting to accurately reconstruct the original hues of the animal. As the pigment appears to be restricted to the feathers in *Sinosauropteryx*, the complexities of colour production found in other integumentary structures, such as the chromatophores found in the skin of reptiles (Vinther 2015*a*), do not apply in this case. Melanosomes are transported to the feather keratin as it develops after which time it cannot be altered (other than through bleaching; Chapter 1.1; Prum and Williamson 2002). Pigment remains in the fossil should therefore represent the original distribution of melanin in the animal's plumage at the time of death.

4.2.4. 3D abdominal modelling

From the illustrations of IVPP V12415 and NIGP 127586, the best-preserved ribs, gastralia and vertebrae from the anterior end of each animal's abdomen were used to create two-

dimensional reconstructions of the ribcages in cross section (Fig. 4.1c and f). The ribs and gastralia were mirrored for symmetry from single bones in each specimen. A layer representing the skin and musculature of the abdomen was added around the bones. The extent of the tissues surrounding the abdominal skeleton is unknown, but from the proximity of the feathers to the bones across the fossils and through comparison to modern animals it is likely that musculature was minimal in this region and therefore the cross section of the abdomen would match well to the shape of the bones themselves, minimising any effects of overlying tissue being over or underestimated. The outlines of the abdominal cross sections were used to create 3D reconstructions of the abdomen of each individual using the software Blender (Blender Foundation). The abdomen length and height (both posterior and anterior) were taken directly from the fossils and the width was extrapolated from the curvature of the ribs and gastralia. This method produced consistent relative proportions in each model despite a difference in the overall size of each.

Each abdomen was taller at the posterior end than the anterior in both specimens, and so the models were tapered according to the exact dimensions measured from each fossil (6% in IVPP V12415 and 15% in NIGP 127586). The difference in the degree of tapering may represent ontogenetic differences, as NIGP 127586 is a much smaller individual than IVPP V12415. The two 3D models were then printed by Shapeways (New York, NY, USA) in grey polylactic acid (PLA) and sanded using increasing grit sandpaper to smooth the surfaces. To replicate the feathers, unicolour synthetic fur (White Ape, Mohair Bear Making Supplies Ltd, Telford, Shropshire, UK) was used to wrap around each model and the filament length trimmed based on the lengths of the feather filaments measured from each fossil.

4.2.5. Predicting lighting environment

The 3D models of the two *Sinosauropteryx* abdomens were printed uniformly grey to allow assessment of the position of self-shadows depending on different lighting conditions, independent of actual colour patterns (Allen et al. 2012; Vinther et al. 2016). The models were mounted on sticks attached horizontally to a tripod to avoid any shadows being cast across

them from other objects. The two models were photographed under different lighting conditions, similar to the recent study of *Psittacosaurus* (Vinther et al. 2016). A Nikon D5300 SLR camera with an 18-55 mm Nikkor lens (Nikon Corporation, Tokyo, Japan) was used for imaging with the light metering set on the centre of the model and automatic focus used. Images were saved in TIFF format. A colour standard (X-Rite Color Passport; X-Rite Inc. Grands Rapids, MI, USA) was positioned next to and in the same plane as the model. Photographs were taken at the University of Bristol Botanical Gardens at around midday (± two hours) on sunny (<10% cloud cover) and cloudy (complete cloud cover) days in both open and closed environments. The area chosen was populated by plants typical of the Early Cretaceous. The models were placed facing directly towards the sun in both instances, as this is the situation in which symmetrical countershading will be most effective as the illumination gradient will be the same on both flanks (Allen et al. 2012). Previous work has shown that due to variability in the sun's position and the effect that will have on illumination gradients, modern ungulates often show countershading patterns which are a compromise between the range of lighting conditions in which each taxon lives where predation pressure will be experienced (Allen et al. 2012). Each model was therefore also imaged at an angle perpendicular to the sun, with the dorsal side receiving direct illumination to imitate the sun being directly overhead. The models were imaged both as grey uncoated plastic and with the synthetic fur (representing the "protofeathers") tightly wrapped around to test for any differences in the illumination gradients with and without feathers. As with previous work, the shadows cast reduced to two illumination conditions (direct and diffuse) corresponding to whether the light was coming directly from the sun's disk or the sky. Consequently, images taken under cloudy conditions produced the same shadowing patterns as those taken in sunlight under vegetation, making them equivalent, for predictions, to a closed habitat. After imaging, the models were cropped, and the lighting inverted to show where the optimal countershading transition should fall for each lighting condition in order to counterbalance the illumination gradient and thus minimise conspicuousness through self-shadow obliteration. This was carried out in MATLAB (2016). The predicted countershading transitions were then directly compared to the reconstructed colour patterns across the abdomens of both *Sinosauropteryx* specimens.

4.2.6. Quantification of countershading transition

Confidence intervals for the transition points to a lighter belly were estimated as follows. First, transects of the calibrated intensity were taken from dorsal to ventral side. For each transect a cubic spline with 7 degrees of freedom was fitted as a smoother using function smooth.spline() in R 3.4.0 (R Core team 2015). Smoothing was necessary, particularly for the fur-covered models which showed spatial heterogeneity due to irregularities in the lie of the fur; 7 d.f. adequately captured the general trend in gradient without too much smoothing. The point along each transect, in pixels, at which the gradient flattened out was located and converted to a percentage of the distance from dorsal to ventral side. Such estimates were calculated for five replicates of each illumination condition (90° direct sun, 30° direct sun and diffuse illumination), integument ('skin' or 'feathers') and model (n=2). The mean and 95% profile confidence intervals for each illumination condition were estimated using a Linear Mixed Model (Gaussian error) with random effects 'model' and 'integument'. The model was fitted using function lmer in package lme4 (Bates et al. 2014) in R. The final calculated confidence intervals can be found in the Results.

4.3. Results

4.3.1. Plumage distribution

Each specimen shows extensive preservation of dark, presumably organically preserved fibres identified as feathers/feather homologues in distinct areas of the animal (Fig. 4.1a and d and 4.3). Preservation of feathers as organic films is due to the presence of the pigment melanin, and thus only originally pigmented feathers are found preserved in this manner (Chapter 1; Vinther et al. 2008; Vinther 2015*a*). Visible absence of feathers in certain regions of the fossil is therefore likely due to unpigmented plumage that did not preserve, rather than a true absence of feathers in life (Vinther et al. 2008; Vinther 2015*a*). Alternatively, the areas lacking feathers could have been naked (there is no evidence of scales being preserved; Chapter 2.2.4; Smithwick et al. 2017*b*) but would similarly be inferred to have been unpigmented. Since the feathering likely also served an insulatory role, an extensive distribution seems most plausible.

Mapping the distribution of preserved pigmented feathers is therefore considered to reflect the extent of coloured plumage on the animal, with other areas being covered by white (unpigmented) feathers.

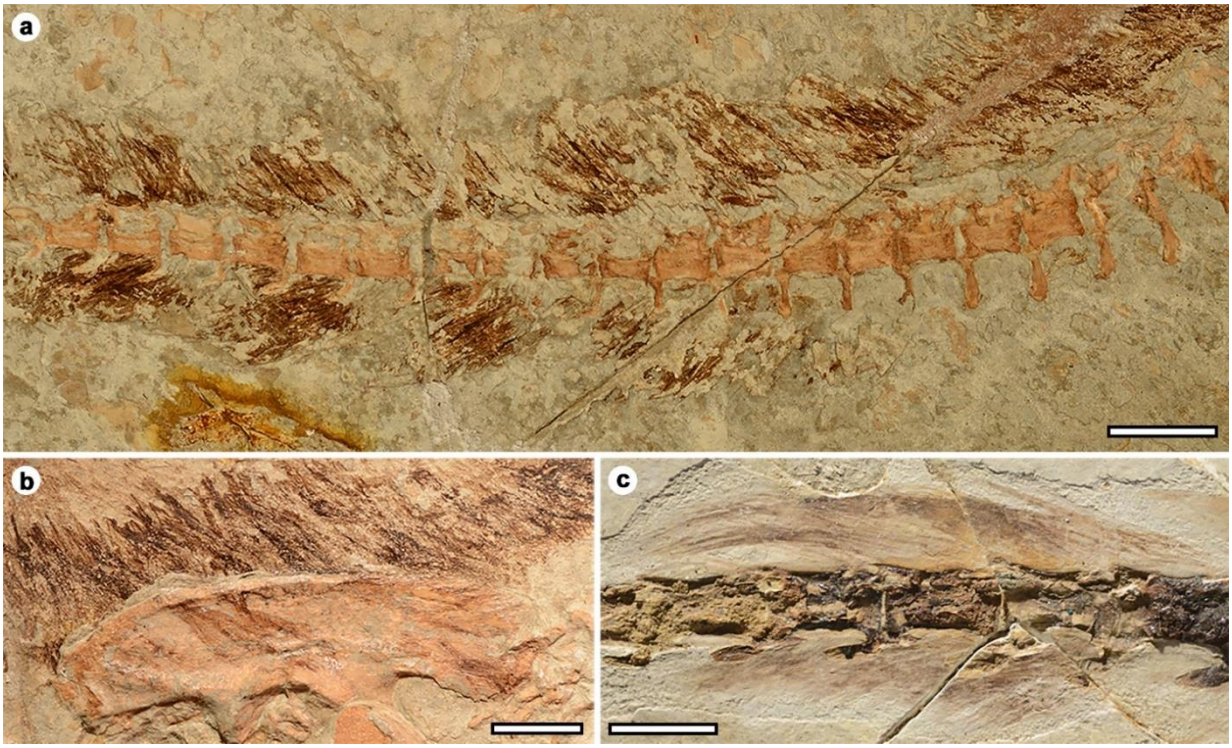

Figure 4.3. Features of the preserved plumage in *Sinosauropteryx*. **a.** The proximal tail region of NIGP 127586 showing the transition into the distinct banding pattern from an unpigmented ventral region and pigmented dorsal region indicative of a countershading pattern. **b.** Detail of pigmented feathers above the hip girdle and overlying the ilium of NIGP 127586. **c.** A single band of pigmented plumage on the tail of IVPP V12415 showing the exceptional feather preservation absent from much of the rest of the specimen. Scale bars represent 10 mm in (a-b) and 5 mm in (c)

NIGP 127586.

The feathers are abundant along the dorsum, beginning on the top of the skull from the anterior end of the orbit, and extending along the back to the tail, where a distinct banding occurs with feathers present in regular blocks with gaps between (Fig. 4.1a). The first pigmented band appears only on the dorsal side of the tail at around the twelfth caudal

vertebra, but all others are present on both the dorsal and ventral sides (Figs. 4.1a and 4.3a). At least 12 distinct bands of pigmented plumage are present on the tail, which transition from being of equal length on the dorsal and ventral sides, to being markedly longer on the dorsal side towards the tip. Some small areas of plumage are present across the skull, which become denser towards the posterior region of the mandible, extending beyond its ventral-most point (Fig. 4.2a). Feathers are also present around the orbit, distinct from the preserved retinal pigment, which extent anteriorly and appear to angle dorsally towards the head crest feathers, likely indicating a stripe across the eye in life (Fig. 4.2a). Across the flank, plumage patches can be seen overlying the abdomen and pelvic girdle (Figs. 4.1a and 4.3b). Preservation of the abdominal contents makes feathers hard to discern in certain areas, however distinct filaments are still clearly visible overlying some organ remains (Fig. 4.2f-g). The feathers do not extend beyond the ventral-most region of the ribcage towards the gastralia. Further patches of plumage occur around the forelimb region.

NIGP 127587.

The plumage is less well preserved than on NIGP 127586, but the areas which are present match well to the other specimen (Fig. 4.1d). Feathers again appear coarsest along the dorsum, from the anterior of the orbit along the top of the skull to the tail. As with NIGP 127586, patches of feathers are present around the orbit extending anteriorly and towards the posterior of the skull running ventrally to the mandible (Fig. 4.2b). Along the tail, feathers are absent on the ventral side until the seventh caudal vertebra. Only around a third of the tail is preserved (24 caudal vertebrae compared to 67 in NIGP 127586), so it is uncertain if the banding pattern seen in NIGP 127586 is also found on NIGP 127587. The length of the feathers appears greater along the dorsal side of the tail to those of the ventral. No feathers are visible around the pelvic girdle, but there are patches associated with the forelimbs, as in NIGP 127586. Across the abdomen, little plumage is present, apart from a patch in the centre of the ribcage. The feathers in this region do not extend ventrally past the bottom of the ribs, conforming to the pattern observed in NIGP 127586.

IVPP V12415.

The plumage of IVPP V12415 is poorly preserved in comparison to the other two specimens, but the general distribution can be determined (Fig. 2.1c). As with the other specimens, the most distinct plumage occurs along the dorsum, but poor preservation in the cervical region and skull make the anterior extent hard to discern. The tail is distinctly banded as in NIGP 127586 (Fig. 2.1c), with an absence of feathers on the ventral side of the tail towards its anterior end. The bands of pigmented plumage appear to continue to the tip of the tail, which is displaced ventrally. The ventral extent of the plumage on the body and the pattern on the skull is difficult to determine due to the preservation.

4.3.2. Colour pattern reconstruction

Illustrations of NIGP 127587 and NIGP 127586 show the pattern of plumage distribution across the fossils (Figs. 4.1b and e). From this distribution, a complete reconstruction was created (Fig. 4.4); this was done blind to any predictions from the modelling of illumination. The consistency of plumage patterns observed across multiple specimens gives confidence to the reconstructed colour pattern. The pattern of pigment across the face appears to show a band of pigmented plumage running from the dorsal area of the head anterioventrally which then angles towards the eye before running to the posterioventral margin of the lower jaw (Fig. 4.2a-e). The banded tail shows a transition from narrow to widely spaced bands from the proximal to distal regions with the ventral pigmentation becoming denser towards the end of the tail. The ventral extent of the pigmented plumage, representing the likely countershading transition, appears to be relatively high on the flank, at around two thirds of the way down the abdomen (Fig. 4.2f-i).

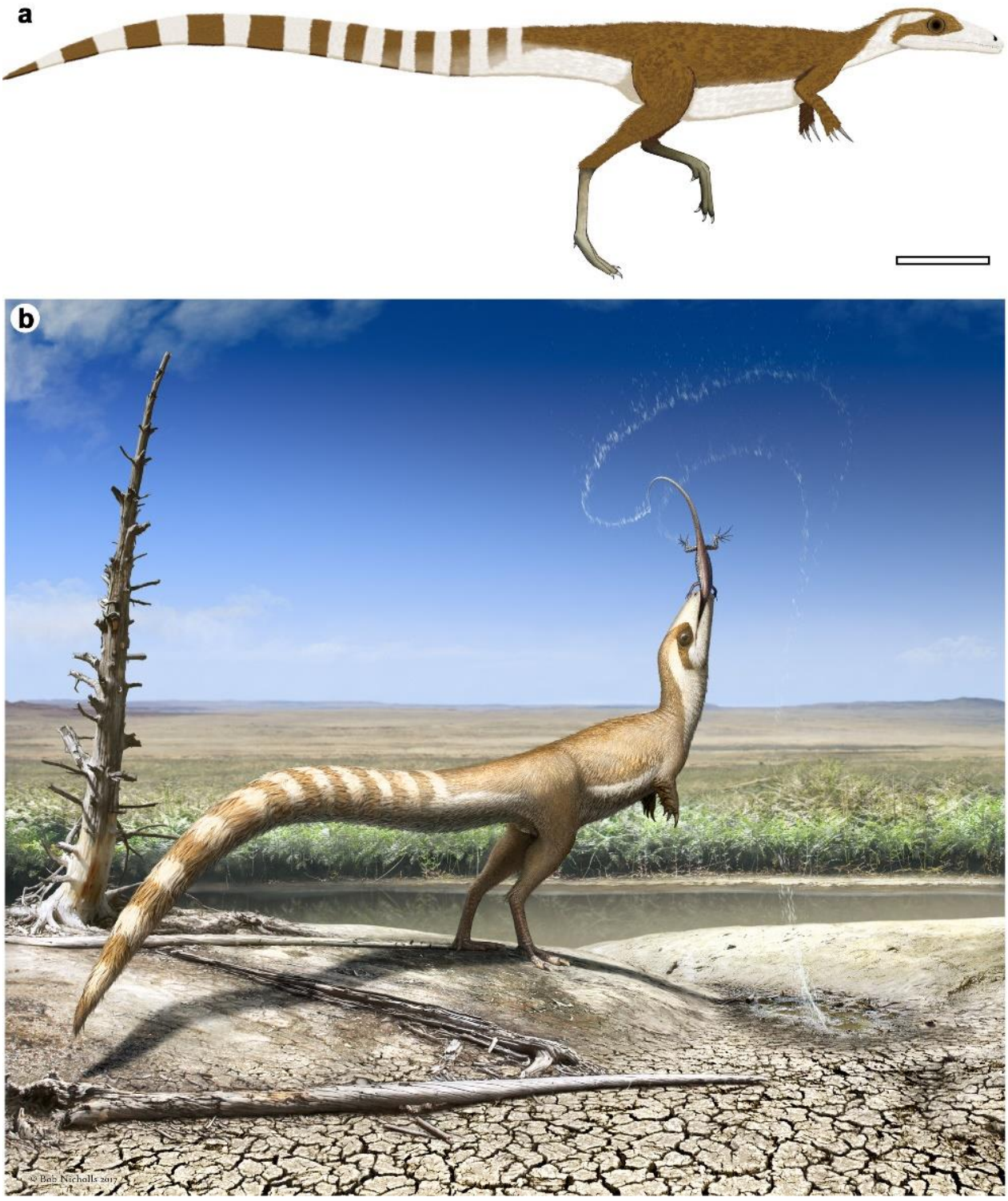

Figure 4.4. Reconstructed colour patterns of *Sinosauropteryx*. **a.** Schematic based on the distribution of pigmented plumage in NIGP 127586 and NIGP 127587 highlighting the level of the countershading transition from a dark dorsum to light ventrum. **b.** Reconstruction of *Sinosauropteryx* in the predicted open habitats in which it lived around the Jehol lakes, preying on the lizard *Dalinghosaurus*. Scale bar in (a) represents 100 mm.

4.3.3. Predicted lighting environment

The reconstructed colour patterns based on NIGP 127586 and NIGP 127587 (Figs. 4.2h-i and 4.4) more closely match the pattern of countershading predicted from images of the models taken under direct light conditions than those of diffuse lighting, indicative of animals living in open habitats (Allen et al. 2012; Vinther et al. 2016). This was true both visually (Fig. 4.5) and quantitatively. For direct overhead sun, the mean predicted transition point to lighter coloration was 72% (95% c.i. 61-83%) of the way from dorsal to ventral side. For direct sun at 30°, it was 60% (95% c.i. 45-75%) and for diffuse illumination 85% (95% c.i. 81-88%). Only the direct illumination confidence intervals include the observed transition point (ca. 67%). The addition of synthetic fur (representing feathers) made little difference to each countershading prediction (Fig. 4.5).

4.4. Discussion

4.4.1. Colour patterns of the face

The presence of pigmented feathers surrounding the orbit and running in a band across the face conforms to “bandit masks” seen in many modern birds and mammals (Fig.I2d-e; Ortolani 1999; Caro 2013). Multiple functions have been proposed for bandit masks in modern taxa (Ficken and Wilmot 1968; Ortolani 1999; Caro 2005, 2009, 2013). One such function is as an anti-glare device (Ortolani 1999; Caro 2013). Reducing the glare from the feathers around the eye would be particularly useful to an animal living in environments with abundant direct sunlight, as is seen often in diurnal extant birds and mammals (Ortolani 1999; Caro 2013). Additionally, it has been suggested that glare is especially high in riparian habitats as light reflectance is increased by proximity to water, as may have been the case in the lacustrine environment in which *Sinosauropteryx* fossils were deposited (Ortolani 1999). Pigmented bands which run directly across the orbital region may also help to mask the presence of the eyes as a form of camouflage against both predators and potential prey (Cuthill and Székely 2009; Kjernsmo et al. 2016). Eye stripes are common in modern birds, which most often also have

dark eyes, making them likely harder for visual predators or prey to detect, and given that eyes elicit responses from both in many situations it is a plausible hypothesis (Bortolotti 2006). Other

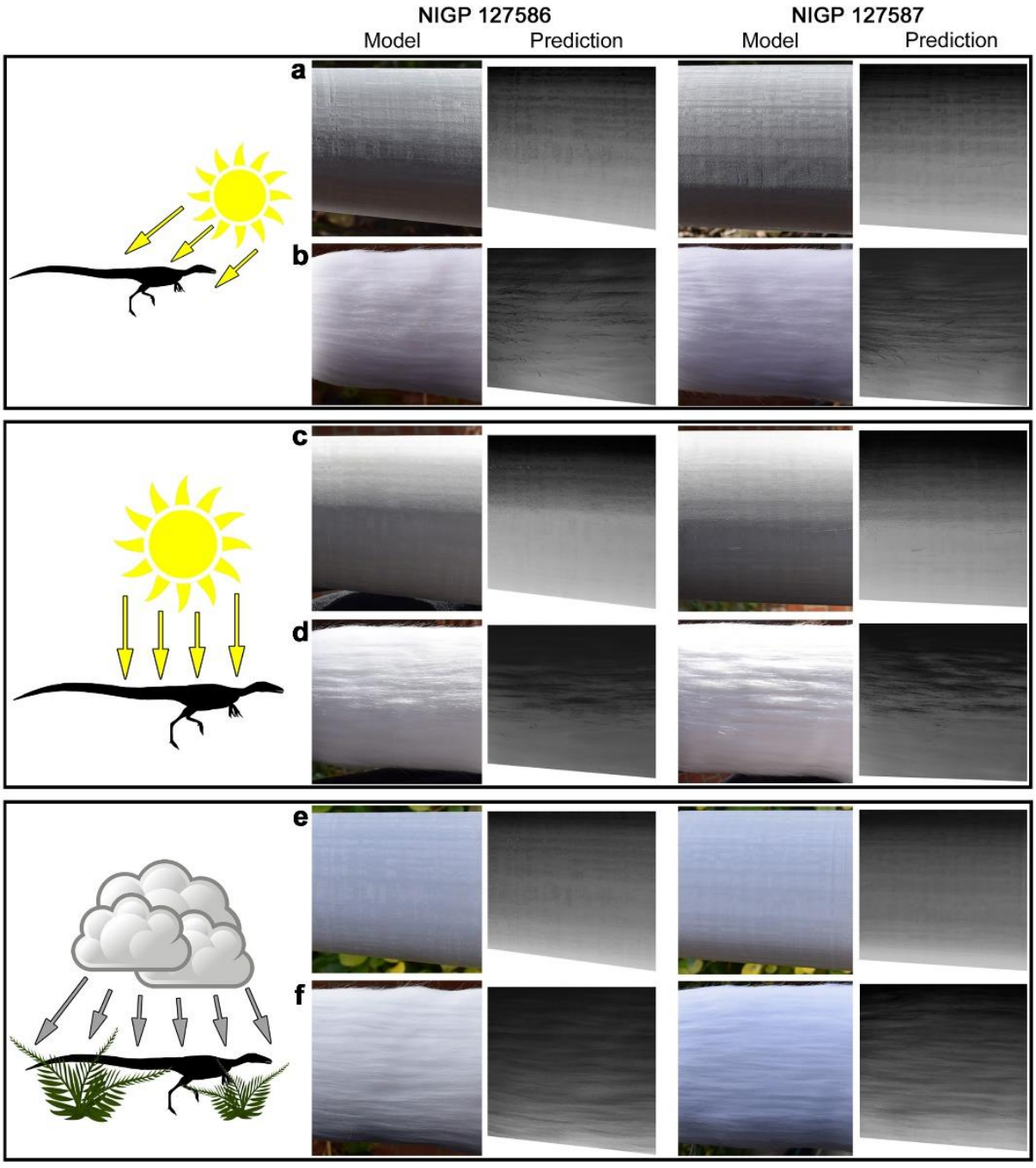

Figure 4.5. The differing pattern of predicted self-shadowing in *Sinosauropteryx.* 3D models of the abdomen of NIGP 127586 and NIGP 127587 imaged under different lighting conditions. 'Model' represents the original photographs taken of the models to show how the self-shadows are cast across each with and without synthetic fur added as a feather analogue. 'Prediction' shows how a gradient of pigment dorsoventrally would be expected

to perfectly counterbalance the illumination gradient caused by self-shadowing. **a-b.** Direct sunlight at an altitude of around 30° on smooth and 'feathered' models. **c-d.** Direct sunlight at an altitude of 90° on smooth and 'feathered' models. **e-f.** Diffuse lighting under 100% cloud cover (which equates to a closed environment) on smooth and 'feathered' models. The ventral position and sharpness of the predicted countershading transition can be seen to be higher and sharper under overhead direct lighting indicative of an open environment (c-d), while under diffuse lighting representing a closed habitat the transition is lower and more gradual (e-f).

possible functions of dark patches around the eyes of extant animals include aposematism and intraspecific signalling (Bortolotti 2006; Caro 2009). Bandit masks have been suggested as being primarily aposematic in mammalian taxa living in exposed open habitats and are especially prevalent in mammalian carnivores, which co-exist with larger carnivores (Newman et al. 2005; Caro 2009; Stankowich et al. 2011), as is likely to have been the situation for *Sinosauropteryx.* A number of modern mammals combine bandit masks with defensive nauseous discharges (Newman et al. 2005), but it is not possible to ascertain if this was the case with *Sinosauropteryx*, and aposematism is generally thought to be rare in modern birds (Bortolotti 2006), making aposematism unlikely in *Sinosauropteryx*. Alternatively, conspicuous face markings could serve as a warning of a physical deterrent, such as a weapon or armour (Newman et al. 2005; Caro 2009; Stankowich et al. 2011). While the theropod had an enlarged claw on each hand (Currie and Chen 2001), the animal's small size makes it unlikely that it posed any real threat to its likely much larger theropod predators, making this function of the bandit mask unlikely.

4.4.2. Function of the banded tail

Banded tails are poorly understood in modern animals, and likely serve several functions including social signalling, dazzle camouflage and outline breaking/disruptive camouflage (Ortolani 1999; Caro 2005, 2009, 2013; Murali and Kodandaramaiah 2016, 2017). Banded tails have been proposed as a way of confusing predators or drawing attention away from more vital body parts (Caro 2013; Murali and Kodandaramaiah 2016, 2017). The tail of *Sinosauropteryx* was the longest of any known theropod relative to body length (Currie and Chen 2001). Due to

this length, it is unlikely that the animal could hold it in a perfectly horizontal position consistently, which would be necessary for a countershaded pattern to be effective. This may explain why the tail is banded rather than showing the countershaded pattern seen on the animal's flanks. The great length of the tail in combination with the distinct and presumably conspicuous colour bands may be explained as a distraction strategy, a method of attracting attention as far from the less conspicuous head and body as possible. Alternatively, the banding could have served as a form of disruptive camouflage as is seen in a number of modern animals, breaking up the outline of the tail to make it less recognisable to potential predators (Ortolani 1999; Caro 2005, 2009, 2013). A combined function of camouflage and instraspecific signalling has also been suggested in some extant bird taxa with banded patterns (Marques et al. 2016). However, no osteological evidence was found for an ability to lift or pose the tail, which would have limited its utility in display.

4.4.3. Countershading in Sinosauropteryx

A clear darker dorsum and absence of pigmented plumage ventrally, with the light ventral side extending to the tail until at least the tenth caudal vertebra conforms to what would be expected for countershaded camouflage adapted to reduce detection from visual predators and from potential prey (Rowland 2009; Allen et al, 2012; Cuthill et al. 2016; Vinther et al. 2016). Visual hunting was likely important for predators of *Sinosauropteryx*. Several tyrannosauroids are contemporaneous with *Sinosauropteryx* (Zhou and Wang 2010). Although these tyrannosauroids were small for the clade (Zhou and Wang 2010), they would have likely been more than capable of tackling the diminutive compsognathid, which appears to have not reached sizes much greater than a metre in length (Currie and Chen 2001). Modern avian predators rely heavily on their exceptional vision to hunt, and as such it is likely that their forebears, the theropods, had similar visual capabilities (Hart 2001). It has been shown that a number of tyrannosauroids had visual capabilities similar to modern raptorial birds (Stevens 2006), and as such strong selection for camouflage would have been likely in their prey. In fact, considering that theropods were most likely tri- or tetra-chromatic, like their extant

counterparts the tetrachromatic birds (Bowmaker 1980; Vorobyev et al. 1998) and the trichromatic crocodiles (Nagloo et al. 2016), colour may have played an even more important role in the Mesozoic predator-prey dynamic than extant terrestrial biotas in which dichromatic mammals are highest in the food chain. It is therefore not surprising to observe camouflage patterns in a small Cretaceous theropod. While many of the vertebrates of the Jehol Biota were arboreal or scansorial, including a number of other theropods (Zhonghe 2006), owing to its anatomy *Sinosauropteryx* was likely restricted to an obligate terrestrial habit and thus did not have the option of retreating to the trees to escape predators. Further, colour patterns beneficial as camouflage would have aided *Sinosauropteryx* in hunting its own prey, which likely also relied, at least in part, on visual cues to detect predators. The hypothesis that its colour patterning was predominantly driven by a need to remain cryptic is therefore parsimonious in *Sinosauropteryx*. Alternative explanations for countershading in modern animals, such as thermoregulation, UV protection and the costs of producing pigmentation could also play a role in the colour patterns observed in *Sinosauropteryx*. The relative importance of these possible functions and their interplay in modern animals is however poorly understood, and so would be difficult to explore in an extinct animal. Despite potential limitations in our understanding of countershading function in modern animals, the correlation between habitat and countershading pattern nuances has been quantitively shown in several extant vertebrate clades (Allen et al. 2012; Ancillotto et al. 2017) and were likely also present in the past.

4.4.4. Habitat preference

The Jehol Biota includes abundant and diverse floral remains alongside its fauna (Zhou et al. 2003; Zhonghe 2006). High palaeotemperatures may have aided the development of lush forested habitats thought to have existed in much of the area (Zhonghe 2006). Speculation has been made about certain taxa inhabiting more or less densely forested areas (Zhonghe 2006) and owing to the volcanic nature of the deposits it is likely that a mosaic of habitats existed in the region, with open areas occurring among denser forested regions (Zhou et al. 2003). The palaeobotanical record of Jehol shows plants adapted for both arid and humid environments,

suggesting climatic fluctuations through time (Barrett and Hilton 2006). As all palaeobotanical remains are allocthonous with no *in situ* plant fossils known, and it is likely that different plant communities existed in the regions around the Jehol lakes and further afield (Barrett and Hilton 2006).

It has been proposed that the larger theropods of Jehol would have likely been found in more open areas, where vegetation was less likely to impede their movement (Zhonghe 2006). The countershading pattern of *Sinosauropteryx* indicates that it too inhabited these more open areas where predation pressure may have been significantly higher due to reduced cover than in the closed areas and background matching camouflage was more difficult to achieve. A need to reduce conspicuousness relative to the environment would therefore have been important to avoid detection from keen visual predators. The diminutive size of *Sinosauropteryx* and its relatively high countershading transition adapted for open areas indicates that it lived in habitats with either few plants or very low vegetation cover.

Further insight may come from the lizard in the stomach of NIGP 127587 (Figs. 4.1d-e and 4.6). Of the known Jehol lizard fauna, the preserved skeletal elements most closely match those of *Dalinghosaurus*, found in the same deposits as *Sinosauropteryx* (the Yixian Formation) (Shu'an and Qiang 2004; Evans and Wang 2005). The tail and hind limbs of *Dalinghosaurus* are exceptionally long relative to its forelimbs, which in modern lizards is a typical morphology of fast-moving terrestrial runners, potentially capable of bipedal locomotion at high speed (Shu'an and Qiang 2004; Olberding et al. 2015). Shorter limbs are generally associated with arboreality (Olberding et al. 2015). Although the slender ungual phalanges of *Dalinghosaurus* indicate that it was likely capable of climbing (Evans and Wang 2005), it appears likely it was better suited to living in the same open habitats inferred herein for the theropod.

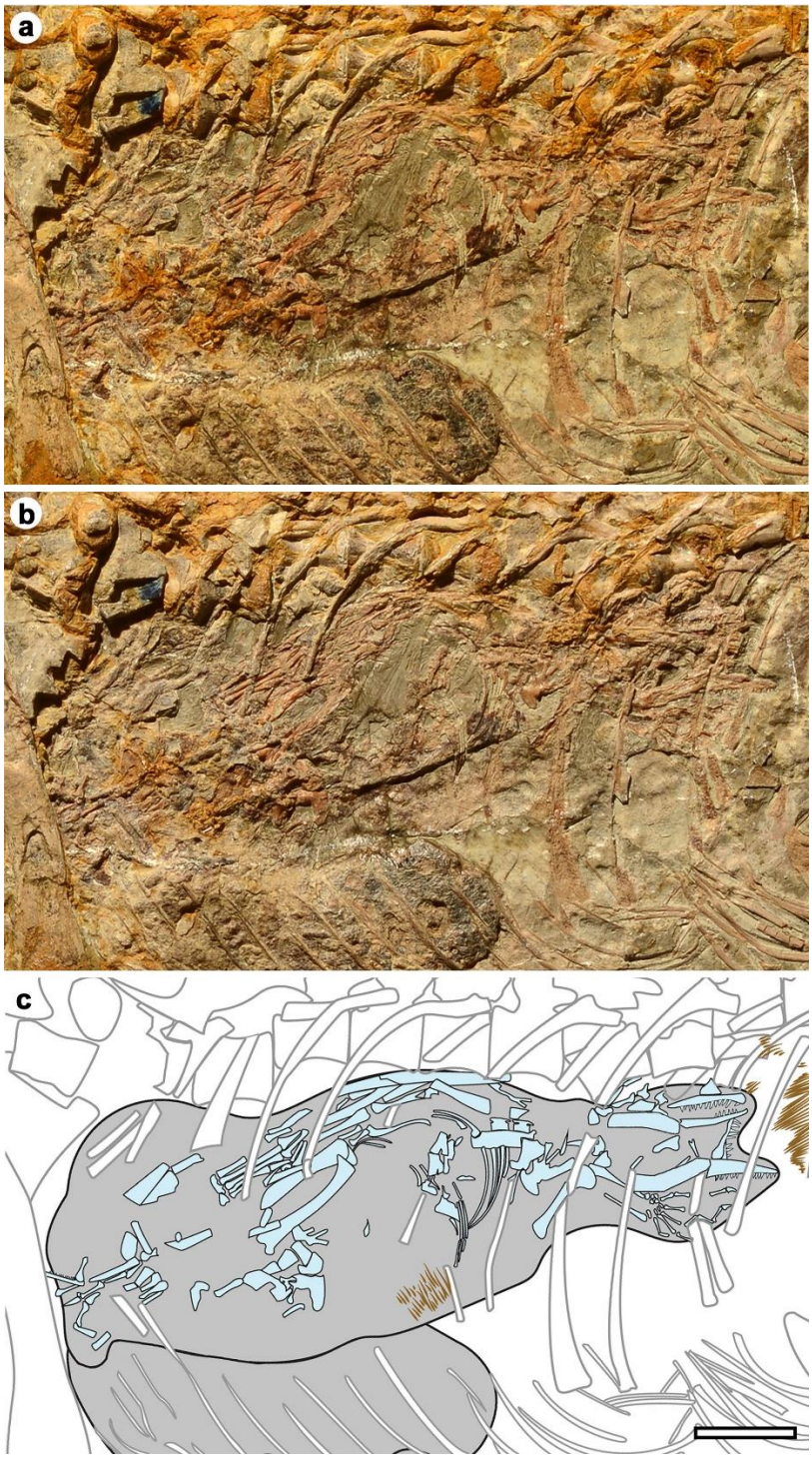

Figure 4.6. The stomach contents of *Sinosauropteryx* NIGP 127587. **a.** Image of the abdomen taken using cross polarization to reduce glare. **b.** Image of the same area taken without cross polarization. **c.** Interpretive drawing of the same area highlighting the lizard inside the abdominal cavity of *Sinosauropteryx* representing its last meal. Bones of *Sinosauropteryx* are outlines in light grey, soft tissues within the abdomen are highlighted in dark grey, feathers are in brown and the bones of the lizard and light blue. Scale bar represents 20 mm.

Most groups of terrestrial vertebrates in Jehol show strong tendency towards forest-living adaptations (Zhonghe 2006). *Sinosauropteryx* however appears to be an exception to this rule. The insight that small theropods like *Sinosauropteryx* may have inhabited open habitats helps build a clearer picture of the environment in which the Jehol animals lived. Jehol was clearly not only rich taxonomically but was also likely varied in the habitats available to animals and consisted of a mosaic of environments, which may explain the area's extraordinary biodiversity (Zhou et al. 2003). Furthermore, the Jehol biota straddles more than 10 million years and is likely to have fluctuated in vegetation cover and landscape. Arboreal taxa and dinosaurs adapted in their colour patterning to closed habitats were present in the forested areas (Zhonghe 2006; Li et al. 2012; Vinther et al. 2016) while larger dinosaurs and their smaller cryptically patterned prey explored open areas with less dense vegetation. The presence of dinosaurs showing camouflage patterns adapted to different habitats indicates that the environment around the Jehol lakes was therefore diverse, varied and hosted different dinosaurian faunas.

Conclusions

From the pattern of countershading and other features of the colouration such as dark eye patches, *Sinosauropteryx* likely inhabited open habitats influenced by direct sunlight. This is contrary to the pattern seen in the contemporaneous dinosaur *Psittacosaurus* which was better adapted to a closed forested habitat suggesting a range of heterogeneous habitats in the Jehol environment. A greater understanding of ancient environments can come from better understanding of the palaeoecology of extinct animals through palaeocolour reconstructions. This work furthers our understanding of how colour patterns have evolved through time and highlights the importance of anti-predator camouflage strategies in deep time.

Chapter 5 – Display, crypsis and putative dimorphism in the plumage of the Early Cretaceous theropod *Caudipteryx.*

Abstract: Colour patterns can serve as camouflage or as conspicuous display features. Often, these contradict one another, meaning a trade-off is required between remaining hidden from predators and being visible to conspecifics. Barred plumage in birds however can act in both signalling and crypsis and is often sexually dimorphic. Similar barred plumage is present on the enigmatic Early Cretaceous oviraptoran theropod *Caudipteryx*, which is well known for its exquisite preservation of presumed display feathers. Here, the plumage of *Caudipteryx* is described in detail and its likely colour patterns reconstructed through analysis of preserved melanosomes. Some individuals show a long distinctly banded tail, while others have a shorter less conspicuous tail, indicating putative dimorphism. Differences in the wing plumage patterns also point to such dimorphism. Melanosome morphologies suggest a dark black dorsum and lighter brown flanks with an unpigmented ventrum in a low countershaded pattern suited to its closed forest habitat. These results suggest that some individuals were more conspicuous while others were drabber, consistent with a sexual dimorphism hypothesis. The similarity of the fine banding to extant birds showing mixed crypsis and display suggests that this phenomenon was present at least as far back as the Early Cretaceous, extending its record back by ~100 million years.

This chapter is currently **unpublished** but is soon to be submitted to a general science journal.

Author contributions – The author devised the chapter concepts along with Jakob Vinther and Steve Brusatte, carried out all analyses, produced the figures and wrote the chapter. Jakob Vinther, Steve Brusatte and Michael Pittman photographed the specimens. Steve Brusatte sampled specimen DNHM D1242, Michael Pittman and Tom Kaye performed the LSF imaging and all authors provided feedback on the writing. Ian Fletcher performed the ToF-SIMS analysis.

5.1. Introduction

Bird plumage colouration serves as both camouflage and display in extant taxa (Baker and Parker 1979; Hill and McGraw 2006*a*; Gluckman and Cardoso 2010). A trade-off must be achieved in the majority of cases between being seen by conspecifics while remaining hidden from predators (Gomez and Théry 2004; Hill and McGraw 2006*a*; Théry 2006; Gomez and Théry 2007; Dreiss et al. 2012; Medina et al. 2017). In general, visual communication signals are thought to compromise camouflage.

Certain plumage colour patterns can however serve as a visual signal to conspecifics while remaining cryptic to predators (Gluckman and Cardoso 2010; Marques et al. 2016). This is seen in birds with fine barring - a common plumage pattern throughout Aves (Gluckman and Cardoso 2010). Fine barring or stripes can appear more conspicuous at close range, while becoming less conspicuous at greater distances as the different colours merge together, a feature noted in fishes as well as birds (Fig. I2e-f; Marshal 2000; Gluckman and Cardoso 2010; Marques et al. 2016). In birds, males tend to have more distinct and regular barring than females or juveniles, consistent with a sexual selection hypothesis (Marques et al. 2016). Therefore, as well as informing of crypsis vs camouflage in birds, fine barring can also indicate sexually dimorphic plumage differences.

Stripes and banding in the plumage of a number of extinct avian and non-avian dinosaur taxa are known from the fossil record (Chapters 1.5 and 4; Vinther 2015*a*; Smithwick et al. 2017*a*). The thick and highly conspicuous tail bands of the non-avian theropod *Sinosauropteryx* from the Early Cretaceous Jehol Biota of China for example (Chapter 4) would certainly have been highly conspicuous. They may have served for display, but it is also possible that they provided a form of outline-breaking camouflage (Zhang et al. 2010; Smithwick et al. 2017*a*). Another theropod from the same deposits, *Caudipteryx*, shows a distinctive tail fan presumed to have been a display feature (Persons et al. 2013) with much finer and subtler banding (Ji et al. 1998; Vinther 2015*a*). Both of these dinosaurs were ground-dwelling but had different sizes and body plans, including different feeding apparatuses. Thus, differences in their banding pattern is of interest and can potentially inform suspected behavioural differences. As a

stemward pennaraptoran, the appearance and ecology of *Caudipteryx* is a much-needed datum that will inform our understanding of these traits across the group, including in the first birds and theropod flyers.

As feathers are generally very well preserved in specimens of *Caudipteryx* (Ji et al. 1998; Zhou et al. 2000), colour patterns can be discerned. Preservation of melanosomes allows colour patterns to be reconstructed (Chapter 1; Vinther 2015*a*). Here, the plumage patterns of *Caudipteryx* are investigated in detail. Through investigation of multiple exceptional specimens using white light and laser stimulated fluorescence (LSF) imaging along with analysis of melanosome morphologies in one specimen, the plumage and pigment distribution *of Caudipteryx* are described in detail. Through comparisons to living animals with similar plumage colour patterns I propose the likely habitat of *Caudipteryx* and reasons for the distinctive barring in certain aspects of its plumage as well as evidence of dimorphism.

5.2. Materials and methods

5.2.1. Institutional abbreviations

DNHM – Dalian Natural History Museum, Dalian, Liaoning Province, China; IVPP - Institute of Vertebrate Palaeontology and Palaeoanthropology, Beijing, China; PMoL – Palaeontological Museum of Liaoning, Liaoning Province, China; NGMC – National Geological Museum of China, Beijing, China; STM, Shandong Tianyu Museum of Nature; BPM – Beipiao Paleontological Museum, Beipiao, China.

Four specimens of *Caudipteryx* were studied in detail, including a new undescribed specimen (DNHM D1242; Fig. 5.1a) from which samples were taken for SEM imaging of melanosomes. The three other specimens (IVPP V12344; Fig. 5.1b, IVPP V12430; Fig. 5.1c, and NGMP97-9-A) were imaged under both white light and LSF but were not sampled for melanosomes. Alongside these specimens, published images of three additional individuals were used for comparative purposes (BPM 0001; PMoL AD00020 and STM4-7).

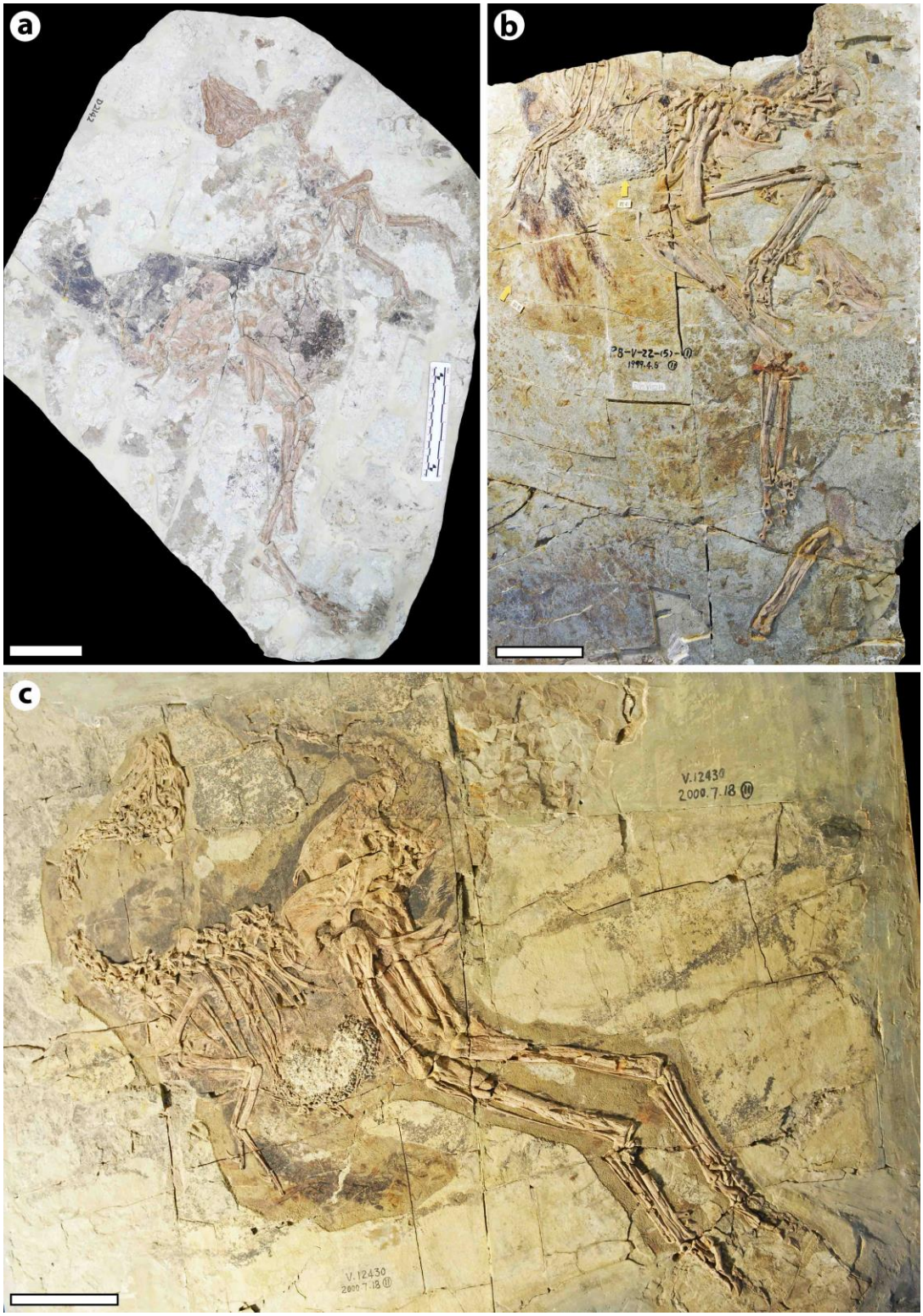

Figure 5.1. The stemward oviraptorosaurian theropod *Caudipteryx* from the Early Cretaceous Jehol Biota of China. **a**. DNHM D1242 – an undescribed complete specimen. **b**. IVPP V 12430 – described as *C. dongi*. **c**. IVPP V 12430 – described as *C. zoui*. Scale bars represent 10 cm.

5.2.2. Specimen photography

The two specimens housed at the IVPP (IVPP V12344 and V12430) were photographed using a Nikon D800 DSLR with a Micro Nikkor 105 mm lens and illuminated with a 3200K halogen light source (Lowell Tota-light, 400W). Cross-polarised lighting was also used for imaging, achieved by mounting a polarising gel in front of the light source and fitting a Tiffen Warm Polariser lens filter to the lens. This technique reduced glare from the surface of the fossil allowing for more detail to be captured (Bengtson 2000). NGMC 97-4-A was photographed with a Nikon D810 DLSR camera with an AF-S Nikkor 28-300mm lens.

5.2.3. LSF imaging

A modified version of a previously devised protocol of Kaye *et al*. (2015) (Wang *et al*. 2017; Kaye et al. 2019) was used to generate LSF imaged. Specimens were imaged using a 405 nm violet laser with a long pass blocking filter incorporated with Nikon D810 DLSR camera lens (which prevents image saturation by the laser). A Laserline Optics Canada lens dispersed the laser into a vertical line. This was mechanically swept over the specimen repeatedly during exposures in a dark room. The resulting images were post-processed (Using Adobe Photoshop CS6) for sharpness, saturation and colour balance. Details of the theory behind LSF imaging can be found in Wang *et al*. (2017).

5.2.4. Sampling information

A total of 17 spot samples were removed from DNHM D1242 using a sterile scalpel. Each sample was around 1-3 mm across and contained dark organic material assumed to be remains of the pigment melanin, known to account for most organic integumentary preservation (Chapter 1; Vinther 2015*a*). No samples were taken from the wings owing to poor preservation and potential issues arising from this area of the fossil being restored. The samples were mounted onto sticky tape (organic side up) and wrapped in clean tissue to be transported to the University of Bristol for investigation. Initial SEM imaging showed an amorphous layer,

around 5-10 µm thick covering the samples (Fig. S5.1), which obscured any microstructural details. This was assumed to be a consolidant applied during preparation of the fossil, most likely Paraloid B72 or similar. As Paraloid is readily soluble in acetone, all samples were submerged in acetone for 24 hours before being removed and dried. After acetone treatment all samples showed exposed microstructural detail of the fossil itself under the SEM.

5.2.5. SEM imaging

Samples were mounted onto SEM stubs using copper tape and sputter coated with gold (10 nm) using a Quorum Q150R ES sputter coater. Samples were then imaged using a Zeiss Evo15 Environmental Scanning Electron Microscope (ESEM) at a working distance of 10 mm and a voltage of 10-20 KeV.

5.2.6. Melanosome measurements

Melanosomes were measured from the SEM images using ImageJ (Abràmoff et al. 2004). Long and short axes were measured, following standard methodology (Chapter 1.5; Li et al. 2010, 2012;). Where possible, 100 melanosomes were measured per sample to give statistical confidence in the data. A small number had fewer than this exposed, and so had as many as possible measured (Table 5.1). It was observed that several (4/17) samples had a mix of 3D melanosomes and mouldic impressions preserved. Melanosomes (and impressions) were only measured if they were fully exposed so the full morphology could be ascertained. Moulds and 3D melanosomes were measured separately, so that possible effects of shrinkage could be taken into consideration (McNamara et al. 2013; Colleary et al. 2015). Where both were present in a single sample, as many as possible were measured. Treating moulds and 3D melanosomes separately gave a total of 19 samples which were added to a previously published dataset of modern melanosomes (Li et al. 2012).

Table 5.1. Measurements of all *Caudipteryx* samples used in the canonical discriminant analyses. N = number of melanosomes

Sample	Preservation	Location	Length (nm)	Length CV	Length skew	Width (nm)	Width CV	Width skew	Aspect ratio	AR skew	N
1	Mould	Neck	1220.179	15.095	0.802	309.307	10.210	0.752	3.986	1.381	28
1b	Mould	Neck	734.262	27.700	0.725	394.279	18.690	-0.033	1.982	1.189	100
2	Mould	Base of neck	936.172	25.091	0.245	312.904	17.933	1.182	3.086	-0.148	100
3	Mould	Base of neck	930.816	26.516	0.191	337.324	19.535	0.809	2.914	-0.042	100
5	Mould	Body	1039.417	28.383	-0.470	298.979	17.439	1.004	3.557	-0.765	94
5	3D	Body	805.711	28.362	-0.299	236.674	17.397	1.398	3.529	-0.308	100
6	Mould	Body	1148.335	19.192	0.144	299.893	15.969	0.660	3.920	0.463	100
7	3D	Body	949.927	28.320	0.049	272.765	12.422	0.037	3.511	0.059	100
8	3D	Tail base	895.516	28.190	0.086	269.686	16.850	0.997	3.410	0.455	100
9	Mould	Middle tail	990.452	23.306	-0.268	316.701	14.294	1.106	3.197	-0.681	100
10	3D	Tail fan	467.671	28.090	0.865	331.224	23.989	1.505	1.472	1.889	100
11	3D	Tail fan	597.170	26.893	1.340	386.111	17.478	0.165	1.596	2.105	100
12	Mould	Tail fan	657.953	25.386	0.849	393.899	19.817	0.314	1.723	1.491	100
12	3D	Tail fan	624.979	22.154	1.010	388.918	17.137	0.395	1.631	1.399	100
13	3D	Tail fan	769.884	28.007	0.469	317.491	16.446	1.139	2.516	0.476	100
15	Mould	Tail base	765.351	34.009	0.397	294.273	19.054	0.517	2.747	0.542	27
15	3D	Tail base	862.570	25.799	-1.076	314.325	18.112	0.184	2.895	-0.446	10
16	3D	Body	653.694	37.441	1.385	314.501	18.120	0.520	2.196	1.523	100
17	Mould	Body	628.967	24.182	1.289	375.972	21.077	0.001	1.769	2.074	25
17	3D	Body	576.737	23.881	1.254	343.713	16.937	0.212	1.749	1.461	100

5.2.7. Colour predictions

Two melanosome measurement datasets were used to predict the likely original colours in each *Caudipteryx* sample through canonical discriminant analyses (CDA) in the statistical software SPSS 25 (IBM Corp) using standard methodological protocol used in previous palaeocolour studies (Li et al. 2010, 2012; Chapter 1.5). CDA allows prediction of group membership of unknown fossil melanosome samples based on the grouping of modern samples by colour category, determined by the measurement variables. The two datasets used were: (1) that published by Li et al. (2012) and (2) a combined dataset of the Li et al. (2012) data and new data collected for Chapter 7.2.7. Melanosome measurement variables (length (nm), width (nm), aspect ratio (length/width), coefficient of variance (CV) of length and width and skew of length, width and aspect ratio) with known associated colours for the modern samples were used to

predict the likely colour category of the fossil samples. Both a forward stepwise model (which only uses the variables explaining the most variance in the modern rata) and a model with all variables considered were run on the data to test for any differences between the methods.

5.2.8. Effects of shrinkage

DNHM D1242 provides a rare opportunity to study the taphonomy of melanosome shrinkage owing to its unusual melanosome preservation in having both 3D melanosomes and mouldic impressions present, often within a single spot sample. As 3D melanosomes and moulds were measured separately, they could be directly compared within a single sample. The relative average size difference and thus percentage difference between 3D melanosomes and moulds were calculated for four samples that contained both types. To further account for possible shrinkage different degrees of size change were modelled by scaling 3D melanosome measurements up by between 5-20% in the CDA.

5.2.9. Anatomical measurements

The anatomy of the fossils was quantified by measuring individual bones and distinctive areas of plumage. These measurements were compiled into a dataset and combined with previously published measurements (Ji et al. 1998; Zhou et al. 2000; Zhou and Wang 2000; Dyke and Norell 2005). Ratios of certain key features were calculated, such as tail fan length to skull length and overall tail length to body length to better understand the key plumage features.

5.2.10. ToF-SIMS analysis

In order to assess the chemical makeup of the organics in the soft tissues, four samples were analysed using ToF-SIMS under the methodology described in Chapter 3.2.4.

Fifty-six mass peaks from the resulting spectra were taken per sample and added to a database of modern and fossil melanin samples and non-melanin controls including those

previously published (Colleary et al. 2015) and new ichthyosaur samples (see Chapter 3.2.4). The data were normalised (see chapter 3.3.5) and a principal component analysis (PCA) was produced to quantitatively compare the samples in the statistical software PAST (Hammer et al. 2001).

5.3. Results

5.3.1. Plumage patterns

Pigmented feathers are well preserved in most of the specimens of *Caudipteryx*. The morphology of the feathers, their distribution and apparent original colour patterns are descried in detail for each specimen by anatomical region.

Tail

A tail fan is preserved in two of the studied specimens (DNHM D1242, NGMC 97-4-A; Fig. 5.2) and present in two further specimens (STM4-7 and PMoL AD00020) with partially preserved tail plumage present in another (BPM 0001). The presence of a tail fan in at least five specimens makes it likely a common trait in the genus (IVPP V 12340 and IVPP V 12430 likely also had this feature, but this region is missing in each fossil). The rectrices comprising the fan appear symmetrical in all specimens where preservation is sufficient to see the details of the vanes (Fig. 5.2). Three individuals (NGMC 97-4-A (Fig. 5.2a-b), PMoL AD00020 and STM4-7) have marked banding preserved in the fan, with presence and absence of dark organic material suggesting pigmented and unpigmented stripes in life. The tail fan of DNHM D1242 does not exhibit the same strong banding but has much subtler stripes at least along the lateral margin of the fan (Fig. 5.2c-d). Some distortion of the fan is present in DNHM D1242, making further colour patterns hard to discern, but the central rectrices appear uniformly pigmented. The total number of rectrices in the tail fans is hard to ascertain due to overlapping and incomplete preservation.

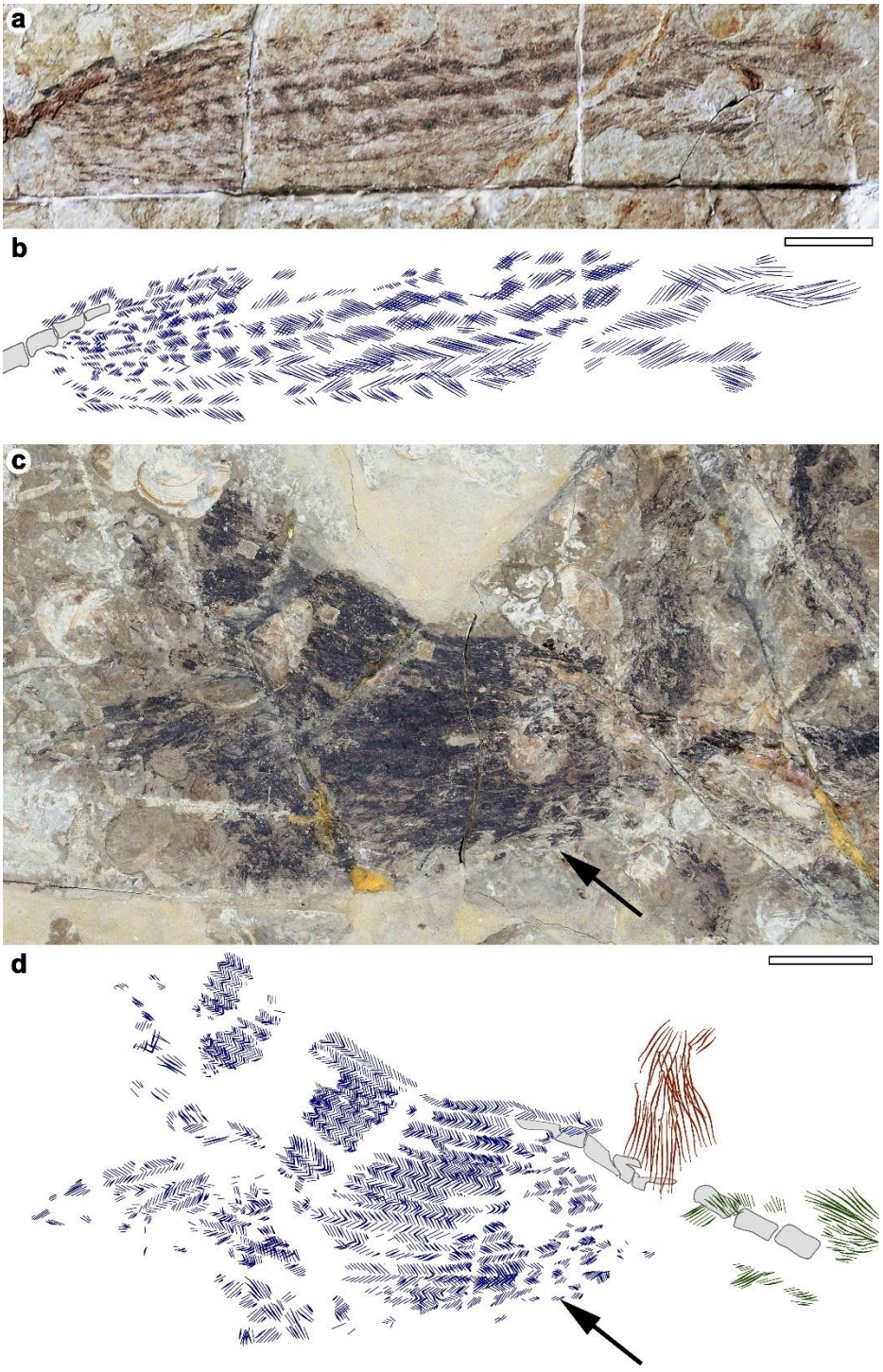

Figure 5.2. Plumage of the two types of tail fan in *Caudipteryx* with interpretive drawings. Bones are outlined in grey, dark blue represents rectrices, green represents plumage from the bony portion of the tail and brown represents body plumage. **a**-**b**. The strongly banded tail of NGMC 97-4-A showing band that become wider distally. **c**-**d**. The tail of DNHM D1242 showing only unpigmented banding on the lateral margin (black arrows) with overlapping rectrices in the middle appearing more uniformly pigmented. Scale bars represent 2 cm.

The relative length of the tail fan differs between individuals with strong banding and DNHM D1242. Those with the strong banding have tail fans around twice the length of the skull (Table 5.2), while DNHM D1242 has a fan length only marginally longer than the skull (Table 5.2). While distortion may account for some of this, the fan appears genuinely shorter than those with more prominent banding. The proportion of total body length comprising the tail (including the bony portion and fan) is greater in specimens with the strong banding (~40%; Table 5.2) compared to DNHM D1242 (~30%; Table 5.2). The caudal vertebrae are highly reduced in length in all specimens when compared to other oviraptorosaurs, making the bony portion of the tail relatively short (Persons et al. 2013; Pittman et al. 2013). Pigmented feathers are present along the dorsal and ventral sides of the bony portion of the tail. Banded plumage is present on the ventral portion of the tail base of NGMC 97-4-A (Fig. 5.3c).

The strongly banded tail fan shows a consistent pattern where the bands are on average finer and narrower at the proximal end (mean 2 mm wide) and then widen progressively towards the distal end (mean 3.5 mm wide), sometimes appearing to lose the banding all together at the tip by ending in a solid area of pigmentation (Fig. 5.2a-b Table 5.3).

Wings

The feathering of the wings is well preserved in at least five specimens (IVPP V12344, IVPP V12430, NGMC 97-4-A, PMOL AD00020 and STM4-7) with BPM 0001 showing poorer preservation compared to the others. The primaries account for the majority of the wing length, are symmetrical in all specimens on which they are preserved (Fig. 5.4) and are all darkly pigmented with no evidence of banding. The remiges have unpigmented rachises in at least IVPP V 12344 (Fig. 5.4c-d) and NGMC 97-4-A (Fig. 5.4e-f). It has been previously noted that the distal ends of the remiges are often not preserved (Ji et al. 1998), and this is seen in multiple specimens (Fig. 5.4). The primaries appear to taper to a point in an unusual fashion in and IVPP V12430 (Fig. 5.4a-b) and there is a gap in the pigment at the distal ends of the primaries in IVPP V12344 and NGMC 97-4-A followed by pigmented tips in some feathers (Fig. 5.4c-f).

Table 5.2. Anatomical measurements of skeletal and plumage features of *Caudipteryx* specimens. Unless stated, all measurements are in mm.

Specimen	D1242	BMP 0001	IVPP V12344	IVPP V12430	NGMC 97-4-A	PMOL AD00020	STM4-7
Described species	*Caudipteryx* sp.	*C. zoui*	*C. dongi*	*Caudipteryx* sp.	*C. zoui*	*Caudipteryx* sp.	*Caudipteryx* sp.
Skull length	92.05	91.30	N/A	99.82	81.72	N/A	84.86
Neck length	119.96	154.11	N/A	169.58	200.13	N/A	173.05
Femur length	137.72	147.72	143.34	153.06	162.96	N/A	149.63
Femur bend	17.78°	5.90°	6.81°	10.55°	11.08°	N/A	13.26°
Tibia length	174.50	190.55	203.98	194.87	233.03	186.66	196.61
Tibia/Femur ratio	1.27	1.29	1.42	1.27	1.43	N/A	1.31
Metatarsal I length	N/A	16.00	19.00	15.00	N/A	N/A	N/A
Metatarsal II length	N/A	105.16	112.00	102.00	N/A	N/A	N/A
Metatarsal III length	N/A	113.00	124.00	112.00	115.00	N/A	N/A
Metatarsal IV length	N/A	107.00	116.00	106.00	N/A	N/A	N/A
Overall leg length	503.09	544.07	542.83	540.66	N/A	N/A	533.37
Leg/body ratio	0.80	0.62	N/A	0.73	N/A	N/A	0.76
Ilium length	112.52	129.43	118.16	112.29	110.19	N/A	108.97
Ilium area (mm^2)	3392.64	4200.67	4278.39	4488.59	4373.82	N/A	5100.47
ischium	59.47	67.32	70.13	71.70	79.73	N/A	57.86
ischium angle	20.83°	23.87°	35.27°	30.11°	30.81°	N/A	13.77°
Pubis length	126.72	124.00	107.89	125.00	138.42	N/A	109.26
Pubis angle	15.57	N/A	20.65	14.71	N/A	N/A	20.58
Sternum length	N/A	29.67	25.00	N/A	36.00	N/A	26.24
Coracoid length	N/A	34.00	N/A	35.00	N/A	N/A	N/A
Scapula length	63.05	82.25	N/A	82.72	84.73	N/A	73.23
Humerus length	60.75	71.89	73.00	69.88	79.30	N/A	71.18
Ulna length	58.69	63.08	59.41	60.82	60.71	N/A	64.98
Metacarpal I length	13.59	11.00	13.00	11.00	N/A	N/A	N/A
Metacarpal II length	29.31	28.00	29.00	28.00	N/A	N/A	N/A
Metacarpal III length	26.18	25.00	27.00	23.00	N/A	N/A	N/A
Bony tail length	94.56	159.32	N/A	172.39	211.66	N/A	162.74
Tail fan length	133.02	144.69	N/A	N/A	196.02	187.00	210.34
Total tail length	227.58	304.01	N/A	N/A	407.67	N/A	373.08
Tail/body ratio	0.29	0.37	N/A	N/A	0.40	N/A	0.41
Fan/bony tail ratio	1.41	0.91	N/A	N/A	0.93	N/A	1.29
Fan/skull ratio	1.45	1.58	N/A	N/A	2.40	N/A	2.48
Tail fan tip to skull tip length	780.45	873.86	N/A	N/A	1028.54	N/A	913.34
Bony tail to skull tip	628.46	815.94	N/A	743.54	808.96	N/A	699.09
Tail type	Subtle banding	Uncertain	N/A	N/A	Strong barring	Strong barring	Strong barring
Secondaries	Uncertain	Uncertain	Barred	Barred	Absent	Absent	Absent
Longest primary	N/A	124.32	173.432	143.016	95.082	N/A	182.23

Two specimens, IVPP V 12344 and IVPP V 12430, show well-preserved secondaries that have clear and distinct banding with ~5.5 mm and ~7.2 mm wide (respectively) pigmented and unpigmented bands that are consistently spaced (Fig. 5.4a-d). All specimens with a strongly-banded tail however show no evidence of secondaries, despite having exceptionally well-preserved primaries (Fig. 5.4e-f).

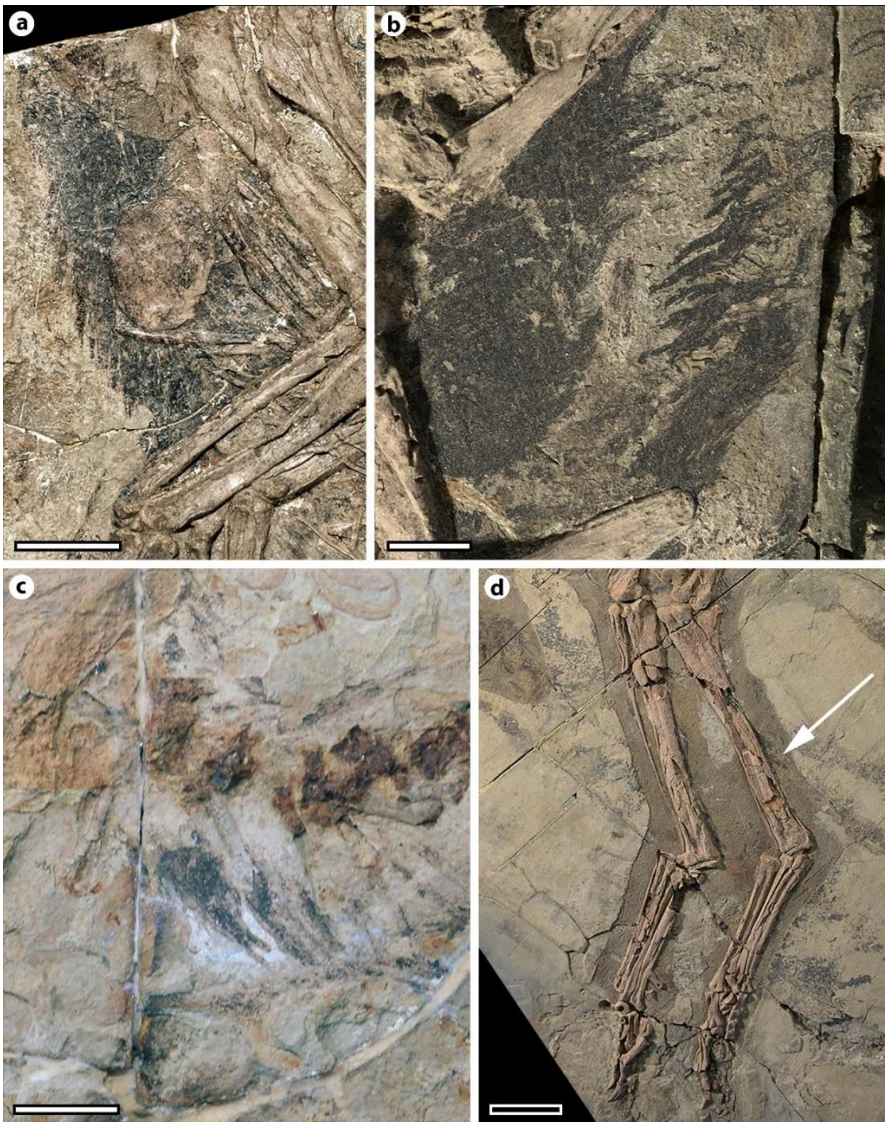

Figure 5.3. Details of the body, ventral tail and leg plumage in *Caudipteryx*. **a**. Filamentous plumage covering the chest of IVPP V12344. **b**. Filamentous plumage in the cloacal region of IVPP V12430. **c**. Strongly banded plumage on the ventral tail base of NGMC 97-4-A. **d**. Pigmented plumage extending to at least the lower-middle tibia in IVPP V 12430. Scale bars represent 2 cm in (a) and (c), 1 cm in (b) and 5 cm in (d).

Body plumage

The quality of plumage preservation across the body varies between specimens, but some common features are present. All specimens show pigmented plumage across the dorsum, with an absence on the ventrum (Figs. 5.1 and 5.5). While there is an absence of pigmented plumage on the ventrum, there are pigmented feathers on the chest (Fig. 5.3a) and under the tail base

(around the cloacal area; Fig. 5.3b), suggesting pigmented plumage would have continued until low on the flank. Pigmented patches of plumage are present on multiple specimens on and between the ribs relatively low down on the body (Fig. 5.5).

Table 5.3. Banding frequency in the tail fans and wings. Individual band width was calculated based on the average number of bands per 10 cm as measured from fossil images.

Tail fan					
Specimen	Region	Measured length (mm)	Pigmented bands	Bands per 10 cm	Band width (mean mm)
NGMC 97-4-A	Proximal	26.02	7	53.81	1.86
	Mid	46.54	7	30.08	3.32
D1242	Proximal	22.61	5	48.99	2.04
STM4-7	Mid	28.47	5	35.13	2.85
	Distal	33.53	4	23.86	4.19
PMoL AD00020	Proximal	36.69	8	43.61	2.29
	Mid	26.23	5	38.12	2.62
	Distal	27.73	5	36.06	2.77
Wing secondaries					
IVPP V 12344	-	82.74	8	20.69	5.52
IVPP V 12430	-	64.41	5	25.76	7.16

The plumage preserved across the body does not show a clear pennaceous feather morphology, instead appearing more filamentous and present in a thick mass (Figs. 5.1, 5.3a-b and 5.5). Distinct patches of plumage such as the chest of IVPP V 12344 (Fig. 5.3a) and under the tail base of IVPP V 12430 (Fig. 5.3b) appear to have been long and flexible in life. A similar feather morphology occurs on the dorsum of multiple specimens where pigmented plumage is particularly dense (e.g., DNHM D1242 and IVPP V 12430). Generally, specimens with more strongly banded tails have less-dense plumage across the body.

Leg plumage

Patches of plumage appear associated with the legs in several specimens. In DNHM D1242, a patch of organic material is present surrounding the tibia/fibula and in IVPP V12430 feathers can be seen extending to at least mid-way down the tibia (Fig. 5.3d).

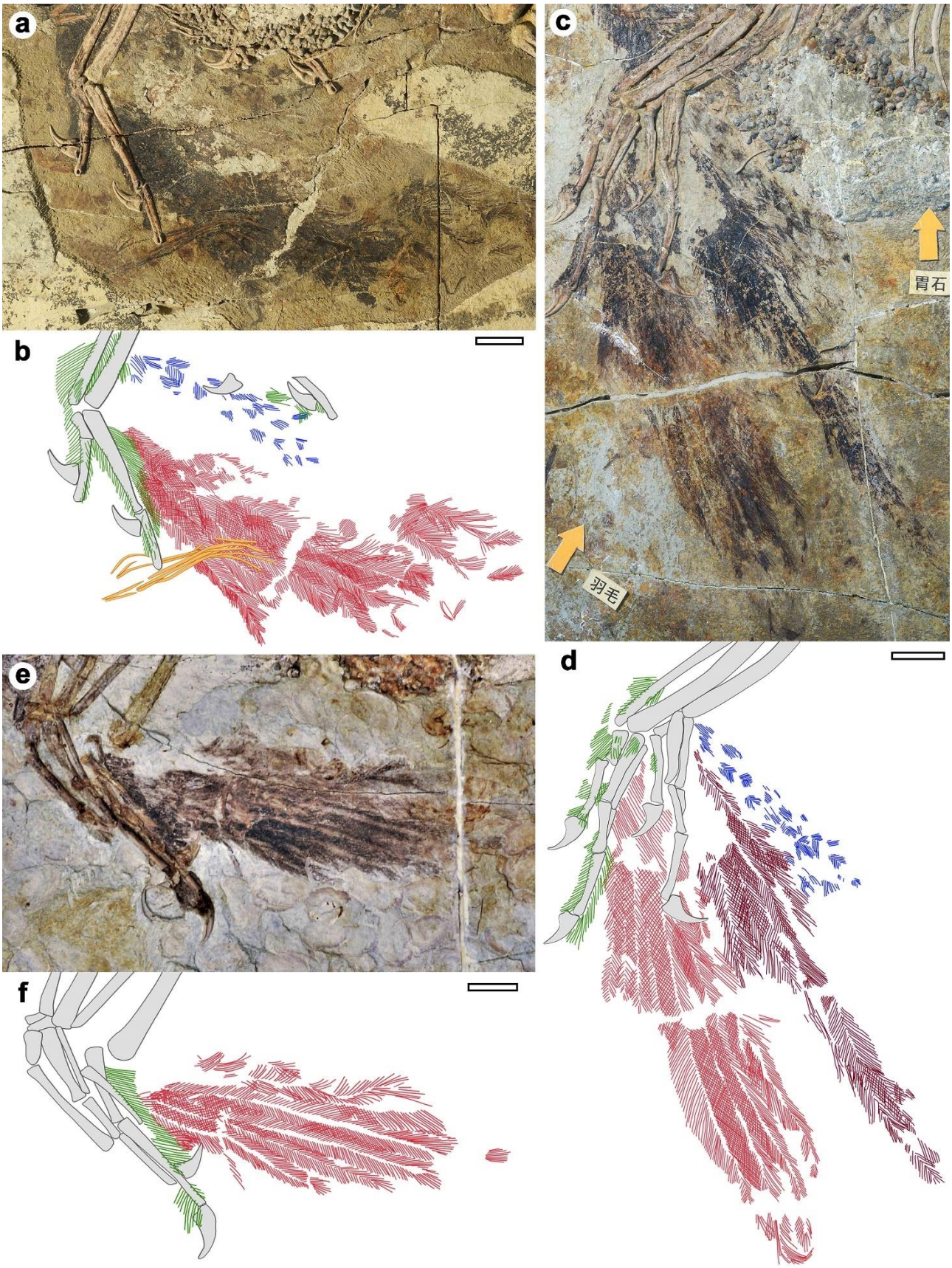
a
b
c
胃石
羽毛
d
e
f

Figure 5.4. Details of the two different wing plumage colour morphs in *Caudipteryx* with interpretive drawings. Bones are outlined in grey, primaries are red (light red for the left wing, dark red for the right wing), secondaries are blue, feathers covering the digits are green and unknown filaments are in orange. **a-b**. IVPP V12344 showing uniformly pigmented primaries with tapering tips and strongly banded secondaries. Large pigmented filaments of unknown origin are present at the distal end of the digits. **c-d**. IVPP V12430 showing the same feather patterning as IVPP V12344 but lacking the large filaments. **e-f**. NGMC 97-4-A showing uniformly pigmented primaries and no secondaries. Scale bars represent 2 cm.

5.3.2. Melanosome preservation and morphology

Two distinct melanosome morphologies were observed in the samples; elongate ovoid resembling eumelanin-rich extant melanosomes (Figs. 1.1b and 5.6a-b) and spherical to oblate morphologies, resembling phaeomelanin-rich extant melanosomes (Figs. 1.1f and 5.6c-d; Vinther 2015*a*). These two types were present as both moulds and 3D melanosomes (Fig. 5.6a-d). The two preservation modes occasionally co-occur in a single sample; however, they were most often present in discrete patches of one or the other without significant mixing (Fig. 5.6c-d). Two samples (4 and 14) did not have sufficient melanosomes preserved/exposed to include in subsequent analyses.

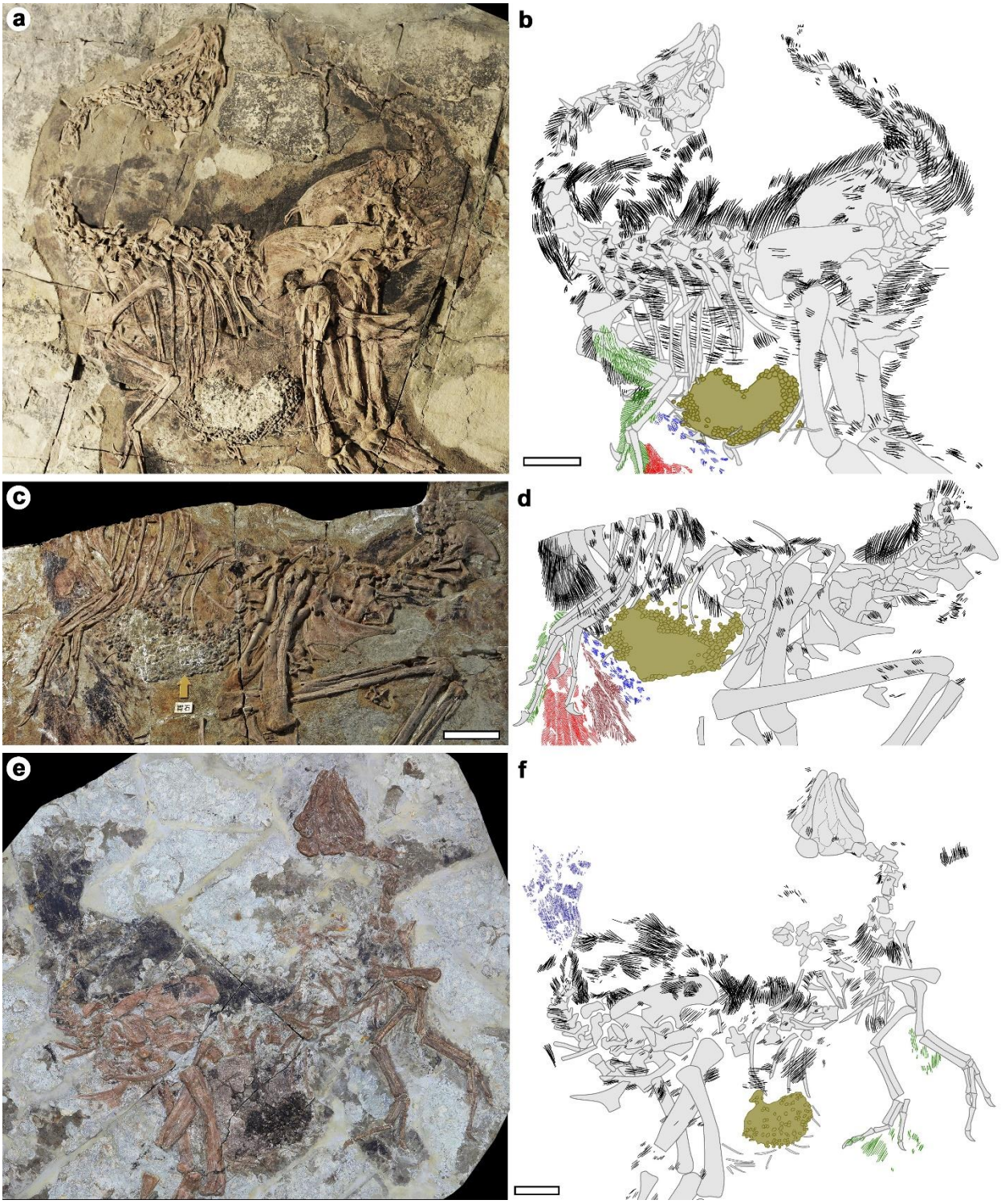

Figure 5.5. Distribution of plumage across the body of multiple *Caudipteryx* specimens. Interpretive drawings: Bones are outlined in grey. Black indicates pigmented body plumage, blue represents the tail fan and secondaries, green represents feathers of the arms and red primaries of the wings. Intestinal contents and gastroliths are presented in olive green. **a-b**. IVPP V12430 and interpretive drawing showing extensive plumage across the body,

neck and tail. There is an absence of pigmented plumage on the ventrum. **c-d**. IVPP V12344 and interpretive drawing with pigmented plumage abundant on the chest and dorsum but absent on the ventrum. **e-f**. DNHM D1242 and interpretive drawing showing pigmented plumage across the dorsum and tail but none on the ventrum. Scale bars represent 5 cm.

5.3.3. Colour predictions

The samples taken from across *Caudipteryx* were predicted as either black or brown with varying degrees of confidence when no shrinkage was modelled (Table 5.4). The first two canonical functions in the CDA accounted for more than 90% of the total observed variance (64.8% and 26% respectively; Table S5.1) and were therefore used to plot the disparity between melanosome colour categories (Fig. 5.6f). The distribution of the predicted colours is shown in (Fig. 5.6). All samples taken from the dorsum were predicted as black and showed typical eumelanosome morphologies (Fig. 5.6e). Conversely, those from the ventral-most plumage along the flank were predicted as being brown, showing more typical phaeomelanin-rich melanosome morphologies (Fig. 5.6e). The tail was predominantly predicted as brown with one black sample near the tip.

5.3.4. Effects of shrinkage

When shrinkage was factored in, no change in the colour predictions was observed for up to 5% shrinkage in either model (Table 5.4). One black prediction changed to grey at 10% shrinkage when all variables were considered with no change in the stepwise results (Table 5.4). A further sample shifted from black to grey at 15% shrinkage in both models. At 20% shrinkage, four of the samples (40%) had changed in the all variables model, and three (30%) in the stepwise model. All but one of these changes was from black to grey likely due to the overlap in morphologies between black and grey melanosomes but generally larger size of grey types (Fig. 1.1a-d).

When both mouldic impressions of melanosomes and 3D melanosomes of the same type were present in a single sample, the size of the moulds relative to 3D melanosomes ranged

from -12.7% to +22.4% (Table 5.5). However, large discrepancies in the sample sizes may explain this wide variation and why in some cases 3D melanosomes were on average larger than moulds in a single sample.

Table 5.4. Palaeocolour predictions for melanosome samples from DNHM D1242 from canonical discriminant analyses (CDA). Predictions are shown "as measured" (colour predictions) and with different degrees of shrinkage modelled. Two different CDA models were used; "all variables" and a "stepwise model". Shrinkage could only be modelled for samples with 3D melanosomes preserved as moulds are thought to retain the original melanosome shape and size. When all variables were considered in the model, more colour prediction changes occurred when shrinkage was tested. "P" indicates probability values.

Sample	Location	Colour prediction	P	5% shrinkage	P	10% shrinkage	P	15% shrinkage	P	20% shrinkage	P
All variables CDA											
1a	Neck	Black	0.88	N/A		N/A		N/A		N/A	
1b	Neck	Brown	0.57	N/A		N/A		N/A		N/A	
2	Neck base	Black	0.90	N/A		N/A		N/A		N/A	
3	Neck base	Black	0.80	N/A		N/A		N/A		N/A	
5	Dorsum	Black	0.92	Black	0.95	Black	0.93	Black	0.90	Black	0.86
6	Dorsum	Black	0.91	N/A		N/A		N/A		N/A	
7	Dorsum	Black	0.96	Black	0.93	Black	0.90	Black	0.85	Black	0.78
8	Tail base	Black	0.92	Black	0.89	Black		Grey	0.80	Grey	0.85
9	Tail base	Black	0.76	N/A		N/A	0.85	N/A		N/A	
10	Tail fan	Brown	0.58	Brown	0.50	Brown	0.42	Brown	0.35	Brown	0.28
11	Tail fan	Brown	0.52	Brown	0.43	Brown	0.35	Brown	0.27	Brown	0.21
12	Tail fan	Brown	0.64	Brown	0.74	Brown	0.65	Brown	0.55	Brown	0.45
13	Tail fan	Black	0.62	Black	0.60	Black	0.58	Black	0.55	Grey	0.59
15	Tail base	Black	0.65	Black	0.66	Grey	0.66	Grey	0.73	Grey	0.80
16	Body	Brown	0.66	Brown	0.58	Brown	0.51	Brown	0.43	Grey	0.37
17	Body	Brown	0.87	Brown	0.90	Brown	0.85	Brown	0.78	Brown	0.70
Stepwise CDA											
1a	Neck	Black	0.60	N/A		N/A		N/A		N/A	
1b	Neck	Brown	0.64	N/A		N/A		N/A		N/A	
2	Neck base	Black	0.90	N/A		N/A		N/A		N/A	
3	Neck base	Black	0.80	N/A		N/A		N/A		N/A	
5	Dorsum	Black	0.94	Black	0.99	Black	0.98	Black	0.97	Black	0.95
6	Dorsum	Black	0.83	N/A		N/A		N/A		N/A	
7	Dorsum	Black	0.95	Black	0.93	Black		Black	0.83	Grey	0.76
8	Tail base	Black	0.91	Black	0.89	Black	0.85	Grey	0.82	Grey	0.88
9	Tail base	Black	0.79	N/A		N/A		N/A		N/A	
10	Tail fan	Brown	0.48	Brown	0.46	Brown	0.44	Brown	0.41	Brown	0.39
11	Tail fan	Brown	0.55	Brown	0.52	Brown	0.48	Brown	0.44	Brown	0.40
12	Tail fan	Brown	0.76	Brown	0.82	Brown	0.78	Brown	0.73	Brown	0.68
13	Tail fan	Black	0.57	Black	0.56	Black	0.55	Black	0.53	Grey	0.54
15	Tail base	Black	0.70	Black	0.81	Black	0.78	Black	0.74	Black	0.69
16	Body	Brown	0.56	Brown	0.49	Brown	0.43	Brown	0.37	Brown	0.32
17	Body	Brown	0.41	Brown	0.87	Brown	0.84	Brown	0.80	Brown	0.76

5.3.5. ToF-SIMS analysis

Key organics associated with melanin in modern samples were observed in the ToF-SIMS data, but only in samples with abundant 3D melanosomes (Fig. 5.6g). Those with predominantly melanosome impressions clustered outside of the fossil melanin region (Fig. 5.6g). This indicates that organics other than melanin dominate where samples contain mainly melanosome impressions while melanin (or diagenetic products derived from melanin) dominates the signal when the sample is mainly composed of 3D melanosomes. The first two PC axes of the PCA accounted for ~61% of the total observed variance (each explaining ~40% and ~21% respectively; Table S5.2) and were used to plot the data in the PCA. Loadings of each variable (mass peak) for the first two PC axes are shown in Figure S5.2.

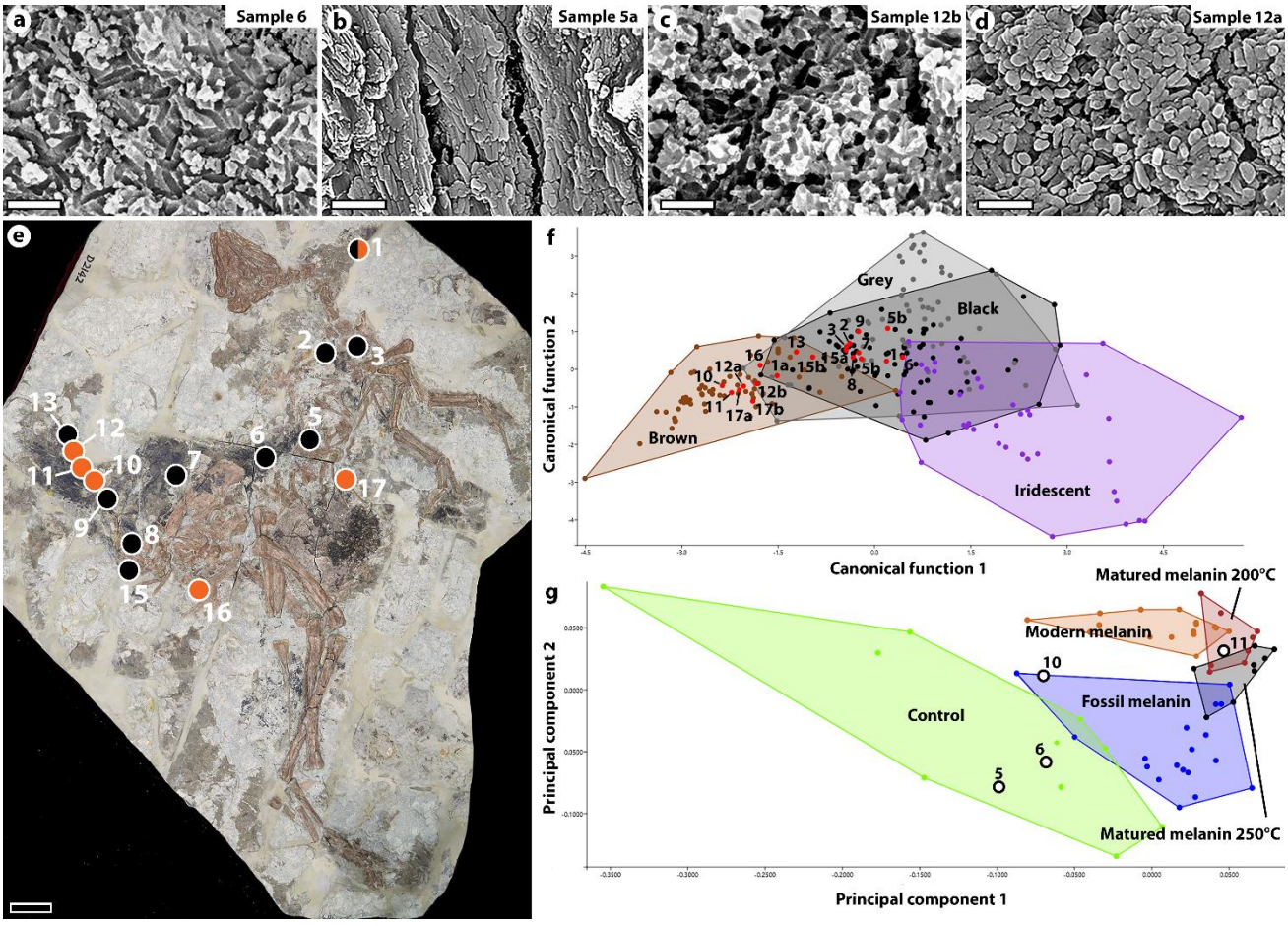

Figure 5.6. Melanosome preservation and palaeocolour predictions in *Caudipteryx* (DNHM D1242). Elongate ellipsoidal melanosomes similar to extant eumelanin-rich melanosomes and predicted as being black are present as both moulds (**a**) and 3D melanosomes (**b**) in certain areas. Smaller spherical melanosomes resembling phaeomelanin-rich modern melanosomes predicted as brown are also common in the fossil as both impressions (**c**) and preserved in 3D (**d**). Colour predictions are mapped out on the fossil (**e**) based on a canonical discriminant analysis (CDA) using modern melanosome data (**f**). Time-of-Flight Secondary Ion Mass Spectrometry (ToF-SIMS) data showing key chemical compounds associated with melanin (based on 54 mass peaks) are shown in a PCA with modern, matured and fossil melanin data along with non-melanin controls (**g**). Numbered points in the CDA and PCA plots correspond to samples from the fossil. Scale bars represent 2 µm in (a-d) and 5 cm in (e).

5.4. Discussion

5.4.1. Feather morphology and plumage colouration of Caudipteryx *– ecological implications*

Caudipteryx shows plumage unlike any other known extinct theropod dinosaur, but with notable similarities to several extant birds. Many features are likely explained by primary flightlessness (Dyke and Norell 2005).

Table 5.5. The difference in melanosomes measurements between moulds and 3D melanosomes when present within a single sample. N = number of melanosomes measured.

Sample	Measurement	Moulds (nm)	N	3D (nm)	N	Difference (nm)	Percentage (%)
5	Length	1039.42	94	805.71	100	233.71	22.48
	Width	298.98	94	236.67	100	62.31	20.84
12	Length	669.2	137	651.29	248	17.91	2.68
	Width	411.69	137	396.2	248	15.49	3.76
15	Length	765.35	27	862.57	10	-97.22	-12.70
	Width	294.27	27	314.33	10	-20.05	-6.81
17	Length	628.97	25	587.96	138	41.00	6.52
	Width	375.97	25	341.26	138	34.71	9.23

Feathers across the body appear more filamentous with no clear vanes, reminiscent of "protofeathers" seen on taxa such as *Sinosauropteryx* (Chapter 4; Chen et al. 1998) or mammal hair (Fig. 5.3c-d). The pennaceous body contour feathers of most extant birds serve, in part, to smooth the surface of the body, reducing drag and increasing aerodynamic efficiency for flight (Homberger and de Silva 2000; Butler et al. 2008). In the flightless *Caudipteryx* there would have been no need for a smooth body profile, and instead a thick shaggy coat of feathers was present. This is similar to extant ratites, many of which also have a similar overall body plan to *Caudipteryx* and are also cursorial runners, as suggested for *Caudipteryx* (Persons et al. 2013). The function of these feathers may have been similar to those of extant ratites owing to their morphological similarity. Ostriches for example use their body feathers for thermoregulation, erecting or flattening them to heat or cool themselves respectively (Louw et al. 1972). The palaeoclimate experienced by the Jehol Biota has been debated, with evidence of cold spells punctuating a generally warm global trend (Amiot et al. 2011; Zhou 2014). It has been suggested that integumentary structures such as feathers being present on many Jehol vertebrates indicates insulatory roles (Amiot et al. 2011), which would support the current interpretation of the body plumage of *Caudipteryx*. Additionally, *Caudipteryx* appears to have had plumage on its legs (Fig. 5.3d), unlike ratites which have naked legs and live in generally hot climates. The lack of feathers preserved on the ventrum of *Caudipteryx* is more likely an artefact of feather taphonomy than an original condition (Vinther 2015*a*). As only originally pigmented regions of feathers preserve in fossils (Chapter 1; Vinther et al. 2008; Vinther 2015*a*), the lack of plumage on the ventrum of *Caudipteryx* (Fig. 5.5) likely represents countershading (Thayer 1896; Rowland 2009, Allen et al. 2012, Vinther et al. 2016; Smithwick et al. 2017*a*).

Countershading has been described in two other Jehol dinosaurs – one herbivore and one carnivore/omnivore (Vinther et al. 2016; Smithwick et al. 2017*a* – Chapter 4) - and therefore appears to be a common colour pattern in the Early Cretaceous, much as it is in modern ecosystems (Thayer 1896; Rowland 2009; Allen et al. 2012). The countershading pattern of *Caudipteryx* can inform the likely habitat it lived in thanks to data on countershading transitions and lighting environment in modern animals (see Chapter 4; Allen et al. 2012;

Vinther et al. 2016; Smithwick et al. 2017*a*). As dark plumage is present low on the chest (Fig. 5.3a) and under the base of the tail (Fig. 5.3b) but absent on the ventral-most abdomen (Fig. 5.5), it seems that the dark-light transition is low on the body. This suggests it was better adapted to living in a closed forested habitat, similar to what has been inferred for the herbivorous ornithischian dinosaur *Psittacosaurus* (Ornithischia: Ceratopsia) (Vinther et al. 2016). As a relatively small suspected herbivore (Zhou and Wang 2000; Norell et al. 2001; Persons et al. 2013), living in a forested habitat and having a countershaded pattern would have afforded *Caudipteryx* some protection in the form of 3D camouflage from the many larger theropods it coexisted with, as in *Psittacosaurus* (Vinther et al. 2016).

Unlike the body feathers, the rectrices and remiges of *Caudipteryx* are pennaceous (Figs. 5.2 and 5.4); the only feathers on the theropod with clear vanes. They are also symmetrical, unlike flight feathers in extant birds which show a distinct asymmetry (Feduccia and Tordoff 1979). In extant birds, feathers used for communication are usually pennaceous where colour patterns can be displayed across the feather vanes (Brush 2000; Li et al. 2010). Without pennaceous feathers, colour patterns can only be generated between, rather than within feathers (Li et al. 2012). Pennaceous feathers can also be held out rigidly from the body to create a display surface in a way not possible with non-pennaceous feathers. That the most striking banding is in the pennaceous wing and tail feathers, features that could likely easily be lifted and erected in display (Persons et al. 2013; Pittman et al. 2013), suggests that *Caudipteryx* used them for communicative purposes. Display has been assumed the most likely function for the wings and tail of *Caudipteryx* owing to its flightless nature (Persons et al. 2013; Pittman et al. 2013; Talori et al. 2018).

The tips of the primaries (Fig. 5.4) may also represent colour patterns. The tapering of some remiges and large gap in pigment in others are likely artefacts of feather taphonomy with gaps representing unpigmented regions in life, although a crack in the matrix of IVPP V12430 could have contributed to loss of soft tissues in this area (Fig. 5.4c-d).

The subtly banded tail of DNHM D1242 was brown and black with some white bands (Fig. 5.2c-d and 5.5). The precise colour patterns of the banding are difficult to determine for

certain with the current number of samples, but general patterns can nevertheless be surmised. As unpigmented gaps only appear obvious on the lateral rectrices, white bands may have been restricted to the margins of the tail fan. Based on melanosome morphologies, the middle of the tail fan was likely banded brown and black (Fig. 5.6). A brown and black banded tail with black and white bands on the lateral margins is therefore considered here to be the most parsimonious reconstruction. While no specimen with a strongly banded tail could be sampled, as the unpigmented gaps are prevalent throughout, they must have been banded white and pigmented. A previous report of melanosomes in PMoL AD00020 found only those predicted as black (Li et al. 2014), making it likely that specimens with strongly banded tails had black and white bands.

The absence of secondaries in all specimens with strongly banded tails (Fig. 5.4e-f) is of note. A genuine absence of these feathers in some but not all specimens would be hard to explain, given that they show exceptional preservation of the primaries. Again, rather than this unlikely scenario, it is more likely that these plumage areas were unpigmented originally (Vinther 2015*a*). Therefore, the specimens with a strongly banded tail may have also had completely unpigmented secondaries, and thus most of the exposed portion of the wing would be white. It is uncertain whether the two specimens showing banded secondaries (IVPP V 12344 and IVPP V 12430) had the tail fan morphotype with strong or subtle banding, but it is possible that this was a condition of those with the weaker banding. Although the wings could not be sampled to determine the likely colour, it is considered likely that due to the similarity of the subtle tail banding in DNHM D1242 to the banded secondaries, they may have been similarly coloured (brown, black and white).

The plumage of *Caudipteryx* therefore appears to have been a mixture of camouflage, with dark earthy colours such as black and brown (often associated with crypsis in extant birds; Gomez and Théry 2007) and countershading, and conspicuous display features like the abundance of barred plumage and white wings. These features may seem at odds with one another, however as observed in extant avians, plumage patterns can serve a dual camouflage and signalling function (Gluckman and Cardoso 2010; Marques et al. 2016). The barring on *Caudipteryx* is in areas that could plausibly also be made less conspicuous when necessary. For

example, the short and deep tail was suited for supporting the tails fan and moving it when it needed to be more conspicuous in display or lowered to be less conspicuous (Persons et al. 2013; Pittman et al. 2013). The conspicuous wings could have been folded away, and barring on the ventral tail base would not be as conspicuous as plumage on the dorsum. In extant birds, barring used for conspecific signalling is more prevalent on the ventrum than the dorsum for the same reason (Gluckman and Cardoso 2010). Additionally, the banding on the tail could have served as a form of disruptive camouflage, helping to break up the outline of the fan (Stevens et al. 2006; Webster et al. 2013). This could particularly be the case for the fan with only white bands at the periphery, as this is a common feature in disruptive camouflage patterns where only the boundary is disrupted (Stevens et al. 2006).

5.4.2. Potential for dimorphic plumage

The two different wing colour patterns in *Caudipteryx* appear to relate to two tail morphs and potentially to differences in the body plumage. It is therefore plausible that dimorphism exists in the plumage of *Caudipteryx,* with one morph having conspicuous white wings and a strongly banded tail fan, while the other morph has less conspicuous banded wings, a more subtly banded tail and thicker pigmented plumage across the body. The hypothesised full reconstruction of the two potential colour morphs are presented in Figure 5.7. Generally, finer barring is invoked in sexual signalling in extant birds (Gluckman and Cardoso 2010; Marques et al. 2016). The finest barring in *Caudipteryx* is on the strongly barred tails, with individuals possessing wing barring showing bands 2-3 times as wide.

Plumage dimorphism, or 'dichromatism' is common in extant birds and is thought to be driven by sexual selection and predation pressure (Kimball and Ligon 1999). It is therefore plausible that the specimens represent both males and females with different plumage patterns. Those with the strongly banded tail and white secondaries could represent males, because males are most often the more conspicuous and showy sex in birds (Kimball and Ligon 1999; Hill and McGraw 2006*a*; Gomez and Théry 2007). The white on the wings is reminiscent of male ostriches that use their wings in "kantling" displays to potential mates and to deter rival

males (Bolwig 1973; Bonato et al. 2009). The strongly banded tail almost certainly represents a display structure (Persons et al. 2013; Pittman et al. 2013) and therefore being more pronounced in the male matches expectations.

Figure 5.7. Reconstructed colour patterns in *Caudipteryx* – two potential colour morphs based on differences seen in the plumage of the fossils. One morph shows a larger strongly banded black and white tail and white secondaries, while the other morph has a smaller more subtly banded tail with rufous bands and banded secondaries. These differences are consistent with a sexually dichromatic hypothesis. Both morphs show a low countershading transition indicative of adaptation to a closed environment.

Alternatively, the occurrence of two morphs could represent ontogenetic changes or taxonomic differences. The only specimen with the subtly banded tail (DNHM D1242) was smaller than all other individuals for which overall body size could be measured (780 mm from the distal tip of the tail fan to the tip of the jaws). However, a range of sizes and relative body

proportions was observed for the other specimens that don't appear to correlate to plumage type (Table 5.2). Additionally, no distinct differences in the plumage were observed between the two described species of *Caudipteryx*; *C. zoui* and *C. dongi.*

5.4.3. Are there two species of Caudipteryx*?*

C. zoui and *C. dongi* were differentiated from one another based on differences in skeletal morphology. Specifically, *C. dongi* was said to have a relatively longer ilium and a relatively smaller sternal plate (Zhou and Wang 2000). However, my compiled dataset of anatomical measurements calls this distinction into question. There is as much variation within the specimens of *C. zoui* as there is between the two proposed species (Table 5.2). I also find that the only described specimen of *C. dongi* has the same banded secondaries present on at least one specimen of *C. zoui* (IVPP V 12430). In the absence of other autapomorphies that I am aware of, I consider all described specimens of *Caudipteryx* to be individuals of a single species, *Caudipteryx zoui*, until further taxonomic work can otherwise demonstrate.

5.4.4. Melanosome taphonomy

Melanosomes preserved in fossils from the Jehol Biota are often preserved as moulds (Fig. 5.6a and c; Zhang et al. 2010). While these moulds are sometimes in mineral grains, they are most often preserved in an unidentified organic matrix. The ToF-SIMS data reveal that only when 3D melanosomes are present in abundance are melanin signals dominant (Fig. 5.6g). Samples with mainly impressions gave spectra of non-melanin organics of unknown origin (Fig. 5.6g). I hypothesis that these organics are likely kerogen, the most common organics found in rocks (Vandenbroucke and Largeau 2007) which have retained the impressions of melanosomes after loss through oxidation or a similar process.

5.5. Conclusions

Through the first comprehensive analysis of the plumage of the oviraptorosaur *Caudipteryx*, I show a range of colour patterns and feather morphologies similar to those seen in living birds

were present. The features of the plumage, including symmetrical wing and tail feathers and a thicker shaggier covering of body feathers are likely related to the flightless nature of *Caudipteryx* and indicate a similar ecology and behaviour to some large living ratite birds. A low countershading transition on the body suggests adaptation to a closed forested habitat and distinctive barred plumage on the tail and wings indicate both display and camouflage functions. Two colour morphs appear to exist, suggesting potential sexual dichromatism, the first record of this in a non-avian theropod.

Chapter 6 – Testing and refining methods for extracting melanosomes from feathers for palaeocolour investigations

Abstract: Imaging melanosomes from extant avian feathers has been key in reconstructing colour in extinct animals. A variety of techniques, including imaging melanosomes in-situ within feather keratin and extracting and isolating them for imaging have been utilised in both palaeocolour work and studies into melanin in living animals. The most relevant of these techniques to palaeocolour is the extraction of melanosomes through enzymatic degradation of feather keratin. However, the enzymes used can degrade phaeomelanin, making the technique inappropriate for extracting phaeomelanin-rich melanosomes, and each extraction is time consuming, making large datasets hard to compile. Here, several techniques for extracting melanosomes from feathers including mechanical splitting/cutting and enzymatic extraction are investigated. While feather barbs can be readily split or cut to reveal melanosomes, those from barbules are difficult to reveal mechanically. Revision of the most commonly used enzymatic protocol by reducing the number of steps allowed phaeomelanin-rich melanosomes to be successfully extracted and SEM imaged. These revisions can aid both palaeocolour and extant melanosome studies by reducing the quantity of enzymes needed and allowing for more samples to be prepared in a shorter space of time, permitting generation of larger datasets.

This chapter is currently **unpublished** but has been submitted for publication along with Chapter 7 as a single paper to the journal *Proceedings of the Royal Society B: Biological Sciences*.

Author contributions – The author devised the concept for this chapter, performed all extractions and SEM imaging, wrote the chapter and produced all figures. Frane Babarović and Zoe Spicer assisted with the resin-setting and mechanical fracturing of the feathers. Chis Neal assisted with resin setting and microtoming of feathers.

6.1. Introduction

Melanin is the most ubiquitous pigment in extant vertebrates, and the fossil record suggests that its importance is likely as old as the clade itself (Chapter 1.1; Hill and McGraw 2006*b*; Vinther 2015*a*). Melanins are found in multiple forms, but the most important in vertebrates are eumelanin, which imparts dark colours including black, and phaeomelanin which imparts lighter browns to rusty reds (Chapter 1.1; McGraw 2006*b*). The chemical structure of these two melanin types is not fully understood, despite over 70 years of study (Mason 1948; Galván and Solano 2016). The process by which melanin is synthesised in vertebrates is however better known (see Chapter 1.1).

Importantly for palaeocolour studies, distinct melanosome morphologies can inform as to the colours they produce in at least birds and mammals (Fig. 1.1.; Chapter 1; Li et al. 2014), allowing colour to be determined through morphological analysis of melanosomes (Liu et al. 2005*a*; Li et al. 2010, 2012). This has been called into question recently (Galván and Solano 2016; Negro et al. 2018) and palaeocolour studies that use melanosome morphology to predict likely colours in extinct taxa have been challenged (Moyer et al. 2014; Negro et al. 2018). In order to better investigate this, melanosomes need to be imaged to allow their shape to be ascertained, which means extracting them from the integumentary tissues in which they sit.

Early investigations of integumentary melanin mainly focussed on human hair (e.g., Birbeck et al. 1956; Arnaud and Bore 1981; Borovanský and Hach 1986; Liu et al. 2003). Over the past 15 years or so, and particularly since the advent of the field of palaeocolour around a decade ago, focus has shifted to other vertebrate systems, particularly avian feathers (e.g., Shawkey et al. 2003; Li et al. 2010, 2012; Colleary et al. 2015). This is in part due to the study of palaeocolour in extinct feathered dinosaurs, whose direct descendants are the birds (Chapter 1; Ostrom 1976). Multiple techniques have been employed to investigate melanin in-situ in extant feathers, for example through the use of transmission electron microscopy (TEM) and tissue staining. These often fail to reveal the 3D morphology of melanosomes, however. For this, melanosomes must be removed from hair or feathers and various methods have been developed to achieve this.

Melanin isolation techniques include using acid/base and enzymatic extractions, both of which aim to degrade keratin in integumentary structures (e.g., hair, feathers and scales) leaving only melanosomes. Many different protocols have been tested over the past half-century with varying degrees of success (Birbeck et al. 1956; Filson and Hope 1957; Roy and Roy 1965; Bolt 1967; Wolfram et al. 1970; Bratosin 1973; Arnaud and Bore 1981; Krol and Lieber 1998; Novellino et al. 2000; Liu et al. 2003; Colleary et al. 2015; Sun et al. 2017). Several of these methods were extensively evaluated by Liu et al. (2003) who confirmed previous observations that acid/base methods showed destruction of melanosomes and alteration of the molecular structure of the melanin, making them inappropriate for investigating melanosomes either morphologically or chemically (Liu et al. 2003). Enzymatic extraction of eumelanin-rich melanosomes using Proteinase K and Papain, based on the original protocol of Novellino et al. (2000), was found to be the least destructive technique, removing keratin without damaging "eumelanosome" structure. This protocol resulted in approximately 2.3% of the mass of the original hair samples remaining as a black pellet that was entirely composed of melanosomes. A follow-up study looking at both black and red human hair utilised the same extraction protocol and showed that eumelanin-rich melanosomes (which dominated black hair samples) had ellipsoidal shapes with smooth surfaces, while phaeomelanin-rich melanosomes (which dominated red hair samples) were smaller and usually more rounded with rougher surfaces (Liu et a. 2005*a*). This study also showed that the enzyme extraction protocol is not well suited to phaeomelanin extraction as "phaeomelanosomes" can lose their structural integrity and were prone to breaking apart due to the action of the enzymes and washing by surfactants and water (Liu et al. 2005*a*).

Despite the issues with phaeomelanin-rich melanosome extraction, the original Liu et al. (2003) enzymatic technique has been subsequently adapted and used in studies looking both at modern melanin and by palaeocolour studies comparing fossil melanosomes to their extant counterparts (Chapter 1; Colleary et al. 2015). Once extracted from keratin, melanin can be analysed using multiple analytical techniques to probe the chemical and physical properties of the pigment. For palaeocolour work, the understanding of both the chemical makeup and morphology of melanosomes is key in extant taxa to allow comparison to fossilised

melanin/melanosomes (Chapter 1; Colleary et al. 2015; Vinther 2015). One of the most important methods for palaeocolour work is scanning electron microscope (SEM) imaging of melanosomes. This method allows morphological measurements to be made to compare extinct with extant quantitatively (see Chapter 1.5).

Alternative methods to the Liu et al. (2003) extraction protocol have been used in several studies involving SEM imaging of melanosomes (including phaeomelanin-rich melanosomes), including setting feathers in resin and fracturing (e.g., Zhang et al. 2010) or cutting them (e.g., Shawkey et al. 2003; Li et al. 2010, 2012). However, these techniques may be limited in scope for palaeocolour work compared to enzymatic extractions because only a single planer area of a feather can be exposed, which may not reveal all of the constituent melanosomes which are often distributed within the 3D volume of the feather rachis, barb and barbule (F.M.S pers. obsv.). Additionally, these techniques often only investigate melanosomes from the barbs (which are easier to cut or split) rather than the barbules, which could limit comparisons to fossils as most of the melanosomes are found in the latter in many cases (Vinther 2015*a*).

Due to the propensity for phaeomelanin-rich melanosome damage during enzymatic extractions and the need to accurately assess melanosome morphology in extant feathers for palaeocolour work, here I explore a number of techniques to reveal melanosomes from within the keratin of modern feathers. These techniques include both mechanical (splitting and cutting of resin-set feathers) and enzymatic extractions. Both black and rufous feathers are used as test cases as they likely represent the extremes of each melanin type in terms of pigment content and so the relative success of each can be compared. The Liu et al. (2003) protocol involves many steps and takes a minimum of seven days to complete per sample, making large sample quantities (important for palaeocolour work) hard to obtain in a short space of time. Devising a technique that allows more samples to be prepared in a shorter space of time will allow for more detailed investigations of extant melanin-bearing integumentary tissues. It will also allow for larger datasets to be produced for palaeocolour studies, increasing the power of subsequent statistical analyses. As over 10,000 extant bird species are known, that exhibit a wide range of melanin-based colours (McGraw 2006*b*), a larger dataset than is currently

available is desirable to gain a better understanding of the relationship between melanosome morphology and the colours produced.

6.2. Material and methods

6.2.1. Sampling

As most palaeocolour studies focus on melanin preserved in feathers, these were the focus of the current work. Feathers from three extant taxa, the wrinkled hornbill (*Rhabdotorrhinus corrugatus*), the common pheasant (*Phasianus colchicus*) and the common kingfisher (*Alcedo atthis*) were used. The feathers of *R. corrugatus* are black, while those of *P. colchicus* and *A. atthis* are rusty red/brown (rufous). Rufous feathers from these two taxa were chosen as they show different feather structure, with those of *A. atthis* being more gracile than those of *P. colchicus* despite them both being coverts. Feathers were obtained from the Zoological Museum, Natural History Museum of Denmark, University of Copenhagen.

6.2.2. Enzyme extraction protocol

To investigate the effectiveness of the enzymatic extraction methodology, each feather type was first subjected to a recently modified version (Colleary et al. 2015) of the original Liu et al. (2003) extraction protocol. A series of experiments using revised steps of the same protocol was then performed on the same feather types. A minimum of seven steps are involved in the original extraction protocol (with some steps repeated if degradation is not sufficient), described here in brief (for the full original process see Liu et al. 2003): (1) small samples from each feather (approximately 1 cm^2) were removed and washed three times in ethanol and once in Purite (Purite Ltd) water, with a few seconds of vortexing after each wash. (2) samples were placed in Eppendorf tubes with a solution of Dithiothreitol (DTT) and phosphate buffered saline (PBS) at a concentration of 10 mg DTT powder to 1 ml PBS. These were incubated in a shaker for 24 hours at 37°C and 200 rpm. (3) The solution was then removed and a new solution of DTT, PBS and Proteinase K added (10 mg DTT, 0.4 mg Proteinase K to 1 ml PBS). This was

incubated as before for 24 hours. After this step, most of the feather structure had degraded and a pellet formed at the bottom of the tube. (4) the supernatant was removed, and the pellet washed six times in Purite, vortexing and centrifuging (at 3300 g) each time to reduce material loss. A solution of DTT, PBS and Papain was added (5 mg DTT, 1 mg Papain to 1 ml PBS) and incubated as before for 24 hours. (5) the supernatant was then removed, and a further six washes were carried out as before with Purite. Another solution of DTT, PBS and Proteinase K was added (2 mg DTT, 0.4 mg Proteinase K to 1 ml PBS) and incubated for 24 hours. (6) the supernatant was removed, and a solution of 2% Triton-X added and stirred for four hours. This solution was removed, and the pellet washed once in ethanol and eight times in Purite. (7) the same solution of DTT, PBS and Proteinase K from step 5 was added and incubated for another 24 hours. (8) after supernatant removal the final pellet was washed three times in Purite. Approximately 1 µl of the pellet was then removed for SEM imaging.

For palaeocolour studies assessing the morphology of preserved melanosomes, it is enough to expose melanosomes to a level where their shape can be quantified. As the full extraction protocol removes all keratin, leaving only melanosomes, it is likely that a shortened procedure would be enough to expose melanosomes from the keratin for SEM imaging. It may also be the case that the degradation of phaeomelanin-rich melanosomes during the extraction process may be due to the long duration samples spend in active enzyme solution. Alternatively, it could be the high number of washes (at least 24 per sample), vortexing and subsequent centrifugation of each sample that results in damage or loss of phaeomelanin-rich melanosomes (Liu et al. 2005*a*). To this end, the extraction protocol was modified using a variety of numbers of steps, different quantities of the enzymes and different amounts of time of exposure to the enzymes. The aim was to determine the minimum number of steps required to expose melanosomes sufficiently to SEM image them and to determine whether phaeomelanin-rich melanosomes could be effectively exposed without damage. Preliminary tests showed that in many cases, a partial or even complete removal of keratin from feather samples could be achieved after the first step involving a solution of DTT, PBS and Proteinase K. Therefore, each experimental run was carried out after washing the samples three times in acetone and once in Purite (step 1) and incubating them in DTT and PBS for 24 hours (step 2).

The third step was modified in 12 different ways to test for the most efficient method (Table 6.1). Each test run produced a pellet that was consistent with the original colour of each feather. Approximately 1 µl of each pellet was mounted on SEM stubs for imaging. Twelve samples could be placed on a single SEM stub (Fig. S6.1a). In addition, some samples were only subjected to the washing (step 1) and incubation in DTT and PBS (step 2) before being SEM imaged to determine whether any degradation of the feather had occurred that would allow melanosomes to be exposed prior to the addition of any enzymes.

Because the main aim of these tests was to determine the minimum number of steps and enzyme quantities required to expose melanosomes for SEM imaging, the chemical purity of the resulting feather residue was not a priority. Additionally, if repeated washing contributes to phaeomelanin-rich melanosome degradation or material loss, minimising the number would be a benefit (it was noted that the amount of material in rufous feather samples reduced with each wash despite careful supernatant removal). Therefore, in addition to revising the steps involved, tests were also run to determine the minimum number of washing steps required to allow melanosomes to be exposed under SEM. To determine this, six examples of the same feather type were subjected to the most effective revised extraction protocol and after step 3 were washed from 1-6 times in Purite with a single sample left unwashed.

In a number of tests, particularly longer exposures of the rufous feathers, it was noted that as well as a pellet at the base of the tube, the supernatant had a rusty hue. To test whether this was due to dispersed melanosomes or melanin, the supernatant from each test was kept. One supernatant sample from the 24-hour test in Proteinase K for each feather type was dried under a fume hood and one of each had a drop of 10% acetic acid added in an attempt to cause any melanin to settle into a pellet. Around 1 µl of the resulting pellet was removed from each for SEM stub mounting (Fig. S6.1b).

Table 6.1. Experimental procedures to test for the minimal amount of time needed to expose melanosomes for SEM imaging and measuring of their shape.

Experiment number	Enzyme used	Quantities used	Time incubated
1	Proteinase K	10 mg DTT, 0.4 mg enzyme to 1 ml PBS	24 hours
2	Papain	10 mg DTT, 0.4 mg enzyme to 1 ml PBS	24 hours
3	Proteinase K	10 mg DTT, 0.4 mg enzyme to 1 ml PBS	Eight hours
4	Papain	10 mg DTT, 0.4 mg enzyme to 1 ml PBS	Eight hours
5	Proteinase K	10 mg DTT, 0.4 mg enzyme to 1 ml PBS	Four hours
6	Papain	10 mg DTT, 0.4 mg enzyme to 1 ml PBS	Four hours
7	Proteinase K	10 mg DTT, 0.4 mg enzyme to 1 ml PBS	Two hours
8	Papain	10 mg DTT, 0.4 mg enzyme to 1 ml PBS	Two hours
9	Proteinase K	20 mg DTT, 1 mg enzyme to 1 ml PBS	24 hours
10	Proteinase K	10 mg DTT, 0.2 mg enzyme to 1 ml PBS	24 hours
11	Proteinase K	20 mg DTT, 1 mg enzyme to 1 ml PBS	Eight hours
12	Proteinase K	10 mg DTT, 0.2 mg enzyme to 1 ml PBS	Eight hours

6.2.3. Resin-setting

To determine whether feathers could be either mechanically fractured or precisely cut to reveal the melanosomes sufficiently to allow SEM imaging and measuring, a series of tests were performed, setting feather samples in different resins and using different technique to split/cut them. Melanosomes are often present in the barbs and barbules of feathers but can also be found in the rachis. However, it is thought that most of the melanosomes that impart colour to feathers are found within the barbules, particularly in species showing iridescence (Maia et al. 2011). In most fossil feathers the barbules often have the highest density of preserved melanosomes (Fig. 1.3). To date, only barbs have successfully been cut or fractured mechanically to reveal melanosomes sufficiently to allow SEM imaging and measurements, and only chemical extraction techniques have allowed reliable SEM imaging of barbule melanosomes. Most analyses of barbule melanosomes have involved in-situ imaging techniques such as TEM and thin-section light microscopy (e.g., Shawkey et al. 2003, 2005; Doucet et al. 2004, 2006; Maia et al. 2010; Li et al. 2010, 2012) which are not suitable for assessing melanosomes 3D morphology. Therefore, a technique that could split or cut the barbules of

modern feathers allowing SEM imaging of the melanosomes within would aid comparisons of fossil and extant samples. This would prove particularly useful for imaging phaeomelanin-rich melanosomes, as it would avoid any potential morphological alteration induced by enzymatic extractions.

Feathers were set into four different resin types. Three of these were used for fracture tests and two for cutting tests based on their known mechanical properties. The resins used for fracture tests were Durcupan 1 (Hayat 1989), Durcupan 2 (Cold Spring Harbour Protocol Mixture) and Epon (TAAB 812). Durcupan 1 and Araldite (Huntsman Advanced Minerals) were used for cutting tests.

Sections of feather measuring around 5 mm in length that included the rachis, barbs and barbules were used. Feather sections were embedded in each resin type in accordance with previously established techniques (Shawkey et al. 2003).

For Durcupan and Epon setting, the feather sections were placed in glass vials and incubated in 0.25 M sodium hydroxide and 0.1% Triton-X for 30 minutes in a shaker. Samples were then moved to ethanol for two and half hours before being dehydrated through incubation twice for ten minutes each time. They were then incubated in either propylene oxide (for Epon) or acetone (for Durcupans 1 and 2). Samples were then infiltrated with successive concentrations of the resins (15%, 50%, 75% and 100%). Each infiltration was allowed to run for 24-48 hours. After the 100% infiltration the glass vials were cured in an oven at 20 °C for 24 hours. For the Araldite setting, Araldite Rapid Epoxy Adhesive was used in accordance with the product guidelines. This two-part resin sets within five minutes and no further treatments were required once the resin had set around the feather.

6.2.4. Mechanical fracturing of resin-set feathers

Resins set in glass vials has all glass removed using a pneumatic air scribe (Ken Mannion Model TT). To mechanically split the feathers set into Durcupans 1 and 2 and Epon, small cuts were first made using a hacksaw (with the sample held firmly in a vice) along the longitudinal plane

of the feather until the blade almost touched the edge of the feather. This was done on all four sides to help direct the fracture along the plane of the feather. Initial experiments without first making these cuts showed that fractures would occur at random in the resin with no control over direction or plane of splitting, with most splitting around the feather rather than through it. A hammer and fine chisel were used to fracture the cut resin block in an attempt to split the feather. In most cases this happened through the feather as desired, but in a few instances the fracture ran conchoidally, sometimes through the feather and sometimes around it. The split resin blocks were assessed to see which had the most feather material exposed on the fresh surface.

6.2.5. Ultramicrotome cutting of resin-set feathers

To determine whether more precision could be obtained in opening the feather to reveal the internal melanosomes, feather samples set in Durcupan 1 and Araldite were cut using a Reichert Jung Ultracut E ultramicrotome with a glass knife. Multiple methods of cutting were employed, with the feather in different orientations. This was to determine whether cutting the barb along different axes would reveal more/fewer melanosomes and would determine differences in the structure of the barbules. Both ultra-thin sections (5 µm) and larger blocks (around 8 mm) were cut.

6.2.6. Mechanical feather breakage

To determine whether melanosomes could be exposed from within feather keratin without the need for enzyme extractions or resin-setting, additional tests were carried out to mechanically fracture feathers. The feathers were washed in acetone and then ground in a mortar and pestle with acetone and the resulting residue removed for SEM imaging.

6.2.7. SEM imaging

Samples from the pellets produced from the enzymatic extraction, resin-set feather samples (both mechanically split and cut) and mechanically ground feathers were mounted on copper tape-covered SEM stubs. These were sputter coated with gold (2.5 nm for the pellets and 10 nm for the resin-set feathers) using a Quorum Q150R ES sputter coater. Samples were then imaged using a Zeiss Evo15 Environmental Scanning Electron Microscope (ESEM) under high vacuum using 10-20 KeV accelerating voltage at a working distance of 10 mm.

6.3. Results

6.3.1. Enzyme extractions

The feathers subjected to the full extraction protocol (Liu et al. 2003; Colleary et al. 2015) showed complete degradation of all keratin. Black feather samples were reduced to a small black pellet in the Eppendorf tubes. Rufous feathers showed no visible material left in the tubes. This occurred from step 5 (the addition of papain) onwards, suggesting that phaeomelanin-rich melanosomes had been lost by this point. Under SEM imaging, black samples were found to be entirely composed of oblong-shaped (presumably eumelanin-rich) melanosomes with no evidence of any other material. Samples from rufous feathers however showed nothing remaining, indicating that all keratin and melanin had been lost during the extraction process. Feathers that had only been subjected to the first and second steps (i.e., with no exposure to enzymes, only DTT and PBS) showed some degradation, but no exposure of melanosomes (Fig. S6.2).

The results of the revised extractions are summarised in Table 6.2. The amount of time spent in the enzyme solution and the type of enzyme used showed high variability in the resulting degradation of the feathers (Fig. 6.1). Comparison between the two enzymes tested, Proteinase K and Papain, shows that only Proteinase K is suitable for reliable melanosome extractions by itself. Papain proved an unreliable enzyme, with some tests resulting in melanosomes being exposed, but many had none exposed (melanosomes were never exposed

from the pheasant feather, Fig. 6.1) and in no case was the feather completely degraded (Table 6.2). The feather types were not affected equally by the enzymes. For example, melanosomes were exposed in every test in the rufous kingfisher feather (Fig. 6.1), but only in 67% of the tests in the rufous pheasant feather. The black hornbill feather had melanosomes exposed in 75% of test cases. In terms of the completeness of the feather degradation, it also seems that feather morphology and/or taxonomy has a strong control. The kingfisher feathers were completely degraded in 42% of the test runs (the same as the hornbill feathers), whereas the pheasant feathers were only completely degraded after the full 24 hours in Proteinase K (Fig. 6.1g), suggesting fundamental differences in the keratin structure. When only half the quantity of Proteinase K was used, feather degradation was less in all samples, but melanosomes were still sufficiently exposed to allow measurements in line with fossil samples.

In terms of the duration of exposure to Proteinase K, the rufous feathers appear to have degraded the fastest. Melanosomes were exposed in all rufous cases with Proteinase K irrespective of duration. The black hornbill feather showed abundant exposed melanosomes in all Proteinase K cases except for the two-hour run where few were exposed from the only partially degraded keratin (Fig. 6.1), suggesting that in this case a minimum of four hours was needed for the enzyme to sufficiently degrade the keratin to expose melanosomes.

Table 6.2. Results from the different tests (step 3) of the extraction protocol. Exposure of melanosomes suitable for measuring (Y = yes, N = no) and level of feather degradation are reported. Partial indicates that the feather was not completely degraded, and some keratin structure remained while complete indicates that no feather/keratin structure remained. Rufous 1 = *Phasianus colchicus; Rufous 2 = Alcedo atthis*; Black = *Rhabdotorrhinus corrugatus.*

			Melanosomes exposed under SEM?			**Feather degradation**		
Experiment	**Enzyme**	**Extraction time**	Rufous 1	Rufous 2	Black	Rufous 1	Rufous 2	Black
1	Proteinase K	24	**Y**	**Y**	**Y**	**Complete**	**Complete**	**Complete**
2	Papain	24	*N*	**Y**	**Y**	*Partial*	*Partial*	*Partial*
3	Proteinase K	8	**Y**	**Y**	**Y**	*Partial*	**Complete**	**Complete**
4	Papain	8	*N*	**Y**	**Y**	*Partial*	*Partial*	*Partial*
5	Proteinase K	4	**Y**	**Y**	**Y**	*Partial*	**Complete**	*Partial*
6	Papain	4	*N*	**Y**	*N*	*Partial*	*Partial*	*Partial*
7	Proteinase K	2	**Y**	**Y**	*Few*	*Partial*	**Complete**	*Partial*
8	Papain	2	*N*	**Y**	*N*	*Partial*	*Partial*	*Partial*
9	Proteinase K (x2)	24	**Y**	**Y**	**Y**	*Partial*	**Complete**	**Complete**
10	Proteinase K (x0.5)	24	**Y**	**Y**	**Y**	*Partial*	*Partial*	**Complete**
11	Proteinase K (x2)	8	**Y**	**Y**	**Y**	*Partial*	**Complete**	**Complete**
12	Proteinase K (x0.5)	8	**Y**	**Y**	**Y**	*Partial*	*Partial*	*Partial*

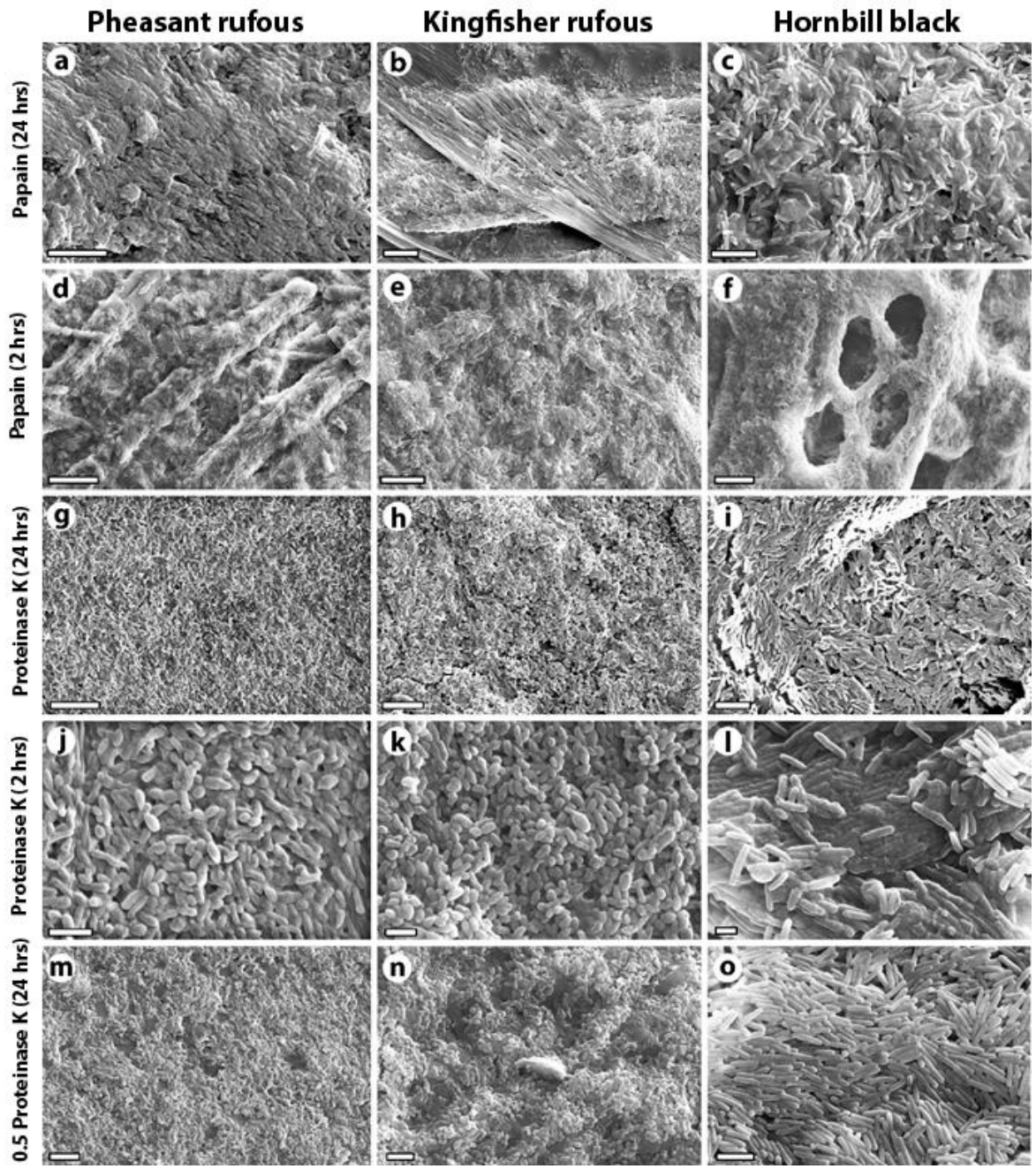

Figure 6.1. SEM images of degraded feather samples subjected to different enzymes and amounts of time under the revised extraction protocol. **a**. Pheasant rufous feather after 24 hours in Papain. While some degradation of the feather has occurred, no melanosomes are exposed. **b**. Kingfisher rufous feather after 24 hours in Papain. Some degradation has occurred, and melanosomes are exposed from all parts of the feather. **c**. Hornbill black feather after 24 hours in Papain showing partial feather degradation and some melanosomes exposed but under amorphous keratin. **d**. Pheasant rufous feather after two hours in Papain. Little degradation has occurred, and no

melanosomes are exposed. **e**. Kingfisher rufous feather after two hours in Papain. Melanosomes are exposed but much keratin remains. **f**. Hornbill black feather after two hours in Papain showing partial feather degradation and some melanosomes exposed. Feather structure can still clearly be seen. **g**. Pheasant rufous feather after 24 hours in Proteinase K showing near-full degradation with mostly melanosomes left. **h**. Kingfisher rufous feather after 24 hours in Proteinase K showing full degradation with mostly melanosomes left. **i**. Hornbill black feather after 24 hours in Proteinase K showing full degradation with only melanosomes left. **j**. Pheasant rufous feather after two hours in Proteinase K showing near-full degradation with mostly melanosomes left. **k**. Kingfisher rufous feather after two hours in Proteinase K showing near-full degradation with mostly melanosomes left. **l**. Hornbill black feather after two hours in Proteinase K showing only partial degradation with some melanosomes exposed but much keratin structure remaining. **m**. Pheasant rufous feather after 24 hours in half-quantity Proteinase K showing near-full degradation with mostly melanosomes left. **n**. Kingfisher rufous feather after 24 hours in half-quantity Proteinase K showing near-full degradation with mostly melanosomes left. **o**. Hornbill black feather after 24 hours in half-quantity Proteinase K showing complete keratin degradation. Scale bars represent 4 µm in (a), (c) and (g-l), 5 µm in (b) and (e), 40 µm in (d), 10 µm in (f), 1 µm in (j-l) and 2 µm in (m-o).

The tests to determine the minimum number of washes required to allow exposure of melanosomes revealed that without any washing, melanosomes were visible but covered in a thin film (likely representing amorphous degraded keratin), interspersed with large salt crystals from the PBS (Fig. 6.2a-b). After just a single wash however, melanosomes were exposed without a film covering them, but remnants of keratin were still present in areas (Fig. 6.2c-d). Subsequent washes showed little change to the overall composition of the samples and exposure of melanosomes, with patches of partially degraded keratin still present after four-six washes (Fig. 6.2e-j). This suggests that to acquire a 100% pure sample of melanin, further enzyme extraction steps would be necessary.

In samples with a rusty hue to the supernatant, no melanosomes were observed even when acetic acid had been added, despite the subsequent formation of a rufous pellet (Fig. S6.3a-b). As the supernatant was the same colour as the original rufous feathers it may be that this is an example of melanin being freed from melanosomes under the action of the enzymes, as has been hypothesised previously (Liu et al. 2005*a*). In some cases, the supernatant had visible material which would not settle under centrifugation. Addition of after acetic acid to these samples also generated a pellet which in these cases included pieces of feather keratin of

variable sizes with melanosomes exposed (Fig. S6.3c-f). When the supernatant was allowed to air dry, a similar result was seen (Fig. S6.3g-h). These results suggest both that melanosomes can be lost at each stage of the extraction protocol and that melanin can be released from melanosomes into the solution.

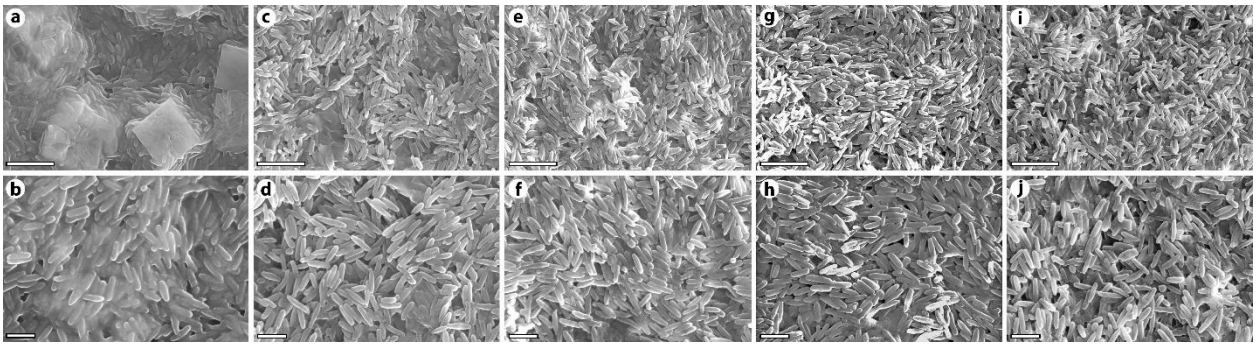

Figure 6.2. SEM images of black feather extracts after 4 hours in Proteinase K having undergone different numbers of washes in Purite. **a-b**. No washes – melanosomes are covered by a layer of presumably degraded keratin and interspersed with salt crystals from the PBS. **c-d**. After a single wash, the keratin covering has gone, and no salt crystals remain. Little changes with two (**e-f**), three (**g-h**) or four (**i-j**) washes. Scale bars represent 5 µm in the top row and 2 µm in the bottom row.

6.3.2. Resin-set feathers

SEM images of mechanically split resin-set feathers showed that the rachis and barbs could easily be opened to reveal the internal structure including in some cases melanosomes (Fig. 6.3a-f). Barbules however were never split longitudinally like the barbs, and only broken cross-sections in a small number of cases showed any internal structures. In none of these cases were melanosomes exposed from the keratin fibril matrix (Fig. 6.3g-h).

Feathers that were cut laterally across both barbs and barbules showed good exposure of the internal surface of the rachis (Fig. 6.4a and c), barbs (Fig. 6.4a-b, e and g) and barbules (Fig. 6.4i-j). While melanosomes could be clearly seen inside the barbs, none were exposed in the barbules. Instead, only a dense layer of keratin fibrils was exposed.

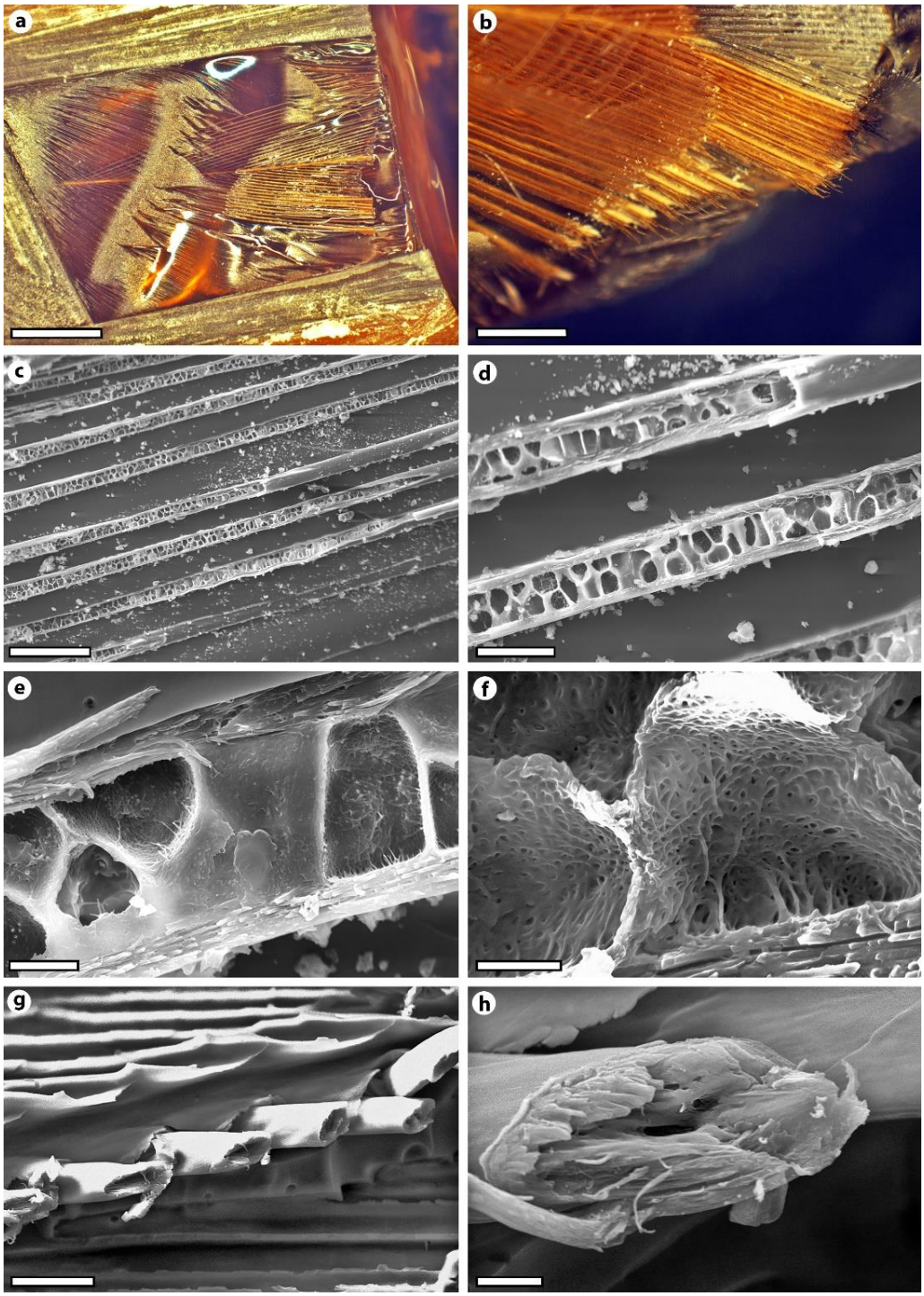

Figure 6.3. Rufous feathers set in resin and mechanically split. **a-b**. The feather after splitting, showing some barbs split longitudinally. **c-d**. Barbs split longitudinally showing their internal structure. **e-f**. Internal structure of the barbs showing keratin fibrils. **g-h**. Barbules split transversely showing keratin fibril internal structure but no exposed melanosomes. Scale bars represent 2 mm in (a), 1 mm in (b), 200 µm in (c), 50 µm in (d), 10 µm in (e), 4 µm in (f), 30 µm in (g) and 5 µm in (h).

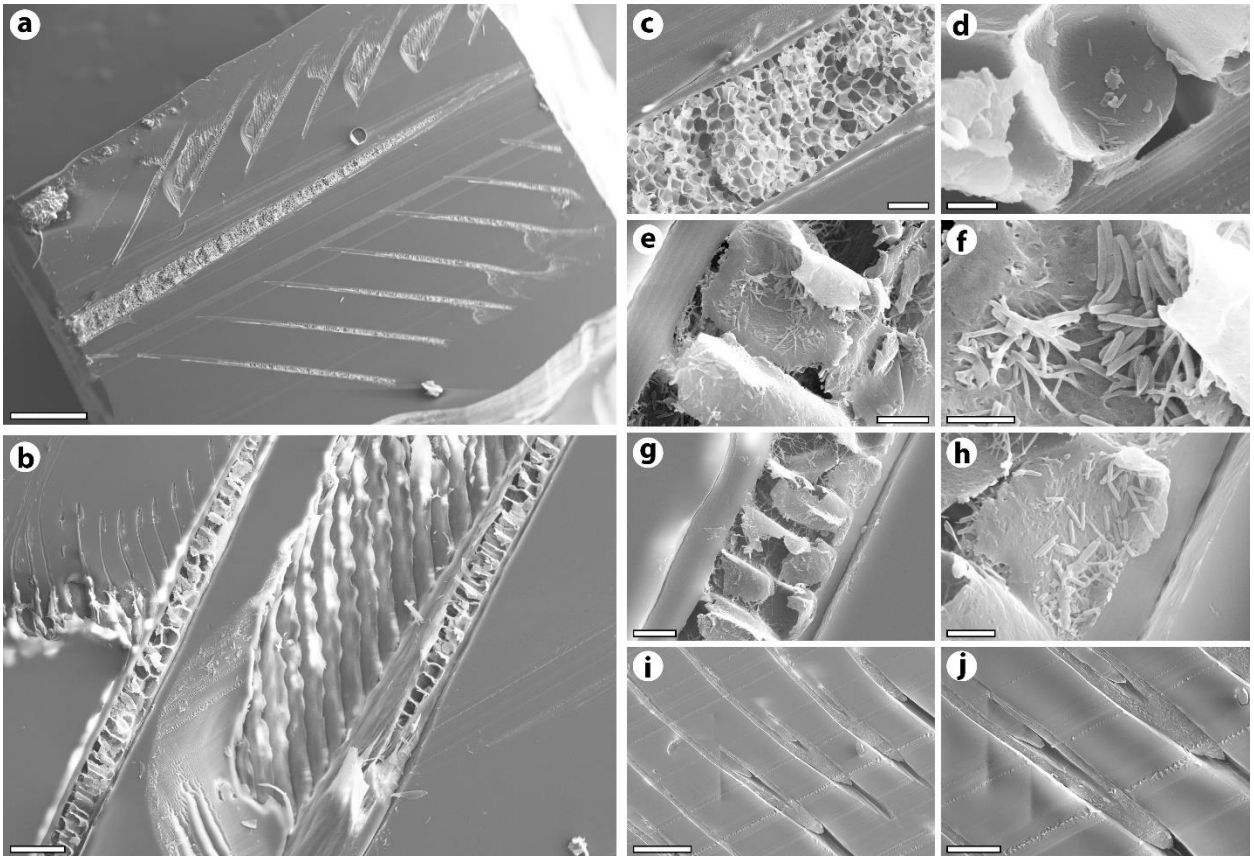

Figure 6.4. SEM images of a black hornbill feather set in resin and cut using an ultramicrotome using a glass knife. **a**. Overview of the whole feather with rachis, barbs and barbules exposed. **b**. Two barbs with exposed internal structure and attached barbules. **c**. The internal keratin structure of the rachis. **d**. Close-up of a single rachis cell with melanosomes inside. **e**. Close-up of a barb cell with melanosomes inside. **f**. Detail of the "eumelanosomes". **g**. Multiple barb cells. **h**. Melanosomes within a cell. **i**. Cut barbules. **j**. Close-up of cut barbules showing tightly packed keratin fibril internal structure and no exposed melanosomes. Scale bars represent 500 µm in (a), 50 µm in (b-c), 5 µm in (d-e), 2 µm in (f), 10 µm in (g) and (j), 3 µm in (h) and 20 µm in (i).

Individual feather barbules that were cut transversely in thin sections showed more promising results (Fig. 6.5). The internal keratinous structure of the barb was well presented (Fig. 6.5a, b, f, g and k) and the internal structure of the barbules visible (Fig. 6.5d, e, h-j, o). In some cases, well-exposed melanosomes could be seen (Fig. 6.5k-n) but in others they had been cut through along with the keratin (Fig. 6.5e and i-j). Only a small number of melanosomes were exposed sufficiently to allow potential measurements to be taken.

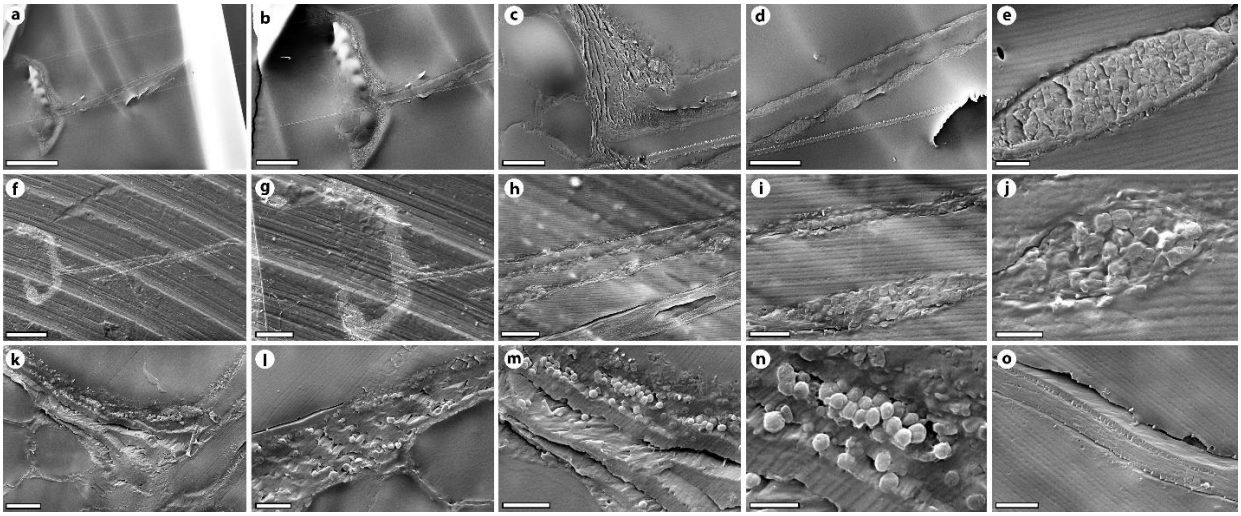

Figure 6.5. SEM images of 5 µm thin sections through a single rufous feather barbule cut transversely. Each row represents one thin section through the same barbule. Two thin sections show melanosomes that have been cut by the knife along with the keratin (**a-e** and **f-j**), therefore making their shape impossible to determine, while one shows some melanosomes exposed from the keratin, presumably as they were pulled free by the action of the knife (**k-o**). In this case they can be seen to be spherical phaeomelanin-rich melanosomes. Scale bars represent 100 µm in (a) and (f), 50 µm in (b) and (g), 10 µm in (c), (h) and (k), 20 µm in (d), 2 µm in (e), (j) and (n), 1 µm in (i), 5 µm in (l-m) and 4 µm in (o).

6.3.3. Mechanically ground feathers

Feathers that had been ground in a mortar and pestle showed extensive damage to feather structure (Fig. 6.6), however melanosomes were only rarely exposed from the rachis and barbs, and never from the barbules (Fig. 6.6g and n). Often, a thin layer of keratin still covered the melanosomes (Fig. 6.6g).

6.4. Discussion

Based on the results of all test runs, the optimal protocol after initial washing and 24-hour exposure to DTT and PBS is for incubation in Proteinase K for four hours. This allowed for melanosomes to be exposed in every case and reduces the risk of overexposing feathers with a

strong phaeomelanin component. As no issues of damage or degradation have been previously reported or observed here for eumelanin-rich melanosomes, black samples could be safely exposed for longer. The quantity of Proteinase K can also be reduced from the original protocol, by at least half. It also appears that the longer the rufous feathers spend in the enzyme, the more melanin is lost into solution (based on the rust-coloured supernatant present after 24 hours in Proteinase K). Therefore, reducing the time and number of steps makes it more likely that phaeomelanin-rich melanosomes can be successfully extracted for SEM imaging. The number of washes required after the enzyme extraction step can also be greatly reduced. The test runs showed that one wash removes enough material for successful SEM imaging of melanosomes. As the supernatant contained remains of the feather with melanosomes (Fig. S6.3), the fewer washes that are performed the better. It was noted that between washing steps the amount of material that formed a pellet during centrifugation reduced each time, and in some cases the pellet was almost completely gone by the fourth wash.

Differences in feather morphology appear to control enzyme effectiveness. The kingfisher feathers are very delicate and gracile, suggesting that there is a lower keratin content compared to the other feathers. This likely explains why melanosomes were exposed in every case and complete feather degradation was more common than for the pheasant feather of the same colour (Table 6.2). The most robust of the feather types was the black hornbill feathers, which also showed the most resistance to degradation under shorter timescales (Table 6.2). While Papain was less suitable for extracting melanosomes and fully degrading feathers, it could prove useful for exposing melanosomes in their original location in the feather. For example, as the feathers were never fully degraded under this enzyme, if differences in melanosome morphology occurred in different parts of the feather they could be treated separately. This could prove particularly useful in the case of multicoloured feathers that are common throughout extant avians, or in feathers with a structural component to their colour (e.g., iridescence; Nordén et al. 2019).

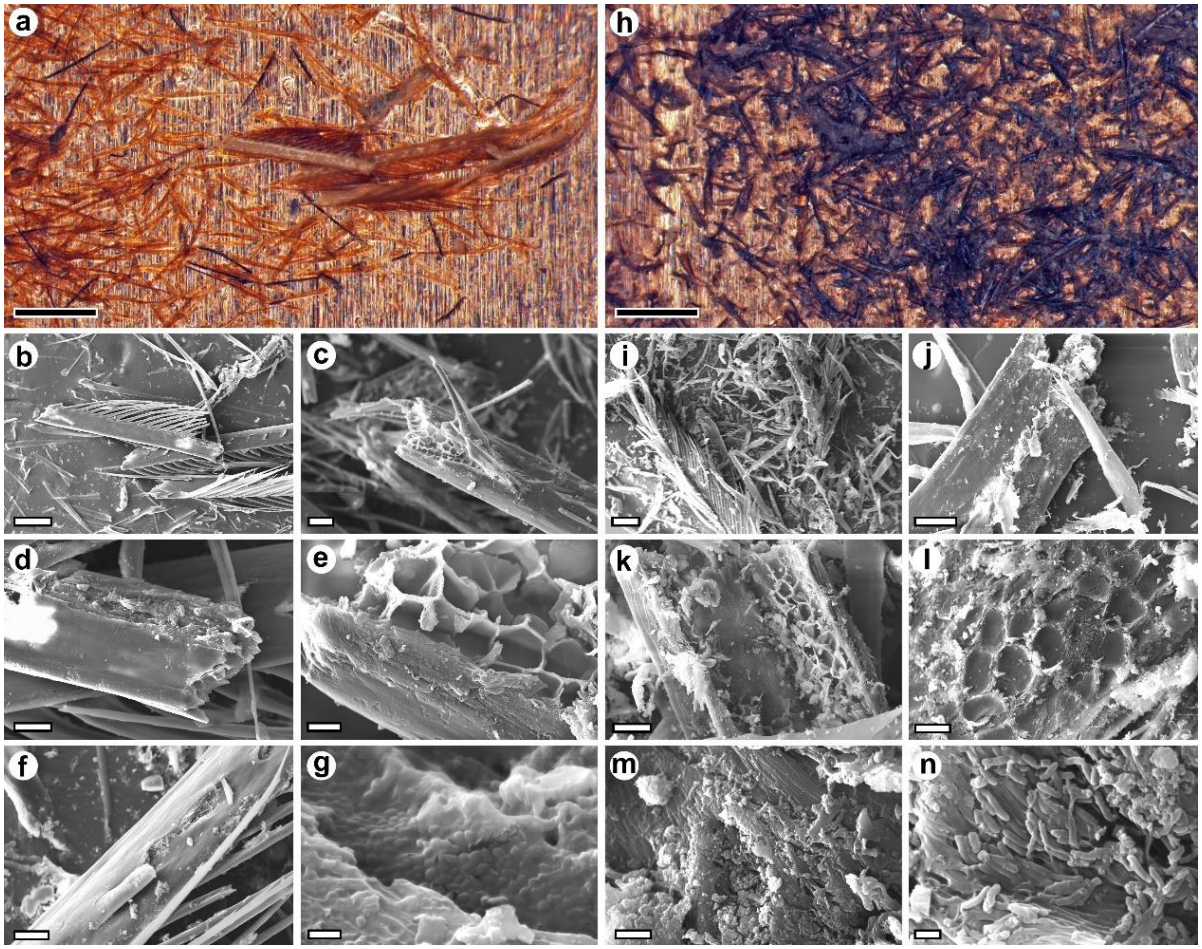

Figure 6.6. Feathers crushed using a mortar and pestle. **a**. Light image of crushed rufous pheasant feathers on a copper tape-mounted SEM stub. **b-g**. SEM images of the pheasant feather showing random exposure of internal structures but few exposed melanosomes. When present, melanosomes often have a thin layer covering them (g). **h**. Light image of crushed black hornbill feathers on a copper tape-mounted SEM stub. **i-n**. SEM images of the black hornbill feather showing similar random exposure of internal structure to the pheasant but with some well-exposed melanosomes (n). Scale bars represent 500 µm in (a) and (h), 200 µm in (b) and (i), 50 µm in (c), 30 µm in (d), (f) and (k), 10 µm in (e), 1 µm in (g) and (n), 100 µm in (j), 20 µm in (l) and 5 µm in (m).

Melanosomes can be exposed sufficiently for SEM imaging with minimal exposure to Proteinase K, rendering most of the full Liu et al. (2003) protocol unnecessary when only morphology is being assessed. Based on the results presented here, a revised protocol for exposing melanosomes from feathers for SEM imaging involving just three steps is proposed: (1) wash feather samples (roughly 1 cm^2) three times in ethanol and once in biomolecular grade

water, vortexing after each wash. (2) add a solution of DTT and (PBS) at a concentration of 10 mg DTT powder to 1 ml PBS and incubate in a shaker for 24 hours at 37°C and 200 rpm. (3) remove the solution of DTT and PBS and add a new solution of DTT, PBS and Proteinase K (10 mg DTT, 0.2 mg Proteinase K to 1 ml PBS) and incubate for four hours as before. If a pellet hasn't formed, incubate for the full 24 hours, if it has, move to the final step. (4) remove the supernatant (keeping this separate in case of material loss) and wash the remaining pellet two times in biomolecular grade water then place around 1 µl of the pellet onto an SEM stub for gold coating and imaging.

This revised protocol should allow for sufficient degradation of most feathers to allow imaging while saving large quantities of enzymes and time. The minimum time required to extract melanosomes from a single sample is 48 hours, rather than the 190 required for the original protocol, the amount of enzyme is reduced by 83.3% from 1.2 mg per sample to 0.2 mg, the amount of DTT is reduced from 29 mg to 20 mg and the number of washes reduced from at least 24 to two. Papain and Triton-X are not needed under the revised protocol. Given the expense of both DTT and in particular Proteinase K, this will prove invaluable to labs looking to extract melanosomes from large numbers of keratinised tissues. Furthermore, the dramatic reduction in the number of washes will minimise material loss and potential melanosome damage from repeated vortexing and centrifugation.

To fully degrade all keratin leaving a pure melanin sample (e.g., for chemical analyses), further enzyme extraction steps and the addition of the Triton X step are needed however and so the decision of which protocol to use should be driven by the types of analyses to be performed on the melanin. After step 3 and subsequent washing, samples can be retained, as only a minimal amount of material is needed for SEM imaging (1 µl). Therefore, samples could be SEM imaged at this stage, and then further steps in the Liu et al. (2003) protocol performed at a later date if chemical analyses are required.

In terms of mechanical exposure of melanosomes, it appears relatively simple to open the rachis and barbs of feathers (Figs. 6.3-5). Melanosomes were shown to be present in both of these structures (Fig. 6.4). However, melanosomes from within barbules were only exposed

in ultra-thin sections and in most cases, they had been cut through along with the keratin (Fig. 6.5), rendering them unsuitable in terms of assessing their 3D morphology. The structure of the barbules appears to be too tight with no air voids like those present in the rachis and barbs that would allow melanosomes to be exposed. It therefore appears that the degree to which air is present in spaces inside the different feather structures dictates the degree to which melanosomes will be exposed through cutting as well as splitting. In the cases where melanosomes had been pulled from the barbules their full shape could be determined, but this appeared to be a somewhat random and unreliable method and the numbers of exposed melanosomes minimal. It appears that the setting of feathers in resin and either mechanically fracturing or cutting them is only suitable for assessing melanosomes within the rachis and barbs or for investigating overall feather internal morphology. To investigate melanosomes within barbules (where most will be found in most cases) their extraction will be necessary from the feather through degradation of the surrounding keratin. In terms of using the crudest methodology, that of grinding the feather, the random nature by which melanosomes become exposed does not make this a suitable technique for melanosomes exposure unless no other means are available.

6.5. Conclusions

The most effective method for revealing melanosomes from the keratin of feathers is through the use of the enzyme Proteinase K. If morphological observations of the melanosomes are all that is required, the full extraction protocol used in previous studies is unnecessary. Instead, a revised protocol is presented involving a single enzyme extraction step and minimal washing that allows melanosomes to be exposed sufficiently for SEM imaging. Along with allowing a greater number of samples to be obtained in a shorter space of time, the revised protocol reduces the amount of Proteinase K required by 83%. For 3D assessment of their morphology, this is currently the only reliable way to expose melanosomes from feather barbules, where the structure of the keratin is so tight and compact that it cannot be easily split or cut. For chemical analyses requiring purified melanin with no remaining protein, the full original extraction protocol will likely be required.

Chapter 7 – Palaeocolour of the early Eocene stem upupiform bird *Messelirrisor*

Abstract: The Eocene deposits of Messel have yielded an important array of fossil birds, many of which are stem group representatives of major extant clades. Among these birds are species of the stem upupiform *Messelirrisor*. Like many Messel birds, specimens of *Messelirrisor* exhibit exceptional preservation of soft tissues including feathers, with some preserving original plumage colour patterns. Here, melanosome morphology from multiple specimens of *Messelirrisor* are analysed and quantitatively compared to a comprehensive new database of feather colours from extant Upupiformes and successive outgroups to predict a likely colouration of mixed blacks and greys, as well as a boldly striped black and white tail in the extinct bird. The new database of melanosomes from close extant relatives of *Messelirrisor* provides strong evidence for the previously proposed, but recently contested link between melanosome morphology and melanin-based colour. The extant members of Upupiformes, hoopoes (Upupidae) and wood hoopoes (Phoeniculidae), exhibit divergent colouration which may be related to their different ecologies. Compared with extant upupiforms, the estimated colouration of *Messelirrisor* shows more similarity to wood hoopoes, which are predominantly arboreal birds. Arboreal habits for *Messelirrisor* are congruent with the presumed forested environment of Messel and predicted perching capabilities based on hindlimb morphology.

This chapter is currently **unpublished** but has been submitted for publication along with Chapter 6 as a single paper to the journal *Proceedings of the Royal Society B: Biological Sciences*.

Author contributions – The author and Jakob Vinther devised this chapter and gathered the fossil data along with Gerald Mayr. The author collected and analysed all modern melanosome data, performed all SEM work, statistical analyses and wrote the manuscript. Lisa Sánchez produced the reconstructions in Figure 7.4. Danial Field and Gerald Mayr aided the anatomical reconstruction and provided feedback on the original manuscript. James Schiffbauer and Tara Selly performed the FIB-SEM.

7.1. Introduction

The Eocene age Messel Formation has long been known not only for its exceptional diversity of fossil taxa, but also for its exquisite degree of fossil preservation (Franzen 1985; Mayr 2017*a*, 2017*b*; O'Reily et al 2017; Schaal et al. 2018). Vertebrate fossils from Messel often exhibit soft tissue preservation, including hair, feathers, skin and even avian wax glands (Mayr 2006; Franzen 1985; O'Reily et al 2017; Schaal et al. 2018). These data on rarely preserved soft tissues can yield unusual insight into the ecologies and behaviours of the ancient animals from Messel, beyond what skeletal anatomy alone can provide. The preservation of integumentary structures in Messel fossils is often associated with original pigments, which in some cases record apparent original colour patterns (Fig. 1.7; Mayr 2006). Extensive work over the past decade on melanin preservation allows original colour patterns to be investigated in vertebrate fossils by analysis of preserved melanosomes (Chapter 1; Vinther 2015*a*).

While the correlation of melanosome shape to colour (Chapter 1.1; Fig 1.1) is thought to be generally independent of phylogeny, it has been little tested (Li et al. 2010, 2012, 2014; Vinther 2015*a*; Eliason et al. 2016) and has been recently questioned (Galván and Solano 2016). To date, most palaeocolour work based on extant melanosome morphology has included data from a wide phylogenetic range of extant taxa (e.g., Li et al. 2010, 2012). This has been necessary as most reconstructions have focused on either non-neornithine theropods or ornithischian dinosaurs, demanding broad sampling across the avian crown group. Investigating melanosomes in extinct members of crown group birds allows for the relationship between melanin-based colours and melanosome morphology to be tested within a more restricted phylogeny. This could help determine whether the association of shape and colour holds true within specific avian clades as well as for Neornithes as a whole.

The avian order Upupiformes comprises two major clades: Phoeniculidae (wood hoopoes) and Upupidae (hoopoes). *Messelirrisor* is the best represented and earliest known stem upupiform (Mayr 2017*b*). Multiple specimens of *Messelirrisor* from the Messel oil shale exhibit exceptional plumage preservation, with some displaying distinctive, and presumably original, colour patterns (Fig. 7.1; Mayr 2006). Extant hoopoes and wood hoopoes show

markedly different colour patterns, with wood hoopoes generally exhibiting dark plumage overall with green or purple iridescence (Fig. 7.2a), while hoopoes have rufous bodies and heads with striking black and white banded wings (Fig. 7.2b). Both hoopoes and wood hoopoes nest in trees but exhibit divergent foraging behaviours. Hoopoes forage on the ground (Barbaro et al. 2007), while woodhoopoes mainly forage along tree trunks probing cracks and crevices (Radford and Du Plessis 2003; Du Plessis et al. 2007).

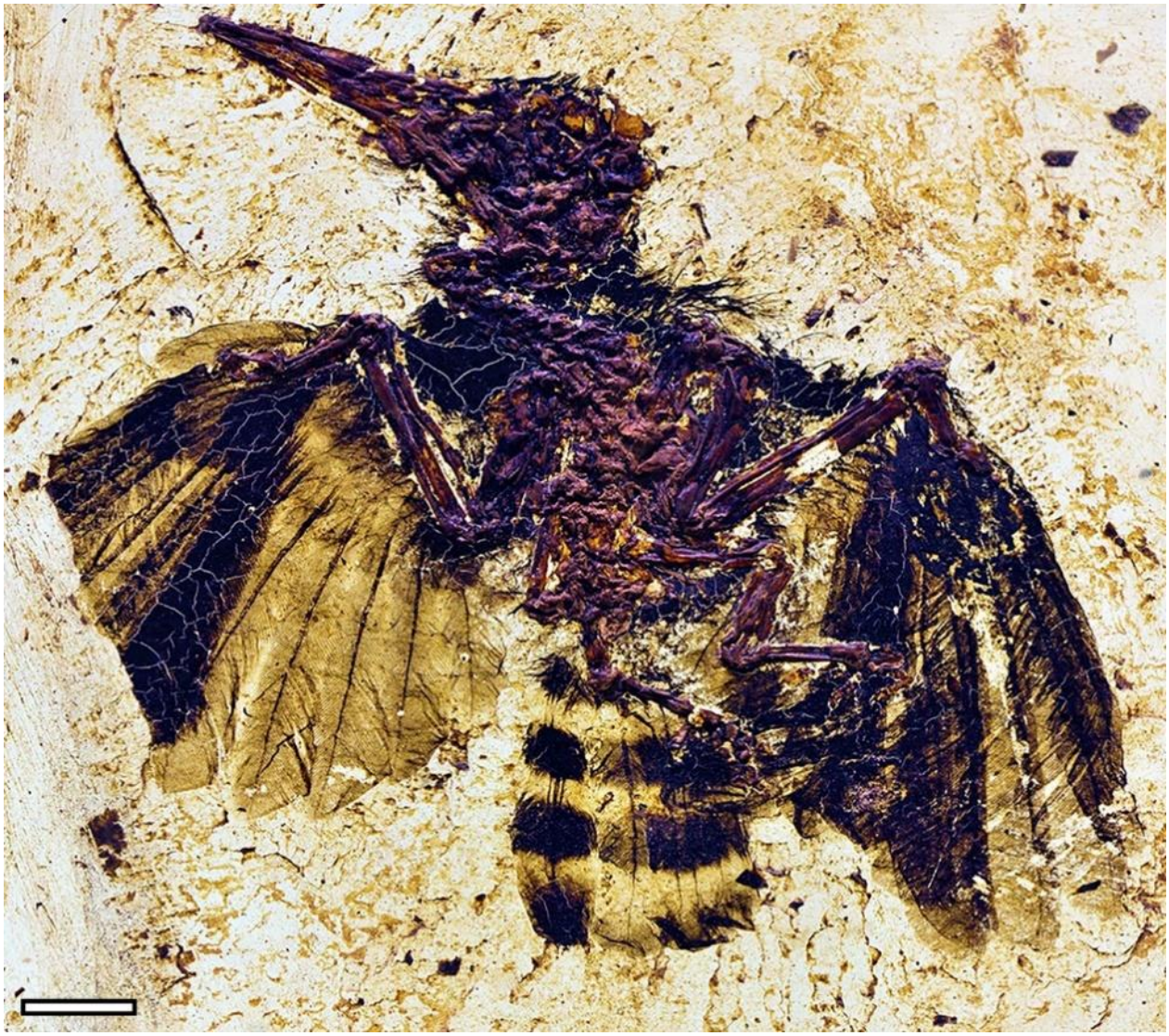

Figure 7.1. The extinct Eocene upupiform *Messelirrisor grandis* (HLMD-Be 178) showing well-preserved plumage including a strongly barred tail. Scale bar represents 10 mm.

Messelirrisor shows many anatomical features similar to modern Upupiformes, including a very long bill (Mayr 1998*a*, 2000, 2006) (Fig. 7.1-7.2). The foot morphology of *Messelirrisor*, however, is different from both hoopoes and wood hoopoes, and suggests that it was a rather generalized perching bird. (Mayr 2006). It has been hypothesised that the evolution of, and eventual competition with passerines drove the more specialised foraging techniques of the predominantly terrestrial hoopoes and the trunk-climbing wood hoopoes (Mayr 2006).

Despite being closely related, the rusty brown and black melanin-based colours of hoopoes relative to the iridescence of woodhoopoes evinces markedly divergent colouration strategies. While both birds exhibit colouration that must serve for display (Ruiz-Rodríguez et al. 2013, 2017), the subtle tones of hoopoes may be related to foraging predominantly in open exposed settings on the ground. The degree of overt display relative to crypsis is a consequence of predation and the degree of vulnerability different habitats offer (Gomez and Théry 2004; Théry 2006; Dreiss et al. 2012; Medina et al. 2017). Habitat, and specifically lighting environment, can drive highly divergent colouration even in closely related taxa (Marchetti 1993; McNaught and Owens 2002).

Through colour pattern reconstructions, I examine whether the plumage colouration of *Messelirrisor* was similar to either of the extant upupiform families, in order to evaluate if either colouration strategy has been conserved from their shared stem lineage or if it is altogether different. Detailed analysis is performed on preserved feather melanosomes through statistical comparison to a comprehensive new database of phylogenetically constrained extant melanosomes alongside previously published data to describe the colour patterning of *Messelirrisor*, helping to place it within the extinct environment of the early Eocene 48 million years ago. Using the large new dataset of melanosome morphologies in Upupiformes and successive outgroups, how well such data predict colour within a phylogenetically restricted sample is also tested.

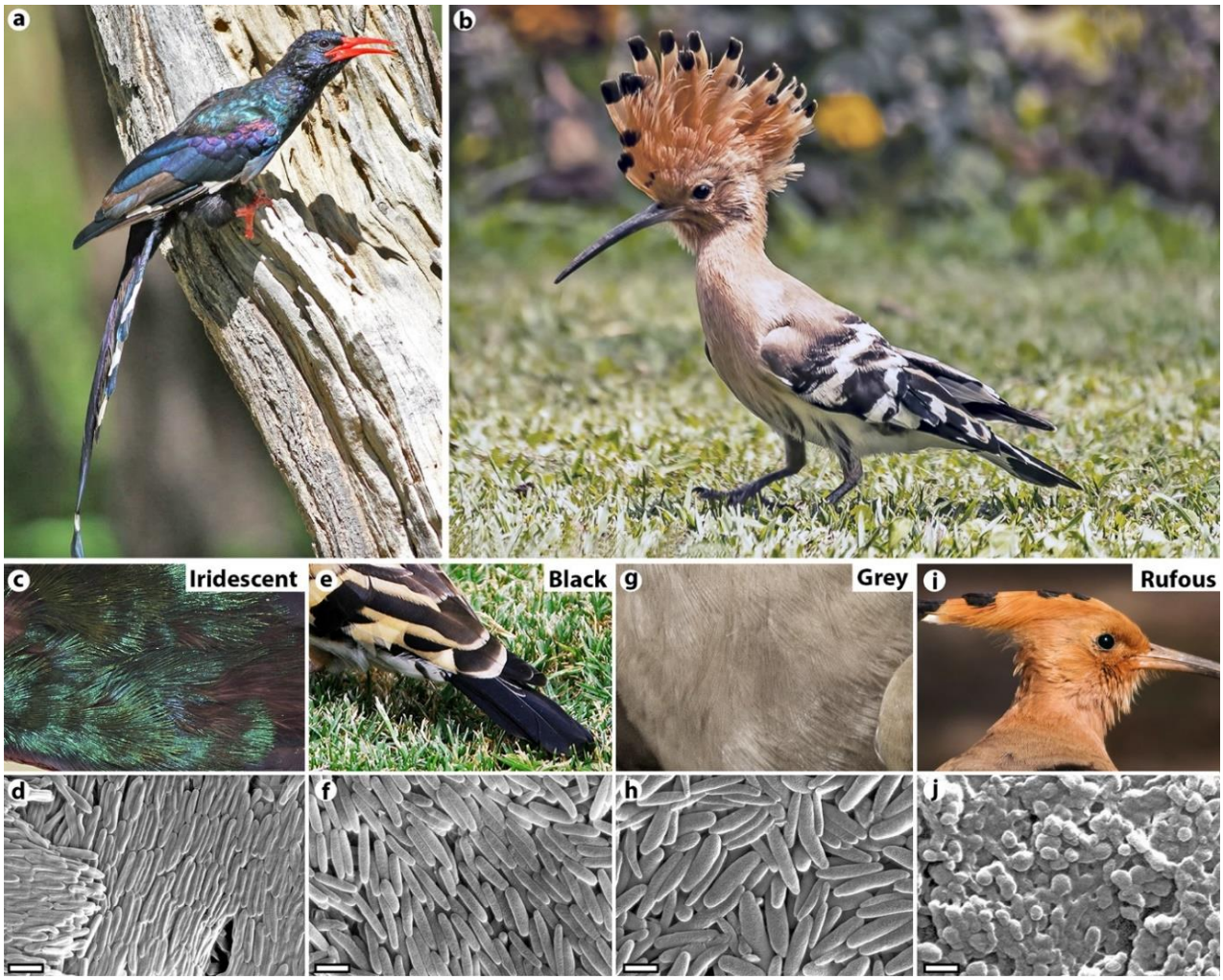

Figure 7.2. Plumage colour patterns and melanosome morphologies in extant Upupiformes. **a**. The Green Wood Hoopoe (*Phoeniculus purpureus)* showing iridescent plumage. **b**. The Eurasian Hoopoe (*Upupa epops*) with a mix of rufous and grey tones with black and white barred tail and wings. **c**. Iridescent feathers on *Phoeniculus purpureus*. **d**. Hollow eumelanin-rich melanosomes from an iridescent wood hoopoe feather. Due to the hollow nature of the melanosomes, the centre has compressed inwards during centrifugation, making hollowness easy to identify. **e**. Black wing and tail feathers in *Upupa epops*. **f**. Oblong shaped eumelanin-rich melanosomes extracted from black feathers of *U. epops.* **g**. Grey plumage on *U. epops*. **h**. Large "eumelanosomes" extracted from a grey feather from *U. epops.* **i**. Rufous plumage on *U. epops*. **j**. Spherical phaeomelanin-rich melanosomes commonly referred to as "phaeomelanosomes" extracted from a rufous feather of *U. epops.* Scale bars represent 1 µm. Extant images: Derek Keats (a), Antony Grossy (b), Fiann M. Smithwick (c), Wikipedia user MinoZig (e, g and i).

7.2. Materials and methods

7.2.1. Institutional abbreviations

HLMD: Hessisches Landesmuseum, Darmstadt, Germany; SMF: Senckenberg Research Institute Frankfurt, Germany; ZMUC: Zoological Museum, University of Copenhagen.

7.2.2. Fossil and modern material

Eight specimens of *Messelirrisor* held in the SMF and HLMD collections were investigated. Specimen numbers are given in Table 7.1. These specimens belong to three species of *Messelirrisor*: *M. halcyrostris*, *M. parvus* and *M. grandis*.

Melanised feathers from all representative genera of the extant Upupiformes (*Upupa*, *Phoeniculus* and *Rhinopomastus*), and members of each family in the Bucerotiformes (sister to Upupiformes; Prum et al. 2015) and successive outgroups (Piciformes and Coraciiformes; Prum et al. 2015) were collected for melanosome sampling. For each taxon, all melanised colours were sampled, yielding a new database of 142 samples from 83 species (and subspecies; Appendix 1). Sampling the taxa most closely related to *Messelirrisor* was considered important, as distinctive variations in melanosome morphology are exhibited by certain clades (e.g., flattened and hollow iridescent melanosomes in hummingbirds, Trochilidae; Fig. 1.1j) which may need to be accounted for when examining fossil melanosomes (Nordén et al. 2019). An existing database of modern feather colours and melanosome measurements (that of Li et al. 2012) comprising 149 colour samples across a wide phylogenetic range of 106 neornithine species was also used. Modern feather samples were obtained from the ZMUC collections.

Table 7.1. Specimens of *Messelirrisor* examined and those that were sampled for SEM imaging.

Specimen number	Taxon	Sampled?	N samples
SMF ME 10987a	*M. halcyrostris*	Y	3
SMF ME 10987b	*M. halcyrostris*	Y	17
SMF ME 11156a	*Messelirrisor* sp.	Y	5
SMF ME 11156b	*Messelirrisor* sp.	Y	3
SMF ME 11117a	*M. halcyrostris*	Y	13
SMF ME 11117b	*M. halcyrostris*	N	N/A
SMF ME 1416a	*M. parvus*	N	N/A
HLMD-Be 178	*M. grandis*	N	N/A

7.2.3. Fossil sampling

Small samples of dark organic feather material were removed from five *Messelirrisor* specimens (Table 7.1) using a scalpel and placed on SEM stubs. Care was taken to avoid any organics from the abdominal region that could be from internal organs, which are known to contain melanin with similar preservation potential to integumentary melanin (McNamara et al. 2018). The stubs were sputter coated with gold for 60 seconds using an Edwards Scancoat Six sputter coater at the Interface Analysis Centre, University of Bristol, Bristol UK.

7.2.4. Specimen photography

Fossils were imaged using a Nikon D800 DSLR with a Micro Nikkor 100 mm VR lens. Photographs were taken illuminated with a 3200K halogen light source (Lowell Tota-light, 400W). An additional set of images were taken using cross-polarised lighting by mounting a polarising gel in front of the light source and using a Tiffen Warm Polariser lens filter on the camera lens. This reduces glare from the fossil surface, allowing soft tissues to stand out with greater contrast from the resin in which the fossils are set (Bengston 2000).

7.2.5. Modern melanosome extraction

Modern feathers were cut from skins and kept in sealed zip-lock bags until being used in the extractions. Melanosomes were extracted from modern feathers using the modified version of the protocol of Liu et al. (2003) described in Chapter 6.4. The final pellets of melanin were plated on an SEM stub and sputter coated in 3 nm of gold using a Quorum Q150R ES sputter coater for SEM imaging.

7.2.6. SEM

Melanosomes were examined via gold-coated fossil and modern feather samples imaged using a Zeiss Evo15 Environmental Scanning Electron Microscope (ESEM) and a Zeiss Sigma VP Field

Emission Gun Scanning Electron Microscope (FEG-SEM) at the University of Bristol. Samples were imaged using an accelerating voltage of 10-20 KeV at a working distance of 8-10 mm. To evaluate the presence of hollow melanosomes, found in woodhoopoes, focused ion beam scanning electron microscopy (FIB-SEM) was utilized to provide site-specific, gallium ion-milled cross-sections of melanosome organization and structure. Using a FEI Scios DualBeam at the University of Missouri Electron Microscopy Core Facility, FIB-SEM methods follow those described in Schiffbauer and Xiao (2009, 2011), and utilized in previous melanosome studies (Vitek et al. 2013; Nordén et al. 2019 - Chapter 1.5). Following initial organometallic platinum deposition to protect the surface, trench-cuts were made to expose the cross-sectional surface of interest. Lower voltage cleaning cross-sections were then conducted to remove trench-cut artefacts from the higher voltage of the ion beam. In-situ secondary electron imaging was conducted to view the exposed cross-sections, using a beam voltage of 10 keV and a working distance of ~7.0 mm. Following FIB-SEM analyses, additional SEM imaging was conducted on a Zeiss Sigma 500 VP FEG-SEM at the University of Missouri X-ray Microanalysis Core Facility.

7.2.7. Melanosome measurements

Melanosomes from both the fossil and modern feather samples imaged via SEM were measured using the methodology of Li et al. (2010, 2012; Chapter 1.5). Measurements of melanosome long and short axes were taken using ImageJ (Abràmoff et al. 2004) and added to the databases of modern feather melanosomes with known associated colours (Li et al. 2010, 2012). With the new data from this study and previous data the total dataset comprised 291 modern samples (Appendix 1).

7.2.8. Statistical colour predictions of fossils

Canonical discriminant analyses (CDA) were run in SPSS 25 (IBM Corp) to determine the colour categories produced by the fossil melanosomes based on the methods described in Chapter 1.5. Melanosome measurement variables input into the analyses were: length (nm), length

coefficient of variance (CV), length skew, width (nm), width CV, width skew, aspect ratio (length divided by width) and aspect ratio skew. This method requires colours of the feathers to be categorised. The predictive power of different colour categories was tested, including splitting the brown category into "dark brown" and "rufous" and grey into "light grey" and "dark grey" as well as using those previously defined (Chapter 1.5).

Iridescence can be generated by multiple mechanisms and is associated with various melanosomes morphologies, including solid types with high aspect ratio (length to width), flattened and hollow morphologies that appear to have evolved multiple times independently within different bird lineages (Fig. 1.1g-j; Prum 2006; Hu et al. 2018; Nordén et al. 2019). In the modern feathers analysed, two melanosome morphologies associated with iridescence were observed: hollow (in members of Phoeniculidae, Fig. 7.2d), and solid with a high aspect ratio (in members of Galbulidae, Fig. 7.3a-b). The hollow melanosomes found in Phoeniculidae are of similar size, shape and aspect ratio to melanosomes categorised as 'black' (Fig. 7.2d and f), with hollowness being the only difference between iridescent melanosomes and black melanosomes in this group. This situation would be problematic under a discriminant analysis due to the overlap in shape between multiple melanosome categories; however, hollowness is easily identified in SEM images of melanosomes and many fossil samples included melanosomes split transversely (Fig. 7.4). Additionally, to determine potential hollowness in fossil melanosomes that were not naturally split, FIB-SEM was performed.

I also tested whether melanosomes from the downy potions of modern feathers are significantly different in their morphology to those from the vane. It is assumed that colour is the only predictor of melanosome morphology, rather than location in the feather. This has not been fully tested, although it has been shown that melanosome concentrations affect feather brightness (Field et al. 2013). In the majority of the studied feathers the down was grey in hue. Melanosomes from the grey downy portions were categorised as "grey" and then as "down" in separate discriminant analyses. If a significant difference was found between downy feather melanosomes and those from the vane, it would have implications for palaeocolour reconstructions as currently the only way to determine these differences is through careful sampling where down and vanes are obviously distinct.

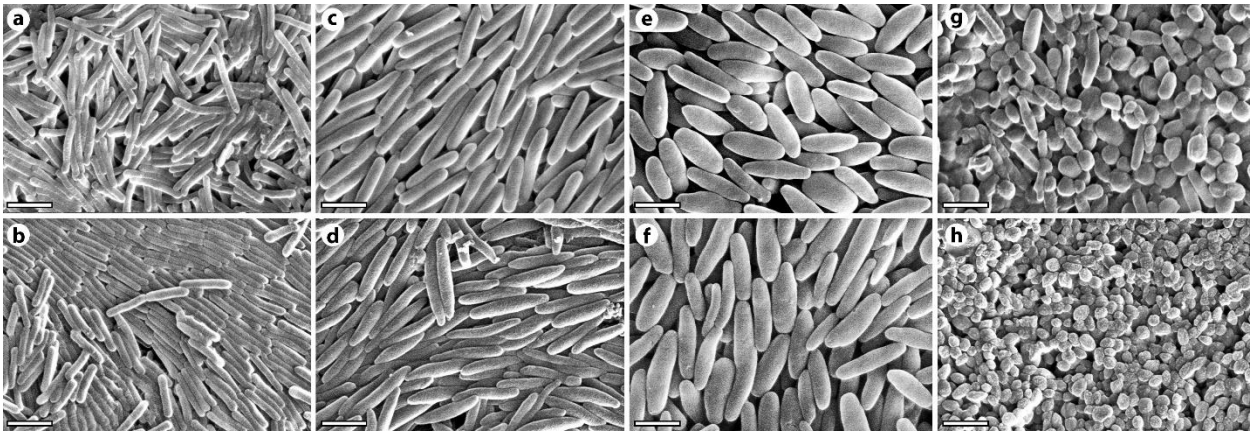

Figure 7.3. Melanosome morphologies observed in extant outgroups of the Upupiformes. Melanosomes extracted from iridescent feathers showing typical high aspect ratio morphologies (**a** - *Jacamerops aureus*: Galbulidae; **b** - *Galbula* leucogastra: Galbulidae). Melanosomes extracted from black feathers showing a typical eumelanin-rich oblong morphology (**c** - *Anthracoceros coronatus*: Bucerotidae; **d -** *Lybius dubius*: Lybiidae). Melanosomes extracted from grey feathers showing a large oblong morphology (**e** - *Semnornis ramphastinus*: Semnornithidae; f - *Sasia africana*: Picidae). Melanosomes extracted from dark brown feathers of *Brachypteracias leptosomus* (Brachypteraciidae) showing a mix of eumelanin-rich oblong melanosomes and spherical phaeomelanin-rich melanosomes. **h**. Melanosomes extracted from rufous feathers of *Galbula ruficauda* (Galbulidae) showing just spherical phaeomelanin-rich melanosomes. Scale bars represent 1 µm.

Three databases were used to predict the likely colour of the fossil samples and to test how using different extant feather data may affect fossil colour predictions: one comprised only the new extant data from Upupiformes and successive outgroups, one used just the Li et al. (2012) data, and one combined both datasets into a more comprehensive combined dataset (all melanosome data can be found in Appendix 1).

Melanosomes can shrink due to dehydration alterations during diagenesis (see Chapter 1.3.1; McNamara et al. 2013; Vinther 2015*a*). To account for this, the fossil melanosome measurements were scaled up by 5, 10, 15 and 20% in alternative statistical analyses to evaluate any effect on colour predictions.

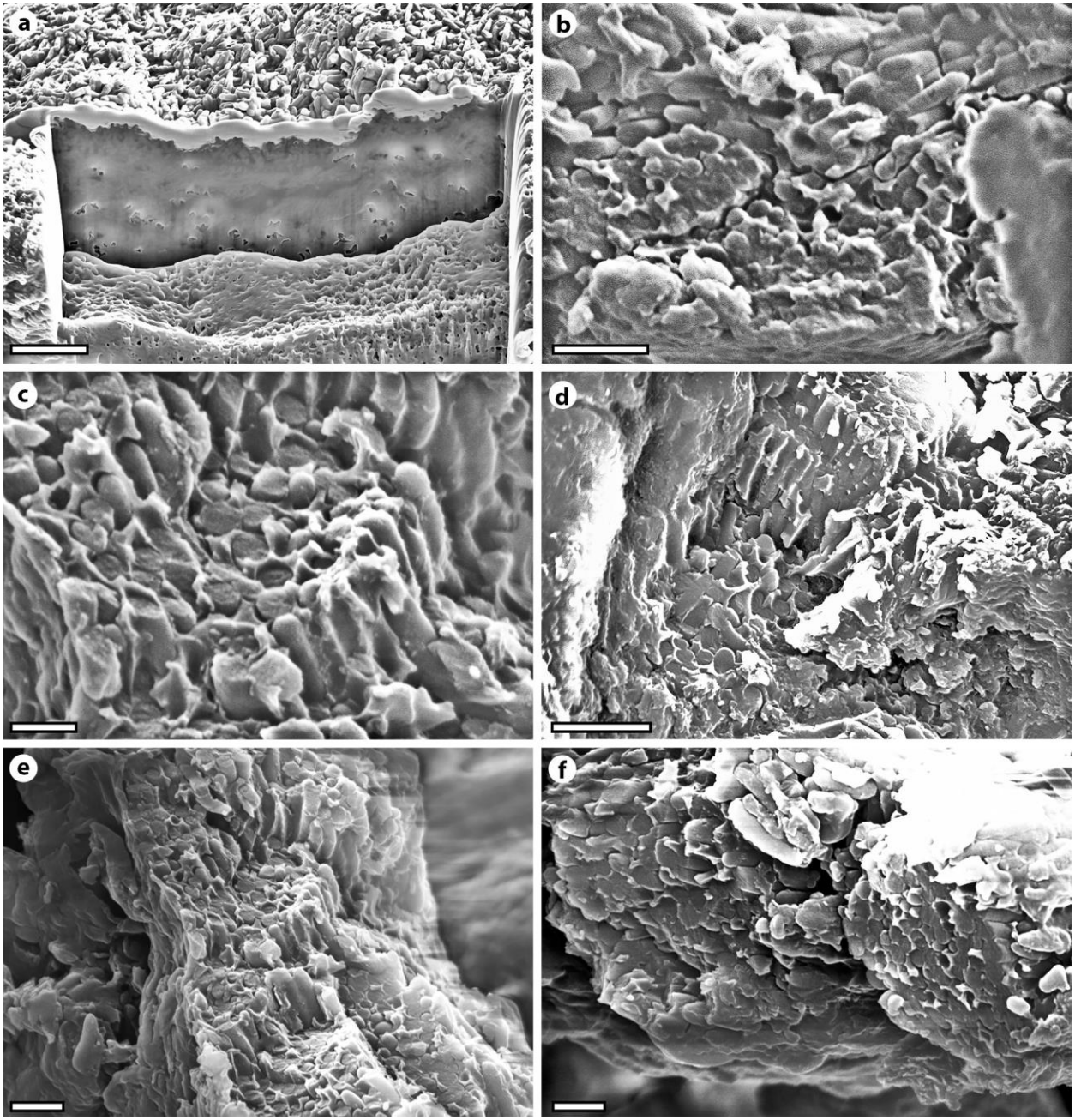

Figure 7.4. FIB-SEM cut (**a**) and naturally split (**b-f**) melanosomes from *Messelirrisor* showing solid internal structure with no evidence of hollowness that would indicate iridescence in the original feathers. Scale bars represent 5 µm in (a), 500 nm in (b), 1 µm in (c) and (e-f) and 2 µm in (d).

One-way ANOVA and Tukey's post hoc tests were also performed on the new database of extant feather melanosomes to determine whether statistically significant difference existed between the colour categories based on the melanosome morphological measurements.

7.3. Results

7.3.1. Messelirrisor *melanosome morphologies*

The samples that contained exposed melanosomes all show oblong morphologies, with no smaller, ovoid melanosomes characteristic of phaeomelanin-rich melanosomes (Figs. 7.4 and 7.5). Eighteen of the samples did not contain exposed melanosomes, due to the presence of lacquer used in the preparation of the fossils that obscure microstructural details. Nineteen samples had sufficient quantities of exposed melanosomes to measure. Both areas of naturally-split and FIB-cut melanosomes show that they are all solid with no evidence of hollowness (Fig. 7.4), rejecting the possibility that they would have exhibited bright iridescence in the same way as in extant Phoeniculidae. There were insufficient regions of well-exposed melanosomes to determine if any differences in melanosome density occurred between samples.

7.3.2. Colour pattern reconstructions in Messelirrisor

The most obvious evidence of colour patterning present in *Messelirrisor* is its banded tail. This is most clear on HLMD-Be 178 (*M. grandis*, Figs. 7.1 and S7.2a) but can also be seen on SMF ME 10987a despite the tail only being partially complete (*M. halcyrostris*, Fig. S7.2b). The other specimens do not show tail feather preservation. The presence of a banded tail in two species suggest that this pattern may have been common to the genus. No other clear colour patterns are discernible with most fossils showing a generally dark plumage throughout, including the wings.

The open wings of HLMD-Be 178 appear to have lighter and darker areas, but these are not consistent between the left and right wings and are therefore likely to reflect overlapping of feathers rather than original colour patterns (Fig. 7.1). Overlapping feathers account for

darker regions while single, or few feathers will appear lighter. While the unpigmented bands in the tail show no feather structure, the lighter areas of the wings still show pigmented feather structure. As the presence of melanin accounts for the preservation of feather structures (Chapter 1; Fig 1.3; Vinther 2015*a*), where visible structure is present it will most likely be due to melanin and therefore that region could not have been unpigmented (white) in life. An apparent stripe running across the right wing of HLMD-Be 178 proximal to the radius appears to be an artefact caused by overlapping coverts on top of the wing (Fig. 7.1). Differences in original melanised colours are generally not apparent in fossils at the macro-scale, with all pigmented feathers being dark. Currently, only SEM analysis of melanosome morphologies can distinguish different pigmentary colours (Chapter 1; Vinther 2015*a*).

All fossil melanosome samples were predicted as black or grey on the basis of melanosome morphology, with subtle variations observed depending on the modern feather data used to inform the predictions (Tables 7.2 and S7.1-2). As the most comprehensive one, the combined dataset is considered to be the most informative for colour predictions and thus this was used as the basis for the full colour reconstruction of *Messelirrisor* (Figs. 7.5 and 7.6). Canonical function loadings can be found in Table S7.3.

Variations in predicted colours were observed among the different *Messelirrisor* specimens. For example, feathers on the crown of SMF ME 11156a are inferred as black, while on SMF ME 10987b they are inferred as grey (Fig. 7.5; Table 7.2). Only one sample from the rectrices of a single specimen (from a dark stripe of SMF ME 10987a) contained exposed melanosomes, and this sample was predicted as black. Another sample predicted as grey came from a smaller feather at the base of the tail of SMF ME 10987b, likely to represent an undertail covert rather than part of the tail fan itself due to its location (Figs. 7.5 and S7.1b). HLMD-Be 178 could not be sampled, but the similarity of the tail banding suggests that it would have been the same as in SMF ME 10987a. Along with the bands of the tail showing absence of pigment (and therefore a probable white colour in life (Chapter 1; Vinther et al. 2008; Field et al. 2013; Vinther 2015*a*), these results suggest that the striking banded tail of *Messelirrisor* was black and white much like extant hoopoes, with no iridescence like that seen in wood hoopoes.

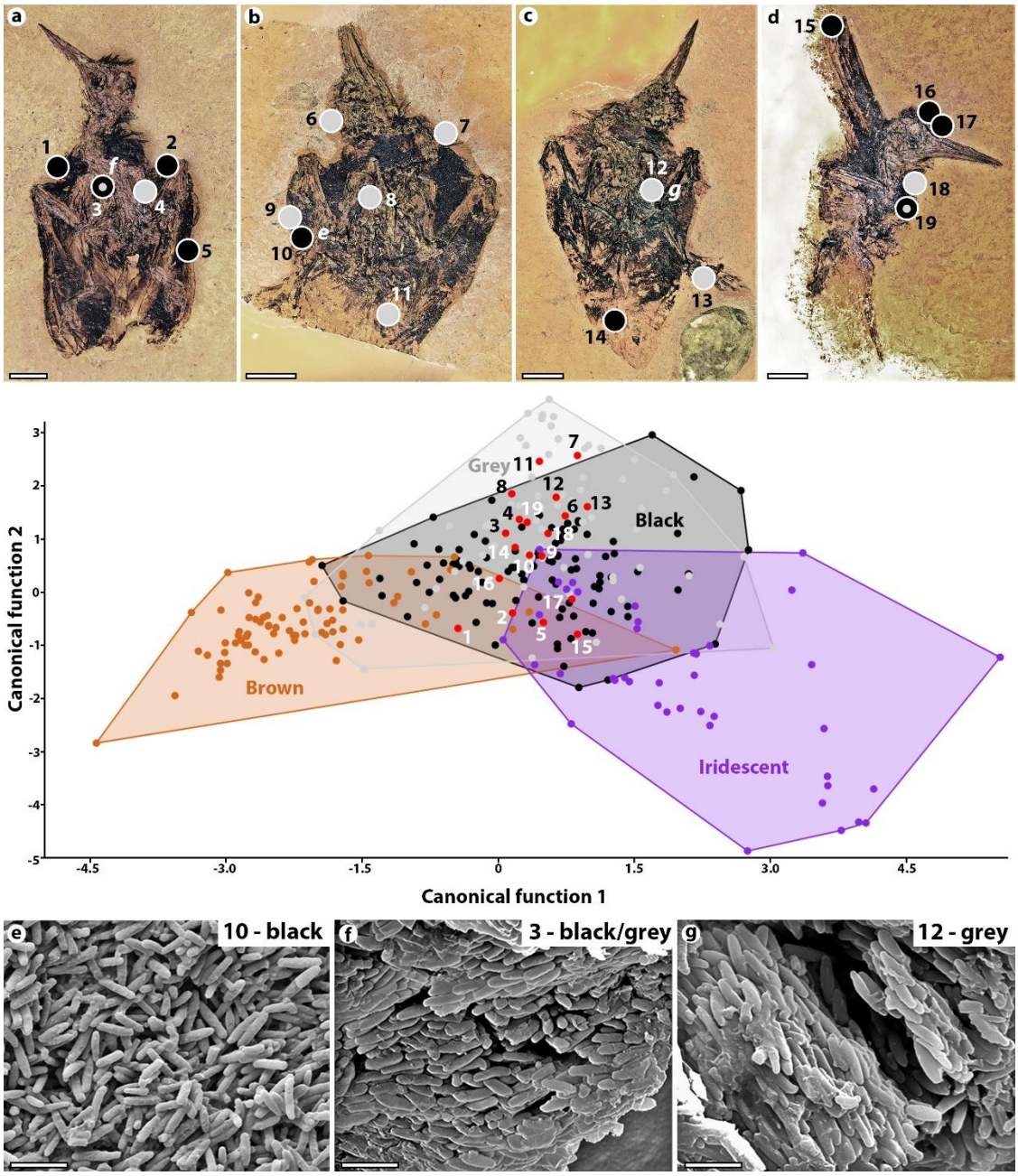

Figure 7.5. Preserved melanosomes in *Messelirrisor* and predicted colour patterns. **a-d**. Sampled *Messelirrisor* specimens: **a**. SMF-ME 11117a (*M. halcyrostris*). **b**. SMF-ME 10987b (*M. halcyrostris*). **c**. SMF-ME 10987a (*M. halcyrostris*). **d**. SMF-ME 11156a (*Messelirrisor* sp.) with predicted colours based on a canonical discriminant analysis (CDA; central panel) represented by coloured circles. All samples were predicted as black or grey. Circles with two colours indicate that the colour predictions changed when 10% melanosome shrinkage was modelled (the outer circle represents the prediction with no shrinkage). Sample numbers correspond to the data points in the CDA and SEM images. **e-g**. SEM images of melanosomes with their respective predicted colour. Scale bars represent 10 mm in (a-d) and 1 µm in (e-g).

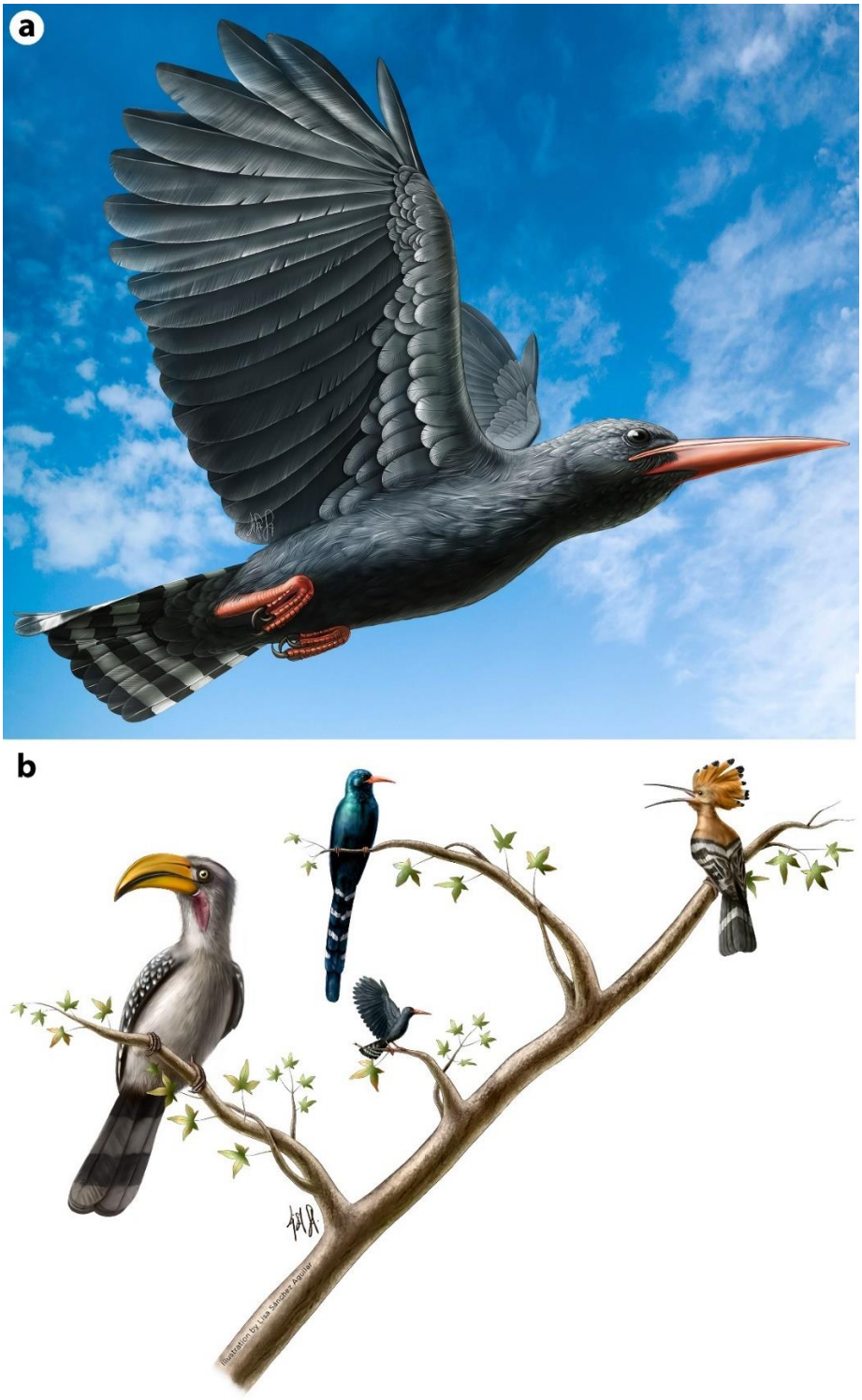

Figure 7.6. Palaeocolour reconstructions of *Messelirrisor*. **a**. Full colour reconstruction based on colour predictions from several fossils. The plumage was a mixture of black and grey with a distinct black and white banded tail. **b**. The phylogenetic position of *Messelirrisor* relative to the extant Upupiformes (hoopoes and wood hoopoes) and Bucerotiformes (hornbills). Each bird is drawn to scale, highlighting the diminutive size of *Messelirrisor*.

Table 7.2. Colour predictions for melanosome samples taken from specimens of *Messelirrisor* based on a combined extant dataset of new upupiform and outgroups and the Li et al. (2012) dataset. The effects of diagenetic shrinkage are modelled by upscaling melanosome measurements by 5-20%. The more shrinkage that is modelled, the more sample predictions change from black to grey. N = number of melanosomes measured.

Sample	no shrinkage	5% shrinkage	10% shrinkage	15% shrinkage	20% shrinkage	N
SMF ME 11117a						
1	Black	Black	Black	Black	Black	6
2	Black	Black	Black	Black	Black	97
3	Black	Black	Grey	Grey	Grey	86
4	Grey	Grey	Grey	Grey	Grey	57
5	Black	Black	Black	Black	Black	21
SMF ME 10987b						
6	Grey	Grey	Grey	Grey	Grey	34
7	Grey	Grey	Grey	Grey	Grey	102
8	Grey	Grey	Grey	Grey	Grey	61
9	Grey	Grey	Grey	Grey	Grey	67
10	Black	Black	Black	Black	Black	141
11	Grey	Grey	Grey	Grey	Grey	19
SMF ME10987a						
12	Grey	Grey	Grey	Grey	Grey	103
13	Grey	Grey	Grey	Grey	Grey	26
14	Black	Black	Black			55
SMF ME 11156a						
15	Black	Black	Black	Black	Black	31
16	Black	Black	Black	Grey	Grey	9
17	Black	Black	Black	Black	Black	7
18	Grey	Grey	Grey	Grey	Grey	35
19	Black	Grey	Grey	Grey	Grey	105

A total of four samples from the wings of two specimens provided enough melanosomes to yield colour predictions. Three out of four of these samples were predicted as black and one as grey, suggesting that the wings of *Messelirrisor* were predominantly black. There is no evidence of banding on the wings of any specimen. This differs from the multiple black and white bands seen in hoopoes or the discrete white bands in some wood hoopoes.

While current methods of colour prediction from melanosome morphology can categorise grey, they cannot distinguish between light grey and dark grey (Table 7.3). As both light and dark greys show overlapping melanosome morphologies, *Messelirrisor* could have displayed a range of grey tones. Differences in grey tones could also have been possible due to

variations in melanosome density (Field et al. 2013). The nuances of black to grey is interspersed across and within the specimens. It is possible that these grey areas derive from the downy portions of feathers rather than feather vanes. However, care was taken during fossil sampling to only take samples from visible feather vanes in most cases.

Melanosomes extracted from downy portions of modern feathers show few differences in morphology relative to those of grey melanosomes from feather vanes, and the existence of a unique "down" category is not supported in the present analyses (Fig. 7.7 and Tables 7.3-7.4). When "down" was included as a category in the CDAs, it reduced the accuracy of grey category predictions to 41%. While melanosomes from the downy portion of the feathers did not differ significantly to grey melanosomes from the vanes (Fig. 7.7 and Table 7.4), their arrangement within the barbs was found to differ. Melanosomes from the down were arranged in distinct clusters with a cylindrical morphology and consistently spaced with regions of only keratin in between (Fig. 7.8). This effectively reduces the concentration of melanosomes compared to the vane of the same feathers.

It is therefore surmised that *Messelirrisor* was broadly black to dark grey in overall tone and no evidence is found that these two tones formed any colour pattern on the bird based on the available sampling.

7.3.3. Effects of shrinkage

When shrinkage was modelled by scaling melanosome measurements, some changes were induced in the colour predictions. While most remained unchanged, a small number of inferences originally predicted as black were predicted as grey (Tables 7.2 and S7.1-2). This appears to be the most common colour shift when shrinkage is modelled, likely because the black and grey colour categories show the most overlap in melanosome morphology (with only width being significantly different between the two, Table 7.4). While it is clearly important to take shrinkage into account (McNamara et al. 2013), the burial history of a deposit can provide insight into the likely extent of alteration during diagenesis. Messel is not considered to have undergone deep burial, being highly immature organically (Hayes et al. 1987; McNamara et al.

2013). Burial temperatures have been estimated as ≤ 40°C for Messel (Hayes et al. 1987; McNamara et al. 2013), while in comparison, the Jehol Biota of China has been subjected to temperatures as high as 185°C (Jiang et al. 2012; McNamara et al. 2013). When shrinkage up to 5% is taken into account (considered here to be most realistic for Messel), only a single sample changed in colour prediction from black to grey in each dataset (Tables 7.2 and S7.1-2).

Table 7.3. The percentage of melanosome colour cases correctly classified in canonical discriminant analyses (CDA) based on different models of melanosome categorisation ordered from top to bottom in terms of level of accuracy. The models are as follows: New extant data – just the new samples from Upupiformes and outgroups. Li et al. (2012) data – a wide phylogenetic spread of avian taxa used in previous palaeocolour studies. Combined data – both of the above datasets combined. Grey split – the new dataset with the grey category split into "light grey" and "dark grey". Brown split – the new dataset with the brown category split into "dark brown" and "rufous". Down category – samples taken from the downy portion of feathers categorised together rather than as their representative colour. Penguin category – the combined dataset with "penguin" retained as a separate category. Splitting the colours into finer categories reduced the accuracy of predictions in the discriminant analyses, as did including the penguin data. Therefore, broader colour categories allowed for more accuracy in predictions of colour based on melanosome morphology. That the new data (restricted phylogeny) and that of Li et al. (2012 – wide phylogenetic range) show such similar results indicates that this is a representative level of accuracy in general for avian melanosome morphology-colour correlation.

Model	Self-test	Cross-validated
New extant data	76.8%	73.9%
Li et al. (2012) data	76.5%	73.8%
Combined data	73.8%	71.7%
Brown split	69.3%	64.8%
Down category	69.2%	67.8%
Penguin category	68.8%	67.5%
Grey split	64.3%	61.7%

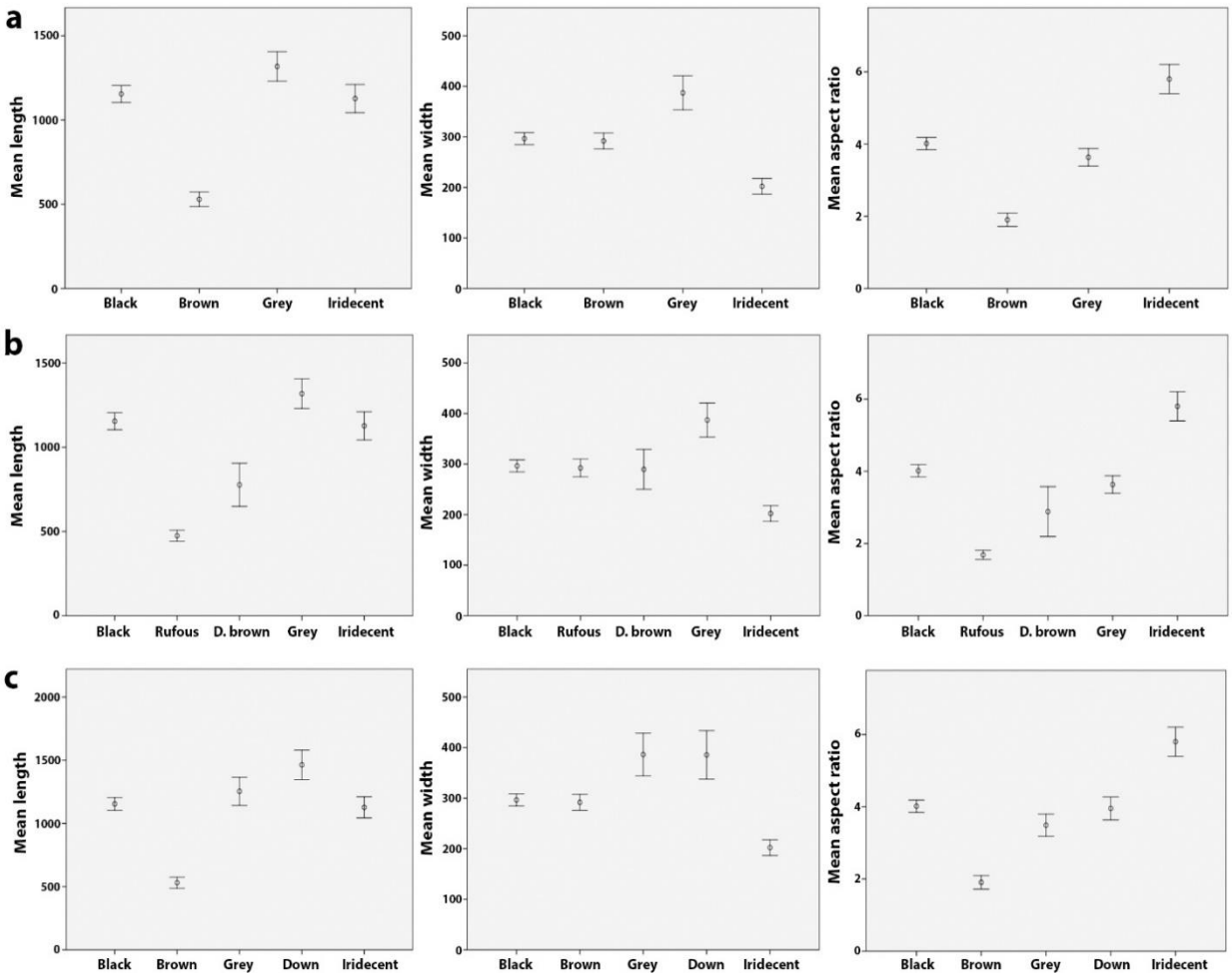

Figure 7.7. Differences in mean length, width and aspect ratios of extant melanosomes when different colour categories are used. 95% confidence intervals (CIs) are displayed. **a**. The data divided into the main four colour categories (black, brown, grey and iridescent) used in other analyses and to predict the palaeocolour of *Messelirrisor*. **b**. Brown feathers split into two categories (rufous and dark brown) to determine whether significant differences exist between different brown hues. The only overlap of confidence intervals is in mean width, indicating that length and aspect ratio can be used to differentiate different hues. Large CIs in dark brown are likely due to low sample size. **c**. Down added as a category to test whether this differs from grey. Overlap occurs in the CIs of all measures, rejecting the categorisation of downy feather melanosomes. All analyses run on the combined new dataset and the Li et al. (2012) dataset.

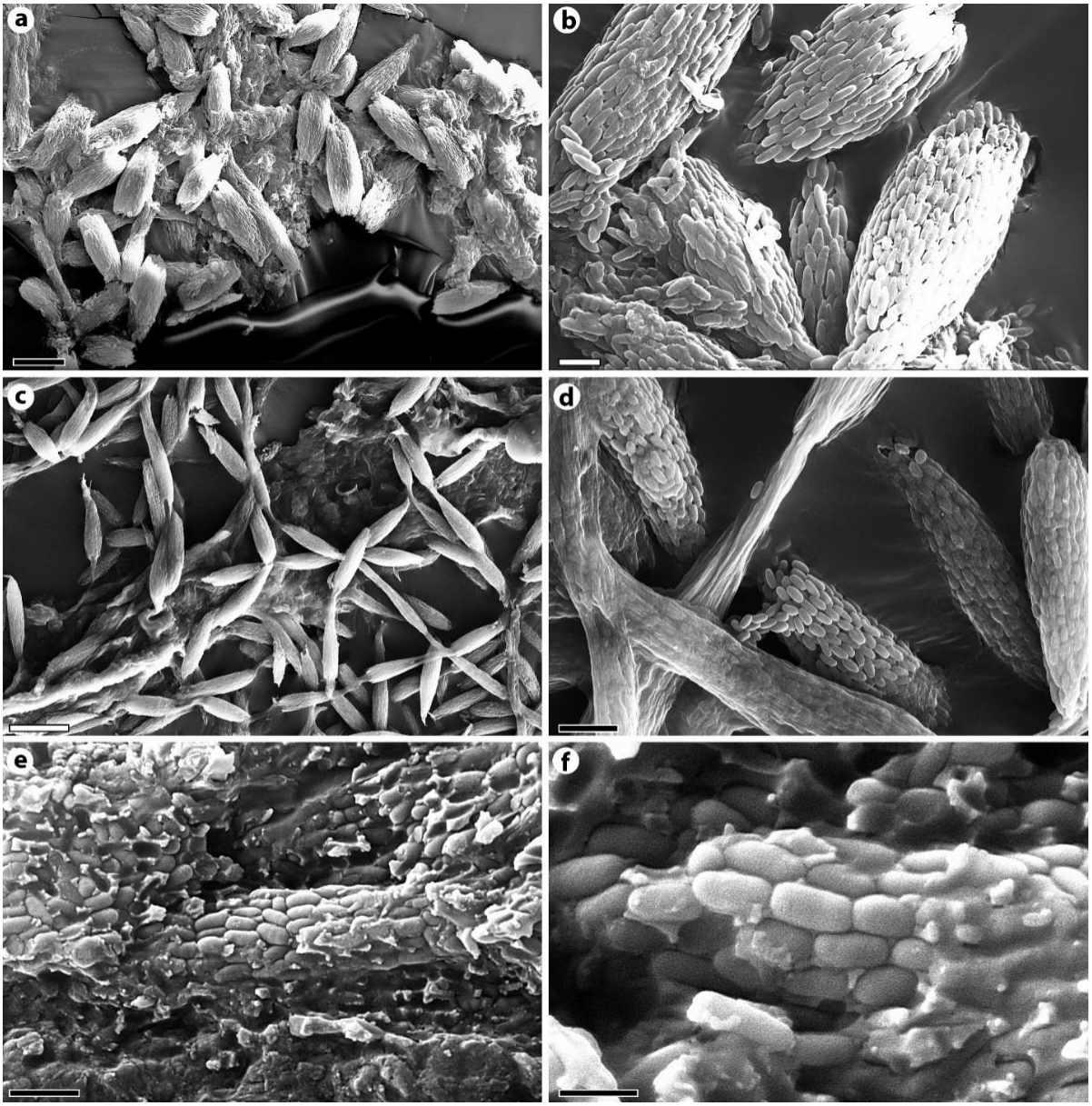

Figure 7.8. Melanosomes partially exposed among degraded keratin but in their original arrangement in the downy portion of extant feathers (**a-d**) revealing the pigment and keratin morphology of downy feathers and fossil examples (**e**-**f**). **a**. Partially degraded down barbs from *Todus mexicanus* (Todidae) showing clusters of melanosomes arranged in cylindrical structures. **b**. Melanosomes in the downy feather barbs of *T. mexicanus* showing a morphology that matches the grey colour they produce. **c**. Overview of partially degraded downy feather barbs from *Brachypteracias leptosomus* (Brachypteraciidae) showing melanosomes arranged in clusters with evenly spaced gaps of just keratin (partially degraded) in between. **d**. Grey-type melanosomes from *B. leptosomus* arranged in the typical downy clusters with degraded keratin in between. **e**-**f**. Fossil melanosomes in the same downy barb arrangement in the Eocene stem swift *Scaniacypselus* from Messel. Scale bars represent 10 µm in (a), 2 µm in (b) and (e), 20 µm in (c), 4 µm in (d) and 1 µm in (f).

Table 7.4. Results from an ANOVA Tukey post-hoc test of different coloured melanosome morphologies in extant Upupiformes and selected outgroups. Different colour groups were compared using the melanosome measurement data including adding "down", "rufous" and "dark brown" as separate categories. P values below 0.05 indicate significant differences between categories for each of the specific measurements.

Down	Black	Brown	Grey	Iridescent
Length	***<0.001***	***<0.001***	***0.028***	***<0.001***
Length CV	1	***0.008***	***0.004***	0.998
Length skew	0.992	***0.028***	0.791	1
Width	***<0.001***	***<0.001***	0.998	***<0.001***
Width CV	0.378	1	0.127	0.689
Width skew	0.977	1	0.791	1
Aspect ratio	1	***<0.001***	0.208	***<0.001***
AR skew	0.625	***<0.001***	0.636	1
Rufous	Black	Dark brown	Grey	Iridescent
Length	***<0.001***	***0.002***	***<0.001***	***<0.001***
Length CV	***<0.001***	0.997	0.992	***0.022***
Length skew	***<0.001***	***0.041***	***<0.001***	***<0.001***
Width	0.998	1	***<0.001***	***<0.001***
Width CV	0.059	0.988	0.337	0.813
Width skew	0.716	0.988	0.31	0.99
Aspect ratio	***<0.001***	***<0.001***	***<0.001***	***<0.001***
AS skew	***<0.001***	***0.011***	***<0.001***	***<0.001***
Dark brown	Black	Rufous	Grey	Iridescent
Length	***<0.001***	***0.002***	***<0.001***	***<0.001***
Length CV	0.054	0.997	0.972	0.146
Length skew	0.998	***0.041***	0.916	1
Width	0.999	1	***0.002***	***0.014***
Width CV	0.854	0.988	0.498	0.767
Width skew	1	0.988	0.969	1
Aspect ratio	***<0.001***	***<0.001***	***0.049***	***<0.001***
AS skew	0.349	***0.011***	0.277	0.928

7.3.4. Melanosome morphology and colour production

Melanosome morphologies observed in the extant clades (Upupiformes, Bucerotiformes, Piciformes and Coraciiformes) generally conform to previous examples dependent on the colours they produce (Figure 7.3 and Table 7.5; Li et al. 2010, 2012). Black feathers (N = 58) showed typical "eumelanosome" morphologies (Fig. 7.3c-d) while brown colours (N = 44) were almost all associated with more spherical "phaeomelanosome" types (Fig. 7.3h). There were a small number of exceptions in the brown category that showed a more oblong "eumelanosome"-like average morphology. However, this is likely due to the samples containing both phaeomelanin-rich and eumelanin-rich melanosomes (Fig. 7.3g). It was noted that this was most common in very dark brown samples. While splitting the "brown" category into "rufous" and "dark brown" reduced the accuracy of the CDA predictions overall, it did result in 89% of samples defined as "rufous" being correctly classified, and the ANOVA results suggest clear morphological differences between rufous and darker brown samples (Table 7.4 and Fig. 7.7). Grey feathers (N = 37) showed "eumelanosome"-type morphologies but were larger than the average black morphology (Fig. 7.3e-f). Iridescent feather melanosomes (N = 6) exhibited higher aspect ratios but were no longer than typical eumelanin-rich melanosomes (Fig. 7.3a-b).

Table 7.5. Average (mean) melanosome measurements for each colour category for extant Upupiformes and outgroups.

Dataset	Colour	Mean length (nm)	Mean width (nm)	Mean Aspect ratio
Upupiformes and outgroups (this study)	Black	1261.505	310.075	4.19
	Brown	559.249	302.227	1.949
	Grey	1386.033	372.482	3.914
	Iridescent	1038.874	164.924	6.462
Li et al. (2012)	Black	1010.597	278.297	3.783
	Brown	496.093	280.105	1.849
	Grey	1248.757	402.455	3.345
	Iridescent	1142.618	208.621	5.689
Combined datasets	Black	1154.683	296.546	4.016
	Brown	529.721	291.884	1.902
	Grey	1318.362	387.257	3.634
	Iridescent	1127.436	202.226	5.802

Results from the ANOVA test showed many significant differences in melanosome measures among colour categories (Table 7.4). The brown colour category was the most morphologically distinct from other colour categories owing to the generally spherical shape of brown phaeomelanin-rich melanosomes (Figs. 7.2h and 7.3g-h). The black and grey categories showed the fewest significant differences with other categories, highlighting their overlap in shape and explaining why these categories are the most commonly misclassified (Appendix 1). The only variable that did not show any significant difference among colour categories was width skew. Aspect ratio and width showed the greatest number of significant differences among categories (suggesting that these are the most informative measures), followed by length and width CV (Table 7.4).

7.4. Discussion

7.4.1. Comparison of colour patterns in Messelirrisor *and extant taxa*

The rufous colour found on the body and head of extant hoopoes is produced by melanosomes which show a distinct spherical morphology, and are presumably therefore phaeomelanin-rich, and measure ~500 nm in diameter on average (Fig. 7.2i-j). This contrasts with the black pigmentation of the wing and tail patches of extant hoopoes, which is produced by typical "eumelanosome"-type morphologies (Fig. 7.2e-f). As no phaeomelanosome-like spherical types were observed in any *Messelirrisor* sample, it seems that this taxon did not exhibit any brown or rufous tones (Fig. 7.5 and Table 7.2). The distinctive head crest of hoopoes is also not present in any *Messelirrisor* fossil (Mayr 1998*a*, 2000). Therefore, in terms of distinctive plumage attributes, *Messelirrisor* apparently only shares a similar black and white banded tail—both in its colour patterns and overall relative proportions—with extant hoopoes.

The dominant melanosomes observed in extant wood hoopoes are hollow oblong melanosomes, producing striking purple/green iridescence (Fig. 7.2c-d). In extant wood hoopoes, little difference was observed between green and purple plumage in terms of melanosome morphology, suggesting that it is the melanosome arrangement and/or overlying keratin that determines the precise hues produced (Prum 2006; Nordén et al. 2019). As no

hollow melanosomes were observed in *Messelirrisor* (Figs. 7.4) and none were high aspect ratio-type (Li et al. 2012) iridescence is unlikely to have contributed to plumage colouration. The non-iridescent areas of pigmented plumage of most wood hoopoe species are predominantly black (produced through typical "eumelanosome" types), much like the types observable throughout the *Messelirrisor* samples (Fig. 7.5). The extant White-headed Wood Hoopoe (*Phoeniculus bollei*), Forest Wood Hoopoe (*P. castaneiceps*) and a subspecies of the Green Wood Hoopoe (*P. purpureus senegalensis*) show some rufous plumage around the head and throat that is produced through phaeomelanin-rich melanosomes. Some unpigmented white plumage is also found in wood hoopoes (e.g., *P. bollei* males); however, the only obvious unpigmented areas of plumage in any *Messelirrisor* specimen is on the banded tail of *M. grandis* and *M. halcyrostris* (Figs. 7.1 and S7.2). The tail feathers of *Messelirrisor* are significantly shorter than those of wood hoopoes but the plumage of the head and body appear similar in gross morphology.

Messelirrisor shows some notable similarities both to hoopoes and wood hoopoes, but the overall plumage type and colour does not directly match either of its extant sister taxa. Certain features being present in the three upupiform clades, such as the banded tail and black plumage, suggests that these were ancestral to Upupiformes in general. Conversely, other features, such as the distinctive crest of hoopoes, not being present in *Messelirrisor* suggests that these are not ancestral to the clade. Being a mixture of black and grey is also reminiscent of extant members of the Bucerotiformes, some of which also show banded black and white tails suggesting that this condition could have been ancestral to this clade (Fig. 7.6b). However, given the general evolutionary lability of plumage colouration (Schutler and Weatherhead 1990; Omlan and Hofmann 2006; Price et al. 2007), these conclusions are not foregone.

Differences in colour predictions between specimens of *Messelirrisor* could indicate difference between sexes or through ontogeny. However, with no osteological correlates to identify sex or age in the fossils it was not possible to investigate this question with the limited sample size available.

7.4.2. Correlation of melanosome morphology to colour

The previously noted correlation between melanosome morphology and colouration has been questioned recently, particularly when relying on these assumptions to predict colour in extinct fossil taxa (Galván and Solano 2016). The new modern melanosome data address these concerns and confirm that melanosome shape strongly predicts colour, whether or not a restricted phylogenetic range of taxa are considered (Tables 7.2, S7.1-2, Fig. 7.7). The significant differences observed among colour categories in all but one variable (Table 7.4) also highlight the predictive power of just a few simple measurements of melanosomes when using extant morphology to predict palaeocolour. Despite some overlap, alternative colouration categories generally exhibit distinct melanosome morphologies (Fig. 7.7 and Tables 7.4-7.5). The new data therefore support previous palaeocolour work relying on melanosome morphology (Chapter 1.5; Li et al. 2010, 2012; Colleary et al. 2015; Brown et al. 2017) and highlights the importance of melanosome shape for predicting melanin-based colouration in both extant and extinct taxa.

The revised extraction protocol (Chapter 6.4) facilitates the extraction of phaeomelanin-rich melanosomes with minimal chance of alteration of melanosome morphology. This allowed many samples with clear rufous colours to be included. The significant difference between average melanosome morphology in the rufous and darker brown samples (Table 7.4) warrants further investigation, which the revised protocol will allow. The retention of keratin in some samples allowed important insights into the arrangement of melanosomes to be determined, such as the spacing of melanosome clusters in downy feather barbs (Fig. 7.8). As it has been shown that melanosome concentration correlates with feather brightness (Field et al. 2013), and the present data show that melanosome morphology doesn't account for observed colour differences between down and vane feather regions, it is plausible that the arrangement of melanosomes in downy barbs can explain the often-observed lighter tone when compared to the vane. Unpigmented feather keratin with randomly dispersed internal air pockets reflects all wavelengths of light, making it appear white (Prum 2006). Having white light-reflecting keratin in between white light-absorbing melanosome clusters will generate brighter/lighter tones than barbs consisting of melanosomes with no regions of just keratin. Furthermore, this should be readily identifiable in fossils if melanosomes are still in their original arrangement, meaning that

feather down does not have to conflate palaeocolour reconstruction. This can be seen in other Messel bird fossils such as the stem swift *Scaniacypselus* (Fig 7.8e-f).

7.4.3. Ecology of extant Upupiformes and implications for Messelirrisor

Recent studies have shown that colour in extinct taxa can inform possible ecologies through direct comparisons between extinct taxa with unknown ecologies to extant taxa with known ecologies (Chapter 1.5; Vinther et al. 2016; Smithwick et al. 2017*a*). Most often, a lack of closely related living taxa however means comparisons must be made with presumed analogous animals, such as mammals for non-avian dinosaurs (Chapter 1.5; Vinther et al. 2016; Brown et al. 2017; Smithwick et al. 2017*a*). Being a member of crown group Aves and having known closely related living taxa means that the possible ecology of *Messelirrisor* can be investigated via direct comparison with extant Upupiformes.

Wood hoopoes are predominantly arboreal, spending most of their time in trees where they forage for insects; these habits are facilitated by a distinct foot morphology specialised for trunk climbing (Radford and du Plessis 2003; Mayr 2006; du Plessis et al. 2007). Even taxa that have been observed foraging on the ground only do so roughly 2% of the time compared to arboreal foraging (du Plessis et al. 2007). Hoopoes, while nesting in trees, often forage in more open areas on ground with low vegetation cover (Barbaro et al. 2007; Podletnik and Denac 2015). Both groups are hole-nesters that lay their eggs and raise their young in tree cavities (Martín-Vivaldi et al. 1999). Predation rates are generally considered low in the nest itself, in part owing to unusual anti-predator defences such as noxious secretions by female hoopoes (Martín-Vivaldi et al. 1999). Predation pressure is therefore likely strongest during foraging, particularly for hoopoes foraging in open areas (Martín-Vivaldi et al. 1999; Ruiz-Rodriguez et al. 2013, 2017).

As camouflage from predators is such a strong driver on animal colouration (Endler 1990; Hill and McGraw 2006*a*), the different colours of hoopoes and wood hoopoes may therefore be related to the observed differences in foraging behaviour and habitat (Gomez and Théry 2004). The often-green iridescence of wood hoopoes could plausibly provide better

background matching in the diffuse lighting environment found high in trees where they generally forage, as seen in other bird taxa (Radford and du Plessis 2003; Gomez and Théry 2004), while also serving for display. The light earthy-browns and blacks of hoopoes are less conspicuous in open scrubland where they most often forage (Barbaro et al. 2007), while their head crest serves for display to both potential predators and intraspecifically (Ruiz-Rodriguez et al. 2017). Hoopoes are known to be preyed upon by diurnal raptors while foraging, and the main predators of wood hoopoes are also raptorial birds of prey along with some arboreal mammals (Ruiz-Rodriguez et al. 2013). It has also been suggested that the striking banded wings of hoopoes, and possibly wood hoopoes, may act as a form of deimatic signalling to confuse or startle predators (Ruiz-Rodriguez et al. 2017).

These findings fit well with the assumption that Messel was a predominantly forested environment (Dunne et al. 2014; Schaal et al. 2018). Being generally dark and more like the predominantly arboreal extant wood hoopoes without the lighter rufous tones of ground-foraging hoopoes in open areas indicates that *Messelirrisor* would have been well suited to living in a forested environment. The lack of iridescence in the plumage of *Messelirrisor*, however, suggests that it may have differed in its exact behaviour and/or ecology, which is also indicated by differences in skeletal morphology (Mayr 1998*a*). It is plausible that black colouration in some birds may be adaptive for activity in less well-lit environments where the colour is less conspicuous, and that iridescence such as that seen in wood hoopoes can appear similarly black in diffuse lighting. Iridescence may therefore be utilised during intermittent display in clearings in the canopy or as green camouflage while foraging on the canopy (Gomez and Théry 2004; Doucet and Meadows 2009; Seymour and Dean 2010).

Corroborating these findings, the skeletal anatomy of *Messelirrisor* suggests that it was better suited to arboreal habits than extant upupiforms (Mayr 1998*a*). The presence of a curved claw on the hallux and fairly short tarsometatarsus of *Messelirrisor* suggests that they would not have foraged on the ground like hoopoes (Mayr 2000).

The strongly banded tail of *Messelirrisor* may have been used as a deimatic signal like the wings of its extant relatives, which would suggest that this startle tactic was in place prior to

the origin of crown Upupiformes and may indicate similar predation pressures. However, the extant clades of raptorial birds that prey on Upupiformes have not been recovered from Messel, and no known raptorial birds from Messel would have been large enough to tackle an adult *Messelirrisor* (Mayr 2017*a*). As both extant subclades of Upupiformes, as well as the closely related Bucerotiformes, Piciformes, and Coraciiformes nest in tree cavities, it is highly likely that *Messelirrisor* was itself a cavity nester. Arboreal mammals are known from Messel (Mayr 2000), which may have been possible predators of *Messelirrisor* either on adults, young or eggs in the nest. The banded tail may have evolved in response to these predation pressures or alternatively could have functioned in intraspecific social signalling, for example signalling quality to the opposite sex, as has been hypothesised for some modern birds (Marques et al. 2016).

7.5. Conclusions

Messelirrisor is a conspicuous representative of the extinct avifauna of Messel with its preserved colour patterning. Through both the use of a new database of modern feather melanosomes from a phylogenetically restricted range of taxa closely related to *Messelirrisor* and data previously published, it is shown that this Eocene stem upupiform showed a mix of black and grey plumage and had a striking black and white banded tail. This colour pattern in comparison with extant relatives and upupiform outgroups along with skeletal correlates, support the hypothesis that *Messelirrisor* was arboreal. This reconstruction also highlights some features, such as a black and white banded tail, also seen in the hornbill outgroup, were likely common to the entire Upupiform lineage.

Chapter 8 – Palaeocolour reconstructions support ancestral nocturnality of strisorian birds

Abstract

Apodiform birds (hummingbirds, swifts and tree swifts) show some of the most remarkable colours in birds. Vivid iridescence present in many apodiforms contrasts strongly with the earthy cryptic tones of their sister taxa, the "Caprimulgiformes". The striking divergence in colour patterns in the two groups is likely related to their activity patterns – caprimulgiforms are nocturnal while apodiforms are diurnal. Apodiformes are nested within the paraphyletic "Caprimulgiformes" and the ancestral condition of the group (Strisores: nocturnal or diurnal) is not known. Two scenarios are possible: all strisorians were ancestrally nocturnal with Apodiformes becoming diurnal, or a fourfold origin of nocturnality in the "Caprimulgiformes". Strisores have a good record of feather-bearing fossils, allowing this to be investigated. Here, I examine melanosomes from the feathers of fossil taxa found at the early Eocene fossil sites of Messel (Germany) and Fur (Denmark), and make quantitative comparisons with a new sample of extant Strisores melanosomes. My results show that no known Eocene fossil Strisores exhibited showy iridescent plumage, and the derived, flattened, and hollow melanosomes exhibited by iridescent taxa such as hummingbirds are absent in these fossils. Instead, all fossil Strisores studied show mixtures of black, brown and grey pigmentation, with some showing patterns such as mottling and banding suggestive of camouflage. These results corroborate the suggestion that the group was originally nocturnal, with crown group Apodiformes diverging into diurnal niches after the Eocene. In addition, I identify new melanosome morphotypes including flat and hollow melanosomes in non-iridescent apodiform feathers, with implications for the morphological evolution of melanosomes and identification of iridescence in fossils.

This chapter is currently **unpublished** but will soon be submitted to a general scientific journal.

Author contributions - The author and Jakob Vinther devised the concept of this chapter and gathered fossil samples along with Gerald Mayr. The author gathered all modern samples and analysed all fossil and modern data, wrote the chapter and produced all figures.

8.1. Introduction

Strisores comprises two major clades, the nocturnal "caprimulgiform" birds (previously Caprimulgiformes - nightjars and allies) and diurnal Apodiformes (hummingbirds and swifts) (Fig. 8.1; Mayr 2010*a*, 2011). While the caprimulgiforms are all cryptic, with earthy colours and behaviours to avoid being seen (Fig. 8.2a-g; Han et al. 2010; White 2017), the Apodiformes display some of the brightest and most saturated iridescent colours of any animal (Fig. 8.2h-m; Greenewalt et al. 1960; Stoddard and Prum 2011; Giraldo et al. 2018; Nordén et al. 2019). The exact topology of the constituent clades within Strisores has long been a topic of debate, but there is strong support for Apodiformes being nested within a paraphyletic "Caprimulgiformes" (Fig. 8.1; Mayr 2002, 2010*a*; Braun and Huddleston 2009; Prum 2015; White 2017 and references therein). Because of this topology, there has also been debate as to whether the ancestral strisorian ecology was predominantly nocturnal or diurnal (Mayr 2010*a*; White 2017). The most parsimonious explanation is that the most recent common ancestor of all crown Strisores was a nocturnal bird (Mayr 2010*a*). This would suggest that Apodiformes secondarily transitioned to a predominantly diurnal lifestyle at some point in their evolutionary history (Mayr 2002, 2011; Hackett et al. 2008; Prum et al. 2015). Alternatively, if the ancestral condition of the group was diurnal, four separate clades (Steatornithidae, Podargidae, Caprimulgi and Aegothelidae) must have independently become nocturnal (Mayr 2010*a*). Strisores have a good fossil record, with multiple taxa known from various deposits including from the Messel Formation of Germany and Fur Formation of Denmark (Mayr 2017*b*). Several of these fossils include well-preserved plumage, enabling hypotheses about ecological transitions through strisorian evolutionary history to be directly assessed.

Direct osteological evidence that could be gleaned from fossils is scant in identifying both the point at which any switches were made between nocturnality and diurnality and the ancestral condition of the Strisores (or any constituent clades). It has been shown that one skeletal feature previously thought to be informative in this regard, the relative size of the eye orbit and/or the sclerotic ring, is not a reliable indicator of activity patterns in compressed vertebrate fossils (such as those from Messel; Hall 2008). In modern nocturnal birds including

Strisores, both the dimensions of the sclerotic ring and the depth of the orbit are required to accurately predict activity patterns, features that can only be determined in three-dimensional fossils (Hall 2008). Plumage features, particularly the preservation of pigments (Chapter 1; Vinther 2015), may provide further data to address the question of ancestral activity patterns in Strisores by allowing colour patterns to be investigated.

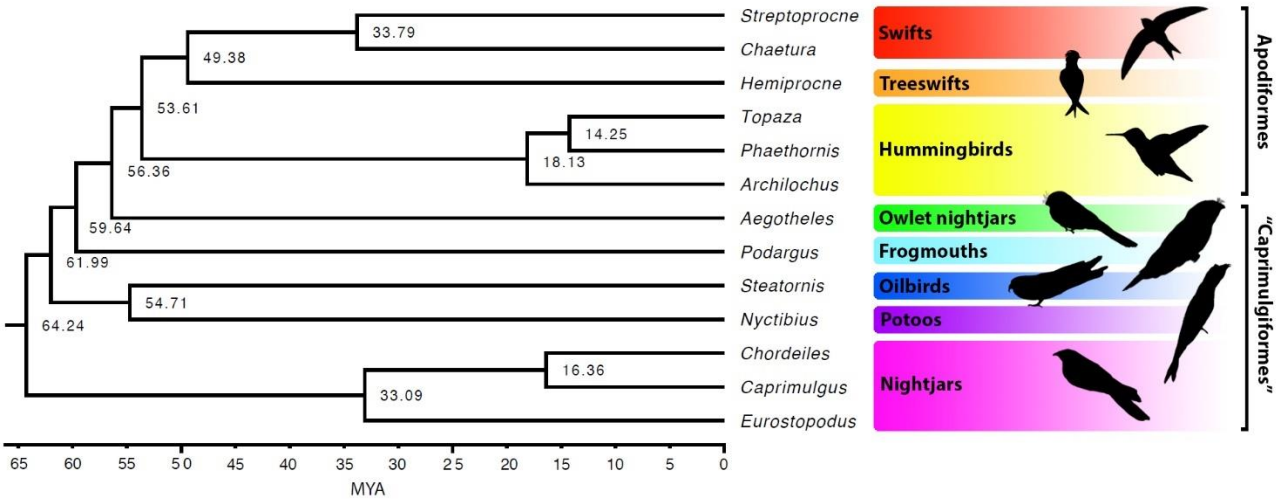

Figure 8.1. A time-calibrated phylogeny for crown Strisores. Extracted from the best-supported phylogenomic topology of Prum et al. (2015). Apodiformes (hummingbirds, swifts, and treeswifts) are deeply nested within Strisores making the "Caprimulgiformes" paraphyletic and implying that the diurnality of crown apodiforms arose from nocturnal strisorian ancestors.

Caprimulgiform birds almost universally display cryptic mottled patterns mainly comprised of different hues of browns, black and grey (Fig. 8.2a-d). Many caprimulgiform families also contain rufous morphs with distinct rust-coloured plumage (Fig. 8.2e-f; Han et al. 2010; Costa et al. 2017), and crypsis-enhancing behaviours such as branch mimicking are prevalent (Figs. I1i and 8.2c; Han et al. 2017; White 2017). Hummingbirds (Trochilidae) and tree swifts (Hemiprocnidae) display mainly showy iridescent colours (Fig. 8.2i-m) while swifts (Apodidae) exhibit both uniformly dark and iridescent members (Fig. 8.2h). Even apparently less showy taxa within Apodiformes, like the rufous hummingbird (*Selasphorus rufus*), often have

patches of iridescence such as throat gorgets that can be flared out to become highly conspicuous (Fig. 8.2l-m). The showy colours of Apodiformes are likely related to social signalling, be it sexual or territorial (Bleiweiss 1985, 1992; Herrera et al. 2008; Doucet and Meadows 2009). In turn, this suggests that their colouration is strongly linked to their diurnal life mode (McNaught and Owens 2002; Théry 2006; White 2017).

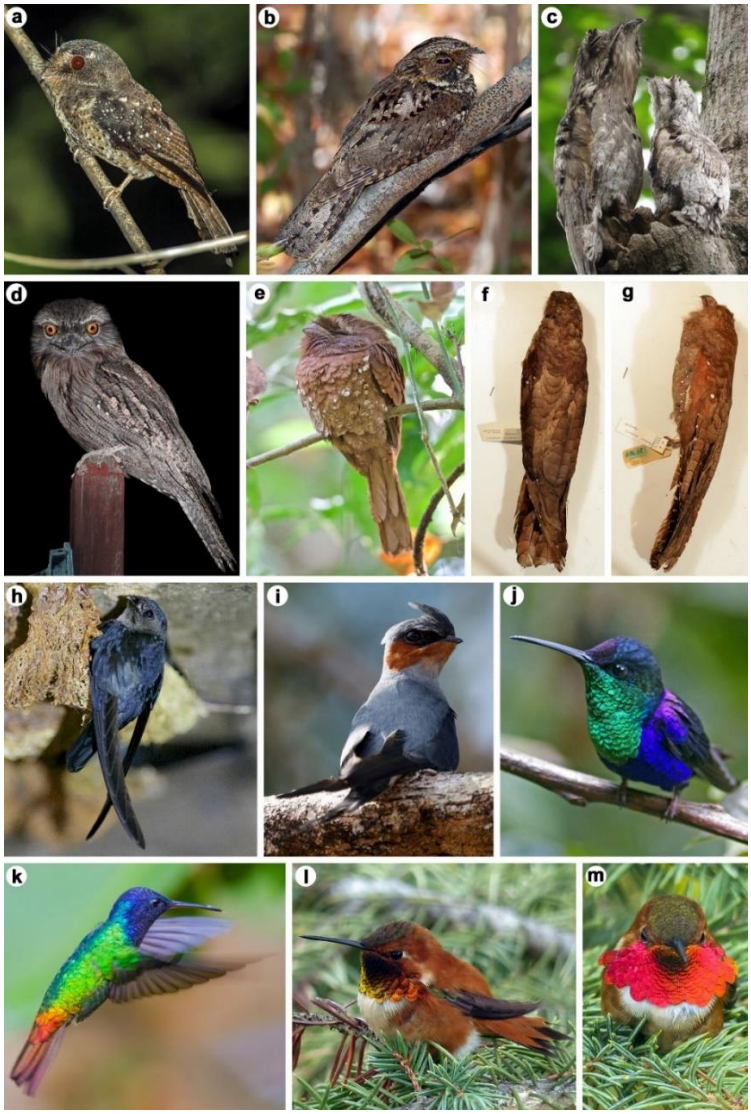

Figure 8.2. Examples of colour patterns exhibited throughout the extant Strisores. **a**-**g**. the nocturnal caprimulgiform birds with highly cryptic mottled and banded plumage with earthy tones. **a**. The Moluccan Owlet-Nightjar (*Aegotheles crinifrons*). **b**. The Puerto Rican Nightjar (*Antrostromus noctitherus*). **c**. The Common Potoo (*Nyctibius griseus*) performing branch mimicking behaviour. **d**. The Tawny Frogmouth (*Podargus strigoides*). **e**. The

Sri Lankan Frogmouth (*Batrachostomus moniliger*) - a rufous frogmouth taxon. **f-g**. The oilbird (*Steatornis caripensis*). **h-i**. The diurnal Apodiformes showing a range of conspicuous colour patterns including bright and saturated iridescence. **h**. The Glossy Swiftlet (*Collocalia esculenta*) showing subtle iridescence. **i**. The Crested Treeswift (*Hemiprocne coronata*). **j**. The Violet-Crowned Woodnymph (*Thalurania colombica*). **k**. The Golden-Tailed Sapphire (*Chrysuronia oenone*) showing remarkable rainbow iridescence. **l-m**. Allen's Hummingbird (*Selasphorus sasin*) with a rufous body and brightly iridescent extendable gorget (throat patch). Image credits: Francesco Veronesi (a), Sidnei Siqueira (b), Christopher Watson (d), Brian Ralphs (e), Thimindu Goonatillake (i), Joseph Boone (j) and Erick Houli (k). All other images either author's own or public domain.

Black, brown and grey colours are all produced through melanosomes with distinct morphologies in birds (Chapter 1; Fig. 1.1; Li et al. 2010, 2012; Vinther 2015). The iridescent colours of Apodiformes are produced using different melanosome types that have presumably evolved independently (Greenewalt et al. 1960; Prum 2006; Giraldo et al. 2018; Nordén et al. 2019). The hummingbirds and tree swifts produce iridescence using hollow and flat melanosomes (Fig. 1.1; Greenewalt et al. 1960; Prum 2006; Giraldo et al. 2018; Nordén et al 2019) while swifts utilise high aspect ratio melanosomes to produce iridescent hues (Nordén et al. 2019).

The melanosome morphologies and their correlated colour patterns found throughout Strisores are therefore linked to their activity patterns and behaviour. Reconstructing the colour patterns of fossil Strisores may allow these features to be determined in extinct members, which will help to understand the ancestral condition of the clade. Here, preserved melanosomes in five extinct strisorian genera from Messel and one from the Fur Formation are investigated and their likely colour patterns reconstructed through quantitative comparison of their melanosome morphologies to a comprehensive new database of melanosomes from all extant strisorian families. The likely ancestral colour patterns for Strisores, and in turn the question of nocturnality vs diurnality are then addressed. In addition, nuances of melanosome morphology in extant taxa, particularly those that produce iridescence are investigated in detail.

8.2. Materials and methods

8.2.1. Institutional abbreviations

HLMD: Hessisches Landesmuseum, Darmstadt, Germany; MGUH: Geological Museum of the University of Copenhagen; SMF: Senckenberg Research Institute Frankfurt, Germany; ZMUC: Zoological Museum, University of Copenhagen.

8.2.2. Fossil sampling

A total of nine fossil Strisores were sampled (12 including part and counterparts) representing six genera; one specimen of *Hassiavis laticauda* (a likely strisorian of currently unknown affinity; Messel Formation; Mayr 1998*b*, 2017*a*)*,* one specimen of the frogmouth (podargiform) *Masillapodargus longipes* (Messel Formation; Mayr 1999, 2017*a*), three specimens of the potoo (nyctibiiform) *Paraprefica* (Messel Formation; Mayr 1999, 2017*a*), one specimen of the stem apodiform *Eocypselus vincenti* (Fur Formation; Mayr 2010*c*), one example of the stem hummingbird (Trochilidae) *Parargornis messelensis* (Messel Formation; Mayr 2003, 2017*a*) and two specimens of the stem swift (Apodidae) *Scaniacypselus szarskii* (Messel Formation; Harrison 1984; Mayr 2017*a*; Table 8.1). Locations of samples are shown in Fig. S8.1.

Small samples (roughly 1 mm^2) were removed from the plumage of each specimen using a sterile scalpel and placed on carbon-coated SEM stubs. Care was taken to only remove organics from plumage rather than putative internal organs (McNamara et al. 2018). Where possible, samples were taken from clear vanes of the feathers to avoid downy regions which would not have contributed to the visible colour of the animal in life (see Chapter 7).

8.2.3. Specimen photography

Fossil specimens were photographed using a Nikon D800 DSLR with a Micro Nikkor 100 mm VR lens under the methodology described in Chapter 7.2.4 under both normal and cross polarised

light. In addition to the fossils that were sampled, further specimens that could not be accessed (for example those on display) were photographed to allow details of the plumage to be assessed.

Table 8.1. Fossil strisorian specimens sampled for melanosome imaging.

Specimen number	Taxon	Number of samples
SMF ME 9047a	*Hassiavis laticauda*	12
SMF ME 9047b	*Hassiavis laticauda*	4
MGUH 26729	*Eocypselus vincenti*	7
SMF ME 1415a	*Masillapodargus longipes*	6
SMF ME 1415b	*Masillapodargus longipes*	12
SMF ME 3727a	*Paraprefica kelleri*	12
SMF ME 3694	*Paraprefica* sp.	11
HLMD Be 10579a	*Paraprefica* sp.	10
HLMD Be 193	*Parargornis messelensis*	11
SMF ME 11345a	*Scaniacypselus starskii*	7
SMF ME 11345b	*Scaniacypselus starskii*	5
SMF ME 599	*Scaniacypselus starskii*	4

8.2.4. Modern feather sampling

Feathers from a total of 108 members of extant strisorians representing each family (and for hummingbirds - tribe; Stiles et al. 2017) were collected from the ZMUC (Appendix 1). For each specimen, every melanised colour including iridescence was sampled. The feathers were subjected to the revised melanosome extraction protocol (Chapter 6.4) and resulting melanin pellets placed on copper tape-coated SEM stubs.

8.2.5. SEM imaging

Both fossil and modern melanin samples were sputter coated with gold (10 nm for the fossils, 3 nm for the modern) using a Quorum Q150R ES sputter coater. Samples were then imaged using

a Zeiss Evo15 Environmental Scanning Electron Microscope (ESEM) at a working distance of 10 mm and an accelerating current of 10-20 KeV.

8.2.6. Colour reconstructions

All modern strisorian sample melanosomes were measured based on the methods described in Chapter 7.2.7 and the data were compiled to make a new database of melanosome colour-morphology. This new database comprises 210 samples from 108 taxa (Appendix 1). Colour reconstructions were performed based on the methodology of Chapter 7.2.8 using the new database in canonical discriminant analyses (CDAs).

It was noted during sampling that all hummingbird and tree swift samples other than those from rufous feathers contained flattened (and likely hollow) melanosomes irrespective of the colours produced (Fig. 8.3a-b). Previously, this melanosome morphology was thought to be only associated with iridescent colour production (Prum 2006; Shawkey 2013; Shawkey et al. 2015; Nordén et al. 2019) but all black, grey, dark brown and iridescent samples contained mainly flat and hollow melanosomes (Fig. 8.3a-e). Because hollowness and flatness are discrete characters, this information could not be incorporated into CDAs (Nordén et al. 2019). When assessing melanosome morphology from 2D SEM images, hollow or flat melanosomes can provide overlapping length and width measurements with solid and cylindrical ones, with only these discrete characters differentiating them (Chapter 7; Nordén et al. 2019). To test the effect this would have on the CDAs, further tests were run with all hollow and/or flat melanosome-containing samples (irrespective of colour) removed.

CDAs were also run using the fossil and modern strisorian data combined with the two modern datasets used in Chapter 7 (the original Li et al. (2012) data and new Upupiformes and outgroup data). For each database, both ‘stepwise’ and ‘all variables included’ models of CDA were used (see Chapter 7.2.8). As a measure of the effectiveness (predictive accuracy) of each database, the proportion of correctly classified modern samples of known colour from self-tests and cross-validated tests were calculated for each CDA (Chapter 7; Li et al. 2010).

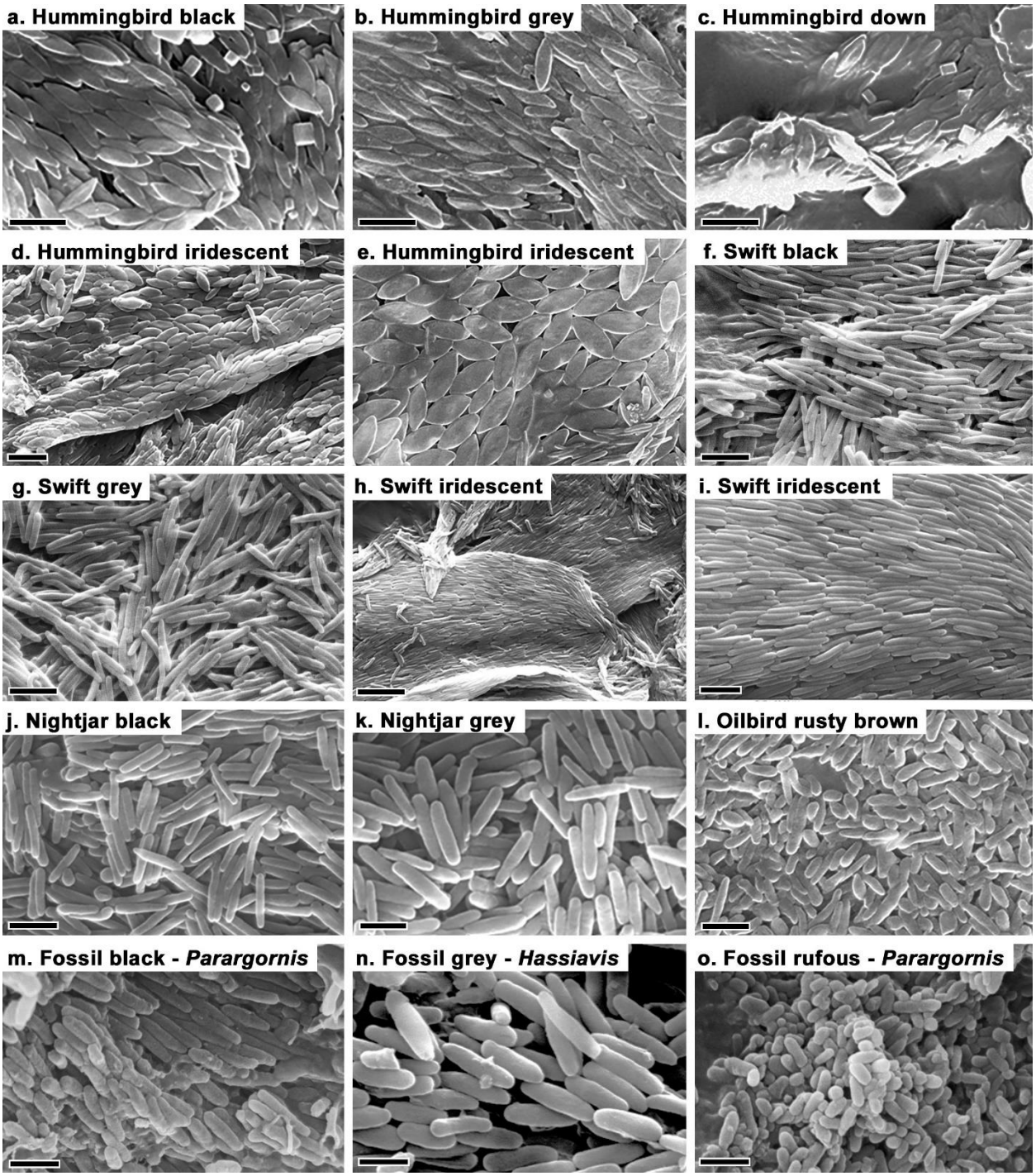

Figure 8.3. SEM images of melanosomes from extant and fossil strisorians. Extant melanosomes were extracted from feathers using the revised protocol (Chapter 6.4). Flat and hollow melanosomes previously thought to only be present in iridescent feathers are present in non-iridescent apodiform samples (**a-c**) and some iridescent hummingbird samples also contain solid and cylindrical melanosomes (**d-e**). Iridescent samples often showed original alignment and layering of melanosomes (d-e). The largest melanosomes yet observed are present in the

hummingbird *Colibri serrirostris* (**e**). Apodidae (swift) melanosomes are all of high aspect ratio-type irrespective of colour (**f-i**) but are more strongly aligned in layers in iridescent samples (**h-i**). Fossil melanosomes (**m-o**) strongly resemble those seen in extant caprimulgiform birds (**j-l**). Scale bars represent 2 µm in (a-d), 3 µm in (e) and (h) and 1 µm in (f-g) and (i-o).

As in previous palaeocolour analyses, potential shrinkage was modelled by scaling fossil melanosome dimensions up. Shrinkage of 5-10% was modelled as this is considered the most realistic for the Messel deposit (see Chapter 7.2.8).

In addition to the CDAs, principal component analyses (PCAs) were performed using the same variables to visualise the disparity in melanosome morphologies. The raw data were Z transformed to make the variables comparable. Without this transformation, length and width account for over 99% of the variance due to their units of measurement being relatively greater resulting in a falsely high variance compared to other variables. Separate PCAs were produced with data grouped by colour and by family to investigate phylogenetic patterns in melanosome morphology as well as separately for individual families to investigate the effect of the unusual melanosome morphologies in Apodiformes.

8.3. Results

8.3.1. Melanosome morphologies in modern strisorians

Melanosomes extracted from the nocturnal caprimulgiform members of Strisores generally conformed to previous observations on melanosome morphology related to the colours they produce (see Chapters 1.1 and 7; Fig 8.3j-l; Table 8.2). The nightjars (Caprimulgidae) show the most diverse array of melanosome morphologies of the nocturnal clades (Fig 8.4c-d). However, they were also the most heavily sampled due to the higher abundance of genera compared to other caprimulgiform families (Appendix 1).

Table 8.2. Melanosome measurements from modern taxa. The average (mean) data for melanosomes in three datasets are compared: (1) only modern strisorian taxa *including* hollow and flat melanosomes; (2) only modern strisorian taxa *excluding* flat and hollow melanosomes; (3) all modern taxa from Chapter 7, this chapter and Li et al. (2012) *excluding* hollow and flat melanosomes. AR = aspect ratio, N = number of melanosomes measured.

Colour category	Length (nm)	Length CV	Length skew	Width (nm)	Width CV	Width skew	Aspect ratio	AR skew	N
Dataset 1									
Black	1191.824	18.385	0.261	252.047	13.110	0.614	5.019	0.429	71
Brown	793.503	29.682	0.857	276.882	16.096	0.707	3.275	1.100	52
Grey	1523.930	17.775	0.213	340.776	15.473	0.506	4.812	0.548	47
High AR iridescent	1119.465	17.681	0.223	186.452	11.950	0.847	6.083	0.171	10
Hollow/flat iridescent	1694.888	15.534	0.493	610.755	19.389	0.489	2.896	0.610	30
Dataset 2									
Black	1190.002	18.484	0.268	249.427	13.108	0.625	5.047	0.421	70
Brown	793.503	29.682	0.857	276.882	16.096	0.707	3.275	1.100	52
Grey	1523.930	17.775	0.213	340.776	15.473	0.506	4.812	0.548	47
High AR iridescent	1119.465	17.681	0.223	186.452	11.950	0.847	6.083	0.171	10
Dataset 3									
Black	1150.447	18.266	0.199	272.221	12.370	0.537	4.422	0.238	149
Brown	636.487	27.214	0.832	288.469	16.123	0.511	2.410	1.257	129
Grey	1375.098	22.522	0.058	365.429	17.196	0.578	4.108	0.209	97
High AR iridescent	1126.570	18.270	0.207	200.512	17.192	0.448	5.832	0.418	46

The diurnal clades show significant divergence from the more typical melanosome morphology-colour relationship of the caprimulgiform birds. Almost every hummingbird and tree swift sample showed abundant flat and hollow melanosomes irrespective of the colours of the feathers they came from (Figs. 8.3a-e and 8.4). Non-fattened and hollow melanosomes were also observed in highly iridescent samples (Fig. 8.3d-e). The only hummingbird samples that consistently showed no flat and hollow melanosomes were those from rufous feathers where the more typical small spherical phaeomelanin-rich melanosomes were the most abundant. When only hummingbird and tree swift samples are compared, these rufous samples can clearly be statistically differentiated (Fig. 8.4g-h). Significant overlap in morphology of iridescent and non-iridescent melanosomes from both hummingbirds and tree swifts can be seen in the PCA plots when all taxa are considered (Figs. 8.4g) but only considering aspect ratio allows differentiation. When data are separated out by phylogeny and compared to the spread of colour categories, a large region of black and grey apodiform melanosomes plot in the same region as iridescent melanosomes (Fig. 8.4). This overlap remains when only hummingbird and tree swifts are compared (Fig. 8.4g).

Due to the revised protocol not always resulting in fully degraded feather structures (see Chapters 6 and 7), certain aspects of the arrangement of melanosomes could be observed. In samples from iridescent feathers, melanosomes were often still in their closely-packed and layered arrangement. This was seen in both hollow and flat types (Fig. 8.3e-d) and high aspect ratio types (Fig. 8.3h-i). Melanosomes were also sometimes still in their original arrangement in non-iridescent feather samples from apodiforms and showed similar layering (Fig. 8.3a-b). In downy portions of these apodiform feathers, melanosomes were sometimes still arranged in the cylindrical clusters identified in Chapter 7.3.4 (Fig. 8.3c) but with hollow and flat melanosomes present along with or instead of the more typical "grey type" (Chapter 1.1; Figs. 1.1 and 8.3c). Some iridescent feather samples from hummingbirds also showed multiple melanosome types within a single sample, sometimes in apparent original arrangement (Fig. 8.3d-e).

In addition to novel nuances of hollow and flat melanosomes in Apodiformes, every sample from modern swifts showed a consistent morphology of high aspect ratio irrespective of hue (Figs. 8.3f-i and 8.4c-f). As with flat and hollow melanosomes, this morphology is thought to be predominantly associated with iridescence, yet in swifts they were associated with black, grey and iridescent feathers. This can be seen in the PCA plots where the high aspect ratio iridescent melanosomes of swifts plot in a restricted region of colourspace well within a region occupied by black, grey and brown melanosomes from the same clade as well as others (Fig. 8.4c and e). This pattern is also clear in the aspect ratio plot where the group occupies a region of greater length to width than other clades and is again restricted in spread (Fig. 8.3d and f). The Apodiformes appear to have diverged from the more expected patterns of melanosome morphology seen in their sister clade and all other studied neognath groups and this appears related to the evolution of iridescence (Chapters 1 and 7; Li et al. 2014; Nordén et al. 2019).

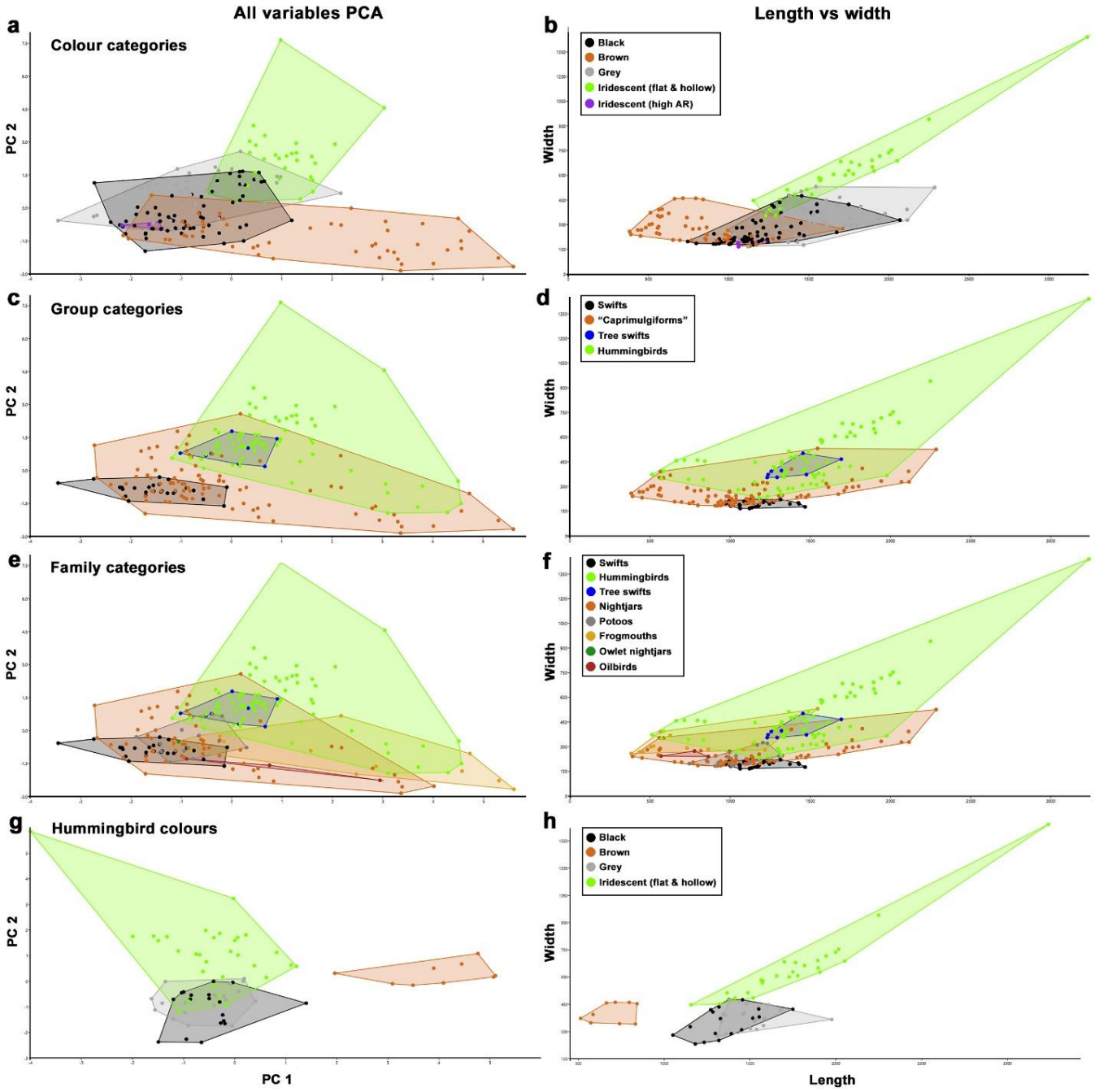

Figure 8.4. Principal component analyses (PCA) based on the first two principal component (PC) scores from all melanosome measurements (z transformed) and length vs width (aspect ratio) plots showing the distribution of melanosome morphologies in extant strisorians. Data are grouped by colour category (**a-b**), clade (with caprimulgiform birds grouped; **c-d**) and family (**e-f**). When comparing the spread of the colour categories to those of the clades, clear patterns emerge in which groups are accounting for certain colour categories. Hummingbird iridescent melanosomes are the most morphologically diverse while the swifts show the most conservative

disparity. When hummingbird melanosomes are considered on their own by colour category, overlap occurs between iridescent and black/grey samples, but brown samples plot in a distinct region in the PCA (**g**) while both iridescent and brown categories become distinct when only aspect ratio is considered (**h**).

8.3.2. Melanosomes and pigment patterns in fossil strisorians

Melanosomes were found in the majority of samples taken from the fossils and mainly consisted of ellipsoidal types but varied widely in overall size (Fig. 8.3m-o and Appendix 1). Only a small number of samples contained melanosomes resembling modern phaeomelanin-rich melanosomes (Fig. 8.3o). Several samples had no melanosomes present most likely due to issues with lacquers and the base resins (see Chapter 7.3.1). No samples contained flat and/or hollow melanosomes indicative of iridescence in modern hummingbirds and tree swifts.

Some of the fossils show colour patterns in their plumage visible to the naked eye. One specimen of the potoo *Paraprefica kelleri* (HLMD Be 164), which couldn't be sampled for melanosomes, shows strong banding on the outer margin of the primaries (Fig. 8.5a-b). This is a feature seen in some modern potoos, such as in *Nyctibius grandis* (Fig. 8.5c). Two specimens of *Hassiavis laticauda* (SMF ME 3545 and HLMD Me 9047) show a strongly banded tail (Fig. 8.5d-f) similar to the banded tails of many modern caprimulgiform birds (Mayr 1998*b*, 2004; Fig. 8.5g). The fossil swift *Scaniacypselus* shows uniformly pigmented wing and tail plumage similar in morphology to extant swifts (Fig. 8.5h-i). The stem hummingbird *Parargornis messelensis* shows pigmented plumage with considerably different morphology to crown group hummingbirds (Mayr 2003; Fig. 8.5j) with no banding or mottling as seen in the caprimulgiform birds (Fig. 8.5a-g).

8.3.3. Palaeocolour reconstructions in Strisores.

Some sample palaeocolour predictions differed when different databases were used (Table S8.1). When hollow and/or flattened melanosomes were included in the modern data, several fossil samples were predicted as being iridescent due to overlap with hummingbird

melanosomes (Table S8.1). However, because the fossil melanosomes were not of the hollow and/or flat type (Fig. 8.3m-o), iridescence could be excluded in these cases. When just modern strisorian data (excluding hollow and flat melanosome data) and all the modern data combined were used to predict palaeocolour, no sample was predicted as iridescent (high aspect ratio type; Figs 8.6-8.7 and Table S8.1). Instead, all fossils showed a mix of black, grey and brown (Fig 8.6; Table S8.1).

The overall level of predictive accuracy of the CDAs also varied depending on the modern dataset used. When just the modern Strisores (including hollow and flat melanosomes) dataset was used, the percentage of correctly classified samples was lowest (Table 8.3). Excluding hollow and flat melanosomes improved the predictive accuracy by almost 4% in self-tests (Table 8.3). When all modern samples were used, the predictive accuracy was around 71%. This is lower than the overall accuracy of the Li et al. (2012) and Upupiformes and outgroups datasets which may be due to the unusual pattern or swift melanosomes all being high aspect ratio irrespective of hue (Table 8.3). Variables loadings on each canonical function also differed depending on which dataset was used (Tables S8.2-8.3).A common pattern in the data between datasets is that more fossil samples are predicted as being brown when only Strisores are used (Table S8.1; Fig. 8.7 c-f) whereas more grey samples are predicted in the total dataset (Table S8.1; Fig. 8.7a-b). This could be due to the large number of brown modern samples from the modern Strisores data with a relative paucity of grey samples (Appendix 1).

Figure 8.5. Plumage details and colour patterns visible to the naked eye in fossil strisorians from Messel. **a-b**. The extinct potoo *Paraprefica kelleri* (HLMD Be 164) showing barred leading edges to the primaries, similar to the extant potoo *Nyctibius grandis* (**c**). **d-f**. The strisorian *Hassiavis laticauda* (d: SMF ME 3545; e: SMF ME 9047a) showing a distinctly barred tail, a feature seen in many extant caprimulgiform birds (e.g., the potoo *Nyctibius griseus*; **g**). **h-i**. The stem swift (Apodidae) *Scaniacypselus szarskii* (i: SMF ME 11345a) with uniformly pigmented wings and tail. **j**. the stem hummingbird *Parargornis messelensis* (HLMD Be 193) showing uniformly pigmented long tail feathers and relatively short wings. Scale bars represent 2 cm in (d), (g) and (j), 1 cm in (e) and (h-i) and 2 mm (f). Scales in (a-c) unknown.

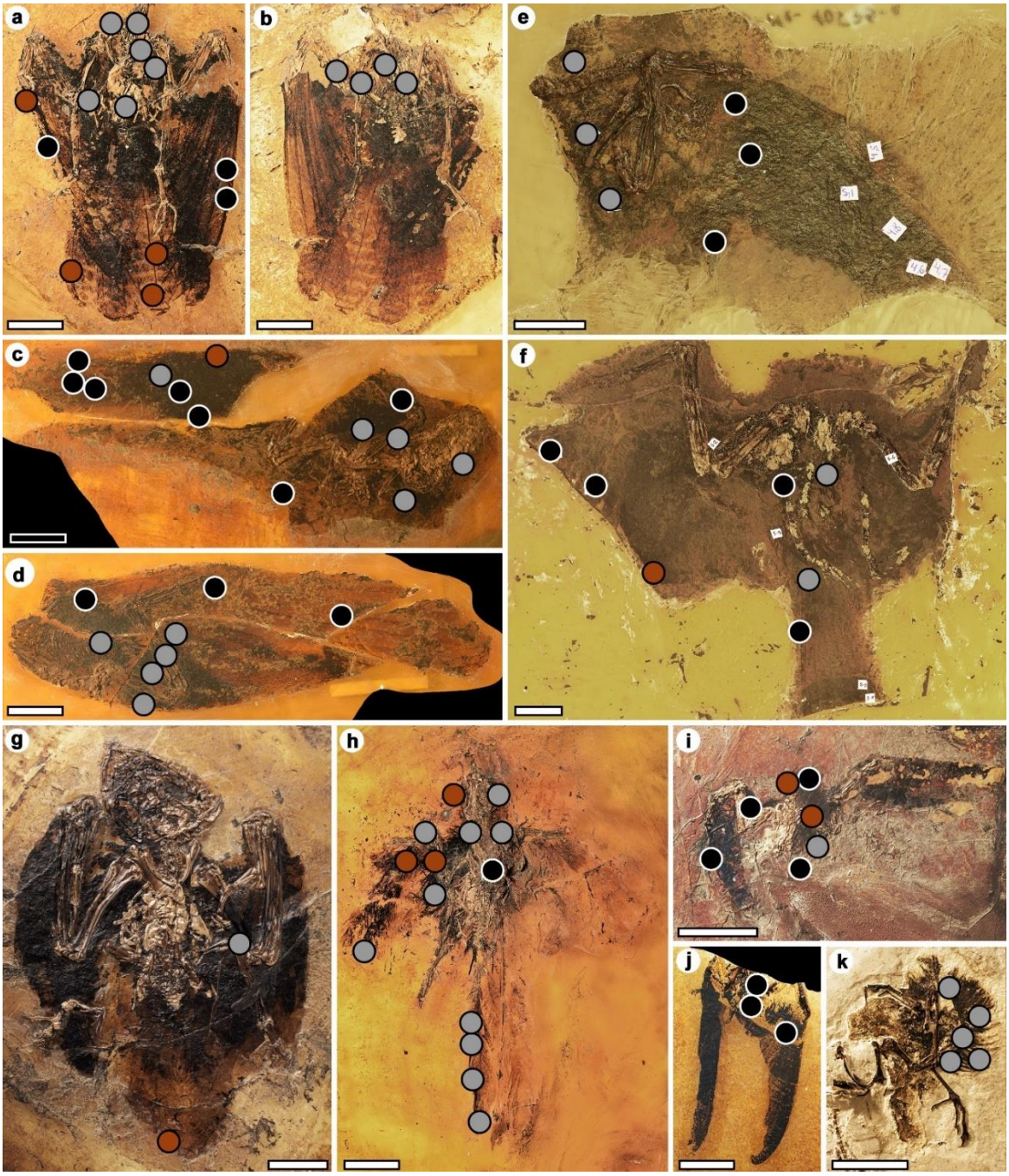

Figure 8.6. Predicted colours of fossil strisorian melanosome samples from canonical discriminant analyses (CDA) using a combined dataset of modern strisorians, taxa from Chapter 7 and those of Li et al. (2012). **a**. *Hassiavis laticauda* (SMF ME 9047a). **b**. *Hassiavis laticauda* (SMF ME 9047b). **c**. *Masillapodargus longipes* (SMF ME 1415a). **d**. *Masillapodargus longipes* (SMF ME 1415b). **e**. *Paraprefica* sp. (HLMD ME 10579a). **f**. *Paraprefica* sp. (SMF ME 3694). **g**. *Paraprefica kelleri* (SMF ME 3727a). **h**. *Parargornis messelensis* (HLMD Be 193). **i**. *Scaniacypselus szarskii* (SMF ME 599). **j**. *Scaniacypselus szarskii* (SMF ME 11345a). **k**. *Eocypselus vincenti* (MGUH 26729). All scale bars represent 2 cm.

Table 8.3. Predictive accuracy of canonical discriminant analyses (CDA) when different datasets of modern melanosome morphologies were used. Each dataset was run under both all "variables considered equally" and "stepwise" CDA models and the number of modern samples correctly classified in terms of colour category calculated based on self-test and cross-validation processes. Datasets including and excluding flat and hollow melanosomes were used to test how these morphologies affected predictive accuracy.

Dataset	All variables CDA		Stepwise CDA	
	Self-test	Cross-validated	Self-test	Cross-validated
Modern Strisores (inc. flat/hollow)	70%	67.6%	69%	68.1%
Modern Strisores (exc. flat/hollow)	73.8%	70.2%	69.5%	69.5%
Li et al. (2012)	76.5%	73.8%	75.3%	72.7%
Upupiformes and outgroups	76.8%	73.9%	75.7%	75.7%
All modern data (exc. flat/hollow)	70.8%	68.5%	70.8%	68.5%

When shrinkage was modelled into the palaeocolour predictions, the number of samples that changed as a result varied depending on the dataset and methods used (Tables 8.4 and S8.1). More samples changed when shrinkage was modelled at both 5% and 10% when only the modern Strisores dataset was used (Table 8.4). Additionally, when all variables were used in the analyses, more samples changed due to shrinkage than under the stepwise method (Table 8.4). As observed in previous analyses (see Chapters 5 and 7), the most common colour shift observed when shrinkage was modelled was from black or brown to grey (Table S8.1). In the colour-melanosome morphology CDA plots this can be seen where each sample moved progressively more towards the region occupied predominantly by grey samples when more shrinkage is modelled without hollow and flat melanosome included (Fig. 8.7c-d). Due to the generally large size of the hollow and flat iridescent melanosomes, when these were included in the modern Strisores data, fossil samples scaled up to account for shrinkage also moved towards the iridescent region of colourspace (Fig. 8.7e-f) and changed to iridescent in colour predictions.

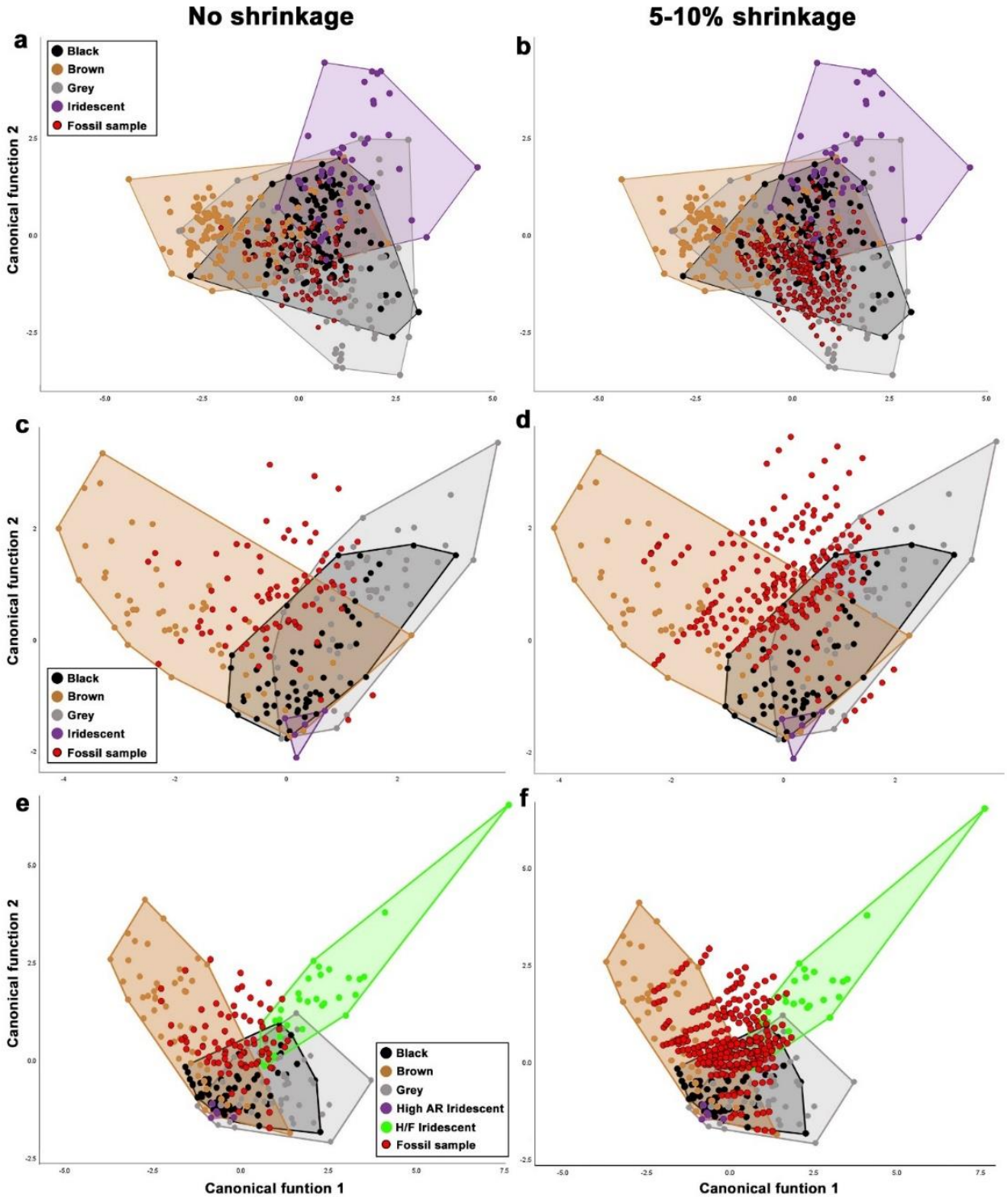

Figure 8.7. Canonical discriminant analysis (CDA) plots showing the distribution of fossil melanosome samples in colour space based on different datasets of melanosome morphologies. Two plots are shown for each dataset; one with no fossil samples scaled up for shrinkage and one with fossils scaled up by 5% and 10% as well as the original measurements. **a-b**. All modern samples including Strisores, data from Chapter 7 and the Li et al. (2012) dataset

with hollow and flat melanosomes excluded. All fossil samples plot within the black, grey and brown regions of colourspace. **c-d**. Only modern Strisores data excluding hollow and flat (H/F) melanosomes. No fossil samples fall within the narrow iridescent region of colourspace. **e-f**. Only modern Strisores data including hollow and flat melanosomes. Several fossil samples plot within the hollow/flat iridescence colourspace despite not being hollow or flat, highlighting the overlap in size of iridescent and non-iridescent melanosomes in hummingbirds and tree swifts. When shrinkage is modelled into the fossil samples, they move towards either the grey (a-d) or flat/hollow iridescence (e-f) regions of colourspace, as these represent the largest morphotypes. AR = aspect ratio.

As the most comprehensive, colour predictions from the combined dataset using a stepwise CDA was used to map out the likely colour patterns of each fossil member of Strisores (Fig. 8.6 and Table S8.1). Each of the caprimulgiform taxa showed a mix of grey, black and brown. *Hassiavis* appears to have had a consistent grey chest and throat region with black and brown wings and a brown and white (absence of pigment) tail (Fig. 8.6a-b). *Masillapodargus* showed mainly black and grey colours with a single brown sample on the wings (Fig. 8.6c-d). *Paraprefica* again showed predominantly black and grey samples with a single brown sample on the wing on one specimen and one on the tail of another (Fig. 8.6e-g). All apodiform and stem apodiform taxa also showed black brown and grey colours. *Parargornis* was predominantly grey with a brown head and proximal wing region (Fig. 8.6h), *Scaniacypselus* was predominantly black with some grey and brown on the body (Fig 8.6i-j) and *Eocypselus* was uniformly grey (Fig. 8.6k).

Table 8.4. The percentage of fossil melanosome samples that changed colour prediction when different levels of shrinkage were modelled using two different datasets and two methods of canonical discriminant analysis (CDA).

	Strisores data		**All modern data**	
Method	**5% shrinkage**	**10% shrinkage**	**5% shrinkage**	**10% shrinkage**
All variables	10.79%	22.54%	8.10%	13.02%
Stepwise	12.38%	20.16%	3.65%	9.37%
Average of both	11.59%	21.35%	5.87%	11.19%

8.4. Discussion

8.4.1. Modern Strisores melanosome morphologies and colour production

Significant divergences in the expected correlation of melanosome morphology to the colours produced in bird feathers exists in certain Strisores families. While the nocturnal caprimulgiform clades appear to show melanosome morphologies generally in line with other bird clades in terms of the colours they generate (see Chapter 1.1), the diurnal Apodiformes show some unexpected and novel patterns. It is shown here for the first time that melanosomes thought to only be involved in iridescent colour production are found in significant numbers in non-iridescent feathers as well as downy portions of iridescent feathers (Fig. 8.3a-e). Therefore, features such as hollowness and flatness do not necessarily indicate that a particular feather shows iridescent colour production (Prum 2006; Nordén et al. 2019). However, the presence of hollow and/or flat melanosomes in a feather sample does appear to show that the bird from which it came has iridescent plumage. Therefore, finding these morphologies in fossil bird feathers would unambiguously show that the animal had iridescent plumage, irrespective of whether that specific sample came from an iridescent feather. In addition, flat and hollow melanosomes from iridescent and non-iridescent hummingbird feathers can be differentiated by size (Fig. 8.4h).

These observations are in line with melanosome arrangement being key to the production of iridescence along with melanosome morphology (Prum 2006; Eliason et al. 2013; Shawkey 2013; Shawkey et al. 2015). Flattened melanosomes are thought to allow for brighter iridescent colours as they allow for closer packing within the barbule, meaning that more layers can be stacked than would be possible with non-flattened melanosomes (Maia et al. 2011; Eliason et al. 2013; Nordén et al. 2019). Having an air space within the melanosomes and thus having multiple layers of melanin, air and keratin in a small volume allows generation of multi-layered reflectors that produce iridescence through coherent light scattering (Prum 2006; Giraldo et al. 2018). Because hummingbirds and tree swifts often have hollow and flat melanosomes in non-iridescent feathers (Figs. 8.3 and 8.4), their size difference and precise arrangement within the keratin of the feather barbule must be key to determining whether any

structural colour is produced (Prum 2006; Eliason et al. 2013; Shawkey 2013; Shawkey et al 2015; Nordén et al. 2019).

The thickness of the keratin that overlies and sits in between layers of melanosomes controls iridescent hues in extant bird feathers (Prum 2006; Eliason et al. 2013; Shawkey et al. 2015). Because the enzymatic extraction protocol degraded keratin in most samples, this could not be studied in detail with the current data. The partial degradation of keratin in some samples did however confirm the tight alignment and arrangement of hollow and flat melanosomes into discrete layers in iridescent hummingbird barbules (Fig. 8.3a-e). The number of and distance between these layers as well as the morphology of the melanosomes must control the precise hues generated (Prum 2006; Eliason et al. 2013; Nordén et al. 2019) as it was also shown that non-iridescent samples also had melanosomes arranged in tightly packed layers (Fig. 8.3a-b).

Studies into the ontogenetic development of iridescence in male Blue-Black Grassquits (*Volatinia jacarina*; Passeriformes) show that no cellular processes are involved in arranging melanosomes within the keratin to allow thin-film refraction iridescence (Maia et al. 2011). Instead, non-metabolic entropic depletion-attraction processes allow melanosomes to migrate to form a layer underneath the keratin at the periphery of the feather barbules. In non-iridescent females, melanised colours are produced through more disordered arrangements of melanosomes. In this case, melanosomes in males are larger and it is thought that size determines whether melanosomes are arranged into iridescence-producing layers or not (Maia et al. 2011). Here, I show that melanosomes associated with iridescence are significantly larger than those associated with non-iridescence in hummingbirds and tree swifts (Figs. 8.3a-e and 8.4h; Table 8.2). In fact, the largest melanosomes of any living vertebrate so far studied are identified here and come from the green iridescent feathers of the hummingbird *Colibri serrirostris* (averaging over 3200 µm in length by 1440 µm wide; Fig. 8.3e). Therefore, a similar depletion-attraction process could explain how iridescence and non-iridescence can both be generated from flat and hollow melanosomes of different sizes within an individual bird.

At present, little data exist on the developmental processes of iridescence in the hummingbirds. In other iridescence-producing taxa, it is only at the final developmental stages that melanosomes become arranged in the precise patterns needed to generate their specific hues (Shawkey et al. 2015). One possible explanation to how iridescence and non-iridescence can be produced using flat and hollow melanosomes in Apodiformes could be the point at which development arrests. If the final stages of melanosome arrangement into multi-layered arrays (Prum 2006) aren't achieved, the resulting colour production would likely be non-iridescent. Only one melanosome type would therefore need to be synthesised yet could result in a vast array of colours, both iridescent and non-iridescent. Similar processes could also explain how swifts can generate iridescence from the same melanosomes that produce non-iridescent hues (Fig. 8.3f-i).

That most hummingbird melanosomes are flat and hollow despite hues produced may account for the remarkable array of iridescent colours within the clade and how patterns such as rainbow hues can be achieved within an individual (Fig. 8.2k). If it is predominantly the arrangement of melanosomes and/or the thickness of the overlying keratin that determines hue, these should be more labile traits than melanosome morphology. In contrast, synthesising different melanosome morphologies may be a more difficult and less parsimonious way to achieve different hues once a novel morphology has been developed (Nordén et al. 2019). The mechanisms by which melanosomes become flattened are currently unknown, and hollowness can be achieved through multiple different pathways that likely evolved independently (Maia et al. 2011; Eliason et al. 2013; Shawkey et al. 2015; D'Alba and Shawkey 2018). The data presented here suggest that more work is needed to understand developmental differences between iridescence and non-iridescence within a group, single taxon and even individual.

The presence of solid and cylindrical melanosomes (those typical of non-iridescent black and grey feathers) in layers associated with flat and hollow melanosome layers in iridescent feathers (Fig. 8.3d) is another important observation. It could not be determined from where these solid melanosome layers derived (barb or barbule). One possibility is that they derive from the rachis or barbs, as this melanosome morphology has been observed in the rachises of iridescent sunbird feathers which also have flattened melanosomes in the barbules (Mahapatra

et al. 2016). It is also plausible that they sit underneath the hollow/flat melanosome layer to absorb any light which passed through all overlying melanosome layers to prevent incoherent scattered light reflecting and thus increase the brightness and/or saturation of the iridescence (Prum 2006). This could be investigated further using in-situ imaging techniques such as TEM imaging (See Chapter 1).

8.4.2. Fossil Strisores melanosomes, palaeocolour reconstructions and palaeoecology

Melanosomes from the fossil taxa all fall within morphologies correlated with black, grey and brown colours in extant birds (Figs. 8.3j-l and Table S8.1). Samples predicted as iridescent based on the data incorporating extant strisorian hollow and flat melanosomes (Fig. 8.7e-f) can be discounted as these distinct morphotypes were not present in any fossil sample. Importantly, no fattened and/or hollow melanosomes were found in the stem hummingbird *Parargornis*, suggesting that this derived morphology evolved later in crown group hummingbirds. The new observations that these melanosome morphologies are present in all pigmented feathers from iridescent members of Trochilidae and Hemiprocnidae irrespective of hue means that iridescence can be conclusively ruled out in the fossils and it is not just a case of insufficient sampling resulting in missed iridescent feathers.

As the lowest predictive power was seen in the modern Strisores data with hollow and flat melanosomes included, the unusual melanosome morphologies in the Apodiformes can clearly distort fossil colour predictions if not treated with caution. This can be mitigated for however because these morphologies can be easily identified in fossils (Chapter 7; Nordén et al. 2019) and removing them from CDA analyses of modern data allows predictive accuracy more in line with the other datasets (Table 8.3).

As with modern caprimulgiform birds, mixes of earthy tones and mottled/banded plumage were prevalent in strisorians from Messel, which would have helped the birds blend in to the forested environment (Gomez and Théry 2007; Mayr 2017*a*; Schaal et al. 2018). While the majority of extant Apodiformes have evolved showy colours presumably related to social

signalling (Fig. 8.2h-m), none of the Messel or Fur Apodiformes appear to have exhibited the same colour features. *Scaniacypselus*, *Eocypselus* and *Parargornis* showed a similar mix of earthy tones to the caprimulgiform taxa, suggesting that they too had colour patterns more likely to be associated with camouflage than conspecific social signalling. In addition, a further species of *Eocypselus* (*E. rowei*) from the Green River Formation in North America has had melanosomes imaged that appear typical of black or grey colours (Ksepka et al. 2013).

These results sharply contrast the trend of dichotomous disparity in colour patterns seen in extant strisorians (Fig. 8.2). Because the colourful and showy plumage of most Apodiformes is likely related to diurnal activity patterns and is absent in Eocene taxa, the most parsimonious ancestral condition for Strisores as a whole is that of nocturnality rather than multiple origins in separate caprimulgiform clades (Fig. 8.1). This is in line with previous interpretations based on phylogeny and skeletal anatomy (Fig. 8.1; Mayr 2010*b*).

The point at which Apodiformes switched to a diurnal habit is still an open question, and all that can be said with the data presented here is that this point was likely post-Eocene. It is of note that in extant birds, multiple clades have converged morphologically and/or behaviourally on similar ecologies to the Apodiformes and have also evolved similarly showy colours, for example swifts/tree swifts and swallows/martins (Passeriformes) and hummingbirds and sunbirds (Passeriformes). The sunbirds have evolved many morphological and behavioural adaptations convergent with hummingbirds including body size, feeding mode (nectivory) and colour patterns (Prinzinger et al 1992). They exhibit bright and showy iridescence, which is produced through flattened melanosomes, another key convergence with hummingbirds (Prum 2006; Nordén et al. 2019). The relationship between these strikingly similar colour patterns and behavioural traits such as feeding modes are poorly understood. It is possible that feeding on brightly coloured flowers, which both clades do, is connected with having bright and showy iridescence. For example, iridescence could help the birds to stand out to conspecifics against varied and saturated flower colours, whether it be for sexual (Herrera et al. 2008) or territorial/competitive signalling (Wolf 1969; Bleiweiss 1985, 1992). Alternatively, iridescence could have evolved due to a form of sensory bias/drive (West-Eberhard 1984; Endler 1992), as iridescent colours are likely widespread in flowers (Whitney et al. 2009). If floral iridescence is

used by hummingbirds and/or sunbirds as a cue during feeding, it is plausible that a preference for iridescence plumage from either sex could evolve in associated at some point after this feeding mode evolved (West-Eberhard 1984; Endler 1992; Fuller et al. 2005). Floral iridescence is thought to be associated with attracting pollinators such as insects (Whitney et al. 2009), and so flowers likely evolved iridescence prior to hummingbirds and sunbirds due to their long coevolution with insect pollinators (Crane et al. 1995). As birds can also perceive UV light, this may also play a role in iridescent signalling as is known in other non-avian animals (Doucet and Meadows 2009). Currently, it is uncertain whether these feeding modes or the presence of showy iridescence evolved first in either clade, which would help to answer these questions.

8.5. Conclusions

Quantitative comparison of preserved melanosomes from six fossil strisorians from Messel along with visible colour patterning reveals that the group showed a mix of earthy hues in the Eocene with none of the showy iridescent colours associated with diurnal members of Strisores today. These palaeocolours suggest that the group was ancestrally nocturnal with the Apodiformes evolving a diurnal habit and showy colours post-Eocene. New information from extant Apodiformes shows that iridescence-associated melanosome morphologies can occur in non-iridescent feathers but only from birds that have evolved and exhibit iridescence. Care must be taken when interpreting putative iridescence in fossils and where possible, melanosome morphologies should be investigated in a clade-specific manner to ensure novel morphologies don’t bias palaeocolour reconstructions.

General discussion and conclusions

The aim of this thesis was to broaden the field of palaeocolour by incorporating both palaeontological and neontological approaches to give a greater understanding of certain diapsid fossils as both geological features and once living organisms. With this thesis I have specifically expanded our understanding of past ecologies of terrestrial theropods by reconstructing the colour patterns of *Sinosauropteryx* and *Caudipteryx*, revealing multiple patterns associated with camouflage and conspicuous signalling. I have explored the evolution of colour patterning and associated ecologies, behaviours and habitat preferences within crown Aves by investigating the evolution of strisorian and upupiform birds in a phylogenetic framework. Through this, I have shown that certain traits have deep origins, like the nocturnal, drab plumage in caprimulgiform birds that in the Eocene included the now showy Apodiformes. I also reveal that Upupiformes departed from an arboreal ancestral condition having black-grey colouration in two separate directions of brighter iridescent and more drab plumage and open habitat preference. Further outside of archosaurs within diapsids, I have specifically targeted ichthyosaur integument and improved our understanding of its taphonomy and found that contrary to previous claims (Lindgren et al. 2014) ichthyosaurs are generally countershaded. I have also developed a revised enzyme extraction protocol that will allow for faster compilation of modern melanosome datasets with higher sample sizes that will aid future palaeocolour research. Through the development of the research themes in this thesis, some general points about the nature of the field, factors that need to be considered in palaeocolour work and areas where more information is needed in future work came to light.

Revealing past environments and predator-prey dynamics through palaeocolour

Animals evolve camouflage and vivid display as a consequence of the eye-of-the-beholder (Guilford and Dawkins 1991; Bortolotti 2006). Whether it is through the mechanisms of survival or passing offspring on, animal colouration can evolve rapidly, as colour is so key to the success of a species. While much work has focussed on how we reveal colours in extinct animals

(Chapter 1), the wider implications of what these can tell us about the animals when they were alive, or the evolution of colour and associated ecologies and/or behaviours in specific clades has thus far been underappreciated (Li et al. 2014; Vinther et al. 2016; Brown et al. 2017; Smithwick et al. 2017*a*). This was a main focus of my research for this thesis. Some have also argued that due to low sample sizes, life history traits cannot be deduced from fossils because of high variability in colour patterns seen in living animals and ambiguity about specific functions (Negro et al. 2018). However, the colour patterns I and others have identified in fossils, such as countershading, banding and eye stripes, still have important implications for the ecology of the animals when alive, irrespective of differences in species, sex or seasonal variation (Negro et al. 2018). While the precise functions of many of the observed colour patterns can be debated, general trends with regard to life history traits can still be inferred. For example, the correlation between countershading and habitat preference in some extant animals holds, irrespective of the precise function or evolutionary origins of the patterning (Allen et al. 2012). The prevalence of countershading, stripes, mottling and other colour patterns in living taxa means that finding it in fossils allows us to investigate life history traits even when only a few or even a single specimen is available.

One of the conclusions I have drawn in writing this thesis is that the general principals governing colour patterning in living animals appear to hold true for extinct taxa. Certain colour pattern strategies seem universal, suggesting that their function was as important in the past as today. While the exact functions of these colour patterns will likely always remain open to question (Bortolotti 2006; Negro et al. 2018), we can draw general inferences by comparisons to a range of living taxa. The prevalence of certain colour patterns in deep time and today suggests that the same or similar drivers were acting on many extinct animals as today's, at least as far back as the Early Jurassic (Chapters 3-5).

All of the colour patterns observed in fossil taxa are present across living animals (Bortolotti 2006; Ruxton et al. 2018). Even in taxa with no direct living descendants (e.g., non-avian theropods and ichthyosaurs) no novel colour patterns outside of those known today were found. The more we understand about the colouration of extinct animals, the more it becomes clear that certain features are consistent throughout time. Countershading appears to be as

common in fossil taxa as it is in living animals (Chapters 3-5). The majority of extinct marine and terrestrial diapsids that have had colours reconstructed show countershading (Chapters 3-5; Vinther et al. 2016; Brown et al. 2017; Smithwick et al. 2017*a*, Lindgren et al. 2018). This is perhaps not surprising, given the ubiquity of the pattern in living animals (Rowland 2011) and the likely function as camouflage driven by the visual capabilities of predators and/or prey in the environment (as well as potentially non-visual factors; Stevens 2007; Rowland 2009, 2011; Allen et al. 2012). The visual cue of a 3D body is a problem that has likely existed since early in the evolution of the eye, potentially when depth perception originated (Goldsmith 1990; Land and Fernald 1992; Fernald 2000; Collins et al. 2003; Nilsson 2009). In turn, because we know that countershading is related to 3D cues requiring a certain level of visual capability, finding countershading in fossil taxa could inform the visual capabilities of predators or prey in the environment at a given time. This highlights the importance of considering the observer/intended receiver when investigating colour pattern evolution (Guilford and Dawkins 1991; Stevens 2007). While colour patterns are generally rare in the fossil record, understanding them can potentially also inform about the types of vision around at any given time.

The types of vision possessed by animals around in the Mesozoic were likely similar to many of today's, albeit with different animals occupying different trophic levels - for example, large theropods with tri- or tetrachromatic vision comparable to extant birds being the apex predators instead of dichromatic mammals (Bowmaker 2006; Stevens 2006). This has been shown to alter the expectations of colour patterns in some regards, for example countershading in animals larger than those that display it today due to the threshold for refuge at large body size being greater due to the large apex predators of the Mesozoic (Brown et al. 2017). Due to the likely good visual capabilities of the animals in places like Jehol, colour patterning appears to have been as important (and likely even more so) for both predators and prey as today. The presence of distinctive colour patterning such as countershading, stripes and banding in two diminutive theropods with different feeding habits and general ecologies in Jehol (*Sinosauropteryx* and *Caudipteryx*) further highlights the importance of camouflage and

signalling in the Mesozoic, likely linked to the strongly visual predator prey landscape at the time.

While we can get a good idea of the types of visual capabilities of animals in the Mesozoic, the further back in time we go, the harder this would likely become as ecosystems become further from what we know and can use comparatively today. If we could investigate palaeocolour back to when eyes were first evolving, we could perhaps learn more about the origins and early evolution of vision in metazoans more generally and build a clearer picture of the visual landscape which is currently limited (Parker 1998, 2000; Fernald 2000; Bowmaker 2006).

Iridescent colour production has been proposed in some Cambrian arthropods (Parker 1998, 2000), suggesting that specific visual cues evolved early on in metazoans, although like with nacreous mollusc shells, iridescence in many invertebrates could be an exaptation of the functional aspect that also create the photonic nanostructure visible to us. Finding other colour patterns known to be related to vision could help build a better picture of the visual world at this time. Conversely, understanding the visual system around at the time could allow predictions about the types of colour patterns animals were displaying. For example, would we expect to find a pattern such as countershading at a time when the main predators possessed compound eyes (Paterson et al. 2011)? If we did, would it advance our understanding of the visual capabilities of these animals, or even suggest that novel visual systems we have not found in fossils existed at the time? Pigments (most likely melanins) are present in some Cambrian fossils (Ma et al. 2012), offering the tantalising opportunity for palaeocolour to be extended back to the early evolution of animals.

Palaeocolour also has great utility in understanding the evolution of colour and associated function and behaviours in the more recent past. It can also provide novel insight at an ecosystem or environmental level. My palaeocolour reconstructions of crown neognaths from Messel (Chapters 7-8) suggest that this Eocene paratropical forest (Mayr 2017*a*) may not have been as colourful as today's tropical forests (Gomez and Théry 2004). This is unexpected given that the diversity of the Messel avifauna approaches modern analogous habitats (Mayr

2017*a*) and visual systems have likely not changed much since the Eocene. As no evidence of iridescence was found in any bird from Messel, in taxa where it may have been presumed likely (Apodiformes and Upupiformes), the majority of Messel birds may have been rather earthy and drab. Alternatively, iridescent colour patterns may have been evolved by other taxa that don't generally display this feature today. This may coincide with differences in other anatomically-related life history traits between Messel birds and their modern relatives, for example, perching ability, flying and feeding (Mayr 2017*a*). Investigations of melanosome morphologies in further Messel taxa may help shed light on this and determine whether any showed derived morphologies associated with iridescence in modern birds (Prum 2006). As these derived morphologies have been evolved many times independently (Prum 2006; Nordén et al. 2019), they may have been present in unexpected avian clades in the Eocene. The presence of isolated feathers showing structural iridescence (Vitek et al. 2013; Fig. 1.8) show that this type of colour was present at the time, but as yet, we do not know to which birds these belonged or how common they were.

Pigmentary colours beyond melanin in palaeocolour

Methods for detecting non-melanin pigments in fossils generally are improving rapidly (Sanger 1988; Vinther 2015*a*; Wiemann et al. 2017). Carotenoids, porphyrins and other pigments such as biliverdin have been detected in fossils (for example egg shells; Wiemann et al. 2017), but as yet have not been recovered from the feathers of fossil birds or confirmed chemically in any vertebrate integument (McNamara et al. 2016*a*). Given the pace of advancement of chemical analytical techniques in palaeontology, I expect this not to be the case for long. These pigments may have contributed to the plumage of some of the taxa investigated in this thesis. For example, carotenoids may have been prevalent in certain Messel birds where we see unpigmented plumage or a lack of plumage preservation altogether. Knowledge on the distribution of these diet-derived pigments in modern bird clades (40% of extant Passeriformes, 13% of non-passeriform birds; Thomas et al. 2014*a*) can help predict their likely occurrence in the Eocene, however. Based on this distribution, I consider it unlikely that any of the Eocene

birds studied in this thesis displayed carotenoid-based colours (Thomas et al. 2014*a*). No extant upupiform or strisorian bird is known to use carotenoids in their displayed colours (Thomas et al. 2014*a*). A few cases exist where some extant birds use carotenoid-based colouration despite it being absent generally in their order or family (Thomas et al. 2014*a*) but based on their rarity this cannot be considered parsimonious in the extinct birds in this thesis. To my knowledge, no pigments outside of melanin have been shown to colour the feathers of any upupiform or strisorian bird, ruling these out as likely in the fossils.

Due to their prevalence across most vertebrates (Bagnara et al. 1968; Jimbow et al. 1986; Landmann 1986), and especially birds (McGraw 2006*a*, 2006*c*), it is likely that further pigments beyond melanin contributed to the colour patterns of dinosaurs in the Mesozoic. For example, patches I have predicted as being unpigmented based on a lack of melanin in the fossils in non-theropod dinosaurs (Chapters 4-5) could have originally contained other pigments that did not preserve. However, again, the limited distribution of carotenoids in modern birds (Thomas et al. 2014*a*) and the clade-specificity of most other avian pigments (McGraw 2006*c*) make it more parsimonious to assume that areas of plumage without melanin were originally unpigmented until evidence suggests otherwise. Could certain non-avian dinosaur clades or even animals like ichthyosaurs have evolved their own specific pigments beyond what we know of today? This is plausible, but difficult to test. Even if chemical data suggested novel pigment classes in fossils, factors such as diagenetic alteration and contamination from exogenous sources would be hard to account for.

Choosing modern analogues for accurate palaeocolour reconstructions

A further feature highlighted by this thesis is the importance of using appropriate extant analogues when examining palaeocolour in extinct taxa. In an ideal situation, both taxa directly related to the animals being studied as well as those not necessarily closely related will give a clearer picture of why certain colour patterns may have been present. This will also provide better information on how and why colour traits have evolved through time. Considering colour patterns and their likely functions in multiple clades made it possible to get a better idea of why

certain patterns may have been present in Jurassic ichthyosaurs (Chapter 3), *Sinosauropteryx* (Chapter 4) and *Caudipteryx* (Chapter 5). None of these taxa have direct living descendants but all show similarities with extant animals from different clades. In these cases, therefore, I used the most appropriate modern analogues based on anatomical and environmental similarities. In the case of taxa with direct living descendants and likely similar ecologies (such as *Messelirrisor* (Chapter 7) and the extinct members of Strisores (Chapter 8)) it is sufficient to rely on modern relatives to build a better idea of why certain colour patterns may have been present. The appropriate analogues therefore should be considered on a case-by-case basis in palaeocolour studies.

Melanosome taphonomy

Several of the specimens studied in this thesis provided samples that can inform melanosome taphonomy. While it is known that melanosomes can shrink during diagenesis (McNamara et al. 2013) and can even be lost altogether leaving just impressions, the precise nuances of these features are poorly understood. Melanosomes from the Strawberry Bank ichthyosaurs provide and interesting case. Some are apparently unaltered, some have shrunk while others have been lost altogether (Chapter 3; Fig. 3.6) despite all being from the same deposit and thus having the same burial history. However, the fossils are heavily weathered and so oxidation may play a role in melanosome loss and/or shrinkage. This is further backed up by the observation that in the Jehol fossils, melanosome impressions are often found in an unidentified organic matrix likely representing kerogen (Chapter 5.4.4; Fig. 3.5). A new mode of preservation is proposed here, whereby melanosomes are initially retained during decay until other organics (e.g., kerogen) create a matrix surrounding them. After the kerogen stabilises, the melanosomes are often lost, possibly through oxidation, leaving impressions/moulds within the now stable kerogen matrix (Fig. D1).

Modern melanosome morphology

During the development of this thesis, I also began questioning how investigating melanosomes in modern birds, initially to allow palaeocolour reconstructions (Chapter 1), may be able to inform about how certain colours have evolved in particular groups. I also wanted to address concerns raised about the previously reported correlation of melanosome morphology to colour (Galván and Solano 2016; Negro et al. 2018). Of particular interest was the evolution of iridescent colours with derived melanosome morphologies in birds. My observations that flat and hollow melanosomes are present in non-iridescent hummingbird feathers and all swift melanosomes are high aspect ratio-type irrespective of colour (Chapter 8) suggest that there is still much to understand about the relationship between melanosome type and colour production in living animals. My observations were only made possible by focussing in and exploring melanosome diversity within each relevant avian clade using large samples. This approach is therefore likely to lead to other novel discoveries if employed on other avian clades.

Recently, palaeocolour studies have been questioned based on an argument that colour in extant birds cannot be determined by melanosome shape (Negro et al. 2018). My new data for modern melanosomes refutes these claims and backs up previous work highlighting distinct morphological differences in melanosomes imparting different colours (Li et al. 2010, 2012; Zhang et al. 2010; Vinther et al. 2016; Hu et al. 2018). While the chemistry of the different morphologies has not yet been fully distinguished, I confirm that there is a general correlation between shape and colour in melanosomes. Additionally, my revised melanosome extraction protocol (Chapter 6) allows phaeomelanin-rich melanosomes to be extracted and confirms their general spherical morphology and smaller size to eumelanin-rich melanosomes, another feature recently questioned (Negro et al. 2018). In almost all of the modern taxa I extracted melanosome from, small spherical phaeomelanin-rich melanosomes were almost exclusively associated with distinctly rufous hues. Other brown tones appear to show a more varied range of morphologies (Appendix 1). Therefore, the presence of the easily distinguishable

phaeomelanin-rich melanosomes will most likely indicate distinct rufous colours when present in fossil birds (Li et al. 2014).

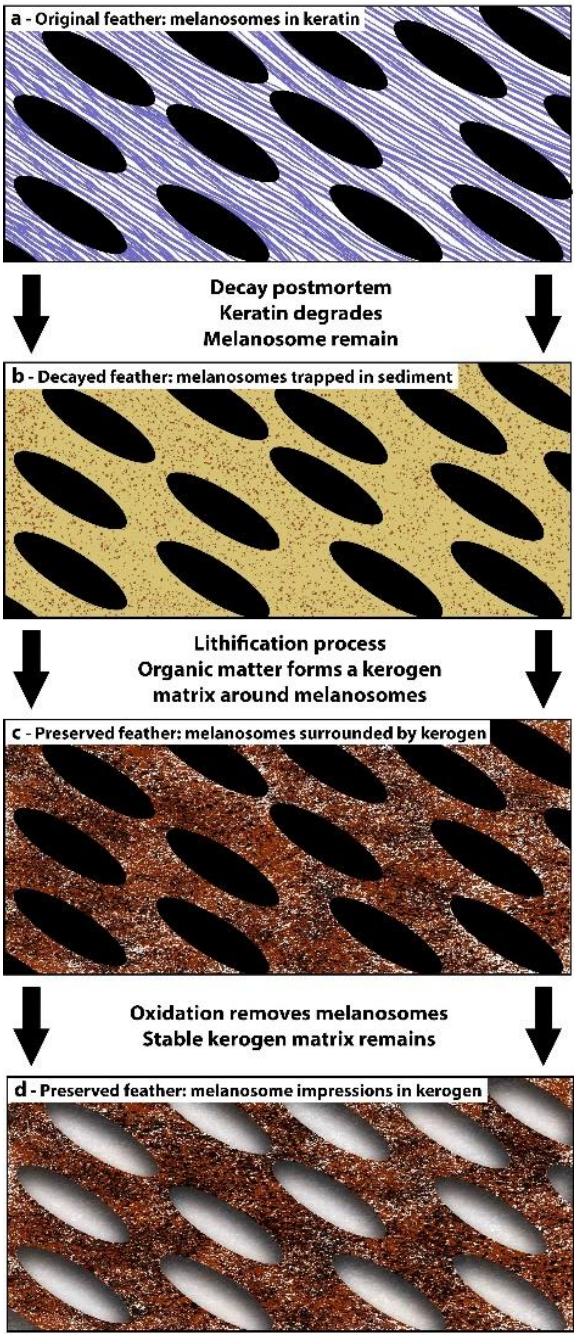

Figure D1. Hypothesised model of melanosome impression formation in deposits such as the Jehol Biota. After decay of feather keratin, organic matter stabilises around the remaining melanosomes held in sediment. This forms a kerogen matrix, which remains when oxidation removes the less stable melanosomes, leaving moulds retaining the original melanosome shape.

The revised protocol also provides an opportunity for broader studies of melanosomes in both a palaeontological and neontological context. Previous techniques required long time periods to gather large datasets for palaeocolour work. Now, hundreds of samples can be obtained in the space of days, opening the door to studies incorporating melanosomes from hundreds, or even thousands of taxa. This will facilitate future palaeocolour studies with more statistical power than previously possible.

Future research directions

There is still much that is not known about colour production in both the past and the present (Colleary et al. 2015; Vinther 2015*a*; Galván and Solano 2016; D'Alba and Shawkey 2018). Palaeocolour provides an ideal opportunity to address many of the unknowns. This is particularly the case when new data on modern colour production are gathered to allow better colour reconstructions.

While melanosome morphology generally correlates to colour in neognath birds (Chapter 7), some nuances, like those seen in Apodiformes (Chapter 8), can complicate palaeocolour work if not fully investigated and taken into account. Therefore, more work is needed on modern clades to determine how prevalent these divergences from the expected melanosome-colour relationship are. If they are only present rarely, then palaeocolour work need not be hampered as long as the phylogenetic position of the extinct taxon is considered carefully. As the revised protocol makes obtaining large melanosome samples straightforward, clade-specific data can easily be included in palaeocolour work where necessary (for example when the relationship of the taxon in question to the crown group is well established, e.g., Chapter 7-8). It is my hope that the revised protocol will aid studies of both palaeocolour and melanosomes in extant animals and allow for large new datasets that can be used to address these concerns. In an ideal world, melanosome data from all extant bird families would prove invaluable to understanding the evolution of melanosomes and colour production. This is within reach using the revised extraction protocol.

The chemistries of modern and fossil melanins are both areas where more work is needed (Colleary et al. 2015; Galván and Solano 2016; McNamara et al. 2016). To better understand what the chemistry of fossil pigments can tell us about colour in extinct animals, a full appreciation of the chemical makeup of modern pigments is needed and is currently incomplete (Galván and Solano 2016). For example, we still do not fully understand how relative concentrations of eumelanin and phaeomelanin contribute to different colours in modern integuments (McGraw et al. 2005). This hampers our understanding of features such as sulphurisation vs original sulphur chemistry in fossil melanin (Chapter 1.3.2; McNamara et al. 2016*b;* Brown et al. 2017). This is in part due to our lack of a full understanding of the precise chemical makeup of each pigment in extant animals (Galván and Solano 2016). While it is assumed that rufous and brown colours are dominated by phaeomelanin, and black and darker tones by eumelanin (Liu et al. 2005*a*; McGraw et al. 2005), more work is needed to confirm this, which was beyond the scope of this thesis. While the revised protocol allows rapid collection of melanosome samples for morphological analysis, it may not be appropriate for chemical work owing to the retention of some keratin (Chapter 6).

Further investigations into potential colour patterns in taxa outside of those already known could improve our picture of ecosystems and predator-prey relationships, particularly in the Mesozoic. Fossil mammals and non-dinosaurian reptiles from the Mesozoic exist with integumentary preservation (Qiang 2002; Rougier et al. 2003; Meng et al. 2006; Evans and Wang 2010) which provide the opportunity to broaden our colour reconstructions. In tandem with work on dinosaur palaeocolour and vision, this could help build a comprehensive picture of the visual landscape in a long extinct ecosystem. Additionally, pursuing palaeocolour in currently unexplored time periods, such as the Cambrian, could prove a novel way of addressing ecological, behavioural and environmental unknowns.

Palaeocolour has the potential to bring extinct animals back to life in more detail than ever before. I am confident that the field will continue to yield surprising results that reveal ever more exciting discoveries about our world in the past. The modern world would be rather dull without the exceptional diversity of colourful animals that inhabit it. The past will become ever more beautiful as we add colour to our once monochrome view of the world.

References

Abràmoff, M. D., Magalhães, P. J. & Ram, S. J. 2004. Image processing with ImageJ. *Biophotonics International*, **11**, 36-42.

Allen, W. L., Baddeley, R., Cuthill, I. C. & Scott-Samuel, N. E. 2012. A quantitative test of the predicted relationship between countershading and lighting environment. *The American Naturalist,* **180**, 762-776.

Allison, P. A. & Briggs, D. E. G. 1993. Exceptional fossil record: Distribution of soft-tissue preservation through the Phanerozoic. *Geology*, **21**, 527-530.

Amiot, R., Wang, X., Zhou, Z., Wang, X., Buffetaut, E., Lécuyer, C., Ding, Z., Fluteau, F., Hibino, T., Kusuhashi, N. & Mo, J. 2011. Oxygen isotopes of East Asian dinosaurs reveal exceptionally cold Early Cretaceous climates. *Proceedings of the National Academy of Sciences*, **108**, 5179-5183.

Ancillotto, L. & Mori, E. 2017. Adaptive significance of coat colouration and patterns of Sciuromorpha (Rodentia). *Ethology Ecology & Evolution*, **29**, 241-254.

Arnaud, J. C. & Bore, P. 1981. Isolation of melanin pigments from human hair. *Journal of the Society of Cosmetic Chemists*, **32**, 137-152.

Bagnara, J. T., Taylor, J. D. & Hadley, M. E. 1968. The dermal chromatophore unit. *The Journal of Cell Biology*, **38**, 67-79.

Baker, R. R. & Parker, G. 1979. The evolution of bird coloration. *Philosophical Transactions of the Royal Society B: Biological Sciences,* **287**, 63-130.

Barbaro L. Couzi L. Bretagnolle V. Nezan J. & Vetillard F. 2007. Multi-scale habitat selection and foraging ecology of the Eurasian Hoopoe (*Upupa epops*) in pine plantations. In *Plantation Forests and Biodiversity: Oxymoron or Opportunity?* Brockerhoff, E. G., Jactel, H., Parrotta, J. A., Quine, C. P., Sayer, J. & Hawkesworth, D. L. (eds.), Springer, Dordrecht, Netherlands, pp. 149-163.

Barden, H. E., Wogelius, R. A., Li, D., Manning, P. L., Edwards, N. P. & Van Dongen, B. E. 2011. Morphological and geochemical evidence of eumelanin preservation in the feathers of the Early Cretaceous bird, Gansus yumenensis. *PLoS One*, **6**, e25494.

Barrett, P. M. & Hilton, J. M. 2006. The Jehol biota (Lower Cretaceous, China): new discoveries and future prospects. *Integrative Zoology*, **1**, 15-17.

Bates, D., Maechler, M., Bolker, B. & Walker, S. 2014. lme4: Linear mixed-effects models using Eigen and S4. *R package version*, **1**, 1-23.

Bengtson, S. 2000. Teasing fossils out of shales with cameras and computers. *Palaeontologica Electronica*, **3**, 14.

Beyermann, K. & Hasenmaier, D. 1973. Identifizierung 180 Millionen Jahre alten, wahrscheinlich unverändert erhaltenen Melanins (Identification of 180 million year old, probably unchanged melanin). *Fresenius' Zeitschrift für Analytische Chemie*, **266**, 202-205.

Birbeck, M. S. C., Mercer, E. H. & Barnicot, N. A. 1956. The structure and formation of pigment granules in human hair. *Experimental Cell Research*, **10**, 505-514.

Blakey, P. R., Earland, C. & Stell, J. G. P. 1963. Calcification of keratin. *Nature*, **198**, 481.

Bleiweiss, R. 1985. Iridescent polychromatism in a female hummingbird: is it related to feeding strategies? *The Auk*, **102**, 701-713.

Bleiweiss, R. 1992. Reversed plumage ontogeny in a female hummingbird: implications for the evolution of iridescent colours and sexual dichromatism. *Biological Journal of the Linnean Society*, **47**, 183-195.

Blender version 2.78. Blender Foundation, Amsterdam, Netherlands. https://www.blender.org.

Bolt, A. G. 1967. Interactions between human melanoprotein and chlorpromazine derivatives I. Isolation and purification of human melanoprotein from hair and melanoma tissue. *Life Sciences*, **6**, 1277-1283.

Bolwig, N. 1973. Agonistic and sexual behavior of the African Ostrich (*Struthio camelus*). *The Condor*, **75**, 100-105.

Bonato, M., Evans, M. R., Hasselquist, D. & Cherry, M. I. 2009. Male coloration reveals different components of immunocompetence in ostriches, *Struthio camelus*. *Animal Behaviour*, **77**, 1033-1039.

Borovanský, J. & Hach, P. 1986. Isolation of melanosomes from keratinous structures: current state of the art. *Archives of Dermatological Research*, **279**, 54-58.

Bortolotti, G. R. 2006. Natural selection and coloration: protection, concealment, advertisement, or deception? In *Bird Coloration, Volume II: Function and Evolution*. Hill, G. E. & McGraw, K. J. (eds.), Harvard University Press, Cambridge, MS, USA, pp. 3–35.

Bowmaker, J. K. 1980. Colour vision in birds and the role of oil droplets. *Trends in Neurosciences*, **3**, 196-199.

Bowmaker, J. K. 2008. Evolution of vertebrate visual pigments. *Vision Research*, **48**, 2022-2041.

Boyle, B. 1992. Fossil detail leaps with double polarization. *Professional Photographers of Canada*, **22**, 10-12.

Bratosin, S. 1973. Disassembly of melanosomes in detergents. *Journal of Investigative Dermatology*, **60**, 224-230.

Braun, M. J. & Huddleston, C. J. 2009. A molecular phylogenetic survey of caprimulgiform nightbirds illustrates the utility of non-coding sequences. *Molecular Phylogenetics and Evolution*, **53**, 948-960.

Briggs, D. E. G. & Kear, A. J. 1993. Fossilization of soft tissue in the laboratory. *Science,* **259**, 1439-1442.

Briggs, D. E. G. & Wilby, P. R. 1996. The role of the calcium carbonate-calcium phosphate switch in the mineralization of soft-bodied fossils. *Journal of the Geological Society*, **153**, 665-668.

Briggs, D. E. G., Kear, A. J., Martill, D. M. & Wilby, P. R. 1993. Phosphatization of soft-tissue in experiments and fossils. *Journal of the Geological Society*, **150**, 1035-1038.

Broili, F. 1942. Vesfestigungen in Integument der Ichthyosaurier. Sitzungsberichte Bayerische Akademie Wissenschaften. *Mathematischen Naturwissenschaftlichen*, 37-52.

Brown, C. M., Henderson, D. M., Vinther, J., Fletcher, I., Sistiaga, A., Herrera, J. & Summons, R. E. 2017. An exceptionally preserved three-dimensional armored dinosaur reveals insights into coloration and Cretaceous predator-prey dynamics. *Current Biology*, **27**, 2514-2521.

Brusatte, S. L., O'Connor, J. K. & Jarvis, E. D. 2015. The origin and diversification of birds. *Current Biology*, **25**, 888-898.

Brush, A. H. 2000. Evolving a protofeather and feather diversity. *American Zoologist*, **40**, 631-639.

Buchholtz, E. A. 2001. Swimming styles in Jurassic ichthyosaurs. *Journal of Vertebrate Paleontology*, **21**, 61-73.

Butler, L. K., Rohwer, S. & Speidel, M. G. 2008. Quantifying structural variation in contour feathers to address functional variation and life history trade-offs. *Journal of Avian Biology*, **39**, 629-639.

Caine, H. & Benton, M. J. 2011. Ichthyosauria from the Upper Lias of Strawberry Bank, England. *Palaeontology*, **54**, 1069-1093.

Carney, R. M., Vinther, J., Shawkey, M. D., D'Alba, L. & Ackermann, J. 2012. New evidence on the colour and nature of the isolated Archaeopteryx feather. *Nature Communications*, **3**, 637.

Caro, T. 2005. The adaptive significance of coloration in mammals. *BioScience*, **55**, 125-136.

Caro, T. 2009. Contrasting coloration in terrestrial mammals. *Philosophical Transactions of the Royal Society B: Biological Sciences*, **364**, 537-548.

Caro, T. 2011. The functions of black-and-white coloration in mammals: review and synthesis. In *Animal Camouflage: Mechanisms and Function.* Stevens, M. & Merilaita, S. (eds.), Cambridge University Press, Cambridge, UK, pp. 298-329.

Caro, T. 2013. The colours of extant mammals. *Seminars in Cell & Developmental Biology*, **24**, 542-552.

Caro, T., Beeman, K., Stankowich, T. & Whitehead, H. 2011. The functional significance of colouration in cetaceans. *Evolutionary Ecology*, **25**, 1231.

Chang, M.-M., Chen, P.-J., Wang, Y.-Q., Wang, Y. & Miao, D.-S. 2003. *The Jehol Fossils: The Emergence of Feathered Dinosaurs, Beaked Birds and Flowering Plants.* Shanghai Scientific & Technical Publishers, Shanghai, China, pp. 208.

Chen, P. J., Dong, Z. M. & Zhen, S. N. 1998. An exceptionally well-preserved theropod dinosaur from the Yixian Formation of China. *Nature*, **391**, 147-152.

Chittenden, R. H. & Albro, A. H. 1899. The formation of melanins or melanin-like pigments from proteid substances. *American Journal of Physiology*, **2**, 291-305.

Clarke, J. A., Zhou, Z. & Zhang, F. 2006. Insight into the evolution of avian flight from a new clade of Early Cretaceous ornithurines from China and the morphology of *Yixianornis grabaui*. *Journal of Anatomy*, **208**, 287-308.

Clarke, J. A., Ksepka, D. T., Salas-Gismondi, R., Altamirano, A. J., Shawkey, M. D., D'Alba, L., Vinther, J., Devries, T. J. & Baby, P. 2010. Fossil evidence for evolution of the shape and color of penguin feathers. *Science*, **330**, 954-957.

Cleland, C. E. 2011. Prediction and explanation in historical natural science. *The British Journal for the Philosophy of Science*, **62**, 551-582.

Clements, T., Dolocan, A., Martin, P., Purnell, M. A., Vinther, J. & Gabbott, S. E. 2016. The eyes of *Tullimonstrum* reveal a vertebrate affinity. *Nature,* **532**, 500-503.

Colleary, C., Dolocan, A., Gardner, J., Singh, S., Wuttke, M., Rabenstein, R., Habersetzer, J., Schaal, S., Feseha, M., Clemens, M., Jacobs, B. F., Currano, E. D., Jacobs, L. L., Sylvestersen, R. L., Gabbott, S. E. & Vinther, J. 2015. Chemical, experimental, and morphological evidence for diagenetically altered melanin in exceptionally preserved fossils. *Proceedings of the National Academy of Sciences,* **112**, 12592-12597.

Collin, S. P., Knight, M. A., Davies, W. L., Potter, I. C., Hunt, D. M. & Trezise, A. E. 2003. Ancient colour vision: multiple opsin genes in the ancestral vertebrates. *Current Biology*, **13**, 864-865.

Conybeare, W. D. 1822. Additional Notices on the Fossil Genera *Ichthyosaurus* and *Plesiosaurus*. *Transactions of the Geological Society of London*, **2**, 103-123.

Costa, T. V., Whitney, B. M., Braun, M. J., White, N. D., Silveira, L. F. & Cleere, N. 2017. A systematic reappraisal of the Rufous Potoo *Nyctibius bracteatus* (Nyctibiidae) and description of a new genus. *Journal of Ornithology*, **159**, 367-377.

Cott, H. B. 1940. *Adaptive Coloration in Animals*. Methuen, London, UK, pp. 508.

Crane, P. R., Friis, E. M. & Pedersen, K. R. 1995. The origin and early diversification of angiosperms. *Nature*, **374**, 27-33.

Currie, P. J. & Chen, P. J. 2001. Anatomy of *Sinosauropteryx prima* from Liaoning, northeastern China. *Canadian Journal of Earth Sciences*, **38**, 1705-1727.

Cuthill, I. C. 2006. Color perception. In *Bird Coloration: Volume I: Mechanisms and Measurements*. Hill G. E. & McGraw, K. J. (eds.), Harvard University Press, Cambridge, MS, USA, pp .3-40.

Cuthill, I. C. & Székely, A. 2009. Coincident disruptive coloration. *Philosophical Transactions of the Royal Society B: Biological Sciences,* **364**, 489-496.

Cuthill, I. C. & Székely, A. 2011. The concealment of body parts through coincident disruptive coloration. In *Animal Camouflage: Mechanisms and Function*. Stevens, M. & Merilaita, S. (eds.), Cambridge University Press, Cambridge, UK, pp. 34-52.

Cuthill, I. C., Bennett, A., Partridge, J. & Maier, E. 1999. Plumage reflectance and the objective assessment of avian sexual dichromatism. *The American Naturalist*, **153**, 183-200.

Cuthill, I. C., Sanghera, N. S., Penacchio, O., Lovell, P. G., Ruxton, G. D. & Harris, J. M. 2016. Optimizing countershading camouflage. *Proceedings of the National Academy of Sciences*, **113**, 13093-13097.

Dal Sasso, C. & Signore, M., 1998. Exceptional soft-tissue preservation in a theropod dinosaur from Italy. *Nature*, **392**, 383-387.

D'Alba, L. & Shawkey, M. D., 2018. Melanosomes: biogenesis, properties, and evolution of an ancient organelle. *Physiological Reviews*, **99**, 1-19.

Dale, J. 2006. Intraspecific variation in coloration. In *Bird Coloration, Volume II: Function and Evolution*. Hill, G. E. & McGraw, K. J. (eds.), Harvard University Press, Cambridge, MS, USA, pp. 36-86.

Damsté, J. S. & Koopmans, M. P. 1997. The fate of carotenoids in sediments: an overview. *Pure and Applied Chemistry*, **69**, 2067-2074.

Darwin, C. 1859. *On the Origin of Species by Natural Selection, or the Preservation of Favoured Races in the Struggle for Life*. John Murray, London, UK, pp. 502.

Darwin, C. 1871. *The Descent of Man: and Selection in Relation to Sex*. John Murray, London, UK, pp. 864.

Davis, P. G. & Briggs, D. E. G. 1995. Fossilization of feathers. *Geology*, **23**, 783-786.

De la Beche, H. T. & Conybeare, W. D. 1821. Notice of the discovery of a new Fossil Animal, forming a link between the *Ichthyosaurus* and Crocodile, together with general remarks on the Osteology of the *Ichthyosaurus*. *Transactions of the Geological Society of London,* **1**, 559-594.

Delair, J. B. 1966. Unusual preservation of fibrous elements in an ichthyosaur skull. *Nature,* **212**, 575.

Demarchi, B., Hall, S., Roncal-Herrero, T., Freeman, C. L., Woolley, J., Crisp, M. K., Wilson, J., Fotakis, A., Fischer, R., Kessler, B. M. & Jersie-Christensen, R. R. 2016. Protein sequences bound to mineral surfaces persist into deep time. *Elife*, **5**, e17092.

Dhouailly, D. 2009. A new scenario for the evolutionary origin of hair, feather, and avian scales. *Journal of Anatomy*, **214**, 587-606.

Dijkstra, P. D., Seehausen, O. & Groothuis, T. G. 2005. Direct male-male competition can facilitate invasion of new colour types in Lake Victoria cichlids. *Behavioral Ecology and Sociobiology*, **58**, 136-143.

Doguzhaeva, L., Mapes, R. & Mutvei, H. 2004. Occurrence of ink in Paleozoic and Mesozoic coleoids (Cephalopoda). *Mitteilungen aus dem Geologisch-Paläontologischen Institut der Universität Hamburg*, **88**, 145-155.

Doucet, S. M. & Meadows, M. G. 2009. Iridescence: a functional perspective. *Journal of The Royal Society Interface*, **6**, 115-132.

Doucet, S. M., Shawkey, M. D., Rathburn, M. K., Mays, H. L. & Montgomerie, R. 2004. Concordant evolution of plumage colour, feather microstructure and a melanocortin receptor gene between mainland and island populations of a fairy–wren. *Proceedings of the Royal Society of London B: Biological Sciences*, **271**, 1663-1670.

Doucet, S. M., Shawkey, M. D., Hill, G. E. & Montgomerie, R. 2006. Iridescent plumage in satin bowerbirds: structure, mechanisms and nanostructural predictors of individual variation in colour. *Journal of Experimental Biology*, **209**, 380-390.

Dove, C. J. & Straker, L. C. 2012. Comment on “A diverse assemblage of Late Cretaceous dinosaur and bird feathers from Canadian amber”. *Science*, **335**, 796-796.

Dreiss, A. N., Antoniazza, S., Burri, R., Fumagalli, L., Sonnay, C., Frey, C., Goudet, J. & Roulin, A. 2012. Local adaptation and matching habitat choice in female barn owls with respect to melanic coloration. *Journal of Evolutionary Biology*, **25**, 103-114.

du Plessis M. A., Simmons R. E. & Radford A. N. 2007. Behavioural ecology of the Namibian Violet Woodhoopoe *Phoeniculus damarensis*. *Ostrich-Journal of African Ornithology*, **78**, 1-5.

Dunne, J. A., Labandeira, C. C. & Williams, R. J. 2014. Highly resolved early Eocene food webs show development of modern trophic structure after the end-Cretaceous extinction. *Proceedings of the Royal Society B: Biological Sciences*, **281**, 20133280.

Dyke, G. J. & Norell, M. A. 2005. *Caudipteryx* as a non-avalian theropod rather than a flightless bird. *Acta Palaeontologica Polonica*, **50**, 101-116.

Edmunds, M. & Dewhirst, R. A. 1994. The survival value of countershading with wild birds as predators. *Biological Journal of the Linnean Society*, **51**, 447-452.

Eglinton G. & Logan G. A. 1991. Molecular preservation. *Philisophical Transactions of the Royal Society B: Biological Sciences*, **333**, 315-328.

Eliason, C. M., Bitton, P. P. & Shawkey, M. D. 2013. How hollow melanosomes affect iridescent colour production in birds. *Proceedings of the Royal Society B: Biological Sciences*, **280**, 20131505.

Eliason C. M., Shawkey M. D. & Clarke J. A. 2016. Evolutionary shifts in the melanin-based color system of birds. *Evolution*, **70**, 445-455.

Endler, J. A. 1990. On the measurement and classification of colour in studies of animal colour patterns. *Biological Journal of the Linnean Society,* **41**, 315-352.

Endler, J. A. 1992. Signals, signal conditions, and the direction of evolution. *The American Naturalist*, **139**, S125-S153.

Endler, J. A., Westcott, D. A., Madden, J. R. & Robson, T. 2005. Animal visual systems and the evolution of color patterns: sensory processing illuminates signal evolution. *Evolution*, **59**, 1795-1818.

Esperante, R., Brand, L., Nick, K. E., Poma, O. & Urbina, M. 2008. Exceptional occurrence of fossil baleen in shallow marine sediments of the Neogene Pisco Formation, Southern Peru. *Palaeogeography, Palaeoclimatology, Palaeoecology*, **257**, 344-360.

Evans, S. E. & Wang, Y. 2005. The early Cretaceous lizard *Dalinghosaurus* from China. *Acta Palaeontologica Polonica*, **50**, 725-742.

Evans, S. E. & Wang, Y. 2010. A new lizard (Reptilia: Squamata) with exquisite preservation of soft tissue from the Lower Cretaceous of Inner Mongolia, China. *Journal of Systematic Palaeontology*, **8**, 81-95.

Farlow, J. O. & Holtz, T. R. 2002. The fossil record of predation in dinosaurs. *The Paleontological Society Papers*, **8**, 251-266.

Feduccia, A. 1999. *The Origin and Evolution of Birds*. Yale University Press, New Haven, CT, USA, pp. 478.

Feduccia, A. 2013. Bird origins anew. *The Auk*, **130**, 1-12.

Feduccia, A. & Tordoff, H. B. 1979. Feathers of *Archaeopteryx*: asymmetric vanes indicate aerodynamic function. *Science*, **203**, 1021-1022.

Feduccia, A., Lingham-Soliar, T. & Hinchliffe, J. R. 2005. Do feathered dinosaurs exist? Testing the hypothesis on neontological and paleontological evidence. *Journal of Morphology*, **266**, 125-166.

Fein, A. & Szuts, E. Z. 1982. *Photoreceptors: Their Role in Vision*. Cambridge University Press, Cambridge, UK, pp. 224.

Ferguson, G. P. & Messenger, J. B. 1991. A countershading reflex in cephalopods. *Proceedings of the Royal Society B: Biological Sciences*, **243**, 63-67.

Fernald, R. D. 2000. Evolution of eyes. *Current Opinion in Neurobiology*, **10**, 444-450.

Ficken, R. W. & Wilmot, L. B. 1968. Do facial eye-stripes function in avian vision? *American Midland Naturalist*, **79**, 522-523.

Field, D. J., D'Alba, L., Vinther, J., Webb, S. M., Gearty, W. & Shawkey, M. D. 2013. Melanin concentration gradients in modern and fossil feathers. *PLoS One*, **8**, e59451.

Filson, A. & Hope, J. 1957. Isolation of melanin granules. *Nature*, **179**, 211.

Foth, C., Tischlinger, H. & Rauhut, O. W. 2014. New specimen of *Archaeopteryx* provides insights into the evolution of pennaceous feathers. *Nature*, **511**, 79-82.

Franzen J. L. 1985. Exceptional preservation of Eocene vertebrates in the lake deposit of Grube Messel (West Germany). *Philosophical Transactions of the Royal Society B: Biological Sciences*, **311**, 181-186.

Frey, E., Tischlinger, H., Buchy, M. C. & Martill, D. M. 2003. New specimens of Pterosauria (Reptilia) with soft parts with implications for pterosaurian anatomy and locomotion. *Geological Society, London, Special Publications*, **217**, 233-266.

Fuller, R. C., Houle, D. & Travis, J. 2005. Sensory bias as an explanation for the evolution of mate preferences. *The American Naturalist*, **166**, 437-446.

Gabbott, S. E., Donoghue, P. C., Sansom, R. S., Vinther, J., Dolocan, A. & Purnell, M. A. 2016. Pigmented anatomy in Carboniferous cyclostomes and the evolution of the vertebrate eye. *Proceedings of the Royal Society B: Biological Sciences*, **283**, 20161151.

Galván, I. & Solano, F. 2016. Bird integumentary melanins: Biosynthesis, forms, function and evolution. *International Journal of Molecular Sciences*, **17**, 520.

Galván, I. & Wakamatsu, K. 2016. Color measurement of the animal integument predicts the content of specific melanin forms. *RSC Advances*, **6**, 79135-79142.

Geist, N. R. 2009. Feathered dinosaurs: the origin of birds. *The Condor*, **150**, 203-204.

Gibbons, A. 1997. Plucking the feathered dinosaur. *Science*, **278**, 1229-1230.

Gioncada, A., Collareta, A., Gariboldi, K., Lambert, O., Di Celma, C., Bonaccorsi, E., Urbina, M. & Bianucci, G. 2016. Inside baleen: exceptional microstructure preservation in a late Miocene whale skeleton from Peru. *Geology*, **44**, 839-842.

Giraldo, M. A., Parra, J. L. & Stavenga, D. G. 2018. Iridescent colouration of male Anna's hummingbird (*Calypte anna*) caused by multilayered barbules. *Journal of Comparative Physiology A*, **204**, 965-975.

Glass, K., Ito, S., Wilby, P. R., Sota, T., Nakamura, A., Bowers, C. R., Vinther, J., Dutta, S., Summons, R. & Briggs, D. E. G. 2012. Direct chemical evidence for eumelanin pigment from the Jurassic period. *Proceedings of the National Academy of Sciences,* **109**, 10218-10223.

Glass, K., Ito, S., Wilby, P. R., Sota, T., Nakamura, A., Bowers, C. R., Miller, K. E., Dutta, S., Summons, R. E. & Briggs, D. E. G. 2013. Impact of diagenesis and maturation on the survival of eumelanin in the fossil record. *Organic Geochemistry,* **64**, 29-37.

Gluckman, T. L. & Cardoso, G. C. 2010. The dual function of barred plumage in birds: camouflage and communication. *Journal of Evolutionary Biology*, **23**, 2501-2506.

Godefroit, P., Sinitsa, S. M., Dhouailly, D., Bolotsky, Y. L., Sizov, A. V., McNamara, M. E., Benton, M. J. & Spagna, P. 2014*a*. A Jurassic ornithischian dinosaur from Siberia with both feathers and scales. *Science*, **345**, 451-455.

Godefroit, P., Sinitsa, S. M., Dhouailly, D., Bolotsky, Y. L., Sizov, A. V., McNamara, M. E., Benton, M. J. & Spagna, P. 2014*b*. Response to Comment on "A Jurassic ornithischian dinosaur from Siberia with both feathers and scales". *Science*, **346**, 434-434.

Goldsmith, T. H. 1990. Optimization, constraint, and history in the evolution of eyes. *The Quarterly Review of Biology*, **65**, 281-322.

Gomez D. & Théry M. 2004. Influence of ambient light on the evolution of colour signals: comparative analysis of a Neotropical rainforest bird community. *Ecology Letters,* **7**, 279-284.

Gomez, D. & Théry, M. 2007. Simultaneous crypsis and conspicuousness in color patterns: comparative analysis of a neotropical rainforest bird community. *The American Naturalist*, **169**, S42-S61.

Gong, E. P., Martin, L. D., Burnham, D. A., Falk, A. R. & Hou, L. H. 2012. A new species of *Microraptor* from the Jehol Biota of northeastern China. *Palaeoworld*, **21**, 81-91.

Gottfried, M. D. 1989. Earliest fossil evidence for protective pigmentation in an actinopterygian fish. *Historical Biology*, **3**, 79-83.

Greenewalt, C. H., Brandt, W. & Friel, D. D. 1960. Iridescent colors of hummingbird feathers. *Journal of the Optical Society of America*, **50**, 1005-1013.

Greenwalt, D. E., Goreva, Y. S., Siljeström, S. M., Rose, T. & Harbach, R. E. 2013. Hemoglobin-derived porphyrins preserved in a Middle Eocene blood-engorged mosquito. *Proceedings of the National Academy of Sciences*, **110**, 201310885.

Gren, J. A., Sjövall, P., Eriksson, M. E., Sylvestersen, R. L., Marone, F., Sigfridsson Clauss, K. G., Taylor, G. J., Carlson, S., Uvdal, P. & Lindgren, J. 2016. Molecular and microstructural

inventory of an isolated fossil bird feather from the Eocene Fur Formation of Denmark. *Palaeontology*. **60**, 73-90.

Griffiths, P. 1996. The isolated *Archaeopteryx* feather. *Archaeopteryx*, **14**, 1-26.

Guilford, T. & Dawkins, M. S. 1991. Receiver psychology and the evolution of animal signals. *Animal Behaviour*, **42**, 1-14.

Hall, M. I. 2008. The anatomical relationships between the avian eye, orbit and sclerotic ring: implications for inferring activity patterns in extinct birds. *Journal of Anatomy*, **212**, 781-794.

Hammer, Ø., Harper, D. & Ryan, P. D. 2001. Past: paleontological statistics software package for education and data analysis. *Palaeontologia Electronica*, **4**, 9.

Han, K. L., Robbins, M. B. & Braun, M. J. 2010. A multi-gene estimate of phylogeny in the nightjars and nighthawks (Caprimulgidae). *Molecular Phylogenetics and Evolution*, **55**, 443-453.

Hanlon, R. T., Chiao, C. C., Mäthger, L. M., Barbosa, A., Buresch, K. C. & Chubb, C. 2008. Cephalopod dynamic camouflage: bridging the continuum between background matching and disruptive coloration. *Philosophical Transactions of the Royal Society B: Biological Sciences*, **364**, 429-437.

Harris J. M. 2004. Binocular vision: moving closer to reality. *Philosophical Transactions of the Royal Society of London A: Mathematical, Physical and Engineering Sciences*, **362**, 2721-2739.

Harrison, C. J. O. 1984. A revision of the fossil swifts (Vertebrata, Aves, Suborder, Apodi), with descriptions of three new genera and two new species. *Mededelingen van de Werkgroep voor Tertiaire en Kwartaire Geologie*, **21**, 157-177.

Hart, N. S. 2001. The visual ecology of avian photoreceptors. *Progress in Retinal and Eye Research*, **20**, 675-703.

Hassanalian, M., Abdelmoula, H., Ayed, S. B. & Abdelkefi, A. 2017. Thermal impact of migrating birds' wing color on their flight performance: Possibility of new generation of biologically inspired drones. *Journal of Thermal Biology*, **66**, 27-32.

Hayat, M. A. 1989. *Principles and Techniques of Electron Microscopy: Biological Applications.* Edward Arnold, London, UK, pp. 522.

Hayes, J. M., Takigiku, R., Ocampo, R., Callot H. J. & Albrecht, P. 1987. Isotopic compositions and probable origins of organic molecules in the Eocene Messel shale. *Nature*, **329**, 48.

Heilmann, G. 1926. *The Origin of Birds.* Appleton, NY, USA, pp. 210.

Herrera, G., Zagal, J. C., Diaz, M., Fernández, M. J., Vielma, A., Cure, M., Martinez, J., Bozinovic, F. & Palacios, A. G. 2008. Spectral sensitivities of photoreceptors and their role in colour discrimination in the green-backed firecrown hummingbird (*Sephanoides sephaniodes*). *Journal of Comparative Physiology A*, **194**, 785.

Hill, G. E. 1990. Female house finches prefer colourful males: sexual selection for a condition-dependent trait. *Animal Behaviour*, **40**, 563-572.

Hill, G. E. 2006. Female mate choice for ornamental coloration. In *Bird Coloration, Volume II: Function and Evolution*. Hill, G. E. & McGraw, K. J. (eds.), Harvard University Press, Cambridge, MS, USA, pp. 137-200.

Hill, G. E & McGraw, K. J. 2006*a*. *Bird Coloration: Vol. 2: Function and Evolution*. Harvard University Press, Cambridge, MA, USA, pp. 544.

Hill, G. E. & McGraw, K. J. 2006*b*. *Bird Coloration: Vol. 1: Mechanisms and Measurements.* Harvard University Press, Cambridge, MA, USA, pp. 496.

Homberger, D. G. & de Silva, K. N. 2000. Functional microanatomy of the feather-bearing integument: implications for the evolution of birds and avian flight. *American Zoologist*, **40**, 553-574.

Horn, B. K. P. 1975. Obtaining shape from shading information. In *The Psychology of Computer Vision.* Winston, P. H. (ed.), McGraw Hill, New York, NY, USA, pp. 115-155.

Howe, S. R., Sharpe, T. & Torrens, H. S. 1981. *Ichthyosaurs: A History of Fossil 'sea-dragons'*. National Museum of Wales, Cardiff, UK, pp. 32.

Hu, D. N., Simon, J. D. & Sarna, T. 2008. Role of ocular melanin in ophthalmic physiology and pathology. *Photochemistry and Photobiology,* **84**, 639-644.

Hu, D., Clarke, J. A., Eliason, C. M., Qiu, R., Li, Q., Shawkey, M. D., Zhao, C., D'Alba, L., Jiang, J. & Xu, X. 2018. A bony-crested Jurassic dinosaur with evidence of iridescent plumage highlights complexity in early paravian evolution. *Nature Communications*, **9**, 217.

Hughes, A. E., Troscianko, J. & Stevens, M. 2014. Motion dazzle and the effects of target patterning on capture success. *BMC Evolutionary Biology*, **14**, 201.

Hultgren, K. M. & Stachowicz, J. J., 2011. Camouflage in decorator crabs: integrating ecological, behavioural and evolutionary approaches. In *Animal Camouflage: Mechanisms and Function*. Stevens, M. & Merilaita, S. (eds.), Cambridge University Press, Cambridge, UK, pp. 212-236.

Huxley, T. H. 1870. Further evidence of the affinity between the dinosaurian reptiles and birds. *Quarterly Journal of the Geological Society*, **26**, 12-31.

Igic, B., D'Alba, L. & Shawkey, M. D. 2016. Manakins can produce iridescent and bright feather colours without melanosomes. *Journal of Experimental Biology,* **219**, 1851-1859.

Ioannou, C. C. & Krause, J. 2009. Interactions between background matching and motion during visual detection can explain why cryptic animals keep still. *Biology Letters*, **5**, 191-193.

Ji, Q. & Ji, S. A. 1996. On the discovery of the earliest fossil bird in China (*Sinosauropteryx* gen. nov.) and the origin of birds. *Chinese Geology*, **233**, 1-4.

Ji, Q., Currie, P. J., Norell, M. A. & Ji, S-A. 1998. Two feathered dinosaurs from northeastern China. *Nature*, **393**, 753.

Ji, S., Gao, C., Liu, J., Meng, Q. & Ji, Q. 2007. New material of *Sinosauropteryx* (Theropoda: Compsognathidae) from western Liaoning, China. *Acta Geologica Sinica*, **81**, 177–182.

Jiang, B., Fürsich, F. T. & Hethke, M. 2012. Depositional evolution of the Early Cretaceous Sihetun Lake and implications for regional climatic and volcanic history in western Liaoning, NE China. *Sedimentary Geology*, **257**, 31-44.

Jimbow, K., Fitzpatrick, T. B. & Quevedo, W. C. 1986. Formation, chemical composition and function of melanin pigments. In *Biology of the Integument*. Bereiter-Hahn, J., Matolsty, A., G. & Richards, K., S. (eds.), Springer, Berlin, Germany, pp. 278-292.

Kamilar, J. M. & Bradley, B. J. 2011. Countershading is related to positional behavior in primates. *Journal of Zoology*, **283**, 227-233.

Kaye, T. G., Falk, A. R., Pittman, M., Sereno, P. C., Martin, L. D., Burnham, D. A., Gong, E., Xu, X. & Wang, Y. 2015. Laser-stimulated fluorescence in paleontology. *PloS one*, **10**, e0125923.

Kaye, T. G., Pittman, M., Mayr, G., Schwarz, D. & Xu, X. 2019. Detection of lost calamus challenges identity of isolated *Archaeopteryx* feather. *Scientific Reports*, **9**, 1182.

Kelley, J. L. & Merilaita, S. 2015. Testing the role of background matching and self-shadow concealment in explaining countershading coloration in wild-caught rainbowfish. *Biological Journal of the Linnean Society*, **114**, 915-928.

Kelley, J. L., Taylor, I. , Hart, N. S. & Partridge, J. C. 2017. Aquatic prey use countershading camouflage to match the visual background. *Behavioral Ecology*, **28**, 1314-1322.

Kellner, A. W. 2002. A review of avian Mesozoic fossil feathers. In *Mesozoic Birds: Above the Heads of Dinosaurs*. Chiappe L. M. (ed.), University of California Press, CA, USA, pp. 389-404.

Kellner, A. W., Wang, X., Tischlinger, H., de Almeida Campos, D., Hone, D.W. & Meng, X. 2010. The soft tissue of *Jeholopterus* (Pterosauria, Anurognathidae, Batrachognathinae) and the structure of the pterosaur wing membrane. *Proceedings of the Royal Society of London B: Biological Sciences*, **277**, 321-329.

Kimball, R. T. & Ligon, J. D. 1999. Evolution of avian plumage dichromatism from a proximate perspective. *The American Naturalist*, **154**, 182-193.

Kjernsmo, K., Grönholm, M. & Merilaita, S. 2016. Adaptive constellations of protective marks: eyespots, eye stripes and diversion of attacks by fish. *Animal Behaviour*, **111**, 189-195.

Koschowitz, M. C., Fischer, C. & Sander, M. 2014. Beyond the rainbow. *Science*, **346**, 416-418.

Krol, E. S. & Liebler, D. C. 1998. Photoprotective actions of natural and synthetic melanins. *Chemical Research in Toxicology*, **11**, 1434-1440.

Ksepka, D. T., Clarke, J. A., Nesbitt, S. J., Kulp, F. B. & Grande, L. 2013. Fossil evidence of wing shape in a stem relative of swifts and hummingbirds (Aves, Pan-Apodiformes). *Proceedings of the Royal Society B: Biological Sciences*, **280**, 20130580.

LaFountain, A. M., Prum, R. O. & Frank, H. A. 2015. Diversity, physiology, and evolution of avian plumage carotenoids and the role of carotenoid–protein interactions in plumage color appearance. *Archives of Biochemistry and Biophysics,* **572**, 201-212.

Land, M. F. & Fernald, R. D. 1992. The evolution of eyes. *Annual Review of Neuroscience*, **15**, 1-29.

Landmann, L. 1986. The skin of reptiles: epidermis and dermis. In *Biology of the Integument*. Bereiter-Hahn, J., Matolsty, A. G. & Richards, K. S. (eds.), Springer, Berlin, Germany, pp. 150-187.

Lee, S.-I., Kim, M., Choe, J. C. & Jablonski, P. G. 2016. Evolution of plumage coloration in the crow family (Corvidae) with a focus on the color-producing microstructures in the feathers: a comparison of eight species. *Animal Cells and Systems*, **20**, 95-102.

Lewis, J. L. & Johnson, S. L. 2001. Collagen architecture and failure processes in bovine patellar cartilage. *Journal of Anatomy*, **199**, 483-492.

Li, W. & DeVries, S. H. 2006. Bipolar cell pathways for color and luminance vision in a dichromatic mammalian retina. *Nature Neuroscience*, **9**, 669.

Li, G., Shen, Y. & Batten, D. J. 2007. *Yanjiestheria*, *Yanshania* and the development of the Eosestheria conchostracan fauna of the Jehol Biota in China. *Cretaceous Research*, **28**, 225-234.

Li, Q., Gao, K.-Q., Vinther, J., Shawkey, M. D., Clarke, J. A., D'alba, L., Meng, Q., Briggs, D. E. G. & Prum, R. O. 2010. Plumage color patterns of an extinct dinosaur. *Science*, **327**, 1369-1372.

Li, Q., Gao, K.-Q., Meng, Q., Clarke, J. A., Shawkey, M. D., D'Alba, L., Pei, R., Ellison, M., Norell, M. A. & Vinther, J. 2012. Reconstruction of *Microraptor* and the evolution of iridescent plumage. *Science,* **335**, 1215-1219.

Li, Q., Clarke, J. A., Gao, K. Q., Zhou, C. F., Meng, Q., Li, D., D'Alba, L. & Shawkey, M. D. 2014. Melanosome evolution indicates a key physiological shift within feathered dinosaurs. *Nature*, **507**, 350.

Lindgren, J., Caldwell, M. W., Konishi, T. & Chiappe, L. M. 2010. Convergent evolution in aquatic tetrapods: insights from an exceptional fossil mosasaur. *PLoS One*, **5**, e11998.

Lindgren, J., Everhart, M. J. & Caldwell, M. W. 2011. Three-dimensionally preserved integument reveals hydrodynamic adaptations in the extinct marine lizard *Ectenosaurus* (Reptilia, Mosasauridae). *PloS One*, **6**, e27343.

Lindgren, J., Uvdal, P., Sjövall, P., Nilsson, D. E., Engdahl, A., Schultz, B. P. & Thiel, V. 2012. Molecular preservation of the pigment melanin in fossil melanosomes. *Nature Communications*, **3**, 824.

Lindgren, J., Sjövall, P., Carney, R. M., Uvdal, P., Gren, J. A., Dyke, G., Schultz, B. P., Shawkey, M. D., Barnes, K. R. & Polcyn, M. J. 2014. Skin pigmentation provides evidence of convergent melanism in extinct marine reptiles. *Nature*, **506**, 484.

Lindgren, J., Moyer, A., Schweitzer, M. H., Sjövall, P., Uvdal, P., Nilsson, D. E., Heimdal, J., Engdahl, A., Gren, J. A., Schultz, B. P. & Kear, B. P. 2015. Interpreting melanin-based coloration through deep time: a critical review. *Proceedings of the Royal Society B: Biological Sciences*, **282**, 20150614.

Lindgren, J., Kuriyama, T., Madsen, H., Sjövall, P., Zheng, W., Uvdal, P., Engdahl, A., Moyer, A. E., Gren, J.A., Kamezaki, N. & Ueno, S. 2017. Biochemistry and adaptive colouration of an exceptionally preserved juvenile fossil sea turtle. *Scientific reports*, **7**, 13324.

Lindgren, J., Sjövall, P., Thiel, V., Zheng, W., Ito, S., Wakamatsu, K., Hauff, R., Kear, B. P., Engdahl, A., Alwmark, C. & Eriksson, M. E. 2018. Soft-tissue evidence for homeothermy and crypsis in a Jurassic ichthyosaur. *Nature*, **564**, 359.

Lingham-Soliar, T. 1999. Rare soft tissue preservation showing fibrous structures in an ichthyosaur from the Lower Lias (Jurassic) of England. *Proceedings of the Royal Society of London B: Biological Sciences*, **266**, 2367-2373.

Lingham-Soliar, T. 2001. The ichthyosaur integument: skin fibers, a means for a strong, flexible and smooth skin. *Lethaia*, **34**, 287-302.

Lingham-Soliar, T. 2003*a*. Evolution of birds: ichthyosaur integumental fibers conform to dromaeosaur protofeathers. *Naturwissenschaften*, **90**, 428-432.

Lingham-Soliar, T. 2003*b*. The dinosaurian origin of feathers: perspectives from dolphin (Cetacea) collagen fibers. *Naturwissenschaften*, **90**, 563-567.

Lingham-Soliar, T. 2010*a*. Dinosaur protofeathers: pushing back the origin of feathers into the Middle Triassic? *Journal of Ornithology*, **151**, 193-200.

Lingham-Soliar, T. 2010*b*. Response to comments by G. Mayr to my paper “Dinosaur protofeathers: pushing back the origin of feathers into the Middle Triassic?”. *Journal of Ornithology*, **151**, 519-521.

Lingham-Soliar, T. 2011. The evolution of the feather: *Sinosauropteryx*, a colourful tail. *Journal of Ornithology*, **152**, 567-577.

Lingham-Soliar, T. 2012. The evolution of the feather: *Sinosauropteryx*, life, death and preservation of an alleged feathered dinosaur. *Journal of Ornithology*, **153**, 699-711.

Lingham-Soliar, T. 2013. The evolution of the feather: scales on the tail of *Sinosauropteryx* and an interpretation of the dinosaur’s opisthotonic posture. *Journal of Ornithology*, **154**, 455-463.

Lingham-Soliar, T. 2014. Comment on “A Jurassic ornithischian dinosaur from Siberia with both feathers and scales”. *Science*, **346**, 434-434.

Lingham-Soliar, T. 2016. Convergence in thunniform anatomy in lamnid sharks and Jurassic ichthyosaurs. *Integrative and Comparative Biology,* **56**, 1323-1336.

Lingham-Soliar, T. & Plodowski, G. 2007. Taphonomic evidence for high-speed adapted fins in thunniform ichthyosaurs. *Naturwissenschaften*, **94**, 65-70.

Lingham-Soliar, T. & Wesley-Smith, J. 2008. First investigation of the collagen D-band ultrastructure in fossilized vertebrate integument. *Proceedings of the Royal Society of London B: Biological Sciences*, **275**, 2207-2212.

Lingham-Soliar, T. & Plodowski, G., 2010. The integument of *Psittacosaurus* from Liaoning Province, China: taphonomy, epidermal patterns and color of a ceratopsian dinosaur. *Naturwissenschaften*, **97**, 479-486.

Lingham-Soliar, T., Feduccia, A. & Wang, X. 2007. A new Chinese specimen indicates that 'protofeathers' in the Early Cretaceous theropod dinosaur *Sinosauropteryx* are degraded collagen fibres. *Proceedings of the Royal Society of London B: Biological Sciences*, **274**, 1823-1829.

Liu, Y. & Simon, J. D. 2005. Metal–ion interactions and the structural organization of *Sepia* eumelanin. *Pigment Cell & Melanoma Research*, **18**, 42-48.

Liu, Y., Kempf, V. R., Brian Nofsinger, J., Weinert, E. E., Rudnicki, M., Wakamatsu, K., Ito, S. & Simon, J. D. 2003. Comparison of the structural and physical properties of human hair eumelanin following enzymatic or acid/base extraction. *Pigment Cell Research*, **16**, 355-365.

Liu, Y., Hong, L., Wakamatsu, K., Ito, S., Adhyaru, B., Cheng, C. Y., Bowers, C. R. & Simon, J. D. 2005*a*. Comparison of structural and chemical properties of black and red human hair melanosomes. *Photochemistry and Photobiology*, **81**, 135-144.

Liu, Y., Hong, L., Wakamatsu, K., Ito, S., Adhyaru, B. B., Cheng, C. Y., Bowers, C. R. & Simon, J. D. 2005*b*. Comparisons of the structural and chemical properties of melanosomes isolated from retinal pigment epithelium, iris and choroid of newborn and mature bovine eyes. *Photochemistry and Photobiology,* **81**, 510-516.

Lomax, D. R. 2010. An *Ichthyosaurus* (Reptilia, Ichthyosauria) with gastric contents from Charmouth, England: first report of the genus from the Pliensbachian. *Paludicola,* **8**, 22-36.

Long, J. A. & Trinajstic, K. 2010. The Late Devonian Gogo Formation lägerstatte of Western Australia: exceptional early vertebrate preservation and diversity. *Annual Review of Earth and Planetary Sciences,* **38**, 255-279.

Louw, H. J., Gideon, N. & Belonje, P. C. 1972. Renal function, respiration, heart rate and thermoregulation in the ostrich (*Struthio camelus*). *Scientific Papers of the Namib Desert Research Station*, **1972**, 43-54.

Ma, X., Hou, X., Aldridge, R. J., Siveter, D. J., Siveter, D. J., Gabbott, S. E., Purnell, M. A., Parker, A. R. & Edgecombe, G. D., 2012. Morphology of Cambrian lobopodian eyes from the Chengjiang Lagerstätte and their evolutionary significance. *Arthropod Structure & Development*, **41**, 495-504.

Mahapatra, B. B., Marathe, S. A., Meyer-Rochow, V. B. & Mishra, M. 2016. A closer look at the feather coloration in the male purple sunbird, *Nectarinia asiatica*. *Micron*, **85**, 44-50.

Maia, R., D'Alba, L. & Shawkey, M. D. 2010. What makes a feather shine? A nanostructural basis for glossy black colours in feathers. *Proceedings of the Royal Society of London B: Biological Sciences*, **278**, 1973-1980.

Maia, R., Macedo, R. H. & Shawkey, M. D. 2011. Nanostructural self-assembly of iridescent feather barbules through depletion attraction of melanosomes during keratinization. *Journal of the Royal Society Interface*, **9**, 20110456.

Mapes, R. H. & Davis, R. A. 1996. Color patterns in ammonoids. In *Ammonoid Paleobiology*. Landman, N. H., Tanabe, K. & Davis, R. A. (eds.), Springer, Boston, MA, USA, pp. 103-127.

Mappes, J., Marples, N. & Endler, J. A. 2005. The complex business of survival by aposematism. *Trends in Ecology & Evolution*, **20**, 598-603.

Marchetti K. 1993. Dark habitats and bright birds illustrate the role of the environment in species divergence. *Nature*, **362**, 149.

Margalida, A., Negro, J. J. & Galván, I. 2008. Melanin-based color variation in the bearded vulture suggests a thermoregulatory function. *Comparative Biochemistry and Physiology Part A: Molecular & Integrative Physiology,* **149**, 87-91.

Marques, C. I., Batalha, H. R. & Cardoso, G. C. 2016. Signalling with a cryptic trait: the regularity of barred plumage in common waxbills. *Royal Society Open Science*, **3**, 160195.

Marshall, N. J. 2000. Communication and camouflage with the same 'bright'colours in reef fishes. *Philosophical Transactions of the Royal Society of London B: Biological Sciences*, **355**, 1243-1248.

Martill, D. M. 1987. Prokaryote mats replacing soft tissues in Mesozoic marine reptiles. *Modern Geology*, **11**, 265-269.

Martill, D. M. 1990. Macromolecular resolution of fossilized muscle tissue from an elopomorph fish. *Nature*, **346**, 171.

Martill, D. M. 1995. An ichthyosaur with preserved soft tissue from the Sinemurian of southern England. *Palaeontology*, **38**, 897-904.

Martin, L. D. & Czerkas, S. A. 2000. The fossil record of feather evolution in the Mesozoic. *American Zoologist*, **40**, 687-694.

Martín-Vivaldi, M., Palomino, J. J., Soler, M. & Soler, J. J. 1999. Determinants of reproductive success in the Hoopoe *Upupa epops*, a hole-nesting non-passerine bird with asynchronous hatching. *Bird Study*, **46**, 205-216.

Mason, H. S. 1948. The chemistry of melanin III. Mechanism of the oxidation of dihydroxyphenylalanine by tyrosinase. *Journal of Biological Chemistry*, **172**, 83-99.

Massare, J. A. 1988. Swimming capabilities of Mesozoic marine reptiles: implications for method of predation. *Paleobiology*, **14**, 187-205.

Massare, J. A. & Young, H. A. 2005. Gastric contents of an ichthyosaur from the Sundance Formation (Jurassic) of central Wyoming. *Paludicola*, **5**, 20-27.

MATLAB and statistics toolbox release R2016a. 2016. The Mathworks, Inc., Natick, Massachusetts, United States. https://mathworks.com/products/matlab/html.

Mayr G. 1998*a*. "Coraciiforme" und "piciforme" Kleinvögel aus dem Mittel-Eozän der Grube Messel (Hessen, Deutschland). *Courier Forschungsinstitut Senckenberg*, **205**, 100.

Mayr, G. 1998*b*. Ein Archaeotrogon (Aves: Archaeotrogonidae) aus dem Mittel-Eozän der Grube Messel (Hessen, Deutschland)? *Journal für Ornithologie*, **139**, 121-129.

Mayr, G. 1999. Caprimulgiform birds from the middle Eocene of Messel (Hessen, Germany). *Journal of Vertebrate Paleontology*, **19**, 521-532.

Mayr G. 2000. Tiny hoopoe-like birds from the Middle Eocene of Messel (Germany). *The Auk*, **117**, 964-970.

Mayr, G. 2002. Osteological evidence for paraphyly of the avian order Caprimulgiformes (nightjars and allies). *Journal für Ornithologie*, **143**, 82-97.

Mayr, G. 2003. A new Eocene swift-like bird with a peculiar feathering. *Ibis*, **145**, 382-391.

Mayr, G. 2004. New specimens of *Hassiavis laticauda* (Aves: Cypselomorphae) and *Quasisyndactylus longibrachis* (Aves: Alcediniformes) from the Middle Eocene of Messel, Germany. *Courier Forschungsinstitut Senckenberg*, **252**, 23-28.

Mayr G. 2006. New specimens of the Eocene Messelirrisoridae (Aves: Bucerotes), with comments on the preservation of uropygial gland waxes in fossil birds from Messel and the phylogenetic affinities of Bucerotes. *Paläontologische Zeitschrift*, **80**, 390-405.

Mayr, G. 2010*a*. Response to Lingham-Soliar: dinosaur protofeathers: pushing back the origin of feathers into the Middle Triassic? *Journal of Ornithology*, **151**, 523-524.

Mayr, G. 2010*b*. Phylogenetic relationships of the paraphyletic 'caprimulgiform'birds (nightjars and allies). *Journal of Zoological Systematics and Evolutionary Research*, **48**, 126-137.

Mayr, G. 2010*c*. Reappraisal of *Eocypselus*—a stem group apodiform from the early Eocene of Northern Europe. *Palaeobiodiversity and Palaeoenvironments*, **90**, 395-403.

Mayr, G. 2011. Metaves, Mirandornithes, Strisores and other novelties–a critical review of the higher-level phylogeny of neornithine birds. *Journal of Zoological Systematics and Evolutionary Research*, **49**, 58-76.

Mayr, G. 2016. The early Eocene birds of the Messel fossil site: a 48 million-year-old bird community adds a temporal perspective to the evolution of tropical avifaunas. *Biological Reviews*. **92**, 1174-1188.

Mayr, G. 2017*a*. The early Eocene birds of the Messel fossil site: a 48 million-year-old bird community adds a temporal perspective to the evolution of tropical avifaunas. *Biological Reviews*, **92**, 1174-1188.

Mayr G. 2017*b*. *Avian Evolution: The Fossil Record of Birds and its Paleobiological Significance*. Wiley-Blackwell, Chichester, UK, pp. 306.

Mayr, G., Peters, S. D., Plodowski, G. & Vogel, O. 2002. Bristle-like integumentary structures at the tail of the horned dinosaur *Psittacosaurus*. *Naturwissenschaften*, **89**, 361-365.

Mayr, G., Pittman, M., Saitta, E., Kaye, T. G. & Vinther, J. 2016, Structure and homology of *Psittacosaurus* tail bristles. *Palaeontology*, **59**, 793-802.

McGowan, C. 1992. Unusual extensions of the neural spines in two ichthyosaurs from the Lower Jurassic of Holzmaden. *Canadian Journal of Earth Sciences*, **29**, 380-383.

McGraw, K. J. 2006*a*. Mechanics of carotenoid-based coloration. In *Bird Coloration, Volume I: Mechanisms and Measurements*. Hill, G. E. & McGraw, K. J. (eds.), Harvard University Press, Cambridge, MS, USA, pp. 177-242.

McGraw, K. J. 2006*b*. Mechanics of melanin-based coloration. In *Bird Coloration, Volume I: Mechanisms and Measurements*. Hill, G. E. & McGraw, K. J. (eds.), Harvard University Press, Cambridge, MS, USA, pp. 243-294.

McGraw, K. J. 2006*c*. Mechanisms of uncommon colors: pterins, porphyrins and psittacofulvins. In *Bird Coloration, Volume I: Mechanisms and Measurements*. Hill, G. E. & McGraw, K. J. (eds.), Harvard University Press, Cambridge, MS, USA, pp. 354-398.

McGraw, K. J. 2008. An update on the honesty of melanin-based color signals in birds. *Pigment Cell & Melanoma Research*, **21**, 133-138.

McGraw, K. J., Safran, R. & Wakamatsu, K. 2005. How feather colour reflects its melanin content. *Functional Ecology,* **19**, 816-821.

McNamara, M. E., Orr, P. J., Kearns, S. L., Alcalá, L., Anadón, P. & Peñalver-Mollá, E. 2006. High-fidelity organic preservation of bone marrow in ca. 10 Ma amphibians. *Geology*, **34**, 641-644.

McNamara, M. E, Orr, P.J., Kearns, S. L., Alcalá, L., Anadón, P. & Peñalver-Mollá, E. 2010. Organic preservation of fossil musculature with ultracellular detail. *Proceedings of the Royal Society of London B: Biological Sciences*, **277**, 423-427.

McNamara, M. E., Briggs, D. E. G., Orr, P. J., Field, D. J. & Wang, Z. 2013. Experimental maturation of feathers: implications for reconstructions of fossil feather colour. *Biology Letters*, **9**, 20130184.

McNamara, M. E., Orr, P. J., Kearns, S. L., Alcalá, L., Anadón, P. & Peñalver, E., 2016*a*. Reconstructing carotenoid-based and structural coloration in fossil skin. *Current Biology*, **26**, 1075-1082.

McNamara, M. E., Dongen, B. E., Lockyer, N. P., Bull, I. D. & Orr, P. J. 2016*b*. Fossilization of melanosomes via sulfurization. *Palaeontology*, **59**, 337-350.

McNamara, M. E., Briggs, D. E. G., Orr, P. J., Field, D. J. & Wang, Z. 2017. Correction to 'Experimental maturation of feathers: implications for reconstructions of fossil feather colour'. *Biology Letters*, **13**.

McNamara, M. E., Kaye, J. S., Benton, M. J., Orr, P. J., Rossi, V., Ito, S. & Wakamatsu, K. 2018. Non-integumentary melanosomes can bias reconstructions of the colours of fossil vertebrates. *Nature Communications*, **9**, 2878.

McNaught M. K. & Owens I. P. 2002. Interspecific variation in plumage colour among birds: species recognition or light environment? *Journal of Evolutionary Biology*, **15**, 505-514.

Medina, I., Delhey, K., Peters, A., Cain, K. E., Hall, M. L., Mulder, R. A. & Langmore, N. E. 2017. Habitat structure is linked to the evolution of plumage colour in female, but not male, fairy-wrens. *BMC Evolutionary Biology*, **17**, 35.

Meng, J., Hu, Y., Wang, Y., Wang, X. & Li, C. 2006. A Mesozoic gliding mammal from northeastern China. *Nature*, **444**, 889.

Merilaita, S. & Lind, J. 2005. Background-matching and disruptive coloration, and the evolution of cryptic coloration. *Proceedings of the Royal Society of London B: Biological Sciences*, **272**, 665-670.

Meyer, W. & Seegers, U. 2012. Basics of skin structure and function in elasmobranchs: a review. *Journal of Fish Biology*, **80**, 1940-1967.

Moore, C. D., Crocker, D. E., Fahlman, A., Moore, M. J., Willoughby, D. S., Robbins, K. A., Kanatous, S. B. & Trumble, S. J. 2014. Ontogenetic changes in skeletal muscle fiber type, fiber diameter and myoglobin concentration in the Northern elephant seal (*Mirounga angustirostris*). *Frontiers in Physiology*, **5**, 217.

Morris, S. C. & Caron, J. B. 2014. A primitive fish from the Cambrian of North America. *Nature*, **512**, 419.

Motani, R. 2002. Scaling effects in caudal fin propulsion and the speed of ichthyosaurs. *Nature*, **415**, 309.

Motta, P. J. 1977. Anatomy and functional morphology of dermal collagen fibers in sharks. *Copeia*, **1977**, 454-464.

Moyer, A. E., Zheng, W., Johnson, E. A., Lamanna, M. C., Li, D. Q., Lacovara, K. J. & Schweitzer, M. H. 2014. Melanosomes or microbes: testing an alternative hypothesis for the origin of microbodies in fossil feathers. *Scientific Reports*, **4**, 4233.

Moyer, A. E., Zheng, W. & Schweitzer, M. H. 2016. Microscopic and immunohistochemical analyses of the claw of the nesting dinosaur, Citipati osmolskae. *Proceedings of the Royal Society B: Biological Sciences*, **283**, 20161997.

Murali, G. & Kodandaramaiah, U. 2016. Deceived by stripes: conspicuous patterning on vital anterior body parts can redirect predatory strikes to expendable posterior organs. *Royal Society open science*, **3**, 160057.

Murali, G. & Kodandaramaiah, U. 2017. Body size and evolution of motion dazzle coloration in lizards. *Behavioral Ecology*, **29**, 79-86.

Nagloo, N., Collin, S. P., Hemmi, J. M. & Hart, N. S. 2016. Spatial resolving power and spectral sensitivity of the saltwater crocodile, *Crocodylus porosus*, and the freshwater crocodile, *Crocodylus johnstoni*. *Journal of Experimental Biology*, **219**, 1394-1404.

Negro, J., Finlayson, C. & Galván, I. 2018. Melanins in fossil animals: is it possible to infer life history traits from the coloration of extinct species? *International Journal of Molecular Sciences*, **19**, 230.

Nelson, J. S., Grande, T. C. & Wilson, M. V. H. 2016. *Fishes of the World.* John Wiley & Sons, Hoboken, NJ, USA, pp. 752.

Newman, C., Buesching, C. & Wolff, J. 2005. The function of facial masks in "midguild" carnivores. *Oikos*. **108**, 623-633.

Nilsson, D. E. 2009. The evolution of eyes and visually guided behaviour. *Philosophical Transactions of the Royal Society B: Biological Sciences*, **364**, 2833-2847.

Nordén, K. K., Faber, J. W., Babarović, F., Stubbs, T. L., Selly, T., Schiffbauer, J. D., Peharec Štefanić, P., Mayr, G., Smithwick, F. M. & Vinther, J. 2019. Melanosome diversity and convergence in the evolution of iridescent avian feathers—Implications for paleocolor reconstruction. *Evolution*, **73**, 15-27.

Norell, M. A. & Xu, X. 2005. Feathered dinosaurs. *Annual Review of Earth and Planetary Sciences*, **33**, 277-299.

Norell, M. A., Makovicky, P. J. & Currie, P.J. 2001. Palaeontology: The beaks of ostrich dinosaurs. *Nature*, **412**, 873.

Novellino, L., Napolitano, A. & Prota, G. 2000. Isolation and characterization of mammalian eumelanins from hair and irides. *Biochimica et Biophysica Acta (BBA)-General Subjects*, **1475**, 295-306.

O'Connor, S., Solazzo, C. & Collins, M. 2015. Advances in identifying archaeological traces of horn and other keratinous hard tissues. *Studies in Conservation*, **60**, 393-417.

Olberding, J. P., Herrel, A., Higham, T. E. & Garland Jr, T. 2016. Limb segment contributions to the evolution of hind limb length in phrynosomatid lizards. *Biological Journal of the Linnean Society*, **117**, 775-795.

Olson, V. A. & Owens, I. P. 1998. Costly sexual signals: are carotenoids rare, risky or required? *Trends in Ecology & Evolution,* **13**, 510-514.

Omland, K. E. & Hofmann, C. M., 2006. Adding color to the past: ancestral-state reconstruction of coloration. In *Bird Coloration, Volume II: Function and Evolution*. Hill, G. E. & McGraw, K. J. (eds.), Harvard University Press, Cambridge, MS, USA, pp. 417–454.

O'Reilly, S., Summons, R., Mayr, G. & Vinther, J. 2017. Preservation of uropygial gland lipids in a 48-million-year-old bird. *Proceedings of the Royal Society B: Biological Sciences*, **284**, 20171050.

Ortolani, A. 1999. Spots, stripes, tail tips and dark eyes: predicting the function of carnivore colour patterns using the comparative method. *Biological Journal of the Linnean Society*, **67**, 433-476.

Osorio, D. & Srinivasan, M. V. 1991. Camouflage by edge enhancement in animal coloration patterns and its implications for visual mechanisms. *Proceedings of the Royal Society B: Biological Sciences*, **244**, 81-85.

Ostrom, J. H. 1976. *Archaeopteryx* and the origin of birds. *Biological Journal of the Linnean Society*, **8**, 91-182.

Owen, R. 1841. A description of some of the soft parts, with the integument, of the hind-fin of the *Ichthyosaurus*, indicating the shape of the fin when recent. *Transactions of the Geological Society of London*, **2**, 199-201.

Owen, P. 1863. On the *Archeopteryx* of von Meyer, with a description of the fossil remains of a long-tailed species, from the lithographic stone of Solenhofen. *Philosophical Transactions of the Royal Society of London*, **153**, 33-47.

Pabst, D. A. 1996. Morphology of the subdermal connective tissue sheath of dolphins: a new fibre-wound, thin-walled, pressurized cylinder model for swimming vertebrates. *Journal of Zoology*, **238**, 35-52.

Pabst, D. A. 2000. To bend a dolphin: convergence of force transmission designs in cetaceans and scombrid fishes. *American Zoologist*, **40**, 146-155.

Palmer, E. & Weddell, G. 1964. The relationship between structure, innervation and function of the skin of the bottle nose dolphin (*Tursiops truncatus*). *Proceedings of the Zoological Society of London*, **143**, 553-568.

Pan, Y., Zheng, W., Moyer, A. E., O'Connor, J. K., Wang, M., Zheng, X., Wang, X., Schroeter, E. R., Zhou, Z. & Schweitzer, M. H. 2016. Molecular evidence of keratin and melanosomes in feathers of the Early Cretaceous bird *Eoconfuciusornis*. *Proceedings of the National Academy of Sciences*, **113**, 7900-7907.

Pan, Y., Zheng, W., Sawyer, R. H., Pennington, M. W., Zheng, X., Wang, X., Wang, M., Hu, L., O'Connor, J., Zhao, T. & Li, Z. 2019. The molecular evolution of feathers with direct evidence from fossils. *Proceedings of the National Academy of Sciences*, 201815703.

Paparella, I., Palci, A., Nicosia, U. & Caldwell, M. W. 2018. A new fossil marine lizard with soft tissues from the Late Cretaceous of southern Italy. *Royal Society Open Science*, **5**, 172411.

Parker, A. R. 1998. Colour in Burgess Shale animals and the effect of light on evolution in the Cambrian. *Proceedings of the Royal Society B: Biological Sciences*, **265**, 967-972.

Parker, A. R. 2000. 515 million years of structural colour. *Journal of Optics A: Pure and Applied Optics*, **2**, R15.

Parry, L. A., Smithwick, F., Nordén, K. K., Saitta, E. T., Lozano-Fernandez, J., Tanner, A. R., Caron, J. B., Edgecombe, G. D., Briggs, D. E. G. & Vinther, J. 2018. Soft-bodied fossils are not simply rotten carcasses–toward a holistic understanding of exceptional fossil

preservation: exceptional fossil preservation is complex and involves the interplay of numerous biological and geological processes. *Bioessays,* **40**, 1700167.

Paterson, J. R., García-Bellido, D. C., Lee, M. S., Brock, G. A., Jago, J. B. & Edgecombe, G. D., 2011. Acute vision in the giant Cambrian predator *Anomalocaris* and the origin of compound eyes. *Nature*, **480**, 237.

Pautard, F. G. E. 1964. Calcification of keratin. In *Progress in the Biological Sciences in Relation to Dermatology. Vol. 2*. Rook, A. & Champion, H. (eds.), Cambridge University Press, Cambridge, UK, pp. 227-240.

Penacchio, O., Lovell, P. G., Cuthill, I. C., Ruxton, G. D. & Harris, J. M. 2015. Three-dimensional camouflage: exploiting photons to conceal form. *The American Naturalist*, **186**, 553-563.

Perrichot, V., Marion, L., Néraudeau, D., Vullo, R. & Tafforeau, P. 2008. The early evolution of feathers: fossil evidence from Cretaceous amber of France. *Proceedings of the Royal Society of London B: Biological Sciences*, **275**, 1197-1202.

Persons IV, W. S., Currie, P. J. & Norell, M. A. 2013. Oviraptorosaur tail forms and functions. *Acta Palaeontologica Polonica*, **59**, 553-567.

Pittman, M., Gatesy, S. M., Upchurch, P., Goswami, A. & Hutchinson, J. R. 2013. Shake a tail feather: the evolution of the theropod tail into a stiff aerodynamic surface. *PloS One*, **8**, e63115.

Podletnik, M. & Denac, D. 2015. Selection of foraging habitat and diet of the Hoopoe *Upupa epops* in the mosaic-like cultural landscape of Goričko (NE Slovenia). *Acrocephalus*, **36**, 109-132.

Prado, G. M., Anelli, L. E., Petri, S. & Romero, G. R. 2016. New occurrences of fossilized feathers: systematics and taphonomy of the Santana Formation of the Araripe Basin (Cretaceous), NE, Brazil. *PeerJ*, **4**, e1916.

Price, J. J., Friedman, N. R. & Omland, K. E. 2007. Song and plumage evolution in the new world orioles (Icterus) show similar lability and convergence in patterns. *Evolution: International Journal of Organic Evolution*, **61**, 850-863.

Prinzinger, R., Schäfer, T. & Schuchmann, K. L. 1992. Energy metabolism, respiratory quotient and breathing parameters in two convergent small bird species: The fork-tailed sunbird *Aethopyga christinae* (Nectariniidae) and the Chilean hummingbird *Sephanoides sephanoides* (Trochilidae). *Journal of Thermal Biology*, **17**, 71-79.

Prum, R. O. 1999. Development and evolutionary origin of feathers. *The Journal of Experimental Zoology*, **285**, 291-306.

Prum, R. O. 2002. Why ornithologists should care about the theropod origin of birds. *The Auk*, **119**, 1-17.

Prum, R. O. 2003. Are current critiques of the theropod origin of birds science? Rebuttal to Feduccia (2002). *The Auk*, **120**, 550-561.

Prum, R. O. 2006. Anatomy, physics, and evolution of structural colors. In *Bird Coloration, Volume I: Mechanisms and Measurements*. Hill, G. E. & McGraw, K. J. (eds.), Harvard University Press, Cambridge, MS, USA, pp.295-353.

Prum, R. O. & Williamson, S. 2002. Reaction–diffusion models of within-feather pigmentation patterning. *Proceedings of the Royal Society B: Biological Sciences*, **269**, 781-792.

Prum, R. O., Berv, J. S., Dornburg, A., Field, D. J., Townsend, J. P., Lemmon, E. M. & Lemmon, A. R. 2015. A comprehensive phylogeny of birds (Aves) using targeted next-generation DNA sequencing. *Nature*, **526**, 569.

Qiang, J. 2002. Discovery of a Mesozoic fossil mammal with hair and soft tissue in western Liaoning, China. *Regional Geology of China*, **1**, 5.

R Core Team 2015. R: A language and environment for statistical computing (R Foundation for Statistical Computing). https://www.r-projects.org/.

Radford A. N. & Du Plessis M. A. 2003. Bill dimorphism and foraging niche partitioning in the green woodhoopoe. *Journal of Animal Ecology*, **72**, 258-269.

Rauhut, O. W., Foth, C., Tischlinger, H. & Norell, M. A. 2012. Exceptionally preserved juvenile megalosauroid theropod dinosaur with filamentous integument from the Late Jurassic of Germany. *Proceedings of the National Academy of Sciences*, **109**, 11746-11751.

Rayner, R. J. 1992. A method of improving contrast in illustrations of coalified fossils. *Palaeontologica Africana*, **29**, 45-49.

Reichlin, T., Wild, A., Dürrenberger, M., Daniels, A. U., Aebi, U., Hunziker, P. R. & Stolz, M. 2005. Investigating native coronary artery endothelium in situ and in cell culture by scanning force microscopy. *Journal of Structural Biology*, **152**, 52-63.

Rieseberg, L. H. & Soltis, D. E. 1987. Flavonoids of fossil Miocene *Platanus* and its extant relatives. *Biochemical Systematics and Ecology*, **15**, 109-112.

Rougier, G. W., Qiang, J. & Novacek, M. J. 2003. A new symmetrodont mammal with fur impressions from the Mesozoic of China. *Acta Geologica Sinica-English Edition*, **77**, 7-14.

Rowland, H. M. 2009. From Abbott Thayer to the present day: what have we learned about the function of countershading? *Philosophical Transactions of the Royal Society of London B: Biological Sciences,* **364**, 519-527.

Rowland, H. M. 2011. The history, theory and evidence for a cryptic function of countershading. In *Animal Camouflage: Mechanisms and Function*. Stevens, M. & Merilaita, S. (eds.), Cambridge University Press, Cambridge, UK, pp. 53-72.

Rowland, H. M., Cuthill, I. C., Harvey, I. F., Speed, M. P. & Ruxton, G. D. 2008. Can't tell the caterpillars from the trees: countershading enhances survival in a woodland. *Proceedings of the Royal Society B: Biological Sciences*, **275**, 2539-2545.

Roy, J. K. & Roy, B. C. 1965. Isolation of some acid soluble protein pigments from dark colored human hair. *Journal and Proceedings of the Institute of Chemistry*, **37**, 257-261.

Ruben, J. A. 2010. Paleobiology and the origins of avian flight. *Proceedings of the National Academy of Sciences*, **107**, 2733-2734.

Ruben, J. A. & Jones, T. D. 2000. Selective factors associated with the origin of fur and feathers. *American Zoologist*, **40**, 585-596.

Ruiz-Rodriguez, M., Avilés, J. M., Cuervo, J. J., Parejo, D., Ruano, F., Zamora-Muñoz, C., Sergio, F., López-Jiménez, L., Tanferna, A. & Martín-Vivaldi, M. 2013. Does avian conspicuous colouration increase or reduce predation risk? *Oecologia*, **173**, 83-93.

Ruiz-Rodríguez, M., Martín-Vivaldi, M. & Avilés, J. M. 2017. Multi-functional crest display in hoopoes *Upupa epops*. *Journal of Avian Biology*, **48**, 1425-1431.

Ruxton, G. D., Speed, M. P. & Kelly, D. J. 2004. What, if anything, is the adaptive function of countershading? *Animal Behaviour*, **68**, 445-451.

Ruxton, G. D., Allen, W. L., Sherratt, T. N. & Speed, M. P. 2018. *Avoiding Attack: The Evolutionary Ecology of Crypsis, Aposematism, and Mimicry*. Oxford University Press, Oxford, UK, pp. 304.

Saitta, E. T., Rogers, C., Brooker, R. A., Abbott, G. D., Kumar, S., O'Reilly, S. S., Donohoe, P., Dutta, S., Summons, R. E. & Vinther, J. 2017. Low fossilization potential of keratin protein revealed by experimental taphonomy. *Palaeontology*, **60**, 547-556.

Saitta, E. T., Fletcher, I., Martin, P., Pittman, M., Kaye, T.G ., True, L. D., Norell, M. A., Abbott, G. D., Summons, R. E., Penkman, K. & Vinther, J. 2018. Preservation of feather fibers from the Late Cretaceous dinosaur *Shuvuuia deserti* raises concern about immunohistochemical analyses on fossils. *Organic Geochemistry*, **125**, 142-151.

Sanger, J. E. 1988. Fossil pigments in paleoecology and paleolimnology. *Palaeogeography, Palaeoclimatology, Palaeoecology*, **62**, 343-359.

Schaal S. K. F. Smith K. & Habersetzer J. 2018. *Messel – An Ancient Greenhouse Ecosystem.* Senckenbergische Naturforschende Gesellschaft, Stuttgart, Germany, pp. 355.

Schaefer, H. M. & Stobbe, N. 2006. Disruptive coloration provides camouflage independent of background matching. *Proceedings of the Royal Society of London B: Biological Sciences*, **273**, 2427-2432.

Schiffbauer, J. D. & Xiao, S. 2009. Novel application of focused ion beam electron microscopy (FIB-EM) in preparation and analysis of microfossil ultrastructures: A new view of complexity in early eukaryotic organisms. *Palaios*, **24**, 616–626.

Schiffbauer, J. D. & Xiao, S. 2011. Paleobiological applications of focused ion beam electron microscopy (FIB-EM): An ultrastructural approach to the (micro)fossil record. In *Quantifying the Evolution of Early Life: Numerical Approaches to the Evaluation of Fossils*

and Ancient Ecosystems. Laflamme, M., Schiffbauer, J. D., & Dornbos, S. Q. (eds.), Springer, NY, USA, pp. 321–354.

Schwieters, J., Cramer, H. G., Heller, T., Jürgens, U., Niehuis, E., Zehnpfenning, J. & Benninghoven, A. 1991. High mass resolution surface imaging with a time-of-flight secondary ion mass spectroscopy scanning microprobe. *Journal of Vacuum Science & Technology A: Vacuum, Surfaces, and Films*, **9**, 2864-2871.

Schweitzer, M. H., Watt, J. A., Avci, R., Forster, C. A., Krause, D. W., Knapp, L., Rogers, R. R., Beech, I. & Marshall, M. 1999. Keratin immunoreactivity in the Late Cretaceous bird *Rahonavis ostromi*. *Journal of Vertebrate Paleontology*, **19**, 712-722.

Schweitzer, M. H., Lindgren, J. & Moyer, A. E. 2015. Melanosomes and ancient coloration re-examined: A response to Vinther 2015. *BioEssays*, **37**, 1174-1183.

Seehausen, O. & Schluter, D. 2004. Male–male competition and nuptial–colour displacement as a diversifying force in Lake Victoria cichlid fishes. *Proceedings of the Royal Society B: Biological Sciences*, **271**, 1345-1353.

Senar, J. C. 2006. Color displays as intrasexual signals of aggression and dominance. In *Bird Coloration, Volume II: Function and Evolution.* Hill, G. E. & McGraw, K. J. (eds.), Harvard University Press, Cambridge, MS, USA, pp. 87-136.

Seymour, C. L. & Dean, W. R. J. 2010. The influence of changes in habitat structure on the species composition of bird assemblages in the southern Kalahari. *Austral Ecology*, **35**, 581-592.

Shawkey, M. D. 2013. How hollow melanosomes affect iridescent colour production in birds. *Proceedings of the Royal Society B: Biological Sciences*, **280**, 20131505.

Shawkey, M. D., Estes, A. M., Siefferman, L. M. & Hill, G. E. 2003. Nanostructure predicts intraspecific variation in ultraviolet–blue plumage colour. *Proceedings of the Royal Society of London B: Biological Sciences*, **270**, 1455-1460.

Shawkey, M. D., Estes, A. M., Siefferman, L. & Hill, G. E. 2005. The anatomical basis of sexual dichromatism in non-iridescent ultraviolet-blue structural coloration of feathers. *Biological Journal of the Linnean Society*, **84**, 259-271.

Shawkey, M. D., D'Alba, L., Xiao, M., Schutte, M. & Buchholz, R. 2015. Ontogeny of an iridescent nanostructure composed of hollow melanosomes. *Journal of Morphology*, **276**, 378-384.

Shu, D. G., Morris, S. C., Han, J., Zhang, Z. F., Yasui, K., Janvier, P., Chen, L., Zhang, X. L., Liu, J. N., Li, Y. & Liu, H. Q. 2003. Head and backbone of the Early Cambrian vertebrate Haikouichthys. *Nature*, **421**, 526.

Shu'an, J. & Qiang, J. 2004. Postcranial anatomy of the Mesozoic *Dalinghosaurus* (Squamata): evidence from a new specimen of western Liaoning. *Acta Geologica Sinica-English Edition*, **78**, 897-905.

Shutler, D. & Weatherhead, P. J. 1990. Targets of sexual selection: song and plumage of wood warblers. *Evolution*, **44**, 1967-1977.

Sinninghe Damsté, J. S., Rijpstra, W. I. C., Kock-Van Dalen, A. C., De Leeuw, J. W. & Schenck, P. A. 1989. Quenching of labile functionalised lipids by inorganic sulphur species: evidence for the formation of sedimentary organic sulphur compounds at the early stages of diagenesis. *Geochimica et Cosmochimica Acta*, **53**, 1343-1355.

Smith, N. A., Chiappe, L. M., Clarke, J. A., Edwards, S. V., Nesbitt, S. J., Norell, M. A., Stidham, T. A., Turner, A., Van Tuinen, M., Vinther, J. & Xu, X. 2015. Rhetoric vs. reality: A commentary on “Bird Origins Anew” by A. Feduccia. *The Auk*, **132**, 467-480.

Smithwick, F. M., Nicholls, R., Cuthill, I. & Vinther, J. 2017*a*. Couthershading and stripes in the theropod dinosaur *Sinosauropteryx* reveal heterogeneous habitats in the Early Cretaceous Jehol Biota. *Current Biology*, **27**, 3337-3343.

Smithwick, F. M., Mayr, G., Saitta, E. T., Benton, M. J. & Vinther, J. 2017*b*. On the purported presence of fossilized collagen fibres in an ichthyosaur and a theropod dinosaur. *Palaeontology*, **60**, 409-422.

Stankowich, T., Caro, T. & Cox, M. 2011. Bold coloration and the evolution of aposematism in terrestrial carnivores. *Evolution*, **65**, 3090-3099.

Stavenga, D. G., Leertouwer, H. L., Marshall, N. J. & Osorio, D. 2010. Dramatic colour changes in a bird of paradise caused by uniquely structured breast feather barbules. *Proceedings of the Royal Society of London B: Biological Sciences*, **278**, 2098-2104.

Stevens, K. A. 2006. Binocular vision in theropod dinosaurs. *Journal of Vertebrate Paleontology*, **26**, 321-330.

Stevens, M. 2007. Predator perception and the interrelation between different forms of protective coloration. *Proceedings of the Royal Society B: Biological Sciences*, **274**, 1457-1464.

Stevens, M. & Merilaita, S. 2008. Animal camouflage: current issues and new perspectives. *Philosophical Transactions of the Royal Society B: Biological Sciences*, **364**, 423-427.

Stevens, M. & Merilaita, S. 2011. *Animal Camouflage: Mechanisms and Function*. Cambridge University Press, Cambridge, UK, pp. 357.

Stevens, M., Stoddard, M. C. & Higham, J. P. 2009. Studying primate color: towards visual system-dependent methods. *International Journal of Primatology*, **30**, 893-917.

Stevens, M., Searle, W. T. L., Seymour, J. E., Marshall, K. L. & Ruxton, G. D. 2011. Motion dazzle and camouflage as distinct anti-predator defenses. *BMC Biology*, **9**, 81.

Stevens, M., Marshall, K. L., Troscianko, J., Finlay, S., Burnand, D. & Chadwick, S. L. 2012. Revealed by conspicuousness: distractive markings reduce camouflage. *Behavioral Ecology*, **24**, 213-222.

Stiles, F. G., Piacentini, V. D. Q. & Remsen Jr, J. V. 2017. A brief history of the generic classification of the Trochilini (Aves: Trochilidae): the chaos of the past and problems to be resolved. *Zootaxa*, **4269**, 396-412.

Stoddard, M. C. & Prum, R. O. 2011. How colorful are birds? Evolution of the avian plumage color gamut. *Behavioral Ecology*, **22**, 1042-1052.

Strausfeld, N. J., Ma, X., Edgecombe, G. D., Fortey, R. A., Land, M. F., Liu, Y., Cong, P. & Hou, X. 2016. Arthropod eyes: The early Cambrian fossil record and divergent evolution of visual systems. *Arthropod Structure & Development*, **45**, 152-172.

Stuart-Fox, D., Moussalli, A. & Whiting, M. J. 2008. Predator-specific camouflage in chameleons. *Biology Letters*, **4**, 326-329.

Summons, R. E. 2014. The exceptional preservation of interesting and informative biomolecules. *The Paleontological Society Papers*, **20**, 217-236.

Sun, X., Wu, B., Zhou, L., Liu, Z., Dong, Y. & Yang, A. 2017. Isolation and characterization of melanin pigment from yesso scallop *Patinopecten yessoensis*. *Journal of Ocean University of China*, **16**, 279-284.

Talori, Y. S., Liu, Y. F., Zhao, J. S., Sullivan, C., O'Connor, J. K. & Li, Z. H. 2018. Winged forelimbs of the small theropod dinosaur *Caudipteryx* could have generated small aerodynamic forces during rapid terrestrial locomotion. *Scientific Reports*, **8**, 17854.

Thayer, A. H. 1896. The law which underlies protective coloration. *The Auk,* **13**, 124-129.

Thayer, G. H. 1909. *Concealing Colouration in the Animal Kingdom*. Macmillan, NY, USA, pp. 407.

Théry M. 2006. Effects of light environment on color communication. In *Bird Coloration, Volume I: Mechanisms and Measurements*. Hill, G. E. & McGraw, K. J. (eds.), Harvard University Press, Cambridge, MS, USA, pp. 148-173.

Thomas, D. B., McGraw, K. J., Butler, M. W., Carrano, M. T., Madden, O. & James, H. F. 2014*a*. Ancient origins and multiple appearances of carotenoid-pigmented feathers in birds. *Proceedings of the Royal Society of London B: Biological Sciences*, **281**, 20140806

Thomas, D. B., Nascimbene, P. C., Dove, C. J., Grimaldi, D. A. & James, H. F. 2014*b*. Seeking carotenoid pigments in amber-preserved fossil feathers. *Scientific Reports*, **4**, 5226.

Turner, D. 2007. *Making Prehistory: Historical Science and the Scientific Realism Debate*. Cambridge University Press, Cambridge, UK, pp. 238.

Vandenbroucke, M. & Largeau, C. 2007. Kerogen origin, evolution and structure. *Organic Geochemistry*, **38**, 719-833.

van der Reest, A. J., Wolfe, A. P. & Currie, P. J. 2016. Reply to comment on: "A densely feathered ornithomimid (Dinosauria: Theropoda) from the Upper Cretaceous Dinosaur Park Formation, Alberta, Canada". *Cretaceous Research*, **62**, 90-94.

Vickerman, J. C. & Briggs, D. 2001. *ToF-SIMS: Surface Analysis by Mass Spectrometry*. IM Publications, Cirencester, UK, pp. 798.

Vinther, J. 2015*a*. A guide to the field of palaeo colour. *BioEssays*, **37**, 643-656.

Vinther, J. 2015*b*. Fossil melanosomes or bacteria? A wealth of findings favours melanosomes. *BioEssays*, **38**, 220-225.

Vinther, J., Briggs, D. E. G., Prum, R. O. & Saranathan, V. 2008. The colour of fossil feathers. *Biology Letters*, **4**, 522-525

Vinther, J., Briggs, D. E. G., Clarke, J., Mayr, G. & Prum, R. O. 2009. Structural coloration in a fossil feather. *Biology Letters*, **6**, rsbl20090524.

Vinther, J., Nicholls, R., Lautenschlager, S., Pittman, M., Kaye, T. G., Rayfield, E., Mayr, G. & Cuthill, I. C. 2016. 3D camouflage in an ornithischian dinosaur. *Current Biology*, **26**, 2456–2462.

Vitek, N. S., Vinther, J., Schiffbauer, J. D., Briggs, D. E. G. & Prum, R. O. 2013. Exceptional three-dimensional preservation and coloration of an originally iridescent fossil feather from the middle Eocene Messel oil shale. *Paläontologische Zeitschrift*, **87**, 493-503.

Voigt, E. 1936. Über das Haarkleid einiger Säugetiere aus der mitteleozänen Braunkohle des Geiseltales. *Nova Acta Leopoldina*, **4**, 317-334.

Voigt, E. 1988. Preservation of soft tissues in the Eocene lignite of the Geiseltal near Halle. *Courier Forschungsinstitut Senckenberg*, **107**, 325-343.

Von Meyer, H. 1861*a*. *Archaeopteryx lithographica*. *Neues Jahrbuch für Mineralogie, Geologie und Paläontologie*, **1861**, 678-679.

Von Meyer, H. 1861*b*. *Archaeopteryx lithographica* (Vogel-Feder) und *Pterodactylus* von Solnhofen. *Neues Jahrbuch für Mineralogie, Geognosie, Geologie und Petrefakten-Kunde*, **1861**, 678-679.

Von Meyer, H. 1862. *Archaeopteryx lithographica* aus dem lithographischen Schiefer von Solenhofen. *Palaeontographica*, **1846-1933**, 53-56.

Vorobyev, M., Osorio, D., Bennett, A. T., Marshall, N. J. & Cuthill, I. C. 1998. Tetrachromacy, oil droplets and bird plumage colours. *Journal of Comparative Physiology A*, **183**, 621-633.

Vukusic, P. 2011. Structural colour: elusive iridescence strategies brought to light. *Current Biology*, **21**, R187-R189.

Wang, X., Pittman, M., Zheng, X., Kaye, T. G., Falk, A. R., Hartman, S. A. & Xu, X. 2017. Basal paravian functional anatomy illuminated by high-detail body outline. *Nature Communications*, **8**, 14576.

Wasmeier, C., Hume, A. N., Bolasco, G. & Seabra, M. C. 2008. Melanosomes at a glance. *Journal of Cell Science*, **121**, 3995-3999.

Webster, R. J., Callahan, A., Godin, J. G. J. & Sherratt, T. N. 2011. Camouflage behaviour and body orientation on backgrounds containing directional patterns. In *Animal Camouflage: Mechanisms and Function*. Stevens, M. & Merilaita, S. (eds.), Cambridge University Press, Cambridge, UK, pp. 101-117.

West-Eberhard, M. J. 1984. Sexual selection, competitive communication and species specific signals in insects. In *Insect Communication*. Lewis, T. (ed.), Academic Press, London, UK, pp. 283-324.

Wiemann, J., Yang, T. R., Sander, P. N., Schneider, M., Engeser, M., Kath-Schorr, S., Müller, C. E. & Sander, P. M. 2017. Dinosaur origin of egg color: oviraptors laid blue-green eggs. *PeerJ*, **5**, e3706.

Whitear, M. 1956. On the colour of an ichthyosaur. *Journal of Natural History*, **9**, 742-744.

White, N. D. 2017. *Unraveling the Evolutionary History of Nocturnality in Birds, with a Focus on Strisores* (Doctoral dissertation, University of Maryland, College Park). Retrieved from the Digital Repository at the University of Maryland (DRUM): https://drum.lib.umd.edu/handle/1903/20337.

Whitney, H. M., Kolle, M., Andrew, P., Chittka, L., Steiner, U. & Glover, B. J. 2009. Floral iridescence, produced by diffractive optics, acts as a cue for animal pollinators. *Science*, **323**, 130-133.

Wilby, P. R. & Briggs, D. E. G. 1997. Taxonomic trends in the resolution of detail preserved in fossil phosphatized soft tissues. *Geobios*, **30**, 493-502.

Williams, M., Benton, M. J. & Ross, A. 2015. The Strawberry Bank Lagerstätte reveals insights into early Jurassic life. *Journal of the Geological Society*, **172**, 683-692.

Wiman, C. 1946. Über Ichthyosaurier und Wale. *Senckenbergiana*, **27**, 1-11.

Wogelius, R. A., Manning, P. L., Barden, H. E., Edwards, N. P., Webb, S. M., Sellers, W. I., Taylor, K. G., Larson, P. L., Dodson, P., You, H. & Da-Qing, L. 2011. Trace metals as biomarkers for eumelanin pigment in the fossil record. *Science,* **333**, 1622-1626.

Wolfenden, R. N. 1884. On certain constituents of the eggs of the Common Frog. *The Journal of Physiology*, **5**, 91-97.

Wolf, L. L. 1969. Female territoriality in a tropical hummingbird. *The Auk*, **86**, 490-504.

Wolfram, L. J., Hall, K. & Hui, I. 1970. The mechanism of hair bleaching. *Journal of the Sociery of Cosmetic Chemistry*, **21**, 875-900.

Wuttke, M. 1983. Weichteil-Erhaltung' durch lithifizierte Mikroorganismen bei mittel-eozänen Vertebraten aus den Ölschiefern der 'Grube Messel' bei Darmstadt. *Senckenbergiana Lethaea*, **64**, 509-527.

Xing, L., Mckellar, R. C., Wang, M., Bai, M., O'Connor, J. K., Benton, M. J., Zhang, J., Wang, Y., Tseng, K., Lockley, M. G. & Li, G. 2016. Mummified precocial bird wings in mid-Cretaceous Burmese amber. *Nature Communications*, **7**, 12089.

Xu, X. 2006. Feathered dinosaurs from China and the evolution of major avian characters. *Integrative Zoology*, **1**, 4-11.

Young, M. F. 2003. Bone matrix proteins: their function, regulation, and relationship to osteoporosis. *Osteoporosis International*, **14**, 35-42.

Young, R. E. & Roper, C. F. 1976. Bioluminescent countershading in midwater animals: evidence from living squid. *Science*, **191**, 1046-1048.

Zhang, F., Zhou, Z. H. & Dyke, G. J. 2006. Feathers and 'feather-like' integumentary structures in Liaoning birds and dinosaurs. *The Journal of Geology* **41**, 395–404

Zhang, F., Kearns, S. L., Orr, P. J., Benton, M. J., Zhou, Z., Johnson, D., Xu, X. & Wang, X. 2010. Fossilized melanosomes and the colour of Cretaceous dinosaurs and birds. *Nature*, **463**, 1075-1078.

Zheng, X.-T., You, H.-L., Xu, X. & Dong, Z.-M. 2009. An Early Cretaceous heterodontosaurid dinosaur with filamentous integumentary structures. *Nature*, **458**, 333-336.

Zhonghe, Z. 2006. Evolutionary radiation of the Jehol Biota: chronological and ecological perspectives. *Geological Journal*, **41**, 377-393.

Zhou, Z. 2014. The Jehol Biota, an Early Cretaceous terrestrial Lagerstätte: new discoveries and implications. *National Science Review*, **1**, 543-559.

Zhou, Z. H. & Wang, X. L. 2000. A new species of *Caudipteryx* from the Yixian Formation of Liaoning, northeast China. *Vertebrata PalAsiatica*, **38**, 113-130.

Zhou, Z. & Wang, Y. 2010. Vertebrate diversity of the Jehol Biota as compared with other lagerstätten. *Science China Earth Sciences*, **53**, 1894-1907.

Zhou, Z. H., Wang, X. L., Zhang, F. C. & Xu, X. 2000. Important features of *Caudipteryx*-evidence from two nearly complete new specimens. *Vertebrata PalAsiatica*, **38**, 243-265.

Zhou, Z. H., Barrett, P. M. & Hilton, J. 2003. An exceptionally preserved Lower Cretaceous ecosystem. *Nature*, **421**, 807-814.

Zylinski, S. & Osorio, D. 2011. What can camouflage tell us about non-human visual perception? A case study of multiple cue use in cuttlefish (*Sepia* spp.). In *Animal Camouflage: Mechanisms and Function*. Stevens, M. & Merilaita, S. (eds.), Cambridge University Press, Cambridge, UK, pp. 164-185.

Supplementary figures

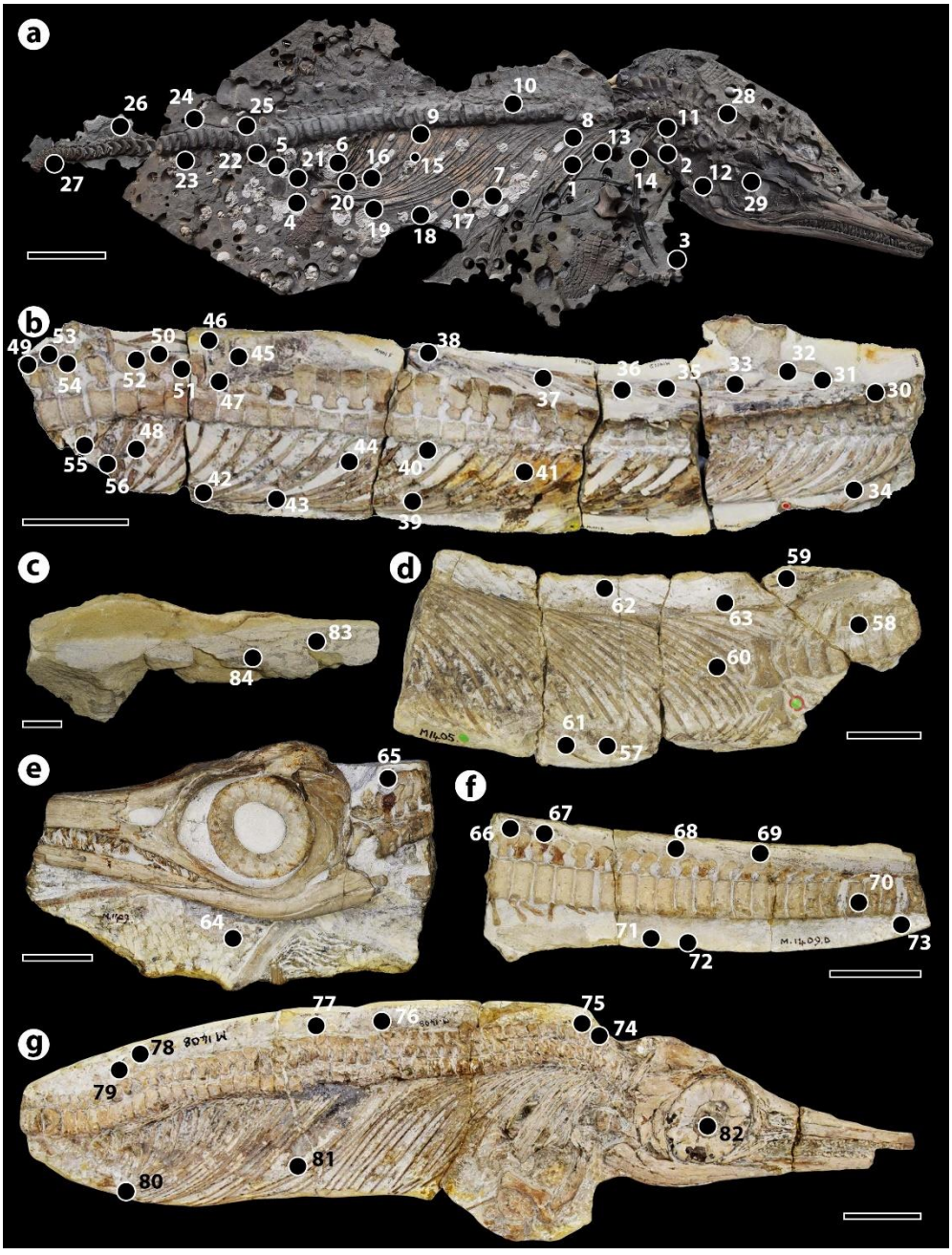

Figure S3.1. Sample locations on the Lyme Regis and Strawberry Bank specimen, numbered in order of sampling. **a**. The Lyme Regis specimen. **b**. The strawberry Bank specimen M1401. **c**. The strawberry Bank specimen 39-20110353. **d**. The strawberry Bank specimen M1405. **e**. The strawberry Bank specimen M1409. **f**. The strawberry Bank specimen M1409D. **g**. The strawberry Bank specimen M1408. Scale bars represent 10 cm in (a) and (b), 10 mm in (c) and 5 cm in (d-g).

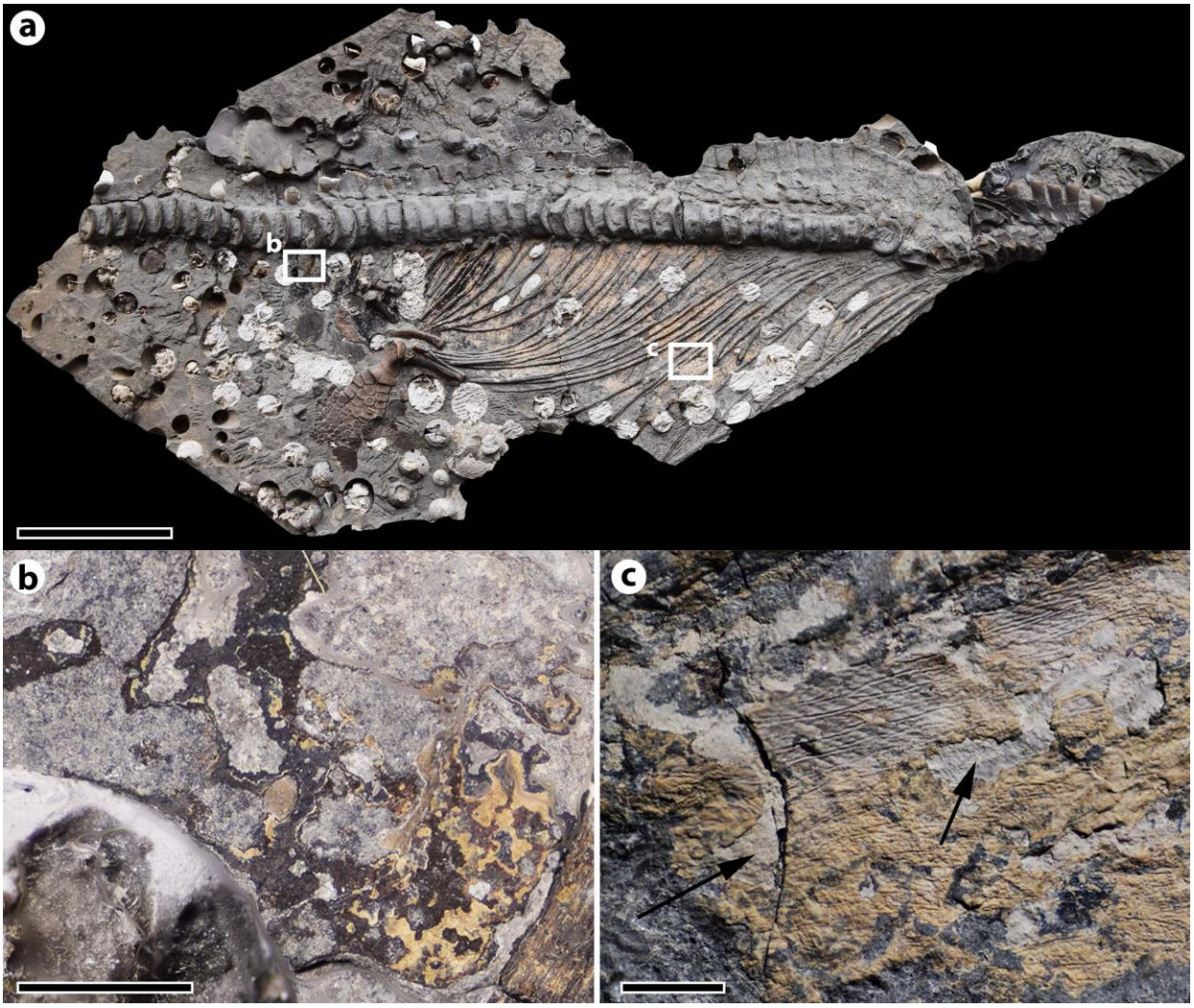

Figure S3.2. Examples of different tissue layers on the Lyme Regis specimen. **a**. Overview showing locations of the close-up panels. **b**. A patch a skin showing organic layers overlying and underlying the phosphatic layers, suggesting both integumentary melanin and internal melanin. **c**. A patch of skin showing multiple layers of fibres as well as an underlying lighter phosphatic layer with an amorphous texture, identified as the hypodermis or superficial fascia. Scale bars represent 10 cm in (a), 5 mm in (b) and 2 mm in (c).

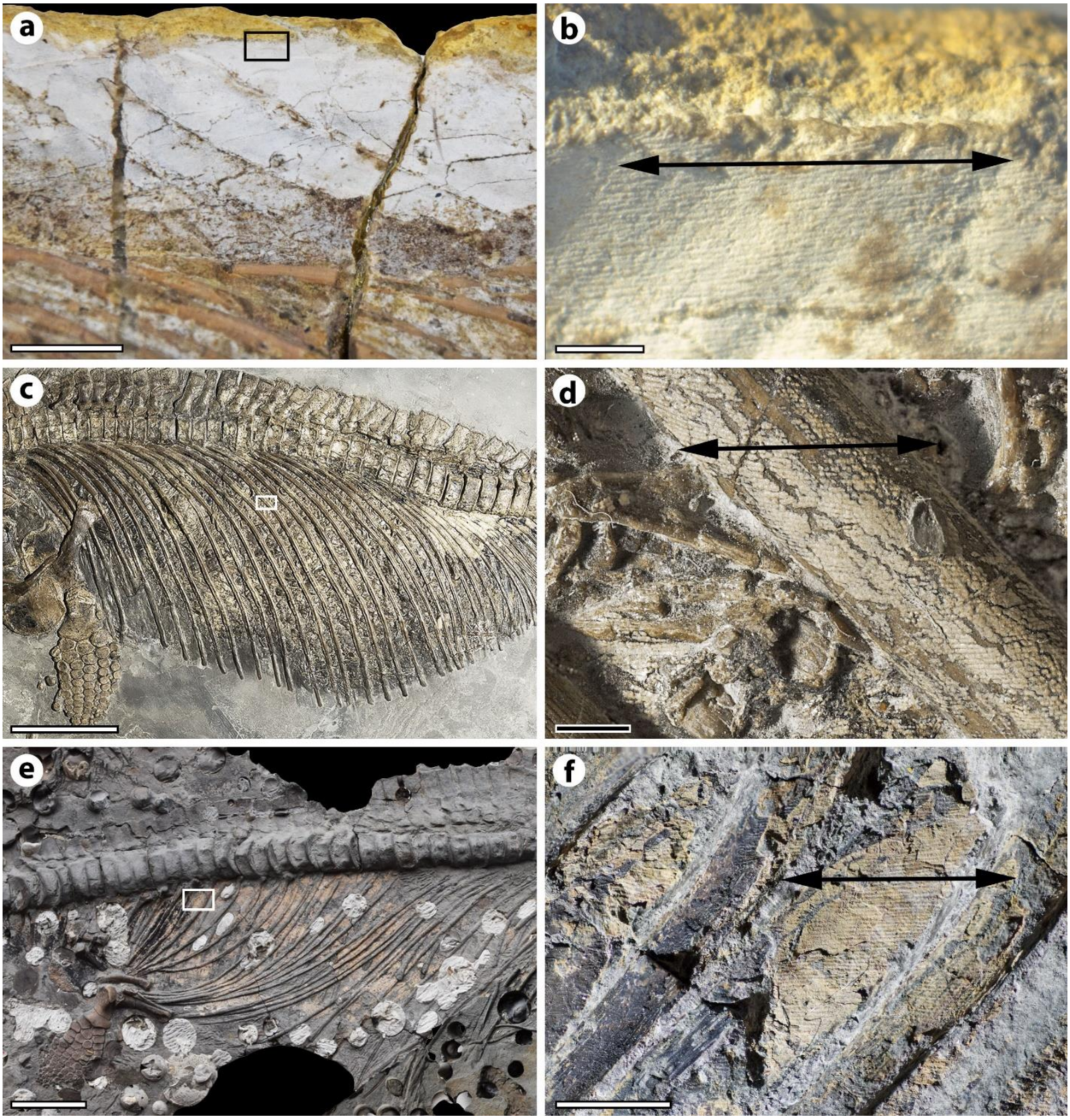

Figure S3.3. Orientations of the dermal fibres to the body axis. All images show the ichthyosaurs with the long axis of the body running horizontally. Rectangles on each overview image show the area of fibres highlighted in the next panel. Arrows indicate the orientation of the fibres. **a**. Strawberry Bank ichthyosaur M1405. **b**. Close up of the fibres running parallel to the body long axis in M1405. **c**. Kimmeridge ichthyosaur K1747. **d**. Close up of the fibres in K1747. **e**. Overview of the Lyme Regis ichthyosaur's abdomen. **f**. Close up of the large parallel-running fibre layer in the Lyme Regis specimen. Scale bars represent 10 mm in (a), 1 mm in (b), 10 cm in (c), 2 mm in (d), 5 cm in (e) and 5 mm in (f).

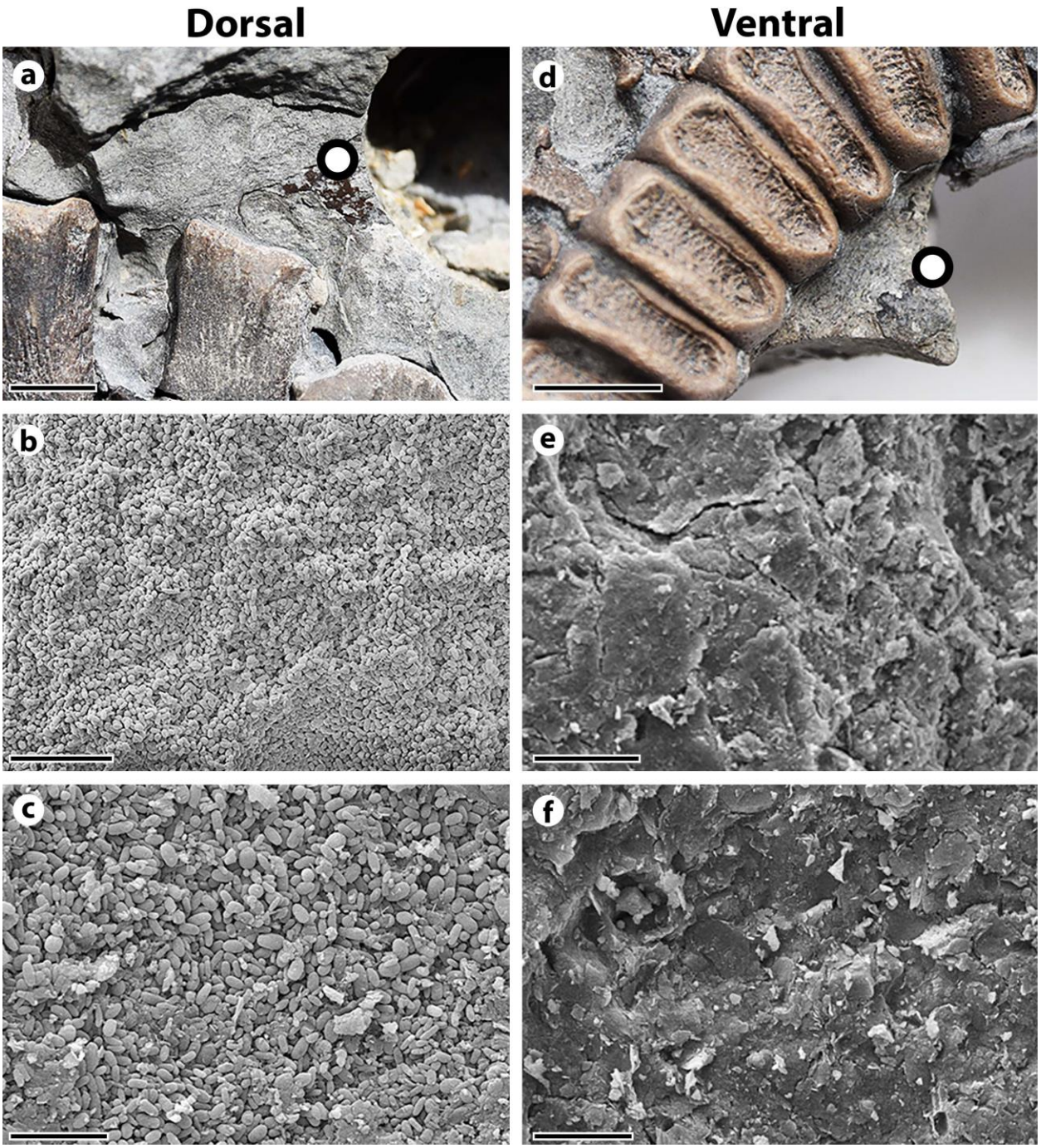

Figure S3.4. Evidence of countershading in the Lyme Regis ichthyosaur. **a**. Dark organics preserved dorsal to the cervical neural spines. **b**. The same patch from (a) under SEM showing abundant melanosomes presumably derived from the integument (dermal chromatophores). **c**. A close up of the melanosomes from (b). **d**. Organics ventral to the caudal vertebrae. **e**. SEM image of the same organics as (d) showing no melanosomes, just amorphous organic material. **f**. A close up of the same material as in (e). Scale bars represent 5 mm in (a) and (d), 10 µm in (b) and (e) and 5 µm in (c) and (f).

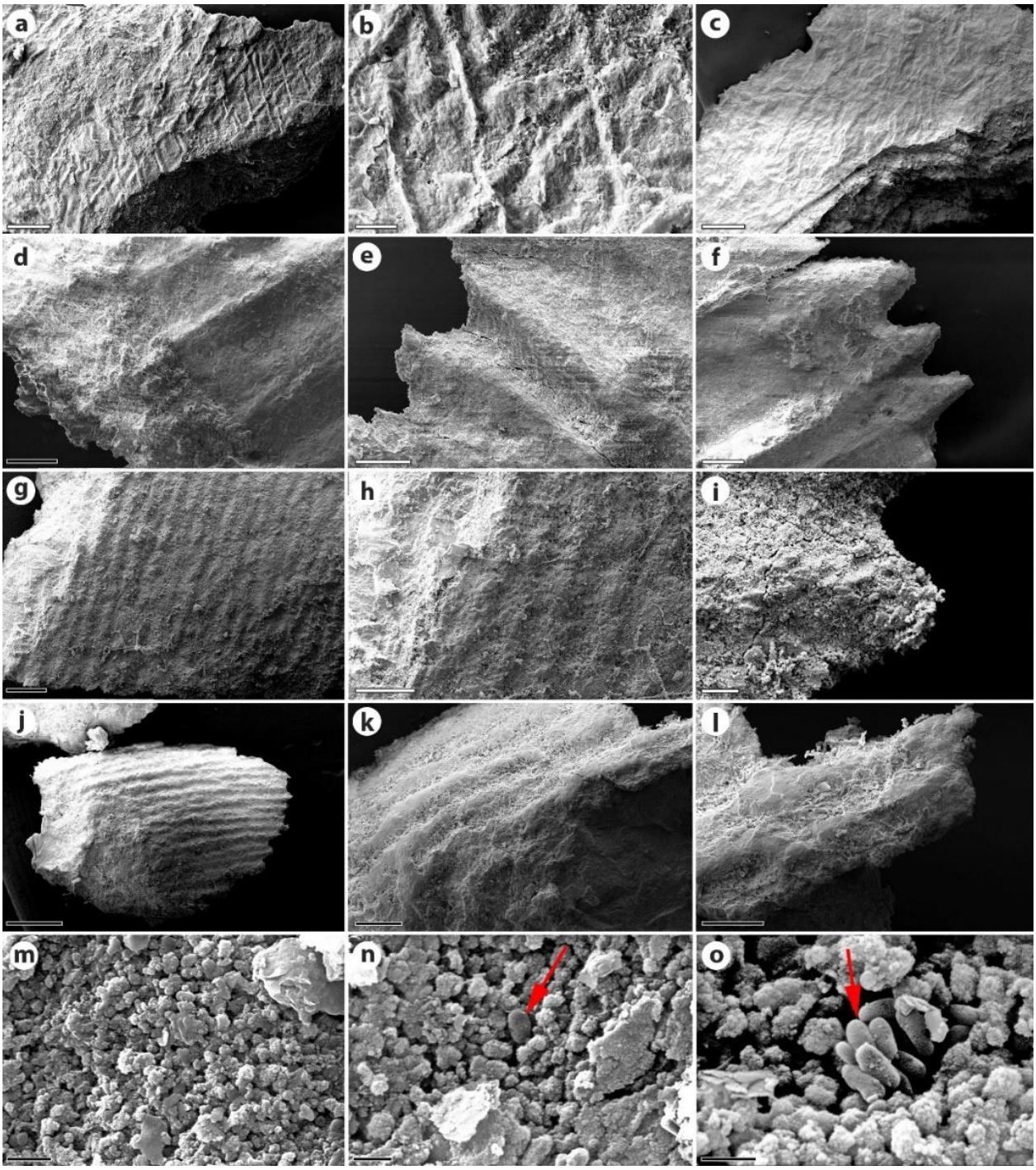

Figure S3.5. SEM images of fibrous layers in the Lyme Regis (a-f) and Strawberry Bank (g-l) ichthyosaurs highlighting their preservation as moulds with no 3D fibres present as well as close ups of the phosphatic texture of the layers (m-o). **a**. Interweaving fibres showing a diamond-hatched effect. **b**. Closer view of the same fibrous layers showing a series of peaks and troughs. **c**. A chip showing distinct layers of fibres with no 3D fibre

preservation. **d**. Close up of the edge of a fibrous layer with no 3D fibres present. **e**. One of the troughs where a fibre once sat. **f**. A series of troughs and peaks at a break in a fibrous layer giving a corrugated appearance. **g**. A series of parallel ridges where fibres once sat. **h**. A closer view of the same ridges showing no 3D fibres. **i**. A close up of the broken edge of a peaked (ridge) with troughs either side of it. **j**. A chip of fibre impressions showing the corrugated texture. **k**. A broken edge of the fibres layer with no 3D fibres present. **l**. A closer view of a broken edge showing only ridges. **m**-**o**. Phosphate mineral grains from the Lyme Regis specimen with occasional melanosomes (red arrows) highlighting the difference in preservation at the micrometre level. Scale bars represent 500 µm in (a), 100 µm in (b), (d), (f) and (h) and (k), 200 µm in (c) and (g), 50 µm in (e) and (l), 20 µm in (i), 400 µm in (j) and 1 µm in (m-o)

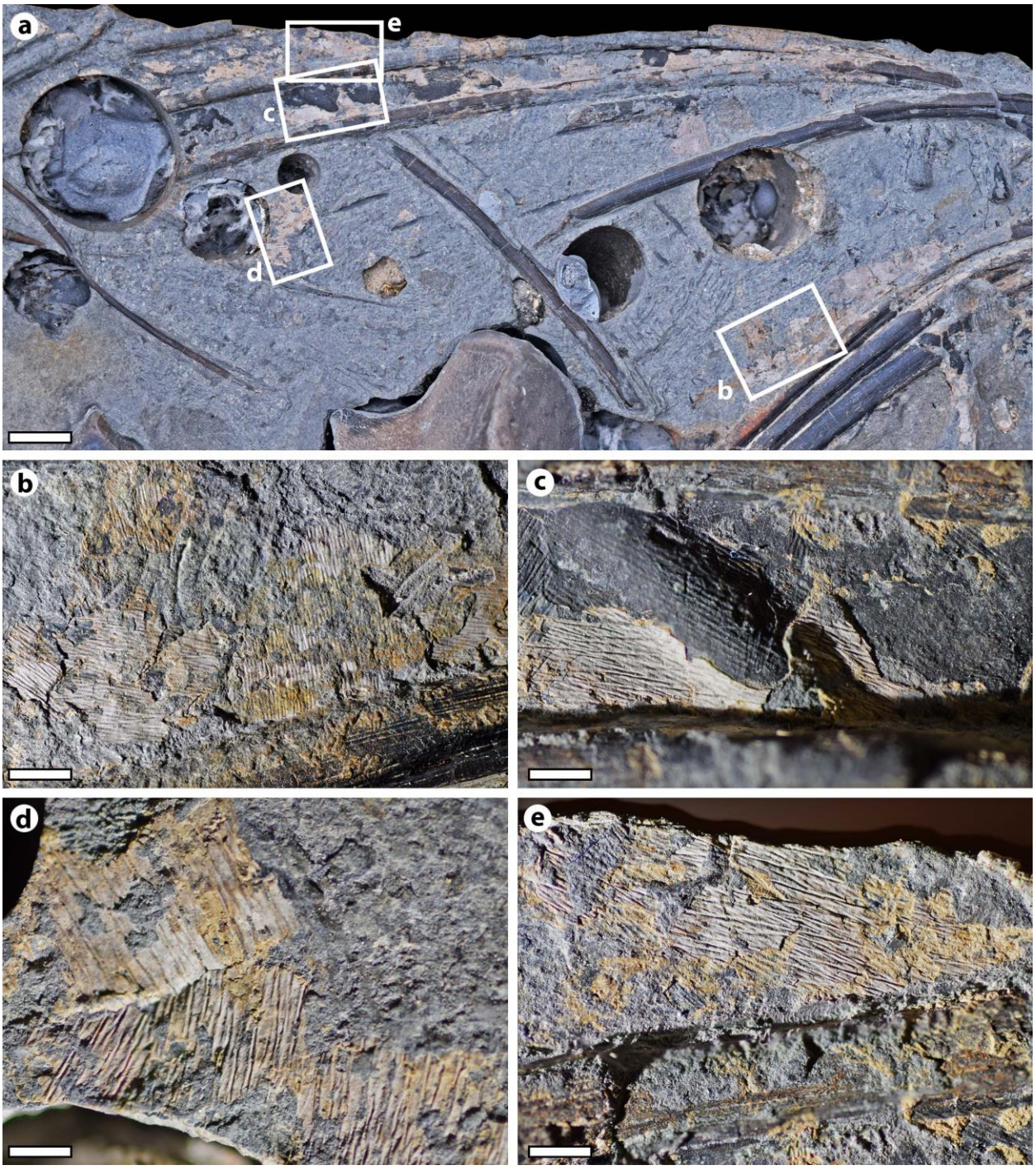

Figure S3.6. Examples of fibrous layers preserved on the Lyme Regis specimen. **a**. Overview of the anterior block containing part of the anterior ribcage and front limb. White rectangles and associated letters indicate regions highlighted in the following panels. **b**. Close up of a patch of soft tissue showing separate layers with different fibre orientations. **c**. Fibrous layers overlying internal organics with different layers showing different orientations. Fibre impressions can be seen in the internal organics. **d**. Two separate fibrous layers overlying one another. **e**. A patch of interweaving fibres. Scale bars represent 1 cm in (a), 2 mm in (b), (c) and (e) and 1 mm in (d).

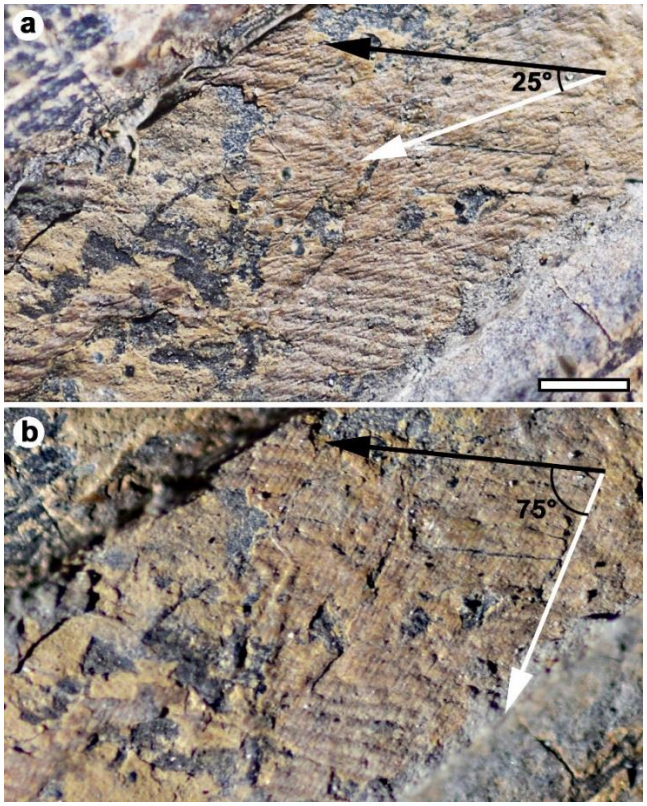

Figure S3.7. A single patch of phosphatised dermal soft tissue from the Lyme Regis specimen illuminated from different angles to highlight the different fibrous fabrics overlying one another. **a**. The patch illuminated from the North-West highlighting a layer of fibres running obliquely at roughly 25° to the main larger layer that runs from right to left (parallel to the body axis). **b**. The same patch illuminated from the North-East highlighting another fibrous fabric running orthogonally at roughly 75° to the main fibrous layer. Scale bar represents 1 mm.

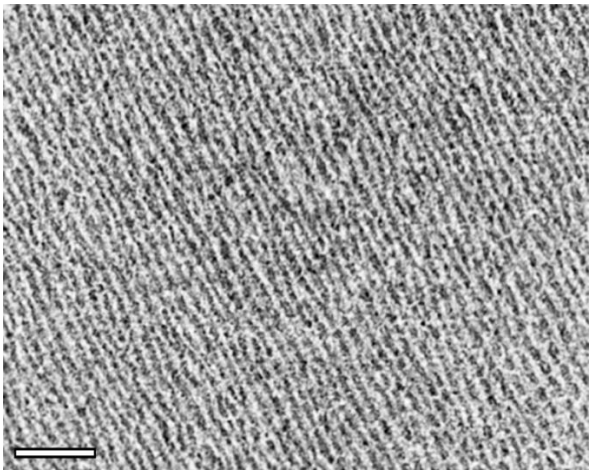

Figure S3.8. CT scan of dermal fibres from an extant harbour porpoise. The fabric appears very similar and is of the same size as the fibres found in the ichthyosaur material. Scale bar represents 1 mm.

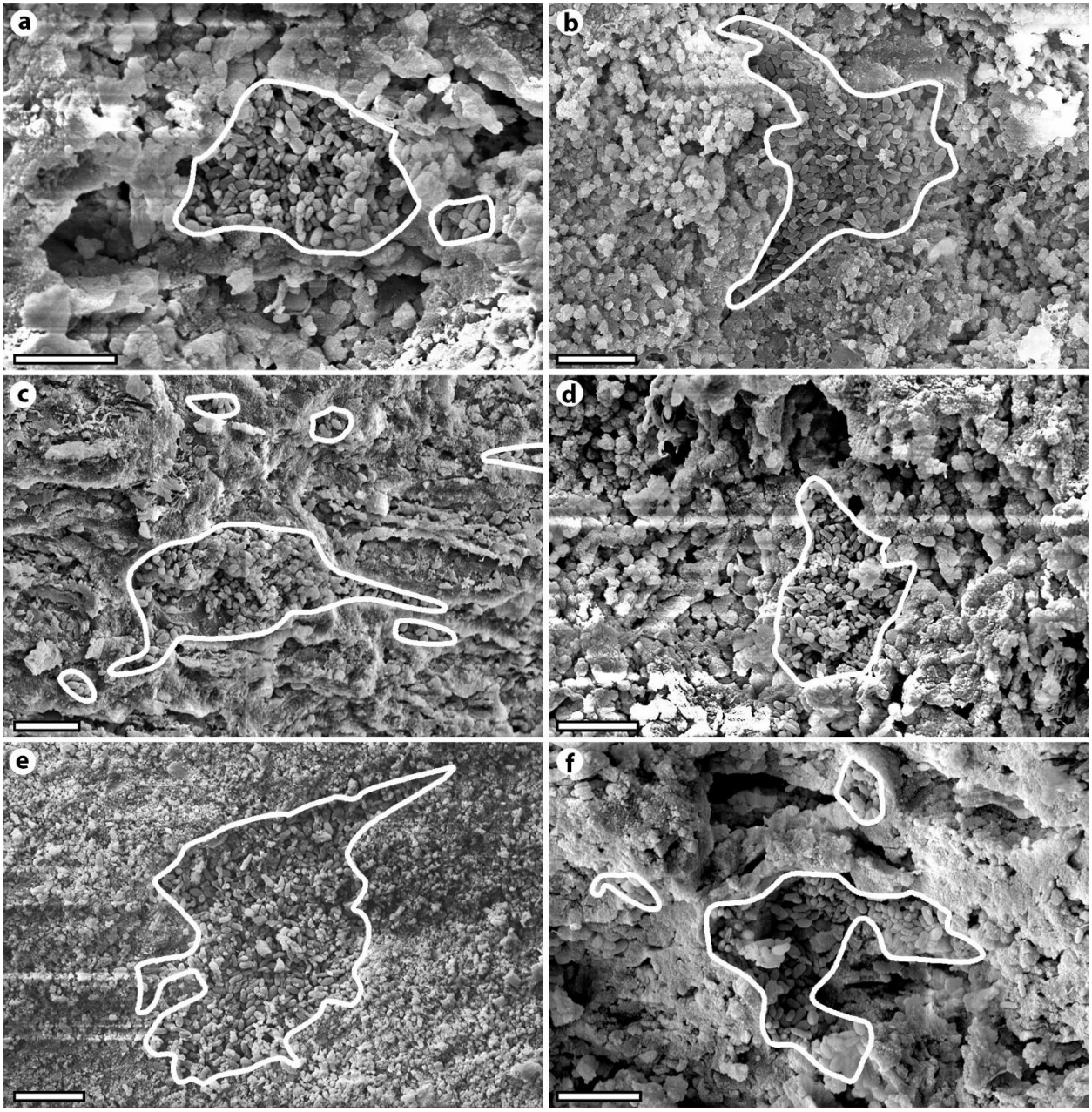

Figure S3.9. SEM images of melanocytes found in the soft tissue (likely phosphatised epidermis) of the Lyme Regis ichthyosaur. **a-f**. Melanocytes with their dendritic shape highlighted by white outlines. Small clusters around the melanocytes likely represent cross sections through the dendritic processes of other melanocytes. Scale bars represent 5 µm.

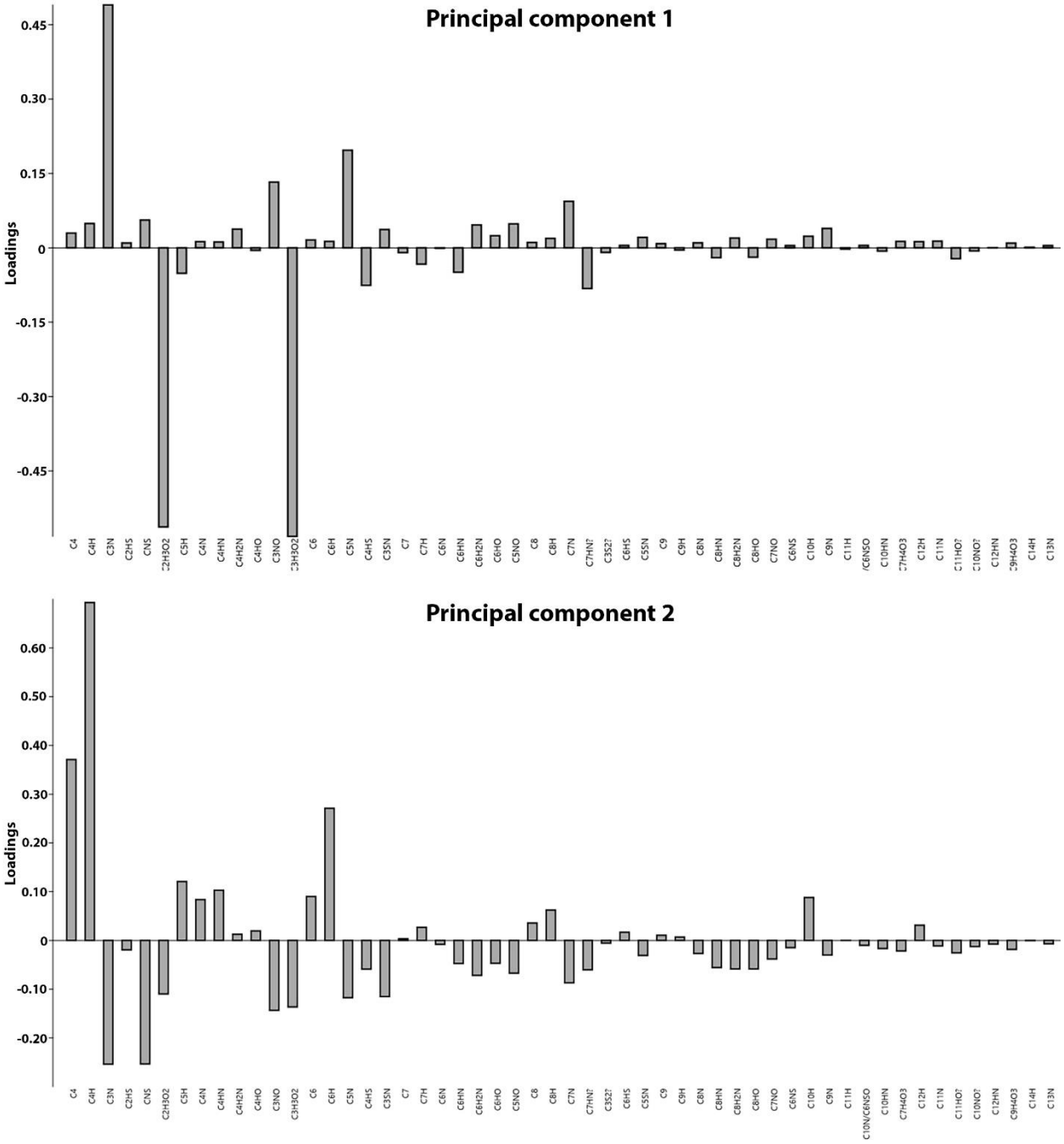

Figure S3.10. Loadings of each variable (mass peak) for the first two principal component (PC) axes from the ToF-SIMS PCA analysis of the Colleary et al. (2015) data and ichthyosaur samples.

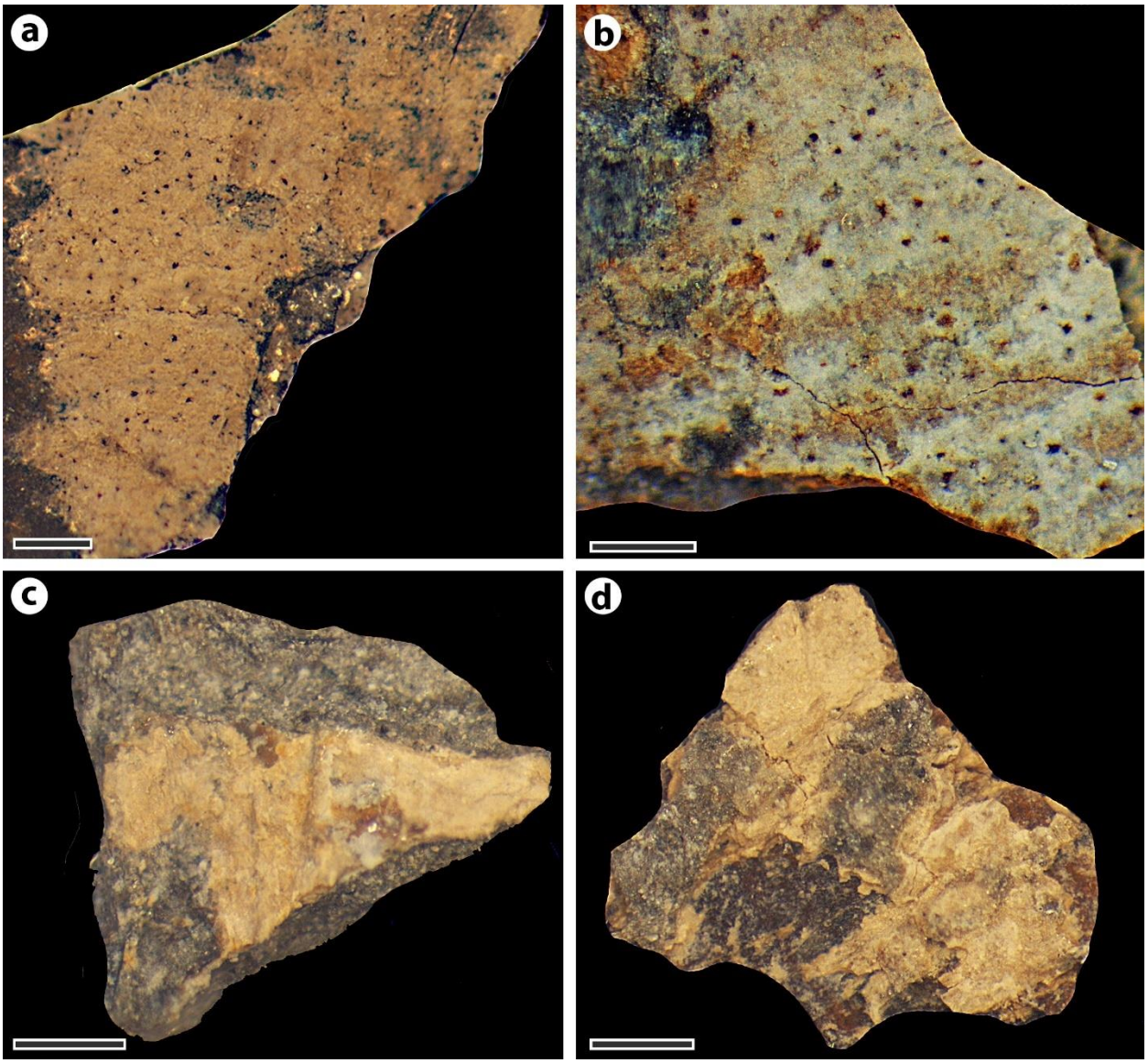

Figure S3.11. Samples of phosphatised epidermal tissue from the Lyme Regis ichthyosaur showing melanocytes (black dots) on those form the dorsal side and flank and none on those from the ventral surfaces. **a**. Epidermis with melanocytes from a patch of skin next to scapula. **b**. Epidermis with melanocytes from near the vertebral column, dorsal to (a). **c**. Epidermis with no melanocytes from the ventral-most phosphatic tissues found at base of ribs. **d**. Epidermis with no melanocytes from further ventral phosphatic tissues at base of ribs. Scale represent 200 µm in (a) and (c-d) and 100 µm in (b).

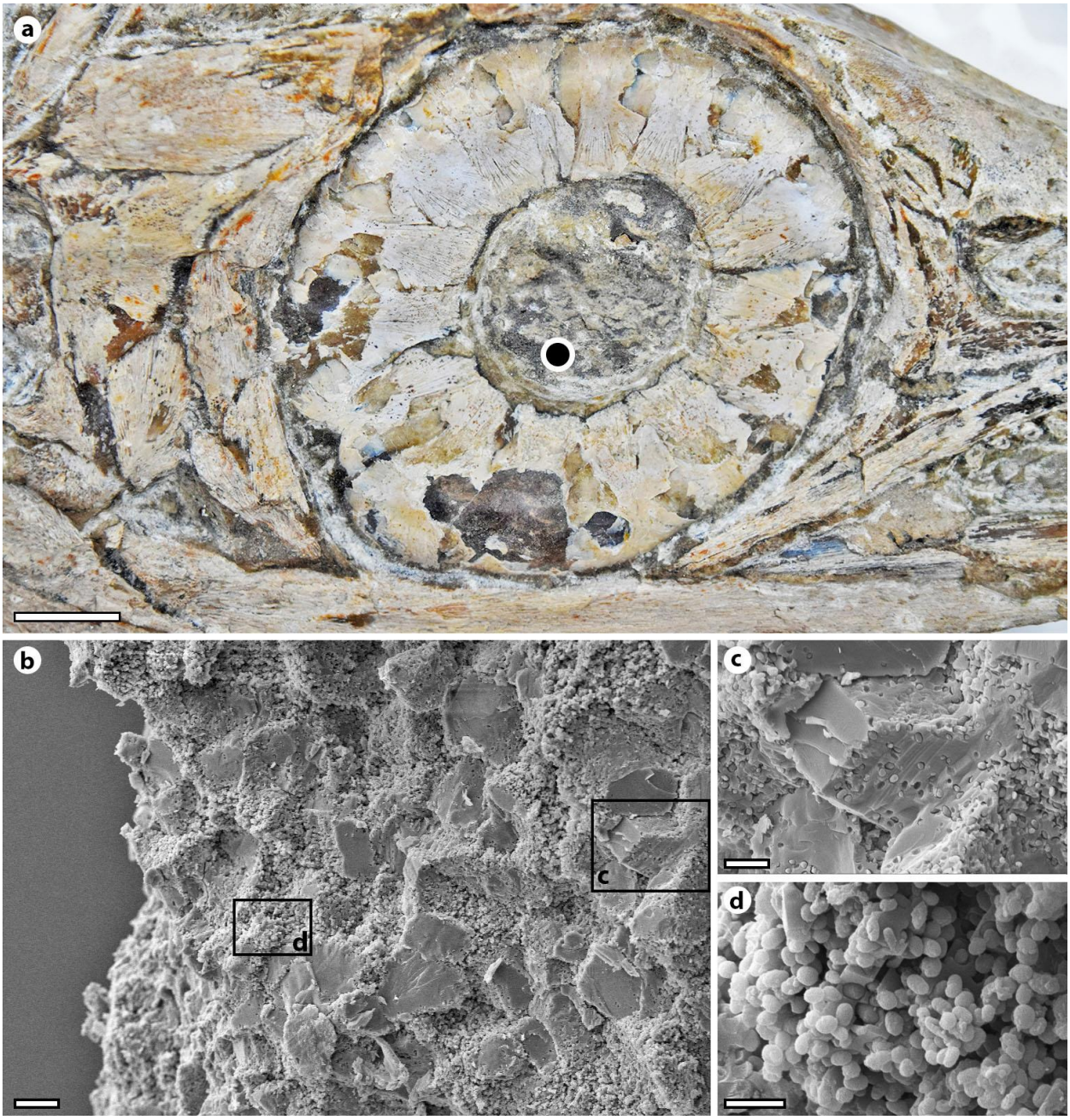

Figure S3.12. Soft tissue from within the eye of a Strawberry Bank ichthyosaur (M1408). Sample location taken for SEM imaging is represented by the black dot. Unlike the Lyme Regis sample, only a single thick layer of oblate melanosomes was observed. **a**. Overview of the eye orbit with in-situ sclerotic ring and dark organics. **b**. Overview SEM image of the eye organics, with melanosomes preserved in an amorphous organic matrix. Rectangles represent areas highlighted in the following panels. **c**. Melanosomes preserved inside the amorphous organic matrix with some only retained as moulds. **d**. 3D melanosomes. Scale bars represent 1 cm in (a), 10 µm in (b) and 2 µm in (c-d).

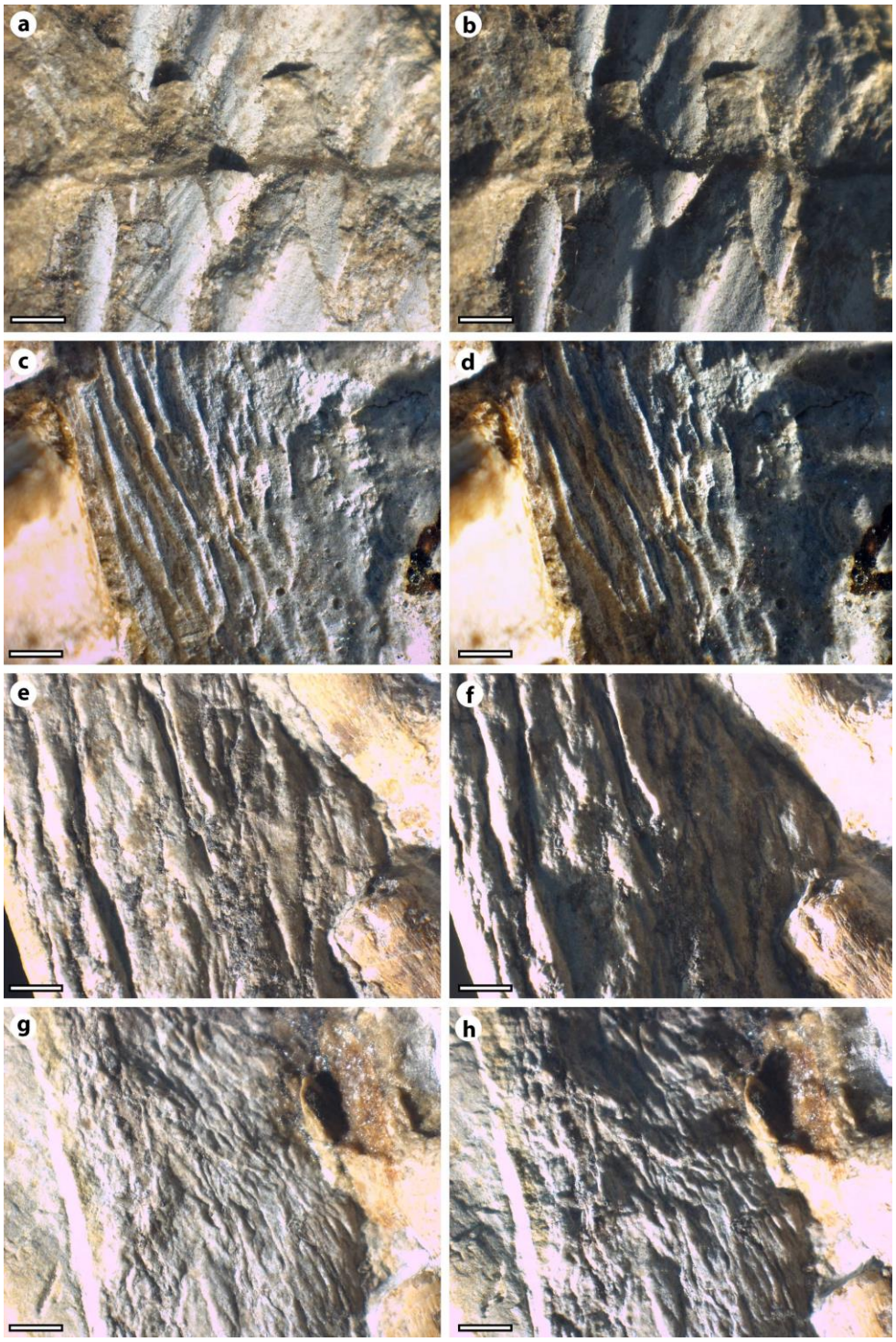

Figure S3.13. Examples of deformation of soft tissues derived from the integument prior to fossilisation in the Strawberry Bank ichthyosaurs. Each area is illuminated from two different angles to highlight the 3D wrinkling of the skin that presumably occurred during decay. **a-b**. Dorsal skin from M1405. **c-d**. Wrinkled ventral skin from M1409D. **e-f**. Wrinkled dorsal skin from M1409D. **g-h**. Wrinkled dorsal skin from M1409D. Scale bars represent 2 mm.

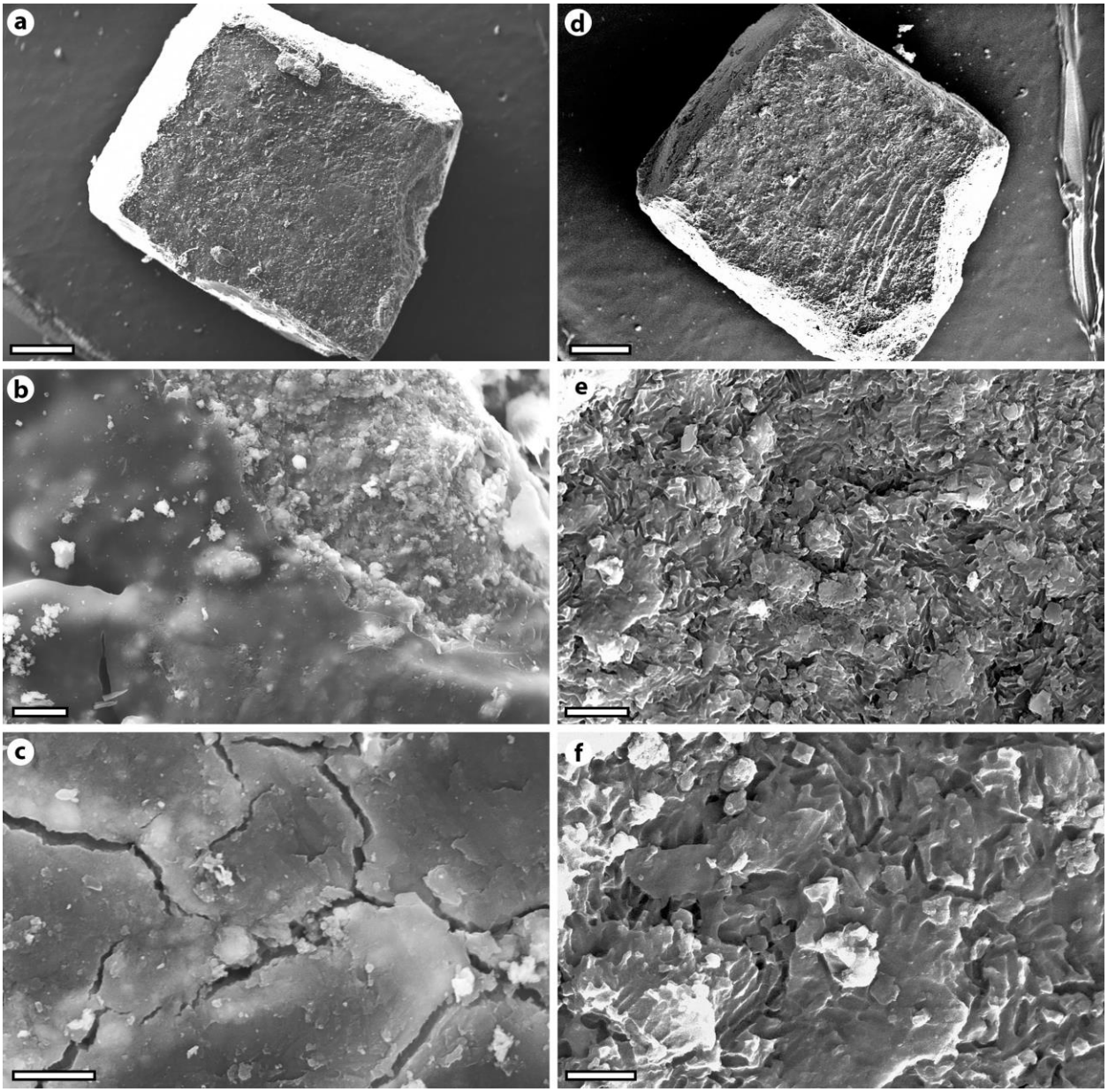

Figure S5.1. SEM images of a sample removed from DNHM D1242 before treatment in acetone (**a-c**) and after (**d-f**). A consolidant (most likely Paraloid B72 or similar) was present on the un-treated samples that obscured any microstructural details. When this was removed with acetone, melanosome impressions were abundant on the fresh surface. Scale bars represent 500 µm in (a) and (d), 10 µm in (b), 4 µm in (c) and (e) and 2 µm in (f).

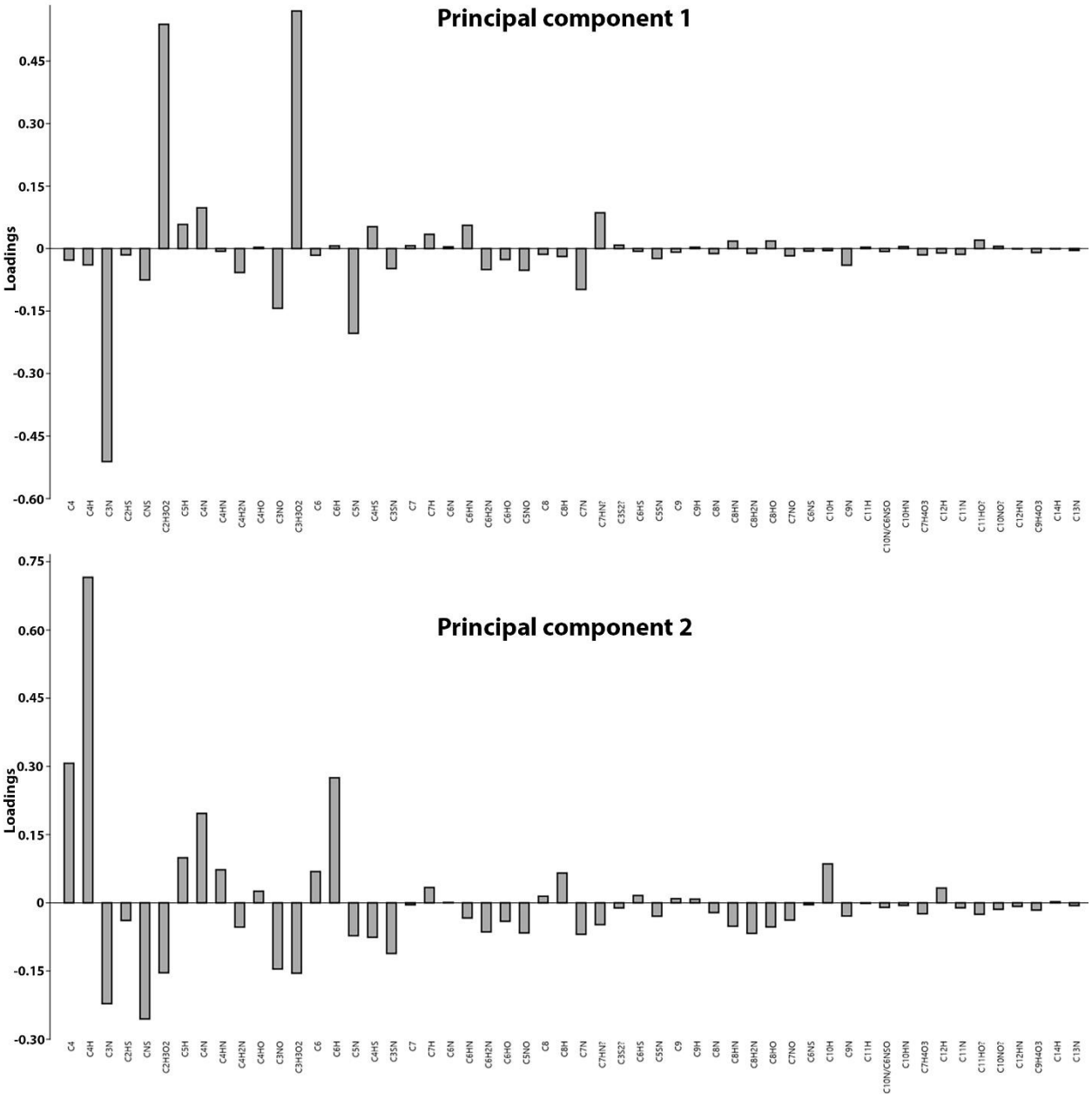

Figure S5.2. Loadings of each variable (mass peak) for the first two principal component (PC) axes from the ToF-SIMS PCA analysis of the Colleary et al. (2015) data and *Caudipteryx* samples.

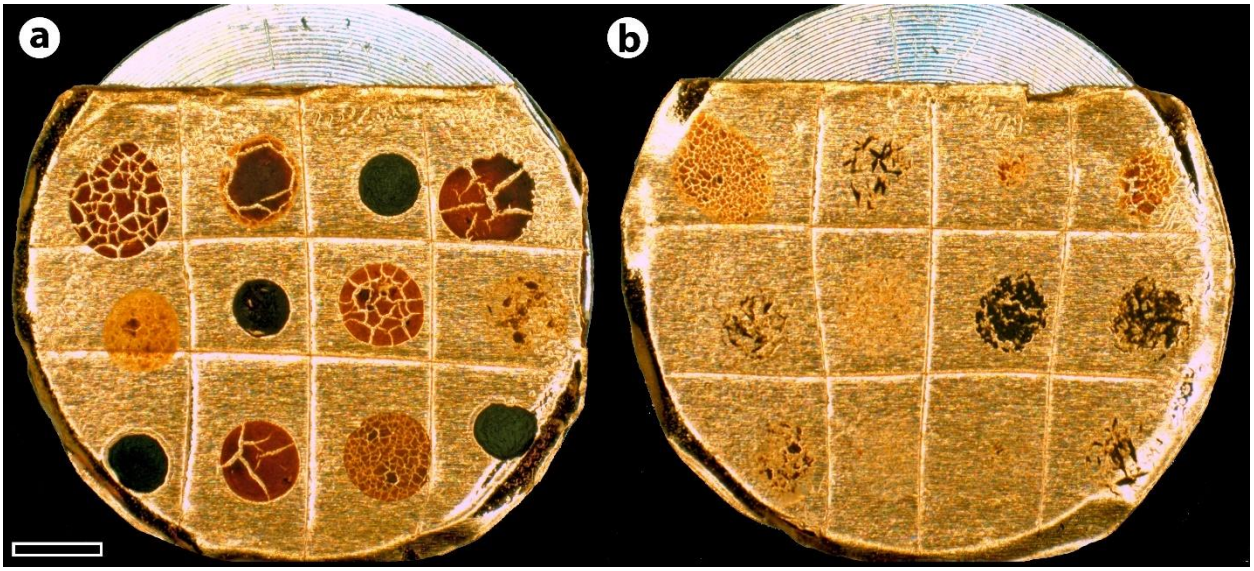

Figure S6.1. Samples from the revised enzymatic extraction protocol mounted on copper tape-coated SEM stubs prior to gold coating. **a**. Extracts from the revised third step of the protocol showing colours indicative of the original feather (rufous – pheasant and kingfisher; black – hornbill). **b**. Drops of removed supernatant after step 3 showing material that would be lost during each washing step. Scale bar represents 2 mm.

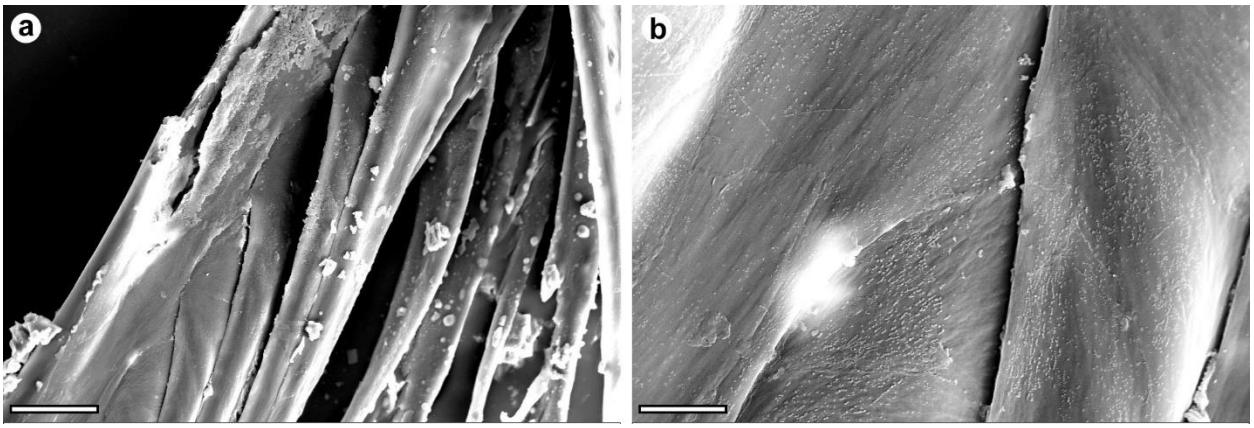

Figure S6.2. Feathers exposed to DTT and PBS for 24 hours without the addition of any enzyme. **a**. The overall structure of the feather has been little degraded. **b**. The keratin is still intact with no melanosomes exposed in any areas. Scale bars represent 50 µm in (a) and 10 µm in (b).

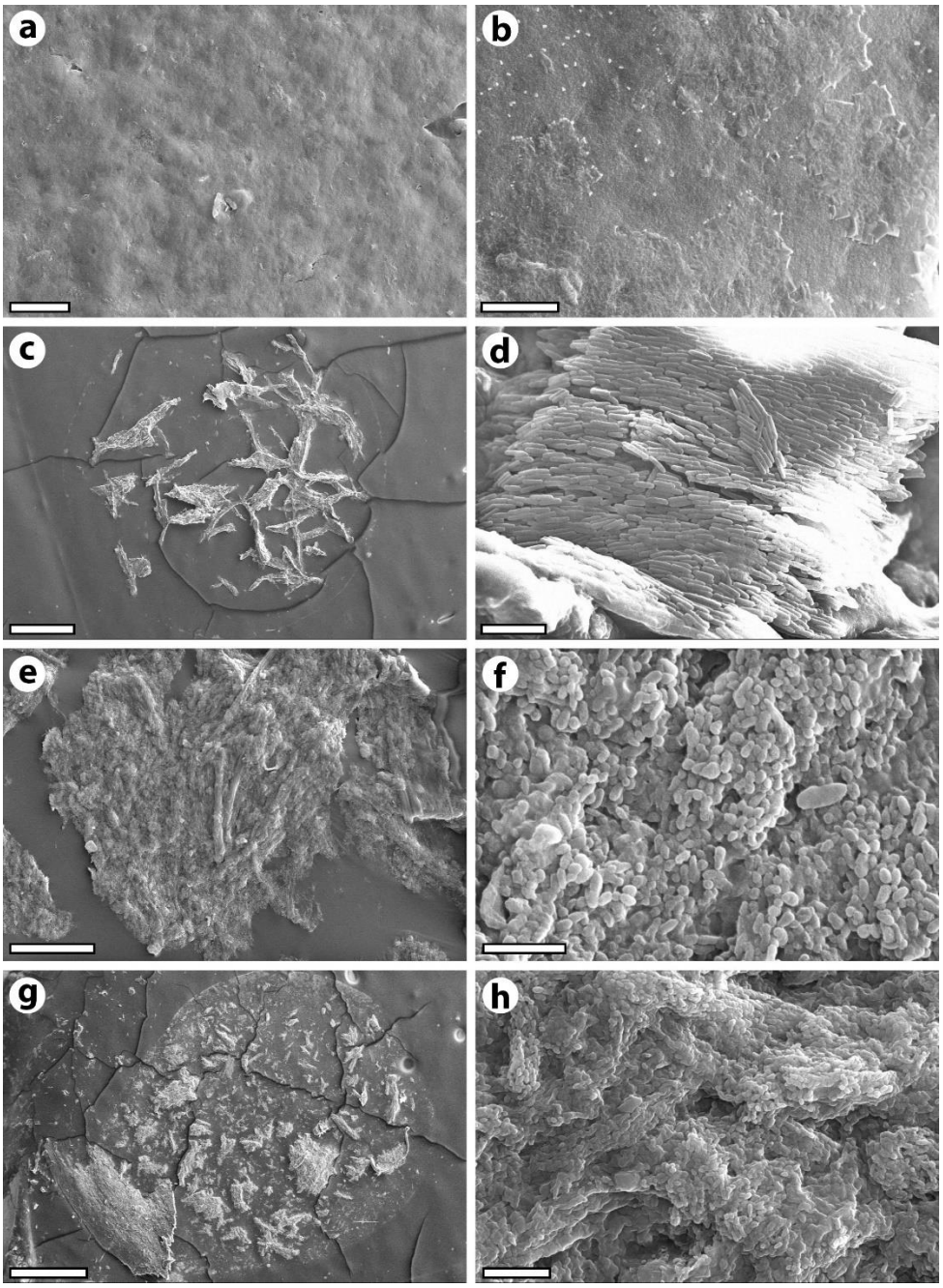

Figure S6.3. SEM images of supernatant removed after step three of the extraction protocol. **a-b**. Rufous pheasant feather extraction supernatant with 10% acetic acid added. No melanosomes are present despite a rusty pellet forming. **c-d**. Supernatant from a black hornbill feather after addition of acetic acid showing partially degraded feather pieces with melanosomes in their original arrangement. **e-f**. Rufous kingfisher feather extraction supernatant with 10% acetic acid added. Large pieces of feather are present with will exposed melanosomes. **g-h**. Rufous kingfisher extract supernatant which was allowed to air dry without acid added. Abundant feather material is present with melanosomes exposed. Scale bars represent 10 µm in (a), 4 µm in (b), (d) and (h), 400 µm in (c) and (g), 40 µm in (e) and 2 µm in (f).

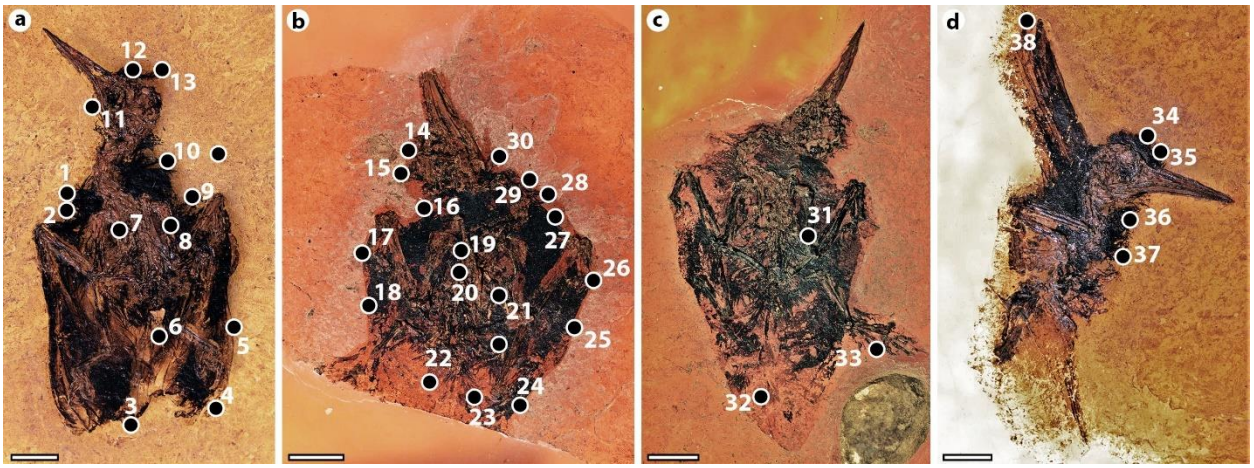

Figure S7.1. Sampling map of *Messelirrisor* specimens. **a**. *M. halcyrostris* (SMF- ME 11117a). **b**. *M. halcyrostris* (SMF- ME 10987b). **c**. *M. halcyrostris* (SMF- ME 10987a). **d**. *Messelirrisor* sp. (SMF- ME 11156a). Scale bars represent 10 mm.

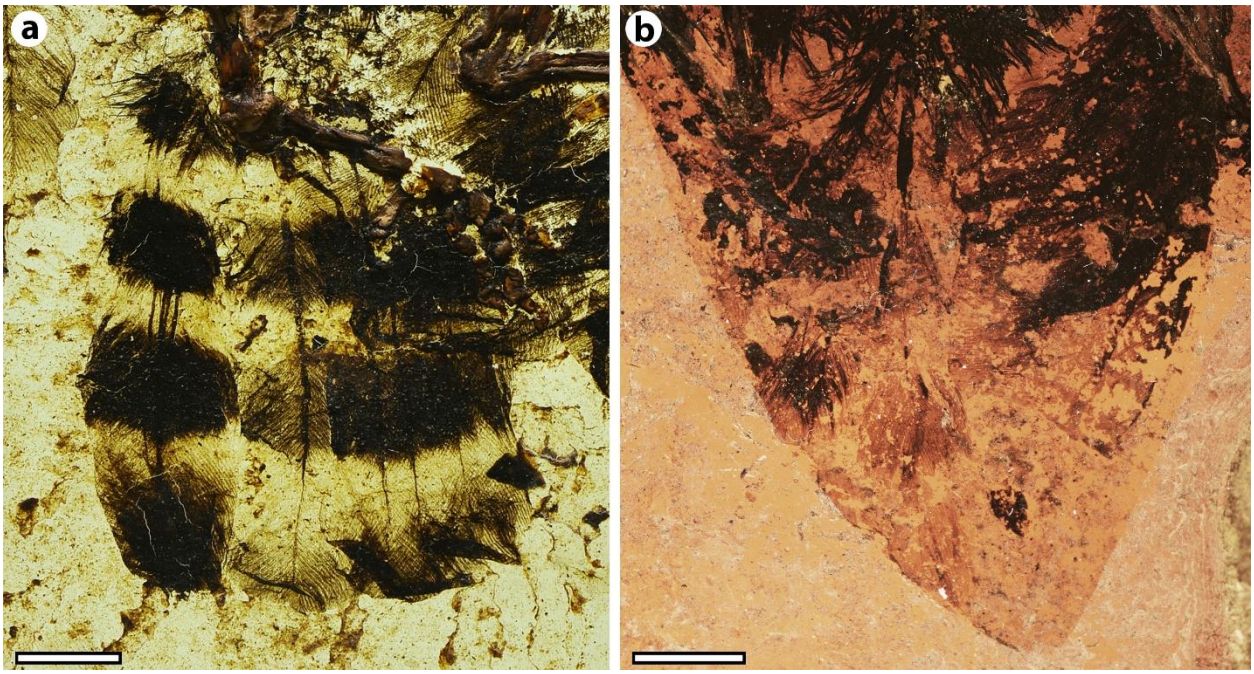

Figure S7.2. The tails of two specimens of *Messelirrisor* showing distinctive banding. **a**. *M. grandis* (HLMD-Be 178) showing a complete tail fanned out with four dark pigmented bands and four unpigmented bands. Only the pigment retains the original structure of the feathers, so where they showed no melanosome-based pigmentation in life no structure remains other than the apparently pigmented rachis. **b**. The tail of *M. halcyrostris* (SMF-ME 10987a) showing at least two pigmented and three unpigmented bands, however the distal tip of the tail is missing making it likely that more bands were present in life. Scale bars represent 5 mm.

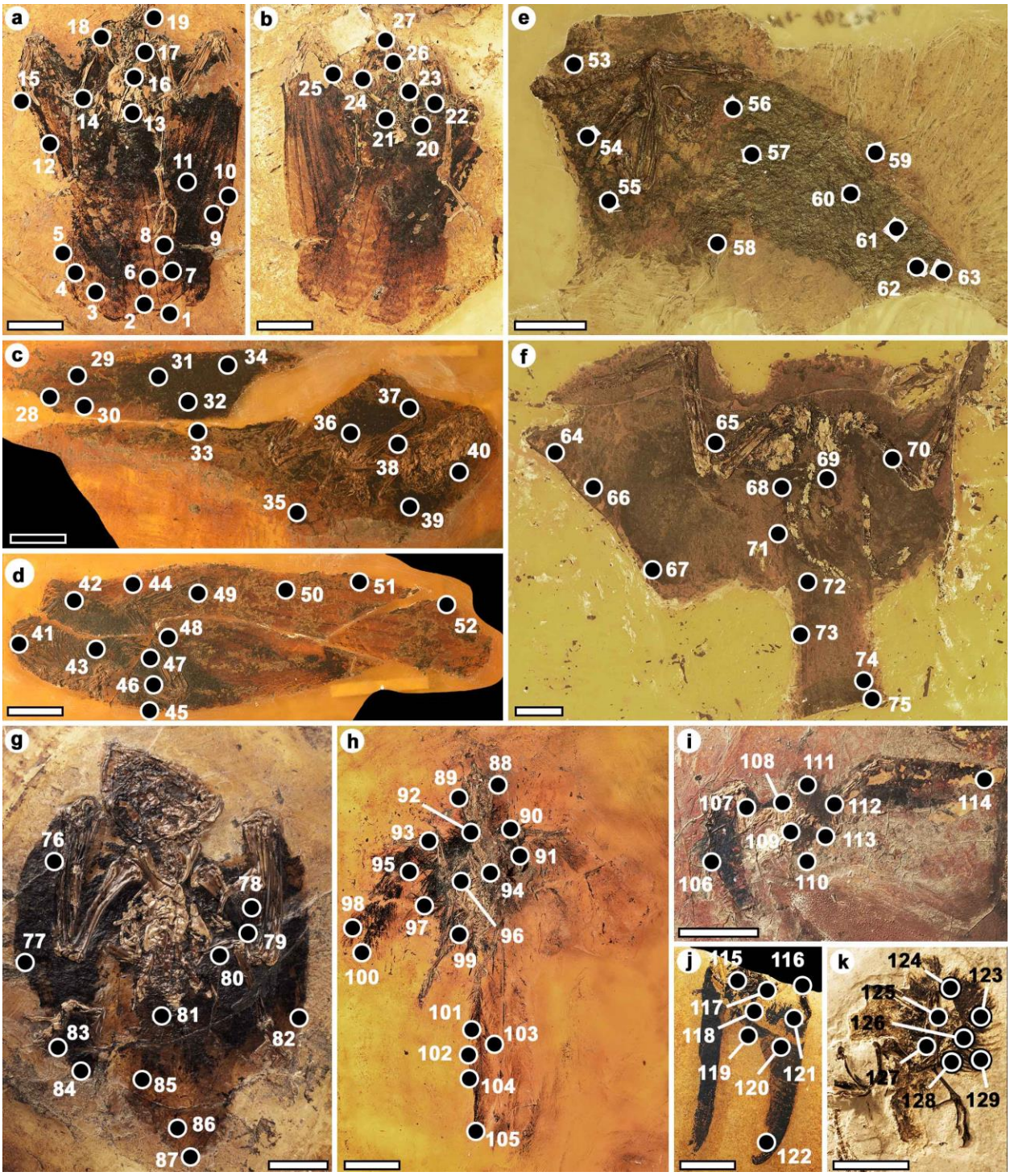

Figure S8.1. Locations of pigment samples removed from fossil strisorians for SEM imaging.

Supplementary tables

Table S3.1. Eigenvalues and percentage of variance explained by each principal component (PC) based on the ToF-SIMS data including ichthyosaur samples and data from Colleary et al (2015). The first two PCs account for almost 70% of the variance and were used to plot the data (Fig. 3.5)

Principal component	Eigenvalue	% variance
1	0.00571	46.58300
2	0.00282	22.98800
3	0.00106	8.69430
4	0.00079	6.46300
5	0.00043	3.55000
6	0.00028	2.35280
7	0.00020	1.63080
8	0.00018	1.47350
9	0.00013	1.06210
10	0.00011	0.91442
11	8.92E-05	0.72719
12	6.09E-05	0.49644
13	4.98E-05	0.40618
14	4.66E-05	0.37941
15	4.06E-05	0.33114
16	3.80E-05	0.30966
17	3.04E-05	0.24776
18	2.42E-05	0.19741
19	2.34E-05	0.19055
20	2.04E-05	0.16597
21	1.77E-05	0.14436
22	1.45E-05	0.11827
23	1.26E-05	0.10255
24	9.32E-06	0.07596
25	7.80E-06	0.06355
26	6.79E-06	0.05532
27	5.28E-06	0.04304
28	4.87E-06	0.03970
29	4.34E-06	0.03537
30	2.99E-06	0.02433
31	2.70E-06	0.02204
32	2.39E-06	0.01949
33	2.13E-06	0.01734
34	1.89E-06	0.01540
35	1.61E-06	0.01309
36	1.17E-06	0.00954
37	1.01E-06	0.00823
38	8.24E-07	0.00671
39	5.78E-07	0.00471
40	4.94E-07	0.00403
41	4.09E-07	0.00333
42	3.23E-07	0.00264
43	2.49E-07	0.00203
44	1.70E-07	0.00139
45	1.58E-07	0.00129
46	1.22E-07	0.00099
47	8.44E-08	0.00069
48	7.38E-08	0.00060
49	3.18E-08	0.00026
50	2.32E-08	0.00019
51	1.97E-08	0.00016
52	1.06E-08	8.61E-05
53	2.91E-09	2.38E-05
54	4.77E-19	3.89E-15

Table S5.1. Loadings of each variable and the amount of variance explained by each canonical function from the canonical function analysis of melanosome morphologies. The largest absolute correlation between each variable and each function is italicised.

	Function 1	Function 2	Function 3
Aspect ratio	***.899***	-0.314	-0.181
Length	***.570***	0.564	-0.147
Width	-0.128	***.683***	0.191
Length CV	0.018	***.365***	0.298
Length skew	0.016	***-.197***	0.146
AR skew	-0.138	-0.308	***.568***
Width CV	0.116	0.168	***.497***
Width skew	0.059	0.115	***-.127***
Variance	65%	26.4%	8.6%

Table S5.2. Eigenvalues and percentage of variance explained by each principal component (PC) based on the ToF-SIMS data including *Caudipteryx* samples and data from Colleary et al (2015).

Principal component	Eigenvalue	% variance
1	0.00532	39.54500
2	0.00297	22.07200
3	0.00138	10.24400
4	0.00096	7.13680
5	0.00074	5.49350
6	0.00049	3.65670
7	0.00026	1.89350
8	0.00022	1.60810
9	0.00020	1.49840
10	0.00017	1.22450
11	0.00013	0.9652
12	0.000109	0.81326
13	8.88E-05	0.66031
14	6.99E-05	0.51951
15	5.70E-05	0.42389
16	4.57E-05	0.33991
17	4.04E-05	0.30007
18	3.47E-05	0.25781
19	2.45E-05	0.18205
20	2.06E-05	0.15325
21	1.72E-05	0.12791
22	1.62E-05	0.12031
23	1.51E-05	0.11192
24	1.38E-05	0.10292
25	1.13E-05	0.08391
26	9.73E-06	0.07233
27	9.09E-06	0.06759
28	7.66E-06	0.05695
29	5.67E-06	0.04212
30	4.66E-06	0.03465
31	4.35E-06	0.03234
32	3.46E-06	0.02569
33	3.19E-06	0.02371
34	2.69E-06	0.02002
35	2.15E-06	0.01595
36	1.68E-06	0.01251
37	1.52E-06	0.01132
38	1.34E-06	0.00994
39	1.11E-06	0.00825
40	1.04E-06	0.00775
41	7.83E-07	0.00582
42	5.22E-07	0.00388
43	4.41E-07	0.00328
44	3.76E-07	0.00280
45	3.07E-07	0.00228
46	2.16E-07	0.00161
47	1.61E-07	0.00119
48	1.45E-07	0.00108
49	1.17E-07	0.00087
50	9.03E-08	0.00067
51	5.60E-08	0.00042
52	2.28E-08	0.00017
53	9.68E-09	7.20E-05
54	1.74E-18	1.29E-14

Table S7.1. Colour predictions for melanosome samples taken from specimens of *Messelirrisor* based on just the new database of extant Upupiformes and outgroups. N = number of melanosomes measured. % = shrinkage.

Sample	Predicted colour	Predicted 5%	Predicted 10%	Predicted 15%	Predicted 20%	N
SMF ME 11117a						
1	Black	Black	Black	Black	Black	6
2	Black	Black	Black	Black	Black	97
3	Black	Black	Grey	Grey	Grey	86
4	Grey	Grey	Grey	Grey	Grey	57
5	Black	Black	Black	Black	Black	21
SMF ME 10987b						
6	Grey	Grey	Grey	Grey	Grey	34
7	Grey	Grey	Grey	Grey	Grey	102
8	Grey	Grey	Grey	Grey	Grey	61
9	Grey	Grey	Grey	Grey	Grey	67
10	Black	Black	Black	Black	Black	141
11	Grey	Grey	Grey	Grey	Grey	19
SMF ME10987a						
12	Grey	Grey	Grey	Grey	Grey	103
13	Grey	Grey	Grey	Grey	Grey	26
14	Black	Black	Black	Black	Black	55
SMF ME 11156a						
15	Black	Black	Black	Black	Black	31
16	Black	Black	Black	Grey	Grey	9
17	Black	Black	Black	Black	Black	7
18	Black	Grey	Grey	Grey	Grey	35
19	Black	Grey	Grey	Grey	Grey	105

Table S7.2. Colour predictions for melanosome samples taken from specimens of *Messelirrisor* based on just the Li et al. (2012) dataset. N = number of melanosomes measured. % = shrinkage.

Sample	no shrinkage	Predicted 5%	Predicted 10%	Predicted 15%	Predicted 20%	N
SMF ME 11117a						
1	Black	Black	Black	Black	Black	6
2	Black	Black	Black	Black	Black	97
3	Black	Black	Grey	Grey	Grey	86
4	Grey	Grey	Grey	Grey	Grey	57
5	Black	Black	Black	Black	Black	21
SMF ME 10987b						
6	Grey	Grey	Grey	Grey	Grey	34
7	Grey	Grey	Grey	Grey	Grey	102
8	Grey	Grey	Grey	Grey	Grey	61
9	Grey	Grey	Grey	Grey	Grey	67
10	Black	Black	Grey	Grey	Grey	141
11	Grey	Grey	Grey	Grey	Grey	19
SMF ME10987a						
12	Grey	Grey	Grey	Grey	Grey	103
13	Grey	Grey	Grey	Grey	Grey	26
14	Black	Black	Grey	Grey	Grey	55
SMF ME 11156a						
15	Black	Black	Black	Black	Black	31
16	Black	Black	Black	Black	Black	9
17	Black	Black	Black	Black	Black	7
18	Black	Black	Grey	Grey	Grey	35
19	Grey	Grey	Grey	Grey	Grey	105

Table S7.1. Loadings of each variable and the amount of variance explained by each canonical function from the canonical function analysis of melanosome morphologies. The largest absolute correlation between each variable and each function is italicised.

	Function 1	Function 2	Function 3
Aspect ratio	***.884***	0.254	-0.209
Length	***.668***	-0.611	0.029
AR skew	***-.331***	0.316	0.208
Length skew	***-.218***	0.196	0.016
Width	-0.084	***-.628***	0.435
Width skew	0.042	***-.102***	0.036
Width CV	0.028	0.006	***.668***
Length CV	-0.152	-0.054	***.491***
Variance	**64.4%**	**28.9%**	**6.7%**

Table S8.1. Full results from colour prediction canonical discriminant analyses (CDA) of fossil strisorians based on modern strisorian melanosome morphologies. Two databases were used: only modern Strisores taxa and all modern strisorians, taxa from Chapter 7 (Upupiformes and outgroups) and the Li et al. (2012) data combined. Two models of CDA were used for each dataset: "all variables" included and a "stepwise" model (Li et al. 2012). Diagenetic shrinkage was modelled by scaling up melanosome measurements by 5-10%. Probability values (p) indicate the level of support for each colour classification.

Only modern Strisores	**All variables model CDA**						**Stepwise model CDA**						
Shrinkage level	**0%**	**p**	**5%**	**p**	**10%**	**p**	**0%**	**p**	**5%**	**p**	**10%**	**p**	**N**
Hassiavis 03_04	Brown	0.813	Brown	0.727	Brown	0.623	Brown	0.978	Brown	0.936	Brown	0.864	34
Hassiavis 03_06	Brown	0.744	Brown	0.724	Brown	0.687	Brown	1.000	Brown	0.995	Brown	0.976	26
Hassiavis 03_11	Grey	0.214	Grey	0.232	Grey	0.229	Grey	0.051	Grey	0.043	Grey	0.034	13
Hassiavis 03_12	Grey	0.199	Grey	0.146	Grey	0.096	Grey	0.246	Grey	0.202	Grey	0.150	58
Hassiavis 04_01	Grey	0.218	Grey	0.184	Grey	0.141	Grey	0.209	Grey	0.189	Grey	0.157	195
Hassiavis 04_02	Grey	0.304	Grey	0.309	Grey	0.289	Grey	0.328	Grey	0.313	Grey	0.275	102
Hassiavis 04_03	Grey	0.351	Grey	0.322	Grey	0.270	Grey	0.375	Grey	0.349	Grey	0.298	204
Hassiavis 04_04	Brown	0.331	Brown	0.225	Grey	0.175	Brown	0.370	Grey	0.254	Grey	0.272	86
Hassiavis 06_01	Grey	0.905	Grey	0.861	Grey	0.763	Grey	0.644	Grey	0.604	Grey	0.520	190
Hassiavis 06_02	Grey	0.948	Grey	0.883	Grey	0.746	Grey	0.321	Grey	0.223	Grey	0.136	119
Hassiavis 06_03	Grey	0.458	Grey	0.362	Grey	0.257	Grey	0.304	Grey	0.236	Grey	0.164	179
Hassiavis 06_04	Brown	0.535	Brown	0.549	Brown	0.547	Brown	0.795	Brown	0.782	Brown	0.751	21
Hassiavis 06_05	Black	0.508	Black	0.481	Black	0.435	Black	0.618	Black	0.584	Black	0.527	21
Hassiavis 06_07	Brown	0.418	Brown	0.342	Brown	0.267	Black	0.741	Black	0.729	Black	0.692	27
Hassiavis 06_08	Brown	0.509	Brown	0.391	Brown	0.284	Brown	0.863	Brown	0.760	Brown	0.632	133
Hassiavis 06_09	Black	0.940	Black	0.854	Black	0.725	Black	0.963	Black	0.902	Black	0.796	108
Hassiavis 06_10	Brown	0.776	Brown	0.756	Brown	0.716	Brown	0.788	Brown	0.758	Brown	0.711	44
Hassiavis 06_11	Grey	0.683	Grey	0.626	Grey	0.525	Grey	0.717	Grey	0.634	Grey	0.508	105
All modern data													
Hassiavis 03_04	Brown	0.796	Brown	0.729	Brown	0.650	Black	0.734	Black	0.759	Black	0.770	34
Hassiavis 03_06	Brown	0.768	Brown	0.717	Brown	0.655	Brown	0.669	Brown	0.635	Brown	0.591	26
Hassiavis 03_11	Grey	0.555	Grey	0.534	Grey	0.488	Grey	0.548	Grey	0.530	Grey	0.485	13
Hassiavis 03_12	Grey	0.672	Grey	0.579	Grey	0.467	Grey	0.803	Grey	0.726	Grey	0.617	58
Hassiavis 04_01	Grey	0.802	Grey	0.743	Grey	0.654	Grey	0.812	Grey	0.754	Grey	0.665	195
Hassiavis 04_02	Grey	0.743	Grey	0.718	Grey	0.663	Grey	0.743	Grey	0.729	Grey	0.684	102
Hassiavis 04_03	Grey	0.815	Grey	0.768	Grey	0.690	Grey	0.834	Grey	0.798	Grey	0.730	204
Hassiavis 04_04	Grey	0.600	Grey	0.629	Grey	0.637	Grey	0.603	Grey	0.638	Grey	0.652	86
Hassiavis 06_01	Grey	0.979	Grey	0.981	Grey	0.957	Grey	0.978	Grey	0.981	Grey	0.957	190
Hassiavis 06_02	Grey	0.807	Grey	0.743	Grey	0.640	Grey	0.892	Grey	0.778	Grey	0.625	119
Hassiavis 06_03	Grey	0.453	Grey	0.371	Grey	0.282	Grey	0.436	Grey	0.374	Grey	0.300	179
Hassiavis 06_04	Black	0.634	Black	0.663	Black	0.680	Black	0.625	Black	0.659	Black	0.682	21
Hassiavis 06_05	Black	0.828	Black	0.832	Black	0.816	Black	0.797	Black	0.806	Black	0.795	21
Hassiavis 06_07	Brown	0.715	Black	0.721	Black	0.711	Black	0.881	Black	0.909	Black	0.920	27
Hassiavis 06_08	Brown	0.526	Grey	0.517	Grey	0.557	Black	0.616	Black	0.588	Black	0.545	133
Hassiavis 06_09	Black	0.998	Black	0.999	Black	0.991	Black	0.995	Black	0.999	Black	0.991	108
Hassiavis 06_10	Brown	0.932	Brown	0.881	Brown	0.814	Brown	0.894	Brown	0.829	Brown	0.750	44
Hassiavis 06_11	Grey	0.813	Grey	0.733	Grey	0.617	Grey	0.830	Grey	0.746	Grey	0.626	105

Only modern Strisores	All variables model CDA						Stepwise model CDA						
Shrinkage level	**0%**	**p**	**5%**	**p**	**10%**	**p**	**0%**	**p**	**5%**	**p**	**10%**	**p**	**N**
Masillapodargus 01_01	Brown	0.876	Brown	0.811	Brown	0.719	Brown	0.907	Brown	0.843	Brown	0.749	187
Masillapodargus 01_02	Black	0.533	Grey	0.590	Grey	0.677	Black	0.455	Grey	0.445	Grey	0.501	148
Masillapodargus 01_03	Brown	0.572	Grey	0.530	Grey	0.640	Brown	0.641	Grey	0.517	Grey	0.614	128
Masillapodargus 01_04	Brown	0.594	Brown	0.575	Brown	0.539	Brown	0.763	Brown	0.740	Black	0.712	37
Masillapodargus 01_05	Black	0.686	Grey	0.832	Grey	0.933	Grey	0.690	Grey	0.819	Grey	0.902	218
Masillapodargus 01_06	Grey	0.041	Grey	0.040	Grey	0.035	Brown	0.028	Grey	0.025	Grey	0.025	256
Masillapodargus 01_07	Grey	0.531	Grey	0.584	Grey	0.597	Grey	0.195	Grey	0.187	Grey	0.165	141
Masillapodargus 01_08	Grey	0.530	Grey	0.520	Grey	0.475	Grey	0.443	Grey	0.450	Grey	0.425	201
Masillapodargus 01_09	Grey	0.221	Grey	0.283	Grey	0.333	Grey	0.043	Grey	0.044	Grey	0.040	12
Masillapodargus 01_10	Grey	0.527	Grey	0.526	Grey	0.486	Grey	0.209	Grey	0.194	Grey	0.163	223
Masillapodargus 01_11	Grey	0.420	Grey	0.496	Grey	0.550	Black	0.339	Black	0.259	Grey	0.277	116
Masillapodargus 01_12	Black	0.238	Grey	0.247	Grey	0.269	Black	0.282	Grey	0.281	Grey	0.294	113
Masillapodargus 01_13	Black	0.091	Grey	0.107	Grey	0.126	Black	0.214	Grey	0.205	Grey	0.219	39
Masillapodargus 06_05	Black	0.004	Black	0.003	Black	0.003	Black	0.000	Black	0.000	Black	0.000	27
Masillapodargus 06_07	Black	0.387	Grey	0.309	Grey	0.367	Black	0.623	Black	0.527	Grey	0.521	64
Masillapodargus 06_08	Brown	0.900	Brown	0.797	Brown	0.665	Brown	0.596	Brown	0.475	Brown	0.357	41
Masillapodargus 06_12	Grey	0.697	Grey	0.641	Grey	0.542	Grey	0.115	Grey	0.105	Grey	0.088	77
Masillapodargus 07_01	Grey	0.709	Grey	0.754	Grey	0.753	Grey	0.308	Grey	0.307	Grey	0.284	147
Masillapodargus 07_02	Brown	0.054	Brown	0.028	Grey	0.018	Brown	0.037	Brown	0.022	Grey	0.013	64
Masillapodargus 07_03	Grey	0.000	Grey	0.000	Grey	0.000	Brown	0.000	Brown	0.000	Brown	0.000	119
Masillapodargus 07_04	Grey	0.108	Grey	0.140	Grey	0.168	Grey	0.137	Grey	0.151	Grey	0.156	171
All modern data													
Masillapodargus 01_01	Black	0.969	Black	0.979	Black	0.976	Black	0.971	Black	0.981	Black	0.978	187
Masillapodargus 01_02	Black	0.951	Black	0.902	Grey	0.824	Black	0.956	Black	0.911	Black	0.835	148
Masillapodargus 01_03	Black	0.992	Black	0.968	Black	0.916	Black	0.988	Black	0.962	Black	0.906	128
Masillapodargus 01_04	Brown	0.742	Black	0.748	Black	0.766	Black	0.730	Black	0.769	Black	0.792	37
Masillapodargus 01_05	Black	0.960	Black	0.899	Black	0.796	Black	0.958	Black	0.894	Grey	0.846	218
Masillapodargus 01_06	Grey	0.875	Grey	0.912	Grey	0.921	Grey	0.853	Grey	0.881	Grey	0.880	256
Masillapodargus 01_07	Grey	0.593	Grey	0.603	Grey	0.584	Grey	0.619	Grey	0.626	Grey	0.603	141
Masillapodargus 01_08	Grey	0.974	Grey	0.993	Grey	0.993	Grey	0.971	Grey	0.989	Grey	0.987	201
Masillapodargus 01_09	Black	0.709	Grey	0.629	Grey	0.652	Grey	0.729	Grey	0.766	Grey	0.773	12
Masillapodargus 01_10	Grey	0.803	Grey	0.799	Grey	0.759	Grey	0.768	Grey	0.770	Grey	0.737	223
Masillapodargus 01_11	Black	0.912	Black	0.858	Grey	0.868	Black	0.950	Black	0.915	Black	0.851	116
Masillapodargus 01_12	Black	0.768	Black	0.657	Grey	0.604	Black	0.761	Black	0.655	Grey	0.588	113
Masillapodargus 01_13	Grey	0.186	Grey	0.197	Grey	0.199	Black	0.184	Black	0.155	Grey	0.150	39
Masillapodargus 06_05	Black	0.279	Black	0.295	Black	0.300	Black	0.209	Black	0.225	Black	0.232	27
Masillapodargus 06_07	Black	0.887	Black	0.825	Black	0.738	Black	0.887	Black	0.836	Black	0.761	64
Masillapodargus 06_08	Black	0.877	Black	0.826	Grey	0.802	Grey	0.795	Grey	0.858	Grey	0.899	41
Masillapodargus 06_12	Grey	0.790	Grey	0.768	Grey	0.714	Grey	0.828	Grey	0.831	Grey	0.800	77
Masillapodargus 07_01	Grey	0.863	Grey	0.894	Grey	0.896	Grey	0.879	Grey	0.908	Grey	0.906	147
Masillapodargus 07_02	Grey	0.948	Grey	0.946	Grey	0.921	Grey	0.925	Grey	0.916	Grey	0.883	64
Masillapodargus 07_03	Grey	0.091	Grey	0.091	Grey	0.086	Grey	0.132	Grey	0.134	Grey	0.129	119
Masillapodargus 07_04	Grey	0.466	Grey	0.497	Grey	0.509	Grey	0.433	Grey	0.471	Grey	0.492	171

Only modern Strisores	All variables model CDA						Stepwise model CDA						
Shrinkage level	**0%**	**p**	**5%**	**p**	**10%**	**p**	**0%**	**p**	**5%**	**p**	**10%**	**p**	**N**
Paraprefica 04_01	Grey	0.534	Grey	0.569	Grey	0.568	Grey	0.470	Grey	0.495	Grey	0.486	42
Paraprefica 04_02	Grey	0.325	Grey	0.257	Grey	0.183	Grey	0.209	Grey	0.174	Grey	0.130	77
Paraprefica 04_03	Grey	0.505	Grey	0.448	Grey	0.364	Grey	0.368	Grey	0.329	Grey	0.268	100
Paraprefica 04_04	Brown	0.865	Brown	0.761	Brown	0.631	Brown	0.621	Brown	0.478	Brown	0.344	12
Paraprefica 04_09	Grey	0.000	Grey	0.000	Grey	0.000	Grey	0.001	Grey	0.001	Grey	0.000	61
Paraprefica 04_10	Grey	0.025	Grey	0.011	Grey	0.004	Grey	0.090	Grey	0.051	Grey	0.025	127
Paraprefica 04_11	Grey	0.147	Grey	0.135	Grey	0.113	Grey	0.160	Grey	0.152	Grey	0.134	8
Paraprefica 04_12	Brown	0.911	Brown	0.847	Brown	0.755	Brown	0.863	Brown	0.754	Brown	0.624	67
Paraprefica 05_02	Black	0.759	Black	0.787	Black	0.784	Black	0.539	Black	0.569	Black	0.573	25
Paraprefica 05_03	Black	0.987	Black	0.954	Black	0.873	Black	0.997	Black	0.965	Black	0.883	9
Paraprefica 05_08	Brown	0.310	Grey	0.276	Grey	0.288	Brown	0.338	Grey	0.243	Grey	0.264	41
Paraprefica 05_10	Black	0.410	Grey	0.408	Grey	0.482	Grey	0.555	Grey	0.653	Grey	0.718	27
Paraprefica 05_11	Black	0.532	Black	0.457	Grey	0.400	Black	0.707	Black	0.638	Black	0.546	112
Paraprefica 05_12	Brown	0.659	Brown	0.591	Brown	0.511	Brown	0.352	Brown	0.339	Brown	0.315	98
Paraprefica 06_01	Brown	0.806	Brown	0.682	Brown	0.538	Brown	0.528	Brown	0.394	Grey	0.341	44
Paraprefica 06_03	Grey	0.865	Grey	0.858	Grey	0.799	Grey	0.840	Grey	0.840	Grey	0.786	9
Paraprefica 09_01	Brown	0.188	Brown	0.146	Brown	0.109	Brown	0.131	Brown	0.120	Brown	0.105	8
Paraprefica 09_09	Grey	0.178	Grey	0.214	Grey	0.239	Brown	0.121	Grey	0.093	Grey	0.112	131
All modern data													
Paraprefica 04_01	Grey	0.881	Grey	0.895	Grey	0.881	Grey	0.852	Grey	0.874	Grey	0.867	42
Paraprefica 04_02	Grey	0.996	Grey	0.968	Grey	0.895	Grey	0.988	Grey	0.941	Grey	0.846	77
Paraprefica 04_03	Grey	0.873	Grey	0.829	Grey	0.749	Grey	0.859	Grey	0.835	Grey	0.776	100
Paraprefica 04_04	Black	0.597	Grey	0.586	Grey	0.648	Grey	0.569	Grey	0.624	Grey	0.662	12
Paraprefica 04_09	Grey	0.096	Grey	0.055	Grey	0.028	Grey	0.211	Grey	0.131	Grey	0.073	61
Paraprefica 04_10	Grey	0.350	Grey	0.226	Grey	0.132	Grey	0.523	Grey	0.365	Grey	0.230	127
Paraprefica 04_11	Grey	0.724	Grey	0.690	Grey	0.629	Grey	0.666	Grey	0.622	Grey	0.553	8
Paraprefica 04_12	Black	0.904	Black	0.912	Black	0.904	Black	0.831	Black	0.821	Black	0.793	67
Paraprefica 05_02	Black	0.603	Black	0.706	Black	0.793	Black	0.592	Black	0.696	Black	0.783	25
Paraprefica 05_03	Black	0.898	Black	0.911	Black	0.896	Black	0.890	Black	0.904	Black	0.889	9
Paraprefica 05_08	Grey	0.740	Grey	0.768	Grey	0.771	Grey	0.742	Grey	0.778	Grey	0.789	41
Paraprefica 05_10	Black	0.865	Black	0.782	Grey	0.809	Black	0.849	Grey	0.829	Grey	0.859	27
Paraprefica 05_11	Black	0.945	Black	0.924	Black	0.880	Black	0.963	Black	0.950	Black	0.916	112
Paraprefica 05_12	Brown	0.666	Brown	0.610	Brown	0.546	Brown	0.683	Black	0.638	Black	0.647	98
Paraprefica 06_01	Black	0.898	Black	0.837	Black	0.750	Black	0.833	Grey	0.856	Grey	0.889	44
Paraprefica 06_03	Grey	0.721	Grey	0.687	Grey	0.618	Grey	0.674	Grey	0.645	Grey	0.583	9
Paraprefica 09_01	Brown	0.502	Brown	0.416	Brown	0.334	Brown	0.758	Brown	0.665	Brown	0.565	8
Paraprefica 09_09	Grey	0.755	Grey	0.846	Grey	0.905	Grey	0.745	Grey	0.841	Grey	0.904	131

Only modern Strisores	All variables model CDA						Stepwise model CDA						
Shrinkage level	**0%**	**p**	**5%**	**p**	**10%**	**p**	**0%**	**p**	**5%**	**p**	**10%**	**p**	**N**
Parargornis 02_01	Grey	0.415	Grey	0.392	Grey	0.342	Grey	0.286	Grey	0.290	Grey	0.269	107
Parargornis 02_03	Grey	0.637	Grey	0.660	Grey	0.644	Grey	0.495	Grey	0.537	Grey	0.546	29
Parargornis 02_04	Grey	0.261	Grey	0.265	Grey	0.249	Grey	0.138	Grey	0.152	Grey	0.154	29
Parargornis 02_05	Grey	0.071	Grey	0.049	Grey	0.030	Grey	0.078	Grey	0.063	Grey	0.046	57
Parargornis 02_06	Grey	0.000	Grey	0.000	Grey	0.000	Brown	0.000	Grey	0.000	Grey	0.000	28
Parargornis 02_07	Brown	0.805	Brown	0.713	Brown	0.602	Brown	0.917	Brown	0.827	Brown	0.709	48
Parargornis 02_08	Grey	0.315	Grey	0.254	Grey	0.183	Grey	0.226	Grey	0.194	Grey	0.149	32
Parargornis 02_11	Grey	0.441	Grey	0.516	Grey	0.569	Brown	0.444	Grey	0.435	Grey	0.475	43
Parargornis 05_01	Grey	0.462	Grey	0.457	Grey	0.421	Grey	0.606	Grey	0.646	Grey	0.645	15
Parargornis 05_02	Grey	0.409	Grey	0.405	Grey	0.378	Brown	0.438	Grey	0.334	Grey	0.378	17
Parargornis 05_04	Brown	0.040	Brown	0.017	Brown	0.007	Brown	0.472	Brown	0.424	Brown	0.371	222
Parargornis 05_05	Grey	0.031	Grey	0.023	Grey	0.015	Grey	0.013	Grey	0.012	Grey	0.009	27
Parargornis 05_08	Brown	0.005	Brown	0.002	Brown	0.001	Brown	0.015	Brown	0.013	Brown	0.011	97
Parargornis 05_10	Black	0.598	Black	0.665	Black	0.711	Black	0.054	Black	0.053	Black	0.049	105
All modern data													
Parargornis 02_01	Grey	0.998	Grey	0.998	Grey	0.978	Grey	0.998	Grey	0.998	Grey	0.982	107
Parargornis 02_03	Grey	0.844	Grey	0.917	Grey	0.957	Grey	0.845	Grey	0.925	Grey	0.970	29
Parargornis 02_04	Grey	0.980	Grey	0.989	Grey	0.980	Grey	0.976	Grey	0.988	Grey	0.980	29
Parargornis 02_05	Grey	0.831	Grey	0.728	Grey	0.596	Grey	0.876	Grey	0.780	Grey	0.649	57
Parargornis 02_06	Grey	0.180	Grey	0.117	Grey	0.070	Grey	0.073	Grey	0.043	Grey	0.024	28
Parargornis 02_07	Brown	0.769	Brown	0.678	Brown	0.578	Brown	0.767	Brown	0.679	Brown	0.582	48
Parargornis 02_08	Grey	0.988	Grey	0.937	Grey	0.834	Grey	0.990	Grey	0.943	Grey	0.843	32
Parargornis 02_11	Grey	0.811	Grey	0.875	Grey	0.913	Grey	0.809	Grey	0.874	Grey	0.913	43
Parargornis 05_01	Grey	0.946	Grey	0.959	Grey	0.948	Grey	0.902	Grey	0.934	Grey	0.938	15
Parargornis 05_02	Grey	0.835	Grey	0.886	Grey	0.910	Black	0.878	Grey	0.928	Grey	0.974	17
Parargornis 05_04	Brown	0.271	Brown	0.179	Brown	0.111	Brown	0.417	Brown	0.296	Brown	0.197	222
Parargornis 05_05	Grey	0.885	Grey	0.821	Grey	0.718	Grey	0.943	Grey	0.897	Grey	0.808	27
Parargornis 05_08	Brown	0.277	Brown	0.201	Brown	0.140	Brown	0.286	Brown	0.208	Brown	0.145	97
Parargornis 05_10	Black	0.541	Black	0.600	Black	0.649	Black	0.548	Black	0.604	Black	0.650	105

Only modern Strisores	All variables model CDA						Stepwise model CDA						
Shrinkage level	**0%**	**p**	**5%**	**p**	**10%**	**p**	**0%**	**p**	**5%**	**p**	**10%**	**p**	**N**
Scaniacypselus 12_08	Black	0.845	Grey	0.647	Grey	0.630	Grey	0.001	Grey	0.001	Grey	0.001	58
Scaniacypselus 12_11	Black	0.021	Black	0.029	Black	0.038	Black	0.010	Black	0.011	Black	0.011	12
Scaniacypselus 13_1	Black	0.051	Black	0.068	Black	0.085	Black	0.008	Black	0.008	Black	0.009	88
Scaniacypselus 13_10	Black	0.917	Black	0.768	Grey	0.703	Black	0.001	Grey	0.001	Grey	0.001	68
Scaniacypselus 13_11	Black	0.988	Black	0.927	Black	0.760	Black	0.001	Black	0.001	Grey	0.001	124
Scaniacypselus 13_12	Black	0.043	Black	0.043	Black	0.040	Black	0.030	Black	0.030	Black	0.028	79
Scaniacypselus 13_07	Black	0.099	Black	0.122	Black	0.140	Black	0.005	Black	0.005	Black	0.005	63
Scaniacypselus 18_01a	Brown	0.044	Grey	0.031	Grey	0.021	Brown	0.322	Brown	0.230	Brown	0.155	240
Scaniacypselus 18_01b	Brown	0.244	Brown	0.315	Brown	0.395	Brown	0.190	Brown	0.204	Brown	0.217	213
Scaniacypselus 18_03	Brown	0.263	Brown	0.308	Brown	0.350	Brown	0.595	Brown	0.619	Brown	0.629	39
Scaniacypselus 19_01	Brown	0.574	Brown	0.433	Grey	0.437	Brown	0.720	Brown	0.589	Brown	0.453	108
Scaniacypselus 19_02	Brown	0.009	Brown	0.004	Grey	0.002	Brown	0.082	Brown	0.059	Brown	0.041	142
Scaniacypselus 19_03	Black	0.602	Black	0.517	Grey	0.490	Black	0.285	Black	0.221	Grey	0.217	69
Scaniacypselus 19_04	Black	0.416	Black	0.372	Black	0.316	Black	0.462	Black	0.417	Black	0.358	140
All modern data													
Scaniacypselus 12_08	Black	0.794	Black	0.814	Black	0.801	Black	0.771	Black	0.774	Black	0.744	58
Scaniacypselus 12_11	Black	0.163	Black	0.192	Black	0.219	Black	0.142	Black	0.169	Black	0.195	12
Scaniacypselus 13_1	Brown	0.432	Brown	0.468	Brown	0.497	Brown	0.310	Black	0.354	Black	0.429	88
Scaniacypselus 13_10	Brown	0.618	Brown	0.618	Brown	0.592	Brown	0.658	Brown	0.647	Brown	0.608	68
Scaniacypselus 13_11	Brown	0.754	Brown	0.783	Brown	0.783	Brown	0.808	Brown	0.822	Brown	0.807	124
Scaniacypselus 13_12	Black	0.668	Black	0.741	Black	0.795	Black	0.532	Black	0.606	Black	0.665	79
Scaniacypselus 13_07	Brown	0.614	Brown	0.622	Black	0.627	Black	0.411	Black	0.489	Black	0.563	63
Scaniacypselus 18_01a	Grey	0.378	Grey	0.371	Grey	0.347	Grey	0.359	Grey	0.348	Grey	0.321	240
Scaniacypselus 18_01b	Brown	0.608	Brown	0.674	Brown	0.737	Brown	0.653	Brown	0.718	Brown	0.779	213
Scaniacypselus 18_03	Black	0.538	Black	0.597	Black	0.651	Black	0.623	Black	0.676	Black	0.722	39
Scaniacypselus 19_01	Black	0.823	Grey	0.838	Grey	0.892	Black	0.913	Black	0.871	Grey	0.835	108
Scaniacypselus 19_02	Grey	0.533	Grey	0.531	Grey	0.511	Grey	0.585	Grey	0.592	Grey	0.579	142
Scaniacypselus 19_03	Black	0.861	Black	0.835	Black	0.786	Black	0.850	Black	0.817	Black	0.761	69
Scaniacypselus 19_04	Black	0.727	Black	0.717	Black	0.688	Black	0.738	Black	0.742	Black	0.728	140

Only modern Strisores	All variables model CDA						Stepwise model CDA						
Shrinkage level	**0%**	**p**	**5%**	**p**	**10%**	**p**	**0%**	**p**	**5%**	**p**	**10%**	**p**	**N**
Eocypselus 01	Grey	0.809	Grey	0.879	Grey	0.889	Grey	0.245	Grey	0.146	Grey	0.076	29
Eocypselus 02	Grey	0.708	Grey	0.644	Grey	0.535	Grey	0.253	Grey	0.169	Grey	0.099	110
Eocypselus 03	Grey	0.511	Grey	0.603	Grey	0.682	Grey	0.380	Grey	0.287	Grey	0.193	50
Eocypselus 04	Grey	0.614	Grey	0.577	Grey	0.503	Grey	0.872	Grey	0.850	Grey	0.773	59
Eocypselus 05	Grey	0.819	Grey	0.669	Grey	0.488	Grey	0.497	Grey	0.339	Grey	0.202	38
Eocypselus 07	Grey	0.668	Grey	0.533	Grey	0.383	Grey	0.715	Grey	0.549	Grey	0.371	62
All modern data													
Eocypselus 01	Grey	0.484	Grey	0.479	Grey	0.441	Grey	0.872	Grey	0.763	Grey	0.614	29
Eocypselus 02	Grey	0.635	Grey	0.872	Grey	0.785	Grey	0.635	Grey	0.887	Grey	0.762	110
Eocypselus 03	Black	0.264	Black	0.194	Grey	0.173	Grey	0.583	Grey	0.530	Grey	0.451	50
Eocypselus 04	Grey	0.789	Grey	0.584	Grey	0.496	Grey	0.626	Grey	0.448	Grey	0.393	59
Eocypselus 05	Grey	0.911	Grey	0.829	Grey	0.702	Grey	0.920	Grey	0.833	Grey	0.700	38
Eocypselus 07	Grey	0.769	Grey	0.658	Grey	0.522	Grey	0.710	Grey	0.620	Grey	0.503	62

Table S8.2. Loadings of each variable and the amount of variance explained by each canonical function from the canonical function analysis of melanosome morphologies for all modern data without hollow and flat iridescent melanosomes included. The largest absolute correlation between each variable and each function is italicised.

	Function 1	Function 2	Function 3
Length	***.833****	-0.452	0.004
Aspect Ratio	***.740****	0.407	-0.137
AR skew	***-.430****	0.143	0.285
Length skew	***-.341****	0.119	0.081
Width	0.002	***-.706****	0.352
Width skew	0.009	***-.065****	-0.014
Width CV	-0.031	-0.020	**.718***
Length CV	-0.303	-0.131	**.436***
Variance	**63.2%**	**27.4%**	**9.3%**

Table S8.3. Loadings of each variable and the amount of variance explained by each canonical function from the canonical function analysis of melanosome morphologies for all modern data with hollow and flat iridescent melanosomes included. The largest absolute correlation between each variable and each function is italicised.

	Function 1	Function 2	Function 3	Function 4
Length	***.885***	0.305	-0.110	-0.063
AR skew	***-.378***	0.160	0.337	0.046
Length skew	***-.318***	0.068	0.173	-0.086
Width	0.213	***.885***	0.277	-0.264
Aspect ratio	0.590	***-.653***	-0.037	0.173
Width skew	-0.009	-0.016	***-.136***	0.109
Width CV	0.006	0.222	0.282	***.758***
Length CV	-0.335	0.151	-0.101	***.693***
Variance	**58.8%**	**28.6%**	**9.7%**	**2.9%**

Appendix 1 - Melanosome measurement data

Total melanosome dataset used in this thesis including a published dataset (Li et al. 2012) and new samples of extant Upupiformes (and outgroups) and Strisores as well as all fossil samples of *Caudipteryx*, *Messelirrisor* and strisorians. Each sample shows the average length (nm), length coefficient of variation (CV), length skew, width (nm), width CV, width skew, aspect ratio and aspect ratio skew taken from 100 melanosomes (or as many as possible in fossil samples) as measured from SEM images.

Latin name	Colour	Length	Len CV	Len skew	Diameter	Diam CV	Diam skew	Aspect ratio	AR skew	N	Hollow	Flat	Database
EXTANT BIRDS													
Spinus tristis	Black	1003.100	24.846	-1.339	244.200	13.110	-0.114	4.100	-1.660	100	No	No	Li et al. (2012)
Falco sparverius	Black	1031.333	10.507	-0.162	363.167	7.677	0.878	2.840	-0.184	100	No	No	Li et al. (2012)
Rhea americana	Black	1129.882	21.503	0.166	316.765	7.729	0.637	3.580	1.200	100	No	No	Li et al. (2012)
Rhea americana	Black	872.080	21.858	-0.312	260.200	8.615	1.226	3.444	-0.790	100	No	No	Li et al. (2012)
Turdus migratorius	Black	1002.300	24.636	-1.361	238.658	13.667	-0.125	4.100	-1.910	100	No	No	Li et al. (2012)
Mareca americana	Black	696.442	63.147	1.989	233.336	14.665	-0.014	2.985	1.989	100	No	No	Li et al. (2012)
Scolopax minor	Black	915.067	25.296	0.321	254.800	18.946	0.404	3.664	0.508	100	No	No	Li et al. (2012)
Scolopax minor	Black	1008.241	6.194	0.205	226.000	5.084	0.222	4.600	0.322	100	No	No	Li et al. (2012)
Synthliboramphus antiquus	Black	992.783	18.877	-0.019	303.739	26.685	0.195	3.333	0.456	100	No	No	Li et al. (2012)
Icterus galbula	Black	956.000	14.121	0.005	236.300	12.641	0.007	4.000	1.580	100	No	No	Li et al. (2012)
Megaceryle alcyon	Black	1233.739	21.647	-0.283	334.130	22.363	0.974	3.784	-0.194	100	No	No	Li et al. (2012)
Francolinus francolinus	Black	970.356	11.319	0.212	218.005	15.619	0.277	4.200	-0.391	100	No	No	Li et al. (2012)
Cepphus grylle	Black	1041.955	15.324	-2.149	216.667	11.224	0.063	4.832	-0.162	100	No	No	Li et al. (2012)
Chlidonias niger	Black	1031.750	21.128	-0.566	283.375	15.527	-0.010	3.629	-0.447	100	No	No	Li et al. (2012)
Tinamus osgoodi	Black	896.996	27.179	-0.291	353.264	14.615	0.671	2.591	-0.366	100	No	No	Li et al. (2012)
Pica hudsonia	Black	934.100	30.196	-0.084	254.300	19.201	-0.194	3.700	0.799	100	No	No	Li et al. (2012)
Coracina novaehollandiae	Black	1174.128	19.816	0.382	361.511	14.627	-0.348	3.281	0.624	100	No	No	Li et al. (2012)
Ramphastos ambiguus	Black	969.700	8.626	0.225	220.300	14.566	0.258	4.400	-0.710	100	No	No	Li et al. (2012)
Sula leucogaster	Black	1136.428	1.317	0.578	267.479	3.701	1.055	4.268	-0.581	100	No	No	Li et al. (2012)
Alectoris chukar	Black	1046.273	31.483	0.310	346.727	16.484	0.339	3.071	1.610	100	No	No	Li et al. (2012)
Gavia immer	Black	893.059	2.370	-0.042	186.932	4.573	-0.382	4.808	-0.143	100	No	No	Li et al. (2012)
Chordeiles minor	Black	1049.956	5.704	-0.764	262.872	8.296	-0.457	4.054	0.276	100	No	No	Li et al. (2012)
Priotelus temnurus	Black	900.031	23.075	-0.677	337.485	13.390	2.211	2.730	-1.299	100	No	No	Li et al. (2012)
Pterocles quadricinctus	Black	709.469	19.352	0.062	262.583	11.110	0.942	2.746	0.425	100	No	No	Li et al. (2012)
Phalacrocorax auritus	Black	954.000	39.368	0.850	342.357	33.327	0.054	2.926	1.940	100	No	No	Li et al. (2012)
Casuarius bennetti	Black	899.896	9.624	0.359	285.532	5.234	0.261	3.152	1.542	100	No	No	Li et al. (2012)
Strix nebulosa	Black	1008.044	16.324	0.249	219.767	12.506	0.227	4.636	0.318	100	No	No	Li et al. (2012)
Ardea cinerea	Black	1260.746	3.128	-0.299	304.573	3.074	0.712	4.171	-0.224	100	No	No	Li et al. (2012)
Fregata magnificens	Black	1146.678	5.423	0.264	232.021	5.873	0.636	5.038	-0.870	100	No	No	Li et al. (2012)
Megapodius reinwardt	Black	899.810	25.596	-0.006	358.040	20.284	0.487	2.643	-0.300	100	No	No	Li et al. (2012)
Struthio camelus	Black	929.527	12.658	0.239	289.376	12.287	0.469	3.213	-0.800	100	No	No	Li et al. (2012)
Probosciger aterrimus	Black	949.912	22.802	-0.599	317.472	12.948	1.011	3.135	-0.609	100	No	No	Li et al. (2012)
Agelaius phoeniceus	Black	1095.200	35.291	-0.512	209.570	19.232	-0.757	3.650	-0.576	100	No	No	Li et al. (2012)
Larus delawarensis	Black	1104.886	1.976	0.659	382.988	14.221	3.526	3.300	-2.185	100	No	No	Li et al. (2012)
Columbia livia	Black	668.833	41.448	0.996	238.667	26.103	1.103	2.920	0.211	100	No	No	Li et al. (2012)
Ardenna grisea	Black	1267.859	4.023	-0.965	245.102	2.757	0.262	5.170	-0.348	100	No	No	Li et al. (2012)
Porzana carolina	Black	948.373	50.896	0.444	191.597	27.187	0.823	5.059	-0.238	100	No	No	Li et al. (2012)
Diomedea exulans	Black	1289.159	3.600	-0.965	393.895	1.996	0.596	3.279	0.382	100	No	No	Li et al. (2012)
Antrostomus vociferus	Black	1043.552	5.974	0.888	201.529	8.776	0.752	5.178	0.888	100	No	No	Li et al. (2012)
Ciconia ciconia	Black	1097.692	2.367	0.650	387.782	19.530	3.483	3.258	-2.538	100	No	No	Li et al. (2012)
Turnix tanki	Black	836.546	22.070	1.331	278.335	15.260	1.102	3.087	0.665	100	No	No	Li et al. (2012)
Cacicus cela	Black	1323.500	22.326	-0.106	221.400	16.102	-0.486	6.000	0.310	100	No	No	Li et al. (2012)
Taeniopygia guttata	Black	1136.300	17.378	0.500	283.990	6.606	-0.204	4.100	0.160	100	No	No	Li et al. (2012)
Rhinopomastus minor	Black	1463.392	13.360	0.065	367.246	14.360	0.367	4.026	0.152	100	No	No	New (Chapter 7)
Upupa epops africana	Black	1390.904	15.600	0.068	275.038	10.577	0.361	5.106	0.051	100	No	No	New (Chapter 7)
Lacedo pulchella	Black	1181.627	13.082	-0.051	486.927	14.118	-0.515	2.459	0.649	100	No	No	New (Chapter 7)
Lybius dubius	Black	1476.915	13.830	-0.059	270.702	12.279	0.270	5.525	0.546	100	No	No	New (Chapter 7)
Anthracoceros malayanus	Black	1208.246	14.602	-0.026	285.848	9.500	-0.171	4.254	0.253	100	No	No	New (Chapter 7)
Dryocopus martius	Black	1716.641	17.060	0.362	275.976	8.473	0.183	6.254	-0.116	100	No	No	New (Chapter 7)
Picoides arcticus	Black	1890.391	14.905	-0.028	330.384	14.242	0.907	5.785	-0.007	100	No	No	New (Chapter 7)
Merops breweri	Black	1022.238	17.958	0.488	295.813	12.729	0.064	3.484	0.362	100	No	No	New (Chapter 7)
Rhyticeros plicatus	Black	1315.150	14.817	-0.857	316.488	7.975	0.498	4.185	-0.896	100	No	No	New (Chapter 7)
Eurystomus glaucurus	Black	1179.236	16.214	0.754	317.008	12.554	0.581	3.765	0.911	100	No	No	New (Chapter 7)
Eurystomus glaucurus	Black	1416.712	15.856	-0.556	347.348	12.123	0.458	4.140	0.401	100	No	No	New (Chapter 7)
Meiglyptes grammithorax	Black	1169.387	22.117	-0.795	301.769	17.578	1.087	3.970	-0.992	100	No	No	New (Chapter 7)

Tanysiptera galatea	Black	940.047	13.950	-0.281	274.199	11.004	0.623	3.450	0.440	100	No	No	New (Chapter 7)
Rhinopomastus cyanomelas	Black	1415.317	15.244	0.521	325.601	14.801	0.294	4.408	1.496	100	No	No	New (Chapter 7)
Rhinopomastus cyanomelus	Black	1512.796	17.012	-0.052	349.191	14.030	0.027	4.373	0.950	100	No	No	New (Chapter 7)
Upupa epops	Black	1111.189	17.438	0.979	257.336	16.742	1.082	4.396	0.826	100	No	No	New (Chapter 7)
Upupa epops	Black	1093.079	20.926	0.428	273.407	10.668	0.645	4.063	0.132	100	No	No	New (Chapter 7)
Upupa epops	Black	1307.953	12.359	-0.190	280.595	9.397	-0.194	4.691	0.407	100	No	No	New (Chapter 7)
Upupa epops	Black	1321.316	13.328	0.059	303.232	10.598	0.638	4.403	0.276	100	No	No	New (Chapter 7)
Upupa epops longirostris	Black	1229.100	19.670	0.048	258.481	11.604	0.406	4.798	-0.079	100	No	No	New (Chapter 7)
Upupa epops senegalensis	Black	1199.715	18.213	-0.075	248.357	10.182	0.420	4.891	0.404	100	No	No	New (Chapter 7)
Capito punctatus	Black	1283.966	19.562	0.083	273.384	14.145	0.306	4.778	0.043	100	No	No	New (Chapter 7)
Dendrocopos major	Black	1627.756	17.865	0.261	311.223	15.483	0.577	5.286	0.380	100	No	No	New (Chapter 7)
Dendrocopos major	Black	2057.070	16.726	0.857	459.841	15.776	-0.209	4.530	1.080	100	No	No	New (Chapter 7)
Chrysocolaptes guttacristatus	Black	1083.507	16.230	0.525	258.190	10.733	0.531	4.238	0.304	100	No	No	New (Chapter 7)
Phoeniculus purpureus	Black	1334.906	10.941	0.252	278.562	8.379	0.072	4.807	0.634	100	No	No	New (Chapter 7)
Phoeniculus purpureus	Black	1160.805	16.481	0.878	255.926	15.411	1.391	4.562	-0.594	100	No	No	New (Chapter 7)
Phoeniculus purpureus	Black	1591.814	12.222	0.147	286.208	11.612	0.425	5.620	0.811	100	No	No	New (Chapter 7)
Halcyon leucocephala	Black	1213.243	17.166	1.143	262.221	9.711	0.149	4.661	0.911	100	No	No	New (Chapter 7)
Selenidera piperivora	Black	1298.170	14.659	0.585	340.484	13.010	0.144	3.843	0.478	100	No	No	New (Chapter 7)
Cittura cyanosis	Black	980.314	13.568	0.051	296.639	12.596	0.409	3.336	0.504	100	No	No	New (Chapter 7)
Anthracoceros melabaricus	Black	1475.170	14.064	-0.072	306.751	7.533	0.188	4.834	0.121	100	No	No	New (Chapter 7)
Penelopides panini	Black	1443.724	15.995	0.124	295.396	9.077	0.456	4.924	0.411	100	No	No	New (Chapter 7)
Penelopides panini	Black	1910.167	19.793	0.625	345.870	9.088	0.103	5.557	0.492	100	No	No	New (Chapter 7)
Merops nubicus	Black	990.028	16.337	0.768	221.759	12.994	0.493	4.553	0.703	100	No	No	New (Chapter 7)
Merops nubicus	Black	905.103	17.470	0.446	250.182	12.099	-0.012	3.682	0.807	100	No	No	New (Chapter 7)
Colaptes auratus	Black	1411.466	14.385	0.109	350.945	12.233	0.624	4.074	0.341	100	No	No	New (Chapter 7)
Eurystomus orientalis	Black	1069.869	19.159	0.002	332.978	13.795	0.934	3.263	-0.459	100	No	No	New (Chapter 7)
Galbula dea	Black	837.765	22.147	0.443	187.076	21.498	1.348	4.569	0.664	100	No	No	New (Chapter 7)
Atelornis pittoides	Black	996.327	18.057	0.368	311.749	12.365	0.235	3.220	-0.187	100	No	No	New (Chapter 7)
Atelornis pittoides	Black	957.409	19.605	0.298	319.252	11.886	-0.028	3.053	0.467	100	No	No	New (Chapter 7)
Campephilus rubricollis	Black	1103.726	13.478	-0.284	297.082	10.779	0.692	3.756	-0.114	100	No	No	New (Chapter 7)
Buceros rhinoceros	Black	1220.699	13.618	-0.085	304.686	8.207	-0.138	4.024	0.193	100	No	No	New (Chapter 7)
Buceros hydrocorax	Black	1182.523	22.144	-0.308	284.238	12.286	3.739	4.215	-0.446	100	No	No	New (Chapter 7)
Barypthengus ruficapillus	Black	803.651	18.995	0.386	330.987	11.286	0.874	2.474	0.428	100	No	No	New (Chapter 7)
Barypthengus ruficapillus	Black	686.958	17.830	0.764	356.423	12.566	0.360	1.963	0.584	100	No	No	New (Chapter 7)
Galbula ruficauda	Black	1122.434	19.540	0.475	258.989	18.497	0.270	4.435	0.806	100	No	No	New (Chapter 7)
Brachypteracias leptosomus	Black	1258.906	18.276	0.889	565.784	19.940	-0.445	2.304	1.041	100	No	No	New (Chapter 7)
Bucorvus leadbeateri	Black	1304.476	12.611	0.237	324.615	8.481	0.224	4.041	0.548	100	No	No	New (Chapter 7)
Selenidera maculirostris	Black	1216.315	18.706	0.166	315.589	9.408	0.380	3.886	0.358	100	No	No	New (Chapter 7)
Selenidera maculirostris	Black	1311.675	17.995	0.324	379.607	15.168	0.839	3.529	0.359	100	No	No	New (Chapter 7)
Semnornis ramphastinus	Black	1013.960	15.818	0.474	329.183	14.619	1.296	3.114	0.452	100	No	No	New (Chapter 7)
Tockus deckeni	Black	1228.160	16.738	-0.118	300.671	12.303	0.215	4.109	-0.268	100	No	No	New (Chapter 7)
Phoeniculus bollei	Black	1449.077	14.446	0.547	354.935	12.542	0.195	4.119	0.044	100	No	No	New (Chapter 7)
Rhyticeros undulatus	Black	1332.839	15.364	0.182	314.133	7.186	0.076	4.251	0.081	100	No	No	New (Chapter 7)
Rhyticeros undulatus	Black	919.706	31.879	1.663	304.738	24.828	0.846	3.164	1.448	100	No	No	New (Chapter 7)
Aceros corrugatus	Black	1476.520	17.686	0.818	292.599	6.622	0.528	5.062	1.002	100	No	No	New (Chapter 7)
Monasa flavirostris	Black	1345.746	22.876	1.355	284.528	8.103	-0.128	4.742	1.028	100	No	No	New (Chapter 7)
Aerodramus amelis	Black	1153.231	26.772	0.791	178.207	14.348	0.690	6.610	0.781	100	No	No	New (Chapter 8)
Aerodramus amelis	Black	1153.231	26.772	0.791	178.207	14.348	0.690	6.610	0.781	100	No	No	New (Chapter 8)
Aeronautes montivagus	Black	1102.913	22.702	0.400	198.802	13.299	0.577	5.678	0.583	100	No	No	New (Chapter 8)
Aeronautes montivagus	Black	972.795	19.181	-0.080	197.592	15.178	1.283	5.021	0.347	100	No	No	New (Chapter 8)
Aeronautes montivagus	Black	1102.913	22.702	0.400	198.802	13.299	0.577	5.678	0.583	100	No	No	New (Chapter 8)
Aeronautes montivagus	Black	972.795	19.181	-0.080	197.592	15.178	1.283	5.021	0.347	100	No	No	New (Chapter 8)
Aerodramus vanikorensis	Black	1132.445	26.355	1.372	221.775	11.436	1.247	5.140	0.450	100	No	No	New (Chapter 8)
Aerodramus vanikorensis	Black	1086.436	18.651	0.132	209.508	13.178	1.584	5.278	0.425	100	No	No	New (Chapter 8)
Aerodramus vanikorensis	Black	1132.445	26.355	1.372	221.775	11.436	1.247	5.140	0.450	100	No	No	New (Chapter 8)
Aerodramus vanikorensis	Black	1086.436	18.651	0.132	209.508	13.178	1.584	5.278	0.425	100	No	No	New (Chapter 8)
Cypsiurus labasiensis pallidor	Black	1211.661	19.166	0.156	210.254	11.490	0.250	5.819	0.406	100	No	No	New (Chapter 8)
Cypsiurus parvus gracilis	Black	1003.902	15.727	0.041	181.303	11.172	1.475	5.587	0.336	100	No	No	New (Chapter 8)
Aerodromus amelis	Black	1205.553	19.282	0.071	203.427	10.071	1.131	5.978	-0.307	100	No	No	New (Chapter 8)
Apus apus	Black	1245.508	19.747	0.026	194.937	13.087	1.245	6.501	0.125	100	No	No	New (Chapter 8)
Apus	Black	1425.194	23.203	0.004	200.397	11.973	1.157	7.239	0.132	100	No	No	New (Chapter 8)
Apus barbatus	Black	1126.894	18.473	0.055	214.178	11.475	2.061	5.299	-0.379	100	No	No	New (Chapter 8)
Apus barbatus	Black	1101.049	17.049	0.463	202.383	9.158	0.450	5.482	0.841	100	No	No	New (Chapter 8)
Nyctibius jamaicensis	Black	906.455	18.620	0.392	183.202	8.500	-0.055	4.982	0.276	100	No	No	New (Chapter 8)
Caprimulgus andamanicus	Black	1096.990	19.484	0.131	196.282	11.091	0.051	5.628	0.318	100	No	No	New (Chapter 8)
Caprimulgus asiaticus	Black	1136.233	16.318	0.309	212.997	14.336	0.562	5.416	0.906	100	No	No	New (Chapter 8)
Caprimulgus climacurus	Black	1033.424	31.066	-0.473	203.635	17.338	1.799	5.319	-0.482	100	No	No	New (Chapter 8)
Caprimulgus indicus	Black	1144.077	16.634	0.209	214.610	9.747	0.041	5.380	0.467	100	No	No	New (Chapter 8)
Caprimulgus macrurus	Black	1242.609	19.112	0.393	211.543	8.657	0.191	5.911	0.665	100	No	No	New (Chapter 8)
Caprimulgus macrurus	Black	1101.170	17.499	0.773	226.300	9.451	0.488	4.889	0.776	100	No	No	New (Chapter 8)
Caprimulgus rufigena	Black	1188.854	19.582	0.483	198.132	11.852	0.253	6.070	0.634	100	No	No	New (Chapter 8)
Caprimulgus vexillarius	Black	1148.125	17.846	-0.148	193.827	9.529	0.550	5.943	-0.108	100	No	No	New (Chapter 8)
Caprimulgus yorki	Black	1113.598	18.003	0.266	198.861	12.756	1.318	5.695	0.047	100	No	No	New (Chapter 8)
Chardeiles nacunda	Black	1674.808	28.845	-0.075	253.753	11.051	0.004	6.692	-0.103	100	No	No	New (Chapter 8)
Chordeiles minor	Black	1015.323	23.266	-0.180	214.844	10.372	0.761	4.786	-0.256	100	No	No	New (Chapter 8)
Chordeiles nacunda	Black	1441.709	21.559	0.103	244.620	11.496	0.615	5.953	-0.004	100	No	No	New (Chapter 8)

Chordeiles virginianus	Black	1471.783	16.634	0.182	234.795	9.975	0.266	6.326	0.643	100	No	No	New (Chapter 8)
Eurostopodus macrotis	Black	942.100	19.093	0.436	212.764	10.579	0.307	4.477	0.421	100	No	No	New (Chapter 8)
Macropsalis creagra	Black	1008.911	17.783	-0.525	187.389	11.579	0.822	5.439	-0.632	100	No	No	New (Chapter 8)
Nyctibius aetherius	Black	1168.766	12.682	-0.188	311.055	13.892	-0.175	3.820	0.632	100	No	No	New (Chapter 8)
Nyctibius grandis	Black	745.106	15.069	0.395	197.682	9.199	-0.311	3.803	1.435	100	No	No	New (Chapter 8)
Nyctibius grandis	Black	1122.238	18.111	-0.354	207.951	10.356	0.165	5.449	-0.144	100	No	No	New (Chapter 8)
Nyctibius griseus	Black	1018.967	15.539	0.125	187.733	8.038	-0.007	5.463	0.366	100	No	No	New (Chapter 8)
Nyctibius jamaicensis	Black	1010.874	21.272	0.139	182.307	8.498	0.103	5.589	0.202	100	No	No	New (Chapter 8)
Nyctidromus albicollis	Black	1180.414	18.891	0.715	254.723	9.524	0.104	4.668	0.805	100	No	No	New (Chapter 8)
Nyctidromus albicollis	Black	798.514	20.434	0.386	186.380	13.267	-0.121	4.369	0.993	100	No	No	New (Chapter 8)
Uropsalis lyra	Black	922.083	22.834	0.329	183.359	9.301	0.183	5.065	0.160	100	No	No	New (Chapter 8)
Uropsalis lyra	Black	941.281	23.687	0.451	185.480	12.232	2.312	5.127	-0.556	100	No	No	New (Chapter 8)
Hydopsalis brasiliana	Black	1109.965	18.332	0.296	223.221	9.920	1.777	5.016	-0.143	100	No	No	New (Chapter 8)
Podargus strigoides	Black	1085.181	15.859	0.428	281.865	11.819	2.085	3.913	0.377	100	No	No	New (Chapter 8)
Podargus strigoides	Black	1217.080	15.948	0.686	281.467	9.636	0.455	4.361	0.252	100	No	No	New (Chapter 8)
Eurostopodus macrotis	Black	909.126	14.467	0.176	244.748	9.719	0.318	3.741	0.505	100	No	No	New (Chapter 8)
Nyciphrynus ocellatus	Black	1133.072	18.899	1.250	242.869	15.531	1.846	4.701	0.243	100	No	No	New (Chapter 8)
Caprimulgus pectoralis	Black	1037.147	19.430	0.272	221.837	9.897	0.828	4.722	0.179	100	No	No	New (Chapter 8)
Aglaectis c. caripennis	Black	1283.654	10.373	0.051	408.098	13.134	0.026	3.181	0.281	100	Uncertain	Yes	New (Chapter 8)
Aglaectis pamela	Black	1456.010	13.871	0.260	475.234	15.042	0.633	3.113	1.323	100	Yes	Yes	New (Chapter 8)
Anthracothorax nigricollis	Black	1180.935	14.467	0.096	231.527	16.761	0.393	5.221	0.839	100	No	Few	New (Chapter 8)
Anthracothorax nicricollis	Black	1749.784	14.130	0.592	423.164	16.909	0.047	4.215	0.702	100	No	Few	New (Chapter 8)
Damophila julie	Black	1318.346	12.849	-0.314	251.008	16.661	0.410	5.398	0.528	100	No	Some	New (Chapter 8)
Discosura longicaudus	Black	1271.124	8.893	0.290	419.909	14.424	-0.001	3.073	0.981	100	Uncertain	Yes	New (Chapter 8)
Doryfera ludovicae	Black	1232.963	13.728	-0.088	240.425	19.881	0.284	5.296	0.650	100	No	Some	New (Chapter 8)
Florisuga fuscus	Black	1550.732	13.715	0.026	424.420	17.390	0.233	3.720	0.588	100	Uncertain	Yes	New (Chapter 8)
Glaucis hirsuta	Black	1451.355	15.954	-0.316	309.572	26.090	0.808	4.917	1.298	100	Yes	Yes	New (Chapter 8)
Lophornis verreauxi	Black	1390.940	14.005	0.973	288.218	15.847	0.552	4.912	0.778	100	No	Few	New (Chapter 8)
Microchera albocoronata	Black	1377.926	15.905	-0.338	476.735	18.868	0.222	2.962	0.990	100	Uncertain	Yes	New (Chapter 8)
Orthorhynchus christatus	Black	1516.204	16.141	0.647	373.640	19.576	0.415	4.180	0.416	100	Uncertain	Yes	New (Chapter 8)
Phaethornis yaruigui	Black	1050.646	13.639	0.294	280.473	17.144	0.073	3.828	0.647	100	No	Most	New (Chapter 8)
Rhamphodon naevius	Black	1297.736	14.496	0.280	289.260	17.409	0.185	4.595	1.295	100	Yes	Some	New (Chapter 8)
Topaza pella	Black	1553.490	16.691	-0.217	380.423	22.896	0.094	4.244	0.733	100	Yes	Yes	New (Chapter 8)
Mearnsia picina	Black	1313.830	20.372	0.372	221.289	12.856	0.360	6.016	-0.143	100	No	No	New (Chapter 8)
Mearnsia picina	Black	1313.830	20.372	0.372	221.289	12.856	0.360	6.016	-0.143	100	No	No	New (Chapter 8)
Eurostopodus macrotis	Black	957.844	27.545	1.070	195.540	10.757	0.212	4.922	0.837	100	No	No	New (Chapter 8)
Macropsalis creagra	Black	2068.831	19.748	-0.572	327.885	15.795	1.349	6.449	-0.552	100	No	No	New (Chapter 8)
Nyctibius aetherius	Black	1203.293	13.331	-0.076	324.979	12.583	0.156	3.750	0.072	100	No	No	New (Chapter 8)
Campylopterus largipennis	Black	1151.649	19.994	1.526	326.731	14.525	0.888	3.550	1.063	100	No	No	New (Chapter 8)
Damophila julie	Black	1319.421	11.487	-0.183	435.443	13.272	-0.160	3.064	0.999	100	Uncertain	Some	New (Chapter 8)
Campylopterus l. largipennis	Black	1327.601	10.881	0.392	371.176	17.706	0.004	3.674	1.108	100	Yes	Yes	New (Chapter 8)
Falco sparverius	Brown	491.833	12.598	-0.203	304.000	22.214	-0.387	1.650	0.510	100	No	No	Li et al. (2012)
Turdus migratorius	Brown	433.666	18.346	-0.119	181.697	20.072	0.091	2.387	0.297	100	No	No	Li et al. (2012)
Spizelloides arborea	Brown	322.734	9.639	0.167	226.072	10.909	-0.067	1.200	2.394	100	No	No	Li et al. (2012)
Alectura lathami	Brown	715.468	19.235	0.103	362.534	15.594	1.237	1.984	-0.261	100	No	No	Li et al. (2012)
Hirundo rustica	Brown	650.300	36.583	0.106	175.900	15.691	1.260	3.700	0.387	100	No	No	Li et al. (2012)
Megaceryle alcyon	Brown	526.600	14.158	-0.521	301.200	15.504	-0.507	1.752	-0.541	100	No	No	Li et al. (2012)
Tinamus osgoodi	Brown	434.845	13.913	-0.140	381.072	13.040	-0.438	1.146	1.314	100	No	No	Li et al. (2012)
Chroicocephalus philadelphia	Brown	924.259	8.901	-0.386	414.084	8.180	-0.877	2.271	0.694	100	No	No	Li et al. (2012)
Pelecanus occidentalis	Brown	938.444	26.135	-0.584	243.333	17.745	-0.414	4.010	0.879	100	No	No	Li et al. (2012)
Callipepla californica	Brown	234.667	24.039	0.902	223.167	48.677	1.271	1.237	0.939	100	No	No	Li et al. (2012)
Alectoris chukar	Brown	318.323	9.013	0.131	227.274	16.069	-0.063	1.300	2.859	100	No	No	Li et al. (2012)
Phasianus colchicus	Brown	448.248	27.440	1.653	227.339	20.053	0.764	2.065	2.071	100	No	No	Li et al. (2012)
Pterocles quadricinctus	Brown	603.252	10.524	-0.180	448.381	12.248	1.924	1.354	0.215	100	No	No	Li et al. (2012)
Phalacrocorax auritus	Brown	888.083	18.412	0.632	340.583	16.964	1.031	2.622	1.611	100	No	No	Li et al. (2012)
Sialia sialis	Brown	322.300	12.783	0.160	223.200	13.620	-0.042	1.400	2.460	100	No	No	Li et al. (2012)
Dendrocygna bicolor	Brown	455.200	21.623	-0.300	233.100	23.843	0.059	2.000	0.456	100	No	No	Li et al. (2012)
Strix nebulosa	Brown	352.320	6.190	0.179	221.477	12.331	-0.067	1.400	2.392	100	No	No	Li et al. (2012)
Tinamus major	Brown	412.535	14.864	0.314	348.553	14.518	0.611	1.203	0.389	100	No	No	Li et al. (2012)
Opisthocomus hoazin	Brown	435.427	20.004	0.205	277.019	9.866	0.252	1.592	1.132	100	No	No	Li et al. (2012)
Coturnix japonica	Brown	411.200	34.334	-0.068	244.200	5.762	0.388	1.700	2.593	100	No	No	Li et al. (2012)
Clangula hyemalis	Brown	358.925	28.383	0.177	158.775	21.938	-0.075	2.261	0.620	100	No	No	Li et al. (2012)
Harpactes fasciatus	Brown	462.079	18.546	0.315	373.041	13.437	-0.050	1.246	0.847	100	No	No	Li et al. (2012)
Anas platyrhynchos	Brown	585.745	30.520	0.407	233.669	13.134	0.718	2.507	0.370	100	No	No	Li et al. (2012)
Megapodius reinwardt	Brown	379.399	16.156	0.207	354.131	9.714	-0.795	1.075	0.767	100	No	No	Li et al. (2012)
Buteo jamaicensis	Brown	530.843	14.363	0.943	368.858	11.604	0.175	1.439	0.963	100	No	No	Li et al. (2012)
Columbia livia	Brown	662.974	23.158	0.487	381.384	11.532	-0.353	1.789	0.937	100	No	No	Li et al. (2012)
Selasphorus rufus	Brown	808.226	7.316	-0.002	228.693	1.063	0.924	3.534	0.702	100	No	No	Li et al. (2012)
Colius striatus	Brown	349.685	16.082	0.225	275.736	13.363	0.438	1.279	1.295	100	No	No	Li et al. (2012)
Baeolophus bicolor	Brown	570.100	15.107	-0.298	291.200	11.801	-0.452	2.000	0.380	100	No	No	Li et al. (2012)
Antrostomus vociferus	Brown	302.900	14.235	0.137	231.455	10.317	-0.017	1.500	2.313	100	No	No	Li et al. (2012)
Sitta carolinensis	Brown	296.238	23.212	0.130	151.530	16.762	0.559	1.595	0.379	100	No	No	Li et al. (2012)
Hylocichla mustelina	Brown	310.383	14.237	0.203	224.211	9.844	-0.028	1.391	2.264	100	No	No	Li et al. (2012)
Coccyzus americanus	Brown	501.300	28.511	1.282	210.200	15.234	0.550	2.400	0.668	100	No	No	Li et al. (2012)
Turnix tanki	Brown	557.530	28.099	1.121	365.502	13.794	-0.009	1.574	1.412	100	No	No	Li et al. (2012)
Taeniopygia guttata	Brown	487.100	21.668	1.201	421.200	15.077	-0.152	1.200	0.508	100	No	No	Li et al. (2012)

Taeniopygia guttata	Brown	376.200	54.218	-0.298	210.000	39.453	-0.514	1.800	-0.443	100	No	No	Li et al. (2012)
Merops breweri	Brown	500.395	38.663	2.115	277.910	13.882	0.259	1.836	1.913	100	No	No	New (Chapter 7)
Merops breweri	Brown	411.895	23.220	0.550	267.229	14.806	0.260	1.555	1.239	100	No	No	New (Chapter 7)
Merops viridis	Brown	529.946	39.825	2.566	286.424	14.394	0.469	1.855	2.029	100	No	No	New (Chapter 7)
Rhyticeros plicatus	Brown	506.377	27.343	0.942	297.413	22.669	1.048	1.763	1.605	100	No	No	New (Chapter 7)
Eurystomus glaucurus	Brown	655.789	29.985	1.968	320.559	13.274	0.293	2.083	1.679	100	No	No	New (Chapter 7)
Eurystomus glaucurus	Brown	628.059	15.478	0.348	452.689	14.614	0.327	1.400	0.866	100	No	No	New (Chapter 7)
Tanysiptera sylvia	Brown	326.390	12.634	-0.352	271.992	12.887	-0.134	1.204	0.690	100	No	No	New (Chapter 7)
Alcedo atthis	Brown	461.024	22.444	0.317	292.053	19.917	1.356	1.612	0.757	100	No	No	New (Chapter 7)
Aulacorhynchus prasinus	Brown	685.188	36.535	1.526	354.362	16.877	0.946	1.983	1.460	100	No	No	New (Chapter 7)
Upupa epops longirostris	Brown	537.249	25.395	0.590	410.327	22.470	0.838	1.315	2.599	100	No	No	New (Chapter 7)
Upupa epops saturina	Brown	485.986	50.356	2.742	304.346	17.938	0.180	1.639	3.102	100	No	No	New (Chapter 7)
Jacamerops aureus	Brown	330.796	16.676	0.448	255.840	15.979	0.358	1.301	1.443	100	No	No	New (Chapter 7)
Phoeniculus purpureus	Brown	662.650	50.123	1.091	320.174	17.167	0.641	2.196	1.093	100	No	No	New (Chapter 7)
Halcyon leucocephala	Brown	354.204	18.088	0.752	258.405	13.901	0.302	1.388	2.346	100	No	No	New (Chapter 7)
Selenidera piperivora	Brown	778.573	41.409	0.910	304.253	15.322	0.557	2.643	0.576	100	No	No	New (Chapter 7)
Coracius benghalensis	Brown	748.404	37.470	1.262	352.695	24.557	0.613	2.197	1.117	100	No	No	New (Chapter 7)
Dacelo novaeguineae	Brown	701.671	44.177	1.267	349.859	14.271	0.320	2.061	1.088	100	No	No	New (Chapter 7)
Dacelo novaeguineae	Brown	857.296	31.615	-0.415	255.404	13.585	0.553	3.425	-0.180	100	No	No	New (Chapter 7)
Dacelo novaeguineae	Brown	675.424	41.734	0.294	268.768	13.820	0.111	2.591	0.767	100	No	No	New (Chapter 7)
Cittura cyanosis	Brown	482.471	51.538	1.822	299.422	14.590	0.232	1.612	1.668	100	No	No	New (Chapter 7)
Merops nubicus	Brown	557.644	37.491	2.331	281.872	15.034	0.696	2.044	2.700	100	No	No	New (Chapter 7)
Chrysocolaptes validis	Brown	853.288	26.051	-0.341	212.106	15.878	0.898	4.171	-0.460	100	No	No	New (Chapter 7)
Chrysocolaptes validis	Brown	496.688	35.357	2.461	284.540	14.628	-0.017	1.820	2.870	100	No	No	New (Chapter 7)
Todus mexicanus	Brown	464.134	34.002	3.540	325.118	16.849	0.608	1.461	3.319	100	No	No	New (Chapter 7)
Campephilus rubricollis	Brown	597.364	16.002	0.716	372.915	20.418	0.825	1.639	1.193	100	No	No	New (Chapter 7)
Jynx ruficollis	Brown	552.349	24.906	1.774	368.187	15.865	0.671	1.529	3.211	100	No	No	New (Chapter 7)
Jynx torquilla	Brown	1219.351	18.229	0.089	212.835	11.145	0.431	5.811	0.341	100	No	No	New (Chapter 7)
Buceros hydrocorax	Brown	923.769	25.254	-0.444	291.919	12.956	0.696	3.232	-0.380	100	No	No	New (Chapter 7)
Buceros hydrocorax	Brown	522.747	34.429	2.107	282.062	12.977	0.540	1.874	2.638	100	No	No	New (Chapter 7)
Buceros hydrocorax	Brown	488.693	23.797	0.817	284.478	13.135	0.316	1.746	1.777	100	No	No	New (Chapter 7)
Sasia abnormis	Brown	427.506	19.827	2.295	318.599	16.588	0.981	1.352	1.169	100	No	No	New (Chapter 7)
Barypthengus ruficapillus	Brown	375.006	28.522	5.415	285.254	16.466	0.116	1.325	5.253	100	No	No	New (Chapter 7)
Barypthengus ruficapillus	Brown	320.852	15.722	0.569	256.028	13.221	0.090	1.256	0.909	100	No	No	New (Chapter 7)
Galbula ruficauda	Brown	303.273	14.742	0.074	217.781	15.859	0.568	1.407	0.187	100	No	No	New (Chapter 7)
Brachypteracias leptosomus	Brown	542.344	27.568	1.354	360.023	21.924	0.342	1.584	1.693	100	No	No	New (Chapter 7)
Clytoceyx rex	Brown	741.279	40.783	0.224	268.790	20.407	0.932	2.969	0.221	100	No	No	New (Chapter 7)
Clytoceyx rex	Brown	324.513	16.949	0.411	255.388	17.134	0.665	1.279	1.719	100	No	No	New (Chapter 7)
Hapaloptila castanea	Brown	292.449	31.013	7.500	222.764	15.717	0.168	1.322	8.210	100	No	No	New (Chapter 7)
Rhyticeros undulatus	Brown	634.504	24.370	0.836	409.577	19.579	0.184	1.591	1.221	100	No	No	New (Chapter 7)
Rhyticeros undulatus	Brown	626.633	27.123	1.205	408.420	18.135	0.358	1.578	2.300	100	No	No	New (Chapter 7)
Galbula albirostris	Brown	345.028	15.325	0.282	272.535	15.962	0.093	1.275	1.350	100	No	No	New (Chapter 7)
Collocalia esculenta	Brown	992.948	14.739	0.875	211.076	12.419	0.556	4.768	0.929	100	No	No	New (Chapter 8)
Hirundapus giganteus	Brown	1172.139	20.004	0.086	179.690	10.899	0.772	6.594	0.749	100	No	No	New (Chapter 8)
Collocalia esculenta	Brown	992.948	14.739	0.875	211.076	12.419	0.556	4.768	0.929	100	No	No	New (Chapter 8)
Hirundapus giganteus	Brown	1172.139	20.004	0.086	179.690	10.899	0.772	6.594	0.749	100	No	No	New (Chapter 8)
Hirundapus caudiculus	Brown	1134.168	21.929	0.105	171.083	13.345	1.730	6.745	0.047	100	No	No	New (Chapter 8)
Hirundapus caudiculus	Brown	1134.168	21.929	0.105	171.083	13.345	1.730	6.745	0.047	100	No	No	New (Chapter 8)
Caprimulgus andamanicus	Brown	995.162	20.689	0.028	201.974	12.222	0.135	4.996	0.225	100	No	No	New (Chapter 8)
Caprimulgus macrurus	Brown	1008.520	37.020	-0.382	226.077	19.202	1.150	4.734	-0.533	100	No	No	New (Chapter 8)
Batrachystomus austris	Brown	863.220	27.841	-0.234	283.685	15.353	0.199	3.085	-0.143	100	No	No	New (Chapter 8)
Caprimulgus donaldsoni	Brown	558.543	20.409	1.101	354.585	12.467	-0.078	1.597	1.089	100	No	No	New (Chapter 8)
Macropsalis creagra	Brown	583.472	21.908	0.955	352.666	16.995	0.511	1.687	1.296	100	No	No	New (Chapter 8)
Nyctibius grandis	Brown	853.533	24.052	0.043	216.646	16.403	1.590	4.065	-0.113	100	No	No	New (Chapter 8)
Nyctibius griseus	Brown	1325.766	17.803	0.506	246.507	14.278	0.739	5.454	0.683	100	No	No	New (Chapter 8)
Batrachystomus septimus	Brown	731.395	17.489	-0.022	291.898	14.711	0.357	2.542	-0.324	100	No	No	New (Chapter 8)
Caprimulgus fraenatus	Brown	1142.270	31.136	0.400	230.938	21.006	0.988	5.026	-0.593	100	No	No	New (Chapter 8)
Caprimulgus rufigena	Brown	1711.758	15.382	0.248	274.837	10.476	0.249	6.289	0.469	100	No	No	New (Chapter 8)
Macropsalis segmentata	Brown	977.080	34.769	-0.139	240.536	15.774	0.546	4.211	-0.323	100	No	No	New (Chapter 8)
Steatornis caripensis	Brown	864.279	25.253	-0.291	240.218	14.979	1.762	3.725	0.026	100	No	No	New (Chapter 8)
Batrachystomus septimus	Brown	522.202	31.109	1.324	304.203	15.881	0.364	1.743	1.751	100	No	No	New (Chapter 8)
Antrostomus rufous	Brown	859.425	17.953	0.435	208.990	11.434	1.744	4.151	-0.443	100	No	No	New (Chapter 8)
Caprimulgus longipennis	Brown	1276.461	22.102	0.711	213.020	13.051	0.328	6.033	0.729	100	No	No	New (Chapter 8)
Caprimulgus macrurus	Brown	971.115	24.120	-0.611	209.044	16.039	2.189	4.793	-0.777	100	No	No	New (Chapter 8)
Eurostopodus macrotis	Brown	653.489	45.208	0.309	207.718	14.340	0.433	3.235	0.420	100	No	No	New (Chapter 8)
Nyctibius aetherius	Brown	990.569	22.834	-0.065	236.949	15.744	1.162	4.302	-0.018	100	No	No	New (Chapter 8)
Nyctidromus albicollis	Brown	696.728	39.168	0.315	205.789	15.636	0.926	3.563	0.475	100	No	No	New (Chapter 8)
Nyctidromus albicollis	Brown	768.505	34.011	0.653	205.995	12.848	0.422	3.827	0.444	100	No	No	New (Chapter 8)
Steatornis caripensis	Brown	777.422	35.547	0.331	273.977	17.388	1.175	2.975	0.411	100	No	No	New (Chapter 8)
Batrachystomus auratus	Brown	505.331	29.546	2.037	300.332	17.514	0.342	1.722	3.512	100	No	No	New (Chapter 8)
Batrachystomus septimus	Brown	456.685	28.516	1.513	267.814	14.750	0.752	1.730	1.364	100	No	No	New (Chapter 8)
Batrachystomus stellatus	Brown	382.833	28.690	2.979	258.174	15.065	0.535	1.508	4.392	100	No	No	New (Chapter 8)
Caprimulgus asiaticus	Brown	450.383	41.566	1.552	231.766	17.824	0.465	2.003	1.962	100	No	No	New (Chapter 8)
Caprimulgus climacurus	Brown	483.717	30.173	1.803	282.110	18.283	0.961	1.784	1.857	100	No	No	New (Chapter 8)
Caprimulgus donaldsoni	Brown	563.571	44.934	1.919	288.987	16.081	0.280	2.050	2.486	100	No	No	New (Chapter 8)
Eurostopodus macrotis	Brown	391.003	25.763	0.905	240.947	18.408	0.755	1.654	2.250	100	No	No	New (Chapter 8)

Macropsalis creagra	Brown	551.875	51.617	1.613	249.214	21.422	0.887	2.270	1.358	100	No	No	New (Chapter 8)
Steatornis caripensis	Brown	568.838	37.127	1.509	243.513	19.273	0.909	2.450	1.810	100	No	No	New (Chapter 8)
Batrachystomus septimus	Brown	433.781	16.237	0.659	267.652	12.206	-0.016	1.640	1.329	100	No	No	New (Chapter 8)
Podargus papuensis	Brown	565.356	24.068	1.524	390.643	14.981	0.006	1.470	4.408	100	No	No	New (Chapter 8)
Podargus strigoides	Brown	626.842	40.614	2.807	368.945	17.577	0.483	1.778	3.314	100	No	No	New (Chapter 8)
Caprimulgus pectoralis	Brown	557.641	39.396	1.582	279.825	15.823	0.594	2.083	2.183	100	No	No	New (Chapter 8)
Amazilia amazilia	Brown	585.216	19.272	1.501	394.315	15.114	0.084	1.512	2.031	100	No	No	New (Chapter 8)
Amazilia fuscicaudata	Brown	571.702	25.662	1.465	348.116	19.443	0.433	1.713	1.725	100	No	No	New (Chapter 8)
Campylopterus falcatus	Brown	841.657	52.593	1.388	453.408	18.967	0.482	1.895	1.697	100	No	No	New (Chapter 8)
Colibri delphinae	Brown	832.136	53.654	1.199	341.617	22.617	0.598	2.668	1.237	100	No	Some	New (Chapter 8)
Glaucis hirsuta	Brown	739.949	53.332	1.673	343.566	24.242	0.100	2.334	1.954	100	No	Some	New (Chapter 8)
Lamprolaima rhami	Brown	714.857	38.873	1.059	461.087	31.542	0.681	1.553	2.266	53	No	No	New (Chapter 8)
Lophornis helenae	Brown	512.597	21.202	2.859	372.807	17.029	0.659	1.394	2.747	100	No	No	New (Chapter 8)
Lophornis stictolopha	Brown	663.401	20.859	2.213	457.591	16.780	0.551	1.475	2.196	100	No	No	New (Chapter 8)
Selasphorus sasia	Brown	795.902	22.570	1.340	460.370	16.642	-0.006	1.751	0.866	82	Uncertain	Yes	New (Chapter 8)
Chordeiles pusillus	Brown	994.807	48.468	0.173	265.974	14.708	0.361	3.830	0.273	100	No	No	New (Chapter 8)
Nyciphrynus ocellatus	Brown	817.109	38.781	-0.068	275.905	17.231	1.652	3.111	-0.112	100	No	No	New (Chapter 8)
Nyctibius jamaicensis	Brown	925.548	30.791	-0.383	203.225	13.938	1.213	4.684	-0.089	100	No	No	New (Chapter 8)
Psittacus erithacus	Grey	1596.797	19.146	-1.809	795.098	15.517	0.033	2.035	-0.260	100	No	No	Li et al. (2012)
Psittacus erithacus	Grey	1667.576	47.515	0.022	326.390	20.013	-0.143	5.000	0.178	100	No	No	Li et al. (2012)
Fulica americana	Grey	1202.240	44.128	-0.016	293.000	22.630	0.404	4.120	0.277	100	No	No	Li et al. (2012)
Falco sparverius	Grey	1681.060	38.485	0.282	574.653	31.891	1.354	2.700	-0.420	100	No	No	Li et al. (2012)
Synthliboramphus antiquus	Grey	1008.220	34.925	0.079	375.780	20.887	0.061	2.697	-0.458	100	No	No	Li et al. (2012)
Beija-Por-Frito-y-Blanco	Grey	1707.377	15.489	-0.616	516.160	16.872	-0.129	3.343	-0.900	100	No	No	Li et al. (2012)
Megaceryle alcyon	Grey	966.000	18.358	-0.732	280.125	13.458	0.785	3.489	0.259	100	No	No	Li et al. (2012)
Chlidonias niger	Grey	1214.000	45.116	0.290	343.333	21.385	-0.633	3.582	0.958	100	No	No	Li et al. (2012)
Coracina novaehollandiae	Grey	1332.536	32.327	-0.200	360.250	23.227	0.285	3.739	-0.234	100	No	No	Li et al. (2012)
Chroicocephalus philadelphia	Grey	1104.833	18.831	-0.608	612.667	15.363	-1.658	1.803	0.143	100	No	No	Li et al. (2012)
Callipepla californica	Grey	1656.845	26.084	0.263	574.726	21.463	1.364	3.000	-0.428	100	No	No	Li et al. (2012)
Alectoris chukar	Grey	1676.241	28.738	0.315	572.847	23.607	1.376	2.800	-0.419	100	No	No	Li et al. (2012)
Junco hyemalis	Grey	1686.945	25.868	0.320	580.347	21.546	1.346	2.800	-0.409	100	No	No	Li et al. (2012)
Ardea herodias	Grey	989.000	17.058	-0.369	217.200	57.164	5.137	4.600	-0.651	100	No	No	Li et al. (2012)
Dumetella carolinensis	Grey	663.100	54.223	0.565	378.100	36.883	-0.237	2.320	0.300	100	No	No	Li et al. (2012)
Ardea cinerea	Grey	1021.623	5.632	-0.075	222.340	2.716	0.255	4.609	1.241	100	No	No	Li et al. (2012)
Opisthocomus hoazin	Grey	951.363	7.942	0.211	218.053	9.590	0.325	2.708	0.702	100	No	No	Li et al. (2012)
Podiceps auritus	Grey	963.286	44.244	-0.476	327.743	52.768	0.226	3.028	-0.345	100	No	No	Li et al. (2012)
Passer domesticus	Grey	300.757	23.635	0.126	141.976	22.659	0.515	2.600	0.355	100	No	No	Li et al. (2012)
Lanius ludovicianus	Grey	407.200	60.481	-0.145	274.500	11.910	-0.237	2.710	0.864	100	No	No	Li et al. (2012)
Clangula hyemalis	Grey	562.280	37.564	0.521	207.488	24.582	0.523	2.710	1.638	100	No	No	Li et al. (2012)
Anas platyrhynchos	Grey	952.951	51.599	0.400	168.276	13.178	0.606	5.663	0.578	100	No	No	Li et al. (2012)
Colaptes auratus	Grey	1185.600	23.667	0.059	313.900	15.229	0.658	3.930	0.294	100	No	No	Li et al. (2012)
Mimus polyglottos	Grey	1691.822	22.157	-0.256	675.242	16.934	1.091	2.506	-0.143	100	No	No	Li et al. (2012)
Podilymbus podiceps	Grey	1705.192	38.049	-0.292	677.579	29.439	1.119	2.300	-0.101	100	No	No	Li et al. (2012)
Pinicola enucleator	Grey	1213.300	22.180	-0.706	252.200	15.799	0.607	4.800	-0.370	100	No	No	Li et al. (2012)
Porphyrio martinicus	Grey	1728.360	10.859	-0.299	299.577	15.402	0.460	5.892	0.378	100	No	No	Li et al. (2012)
Alca torda	Grey	1710.555	9.289	-0.639	523.363	10.393	-0.135	3.200	-0.127	100	No	No	Li et al. (2012)
Antigone canadensis	Grey	514.500	35.212	0.625	275.500	19.757	0.198	1.900	0.918	100	No	No	Li et al. (2012)
Porzana carolina	Grey	1494.345	18.587	0.678	284.103	17.317	-0.082	5.382	0.213	100	No	No	Li et al. (2012)
Egretta tricolor	Grey	1672.856	32.823	0.337	571.760	25.478	1.373	2.900	-0.475	100	No	No	Li et al. (2012)
Baeolophus bicolor	Grey	456.100	37.358	-0.157	283.000	42.509	0.072	1.700	0.532	100	No	No	Li et al. (2012)
Diomedea exulans	Grey	1688.713	24.810	-0.267	676.351	19.219	1.051	2.400	-0.112	100	No	No	Li et al. (2012)
Sitta carolinensis	Grey	1663.306	29.147	0.007	319.587	12.174	-0.181	5.205	0.695	100	No	No	Li et al. (2012)
Coccyzus americanus	Grey	1669.600	27.499	0.289	572.700	22.323	1.361	2.915	-0.452	100	No	No	Li et al. (2012)
Sasia Africana	Grey	1374.531	17.519	-0.452	412.694	19.455	1.053	3.392	-0.045	100	No	No	New (Chapter 7)
Halcyon pileata	Grey	1418.127	17.067	0.458	385.496	14.960	0.730	3.712	0.775	100	No	No	New (Chapter 7)
Halcyon pileata	Grey	1593.353	17.366	-0.033	430.593	18.438	0.314	3.767	0.303	100	No	No	New (Chapter 7)
Merops viridis	Grey	1601.716	18.047	0.180	469.686	15.241	-0.462	3.459	0.261	100	No	No	New (Chapter 7)
Electron platyrhynchum	Grey	958.336	12.528	0.224	333.101	13.407	0.596	2.912	-0.171	100	No	No	New (Chapter 7)
Electron platyrhynchum	Grey	1472.375	19.974	0.281	468.686	19.846	0.168	3.169	0.138	100	No	No	New (Chapter 7)
Eurystomus glaucurus	Grey	1560.608	16.349	0.153	366.439	12.751	2.900	4.319	0.280	100	No	No	New (Chapter 7)
Galbula leucogastra	Grey	1104.681	19.270	0.052	259.225	15.404	0.102	4.320	-0.145	100	No	No	New (Chapter 7)
Alcedo atthis	Grey	1691.672	16.617	0.314	618.917	16.030	0.148	2.784	0.650	100	No	No	New (Chapter 7)
Aulacorhynchus prasinus	Grey	1078.953	14.187	-0.045	318.719	8.833	0.443	3.405	-0.238	100	No	No	New (Chapter 7)
Upupa epops	Grey	1398.324	14.309	-0.357	277.867	9.488	-0.101	5.062	-0.265	100	No	No	New (Chapter 7)
Upupa epops	Grey	1717.854	21.060	-0.380	399.379	26.335	0.866	4.471	-0.356	100	No	No	New (Chapter 7)
Upupa epops	Grey	1883.663	13.477	0.654	546.377	19.416	0.698	3.554	0.722	100	No	No	New (Chapter 7)
Dendrocopos major	Grey	1134.116	25.059	2.161	282.825	19.878	2.660	4.030	0.202	100	No	No	New (Chapter 7)
Phoeniculus purpureus	Grey	1493.827	13.695	-1.173	315.063	10.952	0.107	4.795	-0.560	100	No	No	New (Chapter 7)
Selenidera piperivora	Grey	1483.353	15.742	0.265	382.717	10.530	0.394	3.908	-0.299	100	No	No	New (Chapter 7)
Coracias benghalensis	Grey	1207.020	20.667	0.635	239.737	13.678	1.470	5.124	0.206	100	No	No	New (Chapter 7)
Indicator exilis	Grey	1344.172	23.735	0.505	218.660	25.201	1.251	6.340	0.136	100	No	No	New (Chapter 7)
Tockus griseus	Grey	1032.818	14.425	0.215	316.428	9.129	0.797	3.283	0.077	100	No	No	New (Chapter 7)
Halcyon senegaloides	Grey	1167.847	13.500	-0.397	350.762	10.361	0.253	3.359	-0.135	100	No	No	New (Chapter 7)
Eurystomus orientalis	Grey	1172.960	17.666	-0.265	315.385	18.083	1.167	3.823	0.046	100	No	No	New (Chapter 7)
Todus mexicanus	Grey	1748.166	18.124	-0.531	398.643	16.100	0.041	4.416	0.568	100	No	No	New (Chapter 7)
Todus mexicanus	Grey	1229.969	14.834	-0.114	451.593	16.519	0.931	2.775	-0.256	100	No	No	New (Chapter 7)

Meropogon forsteni	Grey	1035.967	20.227	-0.011	301.782	15.858	0.276	3.484	0.462	100	No	No	New (Chapter 7)
Psilopogon rafflesii	Grey	1486.388	19.327	-0.175	339.831	14.949	0.803	4.392	0.398	100	No	No	New (Chapter 7)
Jynx ruficollis	Grey	1400.944	17.781	-0.062	421.906	11.606	0.104	3.336	0.183	100	No	No	New (Chapter 7)
Jynx torquilla	Grey	1806.287	17.213	0.342	383.768	18.445	-0.007	4.798	0.626	100	No	No	New (Chapter 7)
Jynx torquilla	Grey	1590.436	16.195	0.059	412.091	14.390	0.115	3.922	0.672	100	No	No	New (Chapter 7)
Buceros rhinoceros	Grey	1471.030	16.982	-0.431	343.426	9.882	-0.547	4.297	-0.021	100	No	No	New (Chapter 7)
Merops malimbicus	Grey	1104.873	22.691	1.505	257.647	11.526	1.597	4.327	1.009	100	No	No	New (Chapter 7)
Sasia abnormis	Grey	1026.381	28.874	-0.494	275.219	18.405	1.202	3.854	-0.643	100	No	No	New (Chapter 7)
Barypthengus ruficapillus	Grey	1329.704	20.099	0.284	385.663	11.544	0.306	3.461	0.433	100	No	No	New (Chapter 7)
Pelargopsis capensis	Grey	1852.013	15.433	-0.551	688.579	21.628	0.629	2.771	-0.003	100	No	No	New (Chapter 7)
Semnornis ramphastinus	Grey	1300.585	16.753	0.002	447.377	14.007	0.400	2.968	0.453	100	No	No	New (Chapter 7)
Syma torotoro	Grey	1201.463	26.432	0.303	324.260	32.756	1.000	3.805	-0.067	100	No	No	New (Chapter 7)
Monasa flavirostris	Grey	1422.682	24.870	0.956	268.822	7.272	-0.091	5.325	1.245	100	No	No	New (Chapter 7)
Hemiprocne longipennis	Grey	1693.323	15.173	0.352	466.161	18.002	0.777	3.704	1.781	100	Yes	Yes	New (Chapter 8)
Hemiprocne mystacea	Grey	1476.132	13.596	0.166	372.614	10.350	0.503	3.989	0.026	100	Yes	Yes	New (Chapter 8)
Apus pacificus	Grey	1269.891	23.375	0.405	203.967	12.391	1.101	6.332	0.694	100	No	No	New (Chapter 8)
Apus pacificus	Grey	1429.828	21.050	0.499	194.993	11.970	0.705	7.482	0.677	100	No	No	New (Chapter 8)
Apus pallidus	Grey	1467.613	26.536	-0.797	176.361	16.076	1.246	8.524	-0.710	100	No	No	New (Chapter 8)
Apus pallidus	Grey	1372.803	21.500	-0.401	194.086	13.014	0.798	7.177	-0.488	100	No	No	New (Chapter 8)
Cypsiurus parvus	Grey	1120.653	23.857	-0.090	167.118	19.820	1.426	6.943	-0.046	100	No	No	New (Chapter 8)
Nyctibius grisius	Grey	1036.422	18.163	0.547	243.458	11.462	0.180	4.308	0.553	100	No	No	New (Chapter 8)
Hydopsalis brasiliana	Grey	1416.997	23.537	0.105	233.936	12.537	0.609	6.150	0.011	100	No	No	New (Chapter 8)
Aegotheles cristatus	Grey	996.043	16.823	-0.428	271.672	13.822	1.511	3.752	0.343	100	No	No	New (Chapter 8)
Lamprolaima rhami	Grey	1478.080	16.828	0.554	453.292	15.266	0.795	3.304	0.759	49	Uncertain	Yes	New (Chapter 8)
Caprimulgus europeus	Grey	1488.621	26.294	-0.665	248.515	15.982	1.672	6.145	-0.880	100	No	No	New (Chapter 8)
Nyctibius grandis	Grey	1303.922	14.934	0.206	243.239	10.649	0.155	5.406	0.757	100	No	No	New (Chapter 8)
Aphantochroa cirrochloris	Grey	1608.809	13.679	0.349	447.255	21.419	1.628	3.692	0.398	67	Yes	Yes	New (Chapter 8)
Campylopterus largipennis	Grey	1361.018	14.228	-0.095	287.104	19.208	0.488	4.863	0.678	100	Uncertain	Most	New (Chapter 8)
Colibri delphinae	Grey	1976.861	17.385	0.628	366.570	22.306	0.341	5.564	0.276	34	Yes	Yes	New (Chapter 8)
Lapornis amethystinus	Grey	1456.156	17.653	0.023	394.807	19.297	0.058	3.768	1.032	100	Yes	Yes	New (Chapter 8)
Podargus strigoides	Grey	1143.037	20.759	-0.300	313.374	15.305	2.183	3.750	-0.120	100	No	No	New (Chapter 8)
Hemiprocne comata	Grey	1236.345	15.763	0.886	373.104	11.770	0.468	3.331	1.088	100	Yes	Yes	New (Chapter 8)
Anthracothorax sp	Grey (down)	1335.576	16.657	-0.358	356.047	23.311	0.587	3.880	0.877	100	Uncertain	Yes	New (Chapter 8)
Colibri serrirostris	Grey (down)	1538.474	15.288	0.214	311.297	13.630	-0.078	5.029	1.262	100	No	No	New (Chapter 8)
Damophila julie	Grey (down)	1342.328	14.437	0.572	395.065	21.009	0.277	3.515	0.828	100	Some	Most	New (Chapter 8)
Doryfera ludoviciae	Grey (down)	1526.712	15.342	0.344	357.245	18.685	0.746	4.390	0.901	100	No	Few	New (Chapter 8)
Florisugo mellivora	Grey (down)	1678.109	12.695	-0.052	417.352	15.247	-0.208	4.089	0.620	100	Yes	Most	New (Chapter 8)
Stephanoxis lalandi	Grey (down)	1532.372	14.344	0.384	368.099	21.500	0.773	4.306	1.046	100	Yes	Most	New (Chapter 8)
Hemiprocne mystacea	Grey (down)	1453.871	11.666	0.206	502.229	12.487	-0.204	2.920	0.218	100	No	No	New (Chapter 8)
Caprimulgus andamanicus	Grey (down)	1801.550	20.359	0.147	301.595	13.595	-0.368	6.027	0.389	100	No	No	New (Chapter 8)
Caprimulgus asiaticus	Grey (down)	1824.308	17.643	-0.120	410.183	11.272	-0.212	4.485	0.453	100	No	No	New (Chapter 8)
Caprimulgus donaldsoni	Grey (down)	2285.015	16.045	0.501	525.745	12.422	-0.291	4.386	1.223	100	No	No	New (Chapter 8)
Caprimulgus europeus	Grey (down)	2115.905	17.296	0.659	328.062	11.371	0.035	6.522	1.095	100	No	No	New (Chapter 8)
Caprimulgus europeus	Grey (down)	2113.428	21.929	-0.114	392.524	16.919	0.203	5.447	0.163	100	No	No	New (Chapter 8)
Caprimulgus indicus	Grey (down)	1613.650	21.055	0.197	295.892	18.985	0.408	5.533	0.028	100	No	No	New (Chapter 8)
Caprimulgus macrurus	Grey (down)	1724.794	21.796	0.098	294.797	13.240	-0.482	5.891	0.583	100	No	No	New (Chapter 8)
Caprimulgus vexillarius	Grey (down)	1942.549	18.276	-0.100	332.971	12.065	0.627	5.895	0.438	100	No	No	New (Chapter 8)
Caprimulgus yorki	Grey (down)	1765.003	17.648	-0.207	296.677	14.512	0.555	6.026	0.059	100	No	No	New (Chapter 8)
Nyctidromus albicollis	Grey (down)	1760.946	17.994	0.064	340.169	12.288	0.123	5.221	-0.227	100	No	No	New (Chapter 8)
Podargus strigoides	Grey (down)	1545.452	16.913	1.833	531.184	11.416	0.649	2.931	2.064	100	No	No	New (Chapter 8)
Macropsalis creagra	Grey (down)	1600.392	18.321	0.529	317.298	13.352	1.044	5.067	0.581	100	No	No	New (Chapter 8)
Nyciphrynus ocellatus	Grey (down)	1381.893	20.262	0.730	406.048	13.869	0.504	3.435	0.762	100	No	No	New (Chapter 8)
Amazilia tabaci	Grey (down)	1578.530	15.626	0.548	333.073	17.790	0.498	4.848	0.331	100	No	Few	New (Chapter 8)
Clytolaema rubricauda	Grey (down)	1352.578	15.265	0.673	389.433	16.651	-0.069	3.540	0.714	100	Yes	Yes	New (Chapter 8)
Colibri delphinae	Grey (down)	1503.064	19.829	0.051	316.236	16.297	0.512	4.822	0.125	100	No	Few	New (Chapter 8)
Colibri delphinae	Grey (down)	1584.108	19.252	0.088	371.720	18.410	0.399	4.342	0.335	100	No	No	New (Chapter 8)
Heliodoxa rubinoides	Grey (down)	1386.240	14.095	0.140	475.234	19.537	0.581	2.998	1.312	100	Yes	Yes	New (Chapter 8)
Lophornis verreauxi	Grey (down)	1308.961	15.214	0.716	273.987	17.335	0.489	4.893	1.016	100	No	No	New (Chapter 8)
Threnetes cervinicauda	Grey (down)	1465.249	17.067	0.124	403.520	17.446	0.201	3.664	0.933	71	No	No	New (Chapter 8)
Nyctibius griseus	Grey (down)	1231.091	11.980	0.213	321.179	11.943	-0.153	3.888	0.797	100	No	No	New (Chapter 8)
Florisugo mellivora	Iridescent	1906.744	12.710	0.379	626.783	18.071	0.869	3.091	0.423	100	Yes	Yes	New (Chapter 8)
Amazilia tabaci	Iridescent	1155.580	12.834	0.453	447.392	24.139	0.234	2.703	1.032	100	Yes	Yes	New (Chapter 8)
Amazilia tabaci	Iridescent	1379.827	17.082	-0.991	475.726	28.621	-0.087	3.105	1.362	100	Yes	Yes	New (Chapter 8)
Threnetes cervinicauda	Iridescent	2016.686	11.585	-0.227	753.443	16.613	-0.150	2.712	0.567	100	Yes	Yes	New (Chapter 8)
Glaucis hirsuta	Iridescent	2051.958	16.201	0.100	688.445	19.058	-0.009	3.017	0.481	100	Yes	Yes	New (Chapter 8)
Rhamphodon naevius	Iridescent	1728.192	14.752	0.347	601.677	19.566	0.317	2.924	0.635	100	Yes	Yes	New (Chapter 8)
Anthracothorax nigricollis	Iridescent	1897.144	15.794	1.469	651.037	19.622	1.726	2.946	0.201	100	Yes	Yes	New (Chapter 8)
Campylopterus hemileurus	Iridescent	1321.948	12.346	0.282	451.655	16.789	0.276	2.978	0.673	100	Yes	Yes	New (Chapter 8)
Colibri delphinae	Iridescent	1999.547	12.709	0.550	737.154	13.350	0.649	2.727	0.460	100	Yes	Yes	New (Chapter 8)
Lophornis verreauxi	Iridescent	1366.307	14.983	0.108	512.849	26.107	0.167	2.780	1.227	100	Yes	Yes	New (Chapter 8)
Campylopteryus largipennis	Iridescent	1565.222	13.543	0.135	584.207	17.651	0.051	2.720	0.978	100	Yes	Yes	New (Chapter 8)
Colibri serrirostris	Iridescent	3237.903	11.649	-0.016	1440.872	12.565	-0.235	2.260	0.432	100	Yes	Yes	New (Chapter 8)
Doryfera ludoviciae	Iridescent	2249.601	15.302	0.552	941.149	21.072	-0.476	2.462	2.534	100	Yes	Yes	New (Chapter 8)
Phaethornis yaruigui	Iridescent	1654.806	14.055	0.688	606.440	20.300	0.590	2.777	0.842	100	Yes	Yes	New (Chapter 8)
Amazilia tobaci	Iridescent	1700.297	18.674	0.615	683.890	24.475	0.768	2.531	-0.005	100	Yes	Yes	New (Chapter 8)
Florisugo mellivora	Iridescent	1894.890	20.751	0.384	691.505	26.182	0.526	2.794	0.112	100	Yes	Yes	New (Chapter 8)

Florisuga fuscus	Iridescent	1488.164	11.012	0.689	514.001	17.081	0.608	2.946	0.240	100	Yes	Yes	New (Chapter 8)
Anthracothorax sp	Iridescent	1817.324	20.480	0.351	663.274	27.713	0.228	2.825	1.119	100	Yes	Yes	New (Chapter 8)
Cyanophaia bicolor	Iridescent	1571.293	17.245	1.438	568.658	20.096	1.206	2.812	0.690	100	Yes	Yes	New (Chapter 8)
Topaza pella	Iridescent	1943.245	14.581	0.348	717.012	18.178	0.511	2.745	-0.183	100	Yes	Yes	New (Chapter 8)
Melanerpes formicivorus	Iridescent	1253.200	20.204	0.237	248.900	16.874	0.584	5.100	0.416	100	No	No	Li et al. (2012)
Fulica americana	Iridescent	1688.400	9.130	-0.006	262.800	12.027	-0.261	6.452	-0.247	100	No	No	Li et al. (2012)
Tetrao tetrix	Iridescent	940.838	23.795	-0.010	215.530	45.890	3.283	4.821	-0.389	100	No	No	Li et al. (2012)
Amazonetta brasiliensis	Iridescent	1079.833	11.305	-0.272	140.751	8.394	0.357	7.858	0.700	100	No	No	Li et al. (2012)
Quiscalus quiscula	Iridescent	628.421	12.752	0.362	134.105	14.507	-0.199	4.686	-0.385	100	No	No	Li et al. (2012)
Quiscalus quiscula	Iridescent	1222.300	13.516	-0.213	265.300	7.116	0.179	4.500	0.390	100	No	No	Li et al. (2012)
Corvus corax	Iridescent	1222.300	20.077	-0.225	266.300	11.040	0.179	4.600	0.390	100	No	No	Li et al. (2012)
Anas crecca	Iridescent	1174.219	26.827	1.051	215.256	26.989	-1.201	5.880	1.551	100	No	No	Li et al. (2012)
Rollulus rouloul	Iridescent	1062.997	16.083	1.753	234.046	17.926	1.244	4.727	2.582	100	No	No	Li et al. (2012)
Rollulus rouloul	Iridescent	1324.622	12.000	-0.069	218.882	7.418	-0.445	6.008	0.460	100	No	No	Li et al. (2012)
Priotelus temnurus	Iridescent	1072.746	18.437	-0.033	202.798	24.052	0.704	5.058	1.960	100	No	No	Li et al. (2012)
Chrysococcyx caprius	Iridescent	662.144	18.199	1.202	100.894	22.270	2.332	6.793	0.942	100	No	No	Li et al. (2012)
Phalacrocorax auritus	Iridescent	1127.023	11.213	1.440	268.642	10.704	-0.171	4.195	0.920	100	No	No	Li et al. (2012)
Ptiloris intercedens	Iridescent	1088.082	30.115	2.076	146.557	27.480	0.249	7.732	1.251	100	No	No	Li et al. (2012)
Ducula concinna	Iridescent	842.764	19.237	0.501	200.596	15.599	-0.035	4.315	0.609	100	No	No	Li et al. (2012)
Pica	Iridescent	1242.625	13.891	-1.053	317.833	9.912	-0.133	3.910	-0.249	100	No	No	Li et al. (2012)
Sturnus vulgaris	Iridescent	1098.236	23.007	0.039	199.034	19.770	-0.561	5.725	1.605	100	No	No	Li et al. (2012)
Corvus ossifragus	Iridescent	1102.200	22.313	-0.706	220.200	21.135	0.521	5.000	-0.268	100	No	No	Li et al. (2012)
Plegadis falcinellus	Iridescent	1313.474	10.631	-0.132	211.746	8.202	-0.455	6.001	-0.175	100	No	No	Li et al. (2012)
Quiscalus mexicanus	Iridescent	1101.368	21.765	0.070	192.579	17.249	-0.519	5.719	1.555	100	No	No	Li et al. (2012)
Phasianus versicolor	Iridescent	1440.918	18.833	-0.862	209.907	11.865	-1.099	6.944	-0.535	100	No	No	Li et al. (2012)
Astrapia rothschildi	Iridescent	902.308	25.853	-0.791	126.515	23.449	0.748	7.244	-0.240	100	No	No	Li et al. (2012)
Tauraco corythaix	Iridescent	1239.514	11.524	-0.234	270.233	5.232	0.141	4.609	0.408	100	No	No	Li et al. (2012)
Grallina cyanoleuca	Iridescent	998.200	23.468	0.268	209.320	32.159	-0.091	4.800	1.196	100	No	No	Li et al. (2012)
Anas platyrhynchos	Iridescent	951.731	28.817	0.431	162.197	9.442	0.597	5.668	0.607	100	No	No	Li et al. (2012)
Anas platyrhynchos	Iridescent	1011.571	15.793	0.176	169.000	19.441	0.306	5.986	0.355	100	No	No	Li et al. (2012)
Caloenas nicobarica	Iridescent	751.543	12.038	-0.285	216.492	46.360	3.563	3.796	-1.870	100	No	No	Li et al. (2012)
Pavo cristatus	Iridescent	1739.818	25.720	-0.371	296.136	38.251	0.446	5.884	0.392	100	No	No	Li et al. (2012)
Porphyrio martinicus	Iridescent	1986.800	8.281	-0.553	231.600	15.866	-0.456	8.579	0.121	100	No	No	Li et al. (2012)
Progne subis	Iridescent	952.804	31.116	1.110	169.306	29.933	1.908	5.482	0.897	100	No	No	Li et al. (2012)
Dives warczewiczi	Iridescent	1233.133	12.571	-0.181	263.133	6.741	0.132	4.686	0.300	100	No	No	Li et al. (2012)
Lophorina superba	Iridescent	1094.599	28.589	2.035	149.663	24.862	0.277	7.730	1.293	100	No	No	Li et al. (2012)
Tachycineta bicolor	Iridescent	936.800	49.474	1.099	171.100	47.346	1.947	5.475	0.900	100	No	No	Li et al. (2012)
Cathartes aura	Iridescent	1326.750	9.479	0.278	184.250	12.623	0.675	7.255	0.398	100	No	No	Li et al. (2012)
Aix sponsa	Iridescent	1177.345	17.514	1.068	210.134	17.652	-1.229	5.882	1.137	100	No	No	Li et al. (2012)
Galbula leucogastra	Iridescent	980.752	12.381	-0.286	182.773	7.328	0.539	5.404	-0.061	100	No	No	New (Chapter 7)
Jacamerops aureus	Iridescent	1206.524	14.442	-0.472	151.828	7.641	-0.181	8.010	-0.235	100	No	No	New (Chapter 7)
Jacamerops aureus	Iridescent	1183.913	13.763	0.334	154.688	6.523	-0.026	7.693	0.488	100	No	No	New (Chapter 7)
Jacamerops aureus	Iridescent	1130.499	15.094	0.236	150.798	7.775	-0.028	7.553	-0.202	100	No	No	New (Chapter 7)
Galbula dea	Iridescent	771.953	11.956	0.032	187.573	8.918	1.763	4.146	-0.082	100	No	No	New (Chapter 7)
Galbula ruficauda	Iridescent	959.604	10.822	-0.620	161.883	7.112	0.775	5.967	-0.511	100	No	No	New (Chapter 7)
Hemiprocne longipennis	Iridescent	1256.642	12.460	0.193	392.771	17.731	0.431	3.261	0.700	100	Yes	Yes	New (Chapter 8)
Hemiprocne longipennis	Iridescent	1320.408	13.437	0.137	397.024	12.034	0.531	3.351	0.346	100	Yes	Yes	New (Chapter 8)
Hemiprocne longipennis	Iridescent	1230.897	14.604	0.714	355.035	13.235	0.557	3.492	0.497	100	Yes	Yes	New (Chapter 8)
Hemiprocne mystacea	Iridescent	1292.700	15.116	0.029	355.776	10.965	0.016	3.658	0.392	100	Yes	Yes	New (Chapter 8)
Collocalia esculenta	Iridescent	1178.473	19.728	0.359	185.019	10.888	0.097	6.446	0.247	100	No	No	New (Chapter 8)
Collocalia esculenta	Iridescent	1062.403	16.773	-0.061	166.878	8.012	0.255	6.406	0.022	100	No	No	New (Chapter 8)
Mearnsia picina	Iridescent	1059.488	16.407	0.365	183.964	11.726	1.026	5.817	0.313	100	No	No	New (Chapter 8)
Mearnsia picina	Iridescent	1058.472	18.738	0.055	190.325	15.426	1.399	5.659	0.224	100	No	No	New (Chapter 8)
Collocalia esculenta	Iridescent	1178.473	19.728	0.359	185.019	10.888	0.097	6.446	0.247	100	No	No	New (Chapter 8)
Collocalia esculenta	Iridescent	1062.403	16.773	-0.061	166.878	8.012	0.255	6.406	0.022	100	No	No	New (Chapter 8)
Mearnsia picina	Iridescent	1059.488	16.407	0.365	183.964	11.726	1.026	5.817	0.313	100	No	No	New (Chapter 8)
Mearnsia picina	Iridescent	1058.472	18.738	0.055	190.325	15.426	1.399	5.659	0.224	100	No	No	New (Chapter 8)
Collocalia esculenta	Iridescent	1238.491	16.760	0.398	206.073	13.699	1.458	6.087	0.049	100	No	No	New (Chapter 8)
Collocalia esculenta	Iridescent	1238.491	16.760	0.398	206.073	13.699	1.458	6.087	0.049	100	No	No	New (Chapter 8)
Stephanoxis lalandi	Iridescent	1518.498	18.642	1.692	484.979	20.424	1.212	3.170	0.680	100	Yes	Yes	New (Chapter 8)
Campylopterus hemileurus	Iridescent	1749.861	22.386	0.725	628.484	24.899	0.347	2.828	0.303	100	Yes	Yes	New (Chapter 8)
Damophila julie	Iridescent	1575.146	18.208	1.112	579.049	16.969	1.004	2.728	0.172	100	Yes	Yes	New (Chapter 8)
Thalurania furcata	Iridescent	1412.296	17.282	1.627	484.371	19.397	1.730	2.961	0.572	100	Yes	Yes	New (Chapter 8)
Lamprolaima rhami	Iridescent	1765.393	19.242	0.540	679.980	21.010	0.533	2.630	0.325	100	Yes	Yes	New (Chapter 8)
Topaza pella	Iridescent	1778.129	16.344	0.372	608.016	17.751	0.535	2.944	0.508	100	Yes	Yes	New (Chapter 8)
Pygoscelis adeliae	Penguin	914.500	12.847	-0.546	411.286	7.899	-0.506	2.241	0.621	100	No	No	Li et al. (2012)
Spheniscus demersus	Penguin	761.375	15.905	1.127	458.125	10.248	0.962	1.707	-0.796	100	No	No	Li et al. (2012)
Pygoscelis antarcticus	Penguin	832.417	9.498	0.598	507.833	10.127	0.103	1.657	-0.286	100	No	No	Li et al. (2012)
Pygoscelis antarcticus	Penguin	931.000	5.920	-1.211	314.833	4.749	0.448	2.966	-0.189	100	No	No	Li et al. (2012)
Pygoscelis antarcticus	Penguin	1036.833	15.085	-0.280	354.917	15.574	0.162	2.990	-0.651	100	No	No	Li et al. (2012)
Eudyptula minor	Penguin	841.905	13.195	0.392	468.714	14.708	0.190	1.834	0.996	100	No	No	Li et al. (2012)
Aptenodytes forsteri	Penguin	956.263	10.352	0.572	326.632	12.615	1.184	2.976	-0.188	100	No	No	Li et al. (2012)
Aptenodytes forsteri	Penguin	1035.714	14.830	-0.515	371.000	12.573	0.341	2.811	0.475	100	No	No	Li et al. (2012)
Spheniscus mendiculus	Penguin	892.889	24.822	-0.144	351.778	11.081	0.174	2.606	-1.410	100	No	No	Li et al. (2012)
Spheniscus humboldti	Penguin	1047.071	11.327	-0.885	319.000	9.614	0.028	3.323	0.178	100	No	No	Li et al. (2012)
Aptenodytes patagonicus	Penguin	1005.900	16.604	1.896	285.400	15.341	1.868	3.566	0.361	100	No	No	Li et al. (2012)

Eudyptula minor	Penguin	806.896	15.438	0.591	517.965	13.472	0.314	1.605	1.950	100	No	No	Li et al. (2012)
Eudyptula minor	Penguin	840.588	13.421	0.001	507.412	12.477	0.558	1.692	-0.520	100	No	No	Li et al. (2012)
Eudyptes chrysolophus	Penguin	870.200	20.696	-0.229	534.233	27.667	1.585	1.671	0.283	100	No	No	Li et al. (2012)
Eudyptes chrysolophus	Penguin	758.316	11.177	0.465	529.895	8.095	0.785	1.451	-0.422	100	No	No	Li et al. (2012)
Spheniscus magellanicus	Penguin	1206.857	9.038	0.044	378.214	9.440	0.533	3.234	0.213	100	No	No	Li et al. (2012)
Spheniscus magellanicus	Penguin	1028.556	11.468	-0.339	399.000	7.616	0.265	2.611	-0.474	100	No	No	Li et al. (2012)
Eudyptes chrysocome	Penguin	800.688	12.702	-0.060	543.625	9.066	0.584	1.489	-1.950	100	No	No	Li et al. (2012)
FOSSILS													
Caudipteryx 1a moulds	Unknown	1220.179	15.095	0.802	309.307	10.210	0.752	3.986	1.381	28	No	No	New (Chapter 5)
Caudipteryx 1b moulds	Unknown	734.262	27.700	0.725	394.279	18.690	-0.033	1.982	1.189	100	No	No	New (Chapter 5)
Caudipteryx 2 moulds	Unknown	936.172	25.091	0.245	312.904	17.933	1.182	3.086	-0.148	100	No	No	New (Chapter 5)
Caudipteryx 3 moulds	Unknown	930.816	26.516	0.191	337.324	19.535	0.809	2.914	-0.042	100	No	No	New (Chapter 5)
Caudipteryx 5 moulds	Unknown	1039.417	28.383	-0.470	298.979	17.439	1.004	3.557	-0.765	94	No	No	New (Chapter 5)
Caudipteryx 5 3D	Unknown	805.711	28.362	-0.299	236.674	17.397	1.398	3.529	-0.308	100	No	No	New (Chapter 5)
Caudipteryx 6 moulds	Unknown	1148.335	19.192	0.144	299.893	15.969	0.660	3.920	0.463	100	No	No	New (Chapter 5)
Caudipteryx 7 3D	Unknown	949.927	28.320	0.049	272.765	12.422	0.037	3.511	0.059	100	No	No	New (Chapter 5)
Caudipteryx 8 3D	Unknown	895.516	28.190	0.086	269.686	16.850	0.997	3.410	0.455	100	No	No	New (Chapter 5)
Caudipteryx 9 moulds	Unknown	990.452	23.306	-0.268	316.701	14.294	1.106	3.197	-0.681	100	No	No	New (Chapter 5)
Caudipteryx 10 3D	Unknown	467.671	28.090	0.865	331.224	23.989	1.505	1.472	1.889	100	No	No	New (Chapter 5)
Caudipteryx 11 3D	Unknown	597.170	26.893	1.340	386.111	17.478	0.165	1.596	2.105	100	No	No	New (Chapter 5)
Caudipteryx 12 moulds	Unknown	657.953	25.386	0.849	393.899	19.817	0.314	1.723	1.491	100	No	No	New (Chapter 5)
Caudipteryx 12 3D	Unknown	624.979	22.154	1.010	388.918	17.137	0.395	1.631	1.399	100	No	No	New (Chapter 5)
Caudipteryx 13 3D	Unknown	769.884	28.007	0.469	317.491	16.446	1.139	2.516	0.476	100	No	No	New (Chapter 5)
Caudipteryx 15 moulds	Unknown	765.351	34.009	0.397	294.273	19.054	0.517	2.747	0.542	27	No	No	New (Chapter 5)
Caudipteryx 15 3D	Unknown	862.570	25.799	-1.076	314.325	18.112	0.184	2.895	-0.446	10	No	No	New (Chapter 5)
Caudipteryx 16 3D	Unknown	653.694	37.441	1.385	314.501	18.120	0.520	2.196	1.523	100	No	No	New (Chapter 5)
Caudipteryx 17 moulds	Unknown	628.967	24.182	1.289	375.972	21.077	0.001	1.769	2.074	25	No	No	New (Chapter 5)
Caudipteryx 17 3D	Unknown	576.737	23.881	1.254	343.713	16.937	0.212	1.749	1.461	100	No	No	New (Chapter 5)
Messelirrisor 1	Unknown	926.859	0.106	0.493	258.451	0.113	0.118	3.623	0.658	6	No	No	New (Chapter 7)
Messelirrisor 5	Unknown	952.135	21.075	-0.437	213.376	12.676	0.937	4.478	0.237	21	No	No	New (Chapter 7)
Messelirrisor 7	Unknown	1293.177	13.036	-0.114	387.416	10.024	-0.177	3.361	0.099	86	No	No	New (Chapter 7)
Messelirrisor 8	Unknown	1286.025	19.491	-0.165	382.855	16.182	0.491	3.384	-0.099	57	No	No	New (Chapter 7)
Messelirrisor 9	Unknown	918.571	23.414	0.366	221.493	13.126	0.879	4.167	0.373	97	No	No	New (Chapter 7)
Messelirrisor 15	Unknown	1572.170	17.162	-0.236	422.378	16.987	-0.573	3.780	1.015	34	No	No	New (Chapter 7)
Messelirrisor 17	Unknown	1242.481	28.902	0.716	307.265	23.010	1.435	4.057	1.309	67	No	No	New (Chapter 7)
Messelirrisor 18	Unknown	1159.056	16.847	0.518	303.507	12.668	0.695	3.842	-0.158	141	No	No	New (Chapter 7)
Messelirrisor 19	Unknown	1429.851	17.410	0.760	514.737	13.758	0.101	2.806	0.133	116	No	No	New (Chapter 7)
Messelirrisor 20	Unknown	1418.594	14.294	-0.193	471.657	11.631	0.154	3.026	-0.369	61	No	No	New (Chapter 7)
Messelirrisor 22	Unknown	978.031	16.672	0.316	209.522	16.044	0.967	4.725	1.198	32	No	No	New (Chapter 7)
Messelirrisor 23	Unknown	1572.684	18.093	-1.880	487.083	11.123	-0.790	3.217	-0.763	19	No	No	New (Chapter 7)
Messelirrisor 29	Unknown	1673.404	17.946	-0.426	440.822	12.418	0.084	3.805	-0.266	102	No	No	New (Chapter 7)
Messelirrisor 31	Unknown	1532.450	19.003	-0.427	424.554	17.039	0.429	3.675	0.532	103	No	No	New (Chapter 7)
Messelirrisor 32	Unknown	1060.088	22.550	-0.648	279.105	12.938	1.364	3.836	-0.590	55	No	No	New (Chapter 7)
Messelirrisor 33	Unknown	1553.335	23.729	-0.083	384.402	20.399	-0.122	4.064	0.686	26	No	No	New (Chapter 7)
Messelirrisor 34	Unknown	1137.743	14.528	-0.838	298.339	7.880	0.064	3.837	0.647	9	No	No	New (Chapter 7)
Messelirrisor 35	Unknown	1071.972	2.879	-0.706	251.221	5.718	-0.195	4.279	-1.215	7	No	No	New (Chapter 7)
Messelirrisor 36	Unknown	1339.998	18.776	0.757	375.726	15.225	0.633	3.586	0.368	105	No	No	New (Chapter 7)
Messelirrisor 37	Unknown	1291.934	20.739	-0.863	329.627	12.841	-0.125	3.950	-0.223	35	No	No	New (Chapter 7)
Messelirrisor 38	Unknown	926.080	20.720	-0.756	204.303	15.602	0.296	4.592	-0.434	31	No	No	New (Chapter 7)
Hassiavis 1	Unknown	1372.529	9.647	-0.196	250.070	17.492	1.675	5.597	0.729	3	No	No	New (Chapter 8)
Hassiavis 2	Unknown	772.231	38.495	0.867	300.150	18.908	0.181	2.700	0.848	44	No	No	New (Chapter 8)
Hassiavis 4	Unknown	801.963	27.339	0.216	250.353	15.967	2.307	3.239	0.410	26	No	No	New (Chapter 8)
Hassiavis 8	Unknown	895.015	20.335	0.094	263.022	15.559	1.484	3.447	0.680	34	No	No	New (Chapter 8)
Hassiavis 9	Unknown	799.772	26.246	-0.394	245.532	13.264	0.363	3.268	-0.392	21	No	No	New (Chapter 8)
Hassiavis 10	Unknown	1013.353	18.989	-0.003	254.807	9.964	1.018	4.026	-0.017	21	No	No	New (Chapter 8)
Hassiavis 12*a*	Unknown	956.943	26.879	-0.641	247.649	12.186	-0.213	3.898	0.569	27	No	No	New (Chapter 8)
Hassiavis 12*b*	Unknown	1150.681	18.001	0.493	239.236	11.965	1.334	4.849	0.687	108	No	No	New (Chapter 8)
Hassiavis 13	Unknown	1510.563	17.233	1.110	452.839	13.789	0.025	3.371	0.472	119	No	No	New (Chapter 8)
Hassiavis 14	Unknown	1420.237	17.245	-0.842	462.304	13.704	1.913	3.133	-0.776	179	No	No	New (Chapter 8)
Hassiavis 16	Unknown	1376.600	15.473	-0.017	366.498	13.168	-0.414	3.801	0.576	190	No	No	New (Chapter 8)
Hassiavis 17	Unknown	1351.014	23.231	-0.374	475.779	15.506	0.078	2.843	0.426	58	No	No	New (Chapter 8)
Hassiavis 18	Unknown	1338.808	21.671	-0.539	437.408	8.858	-0.131	3.057	-0.505	13	No	No	New (Chapter 8)
Hassiavis 23	Unknown	1275.683	25.738	-0.389	413.862	13.107	0.097	3.090	-0.033	102	No	No	New (Chapter 8)
Hassiavis 24	Unknown	1301.359	24.270	-0.257	416.431	15.629	0.451	3.130	0.110	204	No	No	New (Chapter 8)
Hassiavis 25	Unknown	1094.716	29.852	-0.161	382.522	15.730	0.326	2.850	0.009	86	No	No	New (Chapter 8)
Hassiavis 26	Unknown	1274.400	24.139	-0.166	468.981	16.667	0.220	2.746	0.043	195	No	No	New (Chapter 8)
Hassiavis 27	Unknown	1443.424	23.154	0.056	368.688	14.961	0.640	3.960	-0.047	105	No	No	New (Chapter 8)
Masillapodargus 28	Unknown	976.740	23.371	0.054	249.887	16.078	0.451	4.016	0.060	187	No	No	New (Chapter 8)
Masillapodargus 29	Unknown	1115.919	20.799	0.013	285.539	15.205	0.126	3.971	0.030	128	No	No	New (Chapter 8)
Masillapodargus 30	Unknown	1144.496	17.492	-0.050	311.526	12.357	0.178	3.715	0.193	148	No	No	New (Chapter 8)
Masillapodargus 31	Unknown	1160.794	20.349	-0.273	344.877	10.553	2.492	3.396	-0.378	39	No	No	New (Chapter 8)
Masillapodargus 32	Unknown	1247.084	19.935	-0.370	313.612	9.820	0.062	3.973	-0.270	113	No	No	New (Chapter 8)
Masillapodargus 33	Unknown	1135.665	16.062	-0.350	318.875	10.716	-0.015	3.591	0.400	116	No	No	New (Chapter 8)
Masillapodargus 34	Unknown	886.273	28.578	0.205	232.033	13.069	0.528	3.860	0.456	37	No	No	New (Chapter 8)
Masillapodargus 35	Unknown	1255.595	19.713	-0.284	386.358	8.094	-1.149	3.278	-0.429	12	No	No	New (Chapter 8)
Masillapodargus 36	Unknown	1256.496	19.099	0.185	379.885	15.948	-0.718	3.359	0.825	201	No	No	New (Chapter 8)

Masillapodargus 38	Unknown	1290.613	15.591	-0.516	395.378	10.571	0.305	3.289	-0.694	141	No	No	New (Chapter 8)
Masillapodargus 39	Unknown	1249.139	15.846	0.368	353.434	22.158	0.195	3.665	0.637	256	No	No	New (Chapter 8)
Masillapodargus 40	Unknown	1338.323	16.386	-0.305	389.563	10.267	0.052	3.463	0.071	223	No	No	New (Chapter 8)
Masillapodargus 42	Unknown	1059.711	0.191	0.125	279.367	0.135	1.466	3.812	0.312	27	No	No	New (Chapter 8)
Masillapodargus 43	Unknown	1238.889	14.307	-0.459	492.321	12.098	0.746	2.533	0.022	77	No	No	New (Chapter 8)
Masillapodargus 45	Unknown	1147.244	26.295	-0.427	381.366	10.898	0.384	3.019	-0.245	171	No	No	New (Chapter 8)
Masillapodargus 46	Unknown	1270.702	16.313	-0.140	380.880	11.595	-0.227	3.358	0.126	147	No	No	New (Chapter 8)
Masillapodargus 47	Unknown	1183.282	24.166	-0.111	340.751	33.597	0.201	3.669	0.935	119	No	No	New (Chapter 8)
Masillapodargus 48	Unknown	1146.763	29.596	-0.261	368.270	22.533	-0.283	3.092	-0.208	64	No	No	New (Chapter 8)
Masillapodargus 49	Unknown	1104.858	21.253	-0.675	283.574	12.540	0.493	3.895	-0.454	64	No	No	New (Chapter 8)
Masillapodargus 50	Unknown	1015.283	29.168	0.018	313.318	18.391	-0.058	3.235	-0.721	41	No	No	New (Chapter 8)
Masillapodargus 51	Unknown	1272.158	18.835	0.210	266.911	15.231	0.907	4.836	-0.039	218	No	No	New (Chapter 8)
Paraprefica 53	Unknown	1550.631	23.512	-0.690	528.204	17.397	0.011	2.938	0.155	127	No	No	New (Chapter 8)
Paraprefica 54	Unknown	1498.735	27.332	-0.911	534.710	23.744	-0.970	2.800	0.304	61	No	No	New (Chapter 8)
Paraprefica 55	Unknown	1227.155	27.726	0.373	459.785	17.581	0.290	2.682	0.393	8	No	No	New (Chapter 8)
Paraprefica 56	Unknown	956.368	21.865	0.826	303.353	15.786	0.230	3.189	0.493	67	No	No	New (Chapter 8)
Paraprefica 57	Unknown	1183.599	14.564	-0.010	221.320	11.767	1.178	5.361	-0.230	9	No	No	New (Chapter 8)
Paraprefica 58	Unknown	1031.704	11.341	0.304	199.437	7.778	0.412	5.204	0.544	25	No	No	New (Chapter 8)
Paraprefica 64	Unknown	1184.921	26.196	0.268	303.422	13.859	0.296	3.950	0.131	27	No	No	New (Chapter 8)
Paraprefica 66	Unknown	1062.539	22.728	-0.160	269.594	13.253	0.474	3.993	0.147	112	No	No	New (Chapter 8)
Paraprefica 67	Unknown	872.964	30.479	0.183	241.742	20.812	0.467	3.736	0.720	98	No	No	New (Chapter 8)
Paraprefica 68	Unknown	1113.518	26.272	0.601	294.690	17.770	0.912	3.794	-0.185	44	No	No	New (Chapter 8)
Paraprefica 69	Unknown	1371.956	16.156	-0.896	327.692	13.788	0.316	4.217	-0.913	9	No	No	New (Chapter 8)
Paraprefica 72	Unknown	1149.916	26.658	0.233	344.201	18.183	1.406	3.412	0.414	41	No	No	New (Chapter 8)
Paraprefica 73	Unknown	1037.568	23.561	-1.741	259.801	14.703	-1.539	3.941	-2.076	4	No	No	New (Chapter 8)
Paraprefica 80	Unknown	1212.354	23.537	-0.286	269.974	20.428	0.002	4.568	0.275	131	No	No	New (Chapter 8)
Paraprefica 87	Unknown	867.642	41.489	0.100	271.404	22.678	0.835	3.231	1.094	8	No	No	New (Chapter 8)
Parargornis 88	Unknown	1407.836	17.348	-0.438	363.151	22.986	0.671	3.966	0.277	27	No	No	New (Chapter 8)
Parargornis 89	Unknown	721.377	18.110	0.299	483.296	18.279	0.868	1.517	1.220	222	No	No	New (Chapter 8)
Parargornis 90	Unknown	1402.025	23.306	0.056	428.165	20.242	0.303	3.295	0.630	57	No	No	New (Chapter 8)
Parargornis 92	Unknown	1265.273	18.710	-0.479	332.046	19.908	0.133	3.897	-0.212	29	No	No	New (Chapter 8)
Parargornis 93*a*	Unknown	1134.302	21.395	0.079	336.872	15.266	0.363	3.376	0.319	43	No	No	New (Chapter 8)
Parargornis 93*b*	Unknown	802.148	31.337	0.737	394.579	25.162	0.571	2.139	1.266	97	No	No	New (Chapter 8)
Parargornis 95	Unknown	945.067	30.320	0.551	283.118	16.189	0.574	3.326	0.931	48	No	No	New (Chapter 8)
Parargornis 96	Unknown	794.216	10.263	0.115	335.787	8.846	0.494	2.386	0.073	105	No	No	New (Chapter 8)
Parargornis 97*a*	Unknown	1442.477	20.249	0.068	374.447	19.183	0.442	3.938	0.484	32	No	No	New (Chapter 8)
Parargornis 97*b*	Unknown	1296.327	13.616	-0.181	424.108	14.885	-0.226	3.064	-0.330	7	No	No	New (Chapter 8)
Parargornis 100	Unknown	1404.115	34.900	0.400	494.739	33.037	0.251	2.881	0.028	28	No	No	New (Chapter 8)
Parargornis 101*a*	Unknown	1224.680	20.991	0.465	340.392	13.068	-0.871	3.601	1.728	29	No	No	New (Chapter 8)
Parargornis 101*b*	Unknown	1150.851	18.194	-0.507	313.712	17.664	0.930	3.740	0.819	17	No	No	New (Chapter 8)
Parargornis 102	Unknown	1255.779	22.770	-0.430	335.882	13.844	-0.024	3.734	0.520	15	No	No	New (Chapter 8)
Parargornis 104	Unknown	812.542	20.495	-0.318	270.378	12.158	0.860	3.032	0.348	5	No	No	New (Chapter 8)
Parargornis 105	Unknown	1333.322	19.953	-0.056	341.271	18.782	0.274	3.965	0.422	107	No	No	New (Chapter 8)
Scaniacypselus 106*a*	Unknown	992.945	18.345	-0.078	290.916	11.172	1.015	3.458	0.353	140	No	No	New (Chapter 8)
Scaniacypselus 106*b*	Unknown	1045.914	0.259	0.267	269.307	0.134	0.102	3.988	1.219	79	No	No	New (Chapter 8)
Scaniacypselus 107	Unknown	903.050	0.187	0.042	342.153	0.167	0.170	2.681	1.574	63	No	No	New (Chapter 8)
Scaniacypselus 108	Unknown	974.648	0.183	0.629	513.888	0.234	0.899	1.954	0.711	68	No	No	New (Chapter 8)
Scaniacypselus 110	Unknown	1102.042	17.165	0.667	329.032	10.762	0.357	3.378	0.735	69	No	No	New (Chapter 8)
Scaniacypselus 111	Unknown	1035.333	20.028	-0.531	301.210	17.381	1.295	3.556	-0.342	108	No	No	New (Chapter 8)
Scaniacypselus 112	Unknown	888.185	0.201	0.674	497.942	0.137	0.435	1.793	0.916	124	No	No	New (Chapter 8)
Scaniacypselus 113	Unknown	971.687	17.287	-0.140	425.378	22.353	1.041	2.375	0.249	142	No	No	New (Chapter 8)
Scaniacypselus 115	Unknown	1043.306	19.151	1.280	407.462	24.525	-0.887	2.713	1.184	6	No	No	New (Chapter 8)
Scaniacypselus 116*a*	Unknown	969.671	14.807	0.335	487.966	17.009	0.192	2.033	0.808	240	No	No	New (Chapter 8)
Scaniacypselus 116*b*	Unknown	448.281	20.484	0.341	247.239	12.145	0.018	1.822	0.557	213	No	No	New (Chapter 8)
Scaniacypselus 117*a*	Unknown	995.769	0.126	0.055	540.058	0.110	-0.230	1.854	0.095	58	No	No	New (Chapter 8)
Scaniacypselus 117*b*	Unknown	839.110	0.177	0.871	286.901	0.151	0.191	2.993	2.176	88	No	No	New (Chapter 8)
Scaniacypselus 118	Unknown	897.739	0.145	0.060	290.066	0.100	1.095	3.120	0.102	12	No	No	New (Chapter 8)
Scaniacypselus 120	Unknown	743.539	29.596	0.291	210.791	12.314	-0.308	3.539	-0.369	39	No	No	New (Chapter 8)
Eocypselus 124	Unknown	1515.452	11.878	-0.072	451.847	11.773	-0.374	3.379	0.342	38	No	No	New (Chapter 8)
Eocypselus 126*a*	Unknown	1547.462	12.516	2.283	482.590	10.964	0.087	3.234	0.852	29	No	No	New (Chapter 8)
Eocypselus 126*b*	Unknown	1476.087	14.274	0.453	478.128	11.090	1.241	3.113	0.586	110	No	No	New (Chapter 8)
Eocypselus 127	Unknown	1485.203	13.330	-0.710	422.730	12.708	0.659	3.552	-0.269	62	No	No	New (Chapter 8)
Eocypselus 128	Unknown	1434.636	11.339	0.799	437.234	10.383	0.328	3.302	-0.785	50	No	No	New (Chapter 8)
Eocypselus 129	Unknown	1350.403	17.418	-1.012	351.940	13.392	1.090	3.882	-0.630	59	No	No	New (Chapter 8)

Appendix 2 - Papers published during my PhD

Papers arising directly from this thesis:

On the purported presence of fossilized collagen fibres in an ichthyosaur and a theropod dinosaur (Chapter 2)

Fiann M. Smithwick, Gerald Mayr, Evan T. Saitta, Michael J. Benton and Jakob Vinther
Published in the journal *Palaeontology* in April 2017.
DOI: https://doi.org/10.1111/pala.12292

Countershading and stripes in the theropod dinosaur *Sinosauropteryx* reveal heterogeneous habitats in the Early Cretaceous Jehol Biota (Chapter 4)

Fiann M. Smithwick, Robert Nicholls, Innes C. Cuthill and Jakob Vinther
Published in the journal *Current Biology* in November 2017
DOI: https://doi.org/10.1016/j.cub.2017.09.032

Papers not directly associated with this thesis but published during my PhD:

Phanerozoic survivors: Actinopterygian evolution through the Permo-Triassic and Triassic-Jurassic mass extinction events

Fiann M. Smithwick and Thomas L. Stubbs
Published in the journal *Evolution* in January 2018.
DOI: https://doi.org/10.1111/evo.13421

Soft-bodied fossils are not simply rotten carcasses – toward a holistic understanding of exceptional fossil preservation

Luke A. Parry, **Fiann Smithwick**, Klara K. Norden, Evan T. Saitta, Jesus Lozano-Fernandez, Alastair R. Tanner, Jean-Bernard Caron, Gregory D. Edgecombe, Derek E. G. Briggs, and Jakob Vinther
Published in the journal *Bioessays* in January 2018.
DOI: https://doi.org/10.1002/bies.201700167

Melanosome diversity and convergence in the evolution of iridescent avian feathers—Implications for paleocolor reconstruction

Klara K. Nordén, Jaeike W. Faber, Frane Babarović, Thomas L. Stubbs, Tara Selly, James D. Schiffbauer, Petra Peharec Štefanić, Gerald Mayr, **Fiann M. Smithwick** and Jakob Vinther
Published in the journal *Evolution* in January 2019.
DOI: https://doi.org/10.1111/evo.13641